University of Barcelona

Faculty of Pharmacy and Food Sciences

G9a, a histone lysine methyltransferase, as a potential target for Alzheimer's disease

Aina Bellver Sanchis

2024

UNIVERSITAT DE BARCELONA

Department of Pharmacology, Toxicology and Therapeutic Chemistry

DOCTORAL THESIS

PhD program in Biotechnology

G9a, a histone lysine methyltransferase, as a potential target for Alzheimer's disease

Dissertation presented by Aina Bellver Sanchis to apply for the doctorate degree at the University of Barcelona.

Director

Dr. Christian Griñán Ferré

Doctoral student

Aina Bellver Sanchis

Aina Bellver Sanchis

2024

This doctoral thesis has been funded by:

Agència de Gestió d'Ajuts Universitaris i de Recerca

Ministerio de Ciencia, Innovación y Universidades (Agencia Estatal de Invesigación)
Fondo Europeo de Desarrollo Regional

Centro de Investigación Biomédica en Red sobre Enfermedades Neurodegenerativa

Fundació Bosch i Gimpera

Institut de Neurociències Universitat de Barcelona

Fundació Montcelimar

International Brain Research Organization

Sociedad Española de Farmacología

A la Lluna,
als de casa,
i a mi mateixa

Acknowledgments

En aquests quasi quatre anys he tingut la sort de compartir molts moments, bons, regulars i dolents. Per sort no he estat sola, i per això m'agradaria dedicar unes paraules a totes les persones que d'una forma o un altre han format part d'aquesta aventura.

En primer lloc, m'agradaria dirigir-me a les persones que em van donar l'oportunitat de poder estar un dia com avui presentant la tesi doctoral. Gràcies Christian, per ser el meu mentor, director i també amic en aquesta etapa. Gràcies per tota la confiança dipositada en mi, per deixar-me acompanyar-te en molts projectes i per totes les oportunitats per poder créixer. Agrair-te la teva paciència i comprensió en els moments de "bajona". Encara ens queden moltes aventures i de fet, no havíem acabat aquesta que ja hem començat la següent. També vull agrair a la Mercè per tota la teva ajuda i suport, tant en l'àmbit personal com professional. Gràcies per ser com ets, per inspirar-me i per ensenyar-me a tenir-ho tot organitzat. El grup té molta sort de tenir-vos, sou tots un referents.

Gràcies a totes les companyes que he tingut en el grup. Júlia i Foteini, per ser la meva motivació a tornar al grup. Per ensenyar-me quan encara jo estudiava Farmàcia i per ajudar-me en els meus primers passos com a estudiant de doctorat. Heu sigut un suport molt important i em fa molt feliç saber que sempre podré comptar amb vosaltres. A l'Alba i a la Júlia, per escoltar-me i tenir tanta paciència. Gràcies per "deixar-me" que us agafés les membranes sense que us enfadeu (jeje) i gràcies per tots els riures fins i tot en els dies més grisos. No vull desaprofitar el moment per també agrair l'ajuda que he tingut de part de les millors estudiants amb qui he treballat. Marta i Iva, us heu guanyat tota la meva confiança i us desitjo molta sort en la vostra etapa doctoral iniciada recentment, ja sabeu que sempre podreu comptar amb mi. Gracias Veronica por tus buenas vibras, yo de mayor quiere ser como tu, tan feliz, positiva y paciente. Y por último Ana, que a pesar de ser la última en llegar al grupo siempre dispuesta a ayudarme, muchísimas gracias.

Agrair a totes les persones que formen o han format part del departament. Especialment gràcies a la Núria, l'Edurne, al Javi i a la Triana. Gràcies per literalment tot. Sense vosaltres tot hauria estat molt difícil. Com sabeu aquesta etapa és una mica muntanya russa i reconec que heu tingut una paciència increïble amb mi. M'heu escoltat parlar de la meva tesis i problemes una vegada i una altra, té el seu mèrit. Heu estat el meu recolzament incondicional, i formeu part de la família que un escull. Tampoc vull deixar de mencionar al Roger i a la Mireia heu estat un gran descobriment en aquest camí. A tots vosaltres, espero que puguem continuar compartint aventures junts i celebrar moltes coses en el futur. No puc estar més orgullosa dels companys amb qui he pogut compartir aquesta aventura.

Una de les coses més importants que he fet durant el doctorat, ha estat marxar a Gainesville. Gràcies Gemma per ensenyar-me i donar-me l'oportunitat, per la teva acollida i per regalar-me moments que difícilment oblidaré com el meu primer Thanksgiving i el primer partit de fútbol americà. Gracias Luis por cuidarme como un hermano mayor, por ser mi mentor y mi gran amigo durante todo ese tiempo. Me regalaste charlas cientificas y filosóficas en la sala de cultivos y como dice la canción, me enseñaste a desaprender lo que había aprendido, para poder crecer. También gracias por presentarme a Rachel y dejarme formar parte en vuestras vidas...sois mi pareja favorita. Thanks to Hannah and Abby for everything we lived together, the nights at the Arcade, my first selfie with an alligator or all the coffees we had together. I also don't want to forget the guys with whom I had so much fun, Lloyd (my honey), Iggy and Julian. I wish you all the best, I miss you all so much! You made me feel at home from day one.

No vull deixar de passar l'oportunitat de fer una menció especial al David. Gracias por tu ayuda en el proceso del set-up del ChiP-seq, y tu generosidad ejemplar.

I would also like to thank those who taught me how to work with the *C. elegans*. Dr. Maciel's group took me in and let me be part of their family when I was just finishing my degree. Thank you for the opportunity and for your willingness to teach me, even from a distance.

Patrícia, Andreia, Joana, Bruna, Daniela C., Daniela V., and Jorge, to all of you thank you very much.

Als meus amics, Júlia T., Jiaming, Rocío, Natalia, Silvia, Cristina, Lorena, Miquel, Marc, Gerard, Denisa, Ferran, Cristina C. i Ari. Gràcies per tots aquells moments de desconnexió del laboratori tan necessaris. Espero poder seguir al vostre costat per seguir veient com anem creixent.

Gracies a tota la meva família. Per preocupar-se i preguntar sobre la tesi en els dinars familiar, o en qualsevol altre moment. A les meves cosines preferides, Farners i Berta, gràcies pels plans que m'han fet sortir del laboratori.

Als de casa, els que han estat sempre amb mi, gràcies per absolutament tot. Sense el vostre suport això no hauria estat possible i en el fons, aquesta tesi doctoral també és vostre. Papa i mama, moltes gràcies per estimar-me, i recolzar-me en totes les aventures (papa, te prometo que la siguiente tesi será sobre los gémenes de los). Gràcies per cuidar-me quan ho he necessitat, sé que sempre estareu al meu costat. A les meves germanes, Laia i Marta, gràcies per ser allà quan ho he necessitat. Per confiar i valorar la meva feina quan jo no ho feia, per estimar-me i preocupar-vos per mi. Soc afortunada de tenir-vos com a germanes. Isaac i Samu, gràcies per la paciència que teniu amb mi i la vostra disposició a ajudar-me sempre. Lluc hauran de passar uns anyets perquè ho puguis entendre i jo estaré encantada de poder-t'ho explicar, però de moment, vull que sàpigues que la teva arribada a casa ha estat una alegria enorme per tots. No deixis mai de somriure. Pau, gràcies per fer-me feliç, cuidar-me, estimar-me i sobretot per tota la paciència que has tingut aquests últims mesos. No em vull deixar al *Chester*, i a la *Fosca*, ja sé que és impossible que ho entengueu, però m'encanta passar temps amb vosaltres. I com no, també vull dedicar-li unes paraules a la *Lluna*, la que es va emportar un trosset del meu cor i trobo molt a faltar. A tots vosaltres us estimo molt.

Statement of Originality

With this statement, I hereby declare that the submitted PhD thesis is my own original work and includes material for five scientific articles that have been previously published in international peer-reviewed journals. All the assistance received in preparing this thesis and sources have been acknowledged.

Aina Bellver Sanchis

March 2024

Abstract

Alzheimer's disease (AD) is the most common cause of dementia that currently lacks effective pharmacological treatment. Identifying new targets to halt disease progression is a pressing need. In most cases, AD has a complex etiology likely to involve multiple susceptibility genes and environmental factors. Epigenetics plays a crucial role in linking the genome to the environment and regulating the transcription of genes related to learning and memory. In particular, G9a is a histone lysine methyltransferase identified as having a critical role in various neurodegenerative diseases, including AD.

On the one hand, I first conducted a study to confirm the involvement of G9a in the neurodegenerative processes that underlie the Senescence Accelerated Mouse-Prone 8 (SAMP8) model at both a behavioural and molecular level. Secondly, we demonstrated the efficacy of G9a inhibition as a therapy for AD using the SAMP8 mouse. We identified its main altered pathways and a novel mechanism of action based on Glia maturation factor beta (GMFB) modulation. The third study validated additional epigenetic mechanisms, specifically microRNAs, that participate in AD and are present in the SAMP8 model. These mechanisms were reversed after the inhibition of G9a. Notably, the downregulation of *miRNA-128* after G9ai partially explains the modulations of pathways related to Peroxisome proliferator-activated receptor gamma (PPARγ).

On the other hand, given the problems associated with G9a inhibitors (G9ai), such as toxicity, poor blood-brain barrier (BBB) permeability, and selectivity, it was decided to focus efforts on the search for chemical structures that would overcome these challenges. The fourth study involved structure-based virtual screening and *in vitro* and *in vivo* screening of the chosen compounds [redacted]

[redacted]

Finally, the drug discovery process is characteristically expensive and lengthy. Therefore, the fifth article focuses on the repurposing technique, which is often less risky, more cost-effective, and can be completed in less time. An *in silico* study proposed a cancer drug, Raltitrexed, as a possible G9ai. This work evaluated its efficacy in inhibiting G9a through *in vitro* and *in vivo* studies using the *C. elegans* model. The results suggest that Raltitrexed could be a candidate for treating AD, although further experiments are required.

Resumen

La enfermedad de Alzheimer (EA) es la causa más común de demencia que actualmente carece de tratamiento farmacológico efectivo. Identificar nuevas dianas para detener la progresión de la enfermedad es una necesidad urgente. En la mayoría de los casos, la EA tiene una etiología compleja que probablemente involucra múltiples genes de susceptibilidad y factores ambientales. La epigenética juega un papel crucial en la conexión del genoma con el medio ambiente y en la regulación de la transcripción de genes relacionados con el aprendizaje y la memoria. En particular, G9a es una lisina metiltransferasa de histona identificada como un elemento crítico en varias enfermedades neurodegenerativas, incluida la EA.

Por un lado, realicé un estudio para confirmar la participación de G9a en los procesos neurodegenerativos que subyacen al modelo *Senescence Accelerated Mouse-Prone 8* (SAMP8) tanto a nivel conductual como molecular. En segundo lugar, demostramos la eficacia de la inhibición de G9a como terapia para la EA utilizando el ratón SAMP8. Identificamos sus principales vías alteradas y un nuevo mecanismo de acción basado en la modulación del factor de *Glia maturation factor beta* (GMFB). El tercer estudio validó mecanismos epigenéticos adicionales, específicamente microARN, que participan en la EA y están presentes en el modelo SAMP8. Estos mecanismos se revirtieron después de la inhibición de G9a. Es importante destacar que la regulación negativa de *miARN-128* después de la inhibición de G9a explica parcialmente las modulaciones de las vías relacionadas con el *Peroxisome proliferator-activated receptor gamma* (PPARγ).

Por otro lado, dado los problemas asociados con los inhibidores de G9a (G9ai), como la toxicidad, la baja permeabilidad de la barrera hematoencefálica y la selectividad, se decidió centrar los esfuerzos en la búsqueda de estructuras químicas que superaran estos desafíos. El cuarto estudio involucró el cribado virtual basado en estructuras y el cribado *in vitro* e *in vivo* de los compuestos elegidos. [redacted]

[redacted]

Finalmente, el proceso de descubrimiento de medicamentos es característicamente costoso y largo. Por lo tanto, el quinto artículo se centra en la técnica de reutilización, que a menudo es menos arriesgada, más rentable y puede completarse en menos tiempo. Un estudio *in silico* propuso un medicamento contra el cáncer, Raltitrexed, como posible G9ai. Este trabajo evaluó su eficacia en la inhibición de G9a a través de estudios *in vitro* e *in vivo* utilizando el modelo *C. elegans*. Los resultados sugieren que Raltitrexed podría ser un candidato para tratar la EA, aunque se requieren más experimentos.

Thesis Structure

The present doctoral dissertation is presented in the following chapters:

Chapter 1- Introduction provides background knowledge and summarizes the existing research of the topic in which this thesis is framed, with special attention to the role of the lysine methyltransferase G9a in Alzheimer's disease.

Chapter 2- Objectives contains the general aim and the specific points that were addressed during the development of this dissertation and at the beginning of each scientific work.

Chapter 3- Methods and Results is divided into four sections, each one of which is based on a separate scientific investigation, already published in international peer-review journals. These sections provide evidence demonstrating the role of G9a in Alzheimer's disease, as well as the beneficial effects following its pharmacological inhibition at both the cognitive and molecular levels. In addition, the last section presents the development of new G9a inhibitors using the nematode C. *elegans*, different cell cultures and the SAMP8 murine model.

Chapter 4- Discussion provides an in-depth interpretation of the results obtained throughout the thesis.

Chapter 5- Conclusions is a set of concluding statements based on the findings collected from the four different investigations.

The Annex contains the following: (a) unpublished results[redacted]; (c) Supplementary figures and tables belonging to the Introduction section "*1.3.5. Rationing, design, and synthesis of G9a inhibitors*".

Below we list the five scientific papers that form the research output of the present dissertation:

Publication 1

Vasilopoulou F*, **Bellver-Sanchis A***, Companys-Alemany J, Jarne-Ferrer J, Irisarri A, Palomera-Ávalos V, Gonzalez-Castillo C, Ortuño-Sahagún D, Sanfeliu C, Pallàs M, Griñán-Ferré C. Cognitive Decline and BPSD Are Concomitant with Autophagic and Synaptic Deficits Associated with G9a Alterations in Aged SAMP8 Mice. Cells. **2022**; 11(16):2603. DOI: 10.3390/cells11162603. *These authors contributed equally to this work.

Publication 2

Bellver-Sanchis A, Geng Q, Navarro G, Ávila-López PA, Companys-Alemany J, Marsal-García L, Larramona-Arcas R, Miró L, Perez-Bosque A, Ortuño-Sahagún D, Ranjan Banerjee D, Singh Choudhary B, Soriano FX, Poulard C, Pallàs M, Du HN, Griñán-Ferré C. G9a inhibition promotes neuroprotection through GMFB regulation in Alzheimer's disease. Aging and disease. **2024**; 15(1):311-337. DOI: 10.14336/AD.2023.0424-2.

Publication 3

Bellver-Sanchis A, Ávila-López PA, Tic I, David Valle-García D, Ribalta-Vilella M, Labrador L, Banerjee DR, Guerrero A, Casadesus G, Poulard C, Pallàs M, Griñán-Ferré C. Neuroprotective effects of G9a inhibition through modulation of PPARγ-dependent pathways by *miR-128*. Neuronal Regeneration Research. **2024**; 10-4103. DOI: 10.4103/1673-5374.393102.

Publication 4

Bellver-Sanchis A*, Singh Choudhary B*, Companys-Alemany J, Sukanya, Ávila-López P, Martínez-Rodríguez AL, Brea Floriani JM, Malik R, Pallàs M, Pérez B, Griñán-Ferré C. Structure based virtual screening, *in vitro* and *in vivo* analysis revealed novel potent methyltransferase G9a inhibitors as prospective anti-Alzheimer's agents. ChemMedChem. **2022**; e202200002. DOI: 10.1002/cmdc.202200002. *These authors contributed equally to this work.

Publication 5

Jana A*, **Bellver-Sanchis A***, Griñán-Ferré C, Banerjee DR. Repurposing of Raltitrexed as an Effective G9a/EHMT2 Inhibitor and Promising Anti-Alzheimer's Agent. ACS Med Chem Lett. **2023**; 14(11):1531-153. DOI: 10.1021/acsmedchemlett.3c00344.*These authors contributed equally to this work.

Furthermore, additional scientific papers have been published during the period of the thesis as a result of the author's participation in other studies carried out by members of the same research group. The content of these publications has not been included in the main document since the author contributed as a collaborator instead of leading the investigation.

Griñán-Ferré C, Jarne-Ferrer J, **Bellver-Sanchis A**, Ribalta-Vilella M, Barroso E, Salvador JM, Jurado-Aguilar J, Palomer X, Vázquez-Carrera M, Pallàs M. Deletion of Gadd45a Expression in Mice Leads to Cognitive and Synaptic Impairment Associated with Alzheimer's Disease Hallmarks. International Journal of Molecular Sciences. **2024**; 25(5):2595. DOI: 10.3390/ijms25052595.

Griñán-Ferré C*, Jarne-Ferrer J*, **Bellver-Sanchis A**, Codony S, Puigoriol-Illamola D, Sanfeliu C, Oh Y, Lee S, Vázquez S, Pallàs M. Novel molecular mechanism driving neuroprotection after soluble epoxide hydrolase inhibition: Insights for Alzheimer's disease therapeutics.CNS Neuroscience & Therapeutics. **2023**; 00:01-20 *These authors contributed equally to this work. DOI: 10.1111/cns.14511.

Jarne-Ferrer J, Griñán-Ferré C, **Bellver-Sanchis A**, Vázquez S, Muñoz-Torrero D, Pallàs M. A Combined Chronic Low-Dose Soluble Epoxide Hydrolase and Acetylcholinesterase Pharmacological Inhibition Promotes Memory Reinstatement in Alzheimer's Disease Mice Models. Pharmaceuticals. **2022**; 15(8):908. DOI: 10.3390/ph15080908.

Griñán-Ferré C*, **Bellver-Sanchis A***, Olivares-Martín M, Bañuelos-Hortigüela O, Pallàs M. Synergistic Neuroprotective Effects of a Natural Product Mixture against AD Hallmarks and

Cognitive Decline in Caenorhabditis elegans and an SAMP8 Mice Model. Nutrients. **2021**; 13:2411. DOI: 10.3390/nu13072411. *These authors contributed equally to this work.

Bellver-Sanchis A, Pallàs M, Griñán-Ferré C. The Contribution of Epigenetic Inheritance Processes on Age-Related Cognitive Decline and Alzheimer's Disease. Epigenomes. **2021**; 5(2):15. DOI: 10.3390/epigenomes5020015.

Pawar S, **Bellver-Sanchis A**, Griñán-Ferré C. RNA-seq and miRNA-seq data from pharmacological inhibition of the G9a/GLP histone methyltransferase complex with UNC0642 in SAMP8 mice. Data in Brief. **2021**; 107114. DOI: 10.1016/j.dib.2021.107114.

Griñán-Ferré C, **Bellver-Sanchis A**, Izquierdo V, Corpas R, Roig-Soriano J, Chillón M, Andres-Lacueva C, Somogyvári M, Sőti C, Sanfeliu C, Pallàs M. The pleiotropic neuroprotective effects of resveratrol in cognitive decline and Alzheimer's disease pathology: from antioxidant to epigenetic therapy. Ageing Research Reviews. **2021**; 101271. DOI: 10.1016/j.arr.2021.101271.

In addition, the author participated in three projects as Entrepreneur researcher and two patent applications:

[redacted]

[redacted]

[redacted]

Abbreviations

5-hmC: hydroxymethylation of cytosine

5-mC: DNA methylation

7βS: Seven β-strand

ABCA7: ATP Binding Cassette Subfamily A Member 7

AchE: acetylcholinesterase

AD: Alzheimer's disease

ADAM10: ADAM Metallopeptidase Domain 10

ADMET: absorption, distribution, metabolism, excretion, and toxicity

Aldh2: Aldehyde dehydrogenase

AML: acute myeloid leukemia

ANK1: Ankyrin 1

Aox1: Aldehyde Oxidase 1

APH1B: Aph-1 Homolog B, Gamma-Secretase Subunit

APOE: Apolipoprotein E

APP: Amyloid Beta Precursor Protein

ARC: Activity regulated cytoskeleton associated protein

Asp: Aspartate

Atg12: Autophagy Related 12

ATM: ataxia telangiectasia-mutated

Aβ: Amyloid beta

BACE1: Beta-Secretase 1

BAT8: HLA-B associated transcript 8

BAX: BCL2 Associated X

BBB: blood-brain barrier

BDNF: Brain Derived Neurotrophic Factor

BECN1: Beclin-1

BIN1: Bridging Integrator 1

BPSD: behavioural and psychological symptoms of dementia

C. elegans: Caenorhabditis elegans

CAMKII: calcium/calmodulin-activated protein kinase II

CASP: Caspase

CAT: Catalase

CCL: C-C Motif Chemokine Ligand

CDK5: Cyclin Dependent Kinase 5

CDP/cut: CCAAT displacement protein/cut

CH3: methylation

ChIP-seq: Chromatin immunoprecipitation-sequencing

CK1: casein kinase 1

CMA: chaperon-mediated autophagy

CNS: central nervous system

Comt: catechol-O-Methyltransferase

Cox2: Cyclooxygenase-2

CpG: cytosine-guanine dimer

CRCs: chromatin remodeling complexes

CREB: CAMP Responsive Element Binding Protein

CRR: cysteine-rich

CXCL: C-X-C Motif Chemokine Ligand

CYCs: Cytochrome C, Somatic

Dcx: Doublecortin

DFE: desferrioxamine

DFO: deferoxamine

DI: discrimination index

DNMT: DNA methyltransferase

DYRK1A: dual-specificity tyrosine-phosphorylation-regulated kinase 1A

EE: environmental enrichment

EGFR: Epidermal Growth Factor Receptor

EHMT1: euchromatic histone N-methyltransferase 1

EHMT2: euchromatic histone N-methyltransferase 2

EOAD: Early-onset AD

EPM:Elevated plus maze

ERG-1: Early Growth Response-1

ERK: Extracellular Signal-Regulated Kinase 2

EWAS: Epigenome-wide association studies

EZH2: Enhancer Of Zeste 2 Polycomb Repressive Complex 2 Subunit

FAD: familial AD

FDA: Food and Drug Administration

Fer-1: ferrostatin-1

FOXO: Forkhead Box O1

G9ai: G9a inhibitor

GABABR2: Gamma-Aminobutyric Acid Type B Receptor Subunit 2

GADD45α: Growth arrest and DNA damage 45 alpha

GFAP: Glial Fibrillary Acidic Protein

GLP: G9a-like protein

GMFBi: GMFB inhibitor

GPX: Glutathione Peroxidase

GSEA: Gene Set Enrichment Analysis

GSH: glutathione

[redacted]

[redacted]

GWAS: Genome-wide association studies

H: Histone

H2O2: hydrogen peroxide

HAT: Histone acetyltransferases

HDAC: histone deacetylase

HDM: histone demethylases

HIFα: Hypoxia Inducible Factor 1 Subunit Alpha

Hmox1: Heme oxygenase decycling 1

HMT: Histone methyltransferase

IBA-1: Ionized calcium binding adaptor molecule 1

IC_{50}: Half maximal inhibitory concentration

IDE: insulin-degrading enzyme

IEG: immediate early genes

IFN-γ: Interferon-gamma

ikb-1: I Kappa B homolog

IL: interleukin

JNK: C-Jun N-Terminal Kinase 1

K: Lysine

K_d: dissociation constant

KD: knock-down

KDAC: lysine deacetylase

KDM: Histone lysine demethylases

KEGG: Kyoto Encyclopedia of Genes and Genomes

KMT: lysine methyltransferase

KO: knock-out

LC3B: Microtubule Associated Protein 1 Light Chain 3 Beta

Leu: Leucine

lncRNA: long non-coding RNA

LOAD: Late-onset AD

LPS: Lipopolysaccharide

LTD: long-term depression

LTP: long-term potentiation

MAPK: Mitogen-Activated Protein Kinase

MARK p110: microtubule affinity-regulated kinase 110

MCI: mild cognitive impairment

MDB: Methyl-CpG Binding Domain

me1: mono-methylated

me2: di-methylated

me3: tri-methylated

MEF2D: Myocyte Enhancer Factor 2D

miRNA-seq: miRNA-sequencing

miRNA: microRNA

MM-GBSA: Mechanics-Generalized Born Surface Area

MM: multiple myeloma

MMP9: matrix metalloproteinase-9

MOF: males-absent-on-the-first

MST1: mammalian STE20-like kinase 1

MTDL: multi-target-directed ligands

MyoD: Myogenic Differentiation 1

NAcSh: nucleus accumbens shell

ncRNA: non-coding RNA

ND: non-demented

NEP: neprilysin

NeuN: Neuronal nurclear antigen

NFTs: Neurofibrillary tangles

NGF: nerve growth factor

NGS: Next-generation sequencing

NLS: nuclear localization signal

NMDA: N-methyl-D-aspartate

NMDAR: N-methyl-D-aspartate receptor

non-PDPK: non-proline-directed protein kinase

NORT: Novel object recognition test

NRF2: Nuclear Factor erythroid-2-Related Factor 2

NRSF: Neuron-restrictive silencer factor

NSD: nuclear receptor-binding SET Domain

NT: neurotrophin

OF: Open Field

OS: Oxidative stress

p75NTR: pan-neurotrophin receptor p75

PAINS: non-Pan assay interreference compounds

PAMPA: Parallel Artificial Membrane Permeation Assays

PCAF: p300/CBP-associated factor

PD: Parkinson’s disease

PDPK: Proline-directed protein kinases

Pe: permeability value

Phe: Phenylalanine

PHF8: PHD Finger Protein 8

PILRA: Paired Immunoglobin Like Type 2 Receptor Alpha

piRNA: piwi-interacting RNA

PKA: Protein kinase A

PKMT: protein lysine methyltransferases

PoC: proof of concept

PPARγ: Peroxisome Proliferator Activated Receptor Gamma

PRC2: Polycomb repressive complex 2

PRDI-BF1: positive regulatory domain I-binding factor 1

PRMTs: arginine methylatrasnferase

PRPs: plasticity-related products

PSD: post-synaptic proteins

Psen: Presenilin

PTK2B: Protein Tyrosine Kinase 2 Beta

PTM: Post-translational modification

PTSD: Post-traumatic stress disorder

QSAR: quantitative structure–activity relationship

R: Arginine

REST: RE1 Silencing Transcription Factor

RI: Resident intruder test

RNA-seq: RNA-sequencing

RNAi: RNAi interference

ROS: reactive oxygen species

SAH: S-adenosyl-L-homocysteine

SAM: S-adenosyl-l-methionine

SAMP8: Senescence-accelerated mouse prone 8

SAMR1: Senescence-Accelerated Resistant Mouse 1

SAR: structure-activity relationship

Ser: serine

SETDB: SET Domain Bifurcated Histone Lysine Methyltransferase

siRNA: Small interfering RNA

SIRT1: Sirtuin 1

Snap25: Synaptosome Associated Protein 25

SOD: superoxide dismutase

SORL1: Sortilin Related Receptor 1

SQSTM1: sequestosome 1

STC: synaptic tagging/capture

SYN: synapsin

SYP: synaptophysin

Tbr1: T-Box Brain Transcription Factor 1

TCT: Three Chamber test

TET: Ten-Eleven Translocation

Tgf:Transforming growth factor

Thr: threonine

TIP60: Tat-interactive protein 60

TNF-a: Tumor Necrosis Factor alpha

TP53INP2: Tumor Protein P53 Inducible Nuclear Protein 2

TREM2: Triggering Receptor Expressed On Myeloid Cells 2

Trk: tyrosine kinase

Tyr: tyrosine

Vgf: VGF Nerve Growth Factor Inducible

VS: Virtual Screening

WIPI1: WD Repeat Domain, Phosphoinositide Interacting 1

ZNF200: Zinc Finger Protein 200

Abbreviations throughout Chapter 3 (Methods and Results) may vary. Each publication contains separate abbreviations section according to the guidelines of the journal.

Contents

Acknowledgments ix

Statement of Originality xii

Abstract (English/Spanish) xv

Thesis Structure xix

Abbreviations xxiii

1 Introduction……1

1.1. Aging, neurodegeneration, and cognitive decline……..2

1.2. Epigenetic landscape in Alzheimer's Disease……4

1.2.1. Understanding Alzheimer's disease…….…….4

1.2.2. Epigenetic insights into Alzheimer's Disease……5

1.2.2.1. DNA methylation…….…….6

1.2.2.2. Histone modifications…….……..8

1.2.2.3. Non-coding RNA (ncRNA) regulation……...11

1.2.3. Chromatin Remodeling, unveiling a potential drug target……...13

1.3. G9a, a lysine methyltransferase…….……...14

1.3.1. Discovery of G9a…….…….14

1.3.2. G9a structure……14

1.3.3. G9a activity…….…….……....17

1.3.4. G9a function…….…….……...18

1.3.5. Rationing, design, and synthesis of G9a inhibitors……..20

[redacted]

1.4. From neuropathology to G9a's role in Alzheimer's disease progression…….27

1.4.1. Clinical symptoms…….……...27

1.4.2. Microscopic features of Alzheimer's disease……..28

1.5. Treatments for Alzheimer's disease…….…….41

1.5.1. Currently approved treatments for Alzheimer's disease……...41

1.5.1.1. Drugs that treat symptoms…….……..41

1.5.1.2. Disease-modifying drugs…….……41

1.5.2. The journey to drug discovery…….……42

1.5.2.1. Drug Discovery: From target to clinical candidate……..42
1.5.2.2. Hit-to-Lead, and Further Optimization……....43
1.5.2.3. Drug repurposing: Challenges and Opportunities……44
1.5.3. Emerging candidates in clinical trials for Alzheimer's disease treatment....44
1.5.4. G9a inhibitors as a promising treatment for Alzheimer's disease…….....45
1.6. Alzheimer's Disease Experimental Models……..46
1.6.1. Caenorhabditis elegans…….....46
1.6.2. SAMP8 mouse model for pathological aging, neurodegeneration, and sporadic Alzheimer's Disease…….....48
2 Objectives……51
3 Methods and Results……...56
3.1. Publication 1……...57
3.2. Publication 2……...87
3.3. Publication 3……..175
3.4. Publication 4……..199
3.5. Publication 5……..231
4 Discussion……...251
4.1. G9a is a potential target for Alzheimer's disease……254
4.2. Effects of G9a on cognitive decline and BPSD in SAMP8, a LOAD mouse model……..256
4.3. Molecular insights into the enhancement of synaptic plasticity by inhibition of G9a in SAMP8……259
4.4. GMFB transduction pathway activation: the key to neuroprotection after G9a inhibition in SAMP8……...263
4.4.1. Rebalancing neuroinflammatory pathways via GMFB after the pharmacological treatment of G9a inhibition……..267
4.4.2. G9a methylation of GMFB promotes neurodegeneration……..268
4.5. G9a inhibition reveals insights into miR-128 dysregulation in SAMP8 Mice ……..269
4.5.1. G9a inhibition induces antioxidant response via PPARγ……271
4.5.2. Upregulation of PPARγ by G9ai could promote the autophagic process..272
4.5.3. GADD45α up-regulation mediated by G9a inhibition ameliorates the DNA damage response and promotes apoptosis……273
4.6. Identifying potent G9a inhibitors for Alzheimer's disease…….274
4.6.1. Compound F: a promising candidate for Alzheimer's disease therapy…..275

4.6.4. The repurposing approach: The Raltitrexed……..…….....279
4.7. Final considerations……..……...…....280
5 Conclusions…….283
6 Bibliography……..…….286
A. Annex……...…….…….…….....341
A3. Supplementary information – Chapter 1. Introduction…….389

List of Figures

Figure 1. Hallmarks of aging. 3
Figure 2. Schematic representation of epigenetics plays a fundamental role as a link between the genome, the environment, and its mechanisms. 6
Figure 3. Schematic representation of human and mouse G9a isoforms.. 17
Figure 4. Part I: Rationing, design, and synthesis of G9a inhibitors. 21
Figure 5. Part II: Rationing, design, and synthesis of G9a inhibitors. 22
Figure 6. Part III: Rationing, design, and synthesis of G9a inhibitors. 23
Figure 7. Putative mechanisms of degeneration in Alzheimer's disease. 28
Figure 8. Findings in AD after pharmacological inhibition or gene edition of G9a. 40
Figure 9. Drug discovery and development process. 43
Figure 10. Experimental models of AD used in this doctoral dissertation. 50
Figure 11. Schematic representations of the beneficial effects of G9a inhibition leading to neuroprotection in the context of Alzheimer's disease. Proposal of different strategies for obtaining G9a inhibitors as candidates for treatment of Alzheimer's disease. 282

List of Tables

Table 1. DNA methylation levels in genes related to AD. 7
Table 2. Histone modifications found in the AD pathology. 10
Table 3. ncRNA alterations found in the AD pathology. 12
Table 4. Selection of the most used G9a inhibitors. 24
Table 5. Multi-target-directed ligands compounds that include G9a as one of the targets. . 26

The figures and tables of the included publications and annexes are not listed.

1 Introduction

1.1. Aging, neurodegeneration, and cognitive decline

Aging is an inevitable process characterized by the progressive functional decline of organisms at the molecular, cellular, and physiological levels (Sen et al., 2016). This is usually associated with physical deterioration that leads to an increased risk of disease and death (Rose, 2009). Of note, there is a link between aging and the process of neurodegeneration, together with genetic and environmental factors, promoting cognitive decline. Hence, among the known risk factors for neurodegenerative diseases, the aging process has the highest impact, so the risk of suffering from such diseases increases with age (Hou et al., 2019). For instance, the most common neurodegenerative diseases, Alzheimer's disease (AD) and Parkinson's disease (PD), are predominantly observed in elderly individuals (Poewe et al., 2017; Gaugler et al., 2022). Nevertheless, there are notable differences between the changes observed in the brains during typical aging (not affecting their daily activities) compared to those in neurodegenerative conditions, where neuronal death is strongly evident (Godin et al., 2018).

In 2013, López-Otin et al. identified nine distinctive "hallmarks of aging" related to the biological mechanism underlying aging, classified into primary, antagonistic, and integrative categories (López-Otín et al., 2013). However, after a decade of research in this field, novel hallmarks have been identified (López-Otín et al., 2023). Firstly, the primary hallmarks encompass genomic instability, telomere attrition, epigenetic alterations, the loss of proteostasis, and disabled macroautophagy. Secondly, antagonistic features, including mitochondrial dysfunction, cellular senescence, and dysregulation of nutrient sensing, represent compensatory or negative responses to primary damage. Integrative hallmarks such as stem cell depletion, impaired intercellular communication, chronic inflammation, and dysbiosis arise due to cumulative damage induced by both direct and antagonistic hallmarks, ultimately contributing to the functional decline associated with aging (López-Otín et al., 2013, 2023) (Figure 1).

The present thesis focuses on epigenetic mechanisms, which play age-related roles in pathologies associated with neurodegenerative diseases. Epigenetic marks strongly influence chromatin activity and function, including transcription and replication, and are an emerging field in neurodegeneration and neuroprotection.

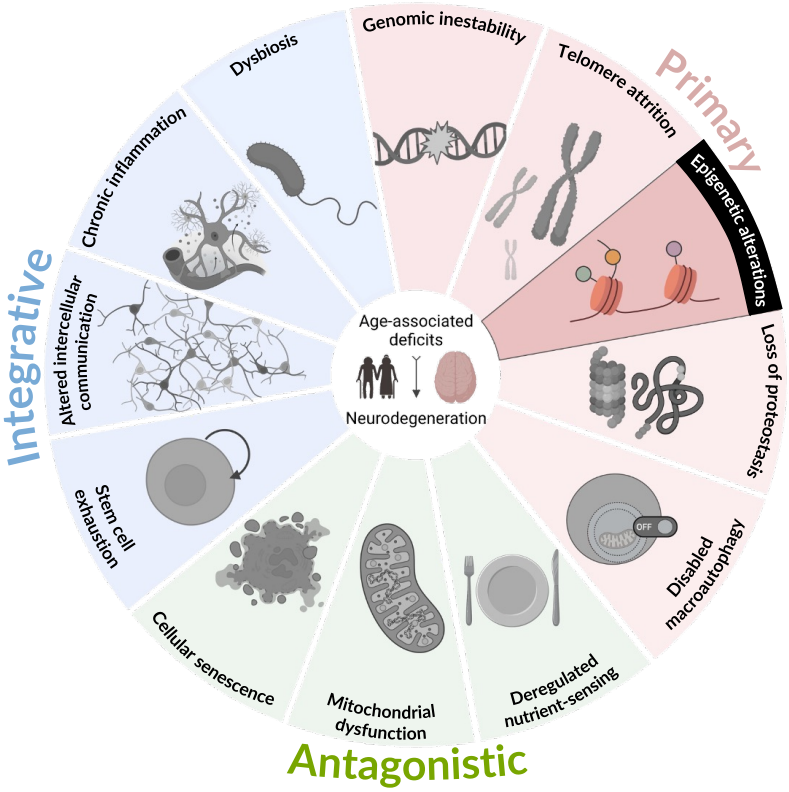

Figure 1. Hallmarks of aging (adapted from López-Otín et al., 2023).

1.2. Epigenetic landscape in Alzheimer's Disease

1.2.1. Understanding Alzheimer's disease

AD is the most common neurodegenerative disease, and the incidence is expected to increase to over 91 million people worldwide by 2050 (Association, 2019). AD is often categorized into familial or early-onset AD (EOAD) and sporadic or late-onset AD (LOAD). EOAD accounts for about 5-10% of all AD cases that develop cognitive impairment before age 65; the remaining 90% of cases are diagnosed as LOAD and develop cognitive impairment after age 65 (Reitz et al., 2020). Approximately 1% of AD instances are attributed to single-gene disorders, distinguished by early onset and inheritance through an autosomal dominant pattern (Migliore and Coppedè, 2022). Unfortunately, most cases of AD present a complex etiology, as the exact mechanism and molecular basis of AD remain unclear.

As aforementioned, rare mutations in genes such as *Amyloid Beta Precursor Protein* (*APP*), *Presenilin 1* (*PSEN1*), and *PSEN2* account for about 1% of AD cases, they are leading to the overproduction and depositio of the amyloid beta (Aβ) peptide (Goate et al., 1991; Rogaev, 1995; Sherrington et al., 1995). While these discoveries support the amyloid cascade hypothesis, they only explain a small fraction of AD cases (Hampel et al., 2021). The *Apolipoprotein E* (*APOE*) *ε4* allele is a significant genetic risk factor, increasing the risk of LOAD up to 15-fold (Genin et al., 2011). Genome-wide association studies (GWAS) have identified over 40 AD risk loci (Migliore and Coppedè, 2022), with genes involved in immune response, Aβ clearance, Tau aggregation, cholesterol metabolism, endocytosis, and protein ubiquitination. Apart from *APOE ε4* and uncommon variations in the *ATP Binding Cassette Subfamily A Member 7* (*ABCA7*), *Sortilin Related Receptor 1* (*SORL1*), and *Triggering Receptor Expressed On Myeloid Cells 2* (*TREM2*) genes, the most common risk variants identified in GWAS make only modest individual contributions to the risk of AD (Sims et al., 2020). Accordingly, studies in animal models and humans show how environmental risk factors - such as diet, lifestyle, alcohol, smoking, and pollutants - induce epigenetic modifications of AD-related genes and pathways (Migliore and Coppedè, 2022).

1.2.2. Epigenetic insights into Alzheimer's Disease

AD is a multifactorial condition that involves several etiopathogenic mechanisms (Iqbal and Grundke-Iqbal, 2010). As the genetic component explains only part of the causal factors, research on the epigenetics of neurodegenerative diseases has become essential to address the limitations of previous candidate gene studies. Genomic sequencing technologies, such as next-generation sequencing (NGS) and GWAS, have facilitated a deeper understanding of the epigenome and its role in disease phenotypes (Gyenesei et al., 2012). Large-scale epigenome-wide association studies (EWAS) effectively identify multiple causal factors associated with AD, including genetic variations and gene-gene interaction effects (van den Hove et al., 2020; Campagna et al., 2021). Recent research indicates that the development of AD is influenced by both environmental and genetic factors and their complex interactions (Eid et al., 2019). Therefore, the development of AD could be effectively elucidated through epigenetic mechanisms, facilitating the interplay between environmental factors and genomic response.

At present, different epigenetic changes have been identified, such as DNA methylation (5-mC) or Post-translational modifications (PTMs) of nucleosomal histones (Figure 2). These modifications alter chromatin structure or recruit histone modifier enzymes, leading to changes in gene expression. Walther Flemming initially introduced the concept of chromatin (Paweletz, 2001). It is composed of nucleosomes, each of them consisting of an octamer of histones (H) (H2A, H2B, H3, and H4) wrapped around 147 base pairs of DNA and the linker histone H1 (Babu and Verma, 1987; Dawson and Kouzarides, 2012; Jiang et al., 2023). The location and arrangement of nucleosomes influence the function of chromatin. Heterochromatin refers to densely packed chromatin, which restricts the accessibility of proteins and transcriptional machinery to the gene promoter regions. However, modifications and transcription processes are allowed when chromatin adopts a relaxed state called euchromatin (Babu and Verma, 1987). Hence, this highly dynamic 3D architecture orchestrates the intricate organization of the genome, acting as an epigenetic regulator of gene expression. Furthermore, microRNAs (miRNAs) are non-coding RNAs (ncRNAs) that act as regulators of their mRNA targets via degradation and translational repression and consequently control gene expression post-transcriptionally (Berson et al., 2018) (Figure 2).

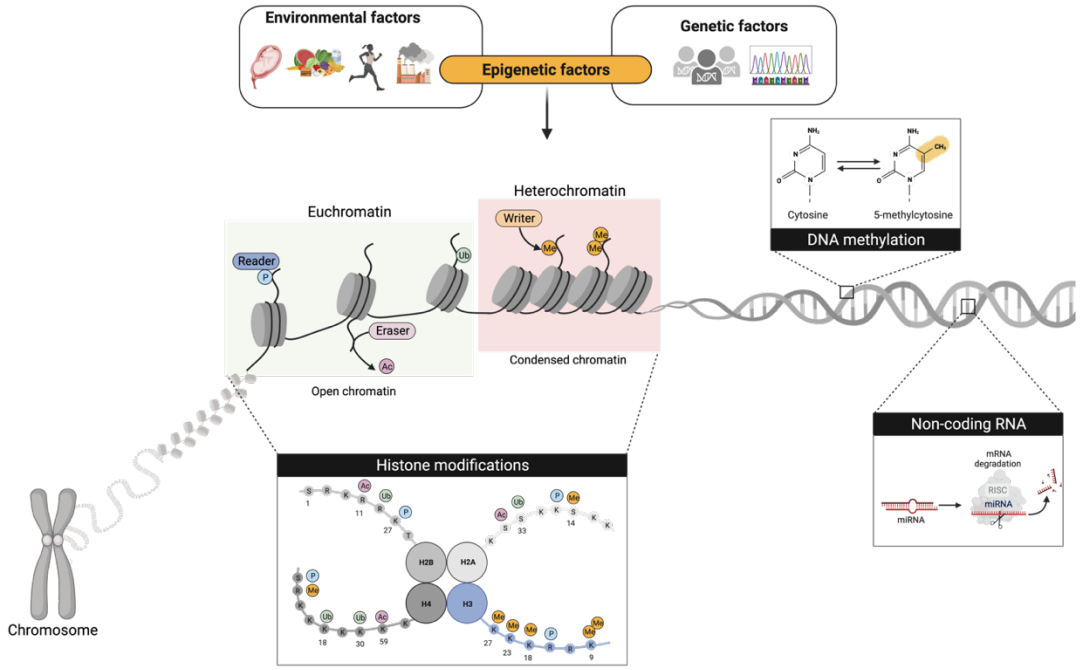

Figure 2. Schematic representation of epigenetics plays a fundamental role as a link between the genome, the environment, and its mechanisms.

1.2.2.1. DNA methylation

DNA methylation of the 5-carbon of a cytosine residue (5-mC) in cytosine-guanine dimers (CpGs) is, within the epigenetic changes, the only one that directly modifies the DNA (Guillaumet-Adkins et al., 2017; Cui and Xu, 2018). These CpG island repeats are very close to gene regulatory regions and commonly appear in the promoters (mostly at housekeeping and transcription start sites). Thus, the effect of 5-mC is to silence gene expression, interfering with transcriptional initiation. This methylation process is catalyzed by the family of DNA methyltransferases (DNMTs). In mammals, three types of DNMTs have been identified: DNMT1, DNMT3a, and DNMT3b. Although the different DNMTs share a similar mechanism, they have different roles. DNMTs are either maintenance (DNMT1) or *de novo* (DNMT3A and DNMT3B) methyltransferases (Sanchez-Mut and Gräff, 2015; Guillaumet-Adkins et al., 2017). Methyl-CpG Binding Domain (MBD) Protein 1 (MBD1), MBD2, MBD3, and MeCP2 are methyl-binding proteins that recognize 5-mC and recruit histone modifiers, so the chromatin remodeling process is enabled (Dawson and Kouzarides, 2012;

Jiang et al., 2023). Furthermore, hydroxymethylation of cytosine (5-hmC) is another modification that directly impacts the DNA, potentially as an intermediary step preceding cytosine demethylation. Enzymes called "Ten-Eleven Translocation family" (TETs), notably TET1, TET2, and TET3, are responsible for this modification (Li et al., 2015).

In the AD human brain, 5mC is one of the most well-studied epigenetic modifications, with a significant increase in its levels positively correlated with Aβ, Neurofibrillary tangles (NFTs,) and ubiquitin load (Coppieters et al., 2014), being also a critical player in brain development (Monti et al., 2020; Jeong et al., 2021). In contrast to 5mC, 5-hmC is related to gene expression activation in the brain (Chen et al., 2012; Mellén et al., 2012; Colquitt et al., 2013). The loss of 5hmC, which results from the downregulation of TET, correlates with abundant Aβ accumulation, and might be closely related to the degree of neurodegeneration during AD (Li et al., 2020) (Table 1).

Table 1. DNA methylation levels in genes related to AD.

DNA methylation status		Target gene	Function	Reference
Hypomethylation	DNMTs	-	Synaptic genes	(Li et al., 2017)
Hypomethylation	-	*APP*	Amyloid precursor protein	(Bakulski et al., 2012)
Hypomethylation	-	*PSEN1*	Component of γ-secretase	(Siegmund et al., 2007; Bakulski et al., 2012; Monti et al., 2020)
Hypomethylation	-	*BACE1*	Aβ production	(Li et al., 2019b)
Hypermethylation	-	*ADAM10*	Aβ production	(Bakulski et al., 2012
Hypomethylation	-	*CDK5*	Tau kinase	(Bakulski et al., 2012
Hypomethylation	-	*BIN1*	Risk genes for AD	(Lang et al., 2022)
Hypermethylation	-	*ANK1*	Encoding for ankyrin-1	(Bakulski et al., 2012)
Hypomethylation	-	*TREM2*	Risk genes for AD	(Ozaki et al., 2017)
Hypermethylation	-	*BDNF*	Nerve growth factor	(Chang et al., 2014; Nagata et al., 2015)
Hypermethylation	-	*ABCA7*	Risk genes for AD	(Bakulski et al., 2012)

DNMT: DNA methyltransferase; APP: Amyloid Beta Precursor Protein; PSEN 1: Presenilin 1; BACE1: Beta-Secretase 1; ADAM10: ADAM Metallopeptidase Domain 10; CDK5: Cyclin Dependent Kinase 5; BIN1: Bridging Integrator 1; ANK1: Ankyrin 1; TREM2: Triggering Receptor Expressed On Myeloid Cells 2; BDNF: Brain Derived Neurotrophic Factor; ABCA7: ATP Binding Cassette Subfamily A Member 7.

1.2.2.2. Histone modifications

Histones are vital proteins in transcription processes susceptible to PTMs, such as acetylation, methylation, phosphorylation, ubiquitination, sumoylation, ADP-ribosylation, citrullination, glycosylation, hydroxylation, and isomerization (Strahl and Allis, 2000).

Among these, the two main modifications are acetylations and methylations. On the one hand, chromatin structure is remodeled by histone acetylation, one of the first histone modifications described. Histone acetyltransferases (HATs) constitute the group of enzymes responsible for adding acetyl-CoA to the lysine (K) residues of H2A, H2B, H3, and H4 histone proteins (Hamilton, 2011; Liu et al., 2023). The addition of acetyl neutralizes the positive charge of lysine aminoacids, making DNA and histones repel each other. This way, nucleosomes turn into a relaxed state in which transcription is activated. In contrast, histone deacetylases (HDACs), also known as lysine deacetylases (KDACs), erase the acetylation mark, negatively regulating transcription and promoting gene silencing. There are three main classes of HATs: the GANT family, the CBP/p300 family, and the MYST family. Additionally, four classes of HDACs (I, IIa, IIb, III, and IV) have been described. The balance between both enzyme groups is needed for controlling gene expression and, especially, DNA repair; if the DNA is damaged and acetylation is dysregulated, it can lead to cell death (Ramazi et al., 2020; Liu et al., 2023).

On the other hand, histone methylation accounts for most of the epigenetic marks that control gene expression through activating or repressing specific genes (Song et al., 2022). Histone methylation occurs at K or arginine (R) residues, which act either as transcriptional activators or repressors, and it is a much more stable modification than acetylation. Both K and R residues undergo different methylations depending on the degree of modification presented. K can be mono- (me1), di- (me2), and tri-methylated (me3). At the same time, R is only methylated with one or two methyl groups both symmetrically and asymmetrically (me1 and me2s or me2a, respectively) (Millán-Zambrano et al., 2022; Song et al., 2022). However, histidine has also been reported to be monomethylated, although little research has focused on its repercussions on gene expression regulation. These PTMs are chemically catalyzed by numerous enzymes classified according to their target. Histone methyltransferases (HMTs),

also known as writers, add the methyl group to histone protein residues. Of relevance for this thesis, protein lysine methyltransferases (PKMTs) catalyze the transfer of a methyl group from the S-adenosyl-l-methionine (SAM) donor to the ε-nitrogen of a K residue on protein substrates. Notably, the ε-amino group of Ks can accept up to three methyl groups, forming me1, me2, or me3 (Tachibana et al., 2001; Dillon et al., 2005). PKMTs are divided into two groups depending on their catalytic methyltransferase domain sequence: SET-containing (Dillon et al., 2005) and non-SET domains, the Seven β-strand (7βS) methyltransferase or class I family (Falnes et al., 2016). The first group, conserving the SET sequence, includes SUV39H1/2, G9a, G9a-like protein (GLP), SMYD, SET Domain Bifurcated Histone Lysine Methyltransferase 1 (SETDB1), and Enhancer Of Zeste 2 Polycomb Repressive Complex 2 Subunit (EZH2), among others (Liu et al., 2023). H3 and H4 proteins, the main targets of these enzymes, present the most relevant methylation marks involved in gene transcription regulation. In particular, K methylation of both histones (H3K4, H3K9, H3K27, H3K36, H3K79, and H4K20) modulates gene expression, either activating or silencing transcription, depending on the type of modification (Barghout et al., 2022). Moreover, R methyltransferases (PRMTs), which target R residues on histones, are divided into three main groups. The first type, including PRMT1, PRMT2, PRMT3, PRMT4, PRMT6 and PRMT8, catalyzes me2a. The second one, including PRMT5 and PRMT9, incorporates me2s (Liu et al., 2023). Lastly, PRMT7, which monomethylates R residues (Barghout et al., 2022). Arginine methylations of H3 and H4 (H3R2, H3R8, H3R17, H3R26 and H4R3) are involved in transcription regulation (Rahman et al., 2021) (detailed in Table 2). As a result, methylation offers the greatest variability of epigenetic changes at the gene expression level, from chromatin structure to on-target loci through the interaction of cell-specific transcription, initiation, and elongation factors. Moreover, methylation affects histones, forming chromatin structures, free histones, and non-histone proteins (Greer and Shi, 2012). In contrast, histone demethylases (HDMs) or erasers, reported afterward, demonstrated that methylation is a dynamic reversible process, and its biological outcome depends on the replacement or establishment of the methylation (Greer and Shi, 2012; Griñán-Ferré et al., 2018). The presence or absence of the mark is recognized by reader proteins activating downstream signaling for gene activation or repression and, therefore, the combination of distinct methylation marks provides a wide variety of epigenetic regulation mechanisms involving

cell cycle regulation, DNA damage repair, stress response, and cell differentiation during brain development (Greer and Shi, 2012).

Additional histone modifications participate in relevant biological processes, including phosphorylation, ubiquitylation, SUMOylation, glycosylation, or ADP-ribosylation (Heerboth et al., 2014; Millar et al., 2019). They all play a crucial role in maintaining genome stability by preventing chromosome dysregulation (Levinsky et al., 2022; Millán-Zambrano et al., 2022), highlighting the importance of histone modifications regarding disease. Recently, the latest developments in mass spectrometry have provided insights into new histone modifications, such as benzoylation, butyrylation, crotonylation, glutarylation, lactylation, etc., which are disrupted in neurodevelopment (Park et al., 2022).

In the last decade, evidence of the link between histone modifications and memory, synaptic plasticity, and cognitive functions has emerged (Park et al., 2022). Interestingly, dysregulation of these processes has been found in mouse models of aging and neurodegenerative diseases, including AD (Table 2).

Table 2. Histone modifications found in the AD pathology.

Chromatin remodeling modification	Biological effect	Writers	Erasers	Reference
H3K9ac ↑ H3K27ac ↑	GA ↓	MOF, PCAF, TIP60	HDACs	(Marzi et al., 2018; Nativio et al., 2020; Santana et al., 2023; Zhao and Huai, 2023)
H4K5ac ↓ H4K8ac ↓	GA ↓	-	-	(Francis et al., 2009; Ricobaraza et al., 2009; Govindarajan et al., 2011)
H4K12ac ↓ H4K16ac ↓	GA ↓	-	-	(Nativio et al., 2020)
-		-	HDAC1 ↓	(Pao et al., 2020)
-		-	HDAC2 ↓	(Gonzalez-Zuniga et al., 2014)
-		-	HDAC3↓	(McQuown et al., 2011; Janczura et al., 2018)
-		-	HDAC6 ↓	(Ding et al., 2008a)

H3K4me2/2 ↑	GA ↑	SETD1A/B	KDMs	(Nativio et al., 2020; Santana et al., 2023; Zhao and Huai, 2023)
H3K9me2 ↑	GR ↑	GLP, G9a,	KDMs	(Nativio et al., 2020; Santana et al., 2023; Zhao and Huai, 2023)
H3K27me3 ↑	GR ↑	G9a/GLP EZH1/2, PRC2	KDM7A, KDM6A/B,	(Nativio et al., 2020; Santana et al., 2023; Zhao and Huai, 2023)
H3K79me 2↓	GA ↓	DOT1L	KDM7, UTY, PHF8	(Nativio et al., 2020)
H3K36me2 ↓	GA ↓	ASH1L, NSD1/3, SMYD, SET2	KDM2A-B, KDM4A-E, NO66	(Nativio et al., 2020)
H2AXS139p (γH2AX) ↑	DRP ↓	ATM, ATR, MST1	PP4	(Myung et al., 2008; Rao et al., 2012)
Total H3 phosphorylation ↑	A, M, DRP, DRC	-	-	(Rao et al., 2012)

Gene repression: GR; Gene activation: GA; Deposition of histones: DH; Activation: A; Mitosis: M; DNA repair: DRP; DNA replication: DRC. MOF: males-absent-on-the-first; PCAF: p300/CBP-associated factor; TIP60: Tat-interactive protein 60; SETDB: SET Domain Bifurcated Histone Lysine Methyltransferase; GLP: G9a-like protein; EZH: Enhancer Of Zeste 2 Polycomb Repressive Complex; PRC2: Polycomb repressive complex 2; NSD: nuclear receptor-binding SET Domain; ATM: ataxia telangiectasia-mutated; MST1: mammalian STE20-like kinase 1; HDAC: histone deacetylase; KDM: Histone lysine demethylases; PHF8: PHD Finger Protein 8.

1.2.2.3. Non-coding RNA (ncRNA) regulation

ncRNAs are RNAs transcribed from DNA but not translated into functional proteins, and they are clustered depending on their cellular function (Santosh et al., 2015). Only 1.5% of the genome is transcribed to mRNA; the rest is mainly considered functional ncRNAs, divided into two groups based on size (either long or short). Among them, the ones that have generated the most interest are miRNAs, between 18-25 nucleotides long and associated with gene repression (blockage of transcription). MiRNAs act on RNA interference (RNAi), resulting in the target mRNA's degradation or translation inhibition (Chuang and Jones, 2007). Furthermore, miRNAs regulate the cell's development, maturation, differentiation, apoptosis, cell signaling, cellular interactions, and homeostasis (Ranganathan and Sivasankar, 2014; Yao et al., 2019). As a consequence, the dysregulation of miRNA-epigenetic mechanisms contributes to a variety of diseases, such as cancer (Di Leva et al., 2014; Peng and Croce, 2016), cardiovascular disease (Barwari et al., 2016; Zhou et al., 2018), diabetes

(Ciccacci et al., 2013; Feng et al., 2016), neurodegenerative diseases (Femminella et al., 2015; Tan et al., 2015), and age-related cognitive decline (Cosín-Tomás et al., 2018; Harman and Martín, 2020). Of note, other ncRNA regulators exist, such as piwi-interacting RNAs (piRNAs) and long non-coding RNAs (lncRNAs).

Some ncRNAs are abnormally expressed during AD. These ncRNAs regulate downstream target genes that play crucial roles in pathophysiological processes contributing to AD (Table 3).

Table 3. ncRNA alterations found in the AD pathology.

Type of ncRNAs	miR-	Expression	Target gene	Reference
microRNAs	*miR-206*	↑	*BDNF* ↓	(Tian et al., 2014; Li et al., 2016)
	miR-613	↑		
	miR-133b	↓	*EGFR*	(Yang et al., 2018)
	miR-214-3p	↓	*Atg12* ↑	(Zhang et al., 2016c)
	miR-132	↑	*SIRT1* ↓	(Hadar et al., 2018)
	miR-212	↑		
	miR-16	↓	*BACE1* ↑	(Hébert et al., 2008; Zhu et al., 2012; Liu et al., 2014; Long et al., 2014; Zhang et al., 2014; Lei et al., 2015; Jiao et al., 2016b; Kim et al., 2016; Zhong et al., 2018)
	miR-29a/b-1	↓		
	miR-107	↓		
	miR-186	↓		
	miR-188-3p	↓		
	miR-195	↓		
	miR-339-5p	↓		
	miR-384	↓		
	miR-128	↑	*PPARγ* ↓	(Liu et al., 2019)
	miR-140-5p	↑	*ADAM10* ↓	(Cheng et al., 2013; Akhter et al., 2018)
	miR-144	↑		
	miR-346	↓	*APP* ↑	(Long and Lahiri, 2011; Liu et al., 2014; Long et al., 2019; Barbato et al., 2020)
	miR-384	↓		
	miR-132	↓	*Tau* ↑	(Santa-Maria et al., 2015; Hernandez-Rapp et al., 2016)
	miR-212	↓		
	miR-219	↓		
	miR-134-5p	↑	CREB ↓	(Baby et al., 2020)

piRNAs	piR_38240 piR_34393	↑ ↑	CYCs ↓	(Roy et al., 2017)
lncRNAs	*BACE1-AS* *BC200*	↑ ↑	*BACE1* ↑	(Mus et al., 2007; Modarresi et al., 2011; Zhang et al., 2018)
	17A	↑	*GABABR2* ↓	(Massone et al., 2011; Wang et al., 2019)

BDNF: Brain Derived Neurotrophic Factor; EGFR: Epidermal Growth Factor Receptor; Atg12: Autophagy Related 12; SIRT1: Sirtuin 1; PPARγ: Peroxisome Proliferator Activated Receptor Gamma; BACE1: Beta-Secretase 1; ADAM10: ADAM Metallopeptidase Domain 10; APP: Amyloid Beta Precursor Protein; CREB: CAMP Responsive Element Binding Protein; CYCs: Cytochrome C, Somatic; GABABR2: Gamma-Aminobutyric Acid Type B Receptor Subunit 2.

1.2.3. Chromatin Remodeling, unveiling a potential drug target

A better understanding of chromatin remodeling mechanisms will foster the development of new drug targets for improved pharmaceutical interventions. The mechanisms driving chromatin remodeling can be divided into two groups: covalent modifications of chromatin components and non-covalent modifications involving ATP-dependent chromatin remodeling complexes (CRCs) (Clapier et al., 2017). Covalent modifications mainly involve PTMs and DNA alterations, as previously discussed (Narlikar et al., 2013; Jiang et al., 2023). In fact, one of the main functions of these remodelers is to relax the chromatin structure, allowing both DNA and histones to become accessible to transcription factors and post-translational modifiers. Chromatin remodeling facilitates changes in gene expression linked to synaptic plasticity during development and adulthood (Santos et al., 2006). This process enables the collaboration of genetic predisposition, experiences, and neuronal activity, modifying cellular and behavioural responses. Moreover, recent discoveries highlight epigenetic dysregulation, particularly histone lysine methylation, in cognitive deficits and neuronal death as part of neurodegenerative diseases, such as AD (Poulard et al., 2021; Padeken et al., 2022).

Among all chromatin remodelers, this thesis focuses on the effect of G9a-mediated methylation in AD. Regarding its function, G9a participates in various mechanisms, with its primary role being the methylation of the histone H3 N-terminal tail, leading to chromatin compaction (Poulard et al., 2021).

1.3. G9a, a lysine methyltransferase

1.3.1. Discovery of G9a

G9a, identified and sequenced in 1990, is a PKMT that catalyzes methyl group transfer to K residues via the SET domain and is likely the primary enzyme responsible for the mono- and di-methylation of H3K9 (H3K9me1 and H3K9me2, respectively) in euchromatin. G9a is also known as lysine methyltransferase-1C (KMT1C), euchromatic histone N-methyltransferase 2 (EHMT2), or BAT8 (HLA-B associated transcript 8) (Poulard et al., 2021).

The SET domain was initially identified in *Drosophila melanogaster* (Jones and Gelbart, 1993) after recognizing a 130 amino acid sequence at the C-terminal end of three gene regulatory factors: Su(var)3-9, Enhancer of zeste, and Trithorax (Alvarez-Venegas and Avramova, 2002). The first discovery of a SET domain-containing histone lysine methyltransferase was Suv39h1, suggesting the association of the SET domain with lysine methylation activity (Rea et al., 2000). Shortly after, G9a emerged as the second protein within the group containing the SET domain of PKMT (Tachibana et al., 2001). A paralog of G9a has been identified and is known as G9a-like protein (GLP), lysine methyltransferase-1D (KMT1D), or euchromatic histone N-methyltransferase 1 (EHMT1). G9a and GLP share approximately 45% of the sequence identity and around 70% of the sequence similarity (Shankar et al., 2013). Their primary difference lies in the N-terminus as opposed to the SET domain, where they maintain a high level of conservation, sharing over 80% sequence identity (Dillon et al., 2005).

1.3.2. G9a structure

G9a mRNA has two isoforms (isoform A, long isoform; isoform B, short isoform) resulting from alternative splicing of its exon 10. Isoform A is the full-length G9a protein, being a product of two transcripts: the *G9a* gene (comprising 24 exons) and the *NG36* gene (containing 4 exons) (Brown et al., 2001; Tachibana et al., 2001). Alternative splicing was identified across all tissues, although the ratio between both isoforms varies. Specifically, G9a isoform B predominates in the kidney, thymus, and testis. A significant accumulation of

isoform B was also observed in epithelial cell lines compared to highly transformed and mesenchymal cell lines. Although no catalytic changes were reported following exon 10 inclusion, alternative splicing might influence subcellular localizations (Mauger et al., 2015). The G9a mouse homolog on chromosome 17 also presents two alternatively spliced isoforms. The long isoform (G9a L) lacks exon 1 but retains exon 2, while the short isoform (G9a S) contains exon 1 but excises a portion of exon 2 (Shankar et al., 2013) (Figure 3).

As aforementioned, G9a is a member of the Su(var)3-9 family of methyltransferases, and a defining feature of this family is the highly conserved SET domain at the C-terminal region (Jenuwein et al., 1998; Zhang et al., 2002a). This SET domain accounts for the methyltransferase function and enables protein-protein interactions thanks to its ankyrin repeats (Dunham et al., 1990; Milner and Campbell, 1993). The human G9a protein exhibits other well-defined domains, including a predominantly disordered N-terminal region and a cysteine-rich (CRR) site (Kerchner et al., 2021).

The SET domain consists of a sequence of β strands that fold into three sheets, encircling a knot-like structure (Taylor et al., 2003). The conserved nucleus of the SET domain is flanked by a pre-SET and a post-SET domain. The pre-SET domain reinforces structural stability through interactions with various structures of the core SET domain. Additionally, a post-SET domain is responsible for establishing a hydrophobic channel through the involvement of an aromatic residue. In contrast to the SET domain, the pre-SET and post-SET domains are not conserved sequences (Qian and Zhou, 2006). G9a adopts a typical fold composed of a conserved SET domain and variable i-SET insert. The i-SET domain serves as a docking platform for the H3 tail, involving a conserved pair of hydrogen bonds between the i-SET domain and the K residue, along with crucial contacts with a primary side chain located upstream of the methyl acceptor. This is likely to ensure the correct positioning of the peptide as lysine enters the active site (Kerchner et al., 2021).

The pre-SET domain comprises nine conserved cysteine residues, organized into two groups: five cysteines and four cysteines, separated by varying numbers of amino acids. These nine cysteines coordinate the formation of an equilateral triangular cluster with three zinc ions. A

fourth zinc ion is also proximate to the SAM binding site. These four structural zinc fingers ensure proper protein folding and enzymatic activity. In the post-SET region, three conserved cysteine residues are noted, and they appear to be crucial for HKMT activity within the SUV39 family (Zhang et al., 2002a).

The ankyrin repeat domain acts as a binding module for mono- and di-methylated lysine, serving as a reader domain critical for protein-protein interactions. Ankyrin repeats adopt helix-turn-helix-β-turn structures, where the H3 peptide is interposed between β-turns and helices found within the fourth and fifth ankyrin repeats (Collins et al., 2008). G9a ankyrin repeats exhibit specific binding to K9-methylated peptides, displaying no affinity for K4- or K27-methylated peptides. Interestingly, GLP and its ankyrin repeats show similar binding patterns to various modified H3 peptides as G9a, with the distinction that GLP displays stronger affinity for H3K9me1 than for H3K9me2 (Collins et al., 2008).

Finally, the CRR domain encompasses an array of conserved cysteine and histidine residues. It assumes a compact fold and is associated with four bound zinc atoms. The C-terminal of the CRR keeps an interesting new gene (RING) domain fold. Typically, RING domains function as protein ubiquitin ligases (Kerchner et al., 2021). Based on existing experimental evidence, it is likely that CRR operates as a novel protein-binding domain facilitating interactions with several other proteins. Notably, these interactions involve cyclin D1, Neuron-restrictive silencer factor (NRSF)/ RE1 Silencing Transcription Factor (REST), the Mediator complex, and Zinc Finger Protein 200 (ZNF200), ultimately resulting in the recruitment of EHMT proteins to specific chromatin loci (Roopra et al., 2004; Nishida et al., 2007; Ding et al., 2008b; Li et al., 2019c; Kerchner et al., 2021).

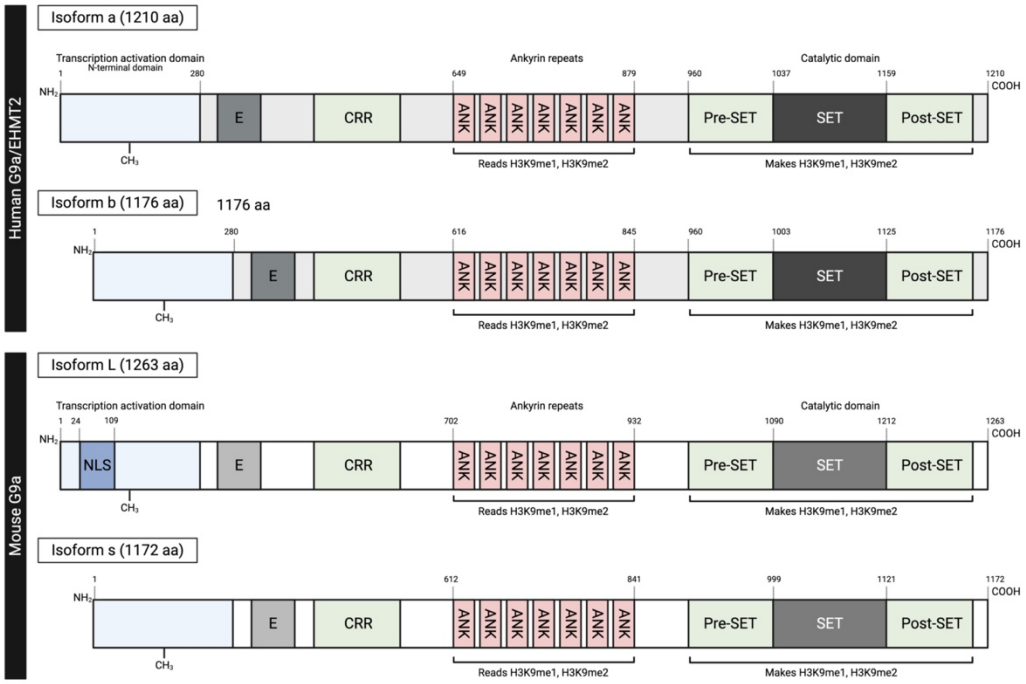

Figure 3. Schematic representation of human and mouse G9a isoforms. CH_3: methylation; NLS: nuclear localization signal; E: glutamic acid rich region; CRR: Cystein rich region; ANK: ankyrin repeats; Catalytic domain: SET domain with flanking Pre-SET and Post-SET regions. Numbers indicate amino acid residues.

1.3.3. G9a activity

As mentioned above, SET-domain proteins exhibit distinctive characteristics compared to other SAM-dependent methyltransferases. Notably, the binding sites for the histone substrate and SAM are situated on opposite faces of the SET domain. These substrate-binding clefts are interconnected through a deep channel traversing the core of the SET domain, facilitating the transfer of the methyl group from SAM to the ε-amino group of the lysine substrate. This unique arrangement of substrate binding sites was initially proposed to enable multiple rounds of lysine methylation without dissociating the protein substrate from the SET domain (Trievel et al., 2002). Within the SET domain, the tyrosine residue Y1154 plays an essential role in the catalytic activity of G9a. This tyrosine likely facilitates the deprotonation of the positively charged ammonium group, favoring the methylation process (Schapira, 2011).

Biochemical characterization of G9a and GLP has revealed that they form both homomeric and heteromeric complexes through their SET domains. However, in various human and mouse cells, endogenous molecules predominantly exist as the stoichiometric G9a–GLP heteromeric complex (Tachibana et al., 2005). Complementation experiments showed that the enzymatic activity of G9a plays a more crucial role in *in vivo* HKMT function than that of GLP. While it remains unclear why G9a and GLP cannot function in isolation as an HKMT *in vivo*, there are several potential mechanistic explanations for the prevalence of the G9a–GLP heterocomplex within cells, despite their ability to also form homodimers (Tachibana et al., 2008).

1.3.4. G9a function

In 2001, Tachibana and colleagues identified histone proteins as the first substrates of G9a (Tachibana et al., 2001). They showed that G9a adds methyl groups to K9 and K27 on H3, unlike Suv39h1, which exclusively methylates K9 (Tachibana et al., 2002; Wu et al., 2011). Moreover, compared to Suv39h1, G9a has higher efficiency in transferring methyl groups to H3 *in vitro*. G9a has been recognized as the significant PKMT for catalyzing mono- and di-methylation of H3K9, well-known for its role in transcriptional silencing (Zhao et al., 2005; Tachibana et al., 2008; Mozzetta et al., 2014). Di-methylation in H3 Lysine (K)9 (H3K9me2) has been associated with the repression of genes related to learning and memory formation (Rea et al., 2000; Gupta-Agarwal et al., 2012). New evidence also points to the repressive role of H3K27 methylation by G9a (Wu et al., 2011; Pan et al., 2018). G9a also methylates H3 at K56 to ensure proper DNA replication, a methylation event induced by DNA damage. Furthermore, Vinson D.A and collaborators in 2022 reported that G9a can catalyze the addition of mono-, di- and tri-methylation on H3K18 and mono- and demethylation on H3K23 (Vinson et al., 2022). Similarly, G9a exhibits variant-specific methylation of histone H1. H1.4 undergoes mono- and di-methylation at H1.4K26, creating a binding site for HP1 and indicating a repressive role in transcription (Trojer et al., 2009). Conversely, G9a demethylates H1.2 at K187; intriguingly, this modification is not recognized by HP1 proteins (Weiss et al., 2010). Notably, Weiss and colleagues demonstrated that G9a does not directly

bind to methylated histone variants, suggesting a mechanism distinct from that observed in H3K9me1/2 methylation (Weiss et al., 2010).

Many non-histone proteins involved in various biological functions have been identified as G9a substrates (Shankar et al., 2013). Although the functional significance of methylation in non-histone proteins remains unclear, G9a-mediated methylation negatively influences the transcriptional activity of several transcription factors and proteins, including C/EBPb (Pless et al., 2008), Myogenic Differentiation 1 (MyoD) (Ling et al., 2012), Myocyte Enhancer Factor 2D (MEF2D) (Choi et al., 2014), p53 (Huang et al., 2010). Specific mediators involved in hypoxia response, such as Pontin, Reptin, and Hypoxia Inducible Factor 1 Subunit Alpha (HIFα), are also subject to regulation through G9a-mediated methylation (Lee et al., 2010, 2011; Bao et al., 2018). Notably, G9a methylation activity affects other methyltransferases, like mAM, suggesting complex regulatory networks (Shankar et al., 2013).

Moreover, it is noteworthy that G9a also represses active gene transcription by recruiting other corepressor proteins (such as alternative PKMTs and chromatin remodelers, EZH2 (Mozzetta et al., 2014), CCAAT displacement protein/cut (CDP/cut) (Nishio and Walsh, 2004), growth factor independent 1 (Gfi1) (Fang et al., 2007), positive regulatory domain I-binding factor 1 (PRDI-BF1) (Győry et al., 2004), NRSF/REST (Roopra et al., 2004; Tahiliani et al., 2007; Mulligan et al., 2008), multi-domain protein UHRF1 (Kim et al., 2009), noncoding RNA Air (Nagano et al., 2008), and HDAC1 (Wang et al., 2017)) and DNA methyltransferases (such as DNMT3a (Chang et al., 2011), and DNMT1 (Estève et al., 2006; Smallwood et al., 2007)). These recruitments completely suppress transcription through histone modifications (Shankar et al., 2013). Thereby, H3K9me2 was required to recruit the silencing chromatin remodeling complex (Fang et al., 2007). By contrast, recent findings suggest that G9a also functions as a coactivator, contributing to gene activation (Lee et al., 2006; Purcell et al., 2012; Oh et al., 2014; Poulard et al., 2019). This switch in function may be influenced by different binding partners (Purcell et al., 2011; Poulard et al., 2017). Its activation domain and auto-methylation are crucial for coactivator function (auto-methylation at a specific site K185 being crucial), regulated by adjacent phosphorylation (T186 site) (Purcell et al., 2011; Poulard et al., 2017).

1.3.5. Rationing, design, and synthesis of G9a inhibitors

In 2007, Kubicek et al. (Kubicek et al. 2007) shortlisted 7 hits from the preselected chemical library containing 125,000 compounds. Among them, **BIX-01294** (**1**), diazepinquinazolin-amine derivatives, emerged as a selective inhibitor of G9a (G9ai) non-competitive cofactor SAM with Half maximal inhibitory concentration (IC_{50}) of 2.7 μM. Moreover, Chang et al. (Chang et al., 2009) published the crystal structure analysis of (**1**) and S-adenosyl-L-homocysteine (SAH) with GLP's catalytic SET region (PDB ID: 2RFI) in which ligand bound with substrate peptide groove positioned near lysine residues, reporting an IC_{50} of 0.7 μM against GLP (Figure 4).

Then, Liu et al. (Liu et al., 2009a, 2010) described the structure-activity relationship (SAR) (Figure 4) and discovered and synthesized derivatives compounds from (**1**). Alterations to the 2-amino within the quinazoline scaffold, (**1**) region were well tolerated (**12-17**) (Figure 4). The authors also evaluated the effect of carbon numbers in the aminoalkoxy side chain on the potency of G9a. They found that carbon numbers 2 to 5 (**18-21**) maintained the potency. In contrast, carbon chain lengths greater than 6 (**22**) decreased potency. This suggests that the 5-carbon number in the aminoalkoxy side chain easily occupies the lysine binding region of G9a, increasing potency and selectivity. The nitrogen atom in the side chain interacts with Leucine (Leu)1086 and Tyrosine (Tyr)1154 via electrostatic and π-cation bonds.

Likewise, Chang et al. reported a potent and less toxic G9ai, **E72** (Chang et al., 2010); however, its cellular potency was lower than that of (**1**). In 2011, Liu et al. (Liu et al., 2011; Vedadi et al., 2011) optimized 7-aminoalkoxy-quinazoline (Figure 5) and evaluated the G9a inhibitory activity, cellular potency and cellular toxicity. Authors assessed the effect of various 2-amino groups of pyrrolidine-1-ylprooxy derivative (**38-47**) and found that all derivatives showed high G9a inhibitory potency against G9a SAHH-coupled assay in which compound (**45-47**) showed high *in vitro* potency along with improved lipophilicity while (**41-47**) showed high cellular potency and lipophilicity. Besides, they evaluated the combined compound encompassing different 4 and 2- amino groups of pyrrolidine analog, where the compound (**50-53**) showed improved lipophilicity, *in vitro* and cellular potency, and low

cellular toxicity. In contrast, compound (**54**) decreased the potency. Among them, compounds (**50/UNC0646**) and (**51/UNC0631**) (Liu et al., 2011) showed high potency and tox/functional ratio but higher toxicity than (**47/UNC0638**). Later, (Liu et al., 2013), incorporated modifications in (**47**), and it was found that 2-(4,4-difluoropiperidin-1-yl) (**55/UNC0642**), 2-(morpholin-4-yl) (**56/UNC1479**) were able to retain the *in vitro* potency (Figure 6). Moreover, Yuan et al. and Sweis et al. (Yuan et al., 2012; Sweis et al., 2014) independently reported **BRD9539** and **A366** as potent and selective G9ais in 2012 and 2014, respectively.

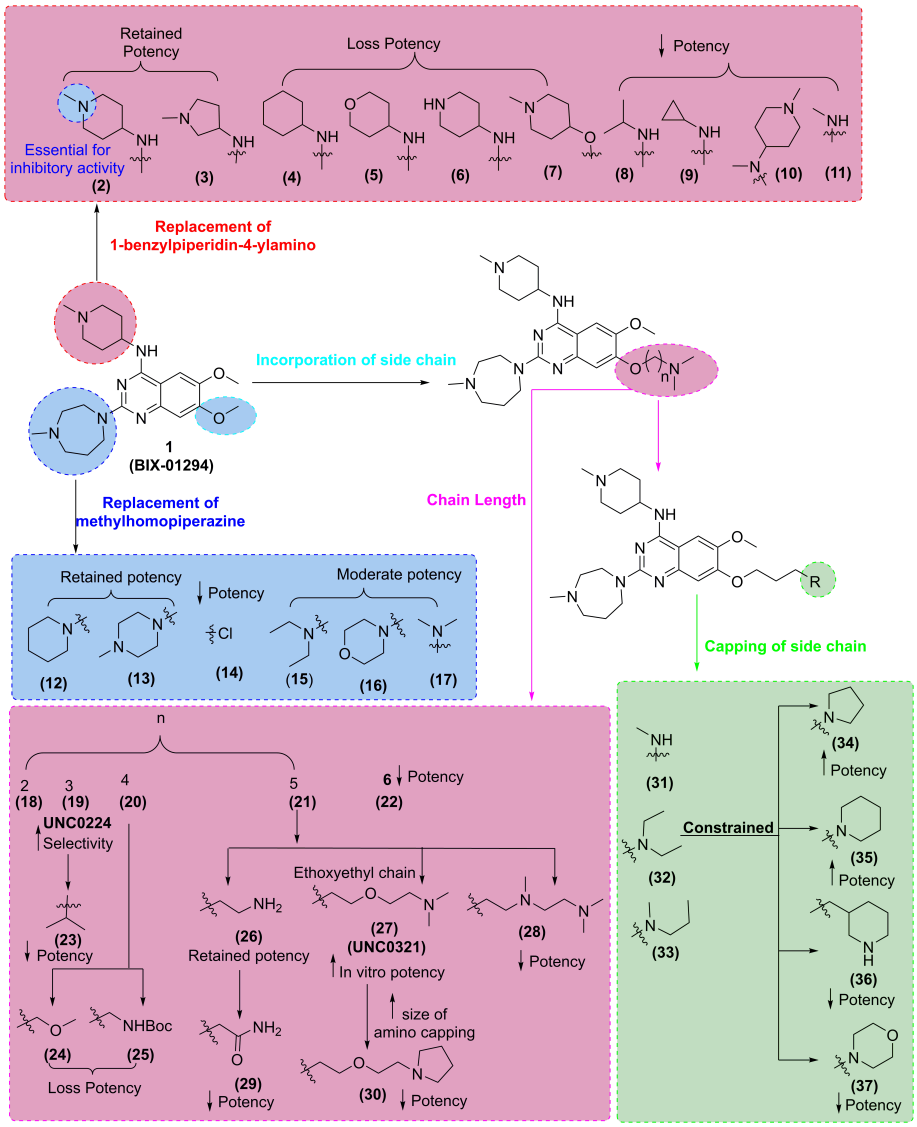

Figure 4. Part I: Rationing, design, and synthesis of G9a inhibitors.

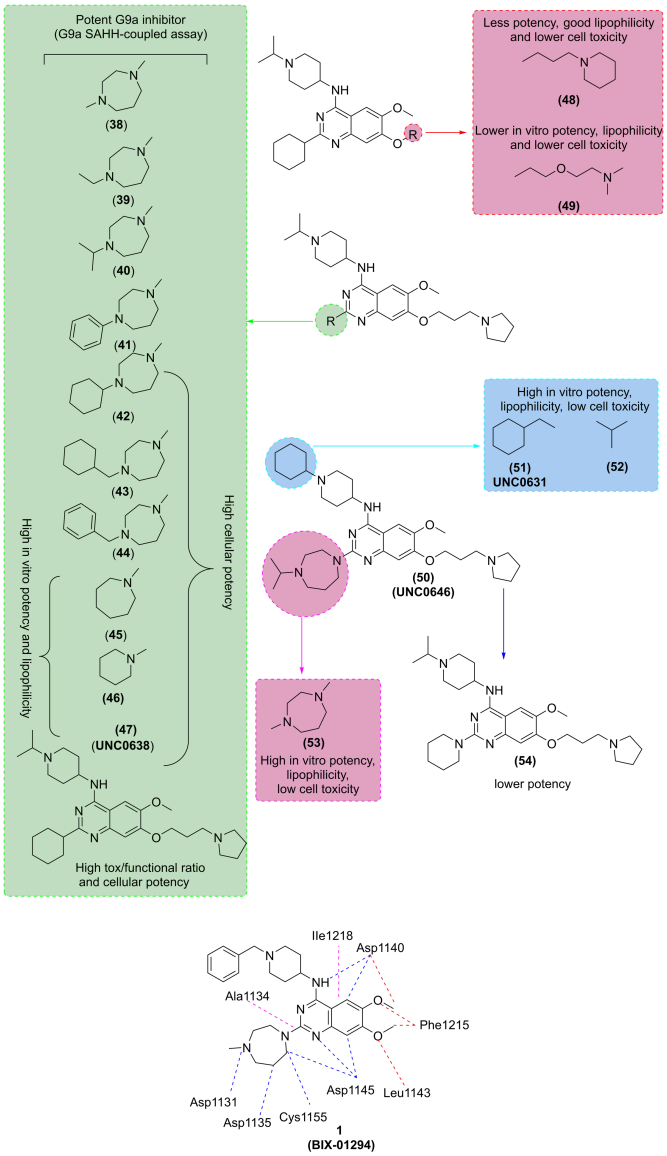

Figure 5. Part II: Rationing, design, and synthesis of G9a inhibitors.

In 2014, Konze et al. (Konze et al., 2014) designed and synthesized (**64/UNC0965**) as a biochemical characterization chemical tool, which is the biotinylated version of **UNC0638** to facilitate the precipitation of G9a from whole cell lysate. Ma et al. (Ma et al., 2014) discovered (**65/UNC0379**) as a substrate competitive inhibitor of PKMTs called SETD8 with selectivity over 15 other methyltransferases. Moreover, Srimongkolpithak et al. (Srimongkolpithak et al., 2014) performed various studies to improve G9a inhibitory activity with knowledge of

pharmacophoric critical features of the **BIX-01294** compound, and they found new quinazoline derivatives such as **HKMTI-1-005, HKMTI-1-022, HKMTI-1-011** (**89-91**) (Supplementary Figures 1 and 2).

Recently, Xiong et al. (Xiong et al., 2017) evaluated the inhibitory activity of GLP and G9a of different derivatives of quinazoline where they evaluated the effect of various 2-amino group, *N*-capping groups of piperidine ring, 6 and 7 methoxy substituents of quinazoline, quinoline scaffold and drawn the SAR of quinazoline derivatives (Supplementary Figure 3). Furthermore, Charles et al. (Charles et al., 2020) performed high throughput screening to discover a novel quinoline-based G9ai called **CSV0C018875** (Supplementary Figure 4). Lastly, following optimization from the initial hit rac-10a obtained from HTS, Nishigaya et al. (Nishigaya et al., 2023) discovered the RK-701, a potent G9a/GLPi (IC_{50} = 27/53 nM).

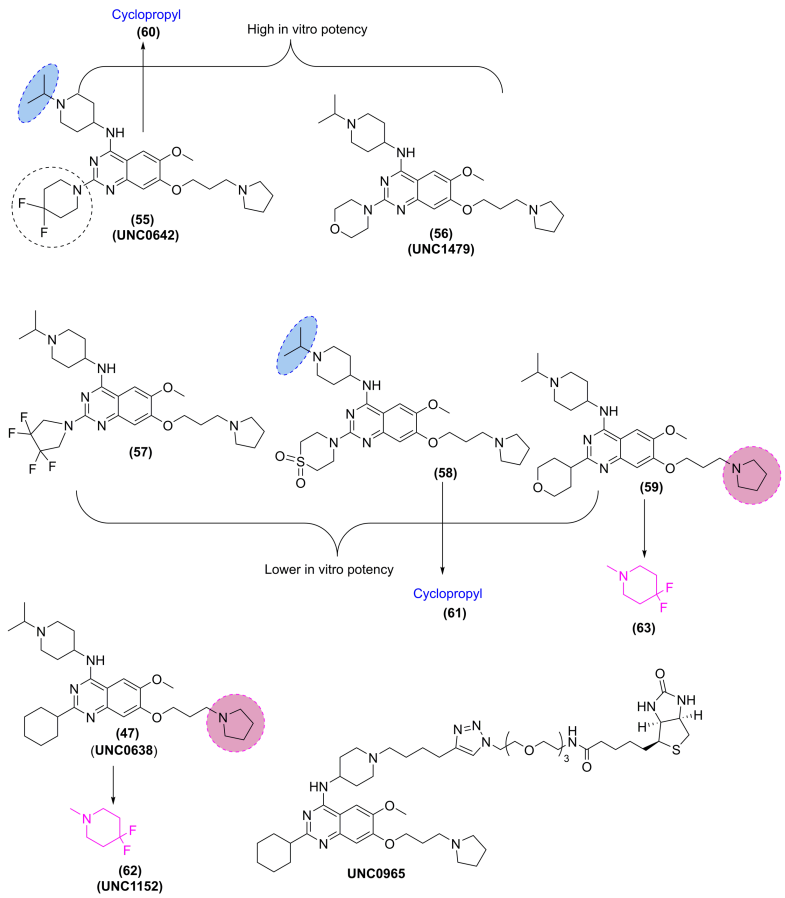

Figure 6. Part III: Rationing, design, and synthesis of G9a inhibitors.

In summary, the following table details the most important compounds during the above process (Table 4). Although many G9ais have been synthesized, their use still has limitations. Achieving specificity only against G9a is a primary concern, as non-specific inhibition could lead to off-target effects and toxicity. For example, the UNC family continues to exhibit high toxicity when used in *in vivo* experiments. UNC0638 is toxic at 5mg/kg, while UNC0642 is toxic at 10mg/kg. Ensuring favorable pharmacokinetic properties is critical for the clinical success of drugs, particularly for central nervous system (CNS) conditions, as they often have a poor blood-brain barrier (BBB) permeability. Therefore, the development of G9ais is essential to overcome current challenges.

Table 4. Selection of the most used G9a inhibitors.

Compound	Derivative from	Type	IC_{50} GLP	IC_{50} G9a	Effects reported in	Reference
BIX-01294		S-Ci	38 μM	1.7 μM	Cancer, AD, Malaria	(Kubicek et al., 2007; Zheng et al., 2019; Vanheer and Kafsack, 2021; García-Domínguez et al., 2022)
UNC0224	BIX-01294	S-Ci	50 nM	15 nM	Cancer, Malaria	(Liu et al., 2011; Vanheer and Kafsack, 2021)
UNC0638	BIX-01294	S-Ci	19 nM	<15 nM	Cancer, AD, PD Malaria	(Vedadi et al., 2011; Sugeno et al., 2016; Vanheer and Kafsack, 2021)
E72	BIX-01294	S-Ci	0.1 μM	nr	nr	(Chang et al., 2010)
UNC0321	UNC0224	S-Ci	15 nM	9 nM	Cancer, Diabetic vascular complication, Malaria	(Liu et al., 2010; Hui and Ye, 2015; Ukaegbu et al., 2015)
UNC0646	UNC0638	S-Ci	nr	6 nM	Cancer, Malaria	(Liu et al., 2011; Gu et al., 2019; Vanheer and Kafsack, 2021)
UNC0642	UNC0638	S-Ci	3.7 nM	<2.5 nM	Cancer, AD, Malaria, PTSD	(Vedadi et al., 2011; Griñán-Ferré et al., 2019; Zheng et al., 2019; Vanheer et al., 2020; Vanheer and Kafsack, 2021; Zhao et al., 2022; Singh et al., 2023)

UN0631	UNC0646	S-Ci	nr	4 nM	Cancer, Malaria	(Liu et al., 2011; Vanheer and Kafsack, 2021)
MS012	BIX-01294, E72,UNC0638	S-Ci	7 ± 2 nM	992 ± 337 nM	nr	(Xiong et al., 2017)
M0124	BIX-01294, E72,UNC0638	S-Ci	13 ± 4 nM	440 ± 63 nM	nr	(Xiong et al., 2017)
A366		S-Ci	38 nM	3.3 nM	Cancer	(Sweis et al., 2014)
HKMTI-1-247		S-Ci	nr	13±1 nM	nr	(Srimongkolpithak et al., 2014)
HKMTI-1-248		S-Ci	nr	31±3 nM	nr	(Srimongkolpithak et al., 2014)
BRD9359		SAM-Ci	nr	6.3 µM	Cancer	(Yuan et al., 2012)
RK-701		S-Ci	53nM	27nM	Cancer	(Nishigaya et al., 2023)

Substrate competitive inhibitors: S-Ci; SAM competitive inhibitors: SAM-Ci; Not reported: nr; AD: Alzheimer's disease; PTSD: Post-traumatic stress disorder.

[redacted]

Recent studies have also identified HDAC and DNMT inhibitors as promising therapeutic agents for neurological diseases. However, many of these inhibitors increase the possibility of off-target side effects and face the challenge of addressing issues related to gene specificity and safety (Yang et al., 2017; Qazi et al., 2018). Zang et al. (Zang et al. 2017) discovered dual inhibitors of G9a and HDAC, in which compound **171** showed the most promising cellular potency for both G9a and HDAC8 with G9a IC_{50} = 7.136 µM (Supplementary Figure 5). Moreover, they (Zheng et al., 2022) also designed and synthesized quinazoline-based

hydroxamic acid derivatives, which produce inhibitory activity against GLP and HDAC (Supplementary Table 5). In parallel fashion, Jose-Eneriz et al. (José-Enériz et al., 2017) discovered a novel dual inhibitor of G9a and DNMT, **CM-272**, which showed the highest G9a/DNMT inhibitory activity with IC_{50} for G9a = 8 nM and 382 nM for DNMT1. It stimulated apoptosis and inhibited cell proliferation to cause cell death. Then, Rabal et al. (Rabal et al., 2018) described their SAR where they modified the quinoline ring's 4, 6, and 7-position and found that any modification in the methoxy group with a small group positioned at the 6-position of the quinoline ring decreases the DNMT1 and G9a activity and modulates the compounds' ADME profile (Supplementary Figure 6). Later, the same group (Rabal et al., 2021) designed and synthesized novel quinoline-based epigenetic inhibitors, which showed potency towards three targets, G9a, DNMT1, and HDAC1/6, and described the different substitution effects on the activity (Supplementary Figure 4). Another dual approach is G9a/EZH2, developed for several cancers, including multiple myeloma (MM) and acute myeloid leukemia (AML) (Ishiguro et al., 2021; Spiliopoulou et al., 2022). Research suggests that inhibitions of both G9a and EZH2 can suppress cancer cell proliferation by regulating various signaling pathways and promoting the differentiation of cancer cells. For instance, the study found that adding the dual inhibitor **HKMTI-1-005** to ATRA (all-trans retinoic acid) is a promising therapeutic approach. **HKMTI-1-005** showed an inhibitory activity with IC_{50} range from 2 to 10 μM (Table 5).

Table 5. Multi-target-directed ligand compounds that include G9a as one of the targets.

Compound	Targets	Type	IC_{50} G9a	IC_{50} Target2	IC_{50} Target3	IC_{50} Target4	Reference
171	G9a/HDAC8	nr	7.1 μM	13.80±1.2* 5.735±1.2#	-	-	(Zang et al., 2017)
CM-272	G9a/DNMT1	S-Ci	8 nM	328 nM	-	-	(José-Enériz et al., 2017)
185	G9a/DNMT1/ HDAC1/ HDAC6	nr	269 nM	1.16 μM	3 nM	152 nM	(Rabal et al., 2021)
HKMTI-1-005	G9a/EZH2	S-Ci	100 nM	2-10 μM	-	-	(Ishiguro et al., 2021; Spiliopoulou et al., 2022)

Substrate competitive inhibitors: S-Ci ; *in Hela cells; #in K562 cells; Not reported: nr**.**

1.4. From neuropathology to G9a's role in Alzheimer's disease progression

1.4.1. Clinical symptoms

From a clinical perspective, patients with AD manifest a widespread decline in cognitive function and memory, leading to subsequent deficits in language and visual skills, often accompanied by behavioural disturbances (Schultz et al., 2004). This decline is progressive, beginning with mild cognitive impairment (MCI), marked by early and noticeable memory disturbances, progressing over time to severe memory loss, learning difficulties, and disorientation.

Moreover, as the disease advances, individuals with AD often exhibit non-cognitive neuropsychiatric symptoms, recognized as behavioural and psychological symptoms of dementia (BPSD) (Shinosaki et al., 2000). BPSD encompasses behavioural issues like aggression, screaming, and agitation, as well as psychological symptoms such as depressive mood, anxiety, and mood hallucinations. Collectively, these symptoms impact the patient's social functioning. However, it remains unclear whether AD-related depression is a symptom, an independent risk factor, or a prodrome for AD (Ownby et al., 2006; Byers et al., 2012).

Looking only at the role of the G9a

Notably, G9ais rescue impaired recognition, working, and spatial memory in aged AD mice models (Griñán-Ferré et al., 2019; Zheng et al., 2019). Moreover, G9a inhibition also correlates with a decrease in anxiety-like behaviours in adult male mice (Wang et al., 2018). Furthermore, treatment with UNC0642 in the 5xFAD mouse model reduces 5-mC levels, contributing to cognitive restoration (Griñán-Ferré et al., 2019).

1.4.2. Microscopic features of Alzheimer's disease

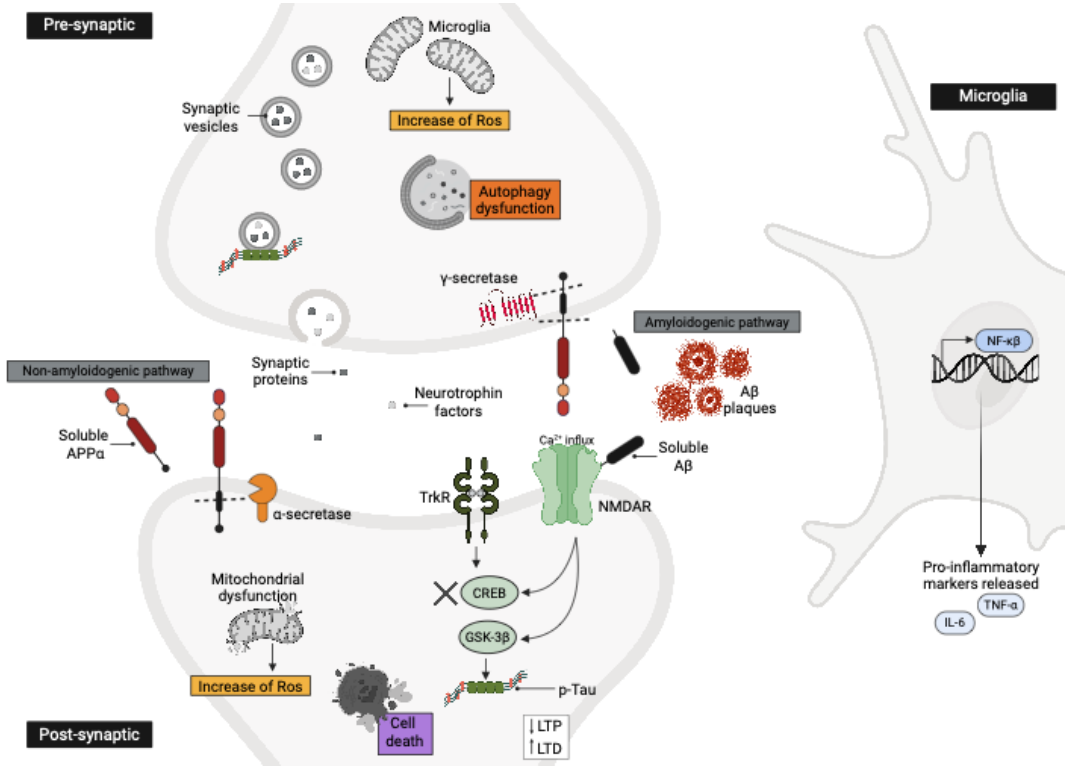

Figure 7. Putative mechanisms of degeneration in Alzheimer's disease.

AD has a complex etiology involving several molecular pathways, and intracellular signaling occurs at the sub/cellular level. The main AD hallmarks are Aβ accumulation and Tau hyperphosphorylation. However, given their evolutionarily conserved physiological and neurotoxic properties, the extent to which dyshomeostasis and abnormal accumulation of Aβ and/or Tau are a cause or consequence of the etiopathogenesis with AD has not been elucidated. Other key events during the pathogenesis of AD include disruption of synaptic plasticity, inflammatory responses, oxidative stress (OS), and dysfunctional proteostasis (Hampel et al., 2021) (Figure 7).

Interestingly, their dysregulation results from a multilayer interaction among genetic, epigenomic, and environmental factors, so epigenetic alterations have emerged as one of the pathogenic mechanisms of AD in recent years (Castrillo and Oliver, 2016). In addition, most

cases are LOAD, probably due to the interaction of environmental influences and individual genetic susceptibility (Gatz et al., 2006). Moreover, increasing evidence suggests an imbalance in epigenetic mechanisms as the basis of abnormal expression of synaptic plasticity- and memory-related genes in AD (Landgrave-Gómez et al., 2015; Bertogliat et al., 2020; Murshid et al., 2022).

Looking only at the role of the G9a

As we pointed out before, aberrant histone methylation is widely associated with AD pathogenesis (Santana et al., 2023). Moreover, post-mortem AD brains show large-scale changes in histone modifications (Klein et al., 2019; Zheng et al., 2019; MacBean et al., 2020). Interestingly, AD brains show increased in the repressive mark H3K9me2 as a result of G9a upregulation. Likewise, in AD mouse models (Tg2576 and familial (FAD)), there are increased global levels of H3K9me2 in the prefrontal cortex (Griñán-Ferré et al., 2019; Zheng et al., 2019). Besides, FAD mice exhibit elevated levels of H3K9me2 in the hippocampus, contrasting with the striatum, where such elevation is not observed (Lithner et al., 2013; Zheng et al., 2019) (Figure 8).

Abnormal amyloid β aggregation

Aβ plaques are extracellular deposits formed mainly by Aβ peptide (36 to 43 amino acid peptide), produced by cleavage of amyloid precursor protein (APP) through β-secretase (BACE1) and γ-secretase (Presenilin (PSENs), nicastrin, anterior pharynx-defective 1 and PSEN enhancer- 2), giving rise to an amyloidogenic carboxy-terminal fragment (C99). Its overproduction drives Aβ to self-assemble into oligomers and, in turn, form toxic Aβ plaques (DeTure and Dickson, 2019), which mainly aggregate in the hippocampus and, during the disease, spread to the cortex and other brain regions. As mentioned, Aβ plaques have different chain lengths, generating first soluble oligomers and then larger insoluble fragments precipitating as amyloid fibrils. Among these, the most well-known species are $A\beta_{40}$ and $A\beta_{42}$, with $A\beta_{40}$ predominant. However, an increase in $A\beta_{40}$ is associated with a decrease in the accumulation of Aβ plaques, as these two species may have opposite effects. While $A\beta_{42}$ promotes plaque accumulation, $A\beta_{40}$ inhibits it (Iwatsubo et al., 1994). Conversely, when the APP is cleaved by α-secretase (ADAM10), Aβ formation is prevented by generating a non-

amyloidogenic carboxy-terminal fragment of APP (C83). Hence, according to the differential cleavage of APP, there are two different pathways: the non-amyloidogenic pathway (regulated by α-secretase) or the amyloidogenic one that leads to the generation of Aβ (β-, and γ-secretase) (O'Brien and Wong, 2011).

Beyond the synthesis of Aβ, its accumulation is also influenced by impaired Aβ clearance or degradation. On the one hand, enzymatic pathways involve Aβ degrading enzymes such as neprilysin (NEP), insulin-degrading enzyme (IDE), matrix metalloproteinase-9 (MMP9), among others. On the other hand, non-enzymatic clearance occurs through microglia or astrocytic phagocytosis, interstitial fluid drainage, and transport across blood vessel walls (Yoon and Jo, 2012). Ultimately, there appears to be a robust connection between AD genetics and Aβ plaque formation, as demonstrated by the impact of high-penetrance AD genetic risk alleles (e.g., *APOEε4*, *APP* mutations, *PSEN1* and *PSEN2* mutations, Down syndrome, *BIN1*, *Aph-1 Homolog B, Gamma-Secretase Subunit* (*APH1B*), *Protein Tyrosine Kinase 2 Beta* (*PTK2B*), and *Paired Immunoglobin Like Type 2 Receptor Alpha* (*PILRA*) etc) on Aβ deposition and plaque formation (Tang and Gershon, 2003).

Looking only at the role of the G9a

As mentioned, G9a is upregulated in the AD brain, which correlates with an increase in the repressive mark H3K9me2 and the Aβ concentration (Zheng et al., 2019). Early *in vitro* studies showed that primary cortical and hippocampal neurons transfected with G9a small interfering RNA (siRNA) promoted hypoxia-induced down-regulation of G9a up-regulation and H3K9me2 expression, restoring levels of NEP, an enzyme vital for Aβ clearance (Wang et al., 2011). Moreover, inhibiting G9a/GLP with BIX-01294 restored excitatory post-synaptic currents in Aβ-treated human stem cell-derived neurons expressing high levels of G9a (Lin et al., 2019). Besides, G9a inhibition decreases β-amyloid plaques in the 5xFAD mouse model (Griñán-Ferré et al., 2019). Although the mechanism has not been elucidated, the reduction of Aβ load after G9a inhibition could be due to the direct modulation of non-amyloidogenic pathway genes, leading to reduced cognitive deficits (Figure 8).

Hyperphosphorylation of Tau protein

NFTs are associated with an abnormally hyperphosphorylated and aggregated form of Tau in the neocortex, hippocampus, and other subcortical structures related to cognition (Arriagada et al., 1992). However, in pathological conditions, its hyperphosphorylation converts Tau from a normal functional protein to a neurotoxic protein, resulting in the aggregation of Tau, synaptic loss, and neuronal dysfunction (Serrano-Pozo et al., 2011). Tau can undergo phosphorylation at various sites, such as in its serine (Ser), threonine (Thr), and tyrosine (Tyr) phosphosites, mainly localized in the proline-rich region (residues 172–251) and the C-terminal tail region (residues 368–441) residues) (Goedert et al., 1989). The progressive pathological accumulation of phosphorylated and aggregated Tau has since been used for the staging of AD and other tauopathies (their density directly correlates with disease severity and dementia) (Iqbal et al., 2016).

In AD, serine/threonine residues followed by proline appear as the most frequently phosphorylated sites, constituting approximately 50% of phosphorylated residues. Proline-directed protein kinases (PDPKs), such as glycogen synthase kinase-3β (GSK-3β), cyclin-dependent-like kinase-5 (CDK5), and dual-specificity tyrosine-phosphorylation-regulated kinase 1A (DYRK1A), play a pivotal role in phosphorylating these sites (Ishiguro et al., 1992; Arioka et al., 1993; Woods et al., 2001; Liu et al., 2008). Conversely, non-proline-directed sites in tau, lacking a subsequent proline, are phosphorylated by several non-proline-directed protein kinases (non-PDPKs), including calcium/calmodulin-activated protein kinase II (CaMKII), microtubule affinity-regulated kinase 110 (MARK p110), protein kinase A (PKA), and casein kinase 1 (CK1) (Baudier and Cole, 1988; Ledesma et al., 1992; Singh et al., 1996a, 1996b; Drewes et al., 1997; Sironi et al., 1998). Several combinations of non-PDPKs and PDPKs have been identified as contributors to the hyperphosphorylation that resembles the p-Tau of AD (Wang et al., 2007). In most of them, it has been linked to NFTs in the brains of AD patients.

[redacted].

Looking only at the role of the G9a in AD

Up to now, G9ai treatments (BIX01294 and UNC0642) have not decreased Tau phosphorylation in AD mouse models (Kametani and Hasegawa, 2018).

Synapse loss and neuronal death

Neurodegeneration leads to synapse loss and neuronal death, which are major functional features of AD and are closely associated with the early manifestations of cognitive impairment (Spires-Jones and Hyman, 2014; Kashyap et al., 2019). Accordingly, cognitive decline and early decreases in verbal fluency in AD are attributed to diminished synaptic density in the hippocampus and medial temporal lobes (Scheff et al., 2006, 2011). Moreover, gene expression studies validate these findings, linking synaptic dysfunction to AD pathology (Overk and Masliah, 2014). Hence, AD-associated alterations involve both pre-synaptic proteins, such as synaptophysin (SYP), and synapsin (SYN), and post-synaptic proteins (PSD), such as PSD95 and PSD93 (Marksteiner et al., 2002; Counts et al., 2006; Scheff et al., 2014). Of note, synaptic alterations serve as a central theme, bridging Aβ and Tau neurotoxicity, AD morphological lesions, and cognitive impairment (Spires-Jones and Hyman, 2014) since it is strongly correlated with cognitive impairment in AD (DeKosky and Scheff, 1990; Terry et al., 1991). Aβ plaques lead to decreased synaptic content, both pre-synaptic and post-synaptic markers, with a substantial number of lost synapses (Spires et al., 2005; Spires-Jones and Hyman, 2014). Similarly, Tau-overexpressing transgenic animals exhibit synaptic loss (Zhou et al., 2017), synergistically amplified in models combining Tau and Aβ mutant transgenes (Busche and Hyman, 2020).

Neurotrophins, such as nerve growth factor (NGF), brain-derived neurotrophic factor (BDNF), neurotrophin (NT) 3 and NT4, play a crucial role in the survival, maintenance, and regeneration of neurons (Huang and Reichardt, 2001). These neurotrophins exert their functions through the pan-neurotrophin receptor p75 (p75NTR) and tyrosine kinase (Trk) receptors (TrkA and TrkB). For instance, NGF promotes and maintains synaptic contact with hippocampal and cortical neurons. At the same time, BDNF is pivotal for the survival and

function of cholinergic and dopaminergic neurons in the hippocampal cortex. Moreover, BDNF emerges as a key player in synaptic plasticity, long-term potentiation (LTP), and memory formation (Lu et al., 2008). A decrease in its levels or its binding to the corresponding receptors contributes to cholinergic atrophy, alterations in LTP and synaptic plasticity, which explains the cognitive and memory deficits observed in the early stages of AD (J Allen et al., 2011; Allen et al., 2013). In addition, transcriptional factor CAMP Responsive Element Binding Protein (CREB) is also involved in pathways and mechanisms activated during memory formation. When phosphorylated through CAMKs cascade, PKA pathway and Mitogen-Activated Protein Kinase (MAPK) pathway, among others, phosphorylated CREB (p-CREB) is also able to regulate BDNF expression (Finkbeiner et al., 1997).

By contrast, cell death can be categorized into necroptosis (Koper et al., 2020; Balusu et al., 2023), apoptosis (Sharma et al., 2021), and ferroptosis (Dixon et al., 2012; Dixon, 2017; Weiland et al., 2019; Chen et al., 2021), among others (Moujalled et al., 2021). On one hand, apoptosis occurs through either an intrinsic (mitochondrial pathway) or an extrinsic apoptotic pathway mediated by death receptors. Both pathways converge on caspase activation, ultimately leading to DNA fragmentation and cell death (Obulesu and Lakshmi, 2014). In AD, an altered expression of critical apoptotic, such as BCL2 Associated X (Bax), Bcl-2, Bcl-xL, and Caspases (CASP) 2, 3, 8, and 9, and anti-apoptotic markers has been observed (Kitamura et al., 1998; Zhang et al., 2002b; Lu et al., 2003; Park et al., 2020). While the precise mechanisms leading to neuronal apoptosis remain unclear, pathological features associated with AD, such as Aβ peptides, calcium dysregulation, OS, and neuroinflammation, have been identified as triggers initiating the process of apoptotic cell death (Bamberger and Landreth, 2002; Calissano et al., 2009; Tönnies and Trushina, 2017). On the other hand, ferroptosis is an iron-dependent form of cell death driven by lipid peroxidation that has emerged as a significant factor in AD pathology (Dixon et al., 2012). It displays unique morphological, biochemical, and genetic features that distinguish it from other cell death mechanisms (Weiland et al., 2019). These features include altered cellular morphology, iron-

dependent lipid peroxide accumulation, glutathione (GSH) depletion, inactivation of Glutathione Peroxidase (GPX)4, and a distinct set of regulated genes (Dixon et al., 2012; Dixon, 2017; Chen et al., 2021). Notably, signatures of ferroptosis have been discovered in the brains of both AD patients and model mice (Zhang et al., 2012; Hambright et al., 2017; Ayton et al., 2020). Specific inhibitors, such as deferoxamine (DFO) and ferrostatin-1 (Fer-1), have effectively targeted ferroptosis. Some inhibitors, such as desferrioxamine (DFE) and vitamin E, have demonstrated clinical benefits in AD (Dixon et al., 2012). Although there is no direct evidence of ferroptosis in AD pathology, its involvement is strongly suggested by the observed signatures and therapeutic responses.

Looking only at the role of the G9a

G9a inhibition could rescue LTP deficits and synaptic tagging/capture by facilitating protein synthesis in the hippocampal CA1 area of the APP/PS1 mouse model of AD (Han et al., 2021). Besides, there is an increased H3K9 methylation in 3xTg-AD (Walker et al., 2013), which correlates with lower levels of *Bdnf* gene expression (Sharma et al., 2017a). Accordingly, pharmacological inhibition of G9a/GLP (BIX-01294) decreases Aβ-induced deficits in long-term plasticity and synaptic tagging/capture in hippocampal pyramidal neurons (Sharma et al., 2017a), suggesting the G9a/GLP complex as a potential target to prevent Aβ-induced plasticity deficits in hippocampal neurons. Thus, G9 inhibition might promote neuronal plasticity gene expression (Lin et al., 2019). A recent study from our group demonstrated that G9a inhibition increased synaptic markers, as SYN, and neurotrophic factors such as *Ngf*, *VGF nerve growth factor inducible* (*Vgf*), and BDNF in 5xFAD (Griñán-Ferré et al., 2019). Moreover, elevated G9a and GLP in the prefrontal cortex and hippocampus in an aged AD mouse model correlate with reduced glutamate receptor transcription and AD-like cognitive deficits (Zheng et al., 2019). In this regard, Chromatin immunoprecipitation-sequencing (ChIP-seq) data indicates that FAD mice show genome-wide enrichment of H3K9me2 at genes involved in neuronal signaling (including glutamate receptors) (Zheng et al., 2019). However, G9a inhibition failed to induce cell-wide priming and synthesis of plasticity-related products (PRPs) in the AD-like condition (Han et al., 2021). This finding contradicts previous studies in

which upregulation of synaptic genes and synaptic transmission was observed in Aβ-affected cortical neurons and in mouse models of AD (Zheng et al., 2019). The discrepancy could be explained by a different duration of the pharmacological inhibition, as G9a activity responds rapidly to external stimuli (Maze et al., 2010). In parallel, findings from the work of Rothammer et al. (Rothammer et al., 2022), suggest that G9a activity represses anti-ferroptosis genes, decreases intracellular GSH levels, and triggers the iron-dependent programmed cell death by ferroptosis pathway (Figure 8).

Inflammatory response

Neuroinflammation is characterized by the activation of glial cells, microglia, and astrocytes, which produces inflammatory factors such as cytokines and chemokines in the brain (Heneka et al., 2015). Microglia, which usually performs surveillance functions and plays a role in neuronal apoptosis and synaptic plasticity, responds to pathological factors by initiating an innate immune response, producing pro-inflammatory cytokines such as Tumor Necrosis Factor alpha (TNF-a) and interleukins (Ils) (e.g., IL-1, IL-6, IL-18), as well as chemokines (e.g., C-C Motif Chemokine Ligand (CCL)1, CCL5, C-X-C Motif Chemokine Ligand (CXCL)10) (Deverman and Patterson, 2009; DiSabato et al., 2016). Similarly, astrocytes, responsible for regulating homeostasis and synaptic plasticity, undergo reactive gliosis in response to pathological insults. Reactive astrocytes, characterized by upregulation of Glial Fibrillary Acidic Protein (GFAP), release cytokines, Ils, and nitric oxide (NO), contribute to the neuroinflammatory response (Rossi and Volterra, 2009; Li et al., 2019a). Consequently, the release of pro-inflammatory molecules can lead to synaptic dysfunction, neuronal death, and inhibition of neurogenesis. For instance, IL-1β induces synaptic loss (Mishra et al., 2012), while TNF causes neuronal death (Micheau and Tschopp, 2003). In contrast, anti-inflammatory cytokines are also produced during neuroinflammation and may serve as a sophisticated mechanism to prevent excessive inflammation (Calsolaro and Edison, 2016). Nevertheless, in the context of neurodegenerative diseases, neuroinflammation tends to persist as a chronic process that fails to resolve by itself, being considered an early characteristic of both neurodegeneration and AD (Heneka et al., 2015).

Looking only at the role of the G9a

G9a pharmacological inhibition also modulates pathways related to neuroinflammation, one of the key events in AD pathogenesis. Accordingly, G9a inhibition decreases Ionized calcium binding adaptor molecule 1 (IBA-1) and GFAP levels in the 5xFAD mouse model (Griñán-Ferré et al., 2019). Furthermore, there is evidence suggesting that epigenetic mechanisms may lead to inflammation by modulating the expression of pro-inflammatory cytokines. Inhibition of an HMT, G9a, reduced gene expression levels of *Il-6*, *Tnf-α*, and *Cxcl10* in a 5xFAD-treated mouse model (Griñán-Ferré et al., 2019) (Figure 8).

Oxidative stress and DNA damage

OS characterized by excessive production of reactive oxygen species (ROS), might play a critical role in AD, acting as both an accelerator of the pathology and one of the earliest events in AD pathogenesis. OS refers to an imbalance between the generation of reactive oxygen/nitrogen species (ROS/RNS) and antioxidant defense mechanisms (Zhao and Zhao, 2013). Under normal conditions, antioxidant enzymes like superoxide dismutase (SOD), GPX, and catalase (CAT), among others, regulate ROS levels by serving as radical scavengers. Among the antioxidants enzymes, SOD is one of the main protective mechanisms, being responsible for the conversion of O_2^- into hydrogen peroxide (H_2O_2) and O_2. The H_2O_2 produced is then transformed into H_2O by CAT action (Wang et al., 2018b). However, an imbalance in OS may lead to functional and organelle deficits, such as those in mitochondria, contributing to synaptic loss and cell death and ultimately manifesting clinical symptoms associated with AD (Tönnies and Trushina, 2017).

Moreover, DNA damage and DNA repair deficiencies are observed in AD. Disruptions in cellular redox conditions play a significant role in causing DNA damage, as the balance of redox homeostasis can either activate or inhibit essential proteins crucial for DNA repair (Nelson and Xu, 2023). Eukaryotic cells have intricate signaling mechanisms collectively known as the DNA damage response to detect, signal, and repair DNA damage, ensuring the

maintenance of genome integrity. However, when DNA lesions go unrepaired, the accumulation of damage triggers various mechanisms of cell death to eliminate cells (e.g., apoptosis, or cellular senescence (Roos and Kaina, 2006; DeVorkin et al., 2014; Radi et al., 2014). Despite a comprehensive characterization of the DNA damage response, the connection between DNA damage and the cellular redox state needs to be better understood, and this relationship has only recently come to light (Shadfar et al., 2023).

Looking only at the role of the G9a

Dysregulation of G9a correlates with increased levels of OS, another factor involved in the AD pathogenesis. G9a promotes OS in neurons (Rothammer et al., 2022), and its inhibition reduces ROS levels and elevates antioxidant enzyme levels (Griñán-Ferré et al., 2019). Additionally, H_2O_2 treatment in cell cultures correlates with a pronounced increase in the repressive mark H3K9me2 (Park et al., 2016). UNC0642 treatment in an AD mouse model modulates OS responses (Griñán-Ferré et al., 2019). Accordingly, increases in the Nuclear Factor erythroid-2-Related Factor 2 (NRF2), *Heme oxygenase decycling 1* (*Hmox1*) gene expression, and a decrease in ROS were also reported in the 5xFAD mice model after G9ai treatment (Griñán-Ferré et al., 2019) (Figure 8).

Dysfunctional proteostasis

Autophagy, a conserved catabolic process in eukaryotic cells, plays a crucial role in degrading defective proteins or organelles within lysosomes and recycling essential components. It is categorized into three main types: macroautophagy, chaperon-mediated autophagy (CMA), and microautophagy (Nixon, 2013). Although the primary function of autophagy is proteostasis, this mechanism also plays a vital role in homeostatic cell signaling, phagocytosis, innate immunity, and synaptic function. Hence, autophagy dysfunction has been closely related to AD. Clearance of damaged proteins is essential to maintain synaptic homeostasis, and the neuronal lysosome plays a vital role in the etiology of AD. Accordingly, a down-regulation of autophagy-related proteins has been demonstrated in AD brains, suggesting defective autophagy (Pickford et al., 2008; Lachance et al., 2019; Heckmann et al., 2020). Autophagy induction is modulated through the VPS34 complex, where Beclin-1

(BECN1), an essential subunit and a critical subunit, is necessary for autophagic vesicle nucleation. Besides, BECN1 is also implicated in receptor recycling and retromer recruitment during Aβ phagocytosis *in vitro* (Lucin and Wyss-Coray, 2013; Lucin et al., 2013). In addition, AMPK promotes autophagy AMPK promotes autophagy through BECN1 (Zhang et al., 2016a). Loss of *Becn1* in an AD mouse model resulted in Aβ load (Pickford et al., 2008). Likewise, sequestosome 1 (SQSTM1)/p62, an autophagy receptor, is crucial in regulating cellular signaling, protein trafficking, and degradation. In AD, reduced SQSTM1/p62 levels in the frontal cortex disrupt signaling pathways, increasing OS and impairing neuronal survival (Salminen et al., 2012).

Looking only at the role of the G9a

G9a directly represses genes known to participate in the autophagic process and inhibition of G9a-mediated epigenetic repression represents an essential regulatory mechanism during autophagy (Shu et al., 2023). G9a can directly interact with the promoters of core autophagy genes, such as Microtubule Associated Protein 1 Light Chain 3 Beta (LC3B,) SQSTM1/p62, Tumor Protein P53 Inducible Nuclear Protein 2 (TP53INP2)/DOR, and WD Repeat Domain, Phosphoinositide Interacting 1 (WIPI1), increasing their histone methylation levels to reduce autophagy levels (Artal-Martinez de Narvajas et al., 2013) (Figure 8).

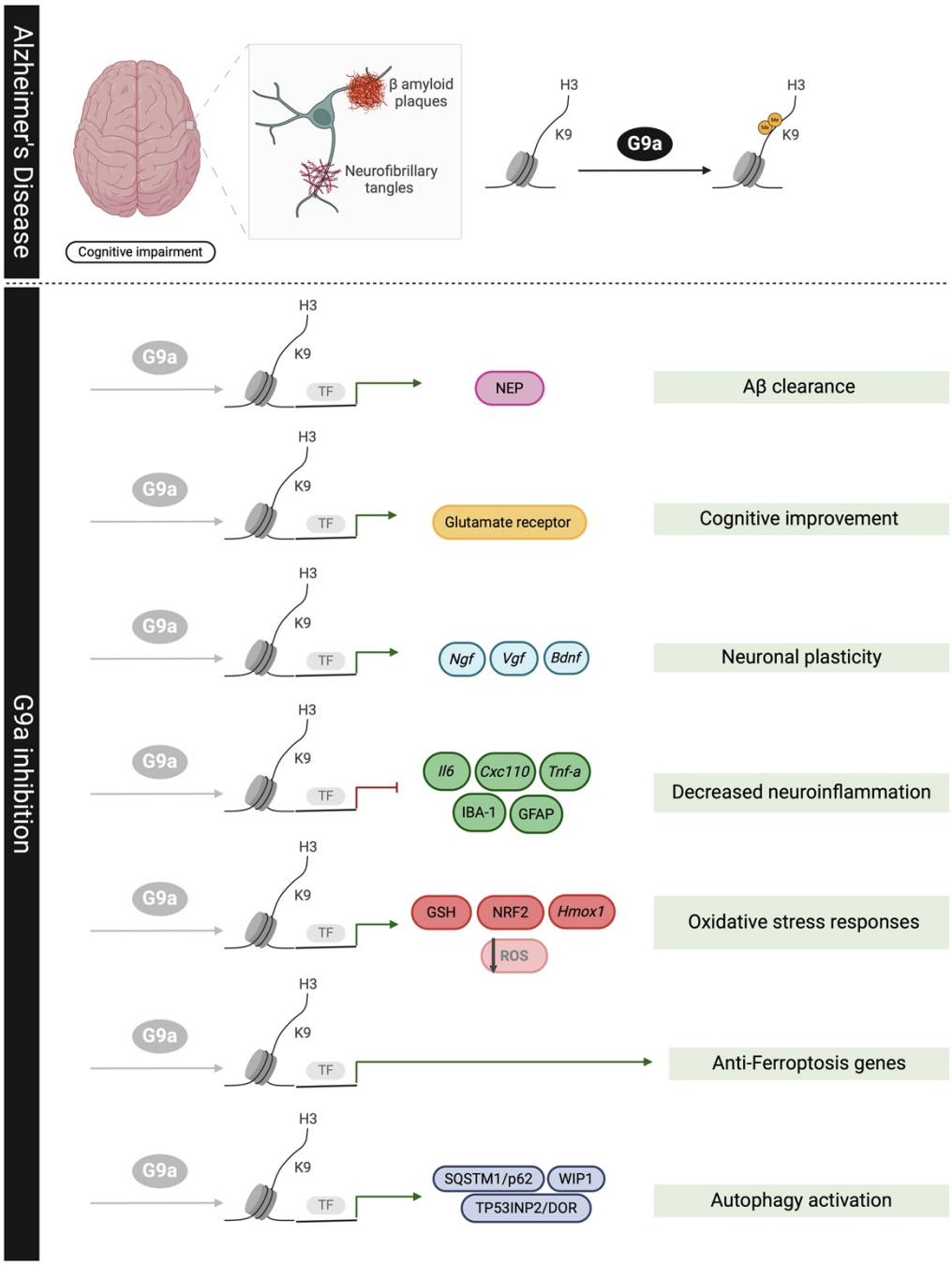

Figure 8. Findings in AD after pharmacological inhibition or gene edition of G9a.

1.5. Treatments for Alzheimer's disease

1.5.1. Currently approved treatments for Alzheimer's disease

As aforementioned, there are an estimated 50 million individuals with AD dementia globally, and this population will grow to 150 million by 2050. Up to now, only 6 drugs have been approved by the Food and Drug Administration (FDA) that fall into two categories: drugs that change disease progression and drugs that may temporarily mitigate some symptoms of AD (Long and Holtzman, 2019).

1.5.1.1. Drugs that treat symptoms

On one hand, acetylcholinesterase (AchE) inhibitors were developed stop the breakdown of acetylcholine by inhibiting the AchE enzyme (Long and Holtzman, 2019). Among them, three drugs were approved the FDA: Donepezil (Aricept®, 1996) (Courtney et al., 2004), Rivastigmine (Exelon®, 2000) (Naik et al., 2009), and Galantamine (Razadyne®, 2001) (Wilcock et al., 2001). On the other hand, in 2003, an N-methyl-D-aspartate (NMDA) receptor (NMDAR) antagonist, Memantine (Ebixa®) (Reisberg et al., 2003), was also approved by FDA to treat moderate-to-severe AD. Memantine is involved in the mitigation of glutamate-induced excitotoxicity. Furthemore, combination therapy of an AchE inhibitor and Memantine has been proposed (Namzaric®, 2014) (US Food and Drug Administration, 2014), improving significatively the cognitive decline. However, none of them cure the disease or reverse its progression, being only symptomatic treaments.

1.5.1.2. Disease-modifying drugs

Recently, the FDA has granted accelerated approval to Aducanumab (Aduhelm®, 2021 – First approved disease-modifying treatment in the history of AD) and Lecanemab (Leqemib®, 2023), both monoclonal antibodies that target Aβ plaques (Sevigny et al., 2016; van Dyck et al., 2023). Nevertheless, plaque reduction has not been a reliable marker for cognitive function in past trials; thus, there is controversy regarding their approval (Knopman et al., 2021).

1.5.2. The journey to drug discovery

The primary objective of the drug discovery and development process is to identify chemical entities with therapeutic potential, particularly for unmet diseases such as AD. Typically, the process begins by identifying a biological target (e.g., receptor, enzyme, protein, gene) involved in a dysfunctional biological pathway in patients.

Drug discovery is a complex, lengthy, and expensive multidisciplinary process, often marked by unsuccessful outcomes. In fact, developing a new drug, from target identification to regulatory approval, takes more than 12 years (DiMasi et al., 2010) and is extremely costly (DiMasi et al., 2016).

1.5.2.1. Drug Discovery: From target to clinical candidate

In the preclinical drug discovery phase, the goal is to produce clinical candidate molecules with evidence of biologic activity at a relevant disease target, along with safety and drug-like properties for human testing. The process often starts in an academic setting, where researchers collaborate to identify and characterize potential targets. Once a target is identified, potential leads are optimized for the target, ensuring the lead molecule has the desired effect on the biological target in *in vitro* and *in vivo* studies. Extensive *in vitro* and *in vivo* studies are conducted during the preclinical research phase to gather safety and efficacy data before initiating human clinical trials (Mohs and Greig, 2017).

Clinical trials proceed in three phases: Phase I focuses on safety, Phase II on efficacy, tolerability, and dosage, and Phase III aims to confirm efficacy and safety in a larger patient population. If the candidate successfully passes these phases, regulatory approval is sought, followed by post-approval follow-up to continue gathering comprehensive efficacy and safety data (Mohs and Greig, 2017) (Figure 9).

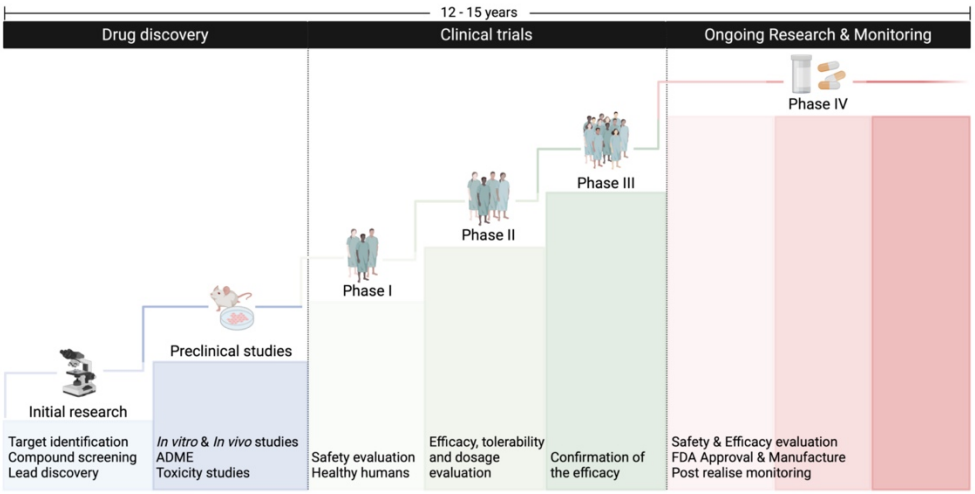

Figure 9. Drug discovery and development process.

1.5.2.2. Hit-to-Lead, and Further Optimization

An essential step in this process is identifying and validating the target, which must be both clinically relevant and "druggable." This involves the target's ability to bind a molecule and elicit a therapeutically useful biological response measurable *in vivo* and *in vitro*. Virtual Screening (VS) is an *in silico* technique with reduced cost that allows to evaluate large collections of chemicals against a molecular target using computational methods. VS includes screening in structure-based, ligand- based, or hybrid approaches (Scholes et al., 2021). When a new hit is identified, validated, and selected for progression, it moves into the hit-to-lead stage (Hit-to-Lead) (de Vink et al., 2019). The hit-to-lead stage aims to improve potency, and computational methods such as Quantitative SAR (QSAR) can be used for chemical optimization (Verma et al., 2010). The lead optimization stage focuses on improving other drug-relevant properties, such as ADMET properties (absorption, distribution, metabolism, excretion, and toxicity) (Fischer et al., 2014; Krönke et al., 2015; Sievers et al., 2018).

1.5.2.3. Drug repurposing: Challenges and Opportunities

Drug repurposing, or repositioning, involves using a drug that has undergone safety and efficacy testing for a different medical indication, whether approved, in advanced clinical stages, or withdrawn from the market. This strategy is beneficial in emergencies like pandemics and for rare diseases with limited drug development in pharmaceutical companies. This approach is well known for potential cost and time savings, along with a higher success rate compared to traditional drug development. Already existing safety and efficacy data, along with available products and supply chains, make it an attractive option. However, drug repurposing faces several challenges, such as limited optimization of the therapeutic molecule without losing potential. In addition, determining the optimal dose and formulation for the new indication can be time-consuming, which can lead to side effects. Besides, the molecules being investigated for reuse are either patented or off-patent, and in some cases the intellectual property protection for the new indication may not be strong enough to undertake such a project (Pushpakom et al., 2019).

1.5.3. Emerging candidates in clinical trials for Alzheimer's disease treatment

Due to the limitations of the approved treatments, there is an urgent need of new drugs that prevent the onset, slow progression, or improve cognitive and behavioural symptoms of AD. There are currently 187 trials evaluating 141 drugs for the treatment of AD (Cummings et al., 2023). The CADRO Translational Research and Clinical Interventions Category outlines various potential targets for clinical therapies addressing AD. These targets include Aβ, Tau, APOE, lipids, neurotransmitter receptors, inflammation, OS, cell death, proteostasis/proteinopathies, metabolism, bioenergetics, vasculature, growth factors, hormones, synaptic plasticity/neuroprotection, gut–brain axis, circadian rhythm, epigenetic regulators, multi-target, unknown target, and other factors. Among Phases I, II, and III, most of the agents are disease-modifying agents (78% of the total number of drugs in the trial), which aim to alter AD biology by targeting its pathological mechanisms and features and hence, deliver neuroprotection. Of the disease-modifying treatments, 44% are biologics, while 56% represent small molecules.

In contrast, 11% of compounds in development are aimed at improving cognition, and drugs targeting the neuropsychiatric and behavioural symptoms of AD also account for 11% (Cummings et al., 2023). Among them, there are two epigenetics drugs: LX1001, Phase II, focused on patients with mild-to-moderate cognitive deficits; and Lamivudine, also in Phase II, focused on prodromal or mild prodromal patients.

In addition, repurposed agents represent 28% of the drugs in the current pipeline. Recent studies demonstrate that antiepileptics and antiretroviral drugs might benefit AD patients through their primary and epigenetic effects (Sun et al., 2021a; Vossel et al., 2021). For instance, in the case of Levetiracetam, its main metabolite promotes histone deacetylation in HeLa cells. Another example is the antiretroviral Lamivudine, which has been found to act as an HDAC inhibitor (He et al., 2022).

1.5.4. G9a inhibitors as a promising treatment for Alzheimer's disease

On the one hand, the first *in vivo* proof of concept (PoC) using BIX-01294 as a G9ai suggests that this pharmacological approach is a potential therapeutic strategy for AD (Zheng et al., 2019). On the other hand, the second *in vivo* PoC was developed by Griñán-Ferré and team the same year (Griñán-Ferré et al., 2019). This study investigated the neuroprotective effects of the G9a/GLP complex inhibition by UNC0642 in a transgenic mouse model of EOAD.

Sbardella an col. Developed in 2019 (Milite et al., 2019) EML741, which is a potent G9a/GLP inhibitor with high *in vitro* and cellular potency. It has an IC_{50} of 23 nM and a dissociation constant (K_d) of 1.13 μM for G9a. EML741 also inhibits DNMT1 with an IC_{50} of 3.1 μM, with no effect on DNMT3a or DNMT3b. EML741 is membrane-permeable histone lysine methyltransferase G9a/GLPi, that crosses the BBB with low cell toxicity. EML741 shows improved inhibitory potency against DNA methyltransferase 1 and improved selectivity against other methyltransferases. The co-crystal structure of GLP in complex with EML741 provides a basis for further development of benzodiazepine based G9a/GLPis. EML741 shows promise as a G9a/GLPi with favorable properties and potential therapeutic applications.

A recent preprint reported the development of a novel brain-penetrant inhibitor of G9a, MS1262, which blocks the G9a-regulated, proteopathic mechanism associated with AD. An intermittent treatment with MS1262 consistently restored both cognitive and non-cognitive functions to healthy levels in multiple AD mouse models, indicating its potential as a neuroprotective agent (Xie et al., 2023).

Overall, these studies highlight the potential of G9ais in the context of AD treatment. Further research is warranted to advance the use of G9ais as anti-AD agents from the bench to the clinic.

1.6. Alzheimer's Disease Experimental Models

1.6.1. *Caenorhabditis elegans*

Caenorhabditis elegans (*C. elegans*) is a free-living, non-parasitic nematode that was first introduced as a model organism by Sydney Brenner in 1963. Key advantages of *C. elegans* in neurodegenerative disease research include its short generation and life cycle, its small and transparent body (1 mm in length), which makes it easy for genetic manipulation, low maintenance costs, and well-characterized nervous system with 302 neurons in hermaphrodite, and 389 neurons in males forming an invariant network (Brenner, 1974) (Figure 10). Moreover, the completion of the *C. elegans* genome sequence in 1998 revealed approximately 38% of worm genes having human orthologs, establishing a foundation for studying AD mechanisms (Consortium, 1998; Shaye and Greenwald, 2011). Along with all the advantages, *C. elegans* has emerged as a powerful *in vivo* tool for neuroprotective compound screening (Olsen et al., 2006; Chen et al., 2015). Furthermore, this model organism is used in the field of transcriptional regulation, contributing to scientific advances in epigenetics and chromatin biology (Wenzel et al., 2011; Padilla et al., 2014; Corsi et al., 2015).

Several transgenic *C. elegans* models of AD have been established by expressing either Aβ human or Tau in specific cell types such as body wall muscle cells and neurons. One of the

well-established AD strain is CL2006, which expresses human $A\beta_{1-42}$ in body-wall muscle with the unc-54 promoter. Of note, CL2006 showed a clear phenotype that consists of progressive paralysis because of the accumulation of toxic Aβ oligomers - usually starting in young adulthood - and premature death (Link, 1995). Interestingly, this strain is widely employed nowadays to illustrate the neuroprotective properties of various natural and synthetic compounds (Chen et al., 2015). Likewise, researchers developed the transgenic strain known as CL2355, a model that employs the promoter of the *C. elegans* synaptobrevin ortholog (*snb-1*) to drive pan-neuronal expression of $A\beta_{1-42}$, and thus producing Aβ deposits between neurons (Zhang et al., 2016b). Remarkably, strain CL2355 shows cognitive alterations due to defects in chemotaxis to benzaldehyde, associative learning, and thrashing assay (Link, 2005). In parallel, an example strain for Tau pathology is BR5706, which presents an accelerated aggregation of insoluble Tau, severe developmental defects of the nervous system, altered pre-synaptic transmission, and very defective locomotion on the first day of adult life (Fatouros et al., 2012).

In addition to its contributions to neurodegenerative disease research, *C. elegans* offers unique insights into the epigenetics field. Like all eukaryotes, *C. elegans*' genomic DNA is packaged with histone proteins to form chromatin, with holocentric chromosomes, making it distinct among genetic model systems (Moore et al., 1999; Cui and Han, 2007). Its germline and embryonic cells provide convenient platforms for studying chromatin modifications, revealing remarkable similarities with higher organisms, including mammals (González-Aguilera et al., 2014). Accordingly, genome-wide analyses have shown significant conservation in the amino acid sequences of core histones between *C. elegans* and humans (Gerstein et al., 2010), indicating the presence of homologs of histone-modifying enzymes such as G9a/SET-25.

Moreover, the possibility of inhibiting gene expression by RNAi boosted *C. elegans* popularity 15 years ago. Notably, RNAi in *C. elegans* is highly efficient, thanks to an inherent amplification step, allowing for robust and scalable genome-wide analyses in a cost-effective and time-efficient manner (Grishok, 2005; Cipriani and Piano, 2011). Research into the RNAi mechanism have led to the revelation of various naturally occurring small RNA-mediated

processes, including transcriptional silencing, messenger RNA degradation, and translational regulation. Interestingly, some of these effects can persist across generations, even without the initial stimulus, suggesting a link to epigenetic modifications (Towbin et al., 2012).

Despite these advantages, *C. elegans* has limitations for modeling certain aspects of human physiology. The absence of some proteins crucial for disease pathogenesis highlights these limitations, as well as the lack of a circulatory system and immune responses.

1.6.2. SAMP8 mouse model for pathological aging, neurodegeneration, and sporadic Alzheimer's Disease

The Senescence-accelerated mouse prone 8 (SAMP8) has been proposed as a neurodegeneration model to study LOAD (Takeda, 1999; E. Morley et al., 2012; Pallàs, 2012; Akiguchi et al., 2017) (Figure 10). This inbred strain was established through phenotypic selection from the AKR/J mice strain and exhibits age-related deterioration in learning and memory abilities compared to the control strain, Senescence-Accelerated Resistant Mouse 1 (SAMR1) (Takeda, 1999; Pallas et al., 2008). SAMP8 mice have a shorter lifespan (10–12 months) compared to SAMR1 mice (19–21 months) and show accelerated aging phenotypes with signs such as hair loss, lordokyphosis, and reduced physical activity. Behavioural studies indicate that SAMP8 mice exhibit cognitive impairment, emotional disorders, reduced anxiety-like behaviour, and altered non-cognitive symptoms. These cognitive and non-cognitive behavioural alterations are evident as early as 4 months, and they increase with age (Chen et al., 2004; Griñan-Ferré et al., 2016a).

SAMP8 is characterized by AD-like pathological traits in the brain, including neuron and dendrite spine loss, cholinergic deficits, synaptic dysfunction, Aβ deposition and impaired clearance (Butterfield and Poon, 2005; Banks et al., 2007; Akiguchi et al., 2017), and aberrant hyperphosphorylation of Tau link to increased activity of specific kinases (e.g. CDK5, GSK-3β, and C-Jun N-Terminal Kinase 1 (JNK1)) (Pallas et al., 2008; Tajes et al., 2008, 2010; Pačesová et al., 2022). Furthermore, the SAMP8 strain demonstrates increased expression of

inflammatory markers, OS, and autophagy dysfunctions (García et al., 2011; Griñan-Ferré et al., 2016a, 2016c).

Noteworthy, the SAMP8 mouse model, being spontaneous and not transgenic, suggests a link to epigenetics. Specifically, alterations in chromatin status are suggested to contribute to the observed abnormalities in senescence and memory function in SAMP8 mice (Griñán-Ferré et al., 2018; Ravanelli et al., 2023). Studies point to age-related epigenetic modifications and neurodegeneration in SAMP8, with evidence that environmental factors such as diet, exercise, environmental enrichment (EE), and resveratrol-enriched diet influence the epigenetic machinery, affecting the acceleration of senescence and the presentation of AD-like processes in these mice (Cosín-Tomás et al., 2014; Griñan-Ferré et al., 2016c; Griñán-Ferré et al., 2018; Izquierdo et al., 2021). Of note, epigenetic mechanisms underlying cognitive impairment in accelerated aging were also evident in the SAMP8 model, resembling findings in an AD mouse model (5xFAD) (Griñán-Ferré et al., 2016; Griñan-Ferré et al., 2016c). For example, EE conditions elevate global 5-mC levels in young SAMP8 mice at 2 months of age while reducing 5-hmC levels, along with alterations in gene expression of *Dnmt3b*, *Hdac1/2*, *Sirt2*, and *Sirtuin (Sirt)6* (Griñan-Ferré et al., 2016c). Moreover, *Dnmt3b* expression was heightened in SAMP8 following erythropoietin injection, highlighting the importance of 5-mC in learning and memory formation (Yu et al., 2015). Additionally, increased acetylation in histones H3 and H4 was noted in the same experimental setting. Furthermore, alterations in histone methylation sites, primarily located on histone H3, were significantly found in the SAMP8 brain compared to SAMR1, indicating a link between post-translational modifications and the senescence process (Griñan-Ferré et al., 2016b; Wang et al., 2017). Similarly, miRNAs such as *miR-16* (Liu et al., 2012) and *miR-139* (Tang et al., 2017) were dysregulated, influencing APP levels and hippocampus-dependent learning and memory formation, respectively. Lastly, alterations in gene expression of various HDAC enzymes and global levels of histone acetylation, along with miRNA expression patterns, were observed in the hippocampus of SAMP8 females at 8 months of age, partially restored with voluntary exercise (Cosín-Tomás et al., 2014).

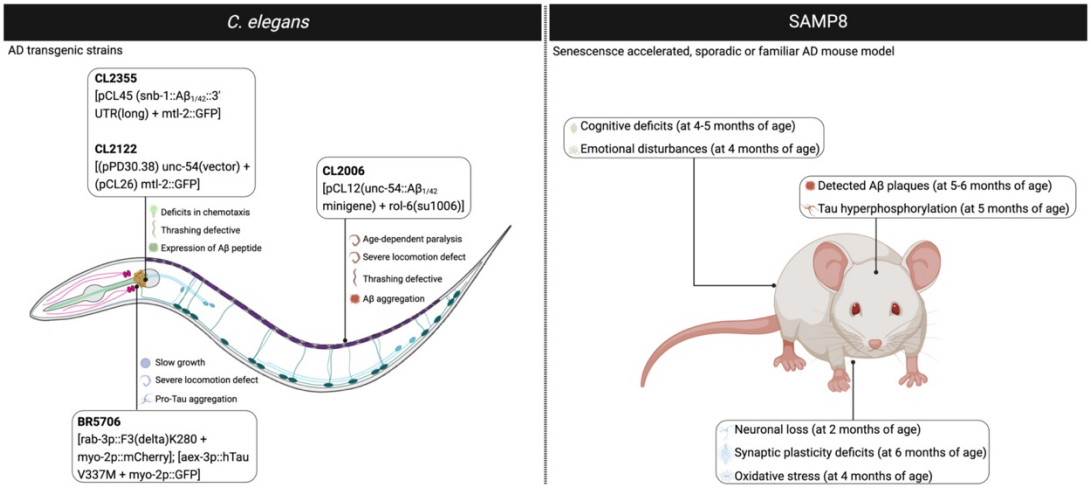

Figure 10. Experimental models of AD used in this doctoral dissertation.

2 Objectives

Given the rapid growth in the proportion of the elderly population worldwide, age-related diseases, such as neurodegenerative disorders, represent an increasing challenge. AD is the most common neurodegenerative disease and the primary form of dementia in the elderly. However, the lack of successful pharmacological treatments to halt AD progression underscores the need for novel therapeutic targets. In recent years, epigenetic modifications, such as post-translational modifications of histone tails, have been increasingly recognized in post-mortem AD brain tissue, suggesting their involvement in disease. Notably, the reversible nature of these epigenetic marks provides a potential avenue for therapeutic interventions, prompting active research to identify effective pharmacological targets.

Overexpression of the G9a and its repressive mark (H3K9me2) has been identified as a driver of the repression of learning memory genes, leading to synaptic plasticity reduction, autophagy dysfunction, increased OS and neuroinflammation, collectively contributing to and/or resulting in cognitive impairment in aging and neurodegenerative diseases, particularly AD. As a result, using small molecules inhibiting G9a can open new avenues for treating age-related cognitive decline and AD. Nevertheless, further research is required because of the side effects of long-term treatment with the available compounds due to their toxicity and scarce stability.

In this context, the main aim of the present doctoral thesis could be divided into two main areas. On the one hand, the role of G9a in AD has been deepened **using *in vitro* and *in vivo* models**. On the other hand, [redacted] improving efficacy, selectivity, and safety parameters, among others. To pursue these main areas, several specific objectives have been established:

1. **Confirm the role of G9a in cognitive decline using AD patient brains as well as in experimental models of AD (*C. elegans* and SAMP8 mouse model).**
    - To determine the G9a levels and their repressive mark, H3K9me2, was used in AD patients' brains, *C. elegans*, and the SAMP8 mouse model.
    - To correlate the H3K9me2, a repressive mark, with an AD hallmark (levels of Aβ) in AD patients' brains, *C. elegans* and SAMP8 mouse model.

- To evaluate the effects of cognitive impairment and Aβ plaque aggregation by different approaches in *C. elegans*: gene editing (generation of a *set-25*-knock-down strain through RNAi technique) and pharmacological inhibition of G9a.

2. Assess the potential role of G9a in age-related cognitive decline, behavioural changes (non-cognitive symptoms), and alterations of molecular mechanisms in aged SAMP8 mice.

- To evaluate cognitive decline and behaviour in 12-month-old male SAMP8 mice.
- To investigate molecular alterations in pathways associated with G9a.

3. Unveil the molecular mechanisms behind the neuroprotective effect of G9a inhibition in the SAMP8 mouse model.

- To assess the effect of G9a inhibition on cognitive and non-cognitive symptoms of AD presented by SAMP8 mouse model.

3.1. Explore transcriptional differences after pharmacological inhibition of G9a in the SAMP8 mouse model.

- To analyze the transcriptome by RNA-sequencing (RNA-seq) after pharmacological inhibition of G9a (UNC0642) in the SAMP8 mouse model.
- To validate the results obtained in the RNA-seq in *vitro* (cell culture and *C. elegans*) and *in vivo* assays.
- To elucidate the neuroprotective mechanism of pharmacological inhibition of G9a by modulating markers related to Aβ levels, neuroinflammation and synaptic plasticity, two of the most critical events in AD pathology.

3.2. Elucidate the effects of the pharmacological inhibition of G9a on miRNA expression in the SAMP8 mouse model.

- To analyze global miRNA expression (miRNA-sequencing, miRNA-seq) after pharmacological inhibition of G9a (UNC0642) in SAMP8 mouse model.

- To validate the results obtained in the miRNA-seq in *in vitro* (cell culture) and *in vivo* assays.
- To elucidate molecular alterations of markers related to mechanisms involved in OS, apoptosis, DNA damage repair and synaptic plasticity.

4. To identify small molecules as G9a inhibitors nd optimize the pharmacokinetic parameters of the commercially available G9a inhibitors.

4.1. Obtain a potential Hit. Structure-based virtual screening of G9a inhibitors:

- To evaluate the selectivity against G9a and GLP of the selected potential inhibitors.
- To assess the efficacy using an AD transgenic *C. elegans* strain.

[redacted]

[redacted]

4.3. Investigate the potential of repurposing techniques for the discovery of a new G9a inhibitor for the treatment of Alzheimer's disease.

3 Methods and Results

3.1. Publication 1

Cognitive decline and BPSD are concomitant with autophagic and synaptic deficits associated with G9a alterations in aged SAMP8 mice.

Foteini Vasilopoulou*, **Aina Bellver-Sanchis***, Júlia Companys-Alemany , Júlia Jarne-Ferrer, Alba Irisarri, Verónica Palomera-Ávalos, Celia Gonzalez-Castillo, Daniel Ortuño-Sahagún, Coral Sanfeliu, Mercè Pallàs and Christian Griñán-Ferré

Cells 2022, 11, 2603.

doi: 10.3390/cells11162603

SUMMARY

Advanced age is the most substantial risk factor for developing age-related neurodegenerative disorders such as AD. In most AD, cases are characterized by cognitive impairment and different non-cognitive deficits known as BPSD. Understanding the mechanisms underlying cognitive decline and BPSD in AD is crucial for addressing this major health issue. Of note, recent findings propose that epigenetic alterations play a pivotal role in the pathophysiology of aging and neurodegeneration. Specifically, it has been suggested that G9a methyltransferase and its repressive histone mark (H3K9me2) play a significant role in influencing learning and memory through the modulation of autophagic activity and synaptic plasticity. Thus, we hypothesize that the aberrant activity of G9a triggers pathological outcomes leading to cognitive and behavioural deficits through synaptic plasticity and autophagic pathways in the aged male SAMP8 mouse model.

Here, we employed a behavioural test battery (Elevated plus maze (EPM), Open Field (OF), Novel object recognition test (NORT), Three-chamber test (TCT), and Resident intruder (RI)) to assess cognitive decline and non-cognitive symptoms in 12-month-old male SAMP8 mice compared to 12-month-old male SAMR1 mice, a healthy control strain. Moreover, a biochemical assessment of AD markers associated with synaptic plasticity and the autophagy process was also performed. Our findings show that aged male SAMP8 mice exhibit increased aggressive and anxiety behaviours, social deficits, and cognitive impairment compared to the SAMR1 mice group. These outcomes were supported by molecular analyses showing altered expression of epigenetic markers, autophagosome markers, and genes related to synaptic plasticity, as well as changes in dendritic branching and spine density. Elevated levels of G9a appear to contribute to the disruption of the JNK pathway in SAMP8 aging, leading to a failure of autophagosome formation and thus contributing to the accumulation of misfolded proteins and neurodegeneration characteristic of AD. Furthermore, repression of the Extracellular Signal-Regulated Kinase 2 (ERK) signaling pathway and its downstream gene targets associated with memory consolidation and decreased dendritic branching and spine density were observed in the SAMP8 mice, suggesting synaptic dysfunction.

In summary, this work provides insights into non-cognitive and cognitive symptoms, along with molecular changes in aged SAMP8, showing the manifestation of AD-like symptoms in this model. Furthermore, our findings suggest that G9a might be playing a key role in autophagy deficits and changes in synaptic plasticity, potentially elucidating the BPSD and cognitive impairment observed in the model.

cells

MDPI

Article

Cognitive decline and BPSD are concomitant with autophagic and synaptic deficits associated with G9a alterations in aged SAMP8 mice

Foteini Vasilopoulou[1,†], Aina Bellver-Sanchis[1,†], Júlia Companys-Alemany[1], Júlia Jarne-Ferrer[1], Alba Irisarri[1], Verónica Palomera-Ávalos[1], Celia Gonzalez-Castillo[2], Daniel Ortuño-Sahagún[3], Coral Sanfeliu[4], Mercè Pallàs[1] and Christian Griñán-Ferré[1,*]

[1] Department of Pharmacology and Therapeutic Chemistry, Faculty of Pharmacy and Food Sciences, Institut de Neurociències, Universitat de Barcelona, Avda. Joan XXIII, 27. 08028 Barcelona, Spain; ftn.vasilopoulou@gmail.com; juliacompanysalemany@gmail.com; abellversanchis@gmail.com; jfjulia97@gmail.com; albairisarrim@gmail.com; veropalomera@ub.edu

[2] Tecnologico de Monterrey, Escuela de Medicina y Ciencias de la Salud, Zapopan, Mexico; celia.glz@tec.mex

[3] Laboratorio de Neuroinmunología Molecular, Instituto de Investigación de Ciencias Biomédicas (IICB) CUCS, Universidad de Guadalajara, Jalisco 44340, México; daniel.ortuno.sahagun@gmail.com

[4] Institut d'Investigacions Biomèdiques de Barcelona (IIBB), CSIC and Institut d'Investigacions Biomèdiques August Pi i Sunyer (IDIBAPS), Barcelona; coral.sanfeliu@iibb.csic.es

[†] These authors have contributed equally to this work and share first authorship

* Correspondence: christian.grinan@ub.edu

Citation: Lastname, F.; Lastname, F.; Lastname, F. Title. *Cells* **2022**, *11*, x. https://doi.org/10.3390/xxxxx

Academic Editor: Firstname Lastname

Received: date
Accepted: date
Published: date

Publisher's Note: MDPI stays neutral with regard to jurisdictional claims in published maps and institutional affiliations.

Copyright: © 2022 by the authors. Submitted for possible open access publication under the terms and conditions of the Creative Commons Attribution (CC BY) license (https://creativecommons.org/licenses/by/4.0/).

Abstract: Behavioural and psychological symptoms of dementia (BPSD) are presented in 95% of Alzheimer's Disease (AD) patients and are also associated with neurotrophin deficits. The molecular mechanisms leading to age-related diseases are still unclear; however, emerging evidence has suggested that epigenetic modulation is a key pathophysiological basis of aging and neurodegeneration. Especially, it has been suggested that G9a methyltransferase, and its repressive histone mark (H3K9me2), are important in shaping learning and memory by modulating autophagic activity and synaptic plasticity. This work deepens our understanding of the epigenetic mechanisms underlying the loss of cognitive function and BPSD in AD. For this purpose, several tasks were performed to evaluate parameters of sociability (three chamber test), aggressiveness (resident intruder), anxiety (elevated plus maze, and open field) and memory (novel object recognition test) in mice, followed by the evaluation of epigenetic, autophagy and

synaptic plasticity markers at the molecular level. The behavioural alterations presented by senescence-accelerated mice prone 8 (SAMP8) of 12 months of age compared to their senescence-accelerated mouse resistant mice (SAMR1), a healthy control strain were accompanied by age-related cognitive deficits and alterations in epigenetic markers. Increased levels of G9a are concomitant to the dysregulation of the JNK pathway in aged SAMP8, driving a failure in autophagosome formation. Furthermore, lower expression of genes involved in the memory consolidation process modulated by ERK was observed in the aged male SAMP8 model, suggesting the implication of G9a. Besides, two of the most important neurotrophins, namely *brain-derived neurotrophic factor (Bdnf)* and *neurotrophin-3 (NT3)* were found reduced, jointly with a decrease in the levels of dendritic branching and spine density presented by SAMP8 mice. Thus, the present study characterizes and provides information regarding the non-cognitive and cognitive states as well as molecular alterations in aged SAMP8, demonstrating AD-like symptoms presented by this model. Besides, our results indicate that higher levels of G9a are associated with autophagic deficits and alterations in synaptic plasticity, which could further explain the BPSD and cognitive decline exhibited by the model.

Keywords: BPSD; aggressivity; cognitive decline; autophagy; epigenetics; G9a; SAMP8.

1. Introduction

Advanced age is the most substantial risk factor for developing age-related neurodegenerative disorders such as Alzheimer's Disease (AD) and other dementias [1]. These pathological conditions manifest as progressive cognitive decline and are often accompanied by non-cognitive alterations, the so-called behavioural and psychological symptoms of dementia (BPSD). BPSD include aggression, agitation, anxiety, and depressive mood, resulting in poor outcomes of AD patients [2–4]. To effectively address this significant health issue, it is crucial to understand the cellular and molecular mechanisms underlying loss of cognitive function and BPSD in AD, driving their clinical manifestation.

Emerging evidence shows that epigenetics is critical in learning and memory processes, and its dysregulation has been associated with the pathogenesis of AD [5–7]. Of note, there are no transgenic mouse lines that model age-related AD, the most important risk factor of AD. However, in this context, the senescence-accelerated mouse 8 (SAMP8) has been proposed as a neurodegenerative mouse model to study late-onset Alzheimer disease (LOAD) associated with aging [8–11]. At the same time, previous studies of our group demonstrated altered epigenetic regulation in AD mouse models, including the SAMP8 model, such as DNA methylation, hydroxymethylation, histone acetylation, and miRNA modifications [12–15]. Additionally, histone modifications can repress or activate genes involved in learning-dependent synaptic plasticity, also demonstrating a role in cognition [6]. In this line of evidence, histone methylation has gained attention in the AD field [16]. Remarkably, we and others have demonstrated that

the aberrant activity of G9a increases its repressive mark by demethylating histone 3 lysine 9 (H3K9me2), triggering pathological outcomes that lead to cognitive and behavioural deficits [17,18]. Remarkably, compelling evidence links G9a to dysregulation of cellular autophagy, repressing genes associated with autophagosome formation [19].

The autophagic process is the primary pathway for degrading defective proteins and organelles and is orchestrated by autophagy-related proteins such as Beclin-1, microtubule-associated protein light chain 3B (LC3B), and p62, among others. Impaired autophagy and dysregulation of the autophagic machinery has been observed in AD patients, with a resulting accumulation of toxic proteins, such as amyloid β [20,21]. Likewise, recent data indicate that autophagy deficiencies correlate with cognitive and behavioural impairments [22]. Furthermore, exciting findings show that autophagy is also involved in maintaining the integrity of synaptic vesicle-dependent transmitter release and organelle quality control, as well as in protein homeostasis of synaptic proteins at postsynaptic sites [23,24]. In AD patients, the synaptic loss is an early critical event intimately linked to cognitive decline and BPSD [25,26].

The above background supports our hypothesis that epigenetic enzymes, especially G9a, might guide cognitive and behavioural symptoms in dementia and AD. Given that sporadic late-onset AD (LOAD) accounts for most human AD cases [27], we used SAMP8 model of age-related neurodegeneration underlying LOAD [10]. This model, established through phenotypic selection from AKR/J mice, presents AD-like cognitive symptoms and behavioural abnormalities, including anxiety-like behaviour, and depression [28,29]. Additionally, SAMP8 brains are characterized by pathological signatures of AD, including neuroinflammation, synaptic deficits, oxidative stress and aberrant epigenetic dysregulation [8,9,11,30]. Thus, we evaluated the behavioural and cognitive state of aged SAMP8 male mice and determined molecular changes in G9a-related autophagic and synaptic plasticity markers compared to their senescence-accelerated mouse resistant mice (SAMR1), a healthy control strain. Our results provide insights for building the relationship among these parameters during age-related cognitive decline.

2. Materials and Methods

2.1. Animals

SAMP8 (n = 13) and SAMR1 (n = 13) male mice aged 12 months were used to perform behavioural experiments. Animals had free access to food and water and were maintained under standard temperature conditions (22 ± 2°C), relative air humidity of about 50% and 12h light-dark cycle (300 lux/0 lux), starting at 8 AM in plastic cages with wood shaving bedding with four animals per cage. After weaning, mice were housed 4-5 per cage, and behavioural tests were performed during the light phase. Mice completed a behavioural test battery at 12 months of age and were tested in the elevated plus-maze (EPM), open field (OF), novel object recognition (NORT) and three-chamber test (TCT), followed by testing the resident intruder (RI). Mice were handled only during weekly cage changes

before the tasks and were acclimated (5 min) to the testing room before the start of each behavioural task. Furthermore, a rest day was left between different tests.

All experimental procedures involving animals were in line with the Directive 2010/63/EU and were approved by the Institutional Animal Care and Generalitat de Catalunya (#10291, 1/28/2018). All efforts were made to minimize the number of mice used and their suffering.

2.2. Behavioural experiments

2.2.1. Elevated Plus Maze (EPM)

The EPM assessed the anxiety-like behaviour in an apparatus which consisted of two open arms (30 x 5 x 15 cm) and two closed arms (30 x 5 x 15 cm) radiating from a central platform (5 × 5 cm). Behaviour was scored as previously described [31]. Parameters recorded included total distance travelled during the 5-min test, time spent in open arms, closed arms and center as well as the number of rearings.

2.2.2. Open Field Test (OF)

Emotional alterations were evaluated by the OF test and performed using a white polywood apparatus (50 × 50 × 25 cm), as previously described [31]. Apparatus' ground was divided into center and peripheral areas. Mice were placed at the center of the open field arena and allowed to explore the apparatus for 5 min. After the session, mice were returned to their home cages, and the open field was cleaned with 70% EtOH and allowed to dry between sessions. The parameters scored included locomotor activity, calculated as the sum of total distance travelled in 5 min, as well as the time spent in centre and periphery zone, and the number of rearings, defecations, and urinations.

2.2.3. Novel Object Recognition Test (NORT)

As previously described, NORT was performed in a 90-degree, two-arm, 25-cm-long, 20-cm- high maze [32]. The walls could be easily removed for cleaning. Briefly, mice were individually habituated to the apparatus for 10 min for 3 consecutive days. On day 4, they were submitted to a 10-min acquisition trial (familiarization phase), during which they were placed in the maze and allowed to explore two identical novel objects (A+A or B+B) placed at the end of each arm. 10-min retention trials (test phase) occurred 2 h after the familiarization phase. During test phase, one of the two identical objects were replaced by a novel one and the time spent exploring the new object (TN) and the old object (TO) were counted manually. The discrimination index (DI) was calculated as (TN-TO/TN+TO).

2.2.4. Three Chamber Test (TCT)

The TCT assesses cognition through sociability and interest in social novelty [33]. The TCT was performed using a box (15 x 15 x 20 cm) divided into three equally dimensioned rooms with openings among them. Testing had a duration of 20 min and occurred in two phases within the TCT apparatus. The animal was placed in the center of the box and allowed to explore the three chambers for 5 min (Habituation phase). The time spent in each room during the habituation phase was counted manually. Then, an intruder (same sex and age) was included to one chamber in a metal cage, and the behaviour of the test subject was assessed for 10 min. In this phase, both the time spent in each room and the time interacting with the intruder (e.g., sniffing, grooming) were measured. The TCT apparatus, the surface, and the metal cages were cleaned with 70% EtOH between the animals' trials to eliminate olfactory cues.

2.2.5. Resident-Intruder Test (RI)

The RI test was performed to evaluate the aggressive behaviour exhibited by the animals, as described previously [34]. Briefly, the test subjects (residents) were isolated in separate cases for 7 days prior to the performance of the test. An intruder animal (C57/BL6 male, 2-month-old) was introduced in the resident home cage on the test day. The entire 20-min session was video-recorded for later analysis. The aggressive behaviour of the residents was evaluated as latency for the first attack, offensive uprights, lateral threats, total number of attacks and the overall time of aggression (%), which was measured manually. In addition, social interaction during the 20-min session was evaluated as the number of rearings.

2.3. RNA extraction and gene expression determination

Total RNA isolation from brain tissue (n=6 mice per group) was carried out using TRIsureTM reagent following the manufacturer's instructions (Bioline Reagent, London, UK). RNA content in the samples was measured at 260 nm, and the purity of the samples was determined by the A260/280 and A260/230 ratio in a NanoDrop™ ND-1000 (Thermo Scientific). Reverse transcription-Polymerase chain reaction (RT-PCR) was performed as previously described [32], to quantify the mRNA expression. The primers are listed in Table S1. Data were analyzed by using the comparative Cycle threshold (Ct) method (ΔΔCt), using β-actin transcript level to normalize differences. Each sample (n = 4–6) was analyzed in duplicate, and the results represented the n-fold difference in transcript levels among different samples.

2.4. Western Blot (WB)

For WB, from brain tissue (n=6 mice per group) were homogenized with lysis buffer containing phosphatase and protease inhibitors (Cocktail II, Sigma, St. Louis, MI, USA) and Bradford's method was used to determine protein concentration. Aliquots of 15 μg of protein were separated by SDS-PAGE (10-16

% gels) and transferred into a PVDF membrane (Millipore, Burlington, MA). Afterward, the membranes were blocked with BSA 5% 1 h at room temperature. The blockage was followed by overnight incubation at 4º C with the primary antibodies (Table S2). The next day, the membranes were washed and incubated with secondary anti-mouse or anti-rabbit antibody for 1 h at room temperature (Table S2). The proteins were revealed using chemiluminescence-based detection kits (Thermofisher and ECL kit, Millipore, Burlington, MA) and the pictures were obtained using an Amersham Imager 680 (BioRad, Hercules, CA). Then, quantitative analysis was carried out by ImageLab Software (Bioke, CA) and results were expressed in Arbitrary Units (AU), considering control group as 100%. To ensure that the differences between the samples was not a result of inaccurate sample preparation, Glyceraldehyde 3-phosphate dehydrogenase (GAPDH) was used as a protein charge control.

2.5. Dendritic length, spine density and Golgi stain protocol

Mice brains (n=5 per group) were removed from the skull after cervical dislocation. Then, Golgi stain protocol was performed using FD Rapid GolgiStain™ kit according to manufactures instructions. Analysis of dendritic branching was performed with images of neurons collected at 20x magnification in an Olympus BX61 microscope coupled to an Olympus DP70 camera. Measurement of neurite length and complexity was carried out with NeuronJ macros and Advanced Sholl Analysis. Then, it was measured the number of intersections or branch points within concentric circles of 10 μm radius and compared between groups. Analysis of spine density was developed using the images acquired in the brightfield microscopy with a 50x oil-objective. All analyzed neurites were around 18 μm and they were at a maximum distance of 150 μm from the soma.

2.6. H3 modification patterns quantification

Global histone H3 methylation from brain tissue (n=6) were detected using an EpiQuik Histone H3 Modification Multiplex Assay Kit (Catalog No. P-3100-96, Epigentek, Farmingdale, NY, USA). Briefly, total core histones were extracted with an EpiQuik Total Histone Extraction Kit according to the manufacturer's protocol (Epigentek, Farmingdale, NY, USA). Histone extracts were used to determine the histone H3 modifications at specific sites. The isolated histones were added to wells coated with antibodies specific for H3K9. The captured histones were detected with a detection antibody, followed by a color development reagent. Absorbance intensity was measured at 450 nm with a microplate reader. The amount of a particular histone modification was calculated as a percentage of the total H3 signal.

2.7. Statistical Analysis

Data are expressed as the mean ± Standard error of the mean (SEM). Statistical analyses were performed using GraphPad Prism ver. 9. The normality of the data distribution was determined using the Kolmogorov-Smirnov normality test, followed by Student's *t*-test (in the case of normal distribution) or Mann-Whitney *U* (in the case of non-normal distribution). Correlations among different parameters were analyzed with Pearson's and Spearman's correlations, for normally and non-normally distributed data, respectively, were used to analyse when it was necessary. Statistical significance was considered when *p*-values were <0.05. Statistical outliers were discriminated using Grubbs' test and were removed from the analysis.

3. Results

3.1. Aged SAMP8 male mice exhibited increased aggressive and anxiety-like behaviours and social deficits

Because emotional and anxiety-like behaviour are associated with cognitive decline and AD [35,36], we determined these behavioural parameters using EPM and OF. In the EPM the SAMP8 group spent significantly more time in the closed arms (Figure 1A) and less time in the center zone compared to the SAMR1 group (Figure 1B). Furthermore, the percentage of time spent in open arms was higher in the SAMP8 group (Table S3), and the number of rearings was decreased (Figure 1C). In the OF, the SAMP8 group presented higher total distance travelled in the arena and vertical activity when compared to the SAMR1 mice (Figures 1D-E). Finally, the SAMP8 mice spent more time in the border area (Figure 1F), whereas the time spent in the center zone tended to decrease compared to the SAMR1 mice (Table S4).

It has been widely described that social behaviour is impaired with age and dementia [37]. To analyze this, we assessed the social behaviour through TCT. Our results in the TCT revealed a relevant difference between strains in terms of sociability. Firstly, we confirmed no preference for any chamber by the two groups, since there are no differences in the time spent in each chamber during the habituation phase (Figure 1G). In the sociability phase, however, the SAMR1 group significantly spent more time in the intruder's chamber, whereas the SAMP8 mice did not show any preference between the empty and the intruder's chamber (Figure 1H). In the same line, the SAMP8 group spent significantly less time exploring the intruder mouse compared to the SAMR1 group (Figure 1I).

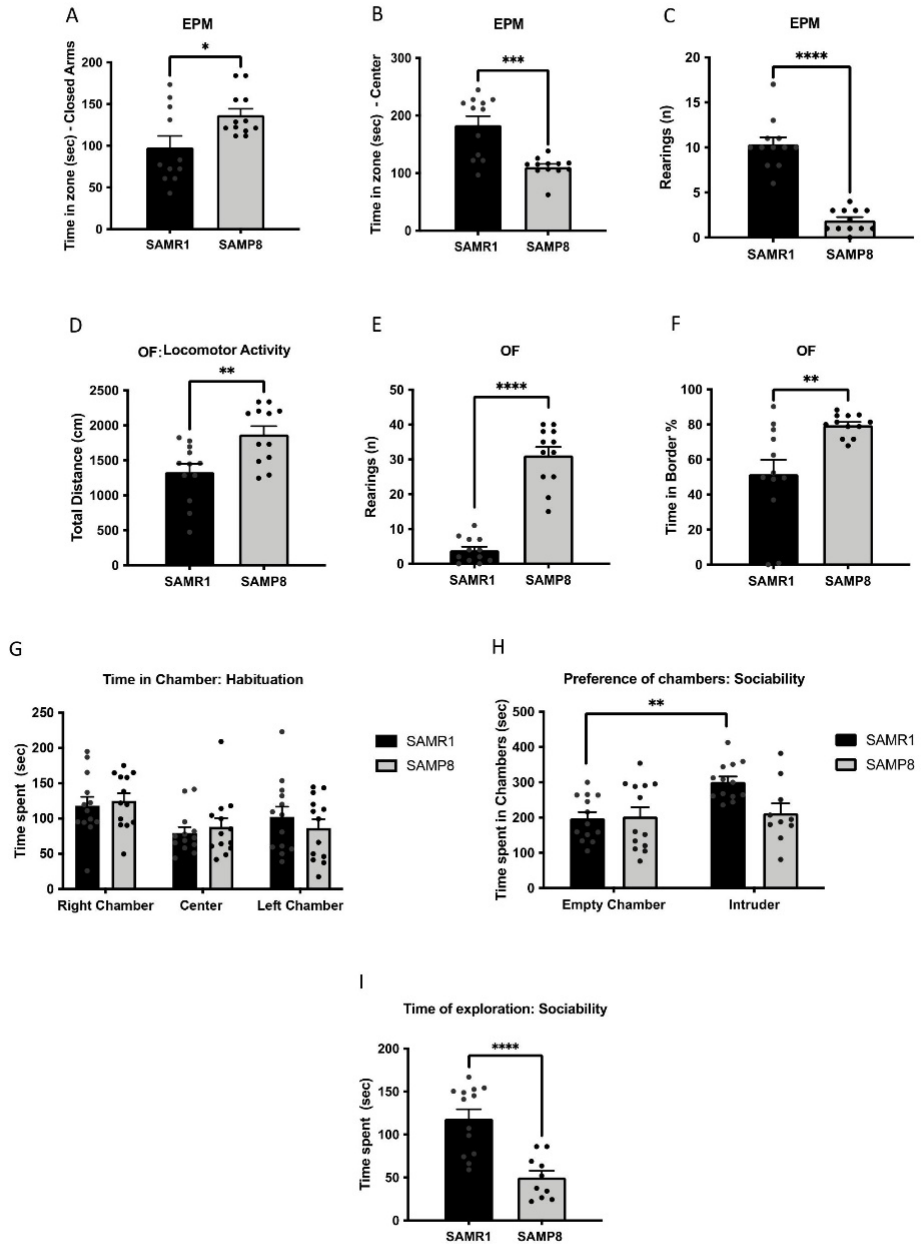

Figure 1. Results of the Elevated Plus Maze (EPM) and Open Field (OF) tests in males SAMR1 and SAMP8 mice at 12 months of age. For EPM: Time spent in closed arms (A), time spent in center (B), number of rearings (C). For OF: Total distance (D), number of rearings (E) and time spent in Border zone (F). Results of the Three-Chamber Test (TCT) in age SAMR1 and SAMP8 male mice. Habituation (G), preference of chambers (H), and time of exploration (I). Bars show mean ± SEM (For EPM and OF: n=11-12 mice per group; Fort

TCT n=13-10 mice per group). Statistical test: t-student analysis (A-G, and I); Two- Way ANOVA followed by Šídák post-hoc test (H). *p<0.05; **p<0.01; ***p<0.001; ****p<0.0001.

3.2. Aged SAMP8 male mice present increased aggressive behaviour

SAMP8 male mice showed higher aggressive behaviour compared to SAMR1. Particularly, the latency to the first attack against the intruder was significantly decreased for the SAMP8 mice, while the total number of aggressive encounters, including attacks and offensive uprights, was higher compared to the SAMR1 group (Figures 2A-C). In addition, SAMP8 mice also presented a higher number of lateral threats and percentage of time of global aggression compared to age-matched SAMR1 mice (Figures 2D-E). Besides, the number of rearings was significantly reduced in the SAMP8 group, suggesting deficits in social interaction (Figure 2F). Finally, behavioural abnormalities between SAMR1 and SAMP8 mice were depicted in a polygonal graph (Figure 2G).

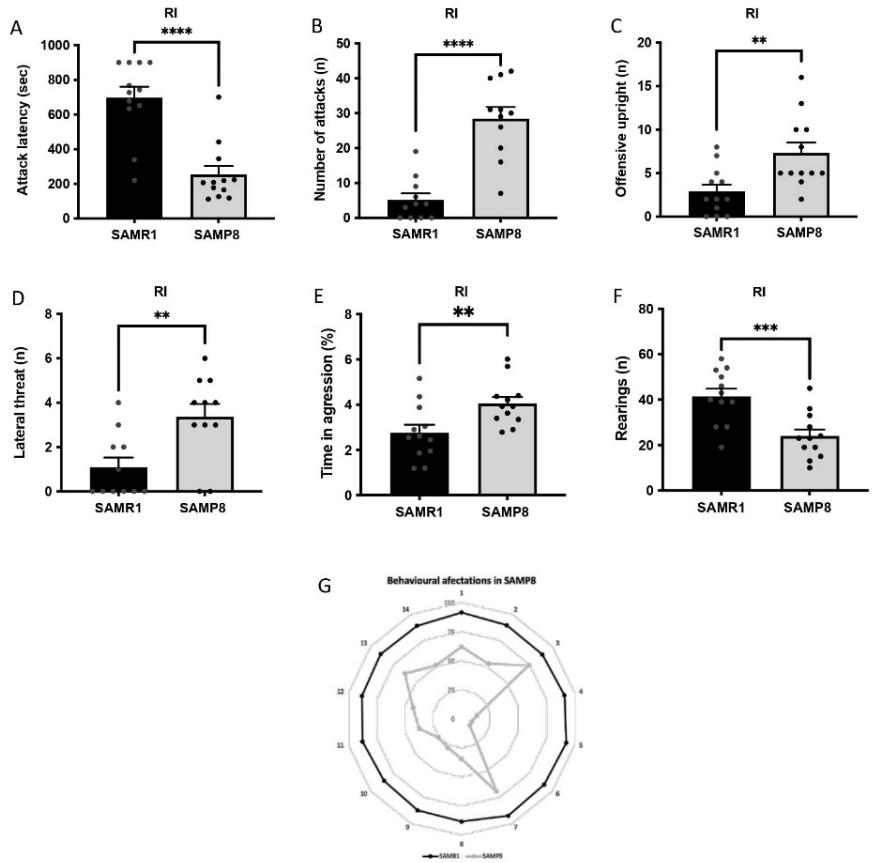

Figure 2. Results of Resident Intruder Test (RI) in males SAMR1 and SAMP8 mice at 12 months of age. Attack latency (A), number of attacks (B), number of offensive upright (C), number of lateral threat (D), time in aggression (E), number of rearings (F). Bars show mean ± SEM (For RI: n=11-12 mice per group). Statistical test: t-student analysis. **p<0.01; ***p<0.001; ****p<0.0001. Polygonal graph presenting a summary of relevant behavioural parameters (G).

3.3. Cognitive deficits correlated with behavioural parameters in aged SAMP8 male mice

In agreement with previous studies of our group and others [34] here, aged SAMP8 male mice presented a weaker cognitive performance than age and sex matched SAMR1, which resulted in significantly lower DI, obtained after the 2h short-memory test (Figure 3A). Then, we sought to determine the relationship between behaviour and cognitive parameters. First, we found a significant positive Pearson's correlation between sociability, expressed as time exploring the intruder mouse in TCT, and the DI evaluated in NORT [$r = 0.4501$, $p = 0.0312$], showing that lower social interaction of SAMP8 is associated with cognitive decline (Figure 3B). Likewise, we showed a significant positive Spearman's correlation between the attack latency of the mice in the RI test and the DI [$r = 0.5675$, $p = 0.0038$], suggesting that higher aggressive behaviour exhibited by aged SAMP8 mice is related to the cognitive impairment (Figure 3C). Regarding the anxiety state of the mice, as assessed with OF and EPM, a positive Pearson's correlation between the distance travelled in center zone, and the DI was determined [$r = 0.4117$, $p = 0.0569$], whereas the time spent in open arms presented a negative Pearson's correlation with the DI [$r = -0.3862$, $p = 0.0623$]. These latter correlations suggest that emotional disturbances of SAMP8 mice related to anxiety are associated with cognitive capabilities (Figures 3D-E).

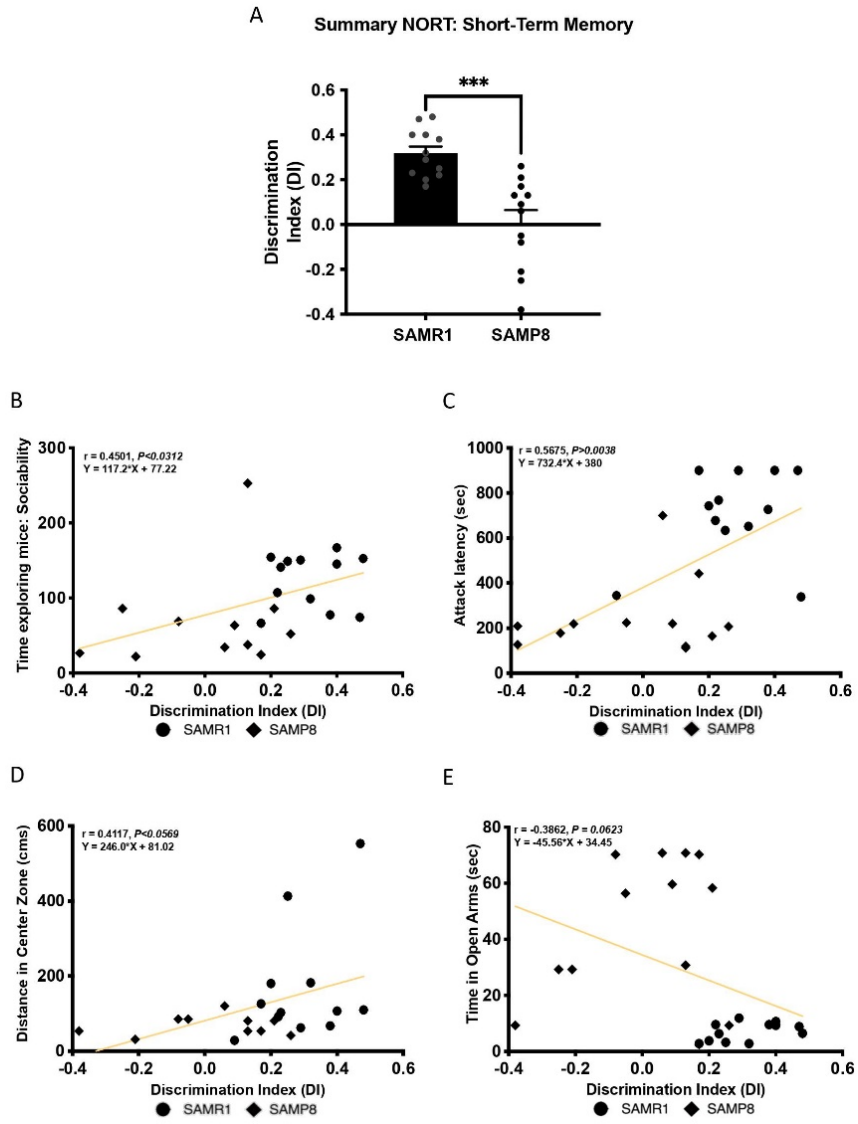

Figure 3. Summary NORT of Short-Term Memory (A). Bars show mean ± SEM (For NORT: n=12 mice per group). Statistical test: t-student analysis. ***p<0.001. Correlations between time exploring mice: sociability (B), attack latency (C), distance in center zone (D), and time in open arms (E) with discrimination index (DI). Pearson's correlations were performed for (time exploring sociability, distance in center zone and time in open arms) and Sperman's correlation was performed for attack latency) in both groups (n = 10-12 mice per group). r and p-values are indicated on graphs.

3.4. Upregulation of G9a correlated with suppression of the JNK-mediated autophagy process in aged SAMP8 mice

G9a activity regulates autophagy in various pathological conditions [38,39]. Thus, we set out to investigate the potential epigenetic regulation of this process by G9a in aged SAMP8 mice. Our results demonstrated increased gene expression of *G9a* (*Ehmt2*) in the brain of SAMP8 mice compared to their SAMR1 counterparts (Figure 4A). Since G9a is an HTM enzyme responsible for depositing methyl groups in H3K9, we also evaluated the H3 patterns. H3K9 methylated marks, including me1, me2 and me3 were found upregulated in SAMP8 mice (Figure 4B). Interestingly, in the neurodegenerative landscape provided by the SAMP8 mice, G9/Ehmt2 overexpression was associated with deficits in the autophagic process. In particular, phosphorylated and, thus, activated Jun N-terminal kinase (JNK) levels were significantly lower in the SAMP8 mouse compared to the SAMR1 strain (Figures 4C-D). Remarkably, JNK downregulation in SAMP8 brains runs parallel with decreases in key autophagic markers, including Beclin-1, p62 and LC3B-II levels, compared to the age-matched SAMR1 mice (Figures 4C, E-G).

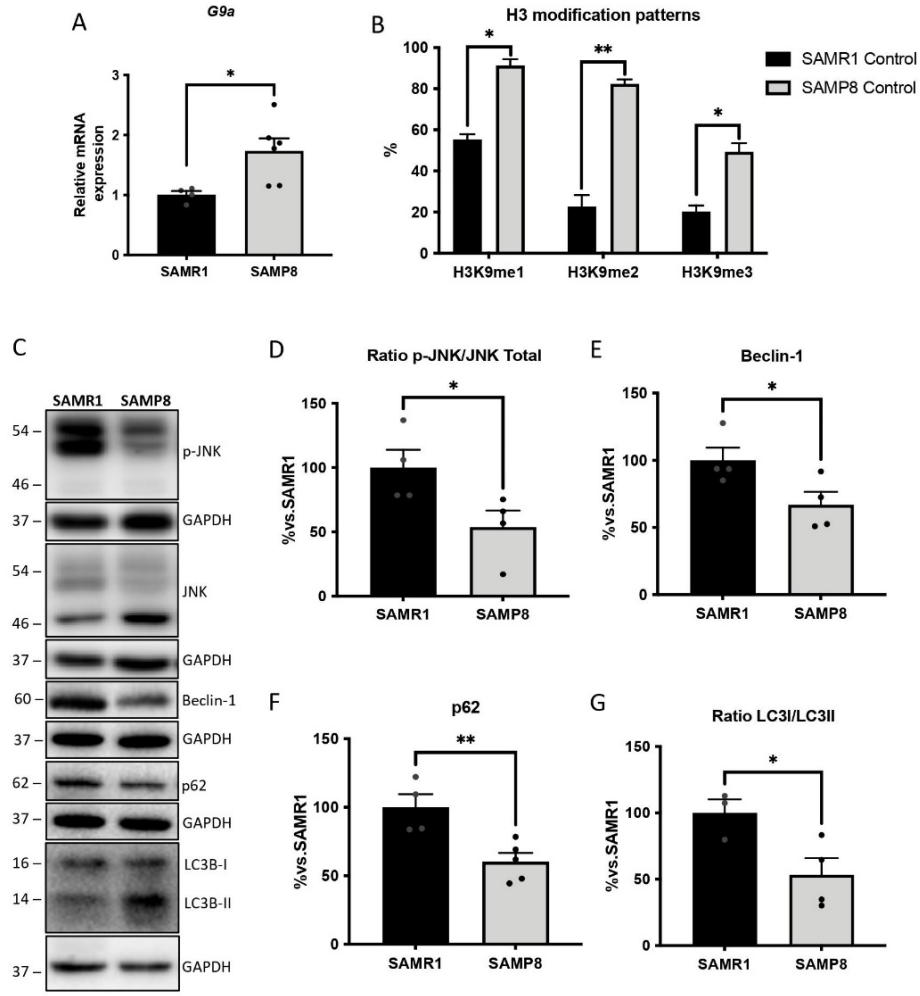

Figure 4. Representative gene expression for *G9a* (A). Gene expression levels were determined by real-time PCR. Representative global H3 modification patterns quantification (B) Bars show mean ± SEM (n=4-6 mice per group); **p*<0.05; ***p*<0.01. Representative WBs (C) and quantification for the ratio p-JNK/JNK total (D), Beclin-1 (E), p-62 (F) and the ratio of LC3I/LC3II (G). Values in bar graphs are adjusted to 100% for protein levels of the SAMR1 group. Bars show mean ± SEM (n=3-5 mice per group). Statistical test: t-student analysis. **p*<0.05; ***p*<0.01.

3.5. ERK activity and its downstream gene targets in memory consolidation are downregulated in aged SAMP8 mice

The activation of the extracellular signal-regulated kinase mitogen-activated protein kinase (ERK MAPK) signalling cascade was evaluated in the brain of aged SAMP8 male mice. The ERK pathway has a crucial role in the induction of neurotrophic factors and immediate early genes (IEGs) [40,41]. As expected, the results showed decreased phosphorylation (p-ERK) levels of ERK in the aged

SAMP8 male mice compared to SAMR1 group (Figures 5A-B). Furthermore, in agreement with the modulation of the ERK signalling pathway, the gene expression of genes modulated by ERK and involved in memory consolidation, including *DNA Methyltransferase 3 alpha* (*Dnmt3a*), *catechol-O-Methyltransferase* (*Comt*), *Zif-268* and *cFos* were found to be reduced in the SAMP8 group compared to age-matched SAMR1 mice (Figures 5C-F).

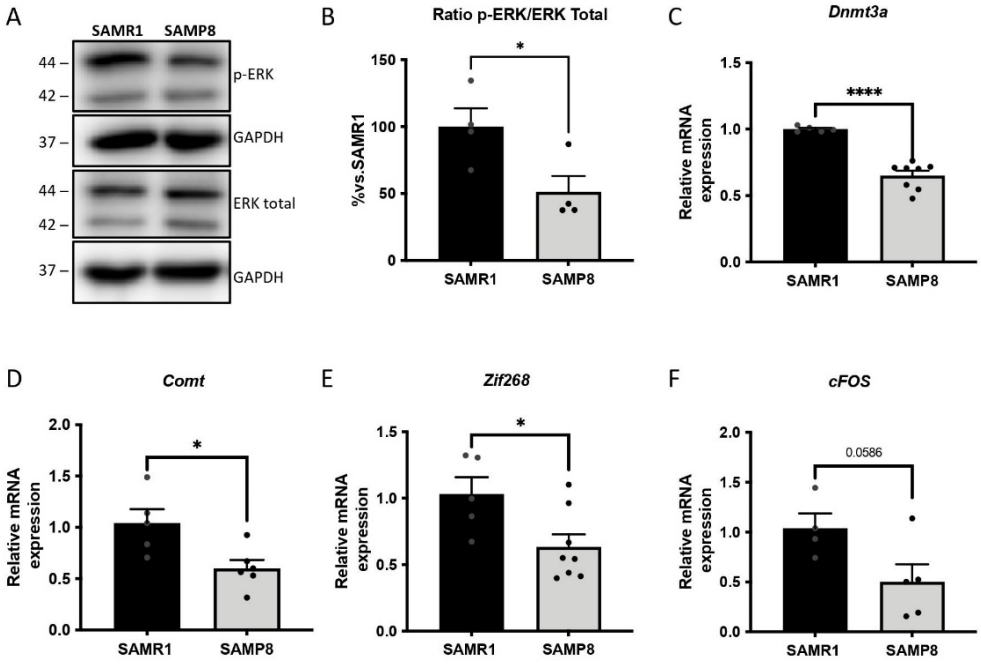

Figure 5. Representative WB (A) and quantification for the ratio p-ERK/ERK total (B). Values in bar graphs are adjusted to 100% for protein levels of the SAMR1 group. Bars show mean ± SEM; *p<0.05. Representative gene expression for *Dnmt3a* (C), *Comt* (D), *Zif-268* (E), and *cFos* (F). Gene expression levels were determined by real-time PCR. Bars show mean ± SEM (n=4-8 mice per group). Statistical test: t-student analysis. *p<0.05; ****p<0.0001.

3.6. Dendritic morphological abnormalities accompanied reduced expression of synaptic plasticity-related genes in aged SAMP8 male mice

The activation of ERK signalling cascade promotes the expression of neurotrophic factors [41]. Thus, we evaluated some important neurotrophins such as brain derived neurotrophic factor (BDNF), *neurotrophin 3* (*NT3*), nerve growth factor (NGF) [42,43]. Strikingly, we found a significant reduction in *NT3*, *Bdnf* and *Ngf* gene expression in the aged SAMP8 group in comparison with the SAMR1 strain (Figures 6A-C). Likewise, we evaluated the gene expression of their receptors, and we obtained that *tropomyosin receptor kinase A* and *B* (*TrkA*, and *TrkB* respectively) gene expression was significantly lower in SAMP8 mice compared to age-matched SAMR1 mice (Figures 6D-E). Furthermore, we stained SAMP8 and SAMR1 brains using Golgi immersion to quantify neurite

arborization through Sholl analysis. The results showed that the SAMP8 strain presents reduced dendritic branching compared to the SAMR1 strain (Figures 6F-G). Furthermore, we also evaluated spine density in the same vein, observing lower levels in the SAMP8 group than in the SAMR1 group (Figures 6H-I).

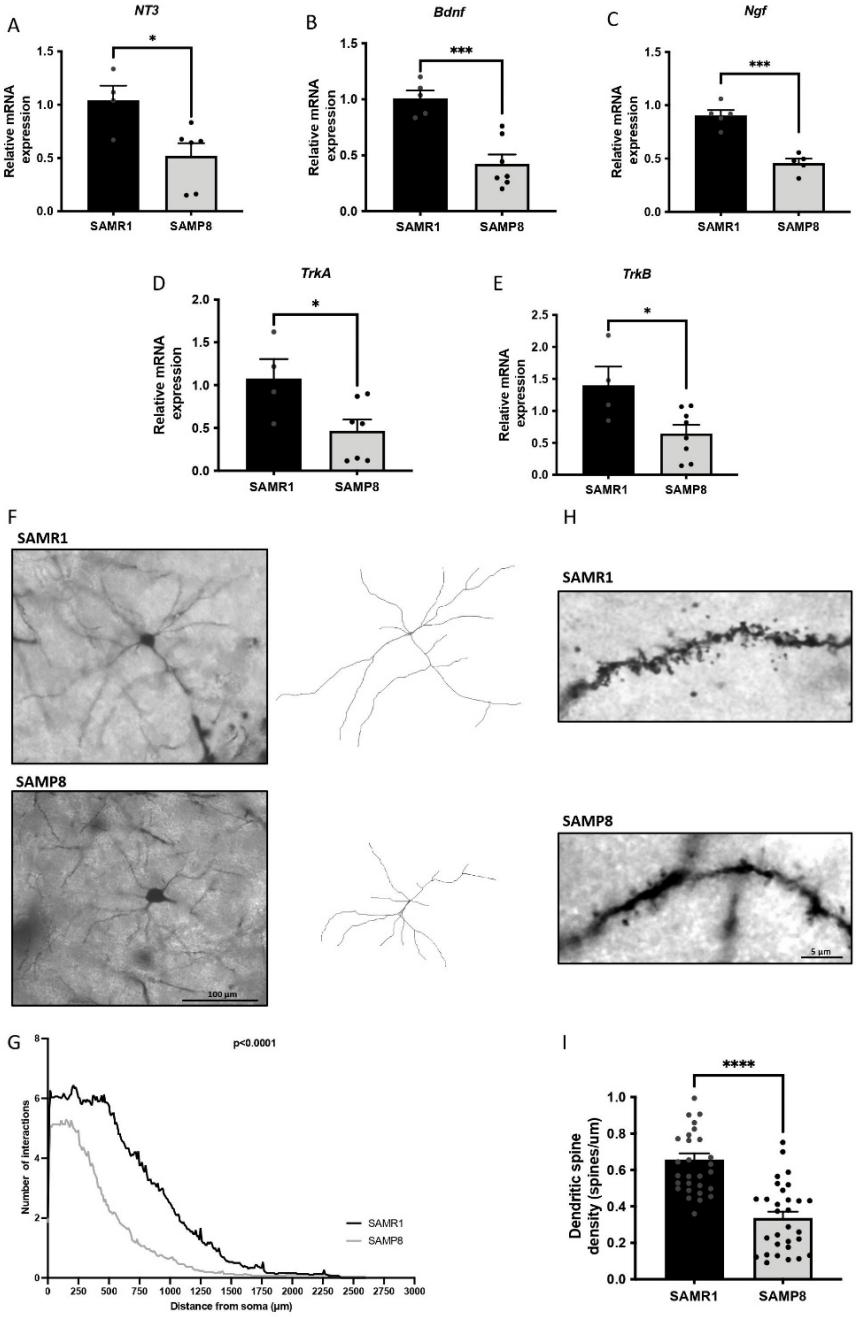

Figure 6. Representative gene expression for *NT3* (A), *Bdnf* (B), *Ngf* (C), *TrkA* (D), and *TrkB* (E). Gene expression levels were determined by real-time PCR. Bars show mean ± SEM (n=4-8 mice per group). Statistical test: t-student analysis. *$p<0.05$; ***$p<0.001$. Representative images and tracings of Golgi-stained cortical neurons from the age SAMR1 male mice group (top) and the age SAMP8 male mice group (bottom); (scale bar = 100 μm) (F). Age SAMP8 male mice showed a reduced in the number of neuronal intersections compared to the SAMR1 Control group through a Sholl analysis (G). Representative images of the spine density of the age SAMR1 male mice group (top) and the age SAMP8 male mice group (bottom) by Golgi staining (H), and quantification (I). Bars show mean ± SEM (n= 28-30 neurons from 6 different mice per each group). Statistical test: t-student analysis. ****$p<0.0001$.

4. Discussion

Most AD patients associate cognitive dysfunction with BPSD [44]. Furthermore, about 95% of AD patients have at least one neuropsychiatric symptom and syndromes, being aggression (76.2%) and depression (68%) the most frequent [44]. However, few studies evaluate these symptoms unique to human beings [45] due to the lack of suitable animal models that can be directly used to study BPSD and age-related emotional alterations. At the same time, a better understanding of the molecular mechanisms underlying cognitive and non-cognitive symptoms in patients could lead to their more accurate pharmacological management. Here, we assessed behavioural and emotional alterations in aged SAMP8 mice using several tasks to go deeper into the cognitive and BPSD-like phenotype of the strain. Furthermore, we established the correlation between behavioural and cognitive deficits and epigenetic alterations in the SAMP8 model.

Enhanced fear and anxiety-like behaviour are frequently associated with aging and AD in rodents [46,47]. Evidence shows that SAMP8 mice present an age-associated emotional disorder characterized by anxiety-like behaviour, which is reported to be either increased or decreased in different studies [48–50]. Accordingly, we obtained mixed results when the OF and EPM were employed. On the one hand, SAMP8 mice spent more time in the OF border zone and slightly less in the centre zone, presented higher locomotor activity and number of rearings, demonstrating a thigmotaxis attitude and corroborating the higher anxiety-like behaviour observed in the SAMP8 strain. On the other hand, SAMP8 spent significantly more time in the open arms of the EPM and less time in the center of the maze, which could indicate lower anxiety-like behaviour levels in the SAMP8 mice. However, data from the same behavioural test indicated that SAMP8 mice tended to spend more time in the closed arms of the maze as well when compared to the SAMR1 mice. These two latter observations suggest that the parallel increases in the time spent in both open and closed maze arms could be due to the higher locomotor activity that SAMP8 showed, making the EPM data interpretation unclear. More important, fear and anxiety-like behaviour have been linked to age-related cognitive deficits in SAMP8 mice [51,52]. Accordingly, we found a potential relationship between anxiety-related parameters and

cognitive performance, indicating the possible association of emotional disturbances with memory impairment in aged male SAMP8 mice.

Social dysfunction observed in human AD patients has been observed in transgenic AD [46,53]. In our study, 12-month-old male SAMP8 mice presented no difference in chamber preference and decreased social interaction exhibiting social behaviour deficits. These findings align with previously published results describing reduced sociability in SAMP8 mice [33,51]. Jointly with social impairments, aggression is one of the most distressing consequences of dementia and of special significance, given its direct influence on social functionality [54]. However, the evaluation of the aggressive behaviour in old SAMP8 male mice has not been reported to our knowledge. Here, we demonstrated that old SAMP8 males displayed higher aggressive behaviour by presenting lower latency to attack and a higher total number of attacks. These results add to the diverse BPSD phenotype of aged SAMP8 mice, the presence of aggressive disturbances and corroborate the manifestation of aggression in advanced age and dementia in this mouse model. Ultimately, when investigated the relationship between social or aggressive behaviour with cognitive performance, we found significant correlations. Social interaction positively correlated with cognitive performance, while a significant negative correlation was determined between aggression and cognitive performance. Consequently, our findings in SAMP8 mice support the consensus that aggression and social impairments in AD and age-related dementias are associated with the degree of cognitive impairment.

Deregulation of epigenetic mechanisms is observed during aging, contributing to progressive deteriorations in cognitive and behavioural status [55]. Indeed, evidence supports the involvement of epigenetic mechanisms in the clinical manifestation of neurodegenerative and neuropsychiatric disorders [56,57]. Besides, *in vivo* animal studies show that transcriptional dysregulation mediated among others by epigenetic mechanisms guides the manifestation of many psychiatric disorders [58–61], thereby suggesting the implication of epigenetic regulation in AD-associated BPSD. In the present study, considering that histone methylation is one of the most critical modifications, we evaluated changes in methylation of H3K9 mediated by the methyltransferase G9a, which is linked to gene silencing [62]. Our results show higher levels of *G9a* gene expression in the aged SAMP8 group, which was correlated with an increase in the overall H3 methylation landscape. Increased histone methylation in the brain of the aged SAMP8 mice is in accordance with previous studies performed in familial AD mice, demonstrating similar increases in H3K9me2 levels in the brain [63]. Likewise, higher levels of H3K9me2 were also described in CA1 of AD patients compared with middle-aged control patients [64]. It is important to note that G9a, as a regulator of chromatin structure in the CNS, has been associated with brain development, memory consolidation process, and cognitive deficits [18,65]. Interestingly, G9a inhibition has been shown to improve cognitive performance in AD models [17,63], improving anxiety-like behaviour in adult mice [66]. This evidence suggests that increased G9a protein levels promoted

epigenetic alterations in the SAMP8 brains that in turn, may account for behavioural abnormalities and age-related cognitive decline.

In the light of these findings, we then investigated alterations in G9a-regulated molecular pathways in the brain of SAMP8 mice. A well-described mechanism by which G9a contributes to neurodegenerative disorders is autophagy repression [19]. It is widely accepted that the balance between protein synthesis and protein turnover is necessary for synaptic plasticity, and this imbalance could be caused by the deregulation of autophagic activity [67]. Previous studies described the binding of G9a within the promoters of core autophagy-associated genes, compromising their activity [19]. Interestingly, genetic depletion or pharmacologic inhibition of G9a, promoted its dissociation of G9a from those inducing LC3BII and p62 expression, fostering autophagosome-like structure formation [19]. Besides, ChIP experiments demonstrated that the loss of G9a and H3K9me2 at the LC3B and p62 promoters was dependent on JNK activity [19]. In line with these findings, lower protein levels of JNK were observed in the aged SAMP8 group, and all the autophagic-related proteins evaluated were downregulated. Thus, increased levels of G9a might be partially responsible for the deregulation of the JNK pathway in the aged SAMP8, leading to autophagic activity deficits, which in turn correlates with the impaired cognitive and behavioural state of SAMP8 mice.

Moreover, it has been described that BDNF, NT3 and NGF neurotrophins are involved in BPSD, such as anxiety, depression and aggressive behaviour [68]. Here, we demonstrated a reduction in *Bdnf, NT3,* and *Ngf* gene expression in aged SAMP8 male mice. In line with these results, cumulative studies with AD animal models showed that lower BDNF and NGF levels lead to neuronal and synaptic dysfunction and eventual cognitive impairment [69–72]. Interestingly, BDNF transcription can be regulated by epigenetics, and particularly, G9a inhibition was shown to increase *Bdnf* expression in AD mice models [18,73]. As aforementioned, G9a has been implicated in memory consolidation mechanisms [65]. Here, we also found lower expression of genes involved in the ERK-modulated memory consolidation process in aged SAMP8, suggesting the participation of G9a. It is also worth mentioning that *Bdnf* expression regulates and is regulated by Erk ½, further supporting the obtained results [74]. In parallel, a remarkable downregulation in the gene expression of *Trk*A and *Trk*B neurotrophin receptors was determined in aged SAMP8 mice, corroborating the deficits in the synaptic function of the SAMP8 strain.

Along with the loss of synapses in the aged brain [75], the dendritic spine density is greatly diminished in AD, and this event is one of the most distinctive features of AD that best correlates with cognitive impairment [76,77]. Remarkably, altered dendritic spine density has been reported in models of other neurological conditions such as depression, stress and aggressive behaviours [78–81]. Hence, dendritic arborization and spine density were vital to assessing cognitive function and behavioural alterations. As expected, we report loss of dendritic spines in the SAMP8 aged cortex and reduced dendritic length compared to the aged SAMR1 group. Interestingly, these results align with a

previous study in which the G9a inhibition promoted the improvement of the structural plasticity of dendritic spines of neurons in the nucleus accumbens [82].

5. Conclusions

Our findings suggest that autophagic and synaptic plasticity impairments in aged SAMP8 male mice might be partially attributable to the epigenetic modulation by G9a, encouraging the conduction of further pharmacological studies to establish a causal relationship between them in SAMP8 mice. Furthermore, we demonstrated that those cognitive alterations were joined with morphological modifications in neurons, and altogether could account for non-cognitive and cognitive alterations exhibited by the mouse model. Additionally, our results agree with previous findings regarding the SAMP8 mouse model and give further support to this senescence model as a gerontological research tool shedding new insight into the suitability of SAM strains for the study of non-cognitive alterations accompanied by cognitive impairment in senescence.

Supplementary Materials: The following supporting information can be downloaded at: www.mdpi.com/xxx/s1, Table S1. Primers used in qPCR studies; Table S2. Antibodies used in Western blot studies. Table S3. Parameters measured in the Elevated Plus Maze (EPM) in male SAMR1 and SAMP8 mice at 12 months of age; Table S4. Parameters measured in the Open Field Test (OF) in male SAMR1 and SAMP8 mice at 12 months of age.

Author Contributions: F.V., J.C.-A., A.B.-S., J.J.-F., A.I. and C.G.-F. performed the experiments. F.V., J.C.-A., A.B.-S., D.O.-S., C.G.-C. and C.G.-F. analyzed the data and drafted the manuscript. C.G.-F., V.P.-A., C.S. and M.P. designed and supervised the study. All authors read and approved the final version of the manuscript.

Funding: This study was supported by the Ministerio de Economía, Industria y Competitividad (Agencia Estatal de Investigación, AEI) and Fondo Europeo de Desarrollo Regional (MINECO-FEDER) by the grants PDC2021-121096/AEI/10.13039/501100011033 and PID2020-118127RB-I00 funded by MCIN/AEI/10.13039/501100011033, and 2017SGR106 and 2019LLAV00017 from AGAUR.

Institutional Review Board Statement: Not applicable.

Informed Consent Statement: Not applicable.

Data Availability Statement: Not applicable.

Acknowledgments: We thank to TEC de Monterrey for supporting the Open Access. J.C.-A. acknowledge the Ministry of Economy and Competitiveness (MINECO) for her FPI fellowship (MDM-2017-0729-19-2). A.B.-S. acknowledge the Agència de Gestió d'Ajuts Universitaris i de Recerca (AGAUR) for her FI-SDUR fellowship (2021 FISDU 00182). Graphical abstract was created with BioRender.com.

Conflicts of Interest: The authors declare no conflict of interest.

References

1. Hou, Y.; Dan, X.; Babbar, M.; Wei, Y.; Hasselbalch, S.G.; Croteau, D.L.; Bohr, V.A. Ageing as a risk factor for neurodegenerative disease. *Nat. Rev. Neurol.* **2019**, *15*, 565–581, doi:10.1038/s41582-019-0244-7.
2. Shinosaki, K.; Nishikawa, T.; Takeda, M. Neurobiological basis of behavioral and psychological symptoms in dementia of the Alzheimer type. *Psychiatry Clin. Neurosci.* **2000**, *54*, 611–620.
3. Fernández, M.; Gobartt, A.L.; Balañá, M. Behavioural symptoms in patients with Alzheimer's disease and their association with cognitive impairment. *BMC Neurol.* **2010**, *10*, 1–9.
4. Bidzan, L.; Bidzan, M.; Pąchalska, M. Aggressive and impulsive behavior in Alzheimer's disease and progression of dementia. *Med. Sci. Monit. Int. Med. J. Exp. Clin. Res.* **2012**, *18*, CR182.
5. Guan, J.-S.; Xie, H.; Ding, X. The role of epigenetic regulation in learning and memory. *Exp. Neurol.* **2015**, *268*, 30–36.
6. Jarome, T.J.; Lubin, F.D. Epigenetic mechanisms of memory formation and reconsolidation. *Neurobiol. Learn. Mem.* **2014**, *115*, 116–127.
7. Day, J.J.; Sweatt, J.D. Epigenetic mechanisms in cognition. *Neuron* **2011**, *70*, 813–829.
8. E Morley, J.; A Farr, S.; B Kumar, V.; J Armbrecht, H. The SAMP8 mouse: a model to develop therapeutic interventions for Alzheimer's disease. *Curr. Pharm. Des.* **2012**, *18*, 1123–1130.
9. Griñán-Ferré, C.; Corpas, R.; Puigoriol-Illamola, D.; Palomera-Ávalos, V.; Sanfeliu, C.; Pallàs, M. Understanding epigenetics in the neurodegeneration of Alzheimer's disease: SAMP8 mouse model. *J. Alzheimer's Dis.* **2018**, *62*, 943–963.
10. Akiguchi, I.; Pallàs, M.; Budka, H.; Akiyama, H.; Ueno, M.; Han, J.; Yagi, H.; Nishikawa, T.; Chiba, Y.; Sugiyama, H. SAMP8 mice as a neuropathological model of accelerated brain aging and dementia: Toshio Takeda's legacy and future directions. *Neuropathology* **2017**, *37*, 293–305.
11. Pallàs, M. Senescence-Accelerated Mice P8: A Tool to Study Brain Aging and Alzheimer's Disease in a Mouse Model. *ISRN Cell Biol.* **2012**, *2012*, 917167, doi:10.5402/2012/917167.
12. Puigoriol-Illamola, D.; Martínez-Damas, M.; Griñán-Ferré, C.; Pallàs, M. Chronic Mild Stress Modified Epigenetic Mechanisms Leading to Accelerated Senescence and Impaired Cognitive Performance in Mice. *Int. J. Mol. Sci.* **2020**, *21*, 1154.
13. Griñán-Ferré, C.; Sarroca, S.; Ivanova, A.; Puigoriol-Illamola, D.; Aguado, F.; Camins, A.; Sanfeliu, C.; Pallàs, M. Epigenetic mechanisms underlying cognitive impairment and Alzheimer disease hallmarks in 5XFAD mice. *Aging (Albany NY)* **2016**, *8*, 664.
14. Griñan-Ferré, C.; Puigoriol-Illamola, D.; Palomera-Ávalos, V.; Pérez-Cáceres, D.; Companys-Alemany, J.; Camins, A.; Ortuño-Sahagún, D.; Rodrigo, M.T.; Pallàs, M. Environmental enrichment modified epigenetic mechanisms in SAMP8 mouse hippocampus by reducing oxidative stress and inflammaging and achieving neuroprotection. *Front. Aging Neurosci.* **2016**, *8*, 241.
15. Cosín-Tomás, M.; Alvarez-López, M.J.; Sanchez-Roige, S.; Lalanza, J.F.; Bayod, S.; Sanfeliu, C.; Pallàs, M.; Escorihuela, R.M.; Kaliman, P. Epigenetic alterations in hippocampus of SAMP8 senescent mice and modulation by voluntary physical exercise. *Front. Aging Neurosci.* **2014**, *6*, 51.
16. Maze, I.; Noh, K.-M.; Allis, C.D. Histone regulation in the CNS: basic principles of epigenetic plasticity. *Neuropsychopharmacology* **2013**, *38*, 3–22.
17. Griñán-Ferré, C.; Marsal-García, L.; Bellver-Sanchis, A.; Kondengaden, S.M.; Turga, R.C.; Vázquez, S.; Pallàs, M. Pharmacological inhibition of G9a/GLP restores cognition and reduces oxidative stress, neuroinflammation and ß-Amyloid plaques in an early-onset Alzheimer's disease mouse model. *Aging (Albany. NY).* **2019**, *11*, 11591–11608, doi:10.18632/aging.102558.

18. Sharma, M.; Dierkes, T.; Sajikumar, S. Epigenetic regulation by G9a/GLP complex ameliorates amyloid-beta 1-42 induced deficits in long-term plasticity and synaptic tagging/capture in hippocampal pyramidal neurons. *Aging Cell* **2017**, *16*, 1062–1072.
19. Artal-Martinez de Narvajas, A.; Gomez, T.S.; Zhang, J.-S.; Mann, A.O.; Taoda, Y.; Gorman, J.A.; Herreros-Villanueva, M.; Gress, T.M.; Ellenrieder, V.; Bujanda, L. Epigenetic regulation of autophagy by the methyltransferase G9a. *Mol. Cell. Biol.* **2013**, *33*, 3983–3993.
20. Pickford, F.; Masliah, E.; Britschgi, M.; Lucin, K.; Narasimhan, R.; Jaeger, P.A.; Small, S.; Spencer, B.; Rockenstein, E.; Levine, B. The autophagy-related protein beclin 1 shows reduced expression in early Alzheimer disease and regulates amyloid β accumulation in mice. *J. Clin. Invest.* **2008**, *118*, 2190–2199.
21. Nixon, R.A.; Wegiel, J.; Kumar, A.; Yu, W.H.; Peterhoff, C.; Cataldo, A.; Cuervo, A.M. Extensive Involvement of Autophagy in Alzheimer Disease: An Immuno-Electron Microscopy Study. *J. Neuropathol. Exp. Neurol.* **2005**, *64*, 113–122, doi:10.1093/jnen/64.2.113.
22. Glatigny, M.; Moriceau, S.; Rivagorda, M.; Ramos-Brossier, M.; Nascimbeni, A.C.; Lante, F.; Shanley, M.R.; Boudarene, N.; Rousseaud, A.; Friedman, A.K. Autophagy is required for memory formation and reverses age-related memory decline. *Curr. Biol.* **2019**, *29*, 435–448.
23. Hwang, J.-Y.; Yan, J.; Zukin, R.S. Autophagy and synaptic plasticity: epigenetic regulation. *Curr. Opin. Neurobiol.* **2019**, *59*, 207–212.
24. Nikoletopoulou, V.; Sidiropoulou, K.; Kallergi, E.; Dalezios, Y.; Tavernarakis, N. Modulation of autophagy by BDNF underlies synaptic plasticity. *Cell Metab.* **2017**, *26*, 230–242.
25. Kashyap, G.; Bapat, D.; Das, D.; Gowaikar, R.; Amritkar, R.E.; Rangarajan, G.; Ravindranath, V.; Ambika, G. Synapse loss and progress of Alzheimer's disease-A network model. *Sci. Rep.* **2019**, *9*, 6555, doi:10.1038/s41598-019-43076-y.
26. Karege, F.; Perret, G.; Bondolfi, G.; Schwald, M.; Bertschy, G.; Aubry, J.-M. Decreased serum brain-derived neurotrophic factor levels in major depressed patients. *Psychiatry Res.* **2002**, *109*, 143–148.
27. Masters, C.L.; Bateman, R.; Blennow, K.; Rowe, C.C.; Sperling, R.A.; Cummings, J.L. Alzheimer's disease. *Nat. Rev. Dis. Prim.* **2015**, *1*, 15056, doi:10.1038/nrdp.2015.56.
28. Vasilopoulou, F.; Bagan, A.; Rodriguez-Arevalo, S.; Escolano, C.; Griñán-Ferré, C.; Pallàs, M. Amelioration of BPSD-Like Phenotype and Cognitive Decline in SAMP8 Mice Model Accompanied by Molecular Changes after Treatment with I2-Imidazoline Receptor Ligand MCR5. *Pharmaceutics* **2020**, *12*, 475.
29. Pérez-Cáceres, D.; Rodrigo, M.T.; Pubill, D.; Camins, A.; Camarasa, J.; Escubedo, E.; Pallàs, M. Depression-like behavior is dependent on age in male SAMP8 mice. *Biogerontology* **2013**, *14*, 165–176.
30. Miyamoto, M. Characteristics of age-related behavioral changes in senescence-accelerated mouse SAMP8 and SAMP10. *Exp. Gerontol.* **1997**, *32*, 139–148.
31. Griñan-Ferré, C.; Palomera-Ávalos, V.; Puigoriol-Illamola, D.; Camins, A.; Porquet, D.; Plá, V.; Aguado, F.; Pallàs, M. Behaviour and cognitive changes correlated with hippocampal neuroinflammaging and neuronal markers in female SAMP8, a model of accelerated senescence. *Exp. Gerontol.* **2016**, *80*, 57–69.
32. Griñán-Ferré, C.; Codony, S.; Pujol, E.; Yang, J.; Leiva, R.; Escolano, C.; Puigoriol-Illamola, D.; Companys-Alemany, J.; Corpas, R.; Sanfeliu, C. Pharmacological inhibition of soluble epoxide hydrolase as a new therapy for Alzheimer's disease. *Neurotherapeutics* **2020**, *17*, 1825–1835.
33. Companys-Alemany, J.; Turcu, A.L.; Bellver-Sanchis, A.; Loza, M.I.; Brea, J.M.; Canudas, A.M.; Leiva, R.; Vázquez, S.; Pallàs, M.; Griñán-Ferré, C. A novel NMDA receptor antagonist protects against cognitive decline presented by senescent mice. *Pharmaceutics* **2020**, *12*, 284.
34. Maes, T.; Mascaró, C.; Rotllant, D.; Lufino, M.M.P.; Estiarte, A.; Guibourt, N.; Cavalcanti, F.; Griñan-Ferré, C.; Pallàs, M.; Nadal, R. Modulation of KDM1A with vafidemstat rescues

memory deficit and behavioral alterations. *PLoS One* **2020**, *15*, e0233468.
35. Pentkowski, N.S.; Rogge-Obando, K.K.; Donaldson, T.N.; Bouquin, S.J.; Clark, B.J. Anxiety and Alzheimer's disease: Behavioral analysis and neural basis in rodent models of Alzheimer's-related neuropathology. *Neurosci. Biobehav. Rev.* **2021**, *127*, 647–658.
36. Kosel, F.; Pelley, J.M.S.; Franklin, T.B. Behavioural and psychological symptoms of dementia in mouse models of Alzheimer's disease-related pathology. *Neurosci. Biobehav. Rev.* **2020**, *112*, 634–647.
37. Boyer, F.; Jaouen, F.; Ibrahim, E.C.; Gascon, E. Deficits in social behavior precede cognitive decline in middle-aged mice. *Front. Behav. Neurosci.* **2019**, *13*, 55.
38. An, P.N.T.; Shimaji, K.; Tanaka, R.; Yoshida, H.; Kimura, H.; Fukusaki, E.; Yamaguchi, M. Epigenetic regulation of starvation-induced autophagy in Drosophila by histone methyltransferase G9a. *Sci. Rep.* **2017**, *7*, 1–14.
39. Li, F.; Zeng, J.; Gao, Y.; Guan, Z.; Ma, Z.; Shi, Q.; Du, C.; Jia, J.; Xu, S.; Wang, X. G9a inhibition induces autophagic cell death via AMPK/mTOR pathway in bladder transitional cell carcinoma. *PLoS One* **2015**, *10*, e0138390.
40. Murphy, L.O.; MacKeigan, J.P.; Blenis, J. A network of immediate early gene products propagates subtle differences in mitogen-activated protein kinase signal amplitude and duration. *Mol. Cell. Biol.* **2004**, *24*, 144–153.
41. Ying, S.-W.; Futter, M.; Rosenblum, K.; Webber, M.J.; Hunt, S.P.; Bliss, T.V.P.; Bramham, C.R. Brain-derived neurotrophic factor induces long-term potentiation in intact adult hippocampus: requirement for ERK activation coupled to CREB and upregulation of Arc synthesis. *J. Neurosci.* **2002**, *22*, 1532–1540.
42. J Allen, S.; J Watson, J.; Dawbarn, D. The neurotrophins and their role in Alzheimer's disease. *Curr. Neuropharmacol.* **2011**, *9*, 559–573.
43. Narisawa-Saito, M.; Wakabayashi, K.; Tsuji, S.; Takahashi, H.; Nawa, H. Regional specificity of alterations in NGF, BDNF and NT-3 levels in Alzheimer's disease. *Neuroreport* **1996**, *7*, 2925–2928.
44. Youn, J.C.; Lee, D.Y.; Jhoo, J.H.; Kim, K.W.; Choo, I.H.; Woo, J.I. Prevalence of neuropsychiatric syndromes in Alzheimer's disease (AD). *Arch. Gerontol. Geriatr.* **2011**, *52*, 258–263.
45. Cerejeira, J.; Lagarto, L.; Mukaetova-Ladinska, E.B. Behavioral and psychological symptoms of dementia. *Front. Neurol.* **2012**, *3*, 73.
46. Kosel, F.; Munoz, P.T.; Yang, J.R.; Wong, A.A.; Franklin, T.B. Age-related changes in social behaviours in the 5xFAD mouse model of Alzheimer's disease. *Behav. Brain Res.* **2019**, *362*, 160–172.
47. Filali, M.; Lalonde, R.; Rivest, S. Cognitive and non-cognitive behaviors in an APPswe/PS1 bigenic model of Alzheimer's disease. *Genes, Brain Behav.* **2009**, *8*, 143–148.
48. Chen, G.-H.; Wang, C.; Yangcheng, H.-Y.; Liu, R.-Y.; Zhou, J.-N. Age-related changes in anxiety are task-specific in the senescence-accelerated prone mouse 8. *Physiol. Behav.* **2007**, *91*, 644–651.
49. Flood, J.F.; Farr, S.A.; Uezu, K.; Morley, J.E. Age-related changes in septal serotonergic, GABAergic and glutamatergic facilitation of retention in SAMP8 mice. *Mech. Ageing Dev.* **1998**, *105*, 173–188.
50. Miyamoto, M.; Takahashi, H.; Ohta, H.; Sakamoto, J. Animal model of brain aging: Senescence-accelerated mouse (SAM). *CNS Drug Rev.* **1998**, *4*, 361–375.
51. Meeker, H.C.; Chadman, K.K.; Heaney, A.T.; Carp, R.I. Assessment of social interaction and anxiety-like behavior in senescence-accelerated-prone and-resistant mice. *Physiol. Behav.* **2013**, *118*, 97–102.
52. Miyamoto, M. Emotional disorders and memory deficits in senescence-accelerated mice, SAMP8 and SAMP10. In Proceedings of the International Congress Series; Elsevier, 2004;

Vol. 1260, pp. 99–106.
53. Vasilopoulou, F.; Rodríguez-Arévalo, S.; Bagán, A.; Escolano, C.; Griñán-Ferré, C.; Pallàs, M. Disease-modifying treatment with I2 imidazoline receptor ligand LSL60101 in an Alzheimer's disease mouse model: a comparative study with donepezil. *Br. J. Pharmacol.* **2021**.
54. Jackson, J.L.; Mallory, R. Aggression and violence among elderly patients, a growing health problem. *J. Gen. Intern. Med.* 2009, *24*, 1167–1168.
55. Harman, M.F.; Martín, M.G. Epigenetic mechanisms related to cognitive decline during aging. *J. Neurosci. Res.* **2020**, *98*, 234–246.
56. Lin, E.; Tsai, S.-J. Epigenetics and depression: an update. *Psychiatry Investig.* **2019**, *16*, 654.
57. Januar, V.; Ancelin, M.-L.; Ritchie, K.; Saffery, R.; Ryan, J. BDNF promoter methylation and genetic variation in late-life depression. *Transl. Psychiatry* **2015**, *5*, e619–e619.
58. Simmons, J.G.; Schwartz, O.S.; Bray, K.; Deane, C.; Pozzi, E.; Richmond, S.; Smith, J.; Vijayakumar, N.; Byrne, M.L.; Seal, M.L. Study protocol: families and childhood transitions study (FACTS)–a longitudinal investigation of the role of the family environment in brain development and risk for mental health disorders in community based children. *BMC Pediatr.* **2017**, *17*, 1–14.
59. Cittaro, D.; Lampis, V.; Luchetti, A.; Coccurello, R.; Guffanti, A.; Felsani, A.; Moles, A.; Stupka, E.; D'Amato, F.R.; Battaglia, M. Histone modifications in a mouse model of early adversities and panic disorder: role for Asic1 and neurodevelopmental genes. *Sci. Rep.* **2016**, *6*, 1–10.
60. Boulle, F.; Van Den Hove, D.L.A.; Jakob, S.B.; Rutten, B.P.; Hamon, M.; Van Os, J.; Lesch, K.P.; Lanfumey, L.; Steinbusch, H.W.; Kenis, G. Epigenetic regulation of the BDNF gene: implications for psychiatric disorders. *Mol. Psychiatry* **2012**, *17*, 584–596.
61. Tsankova, N.; Renthal, W.; Kumar, A.; Nestler, E.J. Epigenetic regulation in psychiatric disorders. *Nat. Rev. Neurosci.* **2007**, *8*, 355–367.
62. Roopra, A.; Qazi, R.; Schoenike, B.; Daley, T.J.; Morrison, J.F. Localized domains of G9a-mediated histone methylation are required for silencing of neuronal genes. *Mol. Cell* **2004**, *14*, 727–738.
63. Zheng, Y.; Liu, A.; Wang, Z.J.; Cao, Q.; Wang, W.; Lin, L.; Ma, K.; Zhang, F.; Wei, J.; Matas, E.; et al. Inhibition of EHMT1/2 rescues synaptic and cognitive functions for Alzheimer's disease. *Brain* **2019**, *142*, 787–807, doi:10.1093/brain/awy354.
64. Hernández-Ortega, K.; Garcia-Esparcia, P.; Gil, L.; Lucas, J.J.; Ferrer, I. Altered machinery of protein synthesis in Alzheimer's: from the nucleolus to the ribosome. *brain Pathol.* **2016**, *26*, 593–605.
65. Gupta-Agarwal, S.; Franklin, A. V.; DeRamus, T.; Wheelock, M.; Davis, R.L.; McMahon, L.L.; Lubin, F.D. G9a/GLP histone lysine dimethyltransferase complex activity in the hippocampus and the entorhinal cortex is required for gene activation and silencing during memory consolidation. *J. Neurosci.* **2012**, *32*, 5440–5453, doi:10.1523/jneurosci.0147-12.2012.
66. Wang, R.; Holsinger, R.M.D. Exercise-induced brain-derived neurotrophic factor expression: therapeutic implications for Alzheimer's dementia. *Ageing Res. Rev.* **2018**, *48*, 109–121.
67. Rosenberg, T.; Gal-Ben-Ari, S.; Dieterich, D.C.; Kreutz, M.R.; Ziv, N.E.; Gundelfinger, E.D.; Rosenblum, K. The roles of protein expression in synaptic plasticity and memory consolidation. *Front. Mol. Neurosci.* **2014**, *7*, 86.
68. Hock, C.; Heese, K.; Müller-Spahn, F.; Hulette, C.; Rosenberg, C.; Otten, U. Decreased trkA neurotrophin receptor expression in the parietal cortex of patients with Alzheimer's disease. *Neurosci. Lett.* **1998**, *241*, 151–154.
69. Buhusi, M.; Etheredge, C.; Granholm, A.-C.; Buhusi, C. V Increased hippocampal ProBDNF contributes to memory impairments in aged mice. *Front. Aging Neurosci.* **2017**, *9*, 284.

70. Jiao, S.S.; Shen, L.L.; Zhu, C.; Bu, X.L.; Liu, Y.H.; Liu, C.H.; Yao, X.Q.; Zhang, L.L.; Zhou, H.D.; Walker, D.G. Brain-derived neurotrophic factor protects against tau-related neurodegeneration of Alzheimer's disease. *Transl. Psychiatry* **2016**, *6*, e907–e907.
71. Lu, B.; Nagappan, G.; Guan, X.; Nathan, P.J.; Wren, P. BDNF-based synaptic repair as a disease-modifying strategy for neurodegenerative diseases. *Nat. Rev. Neurosci.* **2013**, *14*, 401–416.
72. Peng, S.; Garzon, D.J.; Marchese, M.; Klein, W.; Ginsberg, S.D.; Francis, B.M.; Mount, H.T.J.; Mufson, E.J.; Salehi, A.; Fahnestock, M. Decreased brain-derived neurotrophic factor depends on amyloid aggregation state in transgenic mouse models of Alzheimer's disease. *J. Neurosci.* **2009**, *29*, 9321–9329.
73. Ambigapathy, G.; Zheng, Z.; Keifer, J. Regulation of BDNF chromatin status and promoter accessibility in a neural correlate of associative learning. *Epigenetics* **2015**, *10*, 981–993.
74. Alonso, M.; Medina, J.H.; Pozzo-Miller, L. ERK1/2 activation is necessary for BDNF to increase dendritic spine density in hippocampal CA1 pyramidal neurons. *Learn. Mem.* **2004**, *11*, 172–178.
75. Hof, P.R.; Morrison, J.H. The aging brain: morphomolecular senescence of cortical circuits. *Trends Neurosci.* **2004**, *27*, 607–613.
76. Dorostkar, M.M.; Zou, C.; Blazquez-Llorca, L.; Herms, J. Analyzing dendritic spine pathology in Alzheimer's disease: problems and opportunities. *Acta Neuropathol.* **2015**, *130*, 1–19.
77. Masliah, E.; Crews, L.; Hansen, L. Synaptic remodeling during aging and in Alzheimer's disease. *J. Alzheimer's Dis.* **2006**, *9*, 91–99.
78. Patel, M.R.; Weaver, A.M. Astrocyte-derived small extracellular vesicles promote synapse formation via fibulin-2-mediated TGF-β signaling. *Cell Rep.* **2021**, *34*, 108829.
79. Medendorp, W.E.; Petersen, E.D.; Pal, A.; Wagner, L.-M.; Myers, A.R.; Hochgeschwender, U.; Jenrow, K.A. Altered behavior in mice socially isolated during adolescence corresponds with immature dendritic spine morphology and impaired plasticity in the prefrontal cortex. *Front. Behav. Neurosci.* **2018**, *12*, 87.
80. Radley, J.J.; Rocher, A.B.; Rodriguez, A.; Ehlenberger, D.B.; Dammann, M.; McEwen, B.S.; Morrison, J.H.; Wearne, S.L.; Hof, P.R. Repeated stress alters dendritic spine morphology in the rat medial prefrontal cortex. *J. Comp. Neurol.* **2008**, *507*, 1141–1150.
81. Norrholm, S.D.; Ouimet, C.C. Altered dendritic spine density in animal models of depression and in response to antidepressant treatment. *Synapse* **2001**, *42*, 151–163.
82. Maze, I.; Covington III, H.E.; Dietz, D.M.; Laplant, Q.; Renthal, W.; Russo, S.J.; Mechanic, M.; Mouzon, E.; Neve, R.L.; Stephen, J.; et al. Essential Role of the Histone Methyltransferase G9a in Cocaine- induced Plasticity. *Science (80-.).* **2010**, *327*, 213–217, doi:10.1126/science.1179438.Essential.

Table S1. Primers used in qPCR studies.

Syber Green Primers

Target	Forward primer (5'-3')	Reverse primer (5'-3')
NT3	CAGGGTGAAGGGGAAAACTC	AGTTCGGTCATTCAGTCTCGC
G9a	CCAGAGGAGTGAATGGTGT	CTTTCGGTGGCCATACACTT
Dnmt3a	ACGCCAAAGAAGTGTCTGCT	CTTTGCCCTGCTTTATGGAG
Comt	CCCTCCTGTCGGATTACTCA	GGGGGAAGCACATGAGTCTA
Zif-268	TCAGCCTAGTCAGTGGCCTT	AGGTCTCCCTGTTGTTGTGG
cFos	CCCGTAGACCTAGGGAGGAC	CAATACACTCCATGCGGTTG
Bdnf	TGCGAGTATTACCTCCGCCAT	TCACGTGCTCAAAAGTGTCAG
Ngf	GGAGCGCATCGAGTGACTT	CCTCACTGCGGCCAGTATAG
TrkA	CTCCTTCTCGCCAGTGGAC	TGCCCTCAGTAGGGGAAAGA
TrkB	CGTCACTTCGCCAGCAGTAG	CTATACGCCAGGCACCACTC
β-Actin	CAACGAGCGGTTCCGAT	GCCACAGGTTCCATACCCA

Table S2. Antibodies used in Western blot studies.

Antibody	Host	Source/Catalog	WB dilution
GAPDH	Mouse	Millipore/MAB374	1:2000
JNK	Mouse	Santa Cruz/sc-7345	1:500
p-JNK	Rabbit	Cell Signalling/#9251	1:1000
Beclin-1	Rabbit	Cell Signalling/#3738	1:1000
p-62	Mouse	Santa Cruz/sc-28359	1:500
LC3B-I **LC3B-II**	Rabbit	Cell Signalling/2775	1:1000
ERK	Rabbit	Cell Signalling/9102	1:1000
p-ERK	Rabbit	Cell Signalling/9101	1:1000
Goat-anti-mouse HRP conjugated		BioRad/170-5047	1:2000
Goat-anti-rabbit HRP conjugated		BioRad/170-6515	1:2000

Table S3. Parameters measured in the Elevated Plus Maze (EPM) in male SAMR1 and SAMP8 mice at 12 months of age. (n): number of events. Results are expressed as a mean ± Standard error of the mean (SEM). **p*<0.05; ***p*<0.01; ****p*<0.001; *****p*<0.0001.

	SAMR1	**SAMP8**
Locomotor activity (cm)	789,55 ± 44,21	892,42 ± 39,05
Rearings (n)	10,33 ± 0,79	1,92 ± 0,36 ****
Time in Zone (%)- Center	61,21 ± 5,05	36,89 ± 1,74 ***
Time in Zone (%)- Open Arms	2,92 ± 0,56	17,06 ± 2,86 ****
Time in Zone (%)- Closed Arms	35,54 ± 5,04	45,63± 2,52

Table S4. Parameters measured in the Open Field Test (OFT) in male SAMR1 and SAMP8 mice at 12 months of age. (n): number of events. Results are expressed as a mean ± Standard error of the mean (SEM). **p*<0.05; ***p*<0.01; *****p*<0.0001.

	SAMR1	**SAMP8**
Locomotor activity (cm)	1476,18 ± 85,68	1870,07 ± 118,8 *
Rearings (n)	4,7 ± 1,08	31,17 ± 2,41 ****
Time in Zone (%)- Border	61,93 ± 5,42	79,63 ± 1,83 **

3.2. Publication 2

G9a Inhibition Promotes Neuroprotection through GMFB Regulation in Alzheimer's Disease.

Aina Bellver-Sanchis, Qizhi Geng, Gemma Navarro, Pedro A. Ávila-López, Júlia Companys-Alemany, Laura Marsal-García, Raquel Larramona-Arcas, Lluisa Miró, Anna Perez-Bosque, Daniel Ortuño-Sahagún, Deb Ranjan Banerjee, Bhanwar Singh Choudhary, Francesc X Soriano, Coralie Poulard, Mercè Pallàs, Hai-Ning Du, and Christian Griñán-Ferré

Aging and Disease, 2024, 15(1):311-337

doi: 10.14336/AD.2023.0424-2

SUMMARY

In the past decade, numerous studies have shown that inhibiting the enzyme G9a can reduce neurodegeneration and cognitive decline. Its inhibition prevents the formation of Aβ oligomers and promotes LTP and synaptic plasticity by increasing the expression of neurotrophic factors, such as BDNF. However, the exact mechanism by which G9a inhibition provides neuroprotection in age-related diseases, like AD, is not yet fully understood. To support our hypothesis that the G9a inhibition would be a promising therapy for AD, we tried to provide knowledge about the neuroprotective mechanism of its inhibition using the SAMP8 mouse model in this work.

First, we validated the overexpression of G9a and its repressive mark, H3K9me2, in AD human brain, as well as in SAMP8 mice, which are known for accelerated aging and cognitive decline. Then, our attention was mainly directed towards unexplored pathways influenced by G9a inhibition, elucidating how the modification of H3K9me2 contributes to alterations in the CNS's transcriptome. Thus, we treated SAMP8 mice with a well-established G9ai, **UNC0642**. Moreover, this study included behavioural and cognitive tests and a transcriptional profiling analysis (RNA-seq) proceeded by biochemical assays studies were also performed in *C. elegans* and cell cultures to better support our results. Lastly, the re-analysis of ChIP-seq was also conducted, confirming an enrichment of modifications in genes related to neural functions in cells subjected to G9a inhibition.

G9a overexpression in AD patients' brains and H3K9me2 in both AD patients and *C. elegans* AD transgenic strains correlate with cognitive impairment. Accordingly, G9a pharmacological inhibition leads to a reduction in H3K9me2 and AD hallmarks (Aβ levels), improved behavioural and cognitive decline, and restoration of neuronal branching and dendritic spine density in SAMP8 mice. The transcriptional profile analysis after G9ai treatment revealed an unexpectedly increased gene expression of GMFB in SAMP8 mice, which in turn mediated the neuroprotective effects by an increase of neuroplasticity and a reduction of neuroinflammation (via NF-κB). Notably, these neuroprotective effects were reversed when GMFB was pharmacologically inhibited in mice and cell cultures and through

RNAi approach in *C. elegans*. Significantly, our study provides evidence that G9a-mediated lysine methylation controls GMFB activity. Furthermore, we identified that G9a's neurodegenerative role as a GMFB suppressor primarily depends on the methylation of the K25 position of GMFB.

In conclusion, we have revealed a new G9a-mediated mechanism here. When G9a is inhibited, this mechanism activates GMFB and modulates its function, resulting in neuroprotection. Accordingly, our findings indicate that the positive impacts on cognition, neuronal plasticity, and neuroinflammation elicited by *set-25*-knock-down (KD) or pharmacological inhibition of G9a were reversed when GMFB was inhibited. This highlights the crucial role of GMFB as a key player in the neuroprotective effects of G9a inhibition. Additionally, we presented evidence indicating that G9a-mediated methylation acts as a repressive regulator of GMFB, inhibiting its activation and consequently triggering neurodegeneration.

Aging and Disease
www.aginganddisease.org
Volume 15, Number 1; 311-337, February 2024
http://dx.doi.org/10.14336/AD.2023.0424-2

Original Article

G9a Inhibition Promotes Neuroprotection through GMFB Regulation in Alzheimer's Disease

Aina Bellver-Sanchis[1], Qizhi Geng[2], Gemma Navarro[3,4], Pedro A. Ávila-López[5], Júlia Companys-Alemany[1], Laura Marsal-García[6,7], Raquel Larramona-Arcas[8], Lluisa Miró[9], Anna Perez-Bosque[9], Daniel Ortuño-Sahagún[10], Deb Ranjan Banerjee[11], Bhanwar Singh Choudhary[12,13], Francesc X Soriano[8], Coralie Poulard[14,15,16], Mercè Pallàs[1,3], Hai-Ning Du[2], Christian Griñán-Ferré[1,3*]

[1]Department of Pharmacology and Therapeutic Chemistry, Institut de Neurociències-Universitat de Barcelona, 08028 Barcelona, Spain. [2]Hubei Key Laboratory of Cell Homeostasis, Frontier Science Center for Immunology and Metabolism, RNA Institute, College of Life Sciences, Wuhan University, Wuhan 430072, China. [3]Centro de Investigación en Red, Enfermedades Neurodegenerativas (CIBERNED), Instituto de Salud Carlos III, Madrid, Spain. [4]Department Biochemistry and Physiology, Faculty of Pharmacy. Universitat de Barcelona, 08028 Barcelona, Spain. [5]Department of Biochemistry and Molecular Genetics, Feinberg School of Medicine, Northwestern University, Chicago, Illinois, USA. [6]Department of Biochemistry, McGill University, Montréal, Québec, Canada. [7]Rosalind and Morris Goodman Cancer Institute, McGill University, Montréal, Québec, Canada. [8]Department of Cell Biology, Physiology, and Immunology, Celltec-UB, University of Barcelona, Barcelona, Spain, and Institute of Neurosciences, University of Barcelona, 08028 Barcelona, Spain. [9]Departament de Bioquímica i Fisiologia, Facultat de Farmàcia i Ciències de l'Alimentació and Institut de Nutrició i Seguretat Alimentària, Universitat de Barcelona, 08028 Barcelona, Spain. [10]Laboratorio de Neuroinmunología Molecular, Instituto de Investigación de Ciencias Biomédicas (IICB) CUCS, Universidad de Guadalajara, Jalisco 44340, México. [11]Department of Chemistry, National Institute of Technology Durgapur, India. [12]Department of Pharmacy, Central University of Rajasthan, Ajmer, Rajasthan, India. [13]Shree S. K. Patel College of Pharmaceutical Education and Research, Ganpat University, Mehsana, Gujarat, India. [14]Cancer Research Cancer Lyon, Université de Lyon, F-69000 Lyon, France.[15]Inserm U1052, Centre de Recherche en Cancérologie de Lyon, F-69000 Lyon, France. [16]CNRS UMR5286, Centre de Recherche en Cancérlogie de Lyon, F-69000 Lyon, France.

[Received January 22, 2023; Revised April 22, 2023; Accepted April 24, 2023]

ABSTRACT: Epigenetic alterations are a fundamental pathological hallmark of Alzheimer's disease (AD). Herein, we show the upregulation of G9a and H3K9me2 in the brains of AD patients. Interestingly, treatment with a G9a inhibitor (G9ai) in SAMP8 mice reversed the high levels of H3K9me2 and rescued cognitive decline. A transcriptional profile analysis after G9ai treatment revealed increased gene expression of glia maturation factor β (GMFB) in SAMP8 mice. Besides, a H3K9me2 ChIP-seq analysis after G9a inhibition treatment showed the enrichment of gene promoters associated with neural functions. We observed the induction of neuronal plasticity and a reduction of neuroinflammation after G9ai treatment, and more strikingly, these neuroprotective effects were reverted by the pharmacological inhibition of GMFB in mice and cell cultures; this was also validated

***Correspondence should be addressed to:** Dr. Christian Griñán-Ferré: Institut de Neurociències-Universitat de Barcelona, Avda. Joan XXIII, 27, 08028 Barcelona, Spain. Email: christian.grinan@ub.edu.

Copyright: © 2023 Bellver-Sanchis A. et al. This is an open-access article distributed under the terms of the Creative Commons Attribution License, which permits unrestricted use, distribution, and reproduction in any medium, provided the original author and source are credited.

by the RNAi approach generating the knockdown of *GMFB*/*Y507A.10* in *Caenorhabditis elegans*. Importantly, we present evidence that GMFB activity is controlled by G9a-mediated lysine methylation as well as we identified that G9a directly bound GMFB and catalyzed the methylation at lysine (K) 20 and K25 *in vitro*. Furthermore, we found that the neurodegenerative role of G9a as a GMFB suppressor would mainly rely on methylation of the K25 position of GMFB, and thus G9a pharmacological inhibition removes this methylation promoting neuroprotective effects. Then, our findings confirm an undescribed mechanism by which G9a inhibition acts at two levels, increasing GMFB and regulating its function to promote neuroprotective effects in age-related cognitive decline.

Key words: cognitive decline, aging, epigenetics, G9a inhibition, GMFB, SAMP8.

INTRODUCTION

Aberrant epigenetic mechanisms are one of the key drivers of aging and neurodegeneration [1, 2], and are relevant to the progression of age-associated cognitive decline, including Alzheimer's disease (AD) [2]. Transcriptional activation and repression of global histone changes have been observed in different regions of postmortem AD brains [3]. Despite enormous amount of research, none of the clinically approved AD drugs is effective, all providing only symptomatic treatments. Thereby, there is an urgent need to identify new targets based on epigenetic therapies for neurodegenerative diseases [4].

Growing evidence suggests that lysine (K) methyltransferases (KMTs), including G9a, also known as EHMT2 (Euchromatic histone lysine methyltransferase 2), act as a crucial regulator in human diseases [5]. G9a is a KMT that is able to mono- and di-methylate K9 histone H3 (H3K9me1 and H3K9me2), which are marks linked to the repression of genes implicated in synaptic plasticity [6–9], learning, and memory formation [3, 10–12]. Very recently, several studies have shown that G9a can add methyl group doing post-translational modifications (PTMs) in a large number of non-histone proteins, modulating the function and stability of proteins involved in different biological processes [13]. In fact, many biological processes are influenced by PTMs, which have a significant impact on protein structure and dynamics [14], including several human diseases [15, 16]. Aberrant upregulation of G9a in the brain of late-stage familial AD (5XFAD) mice and AD patients has recently been demonstrated [3]. Similarly, another study showed elevated levels of H3K9me2 in the occipital cortex of postmortem AD brains compared to the non-demented (ND) group [17]. In addition, H3K9me2 seems to participate in the pathogenesis of neurodegenerative disorders, such as posttraumatic stress disorder (PTSD) [18] and anxiety-like behavior [19]. Thus, G9a is central to brain age-related diseases.

Over the last decade, several *in vitro* and *in vivo* studies have demonstrated that G9a inhibition reduces neurodegeneration and cognitive impairment [3, 12]. Indeed, inhibition of G9a by BIX01294 prevented the amyloid-β (Aβ) oligomer, and induced late-long term potentiation (LTP), and synaptic plasticity by increasing the gene expression of *brain-derived neurotrophic factor* (*Bdnf)*, which was previously repressed [3, 7, 12, 19]. Subsequently, three selective G9a inhibitors (G9ai) (A-366, UNC0638, and UNC0642) demonstrated neuroprotective effects [20]. Recently, our group demonstrated that pharmacological inhibition of G9a by UNC0642 produced significant neuroprotective effects in an early-onset AD mouse model [12]. However, the precise mechanism by which G9a inhibition promotes neuroprotection remains elusive.

Several pieces of evidence thus indicate the wide involvement of H3K9me2 in the central nervous system (CNS) function and disease. In the present study, we confirmed the high levels of H3K9me2 in samples of AD human patients. Importantly, we focused on undescribed modulated pathways involving G9a inhibition that underlie how H3K9me2 promotes changes in the transcriptome of the CNS. Then, RNA-seq data analysis was performed to further explore differential gene expression under G9a inhibition. Finally, inspection of H3K9me2 chromatin immunoprecipitation assays with sequencing (ChIP-seq) revealed that H3K9me2 is enriched in genes associated with neural functions in cells treated with a G9ai.

Our analysis showed that pharmacological G9a inhibition induces changes in different molecular pathways. Unexpectedly, Glia maturation factor β (GMFB) increased after G9a inhibition in senescence-accelerated mice prone 8 (SAMP8), suggesting its transcriptional regulation by G9a. GMFB is expressed predominantly in the CNS [21]. It is a highly

evolutionarily conserved protein and is expressed in a wide range of animals [22], including invertebrates [21]. Interestingly, GMFB participates in several inflammatory and immune conditions [23]. As mentioned above, PTMs play a crucial role in almost all biological processes [23], and one example is the SUMOylation, which has been considered to play a role in inflammatory processes [24]. A recent study reported that GMFB can be mono-SUMOylated at multiple site by covalent addition of a single SUMO1 protein, fostering the stability and trans-localization of GMFB [23]. Another important clue is that GMFB is implicated in the regulation of neuronal and glial growth and differentiation [25–27]. Furthermore, GMFB expression is altered in several neurodegenerative diseases, suggesting that GMFB may be a suitable disease biomarker [28].

Of note, G9a and GMFB are associated with neuroinflammation, increasing pro-inflammatory cytokines. Likewise, they are known to play a key role in several neurodegenerative diseases [29, 30], and participate in neuronal plasticity, among other degenerative pathways [23, 31, 32]. However, neither the transcriptional regulation of GMFB by G9a nor the G9a-mediated methylation of GMFB have been described. Thus, here we present a previously undescribed mechanism by which G9a inhibition increases GMFB and mediates changes in its function, at the same time directly bound, which in turn mediates the neuroprotective effects.

MATERIAL AND METHODS

Animals and treatment

For the in vivo study, 24-week-old female and male SAMP8 and SAMR1[33, 34] mice (n = 79) were used to perform cognitive and molecular studies. We divided these mice randomly into five groups: SAMR1 (n = 24), SAMP8 control (n = 24), SAMP8 G9ai (UNC0642, 5 mg/Kg); n = 17), SAMP8 treated with GMFBi ((1H-Indazol-4-yl)methanol[35], 12mg/Kg), and SAMP8 treated with G9ai (UNC0642, 5 mg/Kg) + GMFBi ((1H-Indazol-4-yl)methanol, 12mg/Kg) (n = 7). The sample size for the intervention was chosen following previous studies in our laboratory and using one of the available interactive tools (http://www.biomath.info/power/index.html). Experimental groups either received a daily dose of vehicle (2% w/v, (2-hydroxypropyl)-β-cyclodextrin) or a dose of 5 mg/Kg/day of UNC0642 and/or a dose of 12 mg/Kg/day (1H-Indazol-4-yl)methanol dissolved in 2% 2-hydroxypropyl-β-cyclodextrin via oral gavage for 4 weeks. Animals had free access to food and water and were kept under standard temperature conditions (22 ± 2°C) and 12h:12h light-dark cycles (300 lux/0 lux). After the treatment period, cognitive tests were performed on the animals.

C. elegans were cultured according to standard procedures [36], unless otherwise noted. N2 (WT) (Bristol) strain, and the transgenic AD strains (CL2006, CL2355, and its control, CL2122) were used for this study. They were obtained from the Caenorhabditis Genetics Center (CGC), University of Minnesota, Minneapolis, MN, USA. Moreover, KDs of set-25 and Y50D7A.10 strains were generated in this work using the RNAi method in CL2122, CL2355 and CL2006 strains. WT nematodes were propagated at 20°C, while transgenic AD strains were maintained at 16°C in a temperature-controlled incubator on solid nematode growth medium (NGM) seeded with Escherichia coli (E. coli) OP50. To obtain synchronized animals, young adults' laid embryos for 24 hours before being removed from the plates.

RNAi

RNAi was performed using the feeding method as previously described [37]. Bacteria HT115(DE3) carrying IPTG-inducible were incubated at 37°C for 7-8 hours with 100 mg/mL ampicillin. NGM plates were then seeded with 25 mg/mL carbenicillin and 1 mM IPTG with the incubated cultures and left to grow overnight at room temperature. Young adults were plated onto RNAi bacteria at 16ºC. Silenced adults were transferred to fresh OP50 plates to produce subsequent generations 7 days later.

Behavioral and cognitive tests

Chemotaxis assay: Fifteen adult hermaphrodites were left to lay eggs for 24h and then removed from the plates. Eggs were incubated at 16°C for 36h, and then at 23°C for another 48h. Briefly, the assay was performed in 100 mm NGM plates, and 10 µL of control odorant (96% ethanol) was added to the "control" spot. On the opposite side of the plate, 10 µL of odorant (0.025% benzaldehyde in 96% ethanol) was added to the "attractant" spot. Adult worms were washed three times in M9 buffer, and at least 120 worms were placed towards the center of the plate. The test plates were incubated at 23°C for 1.5h, and worms were scored according to the chemotaxis index (CI) as follows: CI = (number of worms at attractant−number of worms at control)/total number of worms.

Three-Chamber Test (TCT):The social behavior of the mice was evaluated in the TCT following a previously described protocol [38]. A box of transparent polyvinyl chloride (15x15x20 cm) divided into three equally dimensioned rooms between openings among them was used. First, each mouse was placed in the center of the box

and allowed to explore the three chambers for 5 min (habituation). Afterwards, an intruder (same-sex and age) was placed in a metal cage in one of the rooms, and the behavior was recorded for 10 min. The time spent in each room and interacting with the intruder (sniffing time) was measured manually. The TCT apparatus was cleaned with 70% ethanol between the trials to eliminate olfactory cues.

Novel object recognition test (NORT): Short- and long-term recognition memory involving cortical areas and the hippocampus was evaluated by NORT. The experimental apparatus used for this test was a 90-degree, two-arm, 25-cm-long, 20-cm-high maze of black polyvinyl chloride. Light intensity in the middle of the field was 30 lux. First, mice were individually habituated to the apparatus for 10 min per day for 3 days. On day 4, the animals were allowed to freely explore two identical objects (A and A or B and B) placed at the end of each arm for a 10 min acquisition trial (first trial-familiarization). Then, a 10-min retention trial (second trial) was carried out 2 h (short-term memory) or 24 h (long-term memory) later. During the Short-term memory retention test, the times that the animal spent exploring the new object (TN) and the old object (TO) was recorded. Twenty-four hours after the acquisition trial, the mice were tested again, with a new object and an object identical to the new one in the previous trial (A and C, or B and C). TN and TO were measured from the video recordings from each trial session. A Discrimination index (DI) was defined as (TN-TO)/(TN+TO). The maze, the surface, and the objects were cleaned with 70% ethanol between the animals' trials to eliminate olfactory cues.

Object Location Test (OLT): The OLT evaluated the spontaneous tendency of rodents to spend more time exploring a novel object location than a familiar object location and recognizing when an object has been relocated. OLT was performed using a white plywood apparatus (50 × 50 × 25 cm), in which three walls were white and one was black. On the first day, animals were just habituated to the empty open field arena for 10 minutes. On the second day, two objects were placed in front of the black wall, equidistant from each other and the wall. The objects were 10 cm high and identical. The animals were placed into the open field arena and allowed to explore both objects and surroundings for 10 minutes. Afterward, animals were returned to their home cages, and the OLT apparatus was cleaned with 70% ethanol. On the third day, one object was moved in front of the opposite white wall to test spatial memory. Trials were recorded using a camera mounted above the open field area, and the total exploration time was determined by scoring TN and TO. DI was calculated, defined as (TN-TO)/(TN+TO).

Biochemical experiments

Brain processing: SAMP8 and SAMR1 mice were euthanized 3 days after completion of the behavioral test by cervical dislocation. Brains were immediately removed from the skull. Cortex and hippocampus were then isolated and frozen on powdered dry ice. They were maintained at -80 °C for biochemical experiments. For the Golgi staining protocol, see the procedure in the section "Spine density and Golgi staining protocol".

Human cases: Tissue samples were obtained from the Institute of Neuropathology-IDIBELL Brain Bank, Hospitalet de Llobregat, following the guidelines of Spanish legislation on this matter and the approval of the local ethics committee (Supplementary Table 1). The postmortem interval between death and tissue processing was 1 to 10 h and samples were processed to minimize postmortem delay artifacts. The brain tissue was immediately frozen on metal plates over dry ice, placed in individual air-tight plastic bags, and maintained at -80 °C for biochemical experiments. The average age in the ND group is 69.16 ± 15.06, and in the AD group is 81.13 ± 7.03. The neuropathologic diagnosis of AD was based on the classification of Braak[39] (Supplementary Table 1).

Reagents: All the reagents and kits used for the protocols described below are listed in Supplementary Table 2.

Protein levels determination by Western blotting (WB)

Protein, histone extraction, and immunoblot analysis were performed as in Vasilopoulou et al. [38] (n = 6 hippocampal samples from mice, or at least 6 samples from human brain per experimental group). Proteins were separated by SDS-PAGE (8-20%) and transferred onto PVDF membranes. Afterwards, membranes were blocked in 5% BSA in 0.1% Tween20-TBS (TBS-T) for 1 h at room temperature (RT), followed by overnight incubation at 4 ºC with the primary antibodies presented in Supplementary Table 3.

Immunoreactive proteins were viewed with a chemiluminescence-based detection kit, following the manufacturer's protocol and digital images were acquired using a ChemiDoc XRS+System. Semi-quantitative analyses were carried out using ImageLab Software and the results were expressed in Arbitrary Units (AU), considering the control mice group as 100%. Protein loading was routinely monitored by immunodetection of GAPDH.

Human Aβ levels quantification by ELISA

Amyloid-β40 and amyloid-β42 protein levels were measured with the human amyloid-β40 ELISA Kit (Invitrogen, #KHB3481) and human amyloid-β42 Ultrasensitive ELISA Kit (Invitrogen, #KHB3544), respectively. The samples were diluted using standard dilution buffer at a percentage of 50% and all procedures followed the manufacturer's instructions. At least 6 human brain samples per experimental group were used for the quantification.

Mouse Aβ levels quantification by ELISA

Mice brains (n= 6 per experimental group) were homogenized in cold 5 M guanidine-HCl/50 mM Tris buffer containing a protease inhibitor cocktail. The quantification of amyloid-β40 (Invitrogen, #KMB3481) and amyloid-β42 (Invitrogen, #KMB3441) was performed using the mouse Aβ40 and Aβ42 ELISA Kits, following the manufacturer's instructions.

RNA extraction and gene expression determination

Total RNA isolation from cortical samples (n = 6 per experimental group) was carried out using TRIsureTM reagent following the manufacturer's instructions (Bioline Reagents, #BIO-38032). The yield, purity, and quality of the RNA were determined spectrophotometrically with a NanoDropTM ND-1000 apparatus and an Agilent 2100B Bioanalyzer. RNAs with 260/280 ratios and RIN higher than 7.5, respectively, were selected.

Reverse transcription-polymerase chain reaction (RT-PCR) was performed using the high-capacity cDNA Reverse Transcription kit. SYBR® Green real-time PCR was performed to quantify the mRNA expression of a set of genes listed in Supplementary Table 4 on a Step One Plus Detection System (Applied-Biosystems, Foster City, CA, USA).

To evaluate the relative changes in gene expression, data were analyzed utilizing the comparative cycle threshold (Ct) method (ΔΔCt). Housekeeping gene level was used to normalize differences in sample loading and preparation. Normalization of expression levels was performed with *β-actin* for the SYBR® Green-based real-time PCR results. Each sample was analyzed in triplicate, and the results represented the n-fold difference of the transcript levels among different groups.

RNA-sequencing

Pools of 4 hippocampal tissue samples from the SAMP8 control and SAMP8 UNC0642 mice (5 mg/Kg) were aligned with the reference genome using Bowtie2[40], and the gene expression level was estimated using RSEM[41]. Differentially expressed genes were identified using the edgeR program[42]. Genes showing altered expression with $p<0.05$ and more than 1.3-fold changes were considered differentially expressed.

KEGG, Gene Ontology, and GSEA[43] were used to perform the enrichment and pathway analysis by using Enrichr database[44]. Raw data were deposited at the Gene Expression Omnibus (accession GSE189250), raw fastq files for RNA-seq on mouse hippocampus SAMP8 (accession GSE189249).

ChIP-seq analysis

Publicly available H3K9me2 ChIP-seq data corresponding to AML12 cells (murine hepatocyte cell line) treated with the selective G9a inhibitor, UNC0638[45] were obtained from the Genome Sequence Archive (GSA: CRA002762)[46]. ChIP-seq analysis was performed as previously described[47]. Briefly, quality control was analyzed in FastQC v0.11.8. The reads were mapped to the reference genome (Mus musculus mm10) with Bowtie2 v2.4.2 using default parameters [40]. The unmapped and duplicate reads were filtered with SAMtools v1.11[48]. The H3K9me2 peaks were determined with MACS2 v2.1.1.2[49]. The ChIP-seq signal was visualized with deepTools2 v3.3.2[50] and the bigwig files were viewed in the IGV genome browser v2.8.12[51].

To determine the annotated genomic region of H3K9me2 peaks and distribution of transcription factors, we used the ChIPseeker package[52]. To determine TF binding at promoters of the genes regulated by H3K9me2 in AML12 cells treated with UNC0638, we used the ENCODE and ChEA Consensus TFs from ChIP-X tool[53]. The detection of transcription factor binding motifs at H3K9me2 peaks was performed with the MEME-ChIP database[54]. Motifs with an E-value<0.05 were considered statistically significant. The protein-protein interaction network between G9a (EHMT2) and transcription factors was determined using the STRING database.

Dendritic length, spine density and Golgi staining protocol

Mice were sacrificed by cervical dislocation and brains were removed from the skull (n=6 whole brain per

experimental group). Then, the Golgi staining protocol was developed using the FD Rapid GolgiStain kit according to the manufacturer's instructions (FD NeuroTechnologies, incs, #PK401). For dendritic branching analysis, images of neurons were collected at 20x magnification in an Olympus BX61 microscope coupled to an Olympus DP70 camera. Measurement of neurite length and complexity was performed using NeuronJ macros and Advanced Sholl Analysis. The number of intersections (branch points) within concentric circles of 10 µm radius was measured and compared between groups. Images for analyzing the spine density were acquired using brightfield microscopy with a 50x oil-objective. All neurites analyzed were around 18 µm and they were at a maximum distance of 150 µm from the soma.

Thioflavin-S staining Aβ aggregation

Adult worms were fixed in 4 % Paraformaldehyde/Phosphate-buffered saline (PBS) (pH 7.5), for 24 hours at 4°C. On the following day, worms were permeabilized in 5 % fresh β-mercaptoethanol, 1 % Triton X-100, 125 mm Tris (pH 7.5), at 37°C for another 24 hours. Then, nematodes were stained with 0.125% Thioflavin-S (ThS) (Sigma, CAS# 1326-12-1) in 50 % ethanol (EtOH) for 2 min, destained in 50 % EtOH for 2 min, washed 3 times with PBS. Approximately 10 L of Fluoromount G was used to prepare the glass slide for microscopy (Electron Microscopy Sciences, CAT#17984-25). Fluorescence images were acquired using a 20Å~ objective of a fluorescence microscope, and Aß in the head region of worms were quantified blindly by counting the number of positive Th-S spots using ImageJ.

Primary cell culture

Primary mixed culture of neurons and microglia was prepared from the cortex and striatum of fetuses from 18-19-day-old C57/BL6 pregnant mice. In brief, samples were dissected, carefully stripped of their meninges, and digested with 0.25% trypsin for 30 min at 37ºC. Cells were brought to a single cell suspension by repeated pipetting followed by passage through a 100 µm-pore mesh and pelleted (7 min, 200g). Neurons and glial cells were resuspended in medium and seeded at a density of 400.000 cells/ml in 6-well plates. Cultures were maintained at 37ºC in a humidified 5% CO2 atmosphere and neurobasal medium supplemented with 2 mM L-glutamine, 5% (v/v) FBS, 100 U/ml penicillin/streptomycin, and 2% (v/v) B27 supplement (Gibco) in a 6-well plate for 12 days.

Cell viability: Then cell viability assay is based on the principle that living cells maintain intact cell membranes that exclude certain dyes, like trypan blue 0.4%. For quantification of live cells, cortical and striatal neurons were gently detached and mixed with an equal volume of trypan blue (0.4%). Neurons (%) were counted with a TC20™ Automated Cell Counter.

Immunocytochemistry: Primary microglial culture cells seeded in coverslips were fixed in 4% paraformaldehyde for 15 min and washed twice with PBS containing 20mM glycine, before permeabilization with PBS-glycine containing 0.2% Triton X-100. Microglial cells were treated for 1 h with PBS containing 1% BSA and labelled with the antibodies listed in Supplementary Table 3. Samples were washed several times and mounted with 30% Mowiol. Samples were observed in a Leica SP2 confocal microscope (Leica Microsystems). Negative control slides stained without primary and/or secondary antibodies were used to identify potential nonspecific, background fluorescence. Scale bar: 30 µm. Fluorescence was quantified using Fiji-Image J software.

Plasmids

The gene encoding the human GMFB was amplified by PCR using the following primers: 5′-CTACGCTGGCCGGCCAGAATTCATGAGTGAGTC TTTGGTTGTTTGTG -3′ (forward) and 5′-CGACTCACTATAGTTCTAGACTAGTGAAAAAAT CCAAGTTTCTCACG-3′ (reverse) from HeLa cDNA. The PCR products were cloned into a pCS2-3xHA vector.

Plasmids used to generate the KD of the GMDB methylation sites are listed in the Supplementary Table 5.

Cell culture, transfection, and treatment

HEK 293T and HeLa S3 cell lines (from passages 1-10) were cultured in DMEM (Dulbecco's modified Eagle's medium) medium, supplemented with 10% fetal bovine serum, 2 mM L-glutamine, penicillin (100 U/mL), and streptomycin (100 µg/mL). The HeLa S3 G9a-KO cell line was maintained in selective medium containing puromycin (0.5 µg/ml). Cells were maintained at 37°C with 5% CO2. Transfections were performed using Lipofectamine 2000 according to the manufacturer's instruction. Cells were harvested 48 hours after transfection and analyzed by immunoprecipitation and WB.

Co-immunoprecipitation and WB

Cells were collected and lysed in immunoprecipitation (IP) buffer [25 mM tris-HCl (pH 7.4), 150 mM NaCl, 5%

glycerol, 1 mM EDTA, and 1% NP-40] containing a protease inhibitor cocktail (BioTool) for 30 min on ice. The Flag resin or HA resin was added into the lysates and incubated at 4°C for 4 hours or overnight with rotation. After washing three times with IP buffer, the resins were resuspended into SDS sample buffer, boiled, and centrifuged. Then, samples were subjected to SDS–polyacrylamide gel electrophoresis (SDS-PAGE), transferred to polyvinylidene difluoride membrane, and immunoblotted with the indicated antibodies (Supplementary Table. 6).

Data analysis

The statistical analysis was conducted using GraphPad Prism version 9.2 statistical software. Group size may differ depending on power analysis and expertise of the authors and statistical analysis was conducted only for studies where the size of each group was at least n = 5-6 samples per group for in vivo studies; and n = 3-5 replicates for in vitro studies. First, Grubb's test was performed to detect outliers, in addition to the Shapiro–Wilk test to verify data normality for all groups. Data were expressed as the mean ± Standard Error of the Mean (SEM). For normally distributed data, means were compared in One-Way or Two-Way ANOVA analysis of variance, (ANOVA), followed by Tukey's post-hoc analysis. Comparison between groups was also performed by two-tailed Student's t-test for independent samples. In contrast, the Mann-Whitney or Kruskal–Wallis test followed by Dunn's post-hoc analysis was used for non-normally distributed data. Statistical significance was considered when p-values were <0.05. The statistical outliers were carried out with Grubss' test and subsequently removed from the analysis. For behavioral tests, a blinded analysis was performed.

RESULTS

G9a overexpression in AD patients' brains and H3K9me2 in both AD patients' and C. elegans AD transgenic strains correlates with cognitive impairment.

Alterations in the histone methylation marks and their enzymes are implicated in senescence, age-related cognitive decline and neurodegenration [1]. However, the precise mechanism remains elusive. As mentioned above, G9a has been implicated in AD, but to date the precise mechanism by which promotes neurodegeneration is not well described. To characterize G9a role in AD, we thus carried out several experiments and bioinformatic analyses (Supplementary Fig. 1) and examined G9a protein levels by WB in human AD patients' brains. We found higher levels of this protein in AD patients' brains compared to the human non-demented (ND) patients' brains (Figs. 1A and B, Supplementary Table 1). Since G9a is a KMT, we also evaluated H3K9me2, the repressive histone mark. Significantly higher H3K9me2 levels were found in human AD patients than in the ND group (Figs. 1A and C). Furthermore, as expected, the ratio of $A\beta_{42}/A\beta_{40}$ was significantly increased in AD patients in comparison with the human ND group (Figs. 1D and E). Of relevance, we also found a strong positive correlation between H3K9me2 levels and Aβ concentration in AD patients (Fig. 1F). Thus, the data reveal that high levels of H3K9me2 are correlated with increased levels of $A\beta_{42}/A\beta_{40}$ in human AD patients' brains, indicating the role of H3K9me2 in the neurodegenerative process of AD.

In *C. elegans* the putative methyltransferase that targets H3K9me2 is SET-25[55], which is homologous to the mammalian G9a protein (28.8% identity, 44.6% similarity)[56]. Thus, to evaluate the role of SET-25 in aging-related diseases, and more specifically in AD, we created the *set-25* knockdown (KD) using the RNAi approach in *C. elegans*. We used the CL2006 strain, which expresses human $A\beta_{1-42}$ under the control of a muscle-specific promoter, and also presents paralysis with age-worsening[57]. First, we confirmed that the gene expression of *set-25* was higher in the transgenic AD strain, CL2006, than in N2 (WT) (Fig. 1G). As expected, *set-25*-KD in CL2006 (*set-25* (RNAi) were almost completely reduced compared to the CL2006 Control group, and this finding is consistent with the observed reduction in H3K9me2 levels (Figs. 1H and I). Then, we examined the effect of *set-25*-KD on cognition in the CL2355 *C. elegans* strain. This strain expresses Aβ in neuronal cells and has a significantly lower chemotaxis index (CI), a memory parameter [57], than the Control strain, CL2122. It is worth noting that *set-25*-KD fostered the restoration of impaired learning and memory in the CL2355 strain, with a similar CI as in Control worms (Fig. 1K, Supplementary Fig. 2). Accordingly, CL2006 had reduced levels of *crh-1c*/cAMP-response element-binding protein (CREB)[58], which plays an important role in development, lifespan, and learning and memory in *C. elegans* and humans[59, 60] . In our study, increased gene expression of *crh-1c* was observed in the CL2006 (*set-25* (RNAi)) strain (Fig. 1J). Next, we showed a reduction in Aβ aggregation in CL2006 (*set-25* (RNAi)) relative to the CL2006 Control group (Figs. 1L and M), suggesting that *set-25* modulates memory formation by reducing AD pathology. Taken together, these results indicate G9a mediates increased H3K9me2 and cognitive impairment, participating in AD pathophysiology (Fig. 1N).

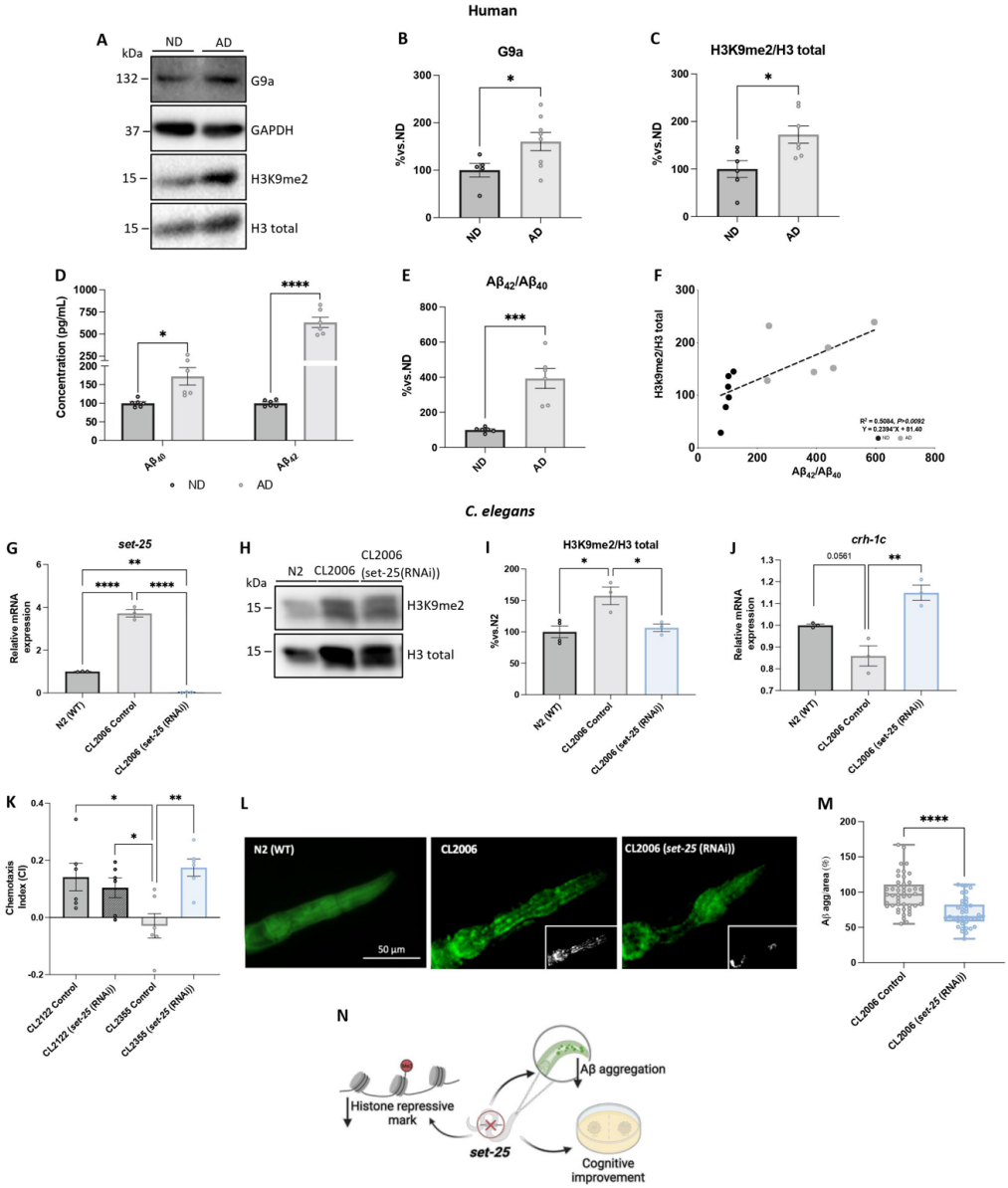

Figure 1. Overexpression of G9a in AD patients' brains and H3K9me2 in both AD patients' and *C. elegans* AD transgenic strains. (A) and **(B)** Representative WB, and quantification of G9a (EHMT2), and **(C)** for histone H3K9me2 in human patients' brains. **(D)** Levels of $A\beta_{40}$ and $A\beta_{42}$. **(E)** The ratio of $A\beta_{42}/A\beta_{40}$ by ELISA in human patients' brains. Values presented are mean ± SEM; (N = 2 groups (ND n = 6, and AD n = 8); Student's t-test; *p<0.05; ***p<0.001). **(F)** Correlation between $A\beta_{42}/A\beta_{40}$ ratio and H3K9me2 (slope = 0.07444). R^2 and p-values are indicated on graphs. **(G)** Representative gene expression of *set-25* in *C. elegans*.**(H)** and **(I)** Representative WB, and quantification of histone H3K9me2 in N2 (WT), CL2006, and CL2006 (*set-25* (RNAi)). **(J)** Representative gene expression of *chr-1c* in *C. elegans*. Gene expression levels were determined by real-time PCR. Values presented are the mean ± SEM; (N = 3 groups; N2 (WT) n = 3, CL2006 Control n = 3, and CL2006 (*set*-25 (RNAi)) n = 3; Each biological replicate with at least 350 worms in each group from whole petri dish); One-Way ANOVA and post-hoc Tukey's test; *p<0.05; **p<0.01; ****p<0.0001).**(K)** Chemotaxis index (CI) calculated for CL2122 (non Aβ strain), CL2355 neuronal Aβ strain), and (CL2355 (*set-25* (RNAi)). Values presented are CI mean ± SEM (N = 4 groups. CL2122 Control n = 5, CL2122 (*set*-25 (RNAi)) n = 6, CL2355 Control n = 6, and CL2355 (*set*-25 (RNAi)) n = 6; Each biological replicate with at least 200 worms for each analysis); (One-Way ANOVAand post-hoc Tukey's test; *p< 0.05; **p<0.01). **(L)** and **(M)** Representative images from each group and quantification of Thioflavin S-positive

particles in the head region of CL2006 strain and CL2006 (*set-25* (RNAi)) strain. Values presented are mean ± SEM (N = 2 groups; CL2006 Control n = 49; CL2006 (*set*-25 (RNAi)) n = 40; Student's t-test; ****$p<0.0001$). **(N)** Representative scheme of the outcomes found in *set-25*-KD. Source data are provided as a Source Data file.

Pharmacological G9a inhibition induced a transcriptional profile that allowed beneficial effects on cognitive performance.

To characterize the transcriptional profile associated with the pharmacological inhibition of G9a, we analyzed the transcriptome by RNA sequencing (RNA-seq) in the SAMP8 control and SAMP8 G9ai groups (Fig. 2A, Supplementary Table 7). Differential expression analysis identified 697 differentially expressed genes (DEG) (fold change cutoff of ≥ 1.3, p-value < 0.05), among which 217 were reduced, and 480 were increased in G9ai-treated SAMP8 mice (Fig. 2B).

Functional analysis showed that these DEGs regulate processes such as neuroactive ligand-receptor interactions, the calcium signaling pathway and the G−protein coupled receptor signaling pathway (Figs. 2C-E and H), all of which are important in regulating the function and plasticity of neural networks in the CNS[61]. Interestingly, we identified an increase in the expression of genes associated with the sensory perception of mechanical stimulus (Figs. 2F and H), which explains the beneficial effects on behavior and cognition induced by G9ai in the SAMP8 mice. On the other hand, we found a reduction in genes associated with the NF-κB signaling pathway (Fig. 2G), hinting that G9a inhibition could reduce neuroinflammation in the late-onset AD mouse model.

A more detailed analysis performed with Gene Set Enrichment Analysis (GSEA) showed enrichment of processes associated with sensory perception in SAMP8 mice treated with G9ai (Supplementary Figs. 3A). These processes include the sensory processing of sound, sensory perception of the light stimulus, and phototransduction of visible light (Supplementary Figs. 3A and B), supporting the idea that G9ai treatment in the SAMP8 model activates genes that promote beneficial effects on behavior and cognition. Interestingly, we found an increase in interleukin 37 (IL-37) signaling in G9ai-treated SAMP8 mice (Supplementary Figs. 3A and B). IL-37 is an anti-inflammatory cytokine that suppresses immune responses and inflammation in different tissues such as the brain[62]. Of note, we observed the enrichment of processes associated with chromatin methylation, such as the regulation of histone modification and H3K9 methylation (Supplementary Fig. 3), confirming the effect of G9ai on histone methylation status. To validate the RNA-seq, we performed RT-qPCR for some DEGs that are known to be associated with G9a and neurodegeneration, such as *synaptosomal-associated protein 25* (*Snap25*)[63], *T-box brain transcription factor 1* (*Tbr1*) [64], and *calcium/Calmodulin dependent protein kinase II gamma* (*Camk2g*) the expression of which was significantly reduced. Furthermore, significantly increased gene expression of *Gmfb* was found (Fig. 2I-L). Interestingly, this transcriptional enhancement of GMFB mediated by G9a inhibition has not been described previously. As mentioned earlier, GMFB is predominantly expressed in the CNS and plays an important role in neuroinflammation, leading to the overproduction of pro-inflammatory cytokines [30]. However, GMFB is a highly conserved brain-enriched protein implicated in neuroplasticity since a peak in these protein levels was correlated with learning and memory formation [65].

Taken together, these data suggest that treatment with G9ai induces a transcriptional profile that has beneficial effects on behavior and cognition.

H3K9me2 enrichment regulates pathways associated with the neuronal system after G9a inhibition.

We next sought to further characterize the dynamics of the histone mark H3K9me2 after treatment with a G9ai. We used public H3K9me2 ChIP-seq data corresponding to AML12 cells (murine hepatocyte cell line) treated with UNC0638, a selective G9ai[45] with the same specificity as UNC0642. Analysis of H3K9me2 enrichment revealed the presence of this histone mark in distal regions (60.78%) and promoters (13.65%) in cells treated with the G9ai (Fig. 3A). Furthermore, H3K9me2 has an enrichment around TSS (Fig. 3B), suggesting a role in transcriptional regulation.

Interestingly, functional analysis showed that H3K9me2 is enriched at promoters of genes associated with nervous tissue such as the neuronal system, transmission across chemical synapses, the neuroactive ligand−receptor interaction, positive regulation of neural precursor cell proliferation, and gamma-aminobutyric acid transport, among others (Figs. 3C and D). Figs. 3E-G shows the H3K9me2 enrichment in cells treated with G9ai compared to the control group treated with dimethyl sulfoxide (DMSO) in the genes *C-X-C motif chemokine ligand 10* (*Cxcl10*), *tumor necrosis factor-alpha* (*Tnf-α*), *heme oxygenase-1* (*Hmox-1*), *hyperpolarization activated cyclic nucleotide-gated potassium channel 1* (*Hcn1*), and *Gmfb.*

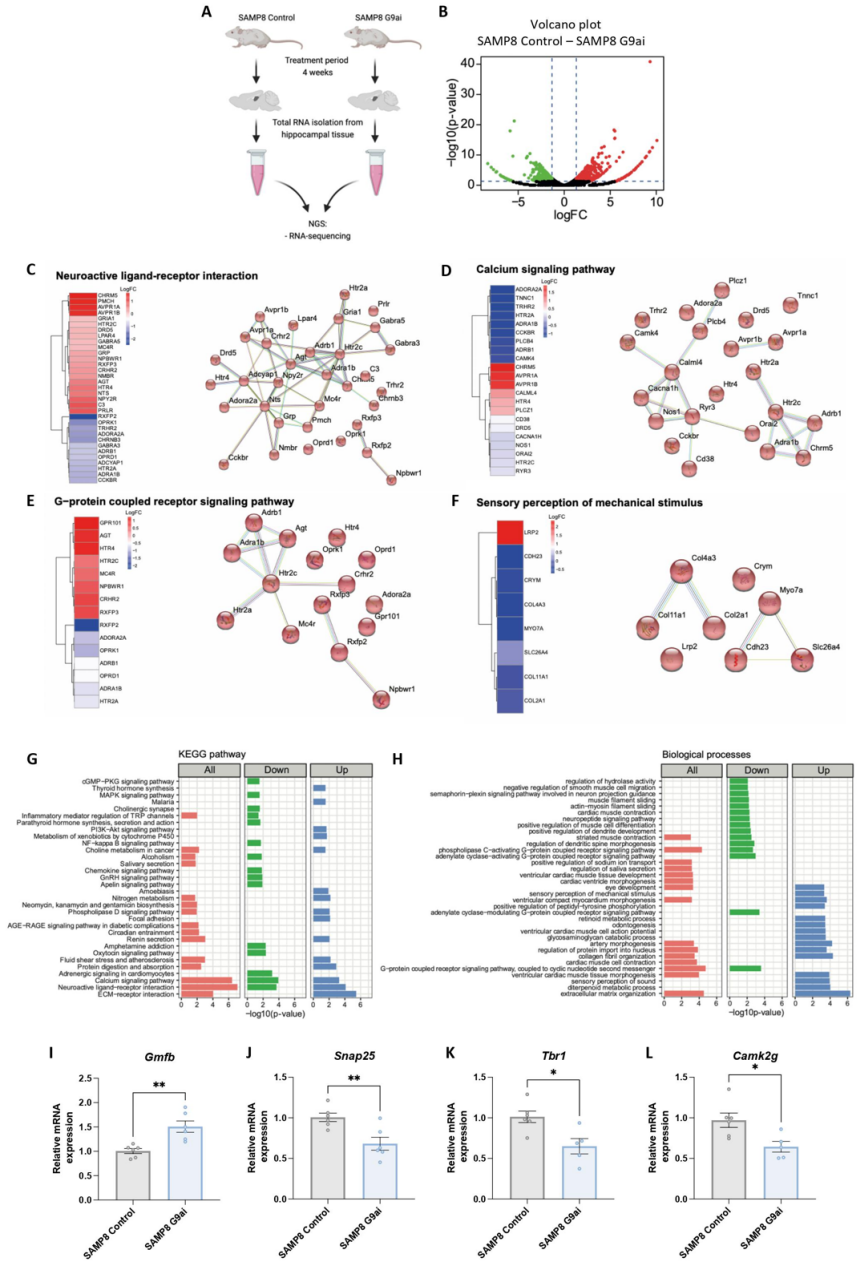

Figure 2. G9a inhibition treatment induced a transcriptional profile that confirmed its neuroprotective effects in the hippocampus of SAMP8 mice. (A) Treatment, hippocampal extraction, and RNA-sequencing in SAMP8 Control and SAMP8 G9ai. **(B)** Volcano plot showing the DEGs (fold change cutoff of ≥ 1.3, *p*-value < 0.05). Downregulated in green and upregulated in red. **(C)** Heatmaps and interaction network of genes associated with affected processes in G9ai-treated SAMP8 mice, such as the neuroactive ligand-receptor interaction. **(D)** Calcium signaling pathway. **(E)** G–protein coupled receptor signaling pathway. **(F)** Sensory perception of mechanical stimulus. The heatmaps show the logFC. **(G)** KEGG pathways regulated by SAMP8 G9ai. **(H)** Biological processes altered by DEGs in SAMP8 mice treated with G9ai (UNC0642, 5mg/Kg). **(I)** Gene expression levels of *Gmfb*, **(J)** *Snap25*, **(K)** *Tbr1,* and **(L)** *Camk2g*. Gene expression levels were determined by RT-qPCR. Values presented are the mean ± SEM; (N = 2 groups (SAMP8 Control n = 6, and SAMP8 G9ai (UNC0642, 5mg/Kg) n = 6); Student's t-test; **p*<0.05; ***p*<0.01). Source data are provided as a Source Data file.

The distribution of the transcription factor motifs relative revealed enrichment of binding motifs around TSS (Supplementary Fig. 5A, and Table 8). To evaluate which transcription factors are associated with H3K9me2, we performed a motif discovery analysis identifying motifs associated with *PR/SET Domain 6* (*Prdm6*), *cytoplasmic polyadenylation element binding protein 1* (*Cpeb1*), and *TATA-Box binding protein associated factor 1* (*Taf1*), among others (Supplementary Fig. 5B). Additionally, an ENCODE and ChEA Consensus TF analysis identified an association with *SUZ12 polycomb repressive complex 2 subunit* (*Suz12*), *enhancer of zeste 2 polycomb repressive complex 2 subunit* (*Ezh2*), *RE1 silencing transcription factor* (*Rest*) and SMAD family member 4 (*Smad4*) (Supplementary Fig. 5C), suggesting a regulatory network associated with transcriptional repression where G9a could be a central regulator (Supplementary Fig. 5D).

Previous results suggest that following G9ai treatment, the H3K9me2 could be reduced, allowing the gene expression. To address this hypothesis in human

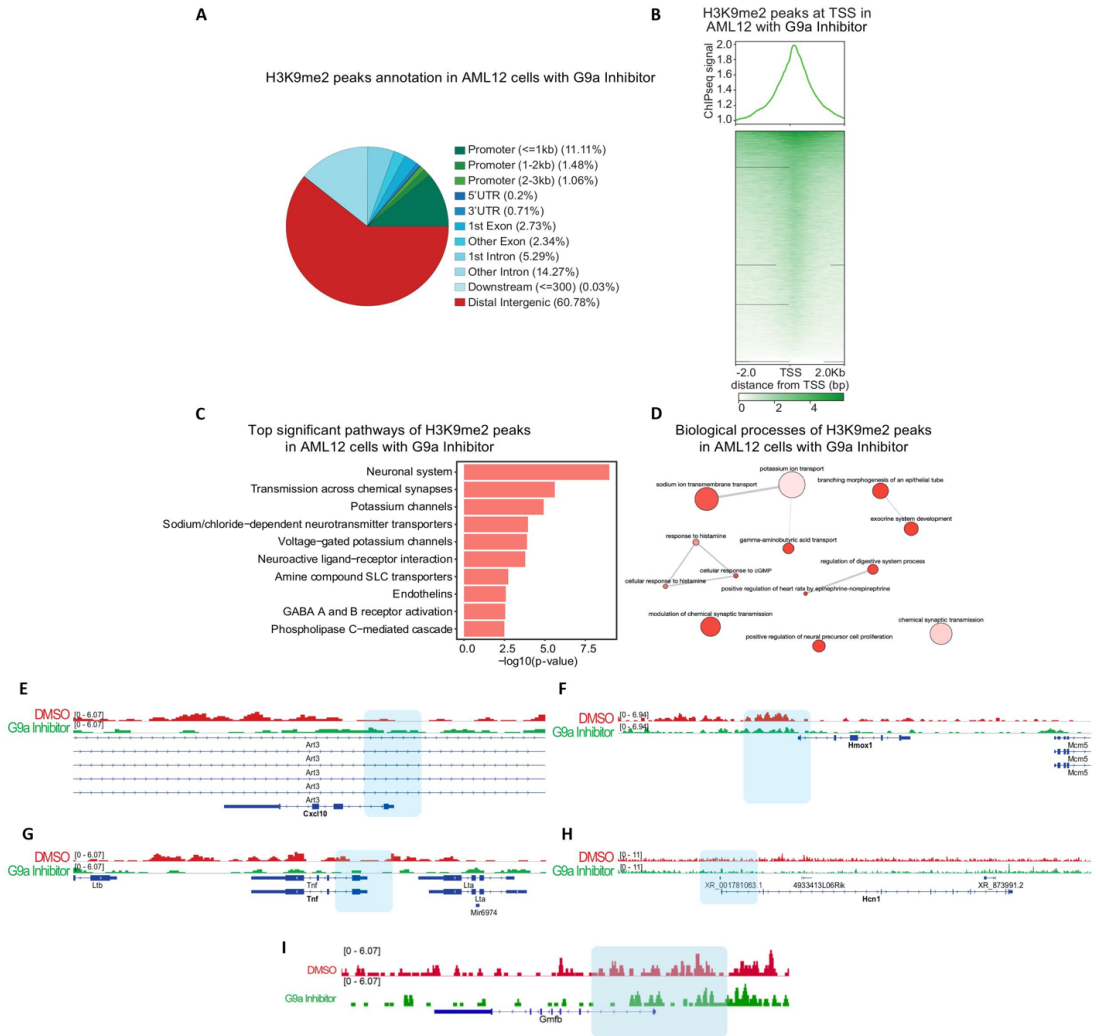

Figure 3. H3K9me2 enrichment in genes associated with the neuronal system after G9a modulation. (A) Genome region annotation of H3K9me2 peaks in AML12 cells treated with the G9ai (UNC0638). **(B)** Heatmap of H3K9me2 enrichment around the TSS regions of the mouse genome (mm10). **(C)** Pathways regulated by the H3K9me2 enriched genes in AML12 cells treated with G9ai. **(D)** Revigo visualization of biological processes analyzed by Gene Ontology (GO). **(E)-(I)** IGV tracks of H3K9me2 enrichment at the promoters of *Cxcl10, Hmox-1*, *Tnf-α*, *Hcn1*, and *Gmfb* in AML12 cells treated with G9ai and DMSO as a control. The blue area defines the promoters.

brain samples, we performed RT-qPCR for several genes, including *CXCL10, TNF-α*, *HMOX-1*, and *HCN1*, which were significantly altered in AD patients (Figs. 6A). Likewise, we evaluated *Cxcl10, Tnf-α,* and *Hmox-1* in G9ai-treated SAMP8 mice, and no changes were found in *Hcn-1* gene expression in the treated group relative to the Control group (Fig. 6B).

Notably, and consistent with our RNA-seq results, we found a reduction of H3K9me2 at TSS and gene body of GMFB after G9a inhibition (Figs. 2I and 3I). This could indicate that G9a inhibition could reduce the levels of the repressive mark H3K9me2 in the GMFB gene which could promote an increase in its expression. Together, these results demonstrate an H3K9me2 enrichment in genes associated with neural function, suggesting that after treatment with a G9ai, the H3K9me2 reduction could allow the expression of genes associated with the correct function of the CNS would be enhanced.

Pharmacological G9a inhibition leads to a reduction in H3K9me2 and AD hallmarks, restoring dendritic spine density in SAMP8 mice.

Because aging is the main risk factor for AD[66], we determined the G9a protein levels in the SAMP8 strain, a well-established AD model for investigating the key mechanisms of age-related cognitive decline with accelerated aging and generated through phenotypic selection from the AKR/J strain of mice[33, 34]. First, we examined protein levels by WB, including in Senescent-Accelerated Resistant 1 mice (SAMR1)[33], a normal aging control. G9a protein expression was higher in the SAMP8 Control group in comparison with the SAMR1 Control group (Figs. 4A and B). Likewise, significantly higher levels of H3K9me2 were only observed in the SAMP8 Control group compared to the SAMP8 mice treated with G9ai (Figs. 4C and D). Interestingly, our results showed a significant increase in $A\beta_{40}$ levels in the SAMR1 and SAMP8 G9ai groups compared to the SAMP8 group, whereas for $A\beta_{42}$ levels, the opposite was observed (Fig. 4E). Therefore, the high $A\beta_{42}/A\beta_{40}$ ratio levels in SAMP8 mice were reduced by G9a inhibition (Fig. 4F). Notably, we found a strong positive correlation between H3K9me2 levels and Aβ levels in SAMP8 mice (Fig. 4G). In agreement with AD patients' data (Fig. 1F), SAMP8 mice data suggest that high H3K9me2 is correlated with increased levels of Aβ in SAMP8, indicating a contribution of the G9a and H3K9me2 to the age-related cognitive decline presented by this AD rodent model.

Aβ levels are associated with behavioral abnormalities and cognitive decline, so we next performed behavioral studies to determine whether pharmacological G9a inhibition could revert them in SAMP8 mice. Firstly, we used the TCT to assess general sociability behavior in mice. In the sociability phase, in all mice groups, the presence of an intruder significantly increased the time spent in the intruder chamber instead of the empty cup chamber on all groups (Supplementary Fig. 7A). Remarkably, we only found a significant increase in the time spent sniffing the intruder mouse in the treated SAMP8 mice, confirming the improvement in social behavior after G9a inhibition (Fig. 4H). To evaluate their working and spatial memories, mice were assessed using the NORT and OLT tests, respectively. During the familiarization phase of the NORT task (Supplementary Fig. 7B) the exploration time was unchanged by G9ai treatment. The task results revealed that SAMP8 treated with G9ai exhibited a significant amelioration in cognitive deficits in both short- and long-term memories (Figs. 4I and J), relative to the SAMP8 Control mice group.

Regarding the OLT results, exploration during the habituation phase (Supplementary Fig. 7C) was unaffected by treatment. The task results showed that SAMP8 treated with G9ai exhibited an increase in the DI compared to the SAMP8 Control group (Fig. 4K), suggesting an improvement in spatial memory. Finally, the polygonal graph depicts differences among SAMR1 and SAMP8 Control, and treated SAMP8 groups in several TCT parameters, the DI of NORT and OLT, and the molecular ratios of H3K9me2 and $A\beta_{42}/A\beta_{40}$ (Fig. 4L). In addition, SAMP8 showed a decrease in the number of neuronal intersections compared to the SAMR1 group. However, this was reverted after G9ai treatment in SAMP8, and this increase was most apparent at intermediate and more distal distances from the soma in a Sholl analysis (Figs. 4M and N). Besides, SAMP8 is known pathologically to present a reduction in neuronal spine density[67]. Accordingly, we found a significant increase in spine density in the brains of SAMP8 mice treated with G9ai, as well as in the SAMR1 group, compared to the SAMP8 Control group, showing the potential of G9a inhibition for improving neuronal plasticity (Figs. 4O and P). This data suggests that G9a inhibition promotes beneficial effects on behavior and cognition.

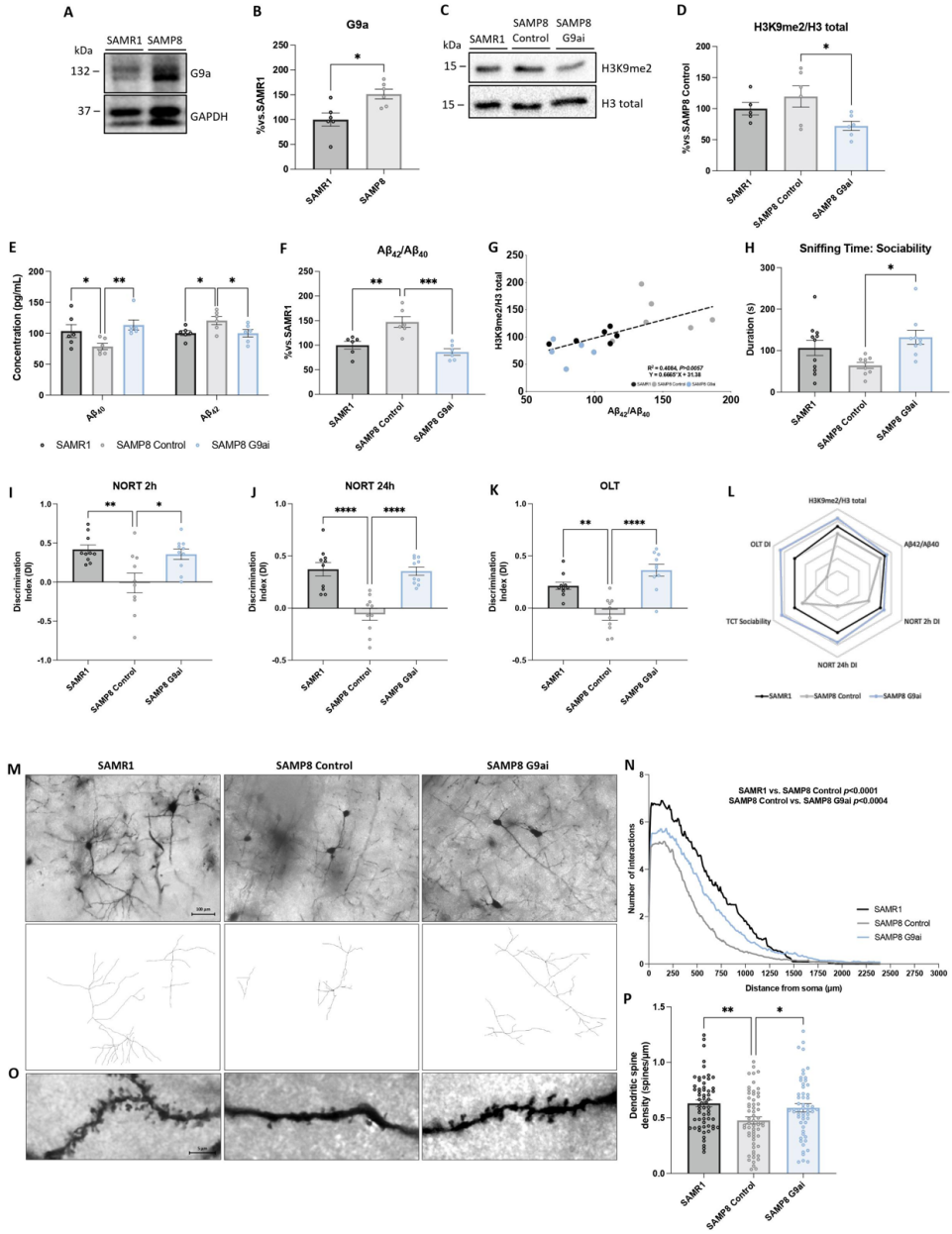

Figure 4. Pharmacological G9a inhibition leads to a reduction in H3K9me2 and AD hallmarks, restoring dendritic spine density in SAMP8 mice. (A) and **(B)** Representative WB, and quantification of G9a in the hippocampus of SAMR1 and SAMP8 mice. **(C)** and **(D)** Representative WB, and quantification of H3K9me2 in SAMR1, SAMP8 and SAMP8 mice treated with G9ai. **(E)** Levels of Aβ40 and Aβ42. **(F)** Ratio of Aβ42/Aβ40 by ELISA. Values presented are mean ± SEM; (N = 3 groups (SAMR1 n = 6, SAMP8 Control n = 6, and SAMP8 G9ai (UNC0642, 5mg/Kg) n = 6); Parametric tests: Student's t-test analysis, or One-Way ANOVA and post-hoc Tukey's test, Non-parametric tests: Mann-Whitney test, or Kruskal-Wallis and post-hoc Dunn's test; *p<0.05; **p<0.01; ***p<0.001). **(G)** Correlation between Aβ42/Aβ40 ratio and H3K9me2 (slope = 0.2071). R2 and p-values are indicated on graphs. For TCT: **(H)** Sniffing time: sociability with the intruder animal. For NORT: **(I)** Short-term memory evaluation after 2 h, and **(J)** long-term evaluation after 24 h in the acquisition trial by Discrimination Index (DI) after exposure of SAMR1, SAMP8 and SAMP8 mice G9ai to novel objects. For OLT: **(K)** OLT evaluation by DI after changing the location of one object. Values presented are the mean ± SEM; (N = 3 groups (SAMR1 n = 10, SAMP8 Control n = 10, and SAMP8 G9ai (UNC0642, 5mg/Kg) n = 10); One-Way ANOVA and post-hoc Tukey's test; *p<0.05; **p<0.01; ***p<0.001; ****p<0.0001).

(L) The polygonal graph presents complete parameters obtained by TCT, NORT, WB and ELISA. **(M)** Representative images and tracings of Golgi-stained neurons from the different experimental groups (scale bar = 100 μm). **(N)** Number of neuronal intersections. Values presented are the mean ± SEM; (N = 3 groups (SAMR1 n = 89, SAMP8 Control n = 98, and SAMP8 G9ai (UNC0642, 5mg/Kg) n = 100); Kruskal-Wallis and post-hoc Dunn's test; *p*-values represented in the graph). **(O)** Representative images of the spine density of the different experimental groups by Golgi staining. **(P)** Spine density quantification of neurons. Values presented are the mean ± SEM; (N = 3 groups; SAMR1 n= 60, SAMP8 Control n = 60, and SAMP8 G9ai (UNC0642, 5mg/Kg) n = 56 dendrites (of different neurons) were analyzed from 6 mice per group; One-Way ANOVA and post-hoc Tukey's test; **p*<0.05; ***p*<0.01). Source data are provided as a Source Data file. Data information: Note that experiments in Figs 4N and 5N, and 4P and 5P were performed at the same time, so the values of SAMR1 and SAMP8 Control are the same but the figures have been split in two for the sake of linearity.

G9a inhibition increased the GMFB transduction pathway, which in turn mediated the neuroprotective effects in SAMP8 mice.

GMFB is implicated in neuronal plasticity. Thus, to further confirm GMFB pathway activation after G9a inhibition in SAMP8, we examined GMFB protein levels and the downstream effector proteins using WB. Strikingly, a significant increase in GMFB was observed in SAMP8 mice treated with G9ai (UNC0642, 5mg/Kg) in comparison with the SAMP8 Control mice (Figs. 5A and B). Furthermore, as GMFB is an enhancer of p38[68] that plays important roles in synaptic plasticity[69], we evaluated the p-p38/p38 ratio and CREB protein levels. A significant increase in p-p38 protein levels was found in the SAMP8 mice treated with G9ai (Figs. 5A and C). Likewise, the p-CREB/CREB ratio was also augmented but did not differ significantly between groups (Figs. 5A and D). Finally, we also evaluated the protein levels of BDNF and its receptor, tropomyosin-related kinase B (TrkB).

Regarding the ratio of protein levels of p-TrkB/TrkB**,** we observed a significant increase in treated SAMP8 mice compared to the SAMP8 Control group (Supplementary Figs. 8A and B). Accordingly, an increase in BDNF protein levels was found in the SAMP8 G9ai mice (Figs. 5A and E, Supplementary Fig. 8C). These findings suggest, for the first time, that G9a inhibition promotes neuronal plasticity through modulation of the GMFB molecular pathway (Fig. 5F). Thus, to demonstrate that GMFB mediates the neuroprotective effects promoted by G9ai, we evaluated cognition, neuronal plasticity and neuroinflammation status after dual treatment with GMFB and G9a inhibitors in SAMP8 mice. First, we evaluated the effect of GMFB inhibitor (GMFBi) and dual treatment on behavior and cognitive impairment. In TCT, social interaction was significantly decreased in treated SAMP8 group, as it was in the SAMP8 Control group compared to the SAMR1 Control group (Fig. 5G, Supplementary Fig. 9A). Similarly, the DI of short- or long-term memory was lower in GMFBi-treated groups (Figs. 5H and E, Supplementary Fig. 9B). Correspondingly, GMFBi-treated showed a decrease in OLT DI compared to the SAMR1 Control group (Fig. 5J, Supplementary Fig. 9C).

Moreover, since we had previously found that GMFB orchestrated the enhancement of synaptic plasticity by increasing p-p38, this marker was also evaluated. We found a reduction in p-p38/p38 levels in the SAMP8 Control group and the GMFBi-treated groups (Figs. 5K and L). Last but not least, dendritic spine length (Figs. 5M and N) and density length (Figs. 5O and P) in the brain of GMFBi-treated and dual-treated mice showed a similar profile to the SAMP8 group, presenting lower levels compared to the SAMR1 group in both quantifications.

G9a inhibition ameliorated neuroinflammation, modulating the NF-kB signaling pathway via GMFB.

We have previously shown an increased neuro-inflammatory process in SAMP8 [70]. Interestingly, GMFB may also modulate neuroinflammation via the extracellular signal-regulated kinase (ERK) and nuclear factor kappa B (NF-κB) axis [32]. Of note, the RNA-seq showed a reduction in the activity of the NF-κB signaling pathway (Fig. 3G) and an increase in the anti-inflammatory cytokine *Il-37* in G9ai-treated SAMP8 mice (Supplementary Figs. 4A and B), which suggests that treatment with G9ai could reduce the levels of neuroinflammation in the SAMP8 model. To demonstrate this, we evaluated neuroinflammation status after G9ai treatment. NF-κB is a transcription factor related to the inflammatory response and a master commander in the expression of pro-inflammatory genes, and its signaling is an important mediator of brain inflammation in AD[71]. To investigate the activation levels of NF-κB in the treated SAMP8 mice, we first evaluated the levels of ERK protein, which plays a critical role by inducing NF-κB expression. Strikingly, a significant reduction in the ratio of p-ERK/ERK ratio was found in G9ai-treated SAMP8 mice (Figs. 6A and B), correlating with the ratio of p-NF-κB/ NF-κB protein levels (Figs. 6A and C). Next, we assessed the gene expression of some pro-inflammatory NF-κB targets, such as *interleukin-6 (Il-6), Cxcl10*, and

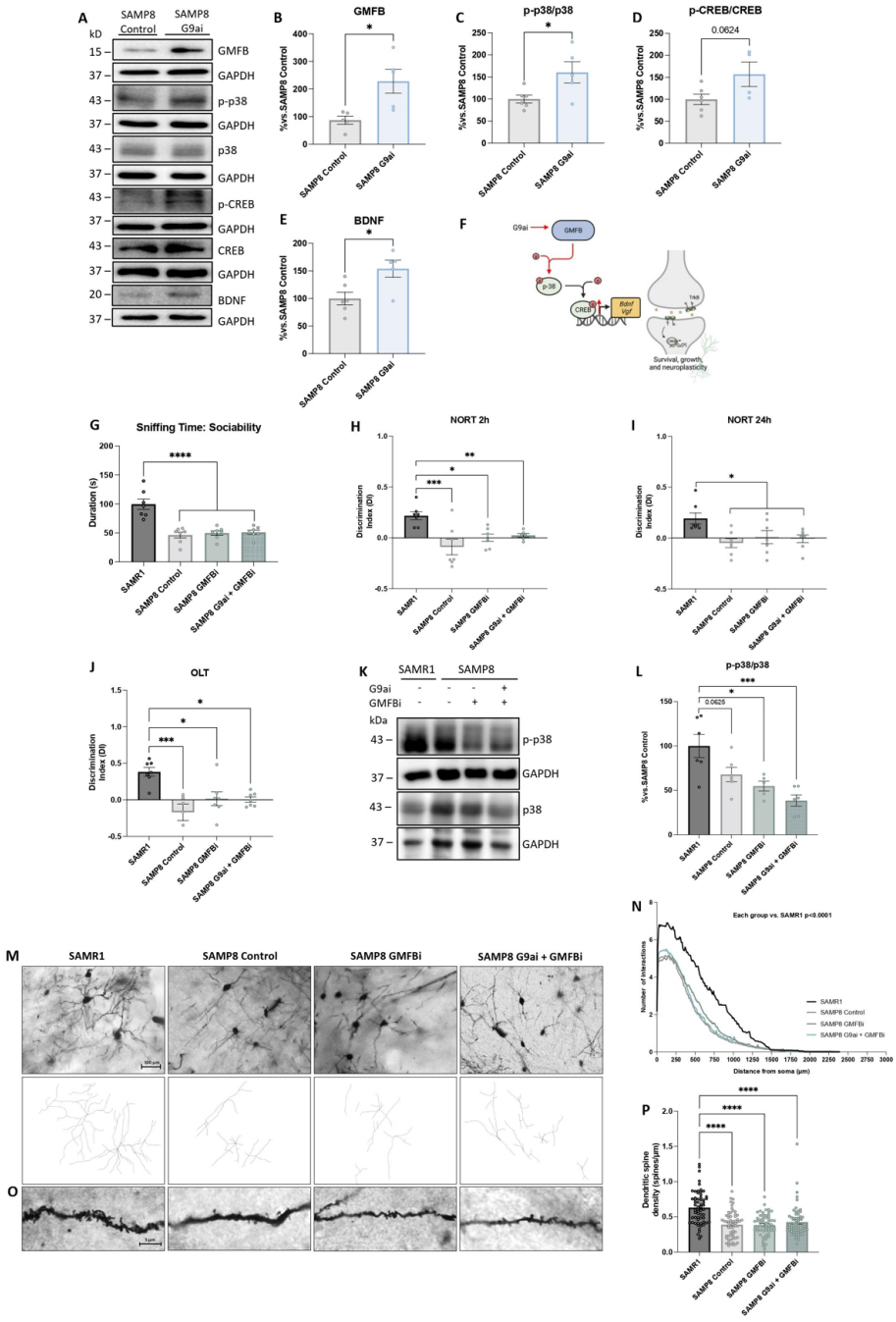

Figure 5. G9a inhibition increased the GMFB transduction pathway, which in turn mediated the neuroprotective effects in SAMP8 mice. (A) and **(B)-(E).** Representative WB, and quantifications of GMFB, the p-p38/p38 ratio, the p-CREB/CREB ratio and BDNF. Values presented are the mean ± SEM; (N = 2 groups (SAMP8 Control n = 6, SAMP8 G9ai (UNC0642, 5mg/Kg) n = 6); Student's t-test analysis; *p<0.05; ***p<0.001). **(F)** Representative scheme of the GMFB molecular signaling modulated after G9ai treatment in SAMP8. For TCT: **(G)** sniffing time: sociability with the intruder animal. For NORT: **(H)** Short-term memory evaluation after 2 h and **(I)** long-term evaluation after 24 h in the acquisition trial by DI after exposure to novel objects. For OLT: **(J)** OLT evaluation by DI after changing the location of one object. **(K)** and **(L)** Representative WB, and quantification of p-p38/p38 protein

levels. Values presented are the mean ± SEM; (N = 4 groups (SAMR1 n = 6-7, SAMP8 Control n = 6-7, SAMP8 GMFBi ((1H-Indazol-4-yl)methanol, 12mg/Kg) n= 6-7, and SAMP8 G9ai (UNC0642, 5mg/Kg) + GMFBi ((1H-Indazol-4-yl)methanol, 12mg/Kg) n = 6-7; Parametric test: One-Way ANOVA and post-hoc Tukey's test; Non-parametric test: Kruskal-Wallis and post-hoc Dunn's test; *p<0.05; **p<0.01; ***p<0.001; ****p<0.0001). **(M)** Representative images and tracings of Golgi-stained neurons (scale bar = 100 µm). **(N)** Reduction in the number of neuronal intersections of the SAMP8 control group and both GMFBi treatments compared to the SAMR1 control group. Values presented are the mean ± SEM; (N = 4 groups (SAMR1 n = 89, SAMP8 Control n = 98, SAMP8 GMFBi ((1H-Indazol-4-yl)methanol, 12mg/Kg) n = 93, and SAMP8 G9ai (UNC0642, 5mg/Kg) + GMFBi ((1H-Indazol-4-yl)methanol, 12mg/Kg) n = 99; One-Way ANOVA and post-hoc Tukey's test). **(O)** Representative images of the spine density by Golgi staining. **(P)** Spine density quantification of neurons. Values presented are the mean ± SEM; (N = 4 groups; SAMR1 n = 60, SAMP8 Control n = 60, SAMP8 GMFBi ((1H-Indazol-4-yl)methanol, 12mg/Kg) n = 60, and SAMP8 G9ai (UNC0642, 5mg/Kg) + GMFBi ((1H-Indazol-4-yl)methanol, 12mg/Kg) n = 60 (of different neurons) were analyzed from 6 mice per group; Kruskal-Wallis and post-hoc Dunn's test ****p<0.0001). Source data are provided as a Source Data file. Data information: Note that experiments in Figs 4N and 5N, and 4P and 5P were performed at the same time, so the values of SAMR1 and SAMP8 Control are the same but the figures have been split in two for the sake of linearity.

Tnf-α. Significantly lower expression of these pro-inflammatory genes was observed in G9ai-treated SAMP8 mice relative to the SAMP8 mice group (Fig. 6D). Additionally, a GSEA analysis demonstrated a reduction in the enrichment of genes associated with the neuroinflammatory response in G9ai-treated SAMP8 mice (Fig. 6E).

Analysis of cell death in a primary mixed culture of neurons and microglia from the cortex and striatum revealed that pretreatment with G9ai significantly decreased cell death after activation with lipopoly-saccharide (LPS) and interferon-gamma (IFN-γ) from the cortex and striatum (Fig. 6F and G). Thus, LPS and IFN-γ induced microglial activation, detected as an increase in fluorescence after one week of treatment. Interestingly, G9ai pretreatment blocked this effect (Figs. 6H-M). Taken together, these data suggest that G9ai treatment enhances neuroinflammation, possibly via GMFB orchestrating transcriptional changes in the NF-κB signaling pathway (Fig. 6N). Our results showed that G9ai treatment was able to reduce these inflammatory markers mainly in pathological conditions (LPS), and thus, we wondered whether GMFB plays an important role in this modulation.

Notably, GMFB is an enhancer of p38, and also orchestrated a reduction in inflammation through the ERK pathway[68, 72]. We thus analyzed cell death by treating cells with a GMFBi, and the combination of a G9ai and a GMFBi. Under normal conditions, no difference was observed between the treated groups and the Control group. However, under LPS exposure, cell survival in those groups treated with a GMFBi was reduced in the same way as in the Control group, the G9ai-treated group being the only one with a significant increase in survival (Fig. 6O). On the other hand, GMFBi treatment increased p-ERK/ERK levels (Figs. 6P and Q). Further investigation of the role of GMFB led us to evaluate the levels of *Il-6* as a pro-inflammatory marker, and an increased in its gene expression levels was observed in the SAMP8 GMFBi group, in the SAMP8 dual treatment group and in the

SAMP8 Control group, relative to the SAMR1 group (Fig. 6R). Therefore, we demonstrated that GMFB modulates changes in the neuroinflammation status after G9a inhibition.

GMFB is methylated by G9a triggering neurodegeneration.

We generated an exogenous G9a construct to perform the co-immunoprecipitation assay. Either empty vector or a Flag-tagged human G9a construct were transfected into HEK 293T cells. The interaction of G9a and GMFB was detected in the Flag-G9a-transfected sample but not in the Control sample (Fig. 7A). Therefore, as G9a can interact with GMFB, and inhibition of G9a affects GMFB functions, we speculate that G9a might methylate GMFB directly. To test this hypothesis, we first examined whether GMFB could be methylated in cells. HA-tagged GMFB was transfected into HEK 293T cells, and protein was enriched by immunoprecipitation using anti-HA antibody. As expected, methylated forms of GMFB were observed using the anti-pan methyl lysine antibody, recognizing both mono and dimethyl substrates (Fig. 7B). To determine whether G9a is the methyltransferase responsible for GMFB methylation, two approaches were utilized. A G9ai (BIX01294, 10 µM) was added to HEK 293T cells that express HA-GMFB and incubated for 3 days. Upon drug incubation, we observed lower levels of methylated GMFB compared with that in DMSO-treated cells (Fig. 7C). Consistently, G9a knockout (KO) also significantly reduced the methylated levels of GMFB compared with that of WT cells (Fig. 7D).

To further identify the potential methylation sites of GMFB by G9a, we first search a consensus methylation site encompassing RK/ARK, which has been indicated to

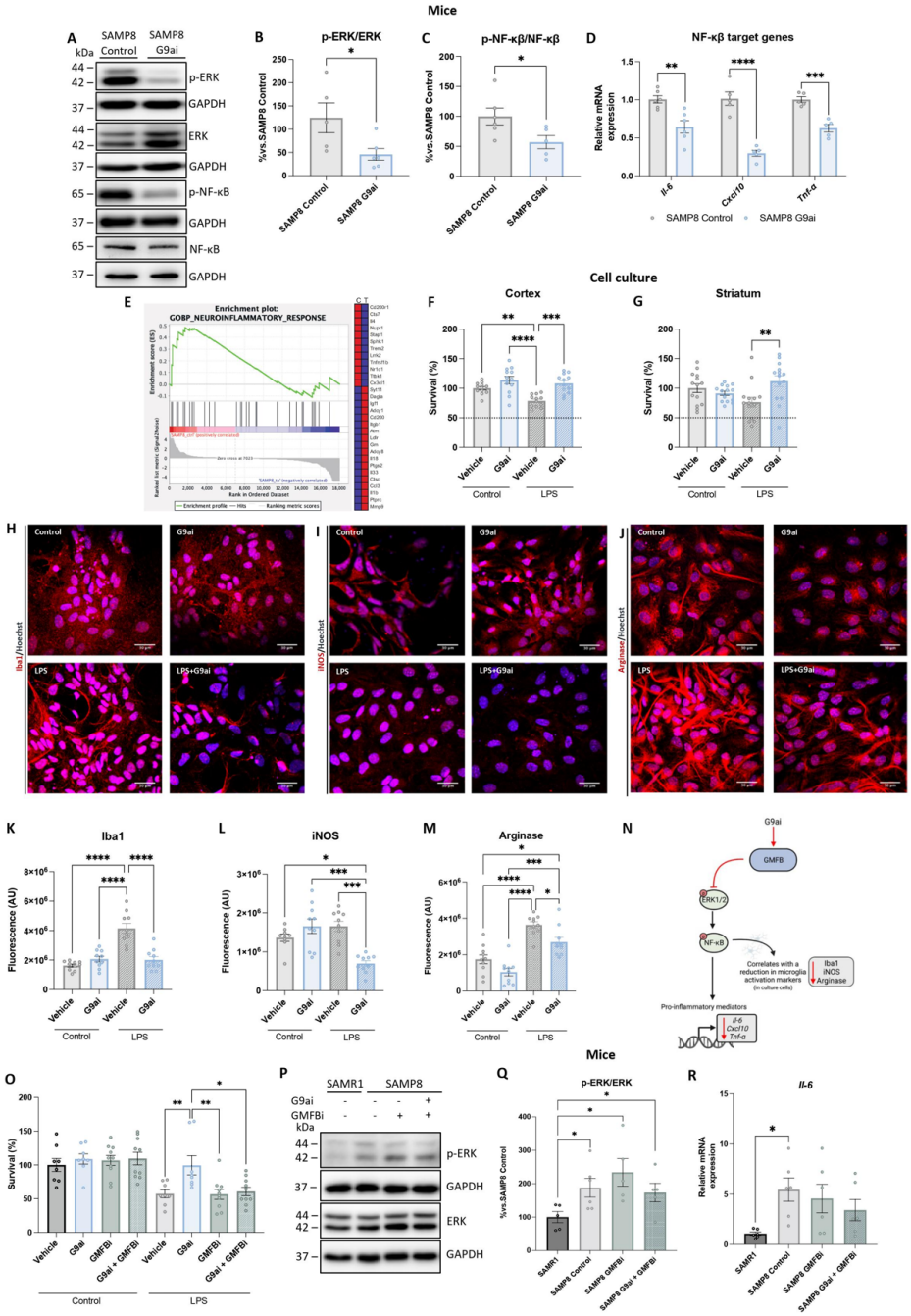

Figure 6. G9ai treatment reduced the inflammatory markers through the modulation of the NF-κB molecular pathway by GMFB. (A) and **(B)-(C)** Representative WB, and quantification of p-ERK/ERK, and NF-κB protein levels in SAMP8 mice. **(D)** Representative gene expression of pro-inflammatory markers of *Il-6, Cxcl10,* and *Tnf-α***.** Gene expression levels were determined by real-time PCR. Values represented are the mean ± SEM; (N = 2 groups (SAMP8 control n = 6, SAMP8 G9ai (UNC0642, 5mg/Kg) n = 6)); Student's t-test analysis; **p<0.01; ***p<0.001; ****p<0.0001). **(E)** GSEA plot of neuroinflammatory response up-regulated in SAMP8 control. **(F)** Neuronal viability of primary mixed culture of neurons and microglia from to cortex and **(G)** striatum stimulated with G9ai (UNC0642, 1 μM) or vehicle, and subsequently treated every 48 h with 1 mM LPS and 200 U/mL IFN-γ for 2 weeks. Values

represented are the mean ± SEM; (N= 4 groups (Control Vehicle n = 12 ; Control G9ai n = 12; LPS Vehicle n = 12; LPS G9ai n = 12)); Two-Way ANOVA and post-hoc Tukey's test; **p<0.01; ***p<0.001; ****p<0.0001). **(H)** and **(K)** IHC of Iba1, **(I)** and **(L)** iNOS, **(J)** and **(M)** Arginase were performed in mice microglial primary cultures treated or not with G9ai (UNC0642, 1 μM). The confocal microscopy images are shown (superimposed sections) in which Iba1, iNOS and Arginase appear as red over Hoechst-stained nuclei. Scale bars = 30 μm. The bars graph shows the number of the red dots/cell (r). The cell nuclei were stained with Hoechst (blue) in all cases. Values presented are the mean ± SEM; (N= 4 groups (Control Vehicle n = 9-10 ; Control G9ai n = 10; LPS Vehicle n = 10; LPS G9ai n = 10)); One-Way ANOVA and post-hoc Tukey's test; *p< 0.05; ***p<0.001; ****p<0.0001). **(N)** Representative scheme of the proposed neuroinflammatory pathway modulated after G9ai treatment in SAMP8. **(O)** Neuronal viability was quantified in primary mixed culture of neurons and microglia was stimulated with GMFBi ((1H-Indazol-4-yl)methanol, 0.67μM) or G9ai (UNC642, 1μM) + GMFBi ((1H-Indazol-4-yl)methanol, 0.67μM), and subsequently treated every 48 h with 1 mM LPS and 200 U/mL IFN-γ for 2 weeks; Values presented are the mean ± SEM; (N = 8 groups (Control Vehicle n = 8; Control G9ai n = 8; Control GMFBi n = 10, Control G9ai + GMFBi n = 10, LPS Vehicle n = 8, LPS G9ai n = 8, LPS GMFBi n = 10, and LPS G9ai + GMFBi n = 10; Kruskal-Wallis and post-hoc Dunn's test; and Mann-Whitney test;*p<0.05; **p<0.001). **(P)** and **(Q)** Representative WB, and quantification of p-ERK/ERK protein levels. **(R)** Representative gene expression of pro-inflammatory markers for *Il-6*. Gene expression levels were determined by real-time PCR. Values presented are the mean ± SEM; (N = 4 groups (SAMR1 n = 5-6, SAMP8 Control n = 6, SAMP8 GMFBi ((1H-Indazol-4-yl)methanol, 12mg/Kg) n = 5-6, and SAMP8 G9ai (UNC0642, 5mg/Kg) + GMFBi ((1H-Indazol-4-yl)methanol, 12mg/Kg) n = 6); One-Way ANOVA and post-hoc Tukey's test*p<0.05). Source data are provided as a Source Data file. Data information: Note that experiments in Supplementary Fig. 6B and Fig. 6D were performed at the same time, so the values regarding gene expression of *Cxcl10* and *Tnf-α* are the same but the figures have been split in two for the sake of linearity.

be a preferred target by G9a [13]. The GPS-MSP method was used to predict all possible methylation sites in GMFB (Fig. 7E, Supplementary Table 9) [73, 74]. In fact, only two proposed residues of GMFB potentially fit the above criteria to be targeted by G9a: Lys20 (K20) and Lys25 (K25) (Fig. 7F). To validate whether they can be methylated by G9a, HA-tagged constructs bearing either a single lysine-to-arginine (K20R, K25R) mutation or double mutations (K20RK25R, referred as 2KR) were generated, and their methylation status by G9a were examined by immunoprecipitation of HA-GMFB followed by WB with anti-pan methyl antibody in HEK 293T cells. Interestingly, we noticed that either K20R, K25R or 2KR mutant significantly reduced methylation levels of GMFB, compared with that of WT construct (Fig. 7G). The methylation signals were specific, as overexpression of empty vectors in cells did not detect any methylated bands (Fig. 7G). Of note, the remaining methylation level of 2KR mutant suggested that there may exist other methylation sites. Nevertheless, we found that K20R and K25R are the two main sites methylated by G9a.

We next sought to investigate the neuroprotective effect of pharmacological G9a inhibition on GMFB binding sites by evaluating cell survival upon LPS exposure in the different cell lines generated. On the one hand, we observed that when we KD K20R in HEK 293T cells, cell viability was only restored after LPS in the G9ai treated group (Fig. 7H). In contrast, the vehicle group as well as the GMFBi treated group did not show any improvement in cell viability, and even exhibited levels similar to those of the vehicle group of control cells. As expected, the group with both treatments showed no cytoprotective effect (Fig. 7H). On the other hand, when K25 of GMFB was mutated in R in the cells, both in the vehicle group and in the G9ai-treated group, a recovery of cell viability was observed upon LPS exposure (Fig.7I). All together these results agreed with the levels observed in the double-mutated cells (2KR) (Fig. 7J). In conclusion, these findings suggest that the neurodegenerative role of G9a as a GMFB suppressor would mainly rely on methylation of the K25 position of GMFB, and thus its pharmacological inhibition removes this methylation promoting neuroprotective effects. Nevertheless, methylation at the K20R position of GMFB by G9a is thought to play a secondary role in the neuroprotective effect.

It is also relevant to note that the activation of GMFB depends on protein kinase A (PKA). GMFB phosphorylated by PKA enhances p-38 activity (almost 60-folds) and inhibits ERK1/ERK2 (IC_{50} = 3 nM) [68, 75, 76]. Interestingly, the consensus motif in PKA substrates (96%) is [R/K][R/K/X]X[S/T][77] and the sequence analysis of GMFB shows that the motif only fits LRKFRFRK25ET27 sequence where the PKA phosphorylation site (T27) is neighboring to G9a methylation site (K25). Moreover, it has been reported before [78] that methylated lysine interferes with the subsequent phosphorylation of GMFB by PKA. Therefore, GMFB gets phosphorylated by PKA under G9a inhibition to activate and perform its subsequent functions (Fig. 7K).

Finally, to demonstrate the potential effects of G9a on GMFB, we generated a KD of *Y50D7A.10* (ortholog of human *Gmfb*) in CL2355 *C. elegans* strain, using the RNAi approach. As expected, our results showed that CL2355 (*set-25*; *Y50D7A.10* (RNAi)) and CL2355 (*Y50D7A.10* (RNAi)) were not able to restore impaired learning and memory (Fig. 7L, Supplementary Fig. 10). In addition, we showed that the single or double KD of

Y50D7A.10 in the CL2006 *C. elegans* strain failed to reduce Aβ aggregation when compared to the CL2006 Control group (Figs. 7M and N). According to the above results in mice, we also evaluated the potential effects of

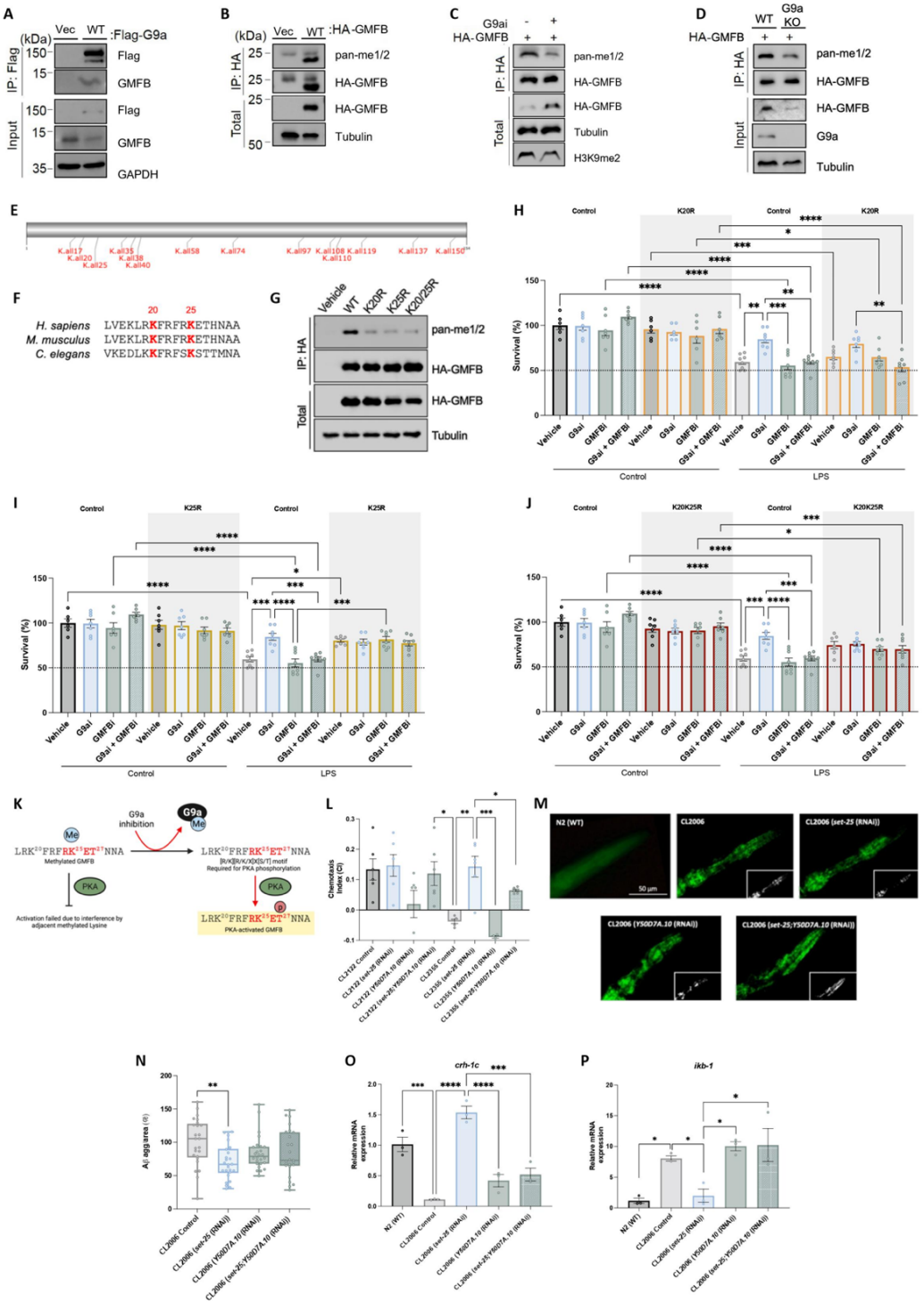

Figure 7. GMFB is lysine methylated by G9a triggering neurodegeneration. (A) Co-IP assay was performed to show that Flag-G9a interacts with GMFB in HEK 293T cells. **(B)** GMFB is capable of being methylated. WB was performed to examine the methylation state of GMFB in HEK 293T cells. **(C)** Inhibition of G9a decreased methylated level of GMFB. **(D)** G9a-KO decreased methylated level of GMFB. **(E)** Predictive lysine methylation sites in GMFB by GSP-MSP method. **(F)** Sequence alignment of human GMFB with selected homologs. **(G)** Methylation state of the different GMFB sites by G9a in the generated HEK 293T cell lines (K20R, K25R, and 2KR mutants). **(H)** Neuronal viability of K20R-KD, **(I)** K25R-KD, and **(J)** 2KR-KD HEK 293T cells with G9ai (UNC0642, 1 μM), GMFBi ((1H-Indazol-4-yl)methanol, 0.67μM), G9ai + GMFBi, or vehicle, and subsequently treated every 48 h with 1 mM LPS (N = 32 groups (Control Vehicle n = 6, Control G9ai n= 7, Control GMFBi n = 6, Control G9ai + GMFBi n = 6, LPS Vehicle n = 8; LPS G9ai n = 8; LPS GMFBi n = 8; LPS G9ai + GMFBi n =8, Control Vehicle K20R-KD n = 6, Control G9ai K20R-KD n = 6, Control GMFBi K20R-KD n = 6, Control G9ai + GMFBi K20R-KD n = 6, LPS Vehicle K20R-KD n = 8; LPS G9ai K20R-KD n = 8, LPS GMFBi K20R-KD n = 8, LPS G9ai + GMFBi K20R-KD n = 8, Control Vehicle K25R-KD n = 6, Control G9ai K25R-KD n = 6, Control GMFBi K25R-KD n = 6, Control G9ai + GMFBi K25R-KD n = 6, LPS Vehicle K25R-KD n = 7, LPS G9ai K25R-KD n = 7, LPS GMFBi K25R-KD n = 8, LPS G9ai + GMFBi K25R-KD n = 8, Control Vehicle K20RK25R-KD n = 6, Control G9ai K20RK25R-KD n = 6, Control GMFBi K20RK25R-KD n = 6, Control G9ai + GMFBi K20RK25R-KD n = 6, LPS Vehicle K20RK25R-KD n = 7, LPS G9ai K20RK25R-KD n = 8, LPS GMFBi K20RK25R-KD n = 8, and LPS G9ai + GMFBi K20RK25R-KD n = 8); Two-Way ANOVA and post-hoc Tukey's test; *p<0.05; **p<0.01;***p<0.001; ****p<0.0001). **(K)** Representative scheme of the hypothesis proposed for the activation of the GMFB. **(L)** CI calculated for CL2122 (non Aβ strain), CL2355 (neuronal Aβ strain), and double and/or single mutant in CL2355 and CL2122. Values presented are CI mean ± SEM; (N = 8 groups (CL2122 Control n = 6, CL2122 (*set-25* (RNAi)) n = 6, CL2122 (*Y50D7A.10* (RNAi)) n = 4, CL2122 (*set-25;Y50D7A.10* (RNAi)) n = 6, CL2355 Control n = 5, CL2355 (*set-25* (RNAi)) n =6, CL2355 (*Y50D7A.10* (RNAi)) n = 5, and CL2355 (*set-25;Y50D7A.10* (RNAi)) n = 6); Each biological replicates with at least 200 worms for each analysis; One-Way ANOVA and post-hoc Tukey's test; *p<0.05; **p<0.01). **(M)** and **(N)** Representative images from each group and quantification of Thioflavin S-positive particles in the head region of CL2006 Control, CL2006 (*set-25* (RNAi)), CL2006 (*Y50D7A.10* (RNAi)) and CL2006 (*set-25;Y50D7A.10* (RNAi)). Values presented are the mean ± SEM. (N = 4 groups (CL2006 Control n = 25, CL2006 (*set-25* (RNAi)) n = 26, CL2006 (*Y50D7A.10* (RNAi)) n = 26, CL2006 (*set-25;Y50D7A.10* (RNAi)) n = 25); Kruskal-Wallis and post-hoc Dunn's test; **p<0.01). **(O)** and **(P)** Representative gene expression of chr-1c, and ikb-1 in C. elegans. Gene expression levels were determined by real-time PCR. Values presented are mean ± SEM. (N = 5 groups (N2(WT) n = 3, CL2006 Control n = 3, CL2006 (*set-25* (RNAi)) n = 3, CL2006 (*Y50D7A.10* (RNAi)) n = 3, CL2006 (*set-25;Y50D7A.10* (RNAi)) n = 3; Each biological replicate with at least 300 worms in each group); One-Way ANOVA and post-hoc Tukey's test; *p<0.05;***p<0.001;***p<0.0001). Source data are provided as a Source Data file.

GMFB on several well-established target genes of G9a. The gene expression of the *crh-1c* decreased (Fig. 7O), while that of *ikb-1* increased (a homolog of human IκB) (Fig. 7P), in those groups that presented *Y50D7A.10*-KD in the same way as in the CL2006 Control group, compared to the N2 group and G9ai-treated group. Thus, *Y50D7A.10*-KD in *C. elegans* reversed all cognitive and behavioral improvements exhibited by the *set-25*-KD strain, indicating a possible role of GMFB in the beneficial effects of G9ai treatment. And for the first time, these results support the hypothesis that G9a interacts with GMFB (regulating it secondarily) to promote neurodegeneration.

DISCUSSION

In the present study, we unraveled an undescribed molecular pathway based on the GMFB transcriptional repression controlled by G9a, which in turn mediates neuroprotection after G9a inhibition. Secondarily, we presented, for the first time, that G9a directly methylates GMFB. We also demonstrated the relevance of G9a and its repressive histone mark H3K9me2 in AD patients, which correlates with an increased levels of the $A\beta_{42}/A\beta_{40}$ ratio, an important hallmark of the disease. First, we used the RNAi method in *C. elegans* as a much cleaner approach than pharmacological inhibition to reduce the off-target effect and elucidate how G9a/SET-25 contributes to the AD pathogenesis. Then, in *C. elegans* AD strains, we showed Aβ aggregation and epigenetic alterations similar to those observed in AD patients that were reversed after *set-25*-KD. These findings confirmed our premise concerning the contribution of G9a to AD-like pathology.

To support our hypothesis that the G9a inhibition would be a promising therapy for AD, we performed an exploratory ChIP-seq analysis, revealing an H3K9me2 enrichment of the distal and promoter regions, suggesting a transcriptional regulation by G9a. In line with our findings, it has been reported that TG2576 mice presented high levels of $A\beta_{40}$ and $A\beta_{42}$ with increased H3K9me2 levels in the cortex and hippocampus [17]. This suggests that treatment with G9ai could restore neural alterations associated with Aβ oligomers by reducing H3K9me2 levels. Consistent with these results, the RNA-seq data revealed alterations in molecular processes associated with chromatin methylation and H3K9me2, which indicates the participation of the proteins associated with the histone mark H3K9me2. This would support the results of the H3K9me2 ChIP-seq analysis in AML12 cells. Thus, based on these findings and previous reports

[7], we suggest that G9a inhibition could improve cognition in AD patients.

In this respect, we demonstrated in SAMP8 mice similar specific epigenetic modifications in G9a and H3K9me2 to those observed in AD patients. Furthermore, we found that the levels of $A\beta_{42}/A\beta_{40}$ ratio decreased after G9ai in SAMP8 mice. Although, we found increased $A\beta_{40}$ levels in both SAMR1 and SAMP8 G9ai groups, it is well established that this amyloid fragment inhibits Aβ deposition *in vivo* [79], and therefore this would partly explain the mechanism by which Aβ aggregation could be reduced after G9a inhibition. However, the mechanism is not explored in depth in this work, but the reduction of Aβ load after G9ai could be as a consequence of direct modulation of non-amyloidogenic pathway genes, reducing cognitive impairment. Furthermore, other molecular pathways that are regulated by G9a could also be responsible, such as autophagy [80] and neuroinflammation [12], among others. More importantly, G9ai treatment restored cognitive status in SAMP8 mice in the same way as is reported in 5XFAD mice [3, 12]. Besides, aggressive behavior has a direct influence on social interaction, and in the same line, the inhibition of G9a has been associated with a decrease in anxiety-like behaviors in adult male mice[19]. Nevertheless, the beneficial effect of G9ai treatment on social performance has not been described previously. Thus, for the first time, we demonstrate that G9a inhibition improved social behavior in SAMP8 mice. Consistently, it has been reported that inhibitors of KTMs lead to the remarkable restoration of cognitive behaviors, such as recognition memory, spatial memory, and working memory [19, 81].

Aberrant gene expression is associated with epigenetic alterations [2], and although some relevant *in vivo* studies are being performed, few have described novel modulated pathways after G9a inhibition in detail [64]. Therefore, one of the main interests of this study was to identify unknown non-canonical pathways by which G9a might act, contributing to transcriptomic changes that lead to neuroprotection. Of note, we focused on validating the GMFB up-regulation in SAMP8 mice after G9ai treatment, because GMFB activation induces the synthesis induction of several important proteins in brain function and promotes neurotrophins production, thus suggesting a role in neuronal growth and regeneration [82], and is correlated with learning and memory formation. Strikingly, GMFB appears to trigger activation of p38 MAPK, followed by activation of the transcription factor CREB, which up-regulates BDNF expression levels, thus confirming the pathway activation in SAMP8 mice [68, 83]. It is noteworthy that p38 MAPK is highly expressed in brain regions that are crucial for learning and memory, and it has been reported that its activation is necessary for BDNF production in the rat hippocampus [69]. In addition, consistent with our results, the generation of GMFB-KO mice revealed its importance in normal cognitive functions since its loss promoted pathological neuroinflammatory disease progression[84]. However, no increase in the expression of neurotrophins, such as BDNF and NGF, expression was observed in the cerebellum of GMFB-KO mice in an *in vivo* study, which displayed impaired of motor and learning skills [84, 85]. Importantly, the activation of p38 MAPK might be correlated with morphological changes in neuronal dendritic spines [86]. Remarkably, Golgi staining analysis revealed an increase in neuronal complexity, which correlated with better cognitive performance after G9ai treatment as well as better cognitive performance in SAMP8 mice. Importantly, therapeutic strategies that would reduce neurodegeneration, and actively promote neuro-regeneration, to better functional phenotype improvement, are of great interest. In this context, G9a has been reported to play a role in axon formation, controlling the expression of genes associated with cAMP and Ca^{2+}-dependent signaling[64]. Although our results on the GMFB-related signaling pathway were beneficial in SAMP8 mice, there are conflicting findings on how GMFB expression is triggered during neuroinflammation and neurodegeneration[29]. As mentioned earlier, GMFB activation promotes NF-κB expression, thus inducing an inflammatory response[87]. Hence, the precise molecular mechanism by which GMFB is involved in neurodegeneration remains unclear[30]. For this reason, the assessment of pro-inflammatory markers was of great importance in this work.

A wealth of evidence confirms the link between increased levels of inflammatory markers and AD pathogenesis, suggesting that neuroinflammation plays a relevant role in neurodegeneration. At first glance, up-regulation of GMFB might compromise the neuroinflammatory state; however, according to our validated *in vivo* results, we can confirm that ERK-NF-κB orchestrates a decrease in pro-inflammatory NF-kB target genes in AD progression in response to G9a inhibition. The ERK pathway triggers the proinflammatory state, thus inducing the NF-κB [88]. Although the relationship between NF-κB and G9a has already been described during an immune response [89], it is still unknown in the context of neuroinflammation [12, 90]. Consistent with our results, clinical research has shown a positive correlation between CXCL10 and cognitive impairment in AD patients [91]. Furthermore, IL-6 is a pleiotropic inflammatory cytokine secreted by activated glia in the CNS, and is involved in the aging process and the pathogenesis of neurodegeneration [92]. Besides, the pro-

inflammatory cytokine TNF-α exacerbates both Aβ and tau pathology. Thus, anti-inflammatory strategies demonstrated amelioration of cognitive function in rodent models of AD [93], consistent with the results of G9ai treatment carried out in SAMP8 mice. Interestingly, clinical imaging studies reported that neuroinflammation in AD patients was characterized by negative correlations between microglial activation and structural integrity or functional activity in the hippocampus of AD patients. As shown by the *in vitro* model of inflammation induced by LPS treatment, the inhibition of G9a reduced microglial-specific marker expression, including Iba-1, iNOS, and Arginase expression. In line with our results, several studies identified increases in Iba-1 expression in AD patients compared with control groups, suggesting that this protein is crucial for activating microglial processes [94]. Moreover, iNOS is mainly expressed by microglia that are activated in different pathological situations, its overexpression being associated with the induction of neuronal death [95]. Thus, these results of lower levels of reactive microglial markers after G9ai treatment *in vitro* reaffirmed the *in vivo* results mentioned above and previously reported in an early-onset AD mouse model by us [12] .

Based on the above, we wondered whether GMFB plays a key role in this modulation. Therefore, we analyzed cell death by treating primary culture cells with a GMFBi, and the combination of a G9ai and a GMFBi. Under normal conditions, there were no differences between treated groups and the control group. Interestingly, we found a reduction in cell survival after neuroinflammatory challenge in those groups treated with a GMFBi compared to the G9ai-treated cell group, suggesting the involvement of the GMFB in this beneficial effect under LPS insult. To the best of our knowledge, this is the first study suggesting this undescribed mechanism and showing the relationship between G9a and GMFB.

We subsequently set out to go further and demonstrate that the beneficial effect following G9a inhibition *in vivo* was orchestrated by increased GMFB protein levels. Thereby, GMFBi treatment and co-treatment with a GMFBi plus G9ai were carried out in SAMP8 mice. Overall, both the SAMP8 group treated with GMFBi and the group treated with both inhibitors showed the same pattern in behavioral tests as that exhibited by the untreated SAMP8 mice. Next, given that GMFB is an enhancer of p38 and inhibitor of ERK, we evaluated their protein levels. In support of our proposed mechanism, our findings showed that SAMP8 groups treated with GMFBi (either alone or in combination) showed a reduction in the p-p38/p38 ratio levels. Accordingly, we found that there was no difference in cortex dendritic arborization and spine density were observed in GMFBi and dual treatment in SAMP8 mice relative to the SAMR1 group, and thus, both treated groups presented the same levels as the untreated SAMP8 group. On the other hand, an increase in the ERK-NF-kB signaling pathway and a subsequent increase in the NF-kB target gene *Il-6* in SAMP8 groups treated with GMFBi

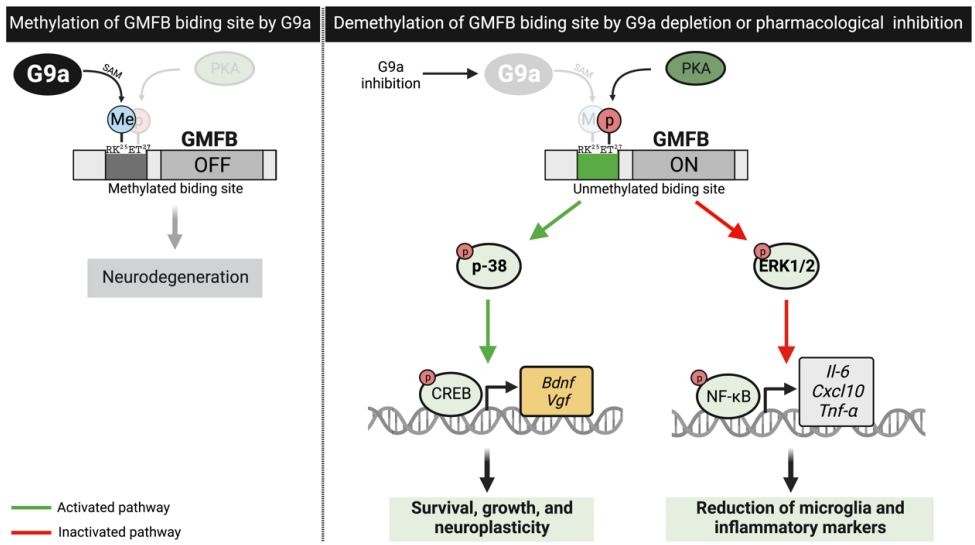

Figure 8. Scheme of the undescribed molecular mechanism, controlled by G9a-mediated methylation of GMFB, which in turn mediates the neuroprotection after G9a inhibition.

(either alone or in combination) were found, thus perpetuating the neuroinflammation in these treated SAMP8 groups. In view of the above, these findings indicate that the neuroprotective effect of G9a inhibition was mediated mainly by GMFB, which increases p38

MAPK activity, favoring synaptic plasticity while decreasing neuroinflammation through the ERK pathway.

In the next phase of our study, the direct protein-protein interaction between G9a and GMFB was evaluated to confirm our findings described above. As aforementioned, G9a can also methylate non-histone proteins [96]. Furthermore, recently it has been proposed a novel direction for the study of GMFB biofunction after being SUMOylated at multiple sites by SUMO1 [23]. But nothing has been described about the link between GMFB and methylation. Our data here observed a remarkable decrease in the methylation level of GMFB upon inhibition or removal of G9a, leaving relatively small amounts of methylated GMFB were. These data suggest that G9a is not the sole methyltransferase for GMFB methylation. It has been reported that G9a forms a heterodimer with G9a-like protein (GLP), and that both can catalyze histone H3K9 mono- and di-methylation. Thus, it is likely that GLP may also contribute to the methylation of GMFB. Further investigation is needed to examine this possibility. Regardless of this, our data supports that G9a is indeed required for GMFB methylation *in vivo*. Going deeper into this hypothesis, we decided to review the literature and found that GMFB has two sites, K20R and K25R, which may be preferentially targeted by G9 methylation [13]. Thus, we generated KDs of K20R, K25R, and 2KR cells to validate G9a's ability to methylate these sites. Our findings suggest that K20R and K25R are the top two sites methylated by G9a. Next, we evaluated the neuroprotective role between the GMFB and G9a binding sites by evaluating cell survival upon LPS exposure in the generated cell lines. Strikingly, our findings suggest that G9a's neurodegenerative role is mainly driven by its methylation at position K25 of GMFB. Conversely, demethylation at position K20R of GMFB by G9a may play a secondary role in the neuroprotective effect. Therefore, pharmacological inhibition of G9a would enhance neuroprotective effects by demethylating this position (K25R). This demethylation at position K25 is required for the phosphorylation of GMFB by PKA, an essential step for GMFB activation. Furthermore, it is noteworthy that GMFB phosphorylated by PKA increases p38 activity and inhibits the ERK pathway [68, 75, 76], as we observed in the SAMP8 group treated with G9ai.

Finally, we generated the *Y50D7A.10*-KD in *C. elegans* AD strains. Consistent with our previous results, we found that CL2355 (*Y50D7A.10* (RNAi)) and CL2355 (*set-25; Y50D7A.10* (RNAi)) were not able to restore cognitive impairment. Likewise, CL2006 (*Y50D7A.10* (RNAi)) and CL2006 (*set-25; Y50D7A.10* (RNAi)) showed no Aβ reduction. Moreover, single, and double KD of *Y50D7A.10* in CL2006 strains presented lower levels of *chr-1c*, and higher levels of *ikb-1*, both well-established target genes of G9a. Therefore, our findings demonstrate that G9a interacts with GMFB, and that the inhibition of G9a is crucial to promote the neuroprotective mechanism through GMFB.

Here, we have highlighted a novel G9a-mediated mechanism. Upon G9a inhibition, this mechanism exhibited two levels of regulation, activating GMFB and modulating its function, to lead to neuroprotection. Hence, we found that the beneficial effects of *set-25*-KD or pharmacological G9a inhibition on cognition, neuronal plasticity and neuroinflammation were abrogated by GMFB inhibition, pinpointing GMFB as a master key in the neuroprotective effects of G9ai. Finally, we also provided evidence showing that repressive regulation of GMFB by G9a methylation inhibits the activation of GMFB triggering neurodegeneration (Fig. 8).

Authors' contributions

C.G.-F. conceived the idea. A.B.-S., C.G.-F., G.N., PA.A.-L., J.C.-A., R.L.-A., L.M-G. and LL.M. performed research. A.B.-S., C.G.-F., Q.G., PA.A.-L., G.N., H.-N.D, J.C.-A., R.L.-A., B.S.C., C.P., A.P.-B. designed the experiments and analyzed the data. A.B.-S., DR.-B., G.N., FX. S., D.O.-S., C.P., M.P. and C.G.-F. wrote the manuscript. All authors read and approved the final manuscript.

Acknowledgments

A.B-S acknowledges the Agència de Gestió d'Ajuts Universitaris i de Recerca (AGAUR) for her FI-SDUR fellowship (2021 FISDU 00182). J.C-A acknowledges the Ministry of Economy and Competitiveness (MINECO) for her FPI fellowship (MDM-2017-0729-19-2). L.M-G was supported by the Mental Health Commission of Canada (MHCC) grant (G254143). Some *C. elegans* strains were provided by the CGC, which is funded by NIH Office of Research Infrastructure Programs (P40 OD010440). All graphical abstracts were created with BioRender.com.

Funding

This study was supported by the Ministerio de Economía, Industria y Competitividad (Agencia Estatal de Investigación, AEI) and Fondo Europeo de Desarrollo

Regional (MINECO-FEDER) (PID2019-106285/AEI/10.13039/501100011033; PDC2021-121096/AEI/10.13039/501100011033), Generalitat de Catalunya (2021 SGR 00357) and the National Natural Science Foundation of China 31770843. This study was co-financed by Secretaria d'Universitats i Recerca del Departament d'Empresa i Coneixement de la Generalitat de Catalunya 2021 (Llavor 00086).

Conflicts of Interest

None of the authors have any disclosures to declare.

Data availability

All data are available in the Source Data File.

Supplementary Materials

The Supplementary data can be found online at: www.aginganddisease.org/EN/10.14336/AD.2023.0424-1.

References

[1] Lardenoije R, Iatrou A, Kenis G, Kompotis K, Steinbusch HWM, Mastroeni D, et al. (2015). The epigenetics of aging and neurodegeneration. Prog Neurobiol, 131:21–64.

[2] Delgado-Morales R, Agís-Balboa RC, Esteller M, Berdasco M (2017). Epigenetic mechanisms during ageing and neurogenesis as novel therapeutic avenues in human brain disorders. Clin Epigenetics, 9:1–18.

[3] Zheng Y, Liu A, Wang Z-J, Cao Q, Wang W, Lin L, et al. (2019). Inhibition of EHMT1/2 rescues synaptic and cognitive functions for Alzheimer's disease. Brain, 142:787–807.

[4] Long JM, Holtzman DM (2019). Alzheimer disease: an update on pathobiology and treatment strategies. Cell, 179:312–339.

[5] Eisenberg CA, Eisenberg LM (2019). G9a and G9a-Like Histone Methyltransferases and Their Effect on Cell Phenotype, Embryonic Development, and Human Disease. DNA, RNA, Histone Methylomes. Springer, 399–433.

[6] Maze I, Covington HE, Dietz DM, LaPlant Q, Renthal W, Russo SJ, et al. (2010). Essential role of the histone methyltransferase G9a in cocaine-induced plasticity. Science (80-), 327:213–216.

[7] Sharma M, Dierkes T, Sajikumar S (2017). Epigenetic regulation by G9a/GLP complex ameliorates amyloid-beta 1-42 induced deficits in long-term plasticity and synaptic tagging/capture in hippocampal pyramidal neurons. Aging Cell, 16:1062–1072.

[8] Sharma M, Razali NB, Sajikumar S (2017). Inhibition of G9a/GLP complex promotes long-term potentiation and synaptic tagging/capture in hippocampal CA1 pyramidal neurons. Cereb Cortex, 27:3161–3171.

[9] Pang KKL, Sharma M, Sajikumar S (2019). Epigenetics and memory: emerging role of histone lysine methyltransferase G9a/GLP complex as bidirectional regulator of synaptic plasticity. Neurobiol Learn Mem, 159:1–5.

[10] Schaefer A, Sampath SC, Intrator A, Min A, Gertler TS, Surmeier DJ, et al. (2009). Control of cognition and adaptive behavior by the GLP/G9a epigenetic suppressor complex. Neuron, 64:678–691.

[11] Kramer JM, Kochinke K, Oortveld MAW, Marks H, Kramer D, de Jong EK, et al. (2011). Epigenetic regulation of learning and memory by Drosophila EHMT/G9a. PLoS Biol, 9:e1000569.

[12] Griñán-Ferré C, Marsal-García L, Bellver-Sanchis A, Kondengaden SM, Turga RC, Vázquez S, et al. (2019). Pharmacological inhibition of G9a/GLP restores cognition and reduces oxidative stress, neuroinflammation and β-Amyloid plaques in an early-onset Alzheimer's disease mouse model. Aging (Albany NY), 11:11591.

[13] Poulard C, Noureddine LM, Pruvost L, Le Romancer M (2021). Structure, Activity, and Function of the Protein Lysine Methyltransferase G9a. Life, 11:1082.

[14] Seo J-W, Lee K-J (2004). Post-translational modifications and their biological functions: proteomic analysis and systematic approaches. BMB Rep, 37:35–44.

[15] Wu Z, Connolly J, Biggar KK (2017). Beyond histones–The expanding roles of protein lysine methylation. FEBS J, 284:2732–2744.

[16] Zhang X, Huang Y, Shi X (2015). Emerging roles of lysine methylation on non-histone proteins. Cell Mol Life Sci, 72:4257–4272.

[17] Lithner CU, Lacor PN, Zhao W-Q, Mustafiz T, Klein WL, Sweatt JD, et al. (2013). Disruption of neocortical histone H3 homeostasis by soluble Aβ: Implications for Alzheimer's disease. Neurobiol Aging, 34:2081–2090.

[18] Zhao M, Zhu Z, Li H, Wang W, Cheng S, Qin X, et al. (2021). Effects of Traumatic Stress in Adolescence on PTSD-like Behaviors, Dendrite Development, and H3K9me2/BDNF Expression in the Amygdala of Male Rats. J. Affect. Disord. .

[19] Wang D, Kosowan J, Samsom J, Leung L, Zhang K, Li Y, et al. (2018). Inhibition of the G9a/GLP histone methyltransferase complex modulates anxiety-related behavior in mice. Acta Pharmacol Sin, 39:866–874.

[20] Kim Y, Lee H-M, Xiong Y, Sciaky N, Hulbert SW, Cao X, et al. (2017). Targeting the histone methyltransferase G9a activates imprinted genes and improves survival of a mouse model of Prader–Willi syndrome. Nat Med, 23:213–222.

[21] Zaheer A, Fink BD, Lim R (1993). Expression of glia maturation factor β mRNA and protein in rat organs and cells. J Neurochem, 60:914–920.

[22] Lim R, Hicklin DJ, Miller JF, Williams TH, Crabtree JB (1987). Distribution of immunoreactive glia maturation

factor-like molecule in organs and tissues. Dev Brain Res, 33:93–100.

[23] Sun W, Wang J, Zhang J, Gao F, Ou Q, Tian H, et al. (2021). SUMOylation of GMFB regulates the stability and function of GMFB in RPE cells under oxidative stress and inflammation. bioRxiv .

[24] Decque A, Joffre O, Magalhaes JG, Cossec J-C, Blecher-Gonen R, Lapaquette P, et al. (2016). Sumoylation coordinates the repression of inflammatory and anti-viral gene-expression programs during innate sensing. Nat Immunol, 17:140–149.

[25] Maheshwari D, Shukla VK, Jain A, Tripathi S, Kumar D, Arora A (2018). Solution structure and dynamics of glia maturation factor from Caenorhabditis elegans. Biochim Biophys Acta (BBA)-Proteins Proteomics, 1866:1008–1020.

[26] Goode BL, Sweeney MO, Eskin JA (2018). GMF as an actin network remodeling factor. Trends Cell Biol, 28:749–760.

[27] Yin G, Du M, Li R, Li K, Huang X, Duan D, et al. (2018). Glia maturation factor beta is required for reactive gliosis after traumatic brain injury in zebrafish. Exp Neurol, 305:129–138.

[28] Yuan Z, Yu Z, Zhang Y, Yang H (2020). Analysis of the clinical diagnostic value of GMFB in cerebral infarction. Curr Pharm Biotechnol, 21:955–963.

[29] Kempuraj D, Khan MM, Thangavel R, Xiong Z, Yang E, Zaheer A (2013). Glia maturation factor induces interleukin-33 release from astrocytes: implications for neurodegenerative diseases. J Neuroimmune Pharmacol, 8:643–650.

[30] Zaheer S, Thangavel R, Sahu SK, Zaheer A (2011). Augmented expression of glia maturation factor in Alzheimer's disease. Neuroscience, 194:227–233.

[31] Zaheer A, Weiss JL, Goyal P, Lim R (1999). Enhanced expression of neurotrophic factors by C6 rat glioma cells after transfection with glia maturation factor. Neurosci Lett, 265:203–206.

[32] Zaheer A, Zaheer S, Sahu SK, Knight S, Khosravi H, Mathur SN, et al. (2007). A novel role of glia maturation factor: induction of granulocyte-macrophage colony-stimulating factor and pro-inflammatory cytokines. J Neurochem, 101:364–376.

[33] Takeda T, Hosokawa M, Higuchi K (1997). Senescence-accelerated mouse (SAM): a novel murine model of senescence. Exp Gerontol, 32:105–109.

[34] Butterfield DA, Poon HF (2005). The senescence-accelerated prone mouse (SAMP8): a model of age-related cognitive decline with relevance to alterations of the gene expression and protein abnormalities in Alzheimer's disease. Exp Gerontol, 40:774–783.

[35] Vattathara JJ, Prakash O, Subhramanian S, Satheeshkumar MK, Xavier T, Anil M, et al. (2020). Substrate Specific Inhibitor Designed against the Immunomodulator GMF-beta Reversed the Experimental Autoimmune Encephalomyelitis. Sci Rep, 10:1–13.

[36] Brenner S (1974). The genetics of Caenorhabditis elegans. Genetics, 77:71–94.

[37] Xiao R, Chun L, Ronan EA, Friedman DI, Liu J, Xu XZS (2015). RNAi interrogation of dietary modulation of development, metabolism, behavior, and aging in C. elegans. Cell Rep, 11:1123–1133.

[38] Vasilopoulou F, Rodríguez-Arévalo S, Bagán A, Escolano C, Griñán-Ferré C, Pallàs M (2021). Disease-modifying treatment with I2 imidazoline receptor ligand LSL60101 in an Alzheimer's disease mouse model: a comparative study with donepezil. Br. J. Pharmacol. .

[39] Braak H, Braak E (1991). Neuropathological stageing of Alzheimer-related changes. Acta Neuropathol, 82:239–259.

[40] Langmead B, Salzberg SL (2012). Fast gapped-read alignment with Bowtie 2. Nat Methods, 9:357–359.

[41] Li B, Dewey CN (2011). RSEM: accurate transcript quantification from RNA-Seq data with or without a reference genome. BMC Bioinformatics, 12:1–16.

[42] Robinson MD, McCarthy DJ, Smyth GK (2010). edgeR: a Bioconductor package for differential expression analysis of digital gene expression data. Bioinformatics, 26:139–140.

[43] Subramanian A, Tamayo P, Mootha VK, Mukherjee S, Ebert BL, Gillette MA, et al. (2005). Gene set enrichment analysis: a knowledge-based approach for interpreting genome-wide expression profiles. Proc Natl Acad Sci, 102:15545–15550.

[44] Duncan A, Heyer MP, Ishikawa M, Caligiuri SPB, Liu X, Chen Z, et al. (2019). Habenular TCF7L2 links nicotine addiction to diabetes. Nature, 574:372–377.

[45] Yan Z, Ji L, Huo X, Wang Q, Zhang Y, Wen B (2020). G9a/GLP-Sensitivity of H3K9me2 Demarcates Two Types of Genomic Compartments. Genomics. Proteomics Bioinformatics .

[46] Wang Y, Song F, Zhu J, Zhang S, Yang Y, Chen T, et al. (2017). GSA: genome sequence archive. Genomics Proteomics Bioinformatics, 15:14–18.

[47] Salmerón-Bárcenas EG, Zacapala-Gómez AE, Lozano-Amado D, Castro-Muñoz LJ, Leyva-Vázquez MA, Manzo-Merino J, et al. (2021). Comprehensive bioinformatic analysis reveals oncogenic role of H2A. Z isoforms in cervical cancer progression. Iran. J. Basic Med. Sci. 24:.

[48] Yang J, Li Z, Lian J, Qi G, Shi P, He J, et al. (2020). Brassicaceae transcriptomes reveal convergent evolution of super-accumulation of sinigrin. Commun Biol, 3:1–8.

[49] Feng J, Liu T, Qin B, Zhang Y, Liu XS (2012). Identifying ChIP-seq enrichment using MACS. Nat Protoc, 7:1728–1740.

[50] Ramírez F, Ryan DP, Grüning B, Bhardwaj V, Kilpert F, Richter AS, et al. (2016). deepTools2: a next generation web server for deep-sequencing data analysis. Nucleic Acids Res, 44:W160–W165.

[51] Robinson JT, Thorvaldsdottir H, Winckler W, Guttman M, Lander ES (2011). Integrative genomics viewer. Nat Biotechnol, 29:24–26.

[52] Yu G, Wang L-G, He Q-Y (2015). ChIPseeker: an R/Bioconductor package for ChIP peak annotation, comparison and visualization. Bioinformatics, 31:2382–2383.

[53] Zhang Y, Jiang C, Trudeau SJ, Narita Y, Zhao B, Teng M, et al. (2020). Histone loaders CAF1 and HIRA restrict Epstein-Barr virus B-cell lytic reactivation. MBio, 11:e01063-20.

[54] Bailey TL, Johnson J, Grant CE, Noble WS (2015). The MEME suite. Nucleic Acids Res, 43:W39–W49.

[55] Towbin BD, González-Aguilera C, Sack R, Gaidatzis D, Kalck V, Meister P, et al. (2012). Step-wise methylation of histone H3K9 positions heterochromatin at the nuclear periphery. Cell, 150:934–947.

[56] Woodhouse RM, Buchmann G, Hoe M, Harney DJ, Low JKK, Larance M, et al. (2018). Chromatin Modifiers SET-25 and SET-32 Are Required for Establishment but Not Long-Term Maintenance of Transgenerational Epigenetic Inheritance. Cell Rep, 25:2259-2272.e5.

[57] Chen X, Barclay JW, Burgoyne RD, Morgan A (2015). Using C. elegans to discover therapeutic compounds for ageing-associated neurodegenerative diseases. Chem Cent J. doi: 10.1186/s13065-015-0143-y.

[58] Lakhina V, Arey RN, Kaletsky R, Kauffman A, Stein G, Keyes W, et al. (2015). Genome-wide functional analysis of CREB/long-term memory-dependent transcription reveals distinct basal and memory gene expression programs. Neuron, 85:330–345.

[59] Kauffman AL, Ashraf JM, Corces-Zimmerman MR, Landis JN, Murphy CT (2010). Insulin signaling and dietary restriction differentially influence the decline of learning and memory with age. PLoS Biol, 8:e1000372.

[60] Kimura Y, Corcoran EE, Eto K, Gengyo-Ando K, Muramatsu M, Kobayashi R, et al. (2002). A CaMK cascade activates CRE-mediated transcription in neurons of Caenorhabditis elegans. EMBO Rep, 3:962–966.

[61] Liu J, Hu A, Zan J, Wang P, You Q, Tan A (2019). Network pharmacology deciphering mechanisms of volatiles of Wendan granule for the treatment of Alzheimer's disease. Evidence-based Complement. Altern. Med. 2019:.

[62] Jia H, Liu J, Han B (2018). Reviews of interleukin-37: functions, receptors, and roles in diseases. Biomed Res. Int. 2018:.

[63] Sugeno N, Jäckel S, Voigt A, Wassouf Z, Schulze-Hentrich J, Kahle PJ (2016). α-Synuclein enhances histone H3 lysine-9 dimethylation and H3K9me2-dependent transcriptional responses. Sci Rep, 6:1–11.

[64] Wilson C, Giono LE, Rozés-Salvador V, Fiszbein A, Kornblihtt AR, Cáceres A (2020). The histone methyltransferase G9a controls axon growth by targeting the RhoA signaling pathway. Cell Rep, 31:107639.

[65] Rahman A, Khan KM, Al-Khaledi G, Khan I, Al-Shemary T (2012). Over activation of hippocampal serine/threonine protein phosphatases PP1 and PP2A is involved in lead-induced deficits in learning and memory in young rats. Neurotoxicology, 33:370–383.

[66] Hou Y, Dan X, Babbar M, Wei Y, Hasselbalch SG, Croteau DL, et al. (2019). Ageing as a risk factor for neurodegenerative disease. Nat Rev Neurol, 15:565–581.

[67] Schouten M, Bielefeld P, Garcia-Corzo L, Passchier EMJ, Gradari S, Jungenitz T, et al. (2020). Circadian glucocorticoid oscillations preserve a population of adult hippocampal neural stem cells in the aging brain. Mol Psychiatry, 25:1382–1405.

[68] Lim R, Zaheer A (1996). In vitro enhancement of p38 mitogen-activated protein kinase activity by phosphorylated glia maturation factor. J Biol Chem, 271:22953–22956.

[69] Katoh-Semba R, Kaneko R, Kitajima S, Tsuzuki M, Ichisaka S, Hata Y, et al. (2009). Activation of p38 mitogen-activated protein kinase is required for in vivo brain-derived neurotrophic factor production in the rat hippocampus. Neuroscience, 163:352–361.

[70] Griñan-Ferré C, Palomera-Ávalos V, Puigoriol-Illamola D, Camins A, Porquet D, Plá V, et al. (2016). Behaviour and cognitive changes correlated with hippocampal neuroinflammaging and neuronal markers in female SAMP8, a model of accelerated senescence. Exp Gerontol, 80:57–69.

[71] Hong JT (2017). NF-kB as a mediator of brain inflammation in AD. CNS Neurol Disord Drug Targets 10:.

[72] Zaheer A, Lim R (1996). In vitro inhibition of MAP kinase (ERK1/ERK2) activity by phosphorylated glia maturation factor (GMF). Biochemistry, 35:6283–6288.

[73] Deng W, Wang Y, Ma L, Zhang Y, Ullah S, Xue Y (2017). Computational prediction of methylation types of covalently modified lysine and arginine residues in proteins. Brief Bioinform, 18:647–658.

[74] Chen H, Xue Y, Huang N, Yao X, Sun Z (2006). MeMo: a web tool for prediction of protein methylation modifications. Nucleic Acids Res, 34:W249–W253.

[75] Fan J, Fong T, Chen X, Chen C, Luo P, Xie H (2018). Glia maturation factor-β: A potential therapeutic target in neurodegeneration and neuroinflammation. Neuropsychiatr Dis Treat, 14:495–504.

[76] Shi Y, Chen L, Liotta LA, Wan H-H, Rodgers GP (2006). Glia maturation factor gamma (GMFG): a cytokine-responsive protein during hematopoietic lineage development and its functional genomics analysis. Genomics Proteomics Bioinformatics, 4:145–155.

[77] Giansanti P, Stokes MP, Silva JC, Scholten A, Heck AJR (2013). Interrogating cAMP-dependent kinase signaling in Jurkat T cells via a protein kinase A targeted immune-precipitation phosphoproteomics approach. Mol Cell Proteomics, 12:3350–3359.

[78] Rea S, Eisenhaber F, O'Carroll D, Strahl BD, Sun Z-W, Schmid M, et al. (2000). Regulation of chromatin structure by site-specific histone H3 methyltransferases. Nature, 406:593–599.

[79] Golde T, McGowan E (2007). Abeta40 inhibits amyloid deposition in vivo. J Neurosci .

[80] Vasilopoulou F, Bellver-Sanchis A, Companys-Alemany J, Jarne-Ferrer J, Irisarri A, Palomera-Ávalos V, et al. (2022). Cognitive decline and BPSD are concomitant with autophagic and synaptic deficits associated with G9a alterations in aged SAMP8 mice. Cells, 11:2603.

[81] Nicolay-Kritter K, Lassalle J, Guillou J-L, Mons N (2021). The histone H3 lysine 9 methyltransferase G9a/GLP complex activity is required for long-term consolidation of spatial memory in mice. Neurobiol Learn Mem, 179:107406.

[82] Zaheer A, Yorek MA, Lim R (2001). Effects of glia maturation factor overexpression in primary astrocytes on MAP kinase activation, transcription factor activation, and neurotrophin secretion. Neurochem Res, 26:1293–1299.

[83] Di Giacomo V, Sancilio S, Caravatta L, Rana RA, Di Pietro R, Cataldi A (2009). Regulation of CREB activation by p38 mitogen activated protein kinase during human primary erythroblast differentiation. Int J Immunopathol Pharmacol, 22:679–688.

[84] Lim R, Zaheer A, Khosravi H, Freeman Jr JH, Halverson HE, Wemmie JA, et al. (2004). Impaired motor performance and learning in glia maturation factor-knockout mice. Brain Res, 1024:225–232.

[85] Zaheer A, Haas JT, Reyes C, Mathur SN, Yang B, Lim R (2006). GMF-knockout mice are unable to induce brain-derived neurotrophic factor after exercise. Neurochem Res, 31:579–584.

[86] Hanley JG (2008). AMPA receptor trafficking pathways and links to dendritic spine morphogenesis. Cell Adh Migr, 2:276–282.

[87] Oeckinghaus A, Ghosh S (2009). The NF-κB family of transcription factors and its regulation. Cold Spring Harb Perspect Biol, 1:a000034.

[88] Lim H-S, Kim YJ, Kim B-Y, Park G, Jeong S-J (2018). The anti-neuroinflammatory activity of tectorigenin pretreatment via downregulated NF-κB and ERK/JNK pathways in BV-2 microglial and microglia inactivation in mice with lipopolysaccharide. Front Pharmacol, 9:462.

[89] Scheer S, Zaph C (2017). The lysine methyltransferase G9a in immune cell differentiation and function. Front Immunol, 8:429.

[90] Chen X, El Gazzar M, Yoza BK, McCall CE (2009). The NF-κB factor RelB and histone H3 lysine methyltransferase G9a directly interact to generate epigenetic silencing in endotoxin tolerance. J Biol Chem, 284:27857–27865.

[91] Galimberti D, Schoonenboom N, Scheltens P, Fenoglio C, Bouwman F, Venturelli E, et al. (2006). Intrathecal chemokine synthesis in mild cognitive impairment and Alzheimer disease. Arch Neurol, 63:538–543.

[92] Quintanilla RA, Orellana DI, González-Billault C, Maccioni RB (2004). Interleukin-6 induces Alzheimer-type phosphorylation of tau protein by deregulating the cdk5/p35 pathway. Exp Cell Res, 295:245–257.

[93] Decourt B, K Lahiri D, N Sabbagh M (2017). Targeting tumor necrosis factor alpha for Alzheimer's disease. Curr Alzheimer Res, 14:412–425.

[94] Hopperton KE, Mohammad D, Trépanier MO, Giuliano V, Bazinet RP (2018). Markers of microglia in post-mortem brain samples from patients with Alzheimer's disease: a systematic review. Mol Psychiatry, 23:177–198.

[95] Mander P, Brown GC (2005). Activation of microglial NADPH oxidase is synergistic with glial iNOS expression in inducing neuronal death: a dual-key mechanism of inflammatory neurodegeneration. J Neuroinflammation, 2:1–15.

[96] Rathert P, Dhayalan A, Murakami M, Zhang X, Tamas R, Jurkowska R, et al. (2008). Protein lysine methyltransferase G9a acts on non-histone targets. Nat Chem Biol, 4:344–346.

SUPPLEMENTARY DATA

G9a Inhibition Promotes Neuroprotection through GMFB Regulation in Alzheimer's Disease

Aina Bellver-Sanchis[1], Qizhi Geng[2], Gemma Navarro[3,4], Pedro A. Ávila-López[5], Júlia Companys-Alemany[1], Laura Marsal-García[6,7], Raquel Larramona-Arcas[8], Lluisa Miró[9], Anna Perez-Bosque[9], Daniel Ortuño-Sahagún[10], Deb Ranjan Banerjee[11], Bhanwar Singh Choudhary[12,13], Francesc X Soriano[8], Coralie Poulard[14,15,16], Mercè Pallàs[1,3], Hai-Ning Du[2], Christian Griñán-Ferré[1,3*]

© 2023. Bellver-Sanchis A. et al. Published online at http://www.aginganddisease.org/EN/10.14336/AD.2023.0424-2

SUPPLEMENTARY DATA

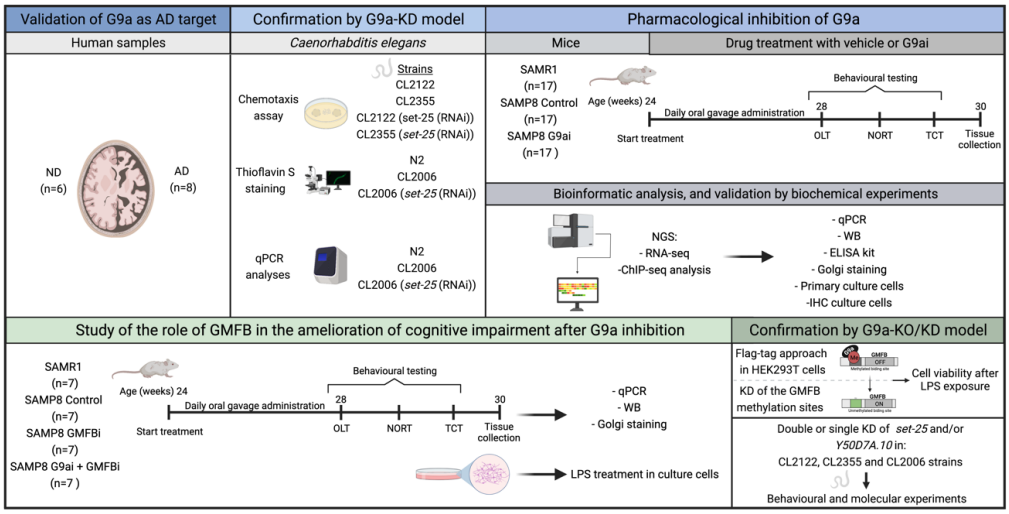

Supplementary Figure 1. Scheme of experimental procedures for *in vitro* and *in vivo* experiments.

© 2023. Bellver-Sanchis A. et al. Published online at http://www.aginganddisease.org/EN/10.14336/AD.2023.0424-2

SUPPLEMENTARY DATA

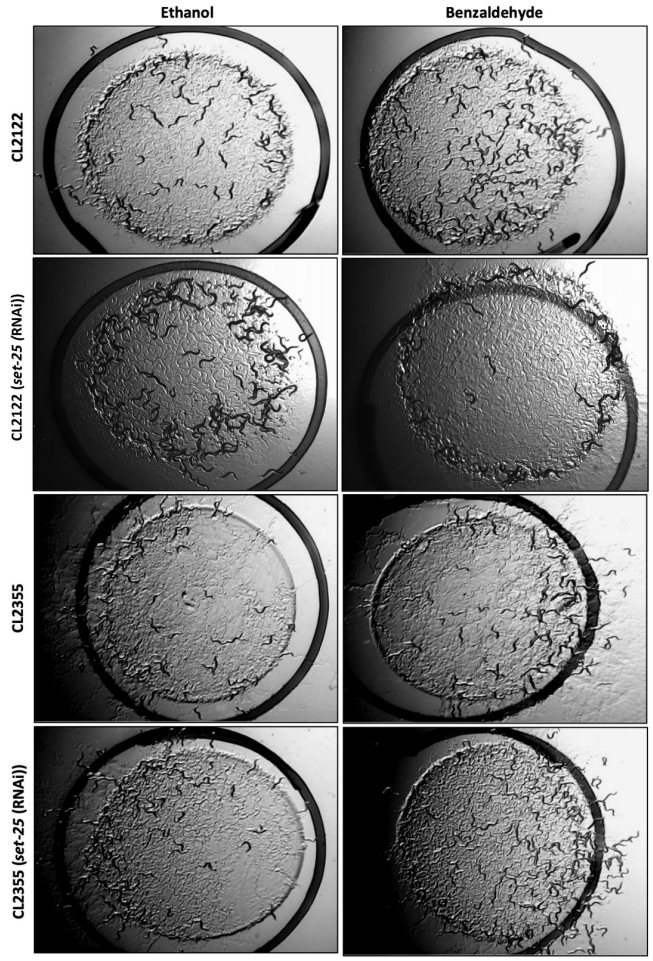

Supplementary Figure 2. Representative image of worms within the attractant (right) or control (left) spot on the chemotaxis assay plates of the different groups.

© 2023. Bellver-Sanchis A. et al. Published online at http://www.aginganddisease.org/EN/10.14336/AD.2023.0424-2

SUPPLEMENTARY DATA

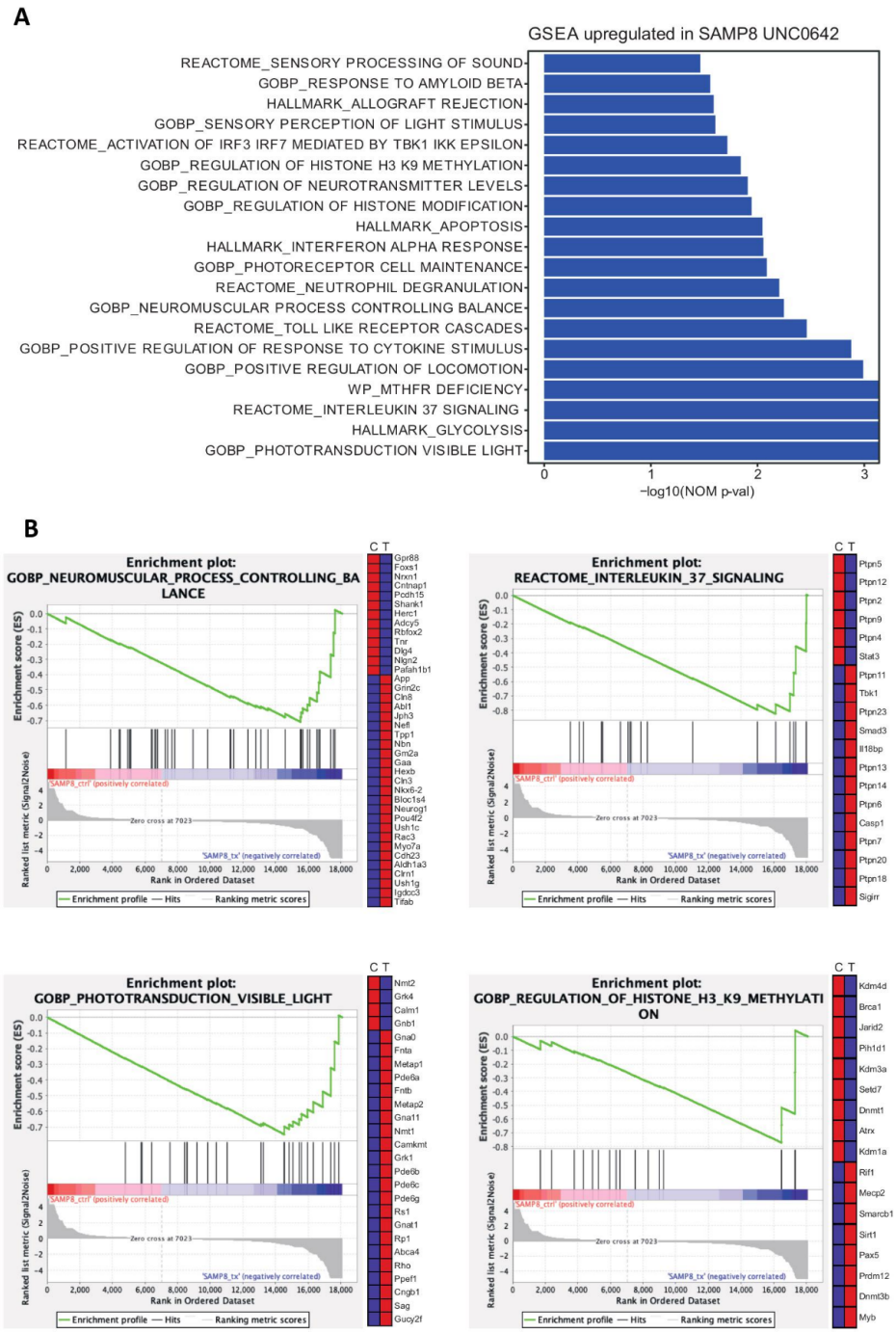

Supplementary Figure 3. **(A)** Bar graph shows the top GSEA pathways upregulated in SAMP8 UNC0642. NOM *p*-value<0.05 were considered statistically significant. **(B=** GSEA plots of the enriched processes in SAMP8 UNC0642.

© 2023. Bellver-Sanchis A. et al. Published online at http://www.aginganddisease.org/EN/10.14336/AD.2023.0424-2

SUPPLEMENTARY DATA

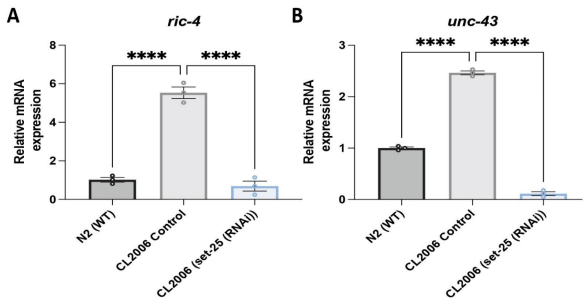

Supplementary Figure 4. (A) Representative gene expression of *ric-4*, **(B)**, and *unc-43*, in *C. elegans*. Gene expression levels were determined by real-time PCR. Values presented are the mean ± SEM; n = 3-5. Each replicate with at least 350 worms in each group from whole petri dish. Groups were compared by One-Way ANOVA and post-hoc Tukey's test; ****$p< 0.0001$).

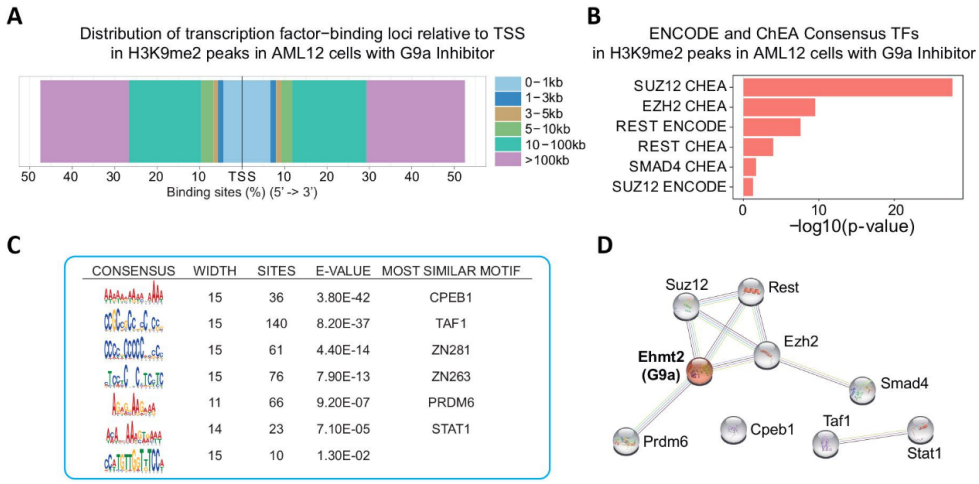

Supplementary Figure 5. (A) Distribution of transcription factor binding relative to TSS in AML12 cells treated with UNC0638 identified within the H3K9me2 peaks. **(B)** Transcription factor binding motifs at H3K9me2 peaks in AML12 cells treated with UNC0638. We considered an adjusted E-value<0.05 as statistically significant. **(C)** ENCODE and ChEA Consensus TFs associated with genes enriched with H3K9me2 at promoters. **(D)** Interaction network of TFs identified in parts (B) and (C).

© 2023. Bellver-Sanchis A. et al. Published online at http://www.aginganddisease.org/EN/10.14336/AD.2023.0424-2

SUPPLEMENTARY DATA

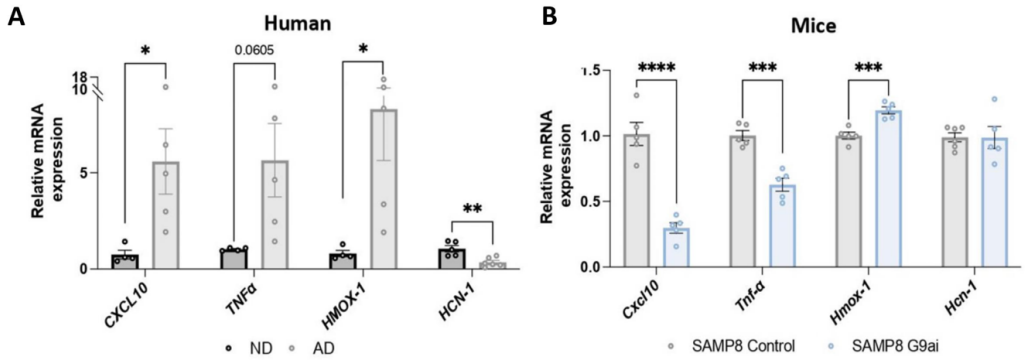

Supplementary Figure 6. (A) Representative gene expression of synaptic plasticity related genes such as CXCL*10, TNF-α, HMOX-1,* and *HCN-1* in human brain. Values presented are the mean ± SEM; (n = 11 (ND = 5, AD n = 6); Student t-test; **p*<0.05, ***p*<0.01). **(B)** Representative gene expression of synaptic plasticity related genes such as *Cxcl10, Tnf-α, Hmox-1,* and *Hcn-1* in SAMP8 mice**.** Values presented are the mean ± SEM (n = 12 (SAMP8 Control = 6, SAMP8 G9ai (UNC0642, 5mg/Kg) n = 6); Student's t-test;****p*<0.001; ****p*<0.001). Data information: Note that experiments in Supplementary Fig. 6B and Fig. 6D were performed at the same time, so the values regarding gene expression of *Cxcl10* and *Tnf-α* are the same but the figures have been split in two for the sake of linearity.

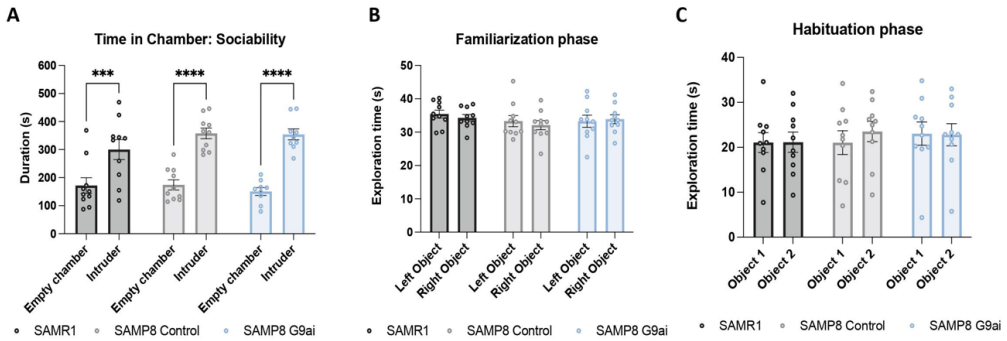

Supplementary Figure 7. For TCT: **(A)** Time spent in chamber. For NORT: **(B)** Familiarization phase. Fort OLT: **(C)** Habituation phase. Values presented are the mean ± SEM; (n = 30 (SAMR1 n = 10, SAMP8 Control n = 10, and SAMP8 G9ai (UNC0642, 5mg/Kg) n = 10); One-Way ANOVA and post-hoc Tukey's test; ****p*<0.001; *****p*<0.0001).

© 2023. Bellver-Sanchis A. et al. Published online at http://www.aginganddisease.org/EN/10.14336/AD.2023.0424-2

SUPPLEMENTARY DATA

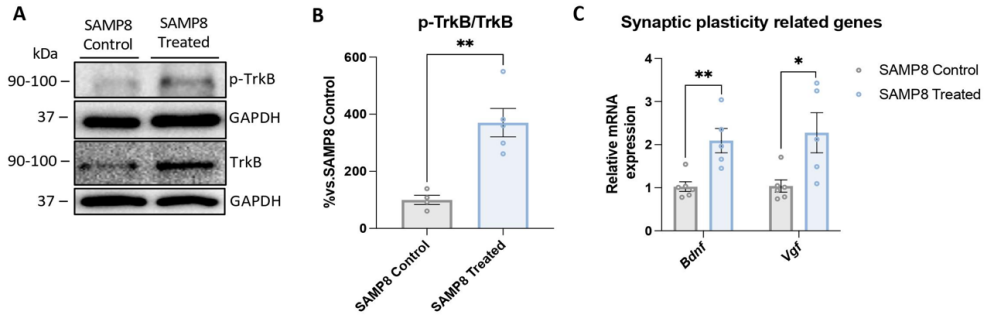

Supplementary Figure 8. (A) and **(B)** Representative WB and quantifications for the ratio of p-TrkB/TrkB. **(C)** Representative gene expression of synaptic plasticity related genes such as *Bdnf,* and *Vgf***.** Values presented are the mean ± SEM; (n = 12 (SAMP8 Control = 6, SAMP8 treated with UNC0642 (5mg/Kg) n = 6)). Groups were compared by Student t-test; **p*<0.05; ***p*<0.01 vs SAMP8 Control.

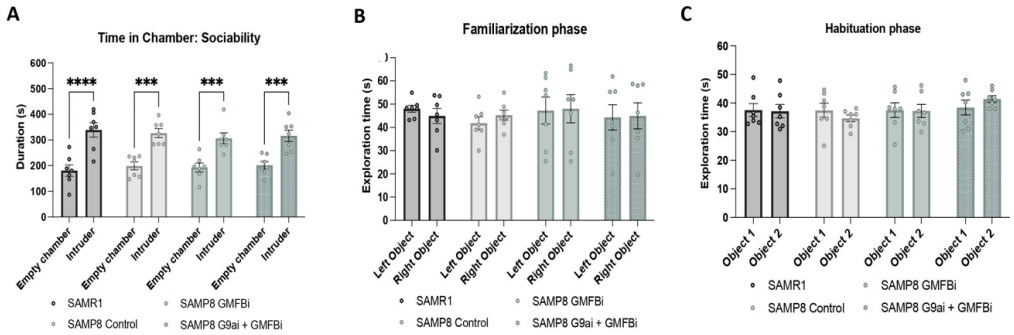

Supplementary Figure 9. For TCT: **(A)** Time spent in chamber. For NORT: **(B)** Familiarization phase. Fort OLT: **(C)** Habituation phase. Values presented are the mean ± SEM; (n = 28-24 (SAMR1 n = 6-7, SAMP8 Control n = 6-7, SAMP8 GMFBi ((1H-Indazol-4-yl)methanol, 12mg/Kg) n= 6-7, and SAMP8 G9ai (UNC0642, 5mg/Kg) + GMFBi ((1H-Indazol-4-yl)methanol, 12mg/Kg) n = 6-7); One-Way ANOVA and post-hoc Tukey's test; ****p*<0.001; *****p*<0.0001.

© 2023. Bellver-Sanchis A. et al. Published online at http://www.aginganddisease.org/EN/10.14336/AD.2023.0424-2

SUPPLEMENTARY DATA

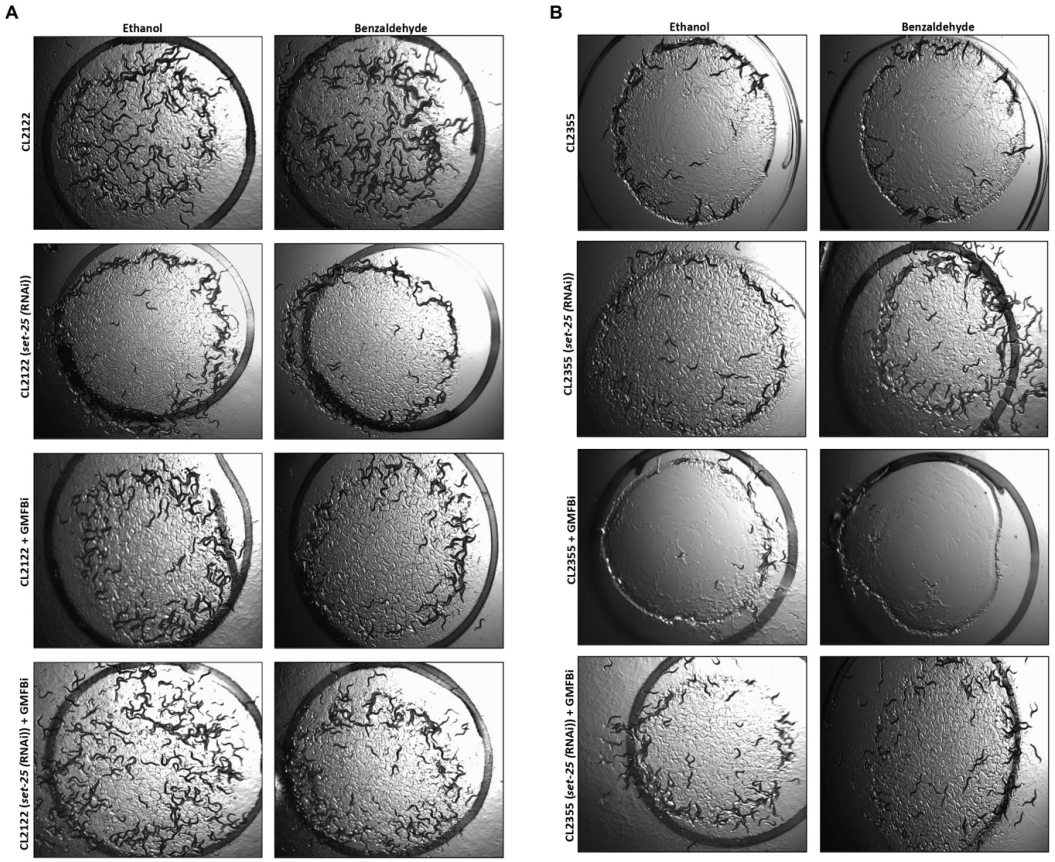

Supplementary Figure 10. Representative image of worms within the attractant (right) or control (left) spot on the chemotaxis assay plates of the different groups **(A)** CL2122 strain, and **(B)** CL2355 strain.

© 2023. Bellver-Sanchis A. et al. Published online at http://www.aginganddisease.org/EN/10.14336/AD.2023.0424-2

SUPPLEMENTARY DATA

Supplementary Table 1. Patients Data.

Gender	Age	Postmortem delay	Diagnosis
Male	85	5 h 45 min	Control
Male	78	2 h 15 min	Control
Male	79	7 h	Control
Male	52	3 h 20 min	Control
Female	72	2 h 45 min	Control
Female	49	5 h	Control
Male	93	7 h 20 min	AD BRAAK STAGE V/C
Male	85	5 h 15 min	AD BRAAK STAGE V/C
Male	74	6 h 30 min	AD BRAAK STAGE V/C
Female	83	3 h 20 min	AD BRAAK STAGE V/C
Female	82	1 h 45 min	AD BRAAK STAGE V/B
Female	72	9 h 30 min	AD BRAAK STAGE V/B
Female	75	4 h 15 min	AD BRAAK STAGE V/B
Female	85	2 h 10 min	AD BRAAK STAGE V/B

Supplementary Table 2. Reagents and kits used in this work.

Reagent, kits, and equipment	Source	Catalog number
Benzaldehyde	Sigma Aldrich	100-52-7
Chemiluminescence-based detection kit	ECL Kit, Millipore	WBKLS0500
EpiQuik Total Histone Extraction HT Kit	EpiGentek	OP-0007-192
Human amyloid-β_{40} ELISA Kit	Invitrogen™	KHB3481
Human amyloid-β_{42} Ultrasensitive ELISA Kit	Invitrogen™	KHB3544
Mouse Aβ_{42} ELISA Kit	Invitrogen™	KMB3441
Mouse Aβ_{40} ELISA Kit	Invitrogen™	KMB3481
TRIsure™	Bioline, Meridian Bioscience	BIO-38032
High Capacity cDNA Reverse Transcription kit	Applied Biosystems™	4368814
Maxima SYBR Green qPCR Master Mix (2X), ROX solution provided	Thermo Scientific™	K0253
mirVana *mi*RNA Isolation kit *with p*henol	Invitrogen™	AM1560
TaqMan miRNA Reverse Transcription kit	Applied Biosystems™	4366596
TaqMan™ Universal PCR Master Mix	Applied Biosystems™	4305719
FD Rapid GolgiStain kit	FD NeuroTechnologies, incs	PK401
Eukitt® Quick-hardening mounting medium	Sigma-Aldrich	25608-33-7
Trypan blue 0,4%	BioRad	1450021
Hoechst	Sigma Aldrich	33258
Thioflavin S	Sigma Aldrich	1326-12-1
Mowiol	Calbiochem	9002-89-5
TC20™ Automated Cell counter	Biorad	1450102

© 2023. Bellver-Sanchis A. et al. Published online at http://www.aginganddisease.org/EN/10.14336/AD.2023.0424-2

SUPPLEMENTARY DATA

Supplementary Table 3. Antibodies used in WB protocol, and in IHC analysis.

Antibody	Host	Source/Catalog	WB dilution
G9a	Rabbit	Abcam/ab40542	1:1000
H3K9me2	Rabbit	Epigentek/A-4035	1:500
Histone H3 total	Rabbit	Cell signaling/#9715	1:1000
GMFB	Mouse	Santa Cruz/ sc-134347	1:500
p38	Mouse	Santa Cruz/sc-81621	1:500
p-p38	Mouse	Santa Cruz/ sc-166182	1:500
CREB	Rabbit	Cell signaling/#4820	1:1000
p-CREB (Ser133)	Rabbit	Cell signaling/#9198	1:1000
BDNF	Rabbit	Bios/BS-4989R	1:1000
NF-κB	Rabbit	Cell signaling/#8242S	1:1000
p- NF-κB	Mouse	Santa Cruz/ sc-136548	1:500
ERK	Rabbit	Cell Signalling/9102	1:1000
p-ERK	Rabbit	Cell Signalling/9101	1:1000
p-TrkB	Mouse	Santa Cruz/sc-8052	1:500
TrkB	Mouse	Santa Cruz/sc-377218	1:500
GAPDH	Mouse	Millipore/MAB374	1:5000
Goat-anti-mouse HRP conjugated	Goat	Biorad/170-5047	1:2000
Goat-anti-rabbit HRP conjugated	Goat	Biorad/170-6515	1:2000
Antibody	**Host**	**Source/Catalog**	**ICH dilution**
iNOS	Mouse	Thermofisher/MA5-17139	1:100
Arginase	Mouse	BD Biosciences/ #610708	1:100
Iba1	Mouse	Abcam/Ab107159	1:100
Cy3-conjugated anti-rabbit	Donkey	Jackson ImmunoResearch/711-165-152	1:200
Cy3-conjugated anti-mouse	Donkey	Jackson ImmunoResearch/711-166-150	1:200

G9a: also called euchromatic histone-lysine N-methyltransferase 2 (EHMT2); H3K9me2: Histone 3 Lysine 9 di-methylated; GMFB: Glia maturation factor beta; p38: mitogen-activated protein kinase; CREB: cAMP response element-binding protein; BDNF: Brain Derived Neurotrophic Factor; NF-κB: Nuclear factor kappa-light-chain-enhancer of activated B cell; ERK: extracellular signal-regulated kinases; TrkB: Tropomyosin receptor kinase B; GAPDH: Glyceraldehyde 3-phosphate dehydrogenase; iNOS: Inducible nitric oxide synthase; Iba1: Ionized calcium binding adaptor molecule 1.

Supplementary Table 4. Primers used in qPCR studies.

Target	Forward primer (5'-3')	Reverse primer (3'-5')	Product length
CXCL10	GCTTCCAAGGATGGACCACA	GCAGGGTCAGAACATCCACT	253
HMOX-1	GTGGTTTTTGAGCCATGCGT	CCACTTCTCCTACCGAGCAC	213
TNF-α	GCTGCACTTTGGAGTGATCG	GGGAGAGTGGATGAAGGCTG	170
HCN-1	CACCAGATTGCTGGGTGTCT	ACTGGATTAAAGCGGTGGCA	210
GAPDH	GGGAGCCAAAAGGGTCAT	GAGTCCTTCCACGATACCAA	181
Gmfb	GGAGAGGTGTTGCAGATTGTTTG	GGAAACCATTTGTGGGAAGTGT	150
Snap25	ACGCATTGAGGAAGGGATGG	ATCTGCTCCCGTTCATCCAC	207
Bdnf	GGGAAATCTCCTGAGCCGAG	AGCTTTCTCAACGCCTGTCA	171
Il-6	ATCCAGTTGCCTTCTTGGGACTGA	TAAGCCTCCGACTTGTGAAGTGGT	134
Cxcl10	GGCTAGTCCTAATTGCCCTTGG	TTGTCTCAGGACCATGGCTTG	104
Tnf-α	TCGGGGTGATCGGTCCCCAA	TGGTTTGCTACGACGTGGGCT	139
Hmox-1	TGACACCTGAGGTCAAGCAC	GTCTCTGCAGGGGCAGTATC	184
Hcn-1	ATCTCATCGATCCCGGTGGA	ACGATACGAAGTGCTCTGGC	92
ß-actin	CAACGAGCGGTTCCGAT	GCCACAGGTTCCATACCCA	190
set-25	GACGAAAACGGATGATGGCG	CCGGGCTCGTAGTATGCAAT	288
*crh-1c**	ATGTCAGCGAAAGGTAACGGATC	TCCTCCGGCTCCTTCTTCATC	173
*ikb-1***	GTCCTCGCGCTCTTTTCCG	GCGATCACCAGCAGATGC	120
ric-4	TTCCAGAGGGTCTTGAGGCT	TCGCAACGCTCAAGTTGTTC	163
unc-43	CTACTGCCATCAGCGTGGAA	AACGGTGTTGGTCCTCATCC	170
daf-16	ATTGTGTTCATTTGCCCCGC	GAAGGGAGCCCATCAATGCTC	131
act-1	ATCACCGCTCTTGCCCCATC	GGCCGGACTCGTCGTATTCTTG	151

© 2023. Bellver-Sanchis A. et al. Published online at http://www.aginganddisease.org/EN/10.14336/AD.2023.0424-2

SUPPLEMENTARY DATA

*Used for ERK phosphorylation assay in cell culture. Cxcl10: C-X-C motif chemokine ligand 10; Hmox-1: Heme Oxygenase-1; Tnf-α: Tumor necrosis factor-alpha; Hcn-1: Hyperpolarization Activated Cyclic Nucleotide Gated Potassium Channel 1; Gapdh: Glyceraldehyde 3-phosphate dehydrogenase; Gmfb: Glia maturation factor beta; Snap25: Synaptosome Associated Protein 25; Bdnf: Brain Derived Neurotrophic Factor; Il-6: Interleukin-6; set-25: SET (trithorax/polycomb) domain containing-25 (ortholog of human G9a); crh-1c: ortholog of human CREB; ikb-1: I Kappa B homolog (ortholog of human NFKB2 (nuclear factor kappa B subunit 2)); ric-4: Resistance to Inhibitors of Cholinesterase (ortholog of human SNAP25 (synaptosome associated protein 25)) ; unc-43: UNCoordinated (ortholog of human CAMK2D (calcium/calmodulin dependent protein kinase II delta)) ; daf-16: abnormal DAuer Formation (ortholog of human FOXO4 (forkhead box O4)); act-1: actin (ortholog of human ACTIN beta)

Supplementary Table 5. Plasmids to generate GMFB methylation site mutants.

Plasmid	Sequence
K20R-KD	CGCCATTCTGCCTGGGGACGTCGGAGCAAGCTTGATTTAGGTGACACTATAGAATACAAGCTACTTGTTCTTTTTGCAGGATCCATGTACCCATACGATGTTCCAGATTACGCTTATCCTTATGACGTACCTGACTATGCAT
	ACCCTTATGATGTACCAGACTACGCTGGCCGGCCAGAATTCATGAGTGAGTCTTTGGTTGTTTGTGATGTTGCCGAAGATTTAGTGGAAAAGCTGAGACGGTTTCGTTTTCGCAAAGAAACGAACAACGCTGCTATTATAA
	TGAAGATTGACAAGGATAAACGCCTGGTGGTACTGGATGAGGAGCTTGAGGGCATTTCACCAGATGAACTTAAAGATGAACTACCTGAACGACAACCTCGCTTCATTGTGTATAGTTATAAATATCAACATGATGATGGA
	AGAGTTTCATATCCTCTGTGCTTTATTTTCTCCAGTCCTGTTGGATGTAAGCCTGAACAACAGATGATGTATGCTGGAAGTAAGAATAAGCTAGTCCAGACAGCTGAACTAACCAAGGTATTTGAAATAAGAAATACCGAA
	GACCTAACTGAAGAATGGTTACGTGAGAAACTTGGATTTTTTCACTAGTCTAGAACTATAGTGAGTCGTATTACGTAGATCCAGACATGATAAGATACATTGATGAGTTTGGACAAACCACAACTAGAATGCAGTGAAAA
	AAATGCTTTATTTGTGAAATTTGTGATGCTATTGCTTTATTTGTAACCATTATAAGCTGCAATAAACAAGTTAACAACAACAATTGCATTCATTTTATGTTTCAGGTTCAGGGGGAGGTGTGGGAGGTTTTTTAATTCGCGGC
	CGCGGCGCCAATGCATTGGGCCCGGTACCCAGCTTTTGTTCCCTTTAGTGAGGGTTAATTGCGCGCTTGGCGTAATCATGGTCATAGCTGTTTCCTGTGTGAAATTGTTATCCGCTCACAATTCCACACAACATACGAGCCG
	GAAGCATAAAGTGTAAAGCCTGGGGTGCCTAATGAGTGAGCTAACTCACATTAATTGCGTTGCGCTCACTGCCCGCTTTCCAGTCGGGAAACCTGTCGTGCCAGCTGCATTAATGAATCGGCCAACGCGCGGGGAGAGGC
	GGTTTGCGTATTGGGCGCTCTTCCGCTTCCTCGCTCACTGACTCGCTGCGCTCGGTCGTTCGGCTGCGGCGAGCGGTATCAGCTCACTCAAAGGCGGTAATACGGTTATCCACAGAATCAGGGGATAACGCAGGAAAGAAC
	ATGTGAGCAAAAGGCCAGCAAAAGGCCAGGAACCGTAAAAAGGCCGCGTTGCTGGCGTTTTTCCATAGGCTCCGCCCCCCTGACGAGCATCACAAAAATCGACGCTCAAGTCAGAGGTGGCGAAACCCGACAGGACTAT
	AAAGATACCAGGCGTTTCCCCCTGGAAGCTCCCTCGTGCGCTCTCCTGTTCCGACCCTGCCGCTTACCGGATACCTGTCCGCCTTTCTCCCTTCGGGAAGCGTGGCGCTTTCTCATAGCTCACGCTGTAGGTATCTCAGTTCG
	GTGTAGGTCGTTCGCTCCAAGCTGGGCTGTGTGCACGAACCCCCCGTTCAGCCCGACCGCTGCGCCTTATCCGGTAACTATCGTCTTGAGTCCAACCCGGTAAGACACGACTTATCGCCACTGGCAGCAGCCACTGGTAAC
	AGGATTAGCAGAGCGAGGTATGTAGGCGGTGCTACAGAGTTCTTGAAGTGGTGGCCTAACTACGGCTACACTAGAAGGACAGTATTTGGTATCTGCGCTCTGCTGAAGCCAGTTACCTTCGGAAAAAGAGTTGGTAGCTC
	TTGATCCGGCAAACAAACCACCGCTGGTAGCGGTGGTTTTTTTGTTTGCAAGCAGCAGATTACGCGCAGAAAAAAAGGATCTCAAGAAGATCCTTTGATCTTTTCTACGGGGTCTGACGCTCAGTGGAACGAAAACTCACG
	TTAAGGGATTTTGGTCATGAGATTATCAAAAAGGATCTTCACCTAGATCCTTTTAAATTAAAAATGAAGTTTTAAATCAATCTAAAGTATATATGAGTAAACTTGGTCTGACAGTTACCAATGCTTAATCAGTGAGGCACCT
	ATCTCAGCGATCTGTCTATTTCGTTCATCCATAGTTGCCTGACTCCCCGTCGTGTAGATAACTACGATACGGGAGGGCTTACCATCTGGCCCCAGTGCTGCAATGATACCGCGAGACCCACGCTCACCGGCTCCAGATTTAT
	CAGCAATAAACCAGCCAGCCGGAAGGGCCGAGCGCAGAAGTGGTCCTGCAACTTTATCCGCCTCCATCCAGTCTATTAATTGTTGCCGGGAAGCTAGAGTAAGTAGTTCGCCAGTTAATAGTTTGCGCAACGTTGTTGCCA
	TTGCTACAGGCATCGTGGTGTCACGCTCGTCGTTTGGTATGGCTTCATTCAGCTCCGGTTCCCAACGATCAAGGCGAGTTACATGATCCCCCATGTTGTGCAAAAAAGCGGTTAGCTCCTTCGGTCCTCCGATCGTTGTCAG
	AAGTAAGTTGGCCGCAGTGTTATCACTCATGGTTATGGCAGCACTGCATAATTCTCTTACTGTCATGCCATCCGTAAGATGCTTTTCTGTGACTGGTGAGTACTCAACCAAGTCATTCTGAGAATAGTGTATGCGGCGACCG
	AGTTGCTCTTGCCCGGCGTCAATACGGGATAATACCGCGCCACATAGCAGAACTTTAAAAGTGCTCATCATTGGAAAACGTTCTTCGGGGCGAAAACTCTCAAGGATCTTACCGCTGTTGAGATCCAGTTCGATGTAACCC
	ACTCGTGCACCCAACTGATCTTCAGCATCTTTTACTTTCACCAGCGTTTCTGGGTGAGCAAAAACAGGAAGGCAAAATGCCGCAAAAAAGGGAATAAGGGCGACACGGAAATGTTGAATACTCATACTCTTCCTTTTTCAA
	TATTATTGAAGCATTTATCAGGGTTATTGTCTCATGAGCGGATACATATTTGAATGTATTTAGAAAAATAAACAAATAGGGGTTCCGCGCACATTTCCCCGAAAAGTGCCACCTAAATTGTAAGCGTTAATATTTTGTTAAA
	ATTCGCGTTAAATTTTTGTTAAATCAGCTCATTTTTTAACCAATAGGCCGAAATCGGCAAAATCCCTTATAAATCAAAAGAATAGACCGAGATAGGGTTGAGTGTTGTTCCAGTTTGGAACAAGAGTCCACTATTAAAGAA
	CGTGGACTCCAACGTCAAAGGGCGAAAAACCGTCTATCAGGGCGATGGCCCACTACGTGAACCATCACCCTAATCAAGTTTTTTGGGGTCGAGGTGCCGTAAAGCACTAAATCGGAACCCTAAAGGGAGCCCCCGATTTA
	GAGCTTGACGGGGAAAGCCGGCGAACGTGGCGAGAAAGGAAGGGAAGAAAGCGAAAGGAGCGGGCGCTAGGGCGCTGGCAAGTGTAGCGGTCACGCTGCGCGTAACCACCACACCCGCCGCGCTTAATGCGCCGCTAC
	AGGGCGCGTCCCATTCGCCATTCAGGCTGCGCAACTGTTGGGAAGGGCGATCGGTGCGGGCCTCTTCGCTATTACGCCAGTCGACCATAGCCAATTCAATATGGCGTATATGGACTCATGCCAATTCAATATGGTGGATCT
	GGACCTGTGCCAATTCAATATGGCGTATATGGACTCGTGCCAATTCAATATGGTGGATCTGGACCCCAGCCAATTCAATATGGCGGACTTGGCACCATGCCAATTCAATATGGCGGACTTGGCACTGTGCCAACTGGGGAG
	GGGTCTACTTGGCACGGTGCCAAGTTTGAGGAGGGGTCTTGGCCCTGTGCCAAGTCCGCCATATTGAATTGGCATGGTGCCAATAATGGCGGCCATATTGGCTATATGCCAGGATCAATATATAGGCAATATCCAATATGG
	CCCTATGCCAATATGGCTATTGGCCAGGTTCAATACTATGTATTGGCCCTATGCCATATAGTATTCCATATATGGGTTTTCCTATTGACGTAGATAGCCCCTCCCAATGGGCGGTCCCATATACCATATATGGGGCTTCCTAA
	TACCGCCCATAGCCACTCCCCCATTGACGTCAATGGTCTCTATATATGGTCTTTCCTATTGACGTCATATGGGCGGTCCTATTGACGTATATGGCGCCTCCCCCATTGACGTCAATTACGGTAAATGGCCCGCCTGGCTCAAT
	GCCCATTGACGTCAATAGGACCACCCACCATTGACGTCAATGGGATGGCTCATTGCCCATTCATATCCGTTCTCACGCCCCCTATTGACGTCAATGACGGTAAATGGCCCACTTGGCAGTACATCAATATCTATTAATAGTA
	ACTTGGCAAGTACATTACTATTGGAAGGACGCCAGGGTACATTGGCAGTACTCCCATTGACGTCAATGGCGGTAAATGGCCCGCGATGGCTGCCAAGTACATCCCCATTGACGTCAATGGGGAGGGGCAATGACGCAAAT
	GGGCGTTCCATTGACGTAAATGGGCGGTAGGCGTGCCTAATGGGAGGTCTATATAAGCAATGCTCGTTTAGGGAAC
K25R-KD	CGCCATTCTGCCTGGGGACGTCGGAGCAAGCTTGATTTAGGTGACACTATAGAATACAAGCTACTTGTTCTTTTTGCAGGATCCATGTACCCATACGATGTTCCAGATTACGCTTATCCTTATGACGTACCTGACTATGCAT
	ACCCTTATGATGTACCAGACTACGCTGGCCGGCCAGAATTCATGAGTGAGTCTTTGGTTGTTTGTGATGTTGCCGAAGATTTAGTGGAAAAGCTGAGAAAGTTTCGTTTTCGCCGAGAAACGAACAACGCTGCTATTATAA
	TGAAGATTGACAAGGATAAACGCCTGGTGGTACTGGATGAGGAGCTTGAGGGCATTTCACCAGATGAACTTAAAGATGAACTACCTGAACGACAACCTCGCTTCATTGTGTATAGTTATAAATATCAACATGATGATGGA
	AGAGTTTCATATCCTCTGTGCTTTATTTTCTCCAGTCCTGTTGGATGTAAGCCTGAACAACAGATGATGTATGCTGGAAGTAAGAATAAGCTAGTCCAGACAGCTGAACTAACCAAGGTATTTGAAATAAGAAATACCGAA
	GACCTAACTGAAGAATGGTTACGTGAGAAACTTGGATTTTTTCACTAGTCTAGAACTATAGTGAGTCGTATTACGTAGATCCAGACATGATAAGATACATTGATGAGTTTGGACAAACCACAACTAGAATGCAGTGAAAA
	AAATGCTTTATTTGTGAAATTTGTGATGCTATTGCTTTATTTGTAACCATTATAAGCTGCAATAAACAAGTTAACAACAACAATTGCATTCATTTTATGTTTCAGGTTCAGGGGGAGGTGTGGGAGGTTTTTTAATTCGCGGC
	CGCGGCGCCAATGCATTGGGCCCGGTACCCAGCTTTTGTTCCCTTTAGTGAGGGTTAATTGCGCGCTTGGCGTAATCATGGTCATAGCTGTTTCCTGTGTGAAATTGTTATCCGCTCACAATTCCACACAACATACGAGCCG
	GAAGCATAAAGTGTAAAGCCTGGGGTGCCTAATGAGTGAGCTAACTCACATTAATTGCGTTGCGCTCACTGCCCGCTTTCCAGTCGGGAAACCTGTCGTGCCAGCTGCATTAATGAATCGGCCAACGCGCGGGGAGAGGC
	GGTTTGCGTATTGGGCGCTCTTCCGCTTCCTCGCTCACTGACTCGCTGCGCTCGGTCGTTCGGCTGCGGCGAGCGGTATCAGCTCACTCAAAGGCGGTAATACGGTTATCCACAGAATCAGGGGATAACGCAGGAAAGAAC
	ATGTGAGCAAAAGGCCAGCAAAAGGCCAGGAACCGTAAAAAGGCCGCGTTGCTGGCGTTTTTCCATAGGCTCCGCCCCCCTGACGAGCATCACAAAAATCGACGCTCAAGTCAGAGGTGGCGAAACCCGACAGGACTAT

© 2023. Bellver-Sanchis A. et al. Published online at http://www.aginganddisease.org/EN/10.14336/AD.2023.0424-2

SUPPLEMENTARY DATA

AAAGATACCAGGCGTTTCCCCCTGGAAGCTCCCTCGTGCGCTCTCCTGTTCCGACCCTGCCGCTTACCGGATACCTGTCCGCCTTTCTCCCTTCGGGAAGCGTGGCGCTTTCTCATAGCTCACGCTGTAGGTATCTCAGTTCG
GTGTAGGTCGTTCGCTCCAAGCTGGGCTGTGTGCACGAACCCCCCGTTCAGCCCGACCGCTGCGCCTTATCCGGTAACTATCGTCTTGAGTCCAACCCGGTAAGACACGACTTATCGCCACTGGCAGCAGCCACTGGTAAC
AGGATTAGCAGAGCGAGGTATGTAGGCGGTGCTACAGAGTTCTTGAAGTGGTGGCCTAACTACGGCTACACTAGAAGGACAGTATTTGGTATCTGCGCTCTGCTGAAGCCAGTTACCTTCGGAAAAAGAGTTGGTAGCTC
TTGATCCGGCAAACAAACCACCGCTGGTAGCGGTGGTTTTTTTGTTTGCAAGCAGCAGATTACGCGCAGAAAAAAAGGATCTCAAGAAGATCCTTTGATCTTTTCTACGGGGTCTGACGCTCAGTGGAACGAAAACTCACG
TTAAGGGATTTTGGTCATGAGATTATCAAAAAGGATCTTCACCTAGATCCTTTTAAATTAAAAATGAAGTTTTAAATCAATCTAAAGTATATATGAGTAAACTTGGTCTGACAGTTACCAATGCTTAATCAGTGAGGCACCT
ATCTCAGCGATCTGTCTATTTCGTTCATCCATAGTTGCCTGACTCCCCGTCGTGTAGATAACTACGATACGGGAGGGCTTACCATCTGGCCCCAGTGCTGCAATGATACCGCGAGACCCACGCTCACCGGCTCCAGATTTAT
CAGCAATAAACCAGCCAGCCGGAAGGGCCGAGCGCAGAAGTGGTCCTGCAACTTTATCCGCCTCCATCCAGTCTATTAATTGTTGCCGGGAAGCTAGAGTAAGTAGTTCGCCAGTTAATAGTTTGCGCAACGTTGTTGCCA
TTGCTACAGGCATCGTGGTGTCACGCTCGTCGTTTGGTATGGCTTCATTCAGCTCCGGTTCCCAACGATCAAGGCGAGTTACATGATCCCCCATGTTGTGCAAAAAAGCGGTTAGCTCCTTCGGTCCTCCGATCGTTGTCAG
AAGTAAGTTGGCCGCAGTGTTATCACTCATGGTTATGGCAGCACTGCATAATTCTCTTACTGTCATGCCATCCGTAAGATGCTTTTCTGTGACTGGTGAGTACTCAACCAAGTCATTCTGAGAATAGTGTATGCGGCGACCG
AGTTGCTCTTGCCCGGCGTCAATACGGGATAATACCGCGCCACATAGCAGAACTTTAAAAGTGCTCATCATTGGAAAACGTTCTTCGGGGCGAAAACTCTCAAGGATCTTACCGCTGTTGAGATCCAGTTCGATGTAACCC
ACTCGTGCACCCAACTGATCTTCAGCATCTTTTACTTTCACCAGCGTTTCTGGGTGAGCAAAAACAGGAAGGCAAAATGCCGCAAAAAAGGGAATAAGGGCGACACGGAAATGTTGAATACTCATACTCTTCCTTTTTCAA
TATTATTGAAGCATTTATCAGGGTTATTGTCTCATGAGCGGATACATATTTGAATGTATTTAGAAAAATAAACAAATAGGGGTTCCGCGCACATTTCCCCGAAAAGTGCCACCTAAATTGTAAGCGTTAATATTTTGTTAAA
ATTCGCGTTAAATTTTTGTTAAATCAGCTCATTTTTTAACCAATAGGCCGAAATCGGCAAAATCCCTTATAAATCAAAAGAATAGACCGAGATAGGGTTGAGTGTTGTTCCAGTTTGGAACAAGAGTCCACTATTAAAGAA
CGTGGACTCCAACGTCAAAGGGCGAAAAACCGTCTATCAGGGCGATGGCCCACTACGTGAACCATCACCCTAATCAAGTTTTTTGGGGTCGAGGTGCCGTAAAGCACTAAATCGGAACCCTAAAGGGAGCCCCCGATTTA
GAGCTTGACGGGGAAAGCCGGCGAACGTGGCGAGAAAGGAAGGGAAGAAAGCGAAAGGAGCGGGCGCTAGGGCGCTGGCAAGTGTAGCGGTCACGCTGCGCGTAACCACCACACCCGCCGCGCTTAATGCGCCGCTAC
AGGGCGCGTCCCATTCGCCATTCAGGCTGCGCAACTGTTGGGAAGGGCGATCGGTGCGGGCCTCTTCGCTATTACGCCAGTCGACCATAGCCAATTCAATATGGCGTATATGGACTCATGCCAATTCAATATGGTGGATCT
GGACCTGTGCCAATTCAATATGGCGTATATGGACTCGTGCCAATTCAATATGGTGGATCTGGACCCCAGCCAATTCAATATGGCGGACTTGGCACCATGCCAATTCAATATGGCGGACTTGGCACTGTGCCAACTGGGGAG
GGGTCTACTTGGCACGGTGCCAAGTTTGAGGAGGGGTCTTGGCCCTGTGCCAAGTCCGCCATATTGAATTGGCATGGTGCCAATAATGGCGGCCATATTGGCTATATGCCAGGATCAATATATAGGCAATATCCAATATGG
CCCTATGCCAATATGGCTATTGGCCAGGTTCAATACTATGTATTGGCCCTATGCCATATAGTATTCCATATATGGGTTTTCCTATTGACGTAGATAGCCCCTCCCAATGGGCGGTCCCATATACCATATATGGGGCTTCCTAA
TACCGCCCATAGCCACTCCCCCATTGACGTCAATGGTCTCTATATATGGTCTTTCCTATTGACGTCATATGGGCGGTCCTATTGACGTATATGGCGCCTCCCCCATTGACGTCAATTACGGTAAATGGCCCGCCTGGCTCAAT
GCCCATTGACGTCAATAGGACCACCCACCATTGACGTCAATGGGATGGCTCATTGCCCATTCATATCCGTTCTCACGCCCCCTATTGACGTCAATGACGGTAAATGGCCCACTTGGCAGTACATCAATATCTATTAATAGTA
ACTTGGCAAGTACATTACTATTGGAAGGACGCCAGGGTACATTGGCAGTACTCCCATTGACGTCAATGGCGGTAAATGGCCCGCGATGGCTGCCAAGTACATCCCCATTGACGTCAATGGGGAGGGGCAATGACGCAAAT
GGGCGTTCCATTGACGTAAATGGGCGGTAGGCGTGCCTAATGGGAGGTCTATATAAGCAATGCTCGTTTAGGGAAC

K20RK2 CGCCATTCTGCCTGGGGACGTCGGAGCAAGCTTGATTTAGGTGACACTATAGAATACAAGCTACTTGTTCTTTTTGCAGGATCCATGTACCCATACGATGTTCCAGATTACGCTTATCCTTATGACGTACCTGACTATGCAT
5R-KD ACCCTTATGATGTACCAGACTACGCTGGCCGGCCAGAATTCATGAGTGAGTCTTTGGTTGTTTGTGATGTTGCCGAAGATTTAGTGGAAAAGCTGAGACGGTTTCGTTTTCGCCGAGAAACGAACAACGCTGCTATTATAA
TGAAGATTGACAAGGATAAACGCCTGGTGGTACTGGATGAGGAGCTTGAGGGCATTTCACCAGATGAACTTAAAGATGAACTACCTGAACGACAACCTCGCTTCATTGTGTATAGTTATAAATATCAACATGATGATGGA
AGAGTTTCATATCCTCTGTGCTTTATTTTCTCCAGTCCTGTTGGATGTAAGCCTGAACAACAGATGATGTATGCTGGAAGTAAGAATAAGCTAGTCCAGACAGCTGAACTAACCAAGGTATTTGAAATAAGAAATACCGAA
GACCTAACTGAAGAATGGTTACGTGAGAAACTTGGATTTTTTCACTAGTCTAGAACTATAGTGAGTCGTATTACGTAGATCCAGACATGATAAGATACATTGATGAGTTTGGACAAACCACAACTAGAATGCAGTGAAAA
AAATGCTTTATTTGTGAAATTTGTGATGCTATTGCTTTATTTGTAACCATTATAAGCTGCAATAAACAAGTTAACAACAACAATTGCATTCATTTTATGTTTCAGGTTCAGGGGGAGGTGTGGGAGGTTTTTTAATTCGCGGC
CGCGGCGCCAATGCATTGGGCCCGGTACCCAGCTTTTGTTCCCTTTAGTGAGGGTTAATTGCGCGCTTGGCGTAATCATGGTCATAGCTGTTTCCTGTGTGAAATTGTTATCCGCTCACAATTCCACACAACATACGAGCCG
GAAGCATAAAGTGTAAAGCCTGGGGTGCCTAATGAGTGAGCTAACTCACATTAATTGCGTTGCGCTCACTGCCCGCTTTCCAGTCGGGAAACCTGTCGTGCCAGCTGCATTAATGAATCGGCCAACGCGCGGGGAGAGGC
GGTTTGCGTATTGGGCGCTCTTCCGCTTCCTCGCTCACTGACTCGCTGCGCTCGGTCGTTCGGCTGCGGCGAGCGGTATCAGCTCACTCAAAGGCGGTAATACGGTTATCCACAGAATCAGGGGATAACGCAGGAAAGAAC
ATGTGAGCAAAAGGCCAGCAAAAGGCCAGGAACCGTAAAAAGGCCGCGTTGCTGGCGTTTTTCCATAGGCTCCGCCCCCCTGACGAGCATCACAAAAATCGACGCTCAAGTCAGAGGTGGCGAAACCCGACAGGACTAT
AAAGATACCAGGCGTTTCCCCCTGGAAGCTCCCTCGTGCGCTCTCCTGTTCCGACCCTGCCGCTTACCGGATACCTGTCCGCCTTTCTCCCTTCGGGAAGCGTGGCGCTTTCTCATAGCTCACGCTGTAGGTATCTCAGTTCG
GTGTAGGTCGTTCGCTCCAAGCTGGGCTGTGTGCACGAACCCCCCGTTCAGCCCGACCGCTGCGCCTTATCCGGTAACTATCGTCTTGAGTCCAACCCGGTAAGACACGACTTATCGCCACTGGCAGCAGCCACTGGTAAC
AGGATTAGCAGAGCGAGGTATGTAGGCGGTGCTACAGAGTTCTTGAAGTGGTGGCCTAACTACGGCTACACTAGAAGGACAGTATTTGGTATCTGCGCTCTGCTGAAGCCAGTTACCTTCGGAAAAAGAGTTGGTAGCTC
TTGATCCGGCAAACAAACCACCGCTGGTAGCGGTGGTTTTTTTGTTTGCAAGCAGCAGATTACGCGCAGAAAAAAAGGATCTCAAGAAGATCCTTTGATCTTTTCTACGGGGTCTGACGCTCAGTGGAACGAAAACTCACG
TTAAGGGATTTTGGTCATGAGATTATCAAAAAGGATCTTCACCTAGATCCTTTTAAATTAAAAATGAAGTTTTAAATCAATCTAAAGTATATATGAGTAAACTTGGTCTGACAGTTACCAATGCTTAATCAGTGAGGCACCT
ATCTCAGCGATCTGTCTATTTCGTTCATCCATAGTTGCCTGACTCCCCGTCGTGTAGATAACTACGATACGGGAGGGCTTACCATCTGGCCCCAGTGCTGCAATGATACCGCGAGACCCACGCTCACCGGCTCCAGATTTAT
CAGCAATAAACCAGCCAGCCGGAAGGGCCGAGCGCAGAAGTGGTCCTGCAACTTTATCCGCCTCCATCCAGTCTATTAATTGTTGCCGGGAAGCTAGAGTAAGTAGTTCGCCAGTTAATAGTTTGCGCAACGTTGTTGCCA
TTGCTACAGGCATCGTGGTGTCACGCTCGTCGTTTGGTATGGCTTCATTCAGCTCCGGTTCCCAACGATCAAGGCGAGTTACATGATCCCCCATGTTGTGCAAAAAAGCGGTTAGCTCCTTCGGTCCTCCGATCGTTGTCAG
AAGTAAGTTGGCCGCAGTGTTATCACTCATGGTTATGGCAGCACTGCATAATTCTCTTACTGTCATGCCATCCGTAAGATGCTTTTCTGTGACTGGTGAGTACTCAACCAAGTCATTCTGAGAATAGTGTATGCGGCGACCG
AGTTGCTCTTGCCCGGCGTCAATACGGGATAATACCGCGCCACATAGCAGAACTTTAAAAGTGCTCATCATTGGAAAACGTTCTTCGGGGCGAAAACTCTCAAGGATCTTACCGCTGTTGAGATCCAGTTCGATGTAACCC
ACTCGTGCACCCAACTGATCTTCAGCATCTTTTACTTTCACCAGCGTTTCTGGGTGAGCAAAAACAGGAAGGCAAAATGCCGCAAAAAAGGGAATAAGGGCGACACGGAAATGTTGAATACTCATACTCTTCCTTTTTCAA
TATTATTGAAGCATTTATCAGGGTTATTGTCTCATGAGCGGATACATATTTGAATGTATTTAGAAAAATAAACAAATAGGGGTTCCGCGCACATTTCCCCGAAAAGTGCCACCTAAATTGTAAGCGTTAATATTTTGTTAAA
ATTCGCGTTAAATTTTTGTTAAATCAGCTCATTTTTTAACCAATAGGCCGAAATCGGCAAAATCCCTTATAAATCAAAAGAATAGACCGAGATAGGGTTGAGTGTTGTTCCAGTTTGGAACAAGAGTCCACTATTAAAGAA
CGTGGACTCCAACGTCAAAGGGCGAAAAACCGTCTATCAGGGCGATGGCCCACTACGTGAACCATCACCCTAATCAAGTTTTTTGGGGTCGAGGTGCCGTAAAGCACTAAATCGGAACCCTAAAGGGAGCCCCCGATTTA
GAGCTTGACGGGGAAAGCCGGCGAACGTGGCGAGAAAGGAAGGGAAGAAAGCGAAAGGAGCGGGCGCTAGGGCGCTGGCAAGTGTAGCGGTCACGCTGCGCGTAACCACCACACCCGCCGCGCTTAATGCGCCGCTAC
AGGGCGCGTCCCATTCGCCATTCAGGCTGCGCAACTGTTGGGAAGGGCGATCGGTGCGGGCCTCTTCGCTATTACGCCAGTCGACCATAGCCAATTCAATATGGCGTATATGGACTCATGCCAATTCAATATGGTGGATCT
GGACCTGTGCCAATTCAATATGGCGTATATGGACTCGTGCCAATTCAATATGGTGGATCTGGACCCCAGCCAATTCAATATGGCGGACTTGGCACCATGCCAATTCAATATGGCGGACTTGGCACTGTGCCAACTGGGGAG
GGGTCTACTTGGCACGGTGCCAAGTTTGAGGAGGGGTCTTGGCCCTGTGCCAAGTCCGCCATATTGAATTGGCATGGTGCCAATAATGGCGGCCATATTGGCTATATGCCAGGATCAATATATAGGCAATATCCAATATGG
CCCTATGCCAATATGGCTATTGGCCAGGTTCAATACTATGTATTGGCCCTATGCCATATAGTATTCCATATATGGGTTTTCCTATTGACGTAGATAGCCCCTCCCAATGGGCGGTCCCATATACCATATATGGGGCTTCCTAA
TACCGCCCATAGCCACTCCCCCATTGACGTCAATGGTCTCTATATATGGTCTTTCCTATTGACGTCATATGGGCGGTCCTATTGACGTATATGGCGCCTCCCCCATTGACGTCAATTACGGTAAATGGCCCGCCTGGCTCAAT
GCCCATTGACGTCAATAGGACCACCCACCATTGACGTCAATGGGATGGCTCATTGCCCATTCATATCCGTTCTCACGCCCCCTATTGACGTCAATGACGGTAAATGGCCCACTTGGCAGTACATCAATATCTATTAATAGTA
ACTTGGCAAGTACATTACTATTGGAAGGACGCCAGGGTACATTGGCAGTACTCCCATTGACGTCAATGGCGGTAAATGGCCCGCGATGGCTGCCAAGTACATCCCCATTGACGTCAATGGGGAGGGGCAATGACGCAAAT
GGGCGTTCCATTGACGTAAATGGGCGGTAGGCGTGCCTAATGGGAGGTCTATATAAGCAATGCTCGTTTAGGGAAC

© 2023. Bellver-Sanchis A. et al. Published online at http://www.aginganddisease.org/EN/10.14336/AD.2023.0424-2

SUPPLEMENTARY DATA

Supplementary Table 6. Reagents and antibodies used in Flag-tag assay.

Reagent, and antibodies	Source	Catalog number
Flag	Sigma Aldrich	F1804
GMFB	Proteintech	10690-1-AP
pan-me1/2 lysine	PTM Biolabs Inc	PTM-602
HA (0906-1)	HuaBio	0906-1
Hemagglutinin (HA) affinity gel (B23301)	BioTools	B23301
Secondary horseradish peroxidase–conjugated mouse or rabbit	Jackson ImmunoResearch Laboratories	
BIX-01294	Selleck	S8006

Supplementary Table 7. RNA-seq transcripts modified in SAMP8 after UNC0642 treatment.

Gene	logFC	PValue
Ipo7	-11,319704	1,97E-02
Krt80	-8,247241566	5,19E-06
Pla2g4b	-7,866249201	2,83E-05
H2-T9	-7,618812145	9,64E-05
Gm7367	-7,345523261	2,91E-04
Gm3488	-7,26862838	2,91E-04
Xntrpc	-6,880387877	2,00E-03
Nxf7	-6,826410991	2,00E-03
Rxfp2	-6,826410991	2,00E-03
Gm14151	-6,809816111	2,00E-03
Hist2h3c2	-6,739123908	2,86E-03
Tnfsf12Tnfsf13	-6,562838958	4,17E-03
Gm21541	-6,552236283	6,15E-03
Olfr112	-6,45170799	6,15E-03
Gm5803	-6,325081966	9,22E-03
Dynlt1f	-6,323524076	9,22E-03
Hist1h2ai	-6,287220269	1,41E-02
Ppp1r1c	-6,133894589	1,41E-02
Gm13304	-6,083240369	2,19E-02
Gm10409	-6,023084641	2,19E-02
Gm9833	-5,993999277	2,19E-02
Ccl21c	-5,974278078	2,19E-02
1700027H10Rik	-5,944181409	3,48E-02

© 2023. Bellver-Sanchis A. et al. Published online at http://www.aginganddisease.org/EN/10.14336/AD.2023.0424-2

SUPPLEMENTARY DATA

Allc	-5,944181409	3,48E-02
B230312C02Rik	-5,944181409	3,48E-02
D6Ertd474e	-5,944181409	3,48E-02
Gm4477	-5,852093062	3,48E-02
Gm20594	-5,76820844	4,97E-11
Gm5424	-5,462817922	2,54E-07
Lars2	-5,313590279	1,83E-11
Muc19	-4,215351762	2,30E-03
Myl4	-3,990040848	2,79E-06
Xirp2	-3,889491181	2,95E-06
Hfe2	-3,749401968	1,02E-02
Igfn1	-3,606724192	2,55E-06
Nlrp5-ps	-3,524547518	3,57E-03
Gm5643	-3,517064631	2,13E-05
Gk2	-3,374698968	2,80E-02
Olfr78	-3,331010331	2,09E-03
Mypn	-3,288097436	2,95E-04
Cd244	-3,224526076	4,00E-02
Slc5a7	-3,224526076	4,00E-02
Zglp1	-3,224526076	4,00E-02
Traf5	-3,219913595	1,64E-03
Rasgef1c	-3,218677094	6,26E-05
Ptprv	-3,134695472	1,28E-02
Vmn2r86	-3,115651197	1,68E-02
Kcnh4	-3,02774823	1,40E-04
Dkkl1	-2,983733289	3,82E-04
Abi3bp	-2,957375368	1,11E-04
Gm11549	-2,9476096	7,34E-05
2310014L17Rik	-2,940859601	1,02E-04
Slc22a13b-ps	-2,926047112	2,22E-02
Oprk1	-2,913448134	4,23E-04
Ccl27b	-2,834395366	1,84E-04
Hist1h3h	-2,827623997	1,44E-02
Rpl31-ps12	-2,762788559	2,22E-02
A830009L08Rik	-2,76236876	8,48E-03
Pou6f2	-2,749118946	1,83E-02
1700085C21Rik	-2,723102438	3,97E-02
Krt20	-2,693593754	2,91E-03
Egr2	-2,675449606	8,59E-04
Chrnb3	-2,673037676	2,27E-03

© 2023. Bellver-Sanchis A. et al. Published online at http://www.aginganddisease.org/EN/10.14336/AD.2023.0424-2

SUPPLEMENTARY DATA

Neu2	-2,667198069	2,32E-02
Pappa2	-2,61255917	6,26E-04
Gm3985	-2,606436327	4,03E-03
Atp6ap1l	-2,597319206	3,02E-03
Col24a1	-2,584296822	6,66E-04
Adora2a	-2,580343929	2,97E-02
Gm20063	-2,580343929	2,97E-02
Exph5	-2,575561176	2,54E-04
Pld5	-2,572825251	1,65E-03
Sowahb	-2,567330995	4,80E-04
Rgs6	-2,551217565	3,67E-04
Tmem196	-2,550598717	1,81E-03
Gm3264	-2,507204987	3,97E-02
Xkr7	-2,475724991	5,47E-03
C730002L08Rik	-2,431806711	2,15E-03
Lamp5	-2,427609086	5,05E-04
AU023762	-2,42583759	3,82E-02
4933413L06Rik	-2,389176057	4,93E-02
Trhr2	-2,388753325	1,96E-02
1700007J10Rik	-2,388152841	4,93E-02
Jmjd7	-2,370999351	3,97E-02
St6gal2	-2,369023519	1,20E-03
Tnnc1	-2,3529406	5,91E-03
Samd15	-2,295804216	1,03E-02
Ankrd34c	-2,280873506	2,88E-03
Hs3st2	-2,272717812	1,40E-03
Kcnh5	-2,269901982	1,08E-03
Gpr88	-2,263528494	1,48E-03
Wisp1	-2,229016499	3,55E-03
Arhgap25	-2,226222407	3,13E-03
Arc	-2,221169172	1,21E-03
C130074G19Rik	-2,211405496	1,70E-03
Gm13308	-2,192470097	2,70E-03
Krt12	-2,192462277	4,07E-03
Tspan11	-2,181411363	7,47E-03
BC061194	-2,144416131	1,68E-02
Scn4b	-2,034037856	3,03E-03
Cbln2	-2,02891944	3,92E-03
Serpinb8	-2,021891763	6,98E-03
Stard8	-2,003007685	4,69E-03

© 2023. Bellver-Sanchis A. et al. Published online at http://www.aginganddisease.org/EN/10.14336/AD.2023.0424-2

SUPPLEMENTARY DATA

Adra1b	-1,991631158	6,41E-03
Fos	-1,987042966	5,52E-03
Car10	-1,979766778	3,87E-03
Foxp2	-1,973387257	5,86E-03
Gfra2	-1,961064736	4,30E-03
Osbpl3	-1,941149408	4,90E-03
Cckbr	-1,930930123	5,89E-03
Fhod3	-1,929933506	4,89E-03
4930429B21Rik	-1,91392892	1,12E-02
Hkdc1	-1,910930565	8,97E-03
Gpr3	-1,909737015	1,83E-02
Usp43	-1,900961817	3,23E-02
Mapk11	-1,891566276	7,05E-03
Pou3f2	-1,878678928	6,33E-03
Sema3a	-1,877945207	7,00E-03
Cobl	-1,859680603	6,29E-03
Satb2	-1,858770834	6,35E-03
Htr2a	-1,856972279	8,06E-03
Egr1	-1,854138555	6,21E-03
40238	-1,844633634	3,80E-02
4930447C04Rik	-1,763484395	1,95E-02
Mef2c	-1,761785966	8,89E-03
Kcnh7	-1,758381824	9,32E-03
Efna5	-1,726954354	1,23E-02
Adcyap1	-1,719312428	1,83E-02
Rasgef1b	-1,704204363	1,33E-02
Arpp19	-1,701397637	1,17E-02
Vmn2r87	-1,695084158	1,91E-02
Cpne5	-1,679116495	1,39E-02
Garnl3	-1,677050991	1,37E-02
Rims3	-1,672379039	1,53E-02
Igsf9b	-1,659970076	1,46E-02
Ipcef1	-1,659839925	1,42E-02
Pamr1	-1,657019084	1,77E-02
Camk2n1	-1,653683615	1,37E-02
Stx1a	-1,64574588	1,52E-02
Ptgfrn	-1,63762731	1,70E-02
Arhgap10	-1,625261678	1,87E-02
Bmp3	-1,624552224	2,59E-02
Grip2	-1,622521862	2,04E-02

© 2023. Bellver-Sanchis A. et al. Published online at http://www.aginganddisease.org/EN/10.14336/AD.2023.0424-2

SUPPLEMENTARY DATA

Hr	-1,60952456	1,91E-02
Medag	-1,608585008	2,13E-02
Gm13298	-1,608414111	1,74E-02
Cabyr	-1,599224655	2,86E-02
Rcan2	-1,596887545	1,77E-02
Ngef	-1,594846191	1,78E-02
Fam78a	-1,589164233	3,51E-02
Chrdl1	-1,58633467	2,93E-02
Rassf3	-1,579060866	2,38E-02
Mybpc1	-1,578174729	3,98E-02
Mkx	-1,575380228	2,52E-02
Lrrc75a	-1,574448832	3,05E-02
E130012A19Rik	-1,56836578	2,20E-02
6430584L05Rik	-1,557203672	4,03E-02
Mtcl1	-1,556561004	2,08E-02
9130024F11Rik	-1,553879452	2,54E-02
Scube1	-1,550612397	2,20E-02
Gm12429	-1,542070281	3,14E-02
Igfbp6	-1,534829786	2,80E-02
Plcb4	-1,522338966	2,49E-02
Syt6	-1,521533946	2,97E-02
Rgs4	-1,518343565	2,33E-02
BC030499	-1,515752203	3,71E-02
Lipg	-1,507916775	4,95E-02
Gcnt4	-1,506121576	3,12E-02
AI414108	-1,504741516	2,59E-02
Tmem132d	-1,496932664	2,74E-02
Coro6	-1,49077425	3,35E-02
Herc6	-1,476398811	3,41E-02
Tbr1	-1,469527657	2,88E-02
Gm3893	-1,465632753	2,80E-02
Cabp1	-1,461096113	3,05E-02
Dusp1	-1,456942559	3,47E-02
Nr4a1	-1,455995478	3,15E-02
Gabra3	-1,448176395	3,10E-02
Fam124a	-1,431013821	3,98E-02
Ephb6	-1,425342563	3,40E-02
Oprd1	-1,416318281	3,97E-02
Snurf	-1,415951731	3,66E-02
Frmd6	-1,412650518	3,67E-02

© 2023. Bellver-Sanchis A. et al. Published online at http://www.aginganddisease.org/EN/10.14336/AD.2023.0424-2

SUPPLEMENTARY DATA

Kcnh1	-1,40845046	3,59E-02
Kcnab3	-1,397977232	3,88E-02
Adrb1	-1,397134587	4,49E-02
Cux1	-1,39425797	3,75E-02
Trib1	-1,393503557	4,43E-02
Myo1b	-1,38344639	4,22E-02
Pdzrn3	-1,380468319	4,39E-02
Plxnd1	-1,37860681	4,15E-02
Rorb	-1,371766378	4,09E-02
Arhgap42	-1,370386924	4,55E-02
Asb13	-1,368731406	4,36E-02
Zfp365	-1,361238403	4,10E-02
Cux2	-1,358237863	4,29E-02
Camkk2	-1,350480895	4,29E-02
Olfm2	-1,346795264	4,92E-02
Ccl27a	-1,341650988	4,63E-02
Camk4	-1,327173604	4,62E-02
Laptm4a	-1,22959717	6,50E-03
Cadm1	-1,15159789	2,56E-02
Clta	-1,10074302	1,89E-02
Sumo2	-1,09268279	3,72E-02
Nfib	-1,04139882	5,89E-03
Tmsb4x	-1,00403317	4,42E-02
Gmfb	-0,9570028	3,47E-02
Tmsb4xp8	-0,94680387	4,29E-02
Actr2	-0,93045666	4,39E-02
Znf706	-0,85797147	1,36E-02
Etv1	-0,8356197	1,95E-02
Rab10	-0,62599276	4,50E-03
Eif4g3	-0,58949328	3,93E-02
Ppp3ca	-0,58501205	3,33E-02
Ik	-0,57854631	9,05E-03
Ptbp2	-0,55903414	2,22E-02
Ac046176.1	-0,44269435	4,29E-02
Cacn2d1	0,5567782	2,65E-02
Pak5	0,60365478	4,81E-02
Pias2	0,72110603	4,81E-02
Pcdh7	0,79407177	1,73E-04
Cxxc4	0,81488799	1,68E-02
Camk2g	0,82033783	3,31E-02

© 2023. Bellver-Sanchis A. et al. Published online at http://www.aginganddisease.org/EN/10.14336/AD.2023.0424-2

SUPPLEMENTARY DATA

R3hdm2	0,8249999	1,09E-03
Strbp	0,96156862	4,72E-03
Nlk	0,98139251	2,29E-02
R3hdm1	1,02742384	3,03E-02
Clk3	1,06161232	7,01E-04
Atp2b2	1,10097339	2,88E-02
Snap25	1,17876809	1,75E-02
Kctd12	1,314599306	4,95E-02
Cacna1h	1,321380915	4,93E-02
Arhgef26	1,340309119	4,80E-02
Nos1	1,357523454	4,52E-02
Tgfbr3	1,361723754	4,67E-02
Scn3b	1,36577581	4,13E-02
Rgs14	1,365999949	4,54E-02
Orai2	1,373671602	4,07E-02
Gfap	1,388464381	3,80E-02
Abca8a	1,389298438	4,95E-02
Lrrtm1	1,389856521	4,13E-02
Sh3d19	1,398160688	4,05E-02
Nr4a3	1,404884869	4,45E-02
Adamtsl1	1,410432647	4,85E-02
Aankrd52	1,41658774	5,91E-03
Golm1	1,417604621	3,68E-02
Fabp7	1,420098959	4,35E-02
Ptpn14	1,430279612	4,10E-02
Thsd7b	1,432412584	4,14E-02
Gm13826	1,436431364	3,44E-02
Dock4	1,442448871	3,09E-02
Cyp7b1	1,4527982	3,92E-02
Foxo1	1,461309285	3,26E-02
Clmn	1,46686559	2,88E-02
Zfp608	1,467426171	3,04E-02
Ogn	1,468064174	4,89E-02
Bhlhe22	1,470806899	3,05E-02
Cgnl1	1,474375015	3,28E-02
Gsta4	1,489770552	3,11E-02
Hba-a1	1,490337224	2,64E-02
Ehd1	1,490725238	3,06E-02
Kcng2	1,500711283	4,53E-02
Rac3	1,501518798	4,77E-02

© 2023. Bellver-Sanchis A. et al. Published online at http://www.aginganddisease.org/EN/10.14336/AD.2023.0424-2

SUPPLEMENTARY DATA

Sertm1	1,507861696	2,74E-02
Fat4	1,508719203	2,52E-02
Myof	1,512484109	3,58E-02
Cnih2	1,517113199	2,44E-02
Cd44	1,520885861	4,96E-02
Crim1	1,528166045	2,35E-02
Htr2c	1,532213836	2,48E-02
Wbscr17	1,533268231	2,30E-02
Nrp1	1,536230503	2,27E-02
Hspb8	1,546246462	4,31E-02
Pip5k1b	1,54800703	2,57E-02
Gria1	1,552777109	2,03E-02
Necab2	1,555117414	2,47E-02
Mr1	1,556333133	4,75E-02
Fzd7	1,556823989	2,87E-02
Car12	1,56052631	2,35E-02
Abca4	1,567315877	3,82E-02
Txnip	1,567521635	2,92E-02
Crtac1	1,570075721	2,19E-02
Fbn1	1,572265918	2,32E-02
Marcksl1	1,575096909	2,30E-02
Pm20d2	1,577273437	2,90E-02
Tenm2	1,578060239	1,89E-02
Cntnap5c	1,580978784	2,22E-02
Pcdh19	1,592734257	1,84E-02
Ccbe1	1,594951246	2,40E-02
Cdh23	1,596398234	4,97E-02
Spidr	1,597960964	4,97E-02
Slc17a6	1,598820985	2,11E-02
Kit	1,602852343	1,82E-02
Dbi	1,605602181	1,91E-02
Cdc42bpg	1,607740001	3,98E-02
Il17rd	1,611729411	2,93E-02
Samd11	1,618113219	4,71E-02
Ryr3	1,619086178	1,63E-02
Tcf7l2	1,62572914	2,30E-02
Rpl34	1,627195298	2,85E-02
2610018G03Rik	1,627335681	4,48E-02
Icosl	1,627335681	4,48E-02
Svep1	1,627335681	4,48E-02

© 2023. Bellver-Sanchis A. et al. Published online at http://www.aginganddisease.org/EN/10.14336/AD.2023.0424-2

SUPPLEMENTARY DATA

Ass1	1,628059642	2,77E-02
Mt2	1,630902141	1,80E-02
Gdpd2	1,638842505	4,29E-02
A330050F15Rik	1,645666076	3,03E-02
Rreb1	1,64906498	1,49E-02
Evc	1,667852592	2,64E-02
Pde3a	1,66959951	4,97E-02
Pigr	1,677854352	3,89E-02
Efcab1	1,67920105	4,22E-02
Cdhr1	1,687624519	2,99E-02
Dgkg	1,690630932	1,24E-02
Hist4h4	1,706866561	1,70E-02
Sipa1l3	1,717846622	1,13E-02
Dock10	1,721396947	1,12E-02
Slc16a12	1,725192307	2,86E-02
Fgl2	1,72831582	4,95E-02
Man1a	1,728701905	1,15E-02
Scn5a	1,733695853	4,67E-02
Spef2	1,733695853	4,67E-02
Gm20754	1,738092944	3,95E-02
Pwwp2b	1,741418367	1,93E-02
Mc4r	1,74484941	3,30E-02
Ntng1	1,747251097	1,09E-02
Nrp2	1,748684236	1,04E-02
Arsj	1,751806582	2,36E-02
Mum1l1	1,751806582	2,36E-02
Arhgap12	1,757303884	9,78E-03
Wipf3	1,763923057	8,94E-03
Mycl	1,764278642	1,37E-02
Gpc4	1,764613729	1,21E-02
Gabra5	1,76693662	9,50E-03
Lpl	1,769577149	9,74E-03
Rbp1	1,774204212	2,65E-02
Il1r1	1,779089412	1,38E-02
Gfra1	1,780769921	9,97E-03
Pcdh8	1,793113432	1,02E-02
Car14	1,796370325	2,41E-02
Trpc4	1,796786576	9,05E-03
Efemp2	1,796799947	2,17E-02
Epha6	1,799844348	7,87E-03

© 2023. Bellver-Sanchis A. et al. Published online at http://www.aginganddisease.org/EN/10.14336/AD.2023.0424-2

SUPPLEMENTARY DATA

Baiap3	1,803358199	2,44E-02
Spint2	1,803906809	1,48E-02
Nr2f2	1,804837999	9,85E-03
Efcab7	1,805603867	3,65E-02
Gm13315	1,810498417	1,84E-02
Zmat5	1,820398379	1,20E-02
Vwc2l	1,826482194	1,10E-02
Pde11a	1,8336279	1,38E-02
Bambi	1,835096877	2,81E-02
Kcnj13	1,845257078	1,09E-02
Efs	1,849508765	1,84E-02
Dpyd	1,854885113	1,22E-02
Zic1	1,858078146	9,90E-03
Drd5	1,867400793	1,71E-02
Cpq	1,867729146	1,36E-02
Tshz2	1,869612826	6,42E-03
Rerg	1,884081883	1,12E-02
Lpar4	1,887209102	2,23E-02
Col4a3	1,89595633	3,48E-02
Crispld2	1,89595633	3,48E-02
Iqgap2	1,898823931	5,40E-03
C1qtnf5	1,908380631	1,49E-02
Gm15713	1,911294901	4,22E-02
Myo7a	1,91675504	1,19E-02
Cachd1	1,917071556	6,14E-03
Rpl26	1,917948419	8,06E-03
Ctxn2	1,920270718	2,95E-02
Hist2h3b	1,940981538	2,75E-02
Prdm5	1,941250233	8,79E-03
Cpne2	1,945159093	7,25E-03
St18	1,948072887	5,34E-03
Rem2	1,954552738	1,50E-02
4930509J09Rik	1,956903912	3,63E-02
A4galt	1,959308722	4,48E-02
Thbs3	1,96151831	1,08E-02
Gm17762	1,962432428	3,23E-02
Cd38	1,988274065	1,52E-02
Gm14092	1,998842623	4,57E-02
Ubxn10	1,998842623	4,57E-02
Wdr52	1,99902718	7,76E-03

© 2023. Bellver-Sanchis A. et al. Published online at http://www.aginganddisease.org/EN/10.14336/AD.2023.0424-2

SUPPLEMENTARY DATA

Aloxe3	2,001115126	3,12E-02
Fzd10	2,001115126	3,12E-02
Itga8	2,005414525	4,60E-03
Fbn2	2,011835915	7,35E-03
Ky	2,014164962	2,64E-02
Kctd4	2,019710386	3,66E-03
Prelp	2,021900917	4,98E-03
Slit1	2,025578174	3,06E-03
D630023F18Rik	2,032326604	1,60E-02
Car4	2,044751843	4,03E-03
Zfp503	2,051509255	2,31E-02
Rnf182	2,057150615	3,71E-03
Col9a3	2,058913103	4,50E-03
Cyp2e1	2,05964904	2,02E-02
Crym	2,060589138	2,96E-03
Hsd11b1	2,061971529	9,37E-03
Myo5b	2,062478747	2,84E-03
Raver1-fdx1l	2,062516706	2,02E-02
Fbxl7	2,072336316	3,65E-02
Trpm3	2,072989999	2,48E-03
Nr3c2	2,07923315	2,43E-03
Ccdc78	2,079963501	3,65E-02
Fgf10	2,08017776	4,08E-03
Serpina3n	2,082235886	2,70E-03
Vamp8	2,082689285	3,23E-02
Zic4	2,08566951	2,33E-02
4933412O06Rik	2,087911228	2,02E-02
Zfp185	2,089658684	1,58E-02
Col8a1	2,112600755	6,82E-03
Chst8	2,119106751	3,77E-03
St6galnac5	2,12068174	2,23E-03
Cd248	2,123417269	1,77E-02
Nek10	2,12615815	2,02E-02
Ttc21a	2,12615815	2,02E-02
Cyp2j12	2,129787371	2,75E-02
Zbtb20	2,132784333	2,05E-03
Ust	2,138764639	2,29E-03
Mdga1	2,139746487	2,16E-03
Tnfaip8l3	2,146021151	2,99E-03
Cd14	2,154410855	4,93E-02

© 2023. Bellver-Sanchis A. et al. Published online at http://www.aginganddisease.org/EN/10.14336/AD.2023.0424-2

SUPPLEMENTARY DATA

Dach2	2,154410855	4,93E-02
Efhc1	2,154410855	4,93E-02
Gm20751	2,154410855	4,93E-02
Sdc1	2,154410855	4,93E-02
Serpinb1b	2,154410855	4,93E-02
Glb1l2	2,165541443	2,02E-02
Col6a5	2,165963172	2,93E-02
Hopx	2,174351615	2,67E-03
Ackr4	2,17600078	2,93E-02
Amigo2	2,182406338	2,93E-03
Clec1a	2,188993254	3,35E-02
Prox1	2,198285179	1,67E-03
Fam160a1	2,200677224	6,00E-03
Csrp2	2,219607596	2,01E-02
Pon3	2,224975374	1,20E-02
Aard	2,241166426	3,82E-02
Gm16998	2,241166426	3,82E-02
Npbwr1	2,241166426	3,82E-02
Stk33	2,241166426	3,82E-02
Prokr2	2,241205379	2,81E-02
Mamdc2	2,241232006	8,73E-03
Ace	2,248521334	1,34E-03
Slc9a2	2,256242367	2,36E-03
Gm21949	2,259219636	2,36E-03
Grp	2,269725303	8,73E-03
Thsd4	2,278168163	1,51E-03
Hist1h2ac	2,291269208	1,99E-02
Gpnmb	2,291593724	2,36E-02
Ecel1	2,304161979	1,48E-02
Tmem255a	2,309782987	1,36E-03
Trpv4	2,313130449	1,15E-02
Gm14685	2,314221849	2,97E-02
Lamb1	2,320208453	1,08E-03
E030013I19Rik	2,32299961	2,97E-02
Rasd1	2,341053926	1,81E-03
Card6	2,351976732	6,20E-03
Slc44a5	2,369505493	1,09E-03
Cpne6	2,391071281	5,51E-04
Figf	2,39233661	1,55E-02
Tanc1	2,39576864	5,55E-04

© 2023. Bellver-Sanchis A. et al. Published online at http://www.aginganddisease.org/EN/10.14336/AD.2023.0424-2

SUPPLEMENTARY DATA

Egf	2,400439122	2,32E-02
Sec14l3	2,400439122	2,32E-02
Col11a1	2,427926047	5,93E-04
Ly6a	2,432988505	1,42E-02
Pcdha4	2,440238373	1,53E-03
Enpp2	2,457199985	3,67E-04
Fam161a	2,465307247	5,07E-03
Sema3b	2,478627816	5,91E-03
Msx1	2,486825244	3,56E-03
Rxfp3	2,502796227	1,03E-02
Tgfb2	2,510147495	4,38E-04
Col5a2	2,511182319	1,32E-03
Lum	2,519617242	4,01E-03
Dnah9	2,521046696	3,91E-04
Efhb	2,521932429	3,97E-02
Hoga1	2,521932429	3,97E-02
Myoc	2,521932429	3,97E-02
Ebf3	2,543863377	1,44E-02
Glis3	2,546897161	7,43E-04
Rph3al	2,561754104	8,74E-03
Sec1	2,565135862	1,13E-02
Cdkn1c	2,579962723	9,09E-04
Pkp2	2,598231944	4,97E-04
Adamts9	2,598897692	1,01E-03
9930014A18Rik	2,600109721	1,92E-03
Crhr2	2,610560385	1,14E-02
Zbbx	2,610560385	1,14E-02
Cidea	2,620553043	2,96E-02
Col2a1	2,620553043	2,96E-02
Pcdh20	2,637568267	1,75E-04
Gramd1c	2,641626037	7,46E-03
Npr1	2,647069141	2,28E-03
Ndst4	2,653975606	3,52E-04
Nnat	2,673915291	1,48E-04
Trp73	2,701182468	4,77E-03
Espl1	2,712861293	2,22E-02
Nmbr	2,712861293	2,22E-02
Frem3	2,717307028	5,47E-03
Dqx1	2,726990723	1,68E-02
Tgtp1	2,732129274	3,42E-03

© 2023. Bellver-Sanchis A. et al. Published online at http://www.aginganddisease.org/EN/10.14336/AD.2023.0424-2

SUPPLEMENTARY DATA

Olfml2b	2,733154203	2,24E-04
Wdr96	2,761669883	1,95E-03
Foxj1	2,764169838	1,33E-03
Gstm6	2,789215043	4,05E-03
Cldn26	2,793933109	7,29E-03
A2m	2,80324447	7,33E-04
Klk8	2,808472316	1,20E-03
Lmo1	2,808472316	1,20E-03
Eomes	2,844331315	1,28E-02
Tnxb	2,850918718	1,37E-04
Xist	2,853211356	2,76E-03
Slc2a12	2,855868508	2,75E-04
Igsf1	2,860975203	1,23E-03
Dnaic2	2,881450049	1,28E-02
Lrrc10b	2,896702224	1,68E-04
Myh8	2,920857723	2,27E-03
Gpx8	2,954229962	1,27E-03
Col4a4	2,956604852	3,83E-03
Arhgap28	2,958889561	9,78E-03
Grem1	2,958889561	9,78E-03
Il20rb	2,958889561	9,78E-03
Stpg1	3,032383254	7,53E-03
Ppl	3,045602891	1,31E-03
Gpr161	3,05499536	8,99E-05
Homer3	3,068169327	1,08E-04
Dnah11	3,07807118	4,44E-04
Slc29a4	3,081356135	1,07E-04
Lrrc18	3,101013938	4,00E-02
Plek2	3,101013938	4,00E-02
Slc39a4	3,101013938	4,00E-02
Ttc16	3,101013938	4,00E-02
Zfp345	3,114890244	1,98E-02
Doc2b	3,146985114	1,67E-05
Slc26a4	3,154500402	1,06E-04
Gm2115	3,158260507	2,68E-05
Cpne7	3,189280277	1,09E-05
1700026D08Rik	3,225092539	2,80E-02
Dgkk	3,225092539	2,80E-02
Gck	3,225092539	2,80E-02
Umodl1	3,225092539	2,80E-02

© 2023. Bellver-Sanchis A. et al. Published online at http://www.aginganddisease.org/EN/10.14336/AD.2023.0424-2

SUPPLEMENTARY DATA

Stra6	3,238742355	2,12E-04
Calb2	3,240373842	2,86E-05
Shisa6	3,252776424	6,68E-06
Cd109	3,275206174	1,93E-04
Hbq1a	3,278772013	1,98E-02
Spag16	3,287353315	1,18E-03
Stac	3,293811338	3,57E-03
Prkcd	3,299168623	1,50E-05
Caps2	3,33933976	1,98E-02
Cndp1	3,33933976	1,98E-02
Fhl4	3,33933976	1,98E-02
Ppic	3,33933976	1,98E-02
Prph	3,33933976	1,98E-02
Agt	3,39908875	3,88E-05
Spink8	3,416966559	2,22E-04
Cabp7	3,427139509	1,27E-05
Rbm47	3,444907994	2,22E-04
Ccl6	3,445199846	1,42E-02
Plcz1	3,445199846	1,42E-02
Egfl6	3,449276862	1,42E-02
Mdfic	3,493698643	1,04E-04
Nts	3,51505529	1,42E-03
Popdc3	3,51505529	1,42E-03
Dynlrb2	3,54382046	1,02E-02
Cldn1	3,55155745	1,29E-04
Fermt1	3,566928427	1,14E-03
Gmnc	3,573107949	2,91E-04
Htr4	3,606232028	1,68E-05
Ccdc153	3,63612871	7,45E-03
Tmem255b	3,722884281	5,48E-03
Vit	3,751049631	4,97E-04
Il16	3,778064678	2,02E-06
Fam212a	3,804717466	4,07E-03
Gja4	3,804717466	4,07E-03
Usp51	3,804717466	4,07E-03
Wdr63	3,804717466	4,07E-03
Lgr6	3,831055529	3,29E-05
2310002F09Rik	3,835604015	3,36E-04
Col8a2	3,872111422	2,69E-05
Mfrp	3,873086203	5,01E-05

© 2023. Bellver-Sanchis A. et al. Published online at http://www.aginganddisease.org/EN/10.14336/AD.2023.0424-2

SUPPLEMENTARY DATA

Lct	3,881980931	6,91E-07
Magel2	3,882156978	3,04E-03
Dcn	3,894310231	4,96E-07
Calml4	3,95315395	4,85E-05
Meig1	3,955650671	2,30E-03
Tuft1	3,955650671	2,30E-03
Cebpd	4,002419518	3,70E-05
Aqp1	4,003660879	3,70E-05
Dlk1	4,003660879	3,70E-05
Wdr16	4,025581232	1,74E-03
Cox6b2	4,092278241	1,33E-03
Gpr101	4,122695007	1,94E-05
Dsc3	4,131558388	9,50E-05
Fibcd1	4,175764988	7,82E-08
Npy2r	4,217207525	2,41E-07
Lbp	4,235389899	9,19E-06
Chst9	4,275650965	7,97E-04
Serpina3h	4,372220136	4,88E-04
Capsl	4,386110582	4,88E-04
Prlr	4,461503752	2,16E-08
Ntf3	4,584496823	1,95E-04
C3	4,630105833	1,57E-04
1500015O10Rik	4,661208562	9,29E-07
Crlf1	4,758871432	8,44E-05
C1ql2	4,853266464	2,43E-06
Slc9a4	5,01436128	1,48E-07
Slitrk6	5,020985524	2,70E-05
Epn3	5,087890476	1,89E-05
Kl	5,530406846	2,68E-11
F5	5,596176696	5,23E-10
Dsp	5,615867008	3,66E-11
Clic6	5,621113392	4,41E-10
Arhgef16	5,729836039	3,48E-02
Ccdc33	5,729836039	3,48E-02
Clec4a3	5,729836039	3,48E-02
Cox8b	5,729836039	3,48E-02
Dmrt3	5,729836039	3,48E-02
Gm16551	5,729836039	3,48E-02
Nespas	5,729836039	3,48E-02
Slc16a8	5,729836039	3,48E-02

© 2023. Bellver-Sanchis A. et al. Published online at http://www.aginganddisease.org/EN/10.14336/AD.2023.0424-2

SUPPLEMENTARY DATA

Slc38a4	5,729836039	3,48E-02
Slco1a5	5,729836039	3,48E-02
Tmem102	5,729836039	3,48E-02
Tmem212	5,729836039	3,48E-02
Hist1h2ap	5,751910039	3,48E-02
Ccdc135	5,776533881	5,12E-07
Gm8989	5,863023466	3,48E-02
4933427G17Rik	5,919079041	2,19E-02
Avpr1b	5,919079041	2,19E-02
Cldn19	5,919079041	2,19E-02
Pemt	5,919079041	2,19E-02
Tbx4	5,919079041	2,19E-02
Fam227b	5,961028766	2,19E-02
Tcfl5	5,986641127	2,19E-02
Nup62-il4i1	6,020098623	2,19E-02
Avpr1a	6,086352426	2,19E-02
Enpp3	6,086352426	2,19E-02
Gm4951	6,086352426	2,19E-02
Prom2	6,086352426	2,19E-02
Rab38	6,086352426	2,19E-02
Trp63	6,086352426	2,19E-02
Tmem140	6,089507778	2,19E-02
Folr1	6,101968665	7,86E-08
Naip6	6,234806451	1,41E-02
Gm19299	6,236230711	1,41E-02
Igbp1b	6,236230711	1,41E-02
Iqch	6,236230711	1,41E-02
Klk10	6,236230711	1,41E-02
Lgals3	6,236230711	1,41E-02
Sec14l4	6,236230711	1,41E-02
Pmch	6,301632819	9,22E-03
Mpzl3	6,371993425	9,22E-03
Pifo	6,371993425	9,22E-03
Ripk4	6,371993425	9,22E-03
Steap4	6,371993425	9,22E-03
Gstp2	6,410350159	6,15E-03
Slc4a5	6,496079135	7,70E-09
Catsperg2	6,509091297	6,15E-03
Krt8	6,610319247	4,17E-03
Scin	6,610319247	4,17E-03

© 2023. Bellver-Sanchis A. et al. Published online at http://www.aginganddisease.org/EN/10.14336/AD.2023.0424-2

SUPPLEMENTARY DATA

Hist2h2aa2	6,672660301	2,86E-03
Kcnh8	6,716179333	2,86E-03
Nek5	6,716179333	2,86E-03
Spint1	6,716179333	2,86E-03
Chrm5	6,814799947	2,00E-03
Lrp2	6,814799947	2,00E-03
Hist2h3c1	6,905318745	1,41E-03
Best3	6,907108198	1,41E-03
Serpina3g	6,941566087	1,41E-03
Krt2	6,993863769	1,01E-03
Wdr86	6,993863769	1,01E-03
Apoc1	7,075696953	7,27E-04
Oca2	7,075696953	7,27E-04
Gm11992	7,153136465	5,30E-04
Ccdc146	7,226630158	3,91E-04
Iyd	7,226630158	3,91E-04
Tmprss11a	7,226630158	3,91E-04
Wfdc2	7,226630158	3,91E-04
Zcchc5	7,363257728	2,18E-04
Prr32	7,602917167	9,64E-05
Krt18	7,657090069	7,45E-05
Tdo2	7,709302194	5,79E-05
Steap1	7,808378224	3,57E-05
Rsc1a1	7,878004917	2,83E-05
Lrrc23	8,070339558	9,48E-06
Rdh5	8,291965011	3,54E-06
Gm3317	8,292649654	3,54E-06
Jmjd7-pla2g4b	8,48043344	1,22E-06
Otx2	8,513699706	1,03E-06
Cldn2	8,852358284	1,68E-07
Kcne2	8,985349371	8,64E-08
Rnaset2b	9,294967611	1,47E-08
Lhx9	9,356998414	9,62E-09
Ttr	9,445444196	1,16E-22
Sostdc1	9,638315625	1,74E-09
Tmem72	10,12514828	9,25E-11

© 2023. Bellver-Sanchis A. et al. Published online at http://www.aginganddisease.org/EN/10.14336/AD.2023.0424-2

SUPPLEMENTARY DATA

Supplementary Table. 8 | H3K9me2 peaks at TSS in AML12 cells treated with UNC0638.

Chr	Star	End	Peak	Score	TSS
chr1	32172176	32173098	H3K9ME2_UNC0638_peak_1	59	*Khdrbs2*
chr1	42952750	42953467	H3K9ME2_UNC0638_peak_2	32	*Gpr45*
chr1	69826896	69827244	H3K9ME2_UNC0638_peak_3	38	*Spag16*
chr1	86703769	86704122	H3K9ME2_UNC0638_peak_4	32	*Dis3l2*
chr1	109983282	109983585	H3K9ME2_UNC0638_peak_5	35	*Cdh7*
chr1	152955282	152955573	H3K9ME2_UNC0638_peak_6	17	*Nmnat2*
chr1	181352292	181353448	H3K9ME2_UNC0638_peak_7	55	*Cnih3*
chr1	33907545	33908234	H3K9ME2_UNC0638_peak_8	36	*Dst*
chr1	46425308	46425654	H3K9ME2_UNC0638_peak_9	32	*Dnah7c*
chr1	55932595	55932886	H3K9ME2_UNC0638_peak_10	27	*9130227L01Rik*
chr1	61306509	61307159	H3K9ME2_UNC0638_peak_11	44	*Gm11587*
chr1	63272940	63273933	H3K9ME2_UNC0638_peak_12	47	*Zdbf2*
chr1	66467924	66468734	H3K9ME2_UNC0638_peak_13	67	-
chr1	75359938	75360478	H3K9ME2_UNC0638_peak_14	28	*Des*
chr1	78310141	78310538	H3K9ME2_UNC0638_peak_15	27	*Sgpp2*
chr1	88318028	88318504	H3K9ME2_UNC0638_peak_16	50	*Trpm8*
chr1	125911610	125912180	H3K9ME2_UNC0638_peak_17	30	*Nckap5*
chr1	132880196	132881157	H3K9ME2_UNC0638_peak_18	41	*Lrrn2*
chr1	134560228	134560814	H3K9ME2_UNC0638_peak_19	27	*Kdm5b*
chr1	151571373	151571664	H3K9ME2_UNC0638_peak_20	17	*Niban1*
chr1	171558852	171559405	H3K9ME2_UNC0638_peak_21	49	*Cd244a*
chr1	174501679	174501970	H3K9ME2_UNC0638_peak_22	38	*Fmn2*
chr1	178530181	178530552	H3K9ME2_UNC0638_peak_23	27	*Kif26b*
chr1	185455088	185455402	H3K9ME2_UNC0638_peak_24	23	*Slc30a10*
chr1	5588745	5589103	H3K9ME2_UNC0638_peak_25	38	*Oprk1*
chr1	12668530	12669260	H3K9ME2_UNC0638_peak_26	48	*Gm17644*
chr1	13844932	13845233	H3K9ME2_UNC0638_peak_27	40	*Gm31195*
chr1	17097006	17097301	H3K9ME2_UNC0638_peak_28	36	-
chr1	17098085	17098400	H3K9ME2_UNC0638_peak_29	38	-
chr1	17727613	17728196	H3K9ME2_UNC0638_peak_30	42	*Crispld1*
chr1	34432350	34432641	H3K9ME2_UNC0638_peak_31	32	*Mir5103*
chr1	34552393	34552789	H3K9ME2_UNC0638_peak_32	40	*Prss40*
chr1	36778555	36778879	H3K9ME2_UNC0638_peak_33	35	*Zap70*
chr1	39650357	39651172	H3K9ME2_UNC0638_peak_34	50	-
chr1	42697541	42698155	H3K9ME2_UNC0638_peak_35	28	*Pou3f3*
chr1	43092196	43092718	H3K9ME2_UNC0638_peak_36	32	-
chr1	54283281	54283777	H3K9ME2_UNC0638_peak_37	25	-

© 2023. Bellver-Sanchis A. et al. Published online at http://www.aginganddisease.org/EN/10.14336/AD.2023.0424-2

SUPPLEMENTARY DATA

chr1	75375352	75375752	H3K9ME2_UNC0638_peak_38	27	*Speg*
chr1	79436072	79436448	H3K9ME2_UNC0638_peak_39	27	*Scg2*
chr1	85112336	85112656	H3K9ME2_UNC0638_peak_40	94	-
chr1	85246996	85247295	H3K9ME2_UNC0638_peak_41	20	*C130026I21Rik*
chr1	88205406	88205697	H3K9ME2_UNC0638_peak_42	22	*Dnajb3*
chr1	89931250	89931600	H3K9ME2_UNC0638_peak_43	27	-
chr1	92831081	92832134	H3K9ME2_UNC0638_peak_44	63	*Gpc1*
chr1	92932595	92932886	H3K9ME2_UNC0638_peak_45	44	*9430060I03Rik*
chr1	93804024	93804315	H3K9ME2_UNC0638_peak_46	50	*Ing5*
chr1	104304415	104304706	H3K9ME2_UNC0638_peak_47	25	*Gm41924*
chr1	105780310	105780783	H3K9ME2_UNC0638_peak_48	22	*Tnfrsf11a*
chr1	120114600	120114913	H3K9ME2_UNC0638_peak_49	22	*Dbi*
chr1	120340534	120341649	H3K9ME2_UNC0638_peak_50	29	*C1ql2*
chr1	130422730	130423060	H3K9ME2_UNC0638_peak_51	32	-
chr1	134298844	134299371	H3K9ME2_UNC0638_peak_52	37	-
chr1	134492941	134493408	H3K9ME2_UNC0638_peak_53	27	*Rabif*
chr1	148711936	148712267	H3K9ME2_UNC0638_peak_54	28	*Gm41966*
chr1	150361741	150362280	H3K9ME2_UNC0638_peak_55	50	-
chr1	151344453	151344786	H3K9ME2_UNC0638_peak_56	38	-
chr1	155244012	155245088	H3K9ME2_UNC0638_peak_57	94	*Gm31102*
chr1	171064454	171064772	H3K9ME2_UNC0638_peak_58	88	*Mir6546*
chr1	171517893	171518533	H3K9ME2_UNC0638_peak_59	45	*Itln1*
chr1	180813983	180814274	H3K9ME2_UNC0638_peak_60	27	-
chr1	185363133	185363509	H3K9ME2_UNC0638_peak_61	38	-
chr1	192855211	192855663	H3K9ME2_UNC0638_peak_62	27	*Gm15867*
chr2	19909691	19909983	H3K9ME2_UNC0638_peak_63	29	-
chr2	31314101	31314466	H3K9ME2_UNC0638_peak_64	17	-
chr2	55436192	55436925	H3K9ME2_UNC0638_peak_65	43	-
chr2	156196944	156197268	H3K9ME2_UNC0638_peak_66	72	*Phf20*
chr2	4717531	4717822	H3K9ME2_UNC0638_peak_67	34	*Bend7*
chr2	4718219	4718714	H3K9ME2_UNC0638_peak_68	55	*Bend7*
chr2	11172175	11172547	H3K9ME2_UNC0638_peak_69	32	*Prkcq*
chr2	14513140	14513746	H3K9ME2_UNC0638_peak_70	38	-
chr2	21877679	21877991	H3K9ME2_UNC0638_peak_71	34	*Gm39767*
chr2	24626125	24626421	H3K9ME2_UNC0638_peak_72	21	*Cacna1b*
chr2	49787570	49788011	H3K9ME2_UNC0638_peak_73	20	*Lypd6b*
chr2	50065985	50066545	H3K9ME2_UNC0638_peak_74	28	*Lypd6*
chr2	70509116	70509621	H3K9ME2_UNC0638_peak_75	27	*Erich2*
chr2	71980942	71981612	H3K9ME2_UNC0638_peak_76	51	*Rapgef4*
chr2	75137654	75138154	H3K9ME2_UNC0638_peak_77	27	*2600014E21Rik*

© 2023. Bellver-Sanchis A. et al. Published online at http://www.aginganddisease.org/EN/10.14336/AD.2023.0424-2

SUPPLEMENTARY DATA

chr2	79255078	79255957	H3K9ME2_UNC0638_peak_78	72	*Itga4*
chr2	106693390	106694023	H3K9ME2_UNC0638_peak_79	31	*Mpped2*
chr2	110362142	110362495	H3K9ME2_UNC0638_peak_80	27	*Fibin*
chr2	133552639	133552992	H3K9ME2_UNC0638_peak_81	32	*Bmp2*
chr2	135659643	135659956	H3K9ME2_UNC0638_peak_82	43	*Plcb4*
chr2	156613736	156614494	H3K9ME2_UNC0638_peak_83	42	-
chr2	156721041	156721378	H3K9ME2_UNC0638_peak_84	64	*Dlgap4*
chr2	157913978	157915252	H3K9ME2_UNC0638_peak_85	125	*Vstm2l*
chr2	165111874	165112247	H3K9ME2_UNC0638_peak_86	21	*Cdh22*
chr2	167096733	167097026	H3K9ME2_UNC0638_peak_87	28	*Kcnb1*
chr2	177320997	177321365	H3K9ME2_UNC0638_peak_88	68	-
chr2	177464802	177465255	H3K9ME2_UNC0638_peak_89	27	*Zfp970*
chr2	14417361	14417896	H3K9ME2_UNC0638_peak_90	30	-
chr2	19445260	19445551	H3K9ME2_UNC0638_peak_91	27	*Ptf1a*
chr2	25706651	25707280	H3K9ME2_UNC0638_peak_92	50	*Bmyc*
chr2	28446924	28447360	H3K9ME2_UNC0638_peak_93	26	-
chr2	31541707	31542253	H3K9ME2_UNC0638_peak_94	43	*Gm32952*
chr2	31670018	31670418	H3K9ME2_UNC0638_peak_95	27	*Exosc2*
chr2	42871218	42871601	H3K9ME2_UNC0638_peak_96	23	*Gm39803*
chr2	56786358	56786649	H3K9ME2_UNC0638_peak_97	17	*Mir195b*
chr2	74668618	74669122	H3K9ME2_UNC0638_peak_98	25	*Hoxd13*
chr2	75434723	75435341	H3K9ME2_UNC0638_peak_99	27	*9430019J16Rik*
chr2	84872034	84872802	H3K9ME2_UNC0638_peak_100	48	*Rtn4rl2*
chr2	85136579	85136977	H3K9ME2_UNC0638_peak_101	22	*Aplnr*
chr2	90889285	90889763	H3K9ME2_UNC0638_peak_102	17	*C1qtnf4*
chr2	92600285	92600606	H3K9ME2_UNC0638_peak_103	29	-
chr2	93642614	93642949	H3K9ME2_UNC0638_peak_104	28	*Alx4*
chr2	93956501	93957010	H3K9ME2_UNC0638_peak_105	51	*Gm13889*
chr2	119594351	119594644	H3K9ME2_UNC0638_peak_106	27	*Oip5os1*
chr2	126552899	126553313	H3K9ME2_UNC0638_peak_107	36	*Slc27a2*
chr2	131040889	131041807	H3K9ME2_UNC0638_peak_108	80	*Gfra4*
chr2	144458357	144458654	H3K9ME2_UNC0638_peak_109	32	*Zfp133-ps*
chr2	146221986	146223758	H3K9ME2_UNC0638_peak_110	43	*Insm1*
chr2	147084285	147085664	H3K9ME2_UNC0638_peak_111	76	*Nkx2-4*
chr2	148395112	148395459	H3K9ME2_UNC0638_peak_112	22	*Sstr4*
chr2	150667935	150668232	H3K9ME2_UNC0638_peak_113	46	*E130215H24Rik*
chr2	151701976	151702389	H3K9ME2_UNC0638_peak_114	38	*Tmem74b*
chr2	153031668	153032952	H3K9ME2_UNC0638_peak_115	63	*Xkr7*
chr2	157078794	157079770	H3K9ME2_UNC0638_peak_116	79	*Tldc2*
chr2	163918616	163918951	H3K9ME2_UNC0638_peak_117	51	*Gm35886*

© 2023. Bellver-Sanchis A. et al. Published online at http://www.aginganddisease.org/EN/10.14336/AD.2023.0424-2

SUPPLEMENTARY DATA

chr2	164168141	164168545	H3K9ME2_UNC0638_peak_118	27	-
chr2	164199756	164200268	H3K9ME2_UNC0638_peak_119	50	*Wfdc15a*
chr2	164804818	164805109	H3K9ME2_UNC0638_peak_120	44	*Zswim3*
chr2	164967912	164968491	H3K9ME2_UNC0638_peak_121	38	*Slc12a5*
chr2	174110346	174110681	H3K9ME2_UNC0638_peak_122	38	*Npepl1*
chr2	178414411	178414806	H3K9ME2_UNC0638_peak_123	33	*Fam217b*
chr2	180892914	180893361	H3K9ME2_UNC0638_peak_124	24	*Mir124a-3*
chr3	34561765	34562056	H3K9ME2_UNC0638_peak_125	36	*Sox2ot*
chr3	8510144	8510435	H3K9ME2_UNC0638_peak_126	26	*Stmn2*
chr3	8510900	8511332	H3K9ME2_UNC0638_peak_127	17	*Stmn2*
chr3	37063597	37063902	H3K9ME2_UNC0638_peak_128	27	-
chr3	37348466	37348874	H3K9ME2_UNC0638_peak_129	50	*Fgf2*
chr3	59005789	59006358	H3K9ME2_UNC0638_peak_130	27	*Med12l*
chr3	62603656	62603992	H3K9ME2_UNC0638_peak_131	25	-
chr3	105452355	105452766	H3K9ME2_UNC0638_peak_132	28	-
chr3	145987948	145988470	H3K9ME2_UNC0638_peak_133	38	*Syde2*
chr3	146220815	146221383	H3K9ME2_UNC0638_peak_134	38	*Lpar3*
chr3	18054677	18055448	H3K9ME2_UNC0638_peak_135	35	*Bhlhe22*
chr3	27371835	27372505	H3K9ME2_UNC0638_peak_136	31	*Ghsr*
chr3	31309800	31310370	H3K9ME2_UNC0638_peak_137	23	-
chr3	35932605	35932896	H3K9ME2_UNC0638_peak_138	22	-
chr3	39277391	39278016	H3K9ME2_UNC0638_peak_139	32	*Gm42214*
chr3	41555841	41556362	H3K9ME2_UNC0638_peak_140	90	*Jade1*
chr3	55181750	55182041	H3K9ME2_UNC0638_peak_141	32	*Sohlh2*
chr3	68869807	68870580	H3K9ME2_UNC0638_peak_142	98	*1110032F04Rik*
chr3	82905219	82905668	H3K9ME2_UNC0638_peak_143	26	*Rbm46os*
chr3	85340864	85341219	H3K9ME2_UNC0638_peak_144	22	*Gm31210*
chr3	87412031	87412382	H3K9ME2_UNC0638_peak_145	28	*Gm40084*
chr3	89773327	89773771	H3K9ME2_UNC0638_peak_146	32	*Ube2q1*
chr3	89830948	89831701	H3K9ME2_UNC0638_peak_147	37	*She*
chr3	94363489	94364279	H3K9ME2_UNC0638_peak_148	38	*C2cd4d*
chr3	94412767	94413058	H3K9ME2_UNC0638_peak_149	22	-
chr3	100472586	100472968	H3K9ME2_UNC0638_peak_150	26	*Tent5c*
chr3	102011590	102013060	H3K9ME2_UNC0638_peak_151	55	*Nhlh2*
chr3	103576358	103576832	H3K9ME2_UNC0638_peak_152	16	*Syt6*
chr3	118434492	118434912	H3K9ME2_UNC0638_peak_153	61	*Mir137*
chr3	121590881	121591428	H3K9ME2_UNC0638_peak_154	64	*Gm33708*
chr3	121952957	121953574	H3K9ME2_UNC0638_peak_155	37	*Arhgap29*
chr3	121953739	121954030	H3K9ME2_UNC0638_peak_156	27	*Arhgap29*
chr4	9269371	9269680	H3K9ME2_UNC0638_peak_157	30	*Clvs1*

© 2023. Bellver-Sanchis A. et al. Published online at http://www.aginganddisease.org/EN/10.14336/AD.2023.0424-2

SUPPLEMENTARY DATA

chr4	17853311	17853817	H3K9ME2_UNC0638_peak_158	50	*Mmp16*
chr4	73790885	73791176	H3K9ME2_UNC0638_peak_159	22	*Gm11240*
chr4	86276617	86276912	H3K9ME2_UNC0638_peak_160	44	-
chr4	114405860	114406219	H3K9ME2_UNC0638_peak_161	71	-
chr4	128654445	128655013	H3K9ME2_UNC0638_peak_162	22	*Phc2*
chr4	128688272	128688655	H3K9ME2_UNC0638_peak_163	22	*Phc2*
chr4	134073036	134073327	H3K9ME2_UNC0638_peak_164	26	*Crybg2*
chr4	136835514	136835808	H3K9ME2_UNC0638_peak_165	35	-
chr4	136836292	136836583	H3K9ME2_UNC0638_peak_166	20	-
chr4	9917002	9917391	H3K9ME2_UNC0638_peak_167	22	*4930448K20Rik*
chr4	11191092	11191383	H3K9ME2_UNC0638_peak_168	57	*Ccne2*
chr4	11385547	11385884	H3K9ME2_UNC0638_peak_169	17	*Gm35631*
chr4	21678809	21680027	H3K9ME2_UNC0638_peak_170	38	*Prdm13*
chr4	41194770	41195197	H3K9ME2_UNC0638_peak_171	44	-
chr4	42916900	42917191	H3K9ME2_UNC0638_peak_172	36	-
chr4	42917368	42917659	H3K9ME2_UNC0638_peak_173	34	-
chr4	87100836	87101307	H3K9ME2_UNC0638_peak_174	26	-
chr4	91371585	91372221	H3K9ME2_UNC0638_peak_175	38	*Mir6402*
chr4	99656561	99657243	H3K9ME2_UNC0638_peak_176	26	*Foxd3*
chr4	101068884	101069239	H3K9ME2_UNC0638_peak_177	50	*Raver2*
chr4	108217335	108217868	H3K9ME2_UNC0638_peak_178	32	-
chr4	114907608	114908038	H3K9ME2_UNC0638_peak_179	22	*Foxd2*
chr4	114925044	114925530	H3K9ME2_UNC0638_peak_180	22	*Foxe3*
chr4	114925685	114926329	H3K9ME2_UNC0638_peak_181	38	*Foxe3*
chr4	119072889	119073309	H3K9ME2_UNC0638_peak_182	44	*Gm35510*
chr4	120854625	120855205	H3K9ME2_UNC0638_peak_183	38	*Rims3*
chr4	122996554	122997014	H3K9ME2_UNC0638_peak_184	48	*Mycl*
chr4	123104957	123105424	H3K9ME2_UNC0638_peak_185	27	*Bmp8b*
chr4	124658377	124658947	H3K9ME2_UNC0638_peak_186	27	*Pou3f1*
chr4	129239044	129239347	H3K9ME2_UNC0638_peak_187	38	-
chr5	117413730	117414317	H3K9ME2_UNC0638_peak_188	44	*Ksr2*
chr5	9266000	9266621	H3K9ME2_UNC0638_peak_189	43	-
chr5	9381168	9381459	H3K9ME2_UNC0638_peak_190	32	-
chr5	14514991	14515450	H3K9ME2_UNC0638_peak_191	38	-
chr5	19226254	19226885	H3K9ME2_UNC0638_peak_192	61	-
chr5	22746374	22746893	H3K9ME2_UNC0638_peak_193	47	-
chr5	36490757	36491339	H3K9ME2_UNC0638_peak_194	22	*Tbc1d14*
chr5	63648773	63649519	H3K9ME2_UNC0638_peak_195	32	*Nwd2*
chr5	63650077	63650608	H3K9ME2_UNC0638_peak_196	36	*Nwd2*
chr5	66745534	66746395	H3K9ME2_UNC0638_peak_197	51	*Limch1*

© 2023. Bellver-Sanchis A. et al. Published online at http://www.aginganddisease.org/EN/10.14336/AD.2023.0424-2

SUPPLEMENTARY DATA

chr5	71700358	71701151	H3K9ME2_UNC0638_peak_198	58	*Gabrb1*
chr5	123076207	123076540	H3K9ME2_UNC0638_peak_199	22	*Tmem120b*
chr5	125532722	125533117	H3K9ME2_UNC0638_peak_200	28	*Tmem132b*
chr5	130384371	130384822	H3K9ME2_UNC0638_peak_201	28	*Caln1*
chr5	147957165	147957486	H3K9ME2_UNC0638_peak_202	42	*Mtus2*
chr5	15470190	15470564	H3K9ME2_UNC0638_peak_203	48	-
chr5	15512179	15512639	H3K9ME2_UNC0638_peak_204	230	*Gm21847*
chr5	15678922	15679504	H3K9ME2_UNC0638_peak_205	43	*Speer4cos*
chr5	22358375	22358685	H3K9ME2_UNC0638_peak_206	30	*Gm42223*
chr5	24473986	24474824	H3K9ME2_UNC0638_peak_207	42	*Agap3*
chr5	24730098	24730683	H3K9ME2_UNC0638_peak_208	62	*Gm42231*
chr5	26006909	26007620	H3K9ME2_UNC0638_peak_209	56	-
chr5	28071231	28071636	H3K9ME2_UNC0638_peak_210	27	*Insig1*
chr5	30587843	30589077	H3K9ME2_UNC0638_peak_211	50	*Kcnk3*
chr5	36967255	36967758	H3K9ME2_UNC0638_peak_212	32	*Wfs1*
chr5	45639315	45639750	H3K9ME2_UNC0638_peak_213	54	*9630001P10Rik*
chr5	64803469	64803773	H3K9ME2_UNC0638_peak_214	38	-
chr5	67391205	67391559	H3K9ME2_UNC0638_peak_215	27	*Bend4*
chr5	72564033	72564607	H3K9ME2_UNC0638_peak_216	22	*Gm34144*
chr5	75075840	75076278	H3K9ME2_UNC0638_peak_217	43	*Gsx2*
chr5	87850743	87851385	H3K9ME2_UNC0638_peak_218	27	*Gm7337*
chr5	98854472	98855174	H3K9ME2_UNC0638_peak_219	36	*Bmp3*
chr5	100728097	100728477	H3K9ME2_UNC0638_peak_220	24	*Gm36619*
chr5	110544851	110545173	H3K9ME2_UNC0638_peak_221	32	*Galnt9*
chr5	110841155	110841446	H3K9ME2_UNC0638_peak_222	44	-
chr5	111558652	111558953	H3K9ME2_UNC0638_peak_223	27	*Gm36274*
chr5	112342974	112343312	H3K9ME2_UNC0638_peak_224	50	*Hps4*
chr5	114130626	114131025	H3K9ME2_UNC0638_peak_225	88	*Ung*
chr5	122092570	122092911	H3K9ME2_UNC0638_peak_226	38	-
chr5	137179118	137179650	H3K9ME2_UNC0638_peak_227	57	-
chr5	139908016	139909036	H3K9ME2_UNC0638_peak_228	84	*Elfn1*
chr5	140607450	140607758	H3K9ME2_UNC0638_peak_229	17	*Lfng*
chr5	142701840	142702724	H3K9ME2_UNC0638_peak_230	96	*Slc29a4*
chr5	142960854	142961174	H3K9ME2_UNC0638_peak_231	37	*Fscn1*
chr5	145231828	145232119	H3K9ME2_UNC0638_peak_232	27	*Zfp655*
chr5	146492781	146493077	H3K9ME2_UNC0638_peak_233	57	-
chr5	150952676	150953104	H3K9ME2_UNC0638_peak_234	34	*Kl*
chr6	125710564	125711128	H3K9ME2_UNC0638_peak_235	31	-
chr6	29347863	29348450	H3K9ME2_UNC0638_peak_236	72	*Calu*
chr6	31399011	31399380	H3K9ME2_UNC0638_peak_237	72	*Mkln1*

© 2023. Bellver-Sanchis A. et al. Published online at http://www.aginganddisease.org/EN/10.14336/AD.2023.0424-2

SUPPLEMENTARY DATA

chr6	45059969	45060299	H3K9ME2_UNC0638_peak_238	34	*Cntnap2*
chr6	48137855	48138234	H3K9ME2_UNC0638_peak_239	26	-
chr6	61180566	61181124	H3K9ME2_UNC0638_peak_240	37	*Ccser1*
chr6	104491346	104491652	H3K9ME2_UNC0638_peak_241	27	*Cntn6*
chr6	110645671	110646145	H3K9ME2_UNC0638_peak_242	36	*Grm7*
chr6	114282731	114283114	H3K9ME2_UNC0638_peak_243	53	*Slc6a1*
chr6	127887683	127888092	H3K9ME2_UNC0638_peak_244	43	-
chr6	145746148	145746578	H3K9ME2_UNC0638_peak_245	50	-
chr6	3764142	3764680	H3K9ME2_UNC0638_peak_246	41	*Gm33576*
chr6	5725688	5726571	H3K9ME2_UNC0638_peak_247	46	*Dync1i1*
chr6	8949438	8949919	H3K9ME2_UNC0638_peak_248	27	*Nxph1*
chr6	14901333	14901782	H3K9ME2_UNC0638_peak_249	36	*Foxp2*
chr6	16525711	16526048	H3K9ME2_UNC0638_peak_250	39	*Gm36503*
chr6	25931131	25931727	H3K9ME2_UNC0638_peak_251	21	*Gm20756*
chr6	30048114	30048412	H3K9ME2_UNC0638_peak_252	32	*Nrf1*
chr6	37331787	37332452	H3K9ME2_UNC0638_peak_253	38	*Creb3l2*
chr6	37871087	37871472	H3K9ME2_UNC0638_peak_254	32	*Trim24*
chr6	38662678	38663527	H3K9ME2_UNC0638_peak_255	44	*Clec2l*
chr6	65381259	65381659	H3K9ME2_UNC0638_peak_256	48	*Qrfprl*
chr6	65778732	65779113	H3K9ME2_UNC0638_peak_257	37	*Prdm5*
chr6	82946263	82947281	H3K9ME2_UNC0638_peak_258	65	*M1ap*
chr6	90309220	90309577	H3K9ME2_UNC0638_peak_259	20	*Chst13*
chr6	91684033	91684391	H3K9ME2_UNC0638_peak_260	32	-
chr6	97616897	97617808	H3K9ME2_UNC0638_peak_261	43	*Gm32247*
chr6	100704602	100705171	H3K9ME2_UNC0638_peak_262	33	*Gxylt2*
chr6	113748876	113749283	H3K9ME2_UNC0638_peak_263	38	*Atp2b2*
chr6	114131114	114131762	H3K9ME2_UNC0638_peak_264	32	*Slc6a11*
chr6	114397637	114398279	H3K9ME2_UNC0638_peak_265	39	*Hrh1*
chr6	115134241	115135711	H3K9ME2_UNC0638_peak_266	131	*Syn2*
chr6	115601269	115601609	H3K9ME2_UNC0638_peak_267	50	*Mkrn2*
chr6	120666218	120667220	H3K9ME2_UNC0638_peak_268	32	*Cecr2*
chr6	125009207	125009541	H3K9ME2_UNC0638_peak_269	64	*4930557K07Rik*
chr6	129459138	129459598	H3K9ME2_UNC0638_peak_270	43	-
chr6	134444870	134445161	H3K9ME2_UNC0638_peak_271	38	*Lrp6*
chr6	141249822	141250172	H3K9ME2_UNC0638_peak_272	32	*Pde3a*
chr6	146888038	146888367	H3K9ME2_UNC0638_peak_273	32	*Ppfibp1*
chr6	148047167	148047772	H3K9ME2_UNC0638_peak_274	37	-
chr6	4003872	4004498	H3K9ME2_UNC0638_peak_275	33	*Gng11*
chr6	4505101	4505665	H3K9ME2_UNC0638_peak_276	82	*Col1a2*
chr6	4600865	4601665	H3K9ME2_UNC0638_peak_277	44	-

© 2023. Bellver-Sanchis A. et al. Published online at http://www.aginganddisease.org/EN/10.14336/AD.2023.0424-2

SUPPLEMENTARY DATA

chr6	7554906	7555396	H3K9ME2_UNC0638_peak_278	46	*Tac1*
chr6	8331870	8332343	H3K9ME2_UNC0638_peak_279	50	*Gm46952*
chr6	10893600	10894003	H3K9ME2_UNC0638_peak_280	41	-
chr6	17065138	17065504	H3K9ME2_UNC0638_peak_281	65	-
chr6	22288382	22288703	H3K9ME2_UNC0638_peak_282	26	*Wnt16*
chr6	26740391	26740939	H3K9ME2_UNC0638_peak_283	57	-
chr6	29031846	29032151	H3K9ME2_UNC0638_peak_284	42	*Lnclep*
chr6	29060154	29060496	H3K9ME2_UNC0638_peak_285	40	-
chr6	30957378	30958411	H3K9ME2_UNC0638_peak_286	79	*Klf14*
chr6	31010145	31010764	H3K9ME2_UNC0638_peak_287	36	*Gm40359*
chr6	35176673	35176964	H3K9ME2_UNC0638_peak_288	32	*Nup205*
chr6	38551437	38551922	H3K9ME2_UNC0638_peak_289	38	*Luc7l2*
chr6	39063330	39063944	H3K9ME2_UNC0638_peak_290	17	*1700025N23Rik*
chr6	39118520	39118910	H3K9ME2_UNC0638_peak_291	44	*4930599N23Rik*
chr6	47121034	47121462	H3K9ME2_UNC0638_peak_292	50	-
chr6	47650566	47651559	H3K9ME2_UNC0638_peak_293	58	-
chr6	47943025	47943522	H3K9ME2_UNC0638_peak_294	21	*Zfp783*
chr6	48024618	48024932	H3K9ME2_UNC0638_peak_295	25	*Zfp777*
chr6	48402813	48403104	H3K9ME2_UNC0638_peak_296	25	*Krba1*
chr6	48765307	48765819	H3K9ME2_UNC0638_peak_297	23	*Gimap3*
chr6	49822185	49822690	H3K9ME2_UNC0638_peak_298	41	*Npy*
chr6	50110304	50110618	H3K9ME2_UNC0638_peak_299	32	*Pals2*
chr6	51432567	51433488	H3K9ME2_UNC0638_peak_300	46	*Nfe2l3*
chr6	51469272	51469698	H3K9ME2_UNC0638_peak_301	22	-
chr6	52190871	52191541	H3K9ME2_UNC0638_peak_302	81	*Hoxa4*
chr6	52246213	52246556	H3K9ME2_UNC0638_peak_303	31	*Hoxa11os*
chr6	52259746	52260296	H3K9ME2_UNC0638_peak_304	37	*Hoxa13*
chr6	53845021	53845361	H3K9ME2_UNC0638_peak_305	31	*Gm16499*
chr6	54429828	54430195	H3K9ME2_UNC0638_peak_306	71	*Wipf3*
chr6	55451783	55452384	H3K9ME2_UNC0638_peak_307	33	*Adcyap1r1*
chr6	55676382	55677250	H3K9ME2_UNC0638_peak_308	53	*Neurod6*
chr6	57022911	57023327	H3K9ME2_UNC0638_peak_309	18	*Vmn1r7*
chr6	57359927	57360284	H3K9ME2_UNC0638_peak_310	24	*Vmn1r17*
chr6	58906705	58907415	H3K9ME2_UNC0638_peak_311	31	*Nap1l5*
chr6	64729706	64730169	H3K9ME2_UNC0638_peak_312	57	*Atoh1*
chr6	67267311	67267602	H3K9ME2_UNC0638_peak_313	38	*Serbp1*
chr6	70956312	70957287	H3K9ME2_UNC0638_peak_314	97	*Foxi3*
chr6	71456720	71457437	H3K9ME2_UNC0638_peak_315	47	*Gm30582*
chr6	71707600	71707961	H3K9ME2_UNC0638_peak_316	51	*Reep1*
chr6	71708531	71708822	H3K9ME2_UNC0638_peak_317	22	*Reep1*

© 2023. Bellver-Sanchis A. et al. Published online at http://www.aginganddisease.org/EN/10.14336/AD.2023.0424-2

SUPPLEMENTARY DATA

chr6	72439582	72439879	H3K9ME2_UNC0638_peak_318	32	*Particl*
chr6	72958365	72958686	H3K9ME2_UNC0638_peak_319	32	*Tmsb10*
chr6	81900013	81900365	H3K9ME2_UNC0638_peak_320	23	*1700009C05Rik*
chr6	81932513	81932841	H3K9ME2_UNC0638_peak_321	32	*Gcfc2*
chr6	83033453	83033800	H3K9ME2_UNC0638_peak_322	38	*Loxl3*
chr6	83069629	83069927	H3K9ME2_UNC0638_peak_323	22	*Tlx2*
chr6	83077801	83078174	H3K9ME2_UNC0638_peak_324	44	*Pcgf1*
chr6	85511889	85512289	H3K9ME2_UNC0638_peak_325	47	*Egr4*
chr6	86526076	86526836	H3K9ME2_UNC0638_peak_326	35	*1600020E01Rik*
chr6	87638341	87638656	H3K9ME2_UNC0638_peak_327	43	*Gm46964*
chr6	87730732	87731097	H3K9ME2_UNC0638_peak_328	35	-
chr6	87980462	87981850	H3K9ME2_UNC0638_peak_329	41	*H1f10*
chr6	88142147	88142705	H3K9ME2_UNC0638_peak_330	61	*Gm38708*
chr6	88166127	88166758	H3K9ME2_UNC0638_peak_331	29	*Gm38708*
chr6	90594291	90595210	H3K9ME2_UNC0638_peak_332	31	-
chr6	100467952	100468343	H3K9ME2_UNC0638_peak_333	31	*Gm38868*
chr6	107529641	107530353	H3K9ME2_UNC0638_peak_334	71	*Lrrn1*
chr6	108828857	108829319	H3K9ME2_UNC0638_peak_335	27	*Edem1*
chr6	113426108	113426575	H3K9ME2_UNC0638_peak_336	32	-
chr6	113494232	113494856	H3K9ME2_UNC0638_peak_337	50	*Prrt3*
chr6	114094350	114094907	H3K9ME2_UNC0638_peak_338	37	*Gm36023*
chr6	115305795	115306345	H3K9ME2_UNC0638_peak_339	32	*Gm38877*
chr6	115526742	115527110	H3K9ME2_UNC0638_peak_340	17	*Gm36355*
chr6	116580122	116580585	H3K9ME2_UNC0638_peak_341	44	*Olfr215*
chr6	117843270	117843725	H3K9ME2_UNC0638_peak_342	57	*Zfp637*
chr6	119175120	119175833	H3K9ME2_UNC0638_peak_343	75	*Dcp1b*
chr6	119479499	119479797	H3K9ME2_UNC0638_peak_344	32	*Fbxl14*
chr6	122873427	122874129	H3K9ME2_UNC0638_peak_345	57	*Necap1*
chr6	124303330	124303629	H3K9ME2_UNC0638_peak_346	23	*Cd163*
chr6	124531016	124531307	H3K9ME2_UNC0638_peak_347	31	*C1s1*
chr6	124625539	124625830	H3K9ME2_UNC0638_peak_348	22	*C1s2*
chr6	124829824	124830541	H3K9ME2_UNC0638_peak_349	27	*Cdca3*
chr6	126939635	126939926	H3K9ME2_UNC0638_peak_350	50	*D6Wsu163e*
chr6	132114656	132115168	H3K9ME2_UNC0638_peak_351	57	-
chr6	132207781	132208078	H3K9ME2_UNC0638_peak_352	33	*Prb1*
chr6	132312250	132312699	H3K9ME2_UNC0638_peak_353	89	*Prpmp5*
chr6	132361404	132362093	H3K9ME2_UNC0638_peak_354	45	*Gm8882*
chr6	132439390	132439874	H3K9ME2_UNC0638_peak_355	86	*Gm5154*
chr6	132710153	132710542	H3K9ME2_UNC0638_peak_356	45	*Tas2r122*
chr6	134397535	134398151	H3K9ME2_UNC0638_peak_357	29	*Bcl2l14*

© 2023. Bellver-Sanchis A. et al. Published online at http://www.aginganddisease.org/EN/10.14336/AD.2023.0424-2

SUPPLEMENTARY DATA

chr6	135309804	135310096	H3K9ME2_UNC0638_peak_358	26	*Pbp2*
chr6	136326955	136327253	H3K9ME2_UNC0638_peak_359	27	*Eif4a3l1*
chr6	136804096	136804389	H3K9ME2_UNC0638_peak_360	38	*H4f16*
chr6	142387009	142387300	H3K9ME2_UNC0638_peak_361	38	-
chr6	143683260	143683555	H3K9ME2_UNC0638_peak_362	33	-
chr6	146725039	146725572	H3K9ME2_UNC0638_peak_363	106	*Stk38l*
chr7	92060984	92061292	H3K9ME2_UNC0638_peak_364	44	*Dlg2*
chr7	57590571	57591187	H3K9ME2_UNC0638_peak_365	22	*Gabrb3*
chr7	87584140	87584624	H3K9ME2_UNC0638_peak_366	47	*Grm5*
chr7	122670857	122671227	H3K9ME2_UNC0638_peak_367	23	*Cacng3*
chr7	4844109	4844976	H3K9ME2_UNC0638_peak_368	85	*Isoc2b*
chr7	10088275	10089170	H3K9ME2_UNC0638_peak_369	27	*Vmn2r51*
chr7	19118080	19118754	H3K9ME2_UNC0638_peak_370	57	*Fbxo46*
chr7	25009963	25010460	H3K9ME2_UNC0638_peak_371	29	*Grik5*
chr7	29064410	29064781	H3K9ME2_UNC0638_peak_372	30	-
chr7	29065849	29066157	H3K9ME2_UNC0638_peak_373	40	-
chr7	46396362	46397093	H3K9ME2_UNC0638_peak_374	39	*Kcnc1*
chr7	49908958	49909249	H3K9ME2_UNC0638_peak_375	46	*Slc6a5*
chr7	54835607	54836122	H3K9ME2_UNC0638_peak_376	35	*Luzp2*
chr7	57386585	57386927	H3K9ME2_UNC0638_peak_377	36	*Gm9962*
chr7	63099224	63099697	H3K9ME2_UNC0638_peak_378	37	*Chrna7*
chr7	63444808	63445159	H3K9ME2_UNC0638_peak_379	35	*Otud7a*
chr7	81213098	81213601	H3K9ME2_UNC0638_peak_380	42	*Pde8a*
chr7	84529026	84529317	H3K9ME2_UNC0638_peak_381	50	-
chr7	86737276	86737567	H3K9ME2_UNC0638_peak_382	27	*Folh1*
chr7	97580120	97580567	H3K9ME2_UNC0638_peak_383	27	-
chr7	101577333	101577837	H3K9ME2_UNC0638_peak_384	49	*Art2b*
chr7	102209624	102210186	H3K9ME2_UNC0638_peak_385	44	*Pgap2*
chr7	105481832	105482322	H3K9ME2_UNC0638_peak_386	32	*Gm36847*
chr7	112679045	112679871	H3K9ME2_UNC0638_peak_387	38	*Tead1*
chr7	113764098	113764538	H3K9ME2_UNC0638_peak_388	22	*Spon1*
chr7	120420885	120421334	H3K9ME2_UNC0638_peak_389	49	*Abca16*
chr7	121864855	121865182	H3K9ME2_UNC0638_peak_390	30	*Scnn1b*
chr7	127512284	127512641	H3K9ME2_UNC0638_peak_391	38	*Srcap*
chr7	128842827	128843212	H3K9ME2_UNC0638_peak_392	47	*Gm39093*
chr7	139977797	139978298	H3K9ME2_UNC0638_peak_393	45	*Adam8*
chr7	141950166	141950645	H3K9ME2_UNC0638_peak_394	59	*Brsk2*
chr7	142967963	142968362	H3K9ME2_UNC0638_peak_395	43	-
chr7	143106948	143107768	H3K9ME2_UNC0638_peak_396	64	*Kcnq1*
chr7	4993604	4994479	H3K9ME2_UNC0638_peak_397	34	*Zfp579*

© 2023. Bellver-Sanchis A. et al. Published online at http://www.aginganddisease.org/EN/10.14336/AD.2023.0424-2

SUPPLEMENTARY DATA

chr7	5146571	5147163	H3K9ME2_UNC0638_peak_398	17	*Vmn1r55*
chr7	6201130	6201612	H3K9ME2_UNC0638_peak_399	27	-
chr7	6440036	6440368	H3K9ME2_UNC0638_peak_400	31	*Olfr1344*
chr7	6488669	6489089	H3K9ME2_UNC0638_peak_401	26	*Olfr1347*
chr7	7300006	7300428	H3K9ME2_UNC0638_peak_402	27	*Mir5620*
chr7	8368787	8369078	H3K9ME2_UNC0638_peak_403	44	*Vmn2r44*
chr7	10578115	10578406	H3K9ME2_UNC0638_peak_404	26	*Vmn1r69*
chr7	12258184	12258490	H3K9ME2_UNC0638_peak_405	31	*Vmn1r81*
chr7	13043765	13044361	H3K9ME2_UNC0638_peak_406	26	*Mzf1*
chr7	16061286	16062005	H3K9ME2_UNC0638_peak_407	76	*Zfp541*
chr7	16816285	16816648	H3K9ME2_UNC0638_peak_408	45	*Strn4*
chr7	18319334	18319836	H3K9ME2_UNC0638_peak_409	37	-
chr7	18674185	18674476	H3K9ME2_UNC0638_peak_410	16	*Psg20*
chr7	18674754	18675139	H3K9ME2_UNC0638_peak_411	32	*Psg20*
chr7	19507218	19507644	H3K9ME2_UNC0638_peak_412	17	*Bloc1s3*
chr7	23384026	23384445	H3K9ME2_UNC0638_peak_413	23	*Nlrp5*
chr7	24432150	24432592	H3K9ME2_UNC0638_peak_414	49	-
chr7	24585532	24586416	H3K9ME2_UNC0638_peak_415	68	*Zfp575*
chr7	24586622	24586954	H3K9ME2_UNC0638_peak_416	19	*Ethe1*
chr7	24869999	24870290	H3K9ME2_UNC0638_peak_417	50	*Dmrtc2*
chr7	25282436	25282735	H3K9ME2_UNC0638_peak_418	25	*Cic*
chr7	28283199	28284063	H3K9ME2_UNC0638_peak_419	283	*Selenov*
chr7	28808807	28809100	H3K9ME2_UNC0638_peak_420	53	*Hnrnpl*
chr7	29773976	29774267	H3K9ME2_UNC0638_peak_421	28	*Mir1964*
chr7	30854931	30855235	H3K9ME2_UNC0638_peak_422	32	*Ffar3*
chr7	30882402	30882905	H3K9ME2_UNC0638_peak_423	49	*D7Ertd128e*
chr7	34522000	34522313	H3K9ME2_UNC0638_peak_424	25	-
chr7	35185143	35185754	H3K9ME2_UNC0638_peak_425	32	-
chr7	35185936	35186791	H3K9ME2_UNC0638_peak_426	59	-
chr7	43768952	43769346	H3K9ME2_UNC0638_peak_427	73	*Klk12*
chr7	44123035	44123326	H3K9ME2_UNC0638_peak_428	21	*Klk1b16*
chr7	45525852	45526190	H3K9ME2_UNC0638_peak_429	32	*Plekha4*
chr7	45628350	45629057	H3K9ME2_UNC0638_peak_430	63	*Rasip1*
chr7	45832536	45834160	H3K9ME2_UNC0638_peak_431	67	-
chr7	46796060	46796409	H3K9ME2_UNC0638_peak_432	22	*Gtf2h1*
chr7	47588372	47589603	H3K9ME2_UNC0638_peak_433	178	*Mrgpra3*
chr7	47981011	47981674	H3K9ME2_UNC0638_peak_434	32	*Mrgpra4*
chr7	59332800	59333238	H3K9ME2_UNC0638_peak_435	22	-
chr7	60155480	60155797	H3K9ME2_UNC0638_peak_436	50	*Gm7367*
chr7	62348882	62349173	H3K9ME2_UNC0638_peak_437	23	*Ndn*

© 2023. Bellver-Sanchis A. et al. Published online at http://www.aginganddisease.org/EN/10.14336/AD.2023.0424-2

SUPPLEMENTARY DATA

chr7	62377574	62378019	H3K9ME2_UNC0638_peak_438	35	*Magel2*
chr7	62378360	62378835	H3K9ME2_UNC0638_peak_439	35	*Magel2*
chr7	66733705	66734331	H3K9ME2_UNC0638_peak_440	22	*Cers3*
chr7	73740203	73741049	H3K9ME2_UNC0638_peak_441	75	*Fam174b*
chr7	79515404	79515849	H3K9ME2_UNC0638_peak_442	44	*Mir9-3hg*
chr7	81933751	81934362	H3K9ME2_UNC0638_peak_443	46	-
chr7	84409490	84410423	H3K9ME2_UNC0638_peak_444	50	*Gm39045*
chr7	91013574	91014410	H3K9ME2_UNC0638_peak_445	57	*Gm39048*
chr7	93079718	93080031	H3K9ME2_UNC0638_peak_446	23	*Fam181b*
chr7	93080435	93081053	H3K9ME2_UNC0638_peak_447	28	*Fam181b*
chr7	99625368	99626962	H3K9ME2_UNC0638_peak_448	115	*Tpbgl*
chr7	101818093	101818682	H3K9ME2_UNC0638_peak_449	33	*Phox2a*
chr7	103938021	103938331	H3K9ME2_UNC0638_peak_450	34	*Olfr632*
chr7	104012427	104012765	H3K9ME2_UNC0638_peak_451	17	*Olfr639*
chr7	104129213	104129842	H3K9ME2_UNC0638_peak_452	20	*Ubqln5*
chr7	105425814	105426227	H3K9ME2_UNC0638_peak_453	22	*Cckbr*
chr7	106752665	106752980	H3K9ME2_UNC0638_peak_454	25	*Olfr698*
chr7	106886166	106886883	H3K9ME2_UNC0638_peak_455	27	*Olfr706*
chr7	109010597	109011430	H3K9ME2_UNC0638_peak_456	69	*Tub*
chr7	109438702	109439290	H3K9ME2_UNC0638_peak_457	61	-
chr7	112186679	112187229	H3K9ME2_UNC0638_peak_458	55	*Gm39071*
chr7	112953683	112954814	H3K9ME2_UNC0638_peak_459	67	*Rassf10*
chr7	112955170	112955587	H3K9ME2_UNC0638_peak_460	53	*Rassf10*
chr7	120917906	120918197	H3K9ME2_UNC0638_peak_461	17	-
chr7	126583783	126584096	H3K9ME2_UNC0638_peak_462	44	*Apobr*
chr7	127026024	127026544	H3K9ME2_UNC0638_peak_463	21	*Kif22*
chr7	127287507	127287831	H3K9ME2_UNC0638_peak_464	17	-
chr7	127967253	127967641	H3K9ME2_UNC0638_peak_465	37	-
chr7	131543268	131544191	H3K9ME2_UNC0638_peak_466	36	*Hmx3*
chr7	132596921	132597783	H3K9ME2_UNC0638_peak_467	31	*Nkx1-2*
chr7	135410178	135410773	H3K9ME2_UNC0638_peak_468	32	*Foxi2*
chr7	135853334	135853755	H3K9ME2_UNC0638_peak_469	22	-
chr7	136352166	136352457	H3K9ME2_UNC0638_peak_470	19	-
chr7	139086053	139086990	H3K9ME2_UNC0638_peak_471	38	*Dpysl4*
chr7	140070223	140070604	H3K9ME2_UNC0638_peak_472	17	*Caly*
chr7	141061364	141061655	H3K9ME2_UNC0638_peak_473	27	*B4galnt4*
chr7	142094662	142095555	H3K9ME2_UNC0638_peak_474	38	-
chr7	143459498	143459998	H3K9ME2_UNC0638_peak_475	53	*Cdkn1c*
chr7	144861242	144862171	H3K9ME2_UNC0638_peak_476	50	*Fgf4*
chr8	33516437	33516789	H3K9ME2_UNC0638_peak_477	38	*Tex15*

© 2023. Bellver-Sanchis A. et al. Published online at http://www.aginganddisease.org/EN/10.14336/AD.2023.0424-2

SUPPLEMENTARY DATA

chr8	33516968	33517426	H3K9ME2_UNC0638_peak_478	22	*Tex15*
chr8	10153761	10154236	H3K9ME2_UNC0638_peak_479	41	*Myo16*
chr8	14096107	14096767	H3K9ME2_UNC0638_peak_480	35	*Dlgap2*
chr8	37564444	37564739	H3K9ME2_UNC0638_peak_481	32	*Sgcz*
chr8	40862364	40862655	H3K9ME2_UNC0638_peak_482	44	*Slc7a2*
chr8	11009054	11009494	H3K9ME2_UNC0638_peak_483	50	*9530052E02Rik*
chr8	36248404	36248923	H3K9ME2_UNC0638_peak_484	43	*Gm35712*
chr8	38660413	38660787	H3K9ME2_UNC0638_peak_485	38	*Gm40493*
chr8	62951457	62952021	H3K9ME2_UNC0638_peak_486	38	*Spock3*
chr8	77723807	77724262	H3K9ME2_UNC0638_peak_487	31	*LOC108167319*
chr8	90248383	90248992	H3K9ME2_UNC0638_peak_488	32	*Tox3*
chr8	95677551	95677988	H3K9ME2_UNC0638_peak_489	45	-
chr8	117498434	117498729	H3K9ME2_UNC0638_peak_490	28	*Plcg2*
chr8	125054058	125054639	H3K9ME2_UNC0638_peak_491	36	*Disc1*
chr8	3089289	3089894	H3K9ME2_UNC0638_peak_492	44	*Gm30220*
chr8	19210000	19210297	H3K9ME2_UNC0638_peak_493	50	*Defa-ps12*
chr8	27227725	27228016	H3K9ME2_UNC0638_peak_494	17	-
chr8	27295310	27295875	H3K9ME2_UNC0638_peak_495	29	*Gm9731*
chr8	31089487	31089834	H3K9ME2_UNC0638_peak_496	31	*Dusp26*
chr8	55347211	55347597	H3K9ME2_UNC0638_peak_497	106	-
chr8	55347761	55348298	H3K9ME2_UNC0638_peak_498	176	-
chr8	66511679	66511970	H3K9ME2_UNC0638_peak_499	29	*Tktl2*
chr8	69902132	69902771	H3K9ME2_UNC0638_peak_500	38	*Tssk6*
chr8	70374696	70375105	H3K9ME2_UNC0638_peak_501	32	*Comp*
chr8	78044688	78045212	H3K9ME2_UNC0638_peak_502	36	*Gm29895*
chr8	83290241	83290545	H3K9ME2_UNC0638_peak_503	29	*Ucp1*
chr8	83389668	83390010	H3K9ME2_UNC0638_peak_504	36	-
chr8	85700696	85701036	H3K9ME2_UNC0638_peak_505	38	*Mir8109*
chr8	88272298	88272714	H3K9ME2_UNC0638_peak_506	32	*Adcy7*
chr8	89042667	89042962	H3K9ME2_UNC0638_peak_507	50	-
chr8	92855361	92855652	H3K9ME2_UNC0638_peak_508	43	*Lpcat2*
chr8	93098761	93099052	H3K9ME2_UNC0638_peak_509	27	*Ces1c*
chr8	95753520	95753929	H3K9ME2_UNC0638_peak_510	32	*Mir7073*
chr8	110101400	110101752	H3K9ME2_UNC0638_peak_511	25	-
chr8	110142434	110142888	H3K9ME2_UNC0638_peak_512	31	*Calb2*
chr8	123041939	123042230	H3K9ME2_UNC0638_peak_513	27	*2810013P06Rik*
chr8	123996726	123997017	H3K9ME2_UNC0638_peak_514	22	-
chr8	129044300	129044616	H3K9ME2_UNC0638_peak_515	21	*Ccdc7a*
chr9	46012759	46013050	H3K9ME2_UNC0638_peak_516	32	*Sik3*
chr9	111118060	111118508	H3K9ME2_UNC0638_peak_517	43	*Lrrfip2*

© 2023. Bellver-Sanchis A. et al. Published online at http://www.aginganddisease.org/EN/10.14336/AD.2023.0424-2

SUPPLEMENTARY DATA

chr9	3532283	3532834	H3K9ME2_UNC0638_peak_518	24	*Gucy1a2*
chr9	3533018	3533453	H3K9ME2_UNC0638_peak_519	27	*Gucy1a2*
chr9	8544084	8544702	H3K9ME2_UNC0638_peak_520	42	*Trpc6*
chr9	8900319	8901440	H3K9ME2_UNC0638_peak_521	44	*Pgr*
chr9	45430648	45431206	H3K9ME2_UNC0638_peak_522	54	*Dscaml1*
chr9	51765248	51765957	H3K9ME2_UNC0638_peak_523	71	*Arhgap20*
chr9	52678958	52679867	H3K9ME2_UNC0638_peak_524	29	*Gm1715*
chr9	58823093	58823508	H3K9ME2_UNC0638_peak_525	17	*Hcn4*
chr9	105774178	105774512	H3K9ME2_UNC0638_peak_526	42	*Col6a6*
chr9	106822011	106822316	H3K9ME2_UNC0638_peak_527	50	*Dcaf1*
chr9	107400305	107400596	H3K9ME2_UNC0638_peak_528	54	*Cacna2d2*
chr9	118606862	118607327	H3K9ME2_UNC0638_peak_529	27	*Itga9*
chr9	4795614	4796420	H3K9ME2_UNC0638_peak_530	59	-
chr9	5156699	5157017	H3K9ME2_UNC0638_peak_531	27	*Gm31429*
chr9	8221655	8222083	H3K9ME2_UNC0638_peak_532	71	*1700128F08Rik*
chr9	8245849	8246199	H3K9ME2_UNC0638_peak_533	20	*Mir1899*
chr9	10904359	10905046	H3K9ME2_UNC0638_peak_534	104	*Gm32710*
chr9	14859956	14860695	H3K9ME2_UNC0638_peak_535	39	*Gpr83*
chr9	19359217	19359824	H3K9ME2_UNC0638_peak_536	38	*Olfr846*
chr9	22188027	22188318	H3K9ME2_UNC0638_peak_537	17	*Zfp872*
chr9	36135335	36135644	H3K9ME2_UNC0638_peak_538	31	*Gm3434*
chr9	39215839	39216186	H3K9ME2_UNC0638_peak_539	37	*Olfr944*
chr9	39548887	39549178	H3K9ME2_UNC0638_peak_540	25	*Olfr958*
chr9	39956144	39956499	H3K9ME2_UNC0638_peak_541	22	-
chr9	40136691	40137136	H3K9ME2_UNC0638_peak_542	37	*Gm35123*
chr9	41890649	41891055	H3K9ME2_UNC0638_peak_543	23	-
chr9	43608144	43608492	H3K9ME2_UNC0638_peak_544	29	*Gm29909*
chr9	46997815	46998317	H3K9ME2_UNC0638_peak_545	19	*Gm4791*
chr9	49340248	49340876	H3K9ME2_UNC0638_peak_546	58	*Drd2*
chr9	54286112	54286620	H3K9ME2_UNC0638_peak_547	25	*Gldn*
chr9	54698944	54699582	H3K9ME2_UNC0638_peak_548	38	*Dnaja4*
chr9	54981400	54981878	H3K9ME2_UNC0638_peak_549	22	*Chrna5*
chr9	55518144	55518435	H3K9ME2_UNC0638_peak_550	22	-
chr9	56796460	56797060	H3K9ME2_UNC0638_peak_551	30	*Gm31586*
chr9	58488186	58488496	H3K9ME2_UNC0638_peak_552	16	*Insyn1*
chr9	58488870	58489245	H3K9ME2_UNC0638_peak_553	25	*Insyn1*
chr9	59577934	59578570	H3K9ME2_UNC0638_peak_554	32	*Celf6*
chr9	60712950	60713576	H3K9ME2_UNC0638_peak_555	39	*Larp6*
chr9	62341161	62341452	H3K9ME2_UNC0638_peak_556	22	*Anp32a*
chr9	62536593	62537119	H3K9ME2_UNC0638_peak_557	60	*Gm39352*

© 2023. Bellver-Sanchis A. et al. Published online at http://www.aginganddisease.org/EN/10.14336/AD.2023.0424-2

SUPPLEMENTARY DATA

chr9	62980419	62980710	H3K9ME2_UNC0638_peak_558	22	*Gm35574*
chr9	65630388	65630927	H3K9ME2_UNC0638_peak_559	27	*Rbpms2*
chr9	73102971	73103489	H3K9ME2_UNC0638_peak_560	29	*Khdc3*
chr9	73103734	73104025	H3K9ME2_UNC0638_peak_561	33	*Khdc3*
chr9	78395885	78396196	H3K9ME2_UNC0638_peak_562	36	*Ddx43*
chr9	85843767	85844536	H3K9ME2_UNC0638_peak_563	47	*Tpbg*
chr9	87015121	87016076	H3K9ME2_UNC0638_peak_564	50	-
chr9	90906202	90906546	H3K9ME2_UNC0638_peak_565	36	*Gm31114*
chr9	91923430	91923721	H3K9ME2_UNC0638_peak_566	17	*Gm31409*
chr9	98902913	98903550	H3K9ME2_UNC0638_peak_567	27	*7420426K07Rik*
chr9	102506099	102506491	H3K9ME2_UNC0638_peak_568	22	*Ky*
chr9	106464903	106465259	H3K9ME2_UNC0638_peak_569	22	*Gpr62*
chr9	106886955	106887246	H3K9ME2_UNC0638_peak_570	26	*Manf*
chr9	108306442	108306733	H3K9ME2_UNC0638_peak_571	27	*Rhoa*
chr9	108826356	108826647	H3K9ME2_UNC0638_peak_572	22	*Celsr3*
chr9	110303926	110304288	H3K9ME2_UNC0638_peak_573	17	*Elp6*
chr9	110532642	110533015	H3K9ME2_UNC0638_peak_574	22	-
chr9	110857629	110858377	H3K9ME2_UNC0638_peak_575	17	-
chr9	111311737	111312265	H3K9ME2_UNC0638_peak_576	95	*Trank1*
chr9	116525829	116526218	H3K9ME2_UNC0638_peak_577	27	*Gm39449*
chr9	118478906	118479591	H3K9ME2_UNC0638_peak_578	57	*Eomes*
chr9	119221865	119222326	H3K9ME2_UNC0638_peak_579	41	*Slc22a13b*
chr9	121777944	121778479	H3K9ME2_UNC0638_peak_580	21	-
chr9	122746927	122747729	H3K9ME2_UNC0638_peak_581	38	*Topaz1*
chr9	123963624	123964131	H3K9ME2_UNC0638_peak_582	17	*Ccr1*
chr9	124439926	124440283	H3K9ME2_UNC0638_peak_583	41	-
chrM	2303	2950	H3K9ME2_UNC0638_peak_584	55	-
chrM	3940	4276	H3K9ME2_UNC0638_peak_585	81	-
chrM	5547	6368	H3K9ME2_UNC0638_peak_586	78	-
chrM	12075	13244	H3K9ME2_UNC0638_peak_587	111	-
chrM	14121	15277	H3K9ME2_UNC0638_peak_588	106	-
chrX	6092126	6092679	H3K9ME2_UNC0638_peak_589	44	-
chrX	6779787	6780078	H3K9ME2_UNC0638_peak_590	17	*Dgkk*
chrX	21714826	21715126	H3K9ME2_UNC0638_peak_591	44	*Slc6a14*
chrX	31243437	31243764	H3K9ME2_UNC0638_peak_592	90	*Gm31556*
chrX	31253984	31254829	H3K9ME2_UNC0638_peak_593	113	*Spin2f*
chrX	33057449	33057846	H3K9ME2_UNC0638_peak_594	62	*Gm2837*
chrX	37571675	37571966	H3K9ME2_UNC0638_peak_595	27	*Rhox2f*
chrX	140061455	140061783	H3K9ME2_UNC0638_peak_596	32	*Dnaaf6b*
chrX	169980503	169980977	H3K9ME2_UNC0638_peak_597	70	*Mid1*

© 2023. Bellver-Sanchis A. et al. Published online at http://www.aginganddisease.org/EN/10.14336/AD.2023.0424-2

SUPPLEMENTARY DATA

chrY	90742078	90743150	H3K9ME2_UNC0638_peak_598	239	-
chr10	4712592	4712965	H3K9ME2_UNC0638_peak_599	29	*Esr1*
chr10	39369954	39370436	H3K9ME2_UNC0638_peak_600	18	*Fyn*
chr10	40222604	40223082	H3K9ME2_UNC0638_peak_601	44	*Rpf2*
chr10	52690652	52691213	H3K9ME2_UNC0638_peak_602	22	*Slc35f1*
chr10	70599076	70600077	H3K9ME2_UNC0638_peak_603	54	-
chr10	84760470	84760761	H3K9ME2_UNC0638_peak_604	21	*Rfx4*
chr10	107271846	107272447	H3K9ME2_UNC0638_peak_605	25	*Lin7a*
chr10	112271435	112271759	H3K9ME2_UNC0638_peak_606	19	*Kcnc2*
chr10	19850243	19851648	H3K9ME2_UNC0638_peak_607	57	*Slc35d3*
chr10	22184524	22184960	H3K9ME2_UNC0638_peak_608	50	-
chr10	26673837	26674223	H3K9ME2_UNC0638_peak_609	27	*Gm8709*
chr10	33222550	33222841	H3K9ME2_UNC0638_peak_610	32	*D830005E20Rik*
chr10	33623977	33624369	H3K9ME2_UNC0638_peak_611	64	-
chr10	39933314	39933767	H3K9ME2_UNC0638_peak_612	50	-
chr10	41071164	41071643	H3K9ME2_UNC0638_peak_613	33	-
chr10	76961469	76962177	H3K9ME2_UNC0638_peak_614	67	*Gm35664*
chr10	77605979	77606282	H3K9ME2_UNC0638_peak_615	16	*Sumo3*
chr10	79716512	79717278	H3K9ME2_UNC0638_peak_616	47	-
chr10	79977550	79978182	H3K9ME2_UNC0638_peak_617	26	-
chr10	82484848	82485139	H3K9ME2_UNC0638_peak_618	27	*Gm1553*
chr10	97692901	97693761	H3K9ME2_UNC0638_peak_619	47	*Ccer1*
chr10	104196750	104197063	H3K9ME2_UNC0638_peak_620	57	*Gm4340*
chr10	127961477	127961813	H3K9ME2_UNC0638_peak_621	32	-
chr10	128035649	128035993	H3K9ME2_UNC0638_peak_622	22	*Naca*
chr11	4947378	4948427	H3K9ME2_UNC0638_peak_623	96	*Ap1b1*
chr11	42420027	42420328	H3K9ME2_UNC0638_peak_624	35	*Gabrb2*
chr11	43775584	43776413	H3K9ME2_UNC0638_peak_625	75	*Adra1b*
chr11	45851979	45852403	H3K9ME2_UNC0638_peak_626	17	-
chr11	49901531	49902344	H3K9ME2_UNC0638_peak_627	62	*Rasgef1c*
chr11	52764451	52765098	H3K9ME2_UNC0638_peak_628	50	*Fstl4*
chr11	54140419	54140847	H3K9ME2_UNC0638_peak_629	336	-
chr11	59012566	59012935	H3K9ME2_UNC0638_peak_630	31	*Obscn*
chr11	60932133	60932424	H3K9ME2_UNC0638_peak_631	17	*Map2k3*
chr11	67454720	67455497	H3K9ME2_UNC0638_peak_632	50	*Gas7*
chr11	67455750	67456150	H3K9ME2_UNC0638_peak_633	36	*Gas7*
chr11	68691665	68692471	H3K9ME2_UNC0638_peak_634	39	*Myh10*
chr11	83752277	83752641	H3K9ME2_UNC0638_peak_635	44	*Heatr6*
chr11	4746156	4747006	H3K9ME2_UNC0638_peak_636	43	*Gm35102*
chr11	5061532	5061950	H3K9ME2_UNC0638_peak_637	37	*Gas2l1*

© 2023. Bellver-Sanchis A. et al. Published online at http://www.aginganddisease.org/EN/10.14336/AD.2023.0424-2

SUPPLEMENTARY DATA

chr11	6415613	6415904	H3K9ME2_UNC0638_peak_638	40	*Ppia*
chr11	11461976	11462531	H3K9ME2_UNC0638_peak_639	38	*Spata48*
chr11	14559582	14560143	H3K9ME2_UNC0638_peak_640	39	*1700046C09Rik*
chr11	16257663	16258069	H3K9ME2_UNC0638_peak_641	33	-
chr11	21992768	21993761	H3K9ME2_UNC0638_peak_642	50	*Otx1*
chr11	24952160	24952641	H3K9ME2_UNC0638_peak_643	44	*Gm39613*
chr11	31965604	31965982	H3K9ME2_UNC0638_peak_644	64	*4930524B15Rik*
chr11	35215366	35215818	H3K9ME2_UNC0638_peak_645	80	-
chr11	35797679	35798081	H3K9ME2_UNC0638_peak_646	44	*Fbll1*
chr11	38492494	38493411	H3K9ME2_UNC0638_peak_647	50	*Gm12130*
chr11	49160360	49160651	H3K9ME2_UNC0638_peak_648	44	*Olfr1394*
chr11	49169041	49169600	H3K9ME2_UNC0638_peak_649	32	*Btnl9*
chr11	49443886	49444440	H3K9ME2_UNC0638_peak_650	64	*Olfr1388*
chr11	49590049	49590565	H3K9ME2_UNC0638_peak_651	32	-
chr11	51048150	51048443	H3K9ME2_UNC0638_peak_652	37	*Olfr1375*
chr11	52098861	52099152	H3K9ME2_UNC0638_peak_653	50	*Ppp2ca*
chr11	52397922	52398284	H3K9ME2_UNC0638_peak_654	27	*9530068E07Rik*
chr11	53350576	53351140	H3K9ME2_UNC0638_peak_655	27	*Aff4*
chr11	58640496	58640831	H3K9ME2_UNC0638_peak_656	36	*Trim58*
chr11	58778537	58778915	H3K9ME2_UNC0638_peak_657	32	*Olfr315*
chr11	60699721	60700093	H3K9ME2_UNC0638_peak_658	22	-
chr11	61022027	61022607	H3K9ME2_UNC0638_peak_659	22	*Kcnj12*
chr11	69088559	69089032	H3K9ME2_UNC0638_peak_660	27	*Vamp2*
chr11	69817021	69817372	H3K9ME2_UNC0638_peak_661	28	*Spem2*
chr11	69837368	69837692	H3K9ME2_UNC0638_peak_662	32	*Tmem256*
chr11	69935798	69936351	H3K9ME2_UNC0638_peak_663	17	-
chr11	69966188	69966792	H3K9ME2_UNC0638_peak_664	24	*Cldn7*
chr11	70086665	70087113	H3K9ME2_UNC0638_peak_665	27	-
chr11	74365242	74365646	H3K9ME2_UNC0638_peak_666	32	*Olfr412*
chr11	74619986	74620385	H3K9ME2_UNC0638_peak_667	27	*Ccdc92b*
chr11	75173259	75173617	H3K9ME2_UNC0638_peak_668	46	*Mir212*
chr11	75795013	75796389	H3K9ME2_UNC0638_peak_669	112	*Gm12339*
chr11	77930932	77931624	H3K9ME2_UNC0638_peak_670	27	*Sez6*
chr11	78165048	78165400	H3K9ME2_UNC0638_peak_671	29	*Nek8*
chr11	78178381	78178672	H3K9ME2_UNC0638_peak_672	27	*Tlcd1*
chr11	84879690	84880075	H3K9ME2_UNC0638_peak_673	38	-
chr11	85885760	85886552	H3K9ME2_UNC0638_peak_674	32	-
chr11	87616718	87617946	H3K9ME2_UNC0638_peak_675	50	*Hsf5*
chr11	95824196	95824496	H3K9ME2_UNC0638_peak_676	50	-
chr11	95862043	95862534	H3K9ME2_UNC0638_peak_677	21	*B4galnt2*

© 2023. Bellver-Sanchis A. et al. Published online at http://www.aginganddisease.org/EN/10.14336/AD.2023.0424-2

SUPPLEMENTARY DATA

chr11	96345730	96346144	H3K9ME2_UNC0638_peak_678	22	-
chr11	96365573	96365864	H3K9ME2_UNC0638_peak_679	43	*Hoxb1*
chr11	96977592	96977883	H3K9ME2_UNC0638_peak_680	32	-
chr11	97280088	97280520	H3K9ME2_UNC0638_peak_681	32	*Gm11592*
chr11	97628404	97629363	H3K9ME2_UNC0638_peak_682	52	*Epop*
chr11	99837432	99837723	H3K9ME2_UNC0638_peak_683	50	*2300003K06Rik*
chr11	99914622	99914945	H3K9ME2_UNC0638_peak_684	29	*Gm11565*
chr11	102665353	102666458	H3K9ME2_UNC0638_peak_685	110	*Meioc*
chr11	103649266	103650108	H3K9ME2_UNC0638_peak_686	31	*Rprml*
chr11	104131776	104132081	H3K9ME2_UNC0638_peak_687	46	*Crhr1*
chr11	104133029	104133352	H3K9ME2_UNC0638_peak_688	34	*Crhr1*
chr11	115053046	115053599	H3K9ME2_UNC0638_peak_689	22	*Cd300e*
chr11	115419874	115420278	H3K9ME2_UNC0638_peak_690	32	-
chr11	116918387	116919576	H3K9ME2_UNC0638_peak_691	67	*Mgat5b*
chr11	119942821	119943159	H3K9ME2_UNC0638_peak_692	34	*Baiap2*
chr11	121146182	121146726	H3K9ME2_UNC0638_peak_693	22	*Tex19.1*
chr11	121259727	121260505	H3K9ME2_UNC0638_peak_694	32	*Foxk2*
chr12	16672293	16672826	H3K9ME2_UNC0638_peak_695	22	*Greb1*
chr12	81781038	81781346	H3K9ME2_UNC0638_peak_696	44	-
chr12	20312537	20312828	H3K9ME2_UNC0638_peak_697	27	-
chr12	24831366	24831978	H3K9ME2_UNC0638_peak_698	64	*Mboat2*
chr12	36381795	36382142	H3K9ME2_UNC0638_peak_699	32	-
chr12	102128702	102129152	H3K9ME2_UNC0638_peak_700	57	-
chr12	102948928	102949219	H3K9ME2_UNC0638_peak_701	32	-
chr12	3236530	3236997	H3K9ME2_UNC0638_peak_702	36	*Rab10os*
chr12	3237149	3237543	H3K9ME2_UNC0638_peak_703	22	*Rab10os*
chr12	11881588	11882057	H3K9ME2_UNC0638_peak_704	31	*Tubb2a-ps2*
chr12	16653335	16653707	H3K9ME2_UNC0638_peak_705	27	-
chr12	30884105	30884963	H3K9ME2_UNC0638_peak_706	38	-
chr12	64472512	64472865	H3K9ME2_UNC0638_peak_707	42	*Fscb*
chr12	72890428	72890725	H3K9ME2_UNC0638_peak_708	38	-
chr12	80518354	80518664	H3K9ME2_UNC0638_peak_709	27	-
chr12	82069705	82069996	H3K9ME2_UNC0638_peak_710	32	*Gm30799*
chr12	110278250	110278748	H3K9ME2_UNC0638_peak_711	21	*Mir1247*
chr12	114513232	114513576	H3K9ME2_UNC0638_peak_712	44	*Mir7094-2*
chr13	15463686	15464501	H3K9ME2_UNC0638_peak_713	49	*Gli3*
chr13	76384010	76384333	H3K9ME2_UNC0638_peak_714	20	*Mctp1*
chr13	119488203	119489292	H3K9ME2_UNC0638_peak_715	161	*Tmem267*
chr13	18948219	18948627	H3K9ME2_UNC0638_peak_716	31	*Amph*
chr13	38345604	38346211	H3K9ME2_UNC0638_peak_717	27	*Bmp6*

© 2023. Bellver-Sanchis A. et al. Published online at http://www.aginganddisease.org/EN/10.14336/AD.2023.0424-2

SUPPLEMENTARY DATA

chr13	46502050	46502578	H3K9ME2_UNC0638_peak_718	42	*Cap2*
chr13	55210231	55210806	H3K9ME2_UNC0638_peak_719	22	*Nsd1*
chr13	109116284	109116953	H3K9ME2_UNC0638_peak_720	44	*Pde4d*
chr13	117602481	117603005	H3K9ME2_UNC0638_peak_721	22	*Hcn1*
chr13	118714985	118715490	H3K9ME2_UNC0638_peak_722	22	*Fgf10*
chr13	3117120	3117610	H3K9ME2_UNC0638_peak_723	72	*Gm46400*
chr13	3478281	3478593	H3K9ME2_UNC0638_peak_724	37	*2810429I04Rik*
chr13	21658666	21659124	H3K9ME2_UNC0638_peak_725	19	*Olfr1361*
chr13	26769262	26769621	H3K9ME2_UNC0638_peak_726	22	*Hdgfl1*
chr13	31625759	31626050	H3K9ME2_UNC0638_peak_727	38	*Foxf2*
chr13	31626601	31626964	H3K9ME2_UNC0638_peak_728	50	*Foxf2*
chr13	47193513	47193874	H3K9ME2_UNC0638_peak_729	32	*Rnf144b*
chr13	49187547	49187838	H3K9ME2_UNC0638_peak_730	43	*Ninj1*
chr13	50657249	50657540	H3K9ME2_UNC0638_peak_731	22	*Gm32038*
chr13	52582815	52583471	H3K9ME2_UNC0638_peak_732	64	*Syk*
chr13	54372102	54372431	H3K9ME2_UNC0638_peak_733	47	*Cplx2*
chr13	54948850	54949671	H3K9ME2_UNC0638_peak_734	78	*Unc5a*
chr13	61157210	61158033	H3K9ME2_UNC0638_peak_735	32	*Ctsr*
chr13	68597463	68597812	H3K9ME2_UNC0638_peak_736	44	*1700001L19Rik*
chr13	68998916	68999327	H3K9ME2_UNC0638_peak_737	33	*Gm35161*
chr13	73846766	73847584	H3K9ME2_UNC0638_peak_738	52	*Gm30303*
chr13	74121190	74121608	H3K9ME2_UNC0638_peak_739	32	*Slc9a3*
chr13	83497186	83497547	H3K9ME2_UNC0638_peak_740	33	*Gm33274*
chr13	92425980	92426385	H3K9ME2_UNC0638_peak_741	21	*Ankrd34b*
chr13	92426707	92427208	H3K9ME2_UNC0638_peak_742	40	*Ankrd34b*
chr13	94876918	94877386	H3K9ME2_UNC0638_peak_743	50	*Otp*
chr13	98354366	98354901	H3K9ME2_UNC0638_peak_744	21	*Foxd1*
chr13	98355344	98355904	H3K9ME2_UNC0638_peak_745	22	*Foxd1*
chr13	103920565	103920899	H3K9ME2_UNC0638_peak_746	17	*D130037M23Rik*
chr13	109903018	109903503	H3K9ME2_UNC0638_peak_747	38	*Mir1904*
chr13	112993625	112994017	H3K9ME2_UNC0638_peak_748	39	*Mcidas*
chr14	40812951	40813374	H3K9ME2_UNC0638_peak_749	17	*Sh2d4b*
chr14	119137721	119138170	H3K9ME2_UNC0638_peak_750	37	*Hs6st3*
chr14	13284468	13285368	H3K9ME2_UNC0638_peak_751	41	*Synpr*
chr14	30715948	30716348	H3K9ME2_UNC0638_peak_752	27	-
chr14	56450420	56450748	H3K9ME2_UNC0638_peak_753	38	*Rnf17*
chr14	63606099	63606876	H3K9ME2_UNC0638_peak_754	74	*Xkr6*
chr14	63607207	63607498	H3K9ME2_UNC0638_peak_755	32	*Xkr6*
chr14	70485973	70486264	H3K9ME2_UNC0638_peak_756	27	-
chr14	70486566	70486935	H3K9ME2_UNC0638_peak_757	57	-

© 2023. Bellver-Sanchis A. et al. Published online at http://www.aginganddisease.org/EN/10.14336/AD.2023.0424-2

SUPPLEMENTARY DATA

chr14	70889673	70890109	H3K9ME2_UNC0638_peak_758	21	*Gfra2*
chr14	103650616	103650998	H3K9ME2_UNC0638_peak_759	52	-
chr14	104460296	104460894	H3K9ME2_UNC0638_peak_760	31	*Pou4f1*
chr14	6497521	6497812	H3K9ME2_UNC0638_peak_761	48	-
chr14	19041996	19042356	H3K9ME2_UNC0638_peak_762	34	*Gm41099*
chr14	24073130	24074084	H3K9ME2_UNC0638_peak_763	93	-
chr14	32158523	32158904	H3K9ME2_UNC0638_peak_764	38	*Ncoa4*
chr14	32377794	32378122	H3K9ME2_UNC0638_peak_765	54	*1700024G13Rik*
chr14	32597788	32598082	H3K9ME2_UNC0638_peak_766	32	-
chr14	33923228	33923652	H3K9ME2_UNC0638_peak_767	19	*Gdf10*
chr14	39471874	39472228	H3K9ME2_UNC0638_peak_768	27	*LOC432842*
chr14	39473465	39473756	H3K9ME2_UNC0638_peak_769	35	*LOC432842*
chr14	44988580	44989705	H3K9ME2_UNC0638_peak_770	40	*Ptger2*
chr14	47472790	47473081	H3K9ME2_UNC0638_peak_771	27	*Fbxo34*
chr14	50345461	50345847	H3K9ME2_UNC0638_peak_772	17	*Olfr735*
chr14	56115872	56116243	H3K9ME2_UNC0638_peak_773	44	*Gzme*
chr14	57035942	57036852	H3K9ME2_UNC0638_peak_774	58	*Gja3*
chr14	59625283	59626255	H3K9ME2_UNC0638_peak_775	55	*Shisa2*
chr14	60379036	60379627	H3K9ME2_UNC0638_peak_776	20	-
chr14	62555572	62556372	H3K9ME2_UNC0638_peak_777	51	*Fam124a*
chr14	68084061	68084720	H3K9ME2_UNC0638_peak_778	40	*Nefl*
chr14	69190590	69191050	H3K9ME2_UNC0638_peak_779	47	*Nkx3-1*
chr14	70443010	70443301	H3K9ME2_UNC0638_peak_780	27	*Mir320*
chr14	70924936	70925358	H3K9ME2_UNC0638_peak_781	33	*Gm34588*
chr14	75845315	75845606	H3K9ME2_UNC0638_peak_782	21	*Tpt1*
chr14	79213251	79213693	H3K9ME2_UNC0638_peak_783	47	*Zfp957*
chr14	102817412	102817852	H3K9ME2_UNC0638_peak_784	26	*Gm34589*
chr14	118012271	118012606	H3K9ME2_UNC0638_peak_785	22	-
chr15	92051491	92052063	H3K9ME2_UNC0638_peak_786	30	*Cntn1*
chr15	66004960	66005422	H3K9ME2_UNC0638_peak_787	25	*Kcnq3*
chr15	4375526	4375978	H3K9ME2_UNC0638_peak_788	17	*Plcxd3*
chr15	10350735	10351050	H3K9ME2_UNC0638_peak_789	19	*Gm41269*
chr15	18077696	18077987	H3K9ME2_UNC0638_peak_790	32	*4921515E04Rik*
chr15	37233901	37234636	H3K9ME2_UNC0638_peak_791	106	*Grhl2*
chr15	39197218	39199162	H3K9ME2_UNC0638_peak_792	58	*Rims2*
chr15	80287651	80288139	H3K9ME2_UNC0638_peak_793	17	*Cacna1i*
chr15	82147176	82147755	H3K9ME2_UNC0638_peak_794	26	*Srebf2*
chr15	82298627	82299377	H3K9ME2_UNC0638_peak_795	43	*Wbp2nl*
chr15	88982798	88983157	H3K9ME2_UNC0638_peak_796	50	*Mov10l1*
chr15	89498923	89499297	H3K9ME2_UNC0638_peak_797	26	*Shank3*

© 2023. Bellver-Sanchis A. et al. Published online at http://www.aginganddisease.org/EN/10.14336/AD.2023.0424-2

SUPPLEMENTARY DATA

chr15	89499945	89500312	H3K9ME2_UNC0638_peak_798	43	*Shank3*
chr15	100038594	100039116	H3K9ME2_UNC0638_peak_799	32	*Dip2b*
chr15	103271722	103272013	H3K9ME2_UNC0638_peak_800	32	-
chr15	7810022	7810515	H3K9ME2_UNC0638_peak_801	38	*Gdnf*
chr15	7810777	7811068	H3K9ME2_UNC0638_peak_802	32	*Gdnf*
chr15	11904407	11905142	H3K9ME2_UNC0638_peak_803	34	*Gm5144*
chr15	12117586	12117877	H3K9ME2_UNC0638_peak_804	27	-
chr15	25364238	25364775	H3K9ME2_UNC0638_peak_805	85	*Basp1*
chr15	29714029	29714460	H3K9ME2_UNC0638_peak_806	72	*Mir3964*
chr15	34838020	34838388	H3K9ME2_UNC0638_peak_807	28	*Kcns2*
chr15	34837387	34837771	H3K9ME2_UNC0638_peak_808	22	*Kcns2*
chr15	36315645	36315948	H3K9ME2_UNC0638_peak_809	27	*Gm41294*
chr15	39006513	39006823	H3K9ME2_UNC0638_peak_810	29	-
chr15	39076943	39077371	H3K9ME2_UNC0638_peak_811	17	-
chr15	44748726	44749017	H3K9ME2_UNC0638_peak_812	22	-
chr15	44787167	44788045	H3K9ME2_UNC0638_peak_813	31	*2310069G16Rik*
chr15	46622018	46622309	H3K9ME2_UNC0638_peak_814	45	*4930548G14Rik*
chr15	66285947	66286540	H3K9ME2_UNC0638_peak_815	33	*Gm27242*
chr15	72968234	72968835	H3K9ME2_UNC0638_peak_816	21	-
chr15	73724653	73725055	H3K9ME2_UNC0638_peak_817	17	-
chr15	75565955	75567034	H3K9ME2_UNC0638_peak_818	89	*Ly6h*
chr15	75746857	75747826	H3K9ME2_UNC0638_peak_819	32	*Mafa*
chr15	76457803	76458094	H3K9ME2_UNC0638_peak_820	32	*Scx*
chr15	78776548	78776859	H3K9ME2_UNC0638_peak_821	48	-
chr15	79109140	79109574	H3K9ME2_UNC0638_peak_822	38	-
chr15	79229325	79229672	H3K9ME2_UNC0638_peak_823	57	-
chr15	80255205	80255729	H3K9ME2_UNC0638_peak_824	102	*Atf4*
chr15	80671357	80672334	H3K9ME2_UNC0638_peak_825	66	*Fam83f*
chr15	84192958	84193539	H3K9ME2_UNC0638_peak_826	32	*Samm50*
chr15	85131347	85132220	H3K9ME2_UNC0638_peak_827	94	-
chr15	86033027	86033444	H3K9ME2_UNC0638_peak_828	27	*Gm34764*
chr15	95653967	95654771	H3K9ME2_UNC0638_peak_829	42	-
chr15	98256259	98257279	H3K9ME2_UNC0638_peak_830	60	*H1f7*
chr15	98313243	98313737	H3K9ME2_UNC0638_peak_831	22	*Olfr285*
chr15	98497268	98498250	H3K9ME2_UNC0638_peak_832	53	*Olfr279*
chr15	99294953	99295244	H3K9ME2_UNC0638_peak_833	27	-
chr15	99393227	99393588	H3K9ME2_UNC0638_peak_834	50	*Tmbim6*
chr15	99590692	99591299	H3K9ME2_UNC0638_peak_835	38	*Aqp5*
chr15	100280690	100280987	H3K9ME2_UNC0638_peak_836	36	*Tmprss12*
chr15	100615639	100615949	H3K9ME2_UNC0638_peak_837	57	*Dazap2*

© 2023. Bellver-Sanchis A. et al. Published online at http://www.aginganddisease.org/EN/10.14336/AD.2023.0424-2

SUPPLEMENTARY DATA

chr15	100728635	100729874	H3K9ME2_UNC0638_peak_838	88	*I730030J21Rik*
chr15	102203744	102204035	H3K9ME2_UNC0638_peak_839	44	*Zfp740*
chr15	102921189	102922206	H3K9ME2_UNC0638_peak_840	117	*Hoxc13*
chr15	102954599	102955567	H3K9ME2_UNC0638_peak_841	52	*Hoxc11*
chr15	102966908	102967214	H3K9ME2_UNC0638_peak_842	22	*Hoxc10*
chr15	103502541	103503623	H3K9ME2_UNC0638_peak_843	66	*Pde1b*
chr16	36693863	36694216	H3K9ME2_UNC0638_peak_844	27	*Ildr1*
chr16	35155848	35156630	H3K9ME2_UNC0638_peak_845	35	*Adcy5*
chr16	92498347	92499061	H3K9ME2_UNC0638_peak_846	22	*Clic6*
chr16	15488452	15488806	H3K9ME2_UNC0638_peak_847	38	*Gm41424*
chr16	16818398	16818851	H3K9ME2_UNC0638_peak_848	17	*Rpl31-ps12*
chr16	18127505	18128182	H3K9ME2_UNC0638_peak_849	44	*Rtn4r*
chr16	36687247	36687765	H3K9ME2_UNC0638_peak_850	64	*Gm41451*
chr16	37916421	37916795	H3K9ME2_UNC0638_peak_851	22	*Gpr156*
chr17	69156709	69157111	H3K9ME2_UNC0638_peak_852	46	*Epb41l3*
chr17	8526791	8527082	H3K9ME2_UNC0638_peak_853	34	*Pde10a*
chr17	14279331	14279804	H3K9ME2_UNC0638_peak_854	51	*Smoc2*
chr17	26715699	26716237	H3K9ME2_UNC0638_peak_855	44	-
chr17	30901675	30902334	H3K9ME2_UNC0638_peak_856	20	*Glp1r*
chr17	42316011	42316313	H3K9ME2_UNC0638_peak_857	31	*Ptchd4*
chr17	43801656	43802336	H3K9ME2_UNC0638_peak_858	101	-
chr17	52601189	52601602	H3K9ME2_UNC0638_peak_859	28	*Kcnh8*
chr17	52601955	52602246	H3K9ME2_UNC0638_peak_860	17	*Kcnh8*
chr17	56751460	56751960	H3K9ME2_UNC0638_peak_861	48	*Nrtn*
chr17	63050512	63051009	H3K9ME2_UNC0638_peak_862	44	*Fbxl17*
chr17	68273531	68273951	H3K9ME2_UNC0638_peak_863	29	*L3mbtl4*
chr17	69439329	69439766	H3K9ME2_UNC0638_peak_864	23	*Akain1*
chr17	8341244	8342227	H3K9ME2_UNC0638_peak_865	50	*Prr18*
chr17	13206400	13206705	H3K9ME2_UNC0638_peak_866	56	*Gm10512*
chr17	24470313	24470604	H3K9ME2_UNC0638_peak_867	22	*Pgp*
chr17	27205009	27205546	H3K9ME2_UNC0638_peak_868	27	*Gm34736*
chr17	34021936	34022624	H3K9ME2_UNC0638_peak_869	39	*Ring1*
chr17	34646431	34646773	H3K9ME2_UNC0638_peak_870	22	*Atf6b*
chr17	34671150	34671465	H3K9ME2_UNC0638_peak_871	31	*Tnxb*
chr17	39847575	39848760	H3K9ME2_UNC0638_peak_872	492	*AY036118*
chr17	39843186	39846706	H3K9ME2_UNC0638_peak_873	544	*AY036118*
chr17	55445692	55446001	H3K9ME2_UNC0638_peak_874	22	-
chr17	55593744	55594162	H3K9ME2_UNC0638_peak_875	27	-
chr17	56123940	56124275	H3K9ME2_UNC0638_peak_876	37	*Sema6b*
chr17	56123190	56123498	H3K9ME2_UNC0638_peak_877	25	*Sema6b*

© 2023. Bellver-Sanchis A. et al. Published online at http://www.aginganddisease.org/EN/10.14336/AD.2023.0424-2

SUPPLEMENTARY DATA

chr17	56776769	56777359	H3K9ME2_UNC0638_peak_878	38	*Rfx2*
chr17	78595649	78596247	H3K9ME2_UNC0638_peak_879	32	-
chr17	80373159	80374055	H3K9ME2_UNC0638_peak_880	64	*Gm10190*
chr17	80944752	80945067	H3K9ME2_UNC0638_peak_881	34	*Tmem178*
chr17	84676046	84676372	H3K9ME2_UNC0638_peak_882	38	*Abcg8*
chr18	12643539	12644009	H3K9ME2_UNC0638_peak_883	36	*Ttc39c*
chr18	12973517	12973808	H3K9ME2_UNC0638_peak_884	21	*Impact*
chr18	22344392	22344739	H3K9ME2_UNC0638_peak_885	64	*Asxl3*
chr18	23310505	23310796	H3K9ME2_UNC0638_peak_886	40	*Dtna*
chr18	31634479	31634807	H3K9ME2_UNC0638_peak_887	44	-
chr18	32938908	32939374	H3K9ME2_UNC0638_peak_888	46	*Camk4*
chr18	36018006	36018594	H3K9ME2_UNC0638_peak_889	26	-
chr18	37356499	37356828	H3K9ME2_UNC0638_peak_890	14	*Pcdhb8*
chr18	65580987	65581585	H3K9ME2_UNC0638_peak_891	49	*Zfp532*
chr18	84209152	84209478	H3K9ME2_UNC0638_peak_892	19	*Zfp407*
chr18	6490169	6490697	H3K9ME2_UNC0638_peak_893	44	*Epc1*
chr18	9213223	9213514	H3K9ME2_UNC0638_peak_894	13	*Fzd8*
chr18	9213811	9215081	H3K9ME2_UNC0638_peak_895	64	*Fzd8*
chr18	19165834	19166276	H3K9ME2_UNC0638_peak_896	27	*Gm31086*
chr18	22334188	22334479	H3K9ME2_UNC0638_peak_897	32	*Gm41676*
chr18	23216677	23217110	H3K9ME2_UNC0638_peak_898	23	*Gm7788*
chr18	27810314	27810635	H3K9ME2_UNC0638_peak_899	61	*Gm33674*
chr18	33241199	33241632	H3K9ME2_UNC0638_peak_900	57	*Gm41683*
chr18	37335407	37335972	H3K9ME2_UNC0638_peak_901	49	*Pcdhb6*
chr18	39773523	39774177	H3K9ME2_UNC0638_peak_902	50	*Pabpc2*
chr18	42395236	42395809	H3K9ME2_UNC0638_peak_903	34	*Pou4f3*
chr18	50220046	50220686	H3K9ME2_UNC0638_peak_904	72	*Gm46613*
chr18	67133345	67133643	H3K9ME2_UNC0638_peak_905	27	*Gnal*
chr18	70568561	70568852	H3K9ME2_UNC0638_peak_906	22	*Mbd2*
chr18	76475901	76476335	H3K9ME2_UNC0638_peak_907	17	-
chr18	80986164	80986597	H3K9ME2_UNC0638_peak_908	23	-
chr19	8356215	8356560	H3K9ME2_UNC0638_peak_909	57	*Slc22a30*
chr19	40893997	40894844	H3K9ME2_UNC0638_peak_910	74	*Zfp518a*
chr19	47178672	47179451	H3K9ME2_UNC0638_peak_911	87	*Neurl1a*
chr19	57610626	57611386	H3K9ME2_UNC0638_peak_912	107	*Atrnl1*
chr19	3767848	3768684	H3K9ME2_UNC0638_peak_913	86	*Kmt5b*
chr19	4712351	4712668	H3K9ME2_UNC0638_peak_914	57	*Sptbn2*
chr19	5106584	5106977	H3K9ME2_UNC0638_peak_915	51	*Klc2*
chr19	8252368	8252974	H3K9ME2_UNC0638_peak_916	30	-
chr19	11912368	11913053	H3K9ME2_UNC0638_peak_917	43	*Patl1*

© 2023. Bellver-Sanchis A. et al. Published online at http://www.aginganddisease.org/EN/10.14336/AD.2023.0424-2

SUPPLEMENTARY DATA

chr19	14398391	14398744	H3K9ME2_UNC0638_peak_918	53	-
chr19	22138798	22139266	H3K9ME2_UNC0638_peak_919	33	*Trpm3*
chr19	23687120	23687663	H3K9ME2_UNC0638_peak_920	27	*Ptar1*
chr19	25236653	25237097	H3K9ME2_UNC0638_peak_921	41	*Kank1*
chr19	28834728	28836174	H3K9ME2_UNC0638_peak_922	77	*Slc1a1*
chr19	32757709	32758165	H3K9ME2_UNC0638_peak_923	38	*Pten*
chr19	36348173	36348575	H3K9ME2_UNC0638_peak_924	50	-
chr19	36554218	36554754	H3K9ME2_UNC0638_peak_925	27	*Hectd2*
chr19	36925885	36926307	H3K9ME2_UNC0638_peak_926	32	*Btaf1*
chr19	37017628	37018539	H3K9ME2_UNC0638_peak_927	31	*Cpeb3*
chr19	41482556	41483573	H3K9ME2_UNC0638_peak_928	43	-
chr19	44147050	44147364	H3K9ME2_UNC0638_peak_929	31	*Pkd2l1*
chr19	44930808	44931498	H3K9ME2_UNC0638_peak_930	36	*Slf2*
chr19	46761499	46761790	H3K9ME2_UNC0638_peak_931	27	-
chr19	53600079	53600792	H3K9ME2_UNC0638_peak_932	72	*Smc3*
chr19	53676716	53677876	H3K9ME2_UNC0638_peak_933	122	*Rbm20*
chr19	53944890	53945560	H3K9ME2_UNC0638_peak_934	57	*Shoc2*
chr19	3388575	3389206	H3K9ME2_UNC0638_peak_935	61	*Tesmin*
chr19	3686128	3686557	H3K9ME2_UNC0638_peak_936	36	-
chr19	3987952	3988306	H3K9ME2_UNC0638_peak_937	18	*Acy3*
chr19	4756321	4756621	H3K9ME2_UNC0638_peak_938	38	*Rbm4b*
chr19	5098245	5098599	H3K9ME2_UNC0638_peak_939	69	*Rab1b*
chr19	5306615	5308113	H3K9ME2_UNC0638_peak_940	160	-
chr19	5367777	5368085	H3K9ME2_UNC0638_peak_941	28	*Eif1ad*
chr19	6194688	6194979	H3K9ME2_UNC0638_peak_942	32	*Majin*
chr19	6364228	6364520	H3K9ME2_UNC0638_peak_943	27	*Sfl*
chr19	6830696	6831050	H3K9ME2_UNC0638_peak_944	26	*Rps6ka4*
chr19	6998328	6998781	H3K9ME2_UNC0638_peak_945	51	*Fermt3*
chr19	7612320	7612999	H3K9ME2_UNC0638_peak_946	144	*Plaat5*
chr19	7671494	7671813	H3K9ME2_UNC0638_peak_947	22	*Slc22a19*
chr19	8618171	8618580	H3K9ME2_UNC0638_peak_948	24	*Slc22a6*
chr19	8757165	8757457	H3K9ME2_UNC0638_peak_949	43	*1700023D09Rik*
chr19	8793371	8793735	H3K9ME2_UNC0638_peak_950	31	*Polr2g*
chr19	8820039	8820470	H3K9ME2_UNC0638_peak_951	23	*Hnrnpul2*
chr19	8966443	8966734	H3K9ME2_UNC0638_peak_952	26	*Eef1g*
chr19	10203820	10204179	H3K9ME2_UNC0638_peak_953	32	*Tmem258*
chr19	10388746	10390069	H3K9ME2_UNC0638_peak_954	84	*Syt7*
chr19	10525537	10525995	H3K9ME2_UNC0638_peak_955	22	*Cpsf7*
chr19	10688837	10689128	H3K9ME2_UNC0638_peak_956	38	-
chr19	11770111	11770550	H3K9ME2_UNC0638_peak_957	38	*Mrpl16*

© 2023. Bellver-Sanchis A. et al. Published online at http://www.aginganddisease.org/EN/10.14336/AD.2023.0424-2

SUPPLEMENTARY DATA

chr19	11868488	11869191	H3K9ME2_UNC0638_peak_958	24	*Olfr1419*
chr19	11965898	11966232	H3K9ME2_UNC0638_peak_959	89	*Osbp*
chr19	12119261	12119626	H3K9ME2_UNC0638_peak_960	41	*Olfr76*
chr19	12119864	12120386	H3K9ME2_UNC0638_peak_961	51	*Olfr76*
chr19	12794965	12795598	H3K9ME2_UNC0638_peak_962	97	-
chr19	12904256	12904584	H3K9ME2_UNC0638_peak_963	27	*Gm5512*
chr19	13837225	13837607	H3K9ME2_UNC0638_peak_964	40	*Olfr1501*
chr19	16872811	16873172	H3K9ME2_UNC0638_peak_965	33	*Foxb2*
chr19	17394132	17394423	H3K9ME2_UNC0638_peak_966	27	*Rfk*
chr19	18671054	18671345	H3K9ME2_UNC0638_peak_967	22	-
chr19	18713097	18713454	H3K9ME2_UNC0638_peak_968	50	-
chr19	21653205	21653496	H3K9ME2_UNC0638_peak_969	32	*Abhd17b*
chr19	24042998	24043332	H3K9ME2_UNC0638_peak_970	46	*Gm41823*
chr19	24897236	24897766	H3K9ME2_UNC0638_peak_971	54	*Foxd4*
chr19	24900093	24900500	H3K9ME2_UNC0638_peak_972	27	*Foxd4*
chr19	27323175	27324058	H3K9ME2_UNC0638_peak_973	78	*Kcnv2*
chr19	29068252	29068569	H3K9ME2_UNC0638_peak_974	38	*Gm9895*
chr19	29251457	29252095	H3K9ME2_UNC0638_peak_975	36	*Jak2*
chr19	29521931	29522603	H3K9ME2_UNC0638_peak_976	49	*Ric1*
chr19	30030620	30031241	H3K9ME2_UNC0638_peak_977	29	-
chr19	31083622	31084308	H3K9ME2_UNC0638_peak_978	61	*Cstf2t*
chr19	32387883	32388294	H3K9ME2_UNC0638_peak_979	24	*2700046G09Rik*
chr19	33122868	33123386	H3K9ME2_UNC0638_peak_980	24	*Gm29946*
chr19	33497327	33497652	H3K9ME2_UNC0638_peak_981	61	*Lipo4*
chr19	36834169	36834696	H3K9ME2_UNC0638_peak_982	73	*Tnks2*
chr19	38124616	38125186	H3K9ME2_UNC0638_peak_983	57	*Gm32440*
chr19	38837069	38837383	H3K9ME2_UNC0638_peak_984	50	*Tbc1d12*
chr19	40830990	40831497	H3K9ME2_UNC0638_peak_985	106	*Ccnj*
chr19	41980751	41981042	H3K9ME2_UNC0638_peak_986	32	*Ubtd1*
chr19	42035973	42036264	H3K9ME2_UNC0638_peak_987	22	*Ankrd2*
chr19	42090506	42090797	H3K9ME2_UNC0638_peak_988	27	*Pi4k2a*
chr19	42779811	42780190	H3K9ME2_UNC0638_peak_989	35	*Gm16244*
chr19	43440220	43441651	H3K9ME2_UNC0638_peak_990	58	-
chr19	43752990	43753326	H3K9ME2_UNC0638_peak_991	44	*Cutc*
chr19	44107004	44107415	H3K9ME2_UNC0638_peak_992	31	*Cwf19l1*
chr19	45150677	45151494	H3K9ME2_UNC0638_peak_993	73	*Tlx1*
chr19	45749112	45749522	H3K9ME2_UNC0638_peak_994	27	*Npm3*
chr19	46305031	46305322	H3K9ME2_UNC0638_peak_995	20	-
chr19	46328826	46329149	H3K9ME2_UNC0638_peak_996	43	-
chr19	47014257	47015815	H3K9ME2_UNC0638_peak_997	55	*Ina*

© 2023. Bellver-Sanchis A. et al. Published online at http://www.aginganddisease.org/EN/10.14336/AD.2023.0424-2

SUPPLEMENTARY DATA

chr19	47067856	47068405	H3K9ME2_UNC0638_peak_998	57	*Taf5*
chr19	47579553	47580083	H3K9ME2_UNC0638_peak_999	44	*Slk*
chr19	47747758	47748304	H3K9ME2_UNC0638_peak_1000	93	*Cfap43*
chr19	52264349	52264978	H3K9ME2_UNC0638_peak_1001	77	*Ins1*
chr19	53903547	53903897	H3K9ME2_UNC0638_peak_1002	27	*Pdcd4*
chr19	54153349	54153698	H3K9ME2_UNC0638_peak_1003	33	*Gm41865*
chr19	56191398	56192114	H3K9ME2_UNC0638_peak_1004	60	*Gm32028*
chr19	56548514	56548954	H3K9ME2_UNC0638_peak_1005	44	*Nhlrc2*
chr19	56722191	56723345	H3K9ME2_UNC0638_peak_1006	94	*Adrb1*
chr19	56826017	56826564	H3K9ME2_UNC0638_peak_1007	61	*Tdrd1*
chr19	57361204	57361561	H3K9ME2_UNC0638_peak_1008	27	*Fhip2a*
chr19	57508051	57508853	H3K9ME2_UNC0638_peak_1009	53	*6720468P15Rik*
chr19	58511770	58512487	H3K9ME2_UNC0638_peak_1010	69	*Ccdc172*
chr19	58606035	58606545	H3K9ME2_UNC0638_peak_1011	33	*1810007D17Rik*
chr19	58729847	58730256	H3K9ME2_UNC0638_peak_1012	25	*Pnliprp1*
chr19	59171835	59172272	H3K9ME2_UNC0638_peak_1013	31	-
chr19	59219176	59220196	H3K9ME2_UNC0638_peak_1014	55	*Kcnk18*
chr19	59260722	59261313	H3K9ME2_UNC0638_peak_1015	25	*Slc18a2*
chr19	59660678	59661121	H3K9ME2_UNC0638_peak_1016	33	*Gm19956*
chr19	61216041	61216505	H3K9ME2_UNC0638_peak_1017	44	*Csf2ra*
chr19	61225150	61226700	H3K9ME2_UNC0638_peak_1018	50	*Csf2ra*
chrUn_JH584304	3801	4165	H3K9ME2_UNC0638_peak_1019	50	*LOC100861749*
chrUn_JH584304	15737	16315	H3K9ME2_UNC0638_peak_1020	154	-
chrUn_JH584304	53233	54410	H3K9ME2_UNC0638_peak_1021	308	*Pisd-ps3*
chr1_GL456211_random	73338	73629	H3K9ME2_UNC0638_peak_1022	38	*LOC102636478*
chr1_GL456211_random	112172	113228	H3K9ME2_UNC0638_peak_1023	114	*LOC100503923*
chr1_GL456211_random	174693	174984	H3K9ME2_UNC0638_peak_1024	59	*LOC100041057*
chr1_GL456212_random	128651	128973	H3K9ME2_UNC0638_peak_1025	44	-
chr1_GL456212_random	67719	68407	H3K9ME2_UNC0638_peak_1026	220	-

© 2023. Bellver-Sanchis A. et al. Published online at http://www.aginganddisease.org/EN/10.14336/AD.2023.0424-2

SUPPLEMENTARY DATA

Supplementary Table. 9 | Prediction of lysine methylation sites in GMFB using the GPS-MSP algorithm.

ID	Position	Peptide	Met-types	Score	Cutoff
AAP35430.1 glia maturation factor, beta [Homo sapiens]	17	VAEDLVE**K**LRKFRFR	K. all	3.45	0.00
AAP35430.1 glia maturation factor, beta [Homo sapiens]	20	DLVEKLR**K**FRFRKET	K. all	0.66	0.00
AAP35430.1 glia maturation factor, beta [Homo sapiens]	25	LRKFRFR**K**ETNNAAI	K. all	2.88	0.00
AAP35430.1 glia maturation factor, beta [Homo sapiens]	35	NNAAIIM**K**IDKDKRL	K. all	0.20	0.00
AAP35430.1 glia maturation factor, beta [Homo sapiens]	38	AIIMKID**K**DKRLVVL	K. all	0.42	0.00
AAP35430.1 glia maturation factor, beta [Homo sapiens]	40	IMKIDKD**K**RLVVLDE	K. all	0.51	0.00
AAP35430.1 glia maturation factor, beta [Homo sapiens]	58	GISPDEL**K**DELPERQ	K. all	1.92	0.00
AAP35430.1 glia maturation factor, beta [Homo sapiens]	74	RFIVYSY**K**YQHDDGR	K. all	0.83	0.00
AAP35430.1 glia maturation factor, beta [Homo sapiens]	97	FSSPVGC**K**PEQQMMY	K. all	0.34	0.00
AAP35430.1 glia maturation factor, beta [Homo sapiens]	108	QMMYAGS**K**NKLVQTA	K. all	1.61	0.00
AAP35430.1 glia maturation factor, beta [Homo sapiens]	110	MYAGSKN**K**LVQTAEL	K. all	0.89	0.00
AAP35430.1 glia maturation factor, beta [Homo sapiens]	119	VQTAELT**K**VFEIRNT	K. all	1.27	0.00
AAP35430.1 glia maturation factor, beta [Homo sapiens]	137	TEEWLRE**K**LGFFTNV	K. all	0.05	0.00
AAP35430.1 glia maturation factor, beta [Homo sapiens]	150	NVNFCVS**K**VFMY***	K. all	0.01	0.00

Reference

1. Dahiya, Y. *et al.* Differential regulation of innate and learned behavior by Creb1/Crh-1 in Caenorhabditis elegans. *J. Neurosci.* **39**, 7934–7946 (2019).
2. Brena, D., Bertran, J., Porta-de-la-Riva, M. *et al.* Ancestral function of Inhibitors-of-kappaB regulates *Caenorhabditis elegans* development. *Sci Rep* **10,** 16153 (2020). https://doi.org/10.1038/s41598-020-73146-5

© 2023. Bellver-Sanchis A. et al. Published online at http://www.aginganddisease.org/EN/10.14336/AD.2023.0424-2

3.3. Publication 3

Neuroprotective effects of G9a inhibition through modulation of peroxisome-proliferator activator receptor gamma-dependent pathways by *miR-128.*

Aina Bellver-Sanchis, Pedro A. Ávila-López, Iva Tic, David Valle-García, Marta Ribalta-Vilella, Luis Labrador, Deb Ranjan Banerjee, Ana Guerrero, Gemma Casadesus, Coralie Poulard,
Mercè Pallàs, and Christian Griñán-Ferré

Neural Regeneration Research, 2024, 19
doi: 10.4103/1673-5374.393102

SUMMARY

Aberrant epigenetic dysregulation is implicated in AD, and notably, miRNAs play a significant role in disease progression, with altered expression linked to neuroinflammation, OS, and synaptic dysfunction. Interestingly, G9a modulation has been shown to alter miRNA expression, although this regulation in the context of AD is poorly explored. Thus, we focus on investigating the interconnections between G9a, miRNAs, OS, and neuroinflammation, with a specific emphasis on AD, using the SAMP8 mouse model. We hypothesize that inhibiting G9a induces alterations in miRNA expression profiles within SAMP8 mice, fostering neuroprotective outcomes.

Our work involved transcriptomic analyses by further validation after pharmacological inhibition of G9a in SAMP8 mice. Additionally, we also employ different bioinformatic tools for pathway analyses to unveil a new mechanism through which G9a inhibition positively affects cognition in the SAMP8 mouse. At first, by integrating transcriptomic analyses, we detected alterations in several miRNAs (*miR-1298*, *miR-669*, *miR-677*, and *miR-128*). Further, subsequent Kyoto Encyclopedia of Genes and Genomes (KEGG) enrichment analyses unveiled the connection between G9a and several pathways, including the cholinergic synapse, axon guidance, cAMP signaling pathway, etc. Among the miRNAs validated, *miR-128* has been involved in the development of the nervous system as well as the regulation of neuronal plasticity, neuronal death, and cognitive impairment, being increased in the hippocampus of AD human brains. In the same line, we observed a downregulation in the expression *miR-128* after the G9a inhibition treatment in SAMP8. Intriguingly, as miR-128 is known to bind to the 3′ untranslated region (3′-UTR) of peroxisome-proliferator activator receptor gamma (PPARG) mRNA, increased levels of *Pparg* gene expression were found in the SAMP8 treated group. As a result, we point out that the observed modulation of OS responses could appear to be

mainly Pparg-driven after treatment with a G9ai. The antioxidant effects after inhibition of G9a were also validated in primary neuron cell cultures. Additionally, the upregulation of PPARγ by the G9a inhibitor was associated with the modulation of markers related to DNA damage responses, apoptosis, autophagy, synaptic plasticity, and neurogenesis.

In summary, our study establishes that inhibiting G9a enhances the gene expression profiles of both mRNAs and miRNAs in the SAMP8 mouse model. Primarily, we propose that the neuroprotective effect of pharmacological G9a inhibition is partially mediated by the modulation of PPARγ-dependent pathways through *miR-128* in the SAMP8 mouse model.

Research Article

NEURAL REGENERATION RESEARCH
www.nrronline.org

Neuroprotective effects of G9a inhibition through modulation of peroxisome-proliferator activator receptor gamma-dependent pathways by *miR-128*

Aina Bellver-Sanchis[1], Pedro A. Ávila-López[2], Iva Tic[1], David Valle-García[3, †], Marta Ribalta-Vilella[1], Luis Labrador[4], Deb Ranjan Banerjee[5], Ana Guerrero[1], Gemma Casadesus[4], Coralie Poulard[6, 7, 8], Mercè Pallàs[1, 9], Christian Griñán-Ferré[1, 9, *]

https://doi.org/10.4103/1673-5374.393102

Date of submission: June 13, 2023

Date of decision: December 17, 2023

Date of acceptance: December 28, 2023

Date of web publication: January 8, 2024

From the Contents

Introduction	2
Methods	3
Results	4
Discussion	7

Graphical Abstract

G9a inhibition modulates PPARγ-dependent pathways through miR-128, enhancing the mechanisms of oxidative stress, autophagy, apoptosis, DNA damage, and synaptic plasticity in Alzheimer's disease

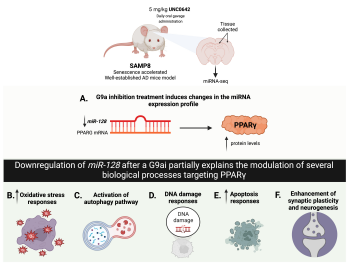

Abstract

Dysregulation of G9a, a histone-lysine N-methyltransferase, has been observed in Alzheimer's disease and has been correlated with increased levels of chronic inflammation and oxidative stress. Likewise, microRNAs are involved in many biological processes and diseases playing a key role in pathogenesis, especially in multifactorial diseases such as Alzheimer's disease. Therefore, our aim has been to provide partial insights into the interconnection between G9a, microRNAs, oxidative stress, and neuroinflammation. To better understand the biology of G9a, we compared the global microRNA expression between senescence-accelerated mouse-prone 8 (SAMP8) control mice and SAMP8 treated with G9a inhibitor UNC0642. We found a downregulation of *miR-128* after a G9a inhibition treatment, which interestingly binds to the 3′ untranslated region (3′-UTR) of peroxisome-proliferator activator receptor γ (PPARG) mRNA. Accordingly, *Pparg* gene expression levels were higher in the SAMP8 group treated with G9a inhibitor than in the SAMP8 control group. We also observed modulation of oxidative stress responses might be mainly driven *Pparg* after G9a inhibitor. To confirm these antioxidant effects, we treated primary neuron cell cultures with hydrogen peroxide as an oxidative insult. In this setting, treatment with G9a inhibitor increases both cell survival and antioxidant enzymes. Moreover, up-regulation of PPARγ by G9a inhibitor could also increase the expression of genes involved in DNA damage responses and apoptosis. In addition, we also described that the PPARγ/AMPK axis partially explains the regulation of autophagy markers expression. Finally, PPARγ/GADD45α potentially contributes to enhancing synaptic plasticity and neurogenesis after G9a inhibition. Altogether, we propose that pharmacological inhibition of G9a leads to a neuroprotective effect that could be due, at least in part, by the modulation of PPARγ-dependent pathways by *miR-128*.

Key Words: aging; cognitive decline; epigenetics; G9a inhibition; microRNAs; miR-128; peroxisome-proliferator activator receptor γ (PPARγ); PPARG; SAMP8

[1]Department of Pharmacology and Therapeutic Chemistry, Institut de Neurociències-Universitat de Barcelona, Barcelona, Spain; [2]Department of Biochemistry and Molecular Genetics, Feinberg School of Medicine, Northwestern University, Chicago, IL, USA; [3]Institute of Biotechnology, National Autonomous University of Mexico, Cuernavaca, Mexico; [4]Department of Pharmacology and Therapeutics, Health Science Center-University of Florida, Gainesville, FL, USA; [5]Department of Chemistry, National Institute of Technology Durgapur, M G Avenue, Durgapur, West Bengal, India; [6]Cancer Research Cancer Lyon, Université de Lyon, Lyon, France; [7]Inserm U1052, Centre de Recherche en Cancérologie de Lyon, Lyon, France; [8]CNRS UMR5286, Centre de Recherche en Cancérlogie de Lyon, Lyon, France; [9]Centro de Investigación en Red, Enfermedades Neurodegenerativas (CIBERNED), Instituto de Salud Carlos III, Madrid, Spain
[†]Current address: Neuroimmunology Department, National Institute of Neurology and Neurosurgery "Manuel Velasco Suárez", Mexico City, Mexico
***Correspondence to:** Christian Griñán-Ferré, PhD, Christian.grinan@ub.edu.
https://orcid.org/0000-0002-5424-9130 (Christian Griñán-Ferré)

Funding: *This study was supported by the Ministerio de Economía, Industria y Competitividad (Agencia Estatal de Investigación, AEI; to CGF and MP) and Fondo Europeo de Desarrollo Regional (MINECO-FEDER) (PID2022-139016OA-I00, PDC2022-133441-I00; to CGF and MP), Generalitat de Catalunya (2021 SGR 00357; to CGF and MP). This study was co-financed by Secretaria d'Universitats i Recerca del Departament d'Empresai Coneixement de la Generalitat de Catalunya 2021 (Llavor 00086; to CGF). AG is the recipient of an Alzheimer's Association Research Fellowship (AARF-21-848511). ABS acknowledges the Agència de Gestió d'Ajuts Universitaris i de Recerca (AGAUR) for her FI-SDUR fellowship (2021FISDU 00182).*

How to cite this article: *Bellver-Sanchis A, Ávila-López PA, Tic I, Valle-García D, Ribalta-Vilella M, Labrador L, Banerjee DR, Guerrero A, Casadesus G, Poulard C, Pallàs M, Griñán-Ferré C (2024) Neuroprotective effects of G9a inhibition through modulation of peroxisome-proliferator activator receptor gamma-dependent pathways by miR-128. Neural Regen Res 19(0):000-000.*

Downloaded from http://journals.lww.com/nrronline by BhDMf5ePHKav1zEoum1tQfN4a+kJLhEZgbsIHo4XMi0hCywCX1AWnYQp/IlQrHD3i3D0OdRyi7TvSFl4Cf3VC4/OAVpDDa8K2+Ya6H515kE= on 01/16/2024

NEURAL REGENERATION RESEARCH
www.nrronline.org

Research Article

Introduction

Dysregulation of epigenetic mechanisms has been widely implicated in various disease states with emphasis on neurodegenerative disorders (Griñán-Ferré et al., 2018). Alzheimer's disease (AD) is a progressive and debilitating neurological disorder characterized by a gradual and permanent decline in intellectual functioning and the ability to carry out daily activities. A complex combination of genetic, environmental, and lifestyle factors has been described as a potential cause of AD (Eid et al., 2019). With aging there are epigenetic alterations that promote dramatic changes in gene pattern profiles related to cognition, learning and memory formation, being relevant for the progression of age-related cognitive decline exhibited in AD pathology (Harman and Martín, 2020). Interestingly, global histone changes related to transcriptional activation and repression have been observed in different regions of postmortem AD brains (Park et al., 2022). Indeed, during aging and senescence, epigenetic alterations are detected, such as DNA methylation (5-mC) and hydroxymethylation changes (5-hmC), and several important chromatin modifications such as H3K4me, H3K9me, H3K27me, H4K16ac, among others (Tecalco-Cruz et al., 2020).

Noteworthily, the expression of non-coding RNA transcripts, including microRNAs (miRNAs) is altered at the epigenetic level in several age-related diseases such as AD (Cosín-Tomás et al., 2018). miRNAs are small noncoding RNAs, comprised of ~22 nucleotides, that negatively regulate gene expression via either degrading the target mRNA or by direct translational inhibition (Ha and Kim, 2014). Regarding AD progression, miRNAs have been identified as one of the crucial players in the constellation of physiological changes presented in AD patients (Cosín-Tomás et al., 2018; Wei et al., 2020). Interestingly, altered miRNA expression has been widely documented in AD and other neurodegenerative diseases, and several studies have linked these to neuroinflammation (Liang and Wang, 2021), oxidative stress (OS; Konovalova et al., 2019), and synaptic dysfunction (Siedlecki-Wullich et al., 2019) among others. Treatment of neuronal cells with histone deacetylase inhibitors, DNA methyltransferase inhibitors (DNMTi), or G9a inhibitors (G9ai) has shown to change miRNA expression pattern profile (Nagaraj et al., 2019; Shukla and Tekwani., 2020).

Epigenetic regulation by the methyltransferase G9a (also called EHMT2, the euchromatic histone methyltransferase 2) acts as a crucial regulator in human diseases and is particularly involved in learning and memory formation (Gupta-Agarwal et al., 2012). G9a mediates the H3K9me2 epigenetic mark, which is mainly associated with transcriptional repression (Shankar et al., 2013). Of note, G9a overexpression in the brain of late-stage familial AD mice (5×FAD) and AD patients has recently been demonstrated (Griñán-Ferré et al., 2019; Zheng et al., 2019). Our group previously demonstrated that pharmacological inhibition of G9a by UNC0642 produced significant neuroprotective effects in an early-onset AD mouse model (Griñán-Ferré et al., 2019; Bellver-Sanchis et al., 2023). On the one hand, we found an uncharacterized mechanism through glia maturation factor beta by which G9a inhibition promotes the reduction of neuroinflammation and increases synaptic plasticity through modifying the transcriptome of senescence-accelerated mouse-prone 8 (SAMP8) mice (Bellver-Sanchis et al., 2023). Moreover, it has been shown that G9a potentiates oxidative stress in neurons, and that its inhibition reduces reactive oxygen species levels and elevates antioxidant enzyme levels (Griñán-Ferré et al., 2019). Additionally, it is noteworthy that hydrogen peroxide (H_2O_2) treatment in cell cultures was shown to be associated with a pronounced increase in the repressive mark H3K9me2 (Rothammer et al., 2022). Then, G9a plays an important role in regulating gene expression with a neuroprotective effect.

Besides epigenetic marks, neuroinflammation (Leng and Edison, 2021) and OS (Ionescu-Tucker and Cotman, 2021) have a great impact on AD. Interestingly, *miR-128* knockout inhibits the progression of AD pathology in mouse models as a consequence of increased peroxisome proliferator-activated receptor gamma (PPARγ) levels (Liu et al., 2019). PPARγ is a ligand-activated transcription factor of the nuclear hormone receptor superfamily, which regulates several essential genes in various metabolic processes and cell fate, and it is also implicated in homeostasis and inflammation (Houseknecht et al., 2002). Of note, PPARγ is implicated in the OS response, inflammation, and apoptosis after brain injury or neurodegenerative disease (Kapadia et al., 2008; Yonutas and Sullivan, 2013). Previous reports demonstrated that PPARγ expression is positively upregulated by several transcription factors such as C/EBP, Krox20, and KLF4, among others (Liu et al., 2006; Cho et al., 2009; Wang et al., 2010; Ge et al., 2016). At the epigenetic level, *Pparg* gene expression is upregulated by H3K4me3. Furthermore, one study traced the repression of *Pparg* gene expression through the G9a-dependent addition of H3K9me2 to the entire *Pparg* gene body (Wang et al., 2013).

SAMP8 is a well-established mouse model to study age-related cognitive decline and AD hallmarks (Butterfield and Poon, 2005; Liu et al., 2020). Thus, the SAMP8 mouse is an interesting tool to unveil epigenetic alterations associated with AD (Griñán-Ferré et al., 2018). Furthermore, some recent studies have confirmed the relevance of epigenetic alterations in the onset and progression of the neurodegenerative process in the SAMP8 mice (Griñán-Ferré et al., 2018; Harman and Martín, 2020; Tecalco-Cruz et al., 2020).

Focusing on individual components of AD pathogenesis, in this study, we aim to explore how G9a, miRNAs, OS, and neuroinflammation are interconnected. Of note, the regulation of miRNA expression by G9a in AD remains elusive. Here, we hypothesize that G9a inhibition promotes changes in miRNA expression profiles in the SAMP8 mice, consequently modulating distinct events relevant to AD and ultimately promoting neuroprotective effects. We explored differentially expressed mRNA and miRNAs after G9a inhibition to find new molecular pathways and targets. Furthermore, using Gene Ontology (GO) database (http://geneontology.org/) and Kyoto Encyclopaedia of Genes and Genomes (KEGG) database (https://www.kegg.jp/) pathway analyses, we unveil a novel mechanism by which G9a inhibition promotes beneficial effects on cognition in the SAMP8 mouse (see results related to cognitive status after G9ai treatment in (Bellver-Sanchis et al., 2023).

Downloaded from http://journals.lww.com/nrronline by BhDMf5ePHKav1zEoum1tQfN4a+kJLhEZgbsIHo4XMi0hCywCX1AWnYQp/IlQrHD3i3D0OdRyi7TvSFl4Cf3VC4/OAVpDDa8K2+Ya6H515kE= on 01/16/2024

Downloaded from http://journals.lww.com/nrronline by BhDMf5ePHKav1zEoum1tQfN4a+kJLhEZgbsIHo4XMi0hCywCX1AWnYQp/IlQrHD3i3D0OdRyi7TvSFl4Cf3VC4/OAVpDDa8K2+Ya6H515kE= on 01/16/2024

Methods

Animals

Female and male SAMP8 24-week-old mice (n = 20; Envigo, Sant Feliu de Codines, Barcelona, Spain, RRID: MGI:2160863) were used to perform cognitive and molecular studies. The mice were randomly allocated into two groups: SAMP8 control (n = 10), and SAMP8 treated with UNC0642 G9a inhibitor (SAMP8 UNC0642 (5 mg/kg); n = 10). The sample size for the intervention was chosen following previous studies (Bellver-Sanchis et al., 2023) in our laboratory and using one interactive tool (http://www.biomath.info/power/index.html). Experimental groups received a daily dose of either vehicle (2% w/v, (2-hydroxypropyl)-β-cyclodextrin) or a dose of 5 mg/kg per day of UNC0642 (BLDpharm, Shangai, China, #BD630326) dissolved in 2% 2-hydroxypropyl-β-cyclodextrin (Atomole Scientific Co. Ltd., Wuhan, Hubei, China, #AT-20762) via oral gavage for 4 weeks (Griñán-Ferré et al., 2019; Bellver-Sanchis et al., 2023). Animals had free access to food and water and were kept under standard temperature conditions (22 ± 2°C) and a 12-hour light-dark cycle (300 lx/0 lx).

All studies and procedures for the mouse behavior tests, brain dissection, and extractions followed the ARRIVE standard ethical guidelines (European Communities Council Directive 2010/63/EU and Guidelines for the Care and Use of Mammals in Neuroscience and Behavioral Research, National Research Council 2003) and were approved by the Institutional Animal Care and Generalitat de Catalunya (#222/18). All efforts were made to minimize the number of mice used and their suffering.

APP/PS1 mice were used as a source of primary cell cultures for *in vitro* experiments. Animals were socially caged (2–4 mice per cage) and maintained on a 12-hour light-dark cycle (lights on at 08:00 and off at 20:00) in a temperature-controlled room (22 ± 2°C). Food and water were available *ad libitum*. The use of these animals for primary culture was approved of under UF IACUC protocol 202011245. The protocol including the collection of fetal tissue was approved 1/19/2021.

Biochemical experiments

Brain processing

An intraperitoneal injection of 10 mg/kg of ketamine (Imalgene 500, Rhone-Merieux) and 1 mg/kg of xylazine (Rompun, Bayer) diluted in NaCl 0.9% was used to euthanize SAMP8 mice 3 days after starting behavioral tests (see results of the behavioral tests in Bellver-Sanchis et al., 2023). Brains were immediately removed from the skull. The cortex and hippocampus were quickly isolated and frozen on powdered dry ice. They were maintained at −80°C for biochemical experiments. All reagents and kits used for the protocols described below are listed in **Additional Table 1**.

miRNA sequencing

Pools of four cortex tissue samples from the SAMP8 control and SAMP8 UNC0642 mice were used. To determine the altered miRNAs after treatment with UNC0642 we used the QIAseqmiRNA platform. TMM normalization and differential expression analysis were carried out using the edgeR program (Wang et al., 2013). The cutoff of differential miRNA was a fold-change threshold of 1.9 and a P-value < 0.05. The miRTarVis tool was used to predict miRNA targets (Jung et al., 2015).

Volcano plot, KEGG, Gene Ontology, and GSEA were used to perform the enrichment and pathway analysis (Subramanian et al., 2005) by using the Enrichr database (http://amp.pharm.mssm.edu/Enrichr; Chen et al., 2013; Kuleshov et al., 2016; Xie et al., 2021), and considering a P-value < 0.05 as statistically significant. Raw data were deposited at the Gene Expression Omnibus for miRNA-seq on mouse hippocampus SAMP8 (accession GSE189248).

miRNA extraction and quantitative reverse transcription-polymerase chain reaction (qRT-PCR)

miRNA was isolated from 100-125 mg of cortex tissue using the mirVana™ miRNA Isolation kit (Applied Biosystems, Foster City, CA, USA, #AM1560) (n = 6 per experimental group). Reverse transcription from RNA to first-strand complementary DNA (cDNA) was obtained using the TaqMan miRNA Reverse Transcription kit (Thermo Fischer Scientific, Waltham, MA, USA, #4366596) following manufacturer indications. Afterwards, amplification was performed from 1.33 µL of cDNA mixed with TaqMan™ Universal PCR Master Mix (Applied Biosystems, Vilnius, Lithuania, #4369016), and 20× RT primer (**Additional Table 2**) using the Step One Plus Detection System (Applied Biosystems, #4376600). Data were analyzed utilizing the ΔΔCt method, where the reference gene for miRNA (*U6 snRNA*) level was used to normalize differences in sample loading and preparation.

RNA extraction and gene expression determination

Total RNA isolation from cortical samples (n = 6 per experimental group) was carried out using TRItidy G™ reagent (PannReac AppliChem, Castellar del Vallès, Barcelona, Spain, #A4051, 0,200) following the manufacturer's instructions. The yield, purity, and quality of the RNA were determined spectrophotometrically with a NanoDrop™ ND-1000 apparatus (Thermo Fisher Scientific, Waltham, MA, USA) and an Agilent 2100B Bioanalyzer (Agilent Technologies, Santa Clara, CA, USA). RNAs with 260/280 ratios and RIN higher than 7.5, respectively, were selected. Reverse transcription-polymerase chain reaction (RT-PCR) was performed using the high-capacity cDNA Reverse Transcription kit (Applied-Biosystems, Vilnius, Lithuania, #4368813). SYBR® Green real-time PCR (Applied-Biosystems, #K0253) was performed to quantify the mRNA expression of a set of genes listed in **Additional Table 3** on a Step One Plus Detection System (Applied-Biosystems, #4376600). Data were analyzed utilizing the comparative cycle threshold (Ct) method (ΔΔCt), where the housekeeping gene level was used to normalize differences in sample loading and preparation. Normalization of expression levels was performed with β-actin for SYBR® Green-based real-time PCR results. Each sample was analyzed in triplicate, and the results represented the n-fold difference of the transcript levels among different groups.

NEURAL REGENERATION RESEARCH
www.nrronline.org

Research Article

Western blotting

Protein extracts were obtained from the hippocampal brain tissue samples taken after behavioral tests (see results of the behavioral tests in (Bellver-Sanchis et al., 2023). Tissues were homogenized in a cold RIPA lysis buffer (Sigma-Aldrich, Saint Louis, MO, USA, #R0278-50ML) supplemented with protease and phosphatase inhibitors, ultrasonicated, and centrifuged (n = 6 mice per group). Firstly, the protein concentration of the supernatants was determined using the Bradford protein assay (Bio-Rad, Hercules, CA, USA, #5000006) while later proteins were separated by SDS-PAGE (12–14%) at 120 V and transferred to PVDF membranes by electroblotting at 200 mA for 120 minutes. Afterward, membranes were blocked in 5% BSA in 0.1% Tween20-TBS (TBS-T) for 1 hour at room temperature (RT), followed by overnight incubation at 4°C with the primary antibodies presented in **Additional Table 4**. By enhancing a chemiluminescence-based detection kit (Millipore, Burlington, MA, USA, #WBKLS0500) and Amersham Imager 680 (GE Healthcare, Chicago, IL, USA), we visualized immunoreactive proteins on digital images. Semi-quantitative analyses were carried out using ImageLab Software (BioRad, Hercules, CA, USA, SCR_014210) and results were expressed in Arbitrary Units (AU), considering the control mice group as 100%. Protein loading was routinely monitored and normalized by immunodetection of glyceraldehyde 3-phosphate dehydrogenase (GAPDH). Antibodies are listed in **Additional Table 4**.

Cell culture

Primary hippocampal neuron cultures were obtained from APP/PS1 mice brains on embryonic day 17. After dissection, the hippocampus was dissociated from the brain and digested with 0.25% trypsin (Gibco, Waltham, MA USA, #25200056). Digestion was stopped by adding DMEM-F12 medium (Gibco, #12400-024) with 10% fetal bovine serum (FBS) (Cytiva, Marlborough, MA, USA, #SH30088.03), after which the tissue was dispersed. The cells were resuspended in DMEM-F12 medium with 10% FBS and plated in poly-D-lysine (Santa Cruz Biotechnology, Dallas, TX, USA, #sc-136156) coated culture dishes at a density 4–5 × 10^5 cells/well. After 3 hours, the medium was replaced with serum-free Neurobasal medium (Gibco, #21103049) supplemented with B27 supplement (Gibco, #17504044), GlutaMAX™ (Gibco, #35050061), and 100× penicillin-streptomycin (P/S) (Gibco, #15140-122). Half of the medium was replaced every 2 days with fresh medium for 14 days allowing differentiation.

Cytotoxicity test

First, the cells were pretreated with a G9a inhibitor or vehicle. After 30 minutes, H_2O_2 was added to some wells at 500 µM. Cell viability was measured 24 hours after both treatments. The cytotoxicity of H_2O_2 was evaluated by the LDH assay (Roche, Indianapolis, IN, USA, #4744926001). Briefly, cell media was collected after each treatment and the collected media was mixed with LDH substrate in a 96-well plate. After incubation for 30 minutes at room temperature, the optical density was measured at 490 nm using a microplate reader (Molecular Devices, Sunnyvale, CA, USA). The measured optical density was then converted after standardization with negative (4% Triton X-100 (Sigma-Aldrich, #9036-19-5; 0% survival) and positive controls (1% Triton X-100; 100% survival).

Data analysis

Data analysis was performed using GraphPad Prism ver.9.2 software (GraphPad Software, San Diego, CA, USA, www.graphpad.com). Data were expressed as the mean ± standard error of the mean (SEM) from at minimum eight samples per group for behavioral tests (see results of the behavioral tests in Bellver-Sanchis et al., 2023) and four samples for molecular techniques. Means were compared with one-way analysis of variance followed by Tukey's *post hoc* analysis. Comparison between groups was also performed by two-tail Student's *t*-test for independent samples. Statistical significance was considered when *P*-values were < 0.05.

Results

G9a inhibition treatment induces changes in the miRNA expression profile

Alterations in miRNAs have been associated with aging and cognitive decline (Cosín-Tomás et al., 2018). Moreover, specific miRNA abnormal levels have been detected in several areas of the AD brain (Wang et al., 2019). Thus, to gain insight into the biology of G9a inhibition treatment, we analyzed the global miRNA expression between SAMP8 control and SAMP8 treated mice with UNC0642 in the whole brain. We identified 44 differentially expressed miRNAs (fold change cutoff of ≥ 1.9, *P*-value < 0.05), of which 27 were up-regulated and 17 were down-regulated in UNC0642 treatment (**Figure 1A**). The top 10 up- and down-regulated miRNAs are shown in **Figure 1B**. Then, we validated the increase in the expression of *mmu-miR-1298-5p* (*P* = 0.0061) and the *mmu-miR-669c-5p* (*P* = 0.0717) and the reduction of the *mmu-miR-677-5p* (*P* = 0.0211) and *mmu-miR-128-3p* (*P* = 0.0213) by qRT-PCR (**Figure 1F–I**). These results suggest that UNC0642 treatment induces an alteration in miRNA expression levels.

To determine co-regulation between miRNAs and mRNAs we used the miRTarVis tool (Jung et al., 2015). To determine alterations in mRNA expression, we used our previously reported RNA sequencing (GSE189249) in SAMP8 control and SAMP8-treated mice with UNC0642. We found several nodes with a high number of miRNAs-associated mRNA molecules in our SAMP8 model (**Figure 1C**). On one hand, the up-regulated miRNAs, *mmu-miR-92b-5p*, *mmu-miR-144-3p*, *mmu-miR-34c-5p*, *mmu-miR-204-3p*, *mmu-miR-539-5p*, *mmu-miR-34c-3p*, *mmu-miR-204-5p*, *mmu-miR-208b-3p*, *mmu-miR-148a-5p*, *mmu-miR-34b-5p*, *mmu-miR-448-3p*, and *mmu-miR-187-5p* are associated with the down-regulation of 145 mRNAs (**Figure 1D** and **Additional Table 5** and **6**). On the other hand, the down-regulated miRNAs, *mmu-miR-34a-3*, *mmu-mir-128-1*, and *mmu-mir-128-2* are associated with the up-regulation of 124 mRNAs (**Figure 1E** and **Additional Table 5** and **6**) according to miRanda algorithm (Betel et al., 2008). Together, these data show that G9a inhibition with UNC0642 treatment causes a transcriptional dysregulation of miRNAs, which could alter biological processes in the SAMP8 model.

Downloaded from http://journals.lww.com/nrronline by BhDMf5ePHKav1zEoum1tQfN4a+kJLhEZgbsIHo4XMi0hCywCX1AWnYQp/IlQrHD3i3D0OdRyi7TvSFl4Cf3VC4/OAVpDDa8K2+Ya6H515kE= on 01/16/2024

Downloaded from http://journals.lww.com/nrronline by BhDMf5ePHKav1zEoum1tQfN4a+kJLhEZgbsIHo4XMi0hCywCX1AWnYQp/IlQrHD3i3D0OdRyi7TvSFl4Cf3VC4/OAVpDDa8K2+Ya6H515kE= on 01/16/2024

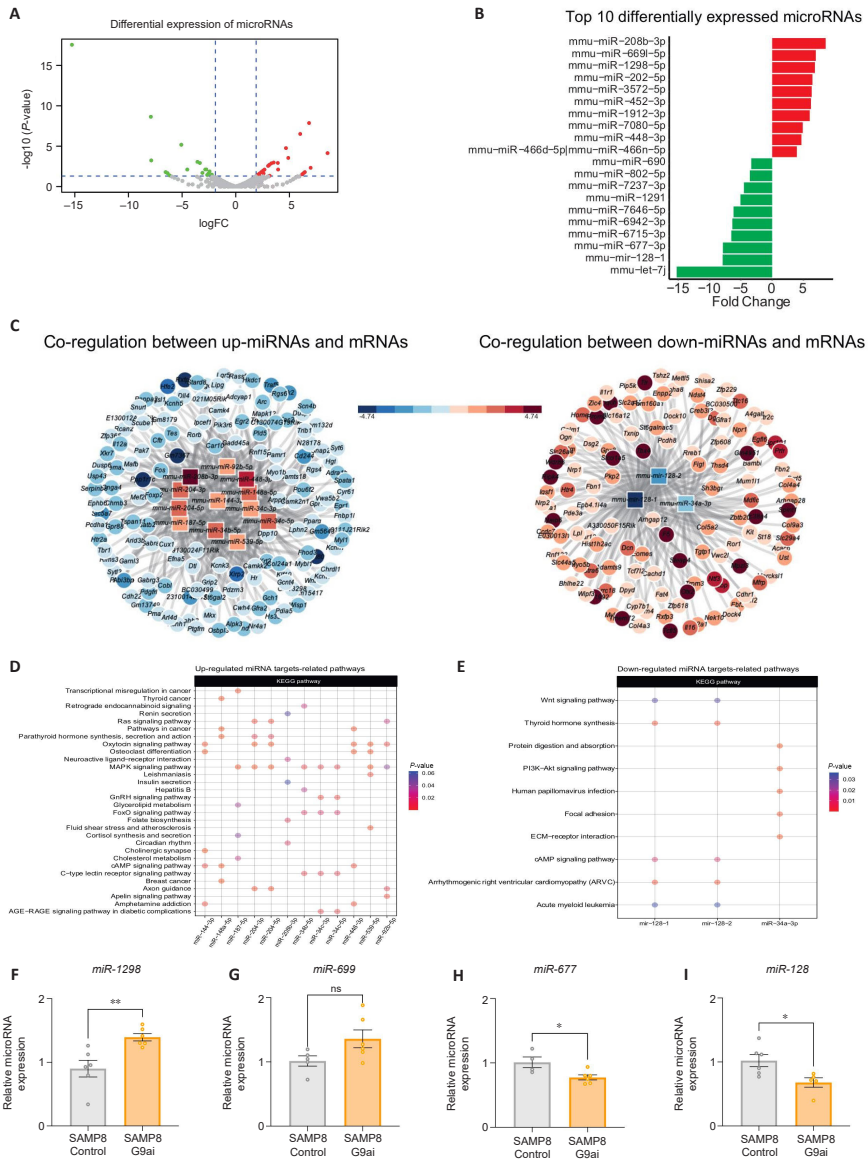

Figure 1 | **G9a inhibition treatment induces changes in the miRNome.**
(A) Volcano plot showing the differentially expressed microRNAs (miRNAs). (B) Top 10 differentially expressed miRNAs; down-regulated in green and up-regulated in red. (C) A representative network between co-regulation of up-miRNAs and down-mRNAs. (D, E) The dot plots show the top KEGG pathways regulated by target mRNAs in SAMP8 UNC0642. A *P*-value < 0.05 was considered statistically significant. (F–I) miRNA expression levels of *miR-1298*, *miR-669*, *miR-677* and *miR-128*. Values are presented as the mean ± SEM (SAMP8 Control $n = 6$, and SAMP8 G9ai (UNC0642, 5 mg/kg) $n = 6$). $^*P < 0.05$, $^{**}P < 0.01$ (Student's *t*-test). ns: Not significant.

Downregulation of *miR-128-3p* after a G9a inhibition partially explains the modulation of oxidative stress responses and autophagy pathway by targeting *Pparg*

To explore the mechanism underlying the neuroprotective effects of G9ai treatment, the potential mRNAs targeted by *miR-128-3p* were examined for being the second most down-regulated miRNA. MiRNAs require complementary binding with 6 consecutive nucleotides in the 3′ UTR of a target mRNA (Agarwal et al., 2015). Based on Target Scan Human 8.0 (Lewis et al., 2005; Grimson et al., 2007; Friedman et al., 2009; Garcia et al., 2011; Agarwal et al., 2015; McGeary et al., 2019) the 3′-untranslated region (3′-UTR) of PPARG mRNA contains a putative 7-nt *miR-128* target sequence (**Figure 2A**). In accordance, higher *Pparg* gene expression levels were statistically significant in the SAMP8 group treated with G9ai ($P = 0.0001$; **Figure 2B**).

Moreover, gene expression of potential PPARγ target genes was evaluated. First, it was observed that the expression of antioxidant genes, such as superoxide dismutase-1 (*Sod1*), heme oxygenase-1 (*Hmox1*), glutathione peroxidase 1 (*Gpx*),

NEURAL REGENERATION RESEARCH
www.nrronline.org

Research Article

and aldehyde oxidase-1 (*Aox1*), was significantly up-regulated after treatment with the G9ai (P = 0.0187, 0.0009, 0.0035, 0.0288, respectively; **Figure 2C**). Accordingly, the gene expression levels of cyclooxygenase-2 (*Cox2*) and aldehyde dehydrogenase-2 (*Aldh2*), both pro-oxidant genes, were significantly downregulated in the treated SAMP8 group (P = 0.0476, 0.0090, respectively; **Figure 2D**). Second, we found an increase in the protein levels of FOXO1a in SAMP8 treated with UNC0642 compared to the SAMP8 control group (**Figure 2F** and **H**). Likewise, we observed a statistically significant increase in the p-AMPK/AMPK ratio in the SAMP8-treated group (P = 0.0370; **Figure 2F** and **G**). We also found increased gene expression of deacetylase sirtuin 1 (*Sirt-1*), which regulates the activity of FOXO transcription factors (P = 0.0493; **Figure 2E**), in treated SAMP8 with UNC0642. Then, we assessed the protein levels of antioxidant enzymes. Catalase-3 (CAT3), GPX, and SOD1 were upregulated in the SAMP8 group treated with G9ai compared with the control group (P = 0.02, 0.0203, respectively; **Figure 2I–L**).

To further confirm the antioxidant effects of the G9a inhibition, we treated primary neuron cell cultures with H_2O_2 as an oxidative insult. In pathological conditions (H_2O_2), we observed a significant increase in cell survival in the group treated with the G9ai *versus* the one treated only with vehicle (P = 0.0003; **Figure 2M**). Then, the antioxidant enzyme glutathione synthetase was upregulated after the pharmacological inhibition of G9a (P = 0.0021; **Figure 2N–O**).

Autophagy can be regulated by the PPARγ/AMPK (Wang et al., 2022). Therefore, we evaluated several autophagy markers. Strikingly, sequestosome-1 (SQSTM1/p62) and Beclin-1 were found upregulated in the SAMP8 treated with the G9ai in comparison with the control (P = 0.0434, 0.0118, respectively; **Figure 3A–C**), suggesting autophagy activation.

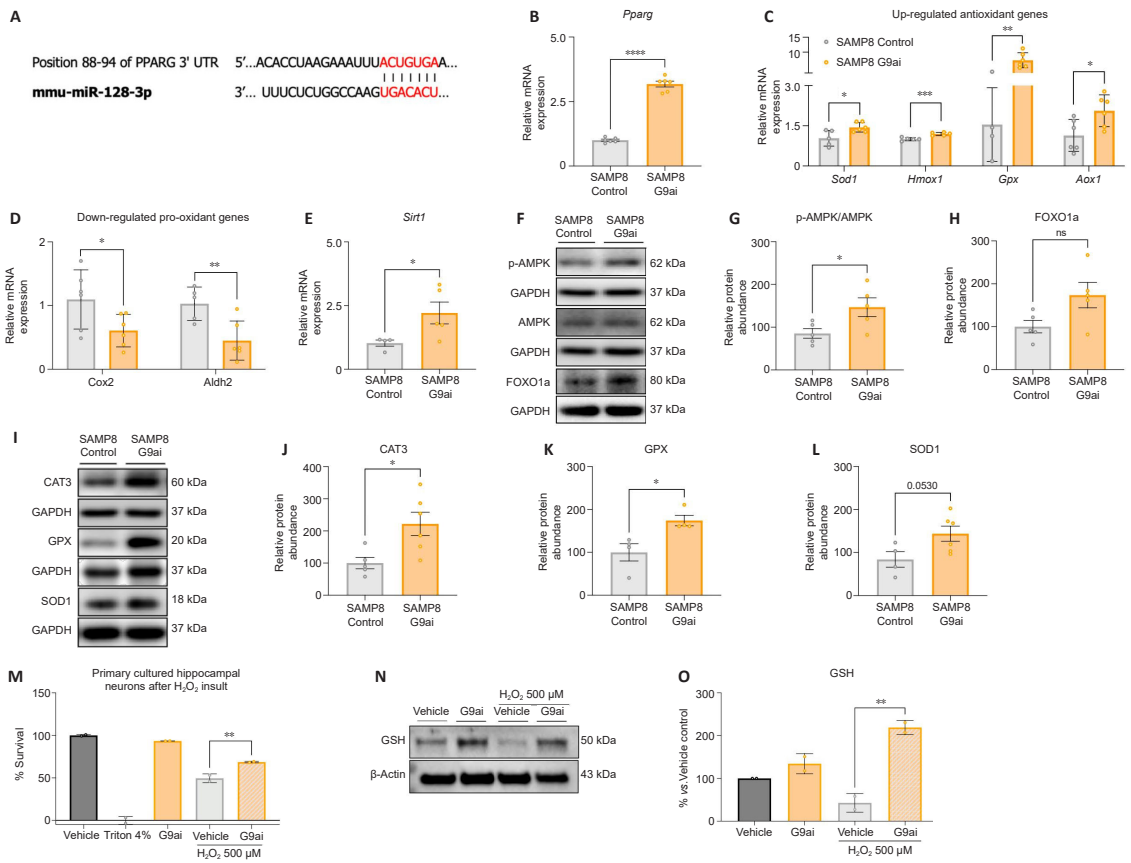

Figure 2 | **Downregulation of *miR-128* after a G9a inhibition partially explains the modulation of treatment modulates oxidative stress responses by targeting peroxisome-proliferator activator receptor γ (Ppary).**

(A) Prediction of *miR-128-3p* and PPARG binding sites based on TargetScan. (B) Gene expression levels of peroxisome-proliferator activator receptor γ (*Pparg*). OS pathway: (C) Representation of the expressions of up-regulated antioxidants genes, such as superoxide dismutase-1 (*Sod1*), heme oxygenase-1 (*Hmox1*), glutathione peroxidase 1 (*Gpx*), and aldehyde oxidase-1 (*Aox1*) (grey: SAMP8 Control; orange: SAMP8 G9ai). (D) Representation of the expressions of down-regulated antioxidants genes, such as cyclooxygenase-2 (*Cox2*) and aldehyde dehydrogenase-2 (*Aldh2*) (grey: SAMP8 Control; orange: SAMP8 G9ai). (E) Gene expression of Sirt1. (F–H) Representative western blot bands and quantification of p-AMPK/AMPK ratio, and FOXO1a protein levels. (I–L) Representative western blot bands and quantification of CAT3, GPX, and SOD1 protein levels. Values presented are the mean ± SEM (SAMP8 Control n = 6, and SAMP8 G9ai (UNC0642, 5 mg/kg) n = 6); Student's t-test; $^*P < 0.05$, $^{**}P < 0.01$). (M) Cell survival after H_2O_2 insult in primary cultured hippocampal neurons. (N, O) Representative western blot bands and quantification of glutathione synthetase (GSH) protein levels. Values are presented as the mean ± SEM (normal conditions: vehicle group n = 2, Triton 4% group n = 2, G9ai 1 μM n = 2; oxidative stress (H_2O_2): vehicle group n = 2, G9ai 1 μM n = 2). $^{**}P < 0.01$ (one-way analysis of variance followed by Tukey's *post hoc* analysis). ns: Not significant; SAMP8: senescence-accelerated mouse-prone 8.

Downloaded from http://journals.lww.com/nrronline by BhDMf5ePHKav1zEoum1tQfN4a+kJLhEZgbsIHo4XMi0hCywCX1AWnYQp/IlQrHD3i3D0OdRyi7TvSFl4Cf3VC4/OAVpDDa8K2+Ya6H515kE= on 01/16/2024

NEURAL REGENERATION RESEARCH
www.nrronline.org

Downloaded from http://journals.lww.com/nrronline by BhDMf5ePHKav1zEoum1tQfN4a+kJLhEZgbsIHo4XMi0hCywCX1AWnYQp/IlQrHD3i3D0OdRyi7TvSFl4Cf3VC4/OAVpDDa8K2+Ya6H515kE= on 01/16/2024

Upregulation of PPARγ by G9ai enhances the expression of genes involved in DNA damage response and apoptosis

The growth arrest and DNA damage 45 alpha (GADD45α) plays an important role in DNA repair (Smith et al., 2000), cell cycle (Vairapandi et al., 2002), apoptosis (Tront et al., 2006), angiogenesis, senescence (Tront et al., 2006), and DNA demethylation (Lee et al., 2012) by recruiting demethylation proteins to CpG island promoters (Arab et al., 2019). Consistent with this, we observed an increase in both *Gadd45a* gene expression and protein levels of GADD45α after the pharmacological inhibition of G9a in SAMP8 mice (P = 0.0119, 0.0408, respectively; **Figure 3D–F** and **Additional Table 6**). As we mentioned before, GADD45α plays an important role in apoptosis (Hildesheim et al., 2002; Tront et al., 2006; Salvador et al., 2013; Kleinsimon et al., 2018). Accordingly, three well-established apoptotic markers, B-cell lymphoma 2 (BCL-2), Bcl-2 Associated X-protein (BAX), and Caspase-3 (CASP3), were significantly upregulated in the treated SAMP8 group compared to the control group (P = 0.042, 0.0223, 0.0964, respectively; **Figure 3G–J**).

PPARγ/GADD45α contributes to the enhancement of synaptic plasticity and neurogenesis after G9a inhibition

Lack of *Gadd45a* promotes alterations in hippocampal memory and long-term potentiation, a phenotype accompanied by reduced levels of memory-related mRNA (Aparisi Rey et al., 2019). Then, we evaluated gene expression levels of immediate early genes (IEGs) after G9ai pharmacological treatment in SAMP8 mice, since they have a relevant role in the regulation of neuronal activity, synaptic plasticity, and neurogenesis (Minatohara et al., 2016; Duclot and Kabbaj, 2017; Kim et al., 2018; Mahringer et al., 2019; Meenakshi et al., 2021). Early growth response 1 (*Egr1*), activity regulated cytoskeleton associated protein (*Arc*), and *Dnmt3a* gene expression levels were found significantly increased in the treated SAMP8 group in comparison with the control SAMP8 group (P = 0.0231, 0.0013, 0.0428, respectively; **Figure 4A**). However, no statistical differences were observed in *Egr2* gene expression levels (P = 0.4063; **Figure 4A**). Synaptic plasticity-related gene expression, such as VGF nerve growth factor inducible (*Vgf*) and transforming growth factor (*Tgf*) were found upregulated after G9ai pharmacological treatment in SAMP8, although the increase was only statistically significant for *Vgf* (P = 0.0007; **Figure 4B**). Likewise, the gene expression of the neurotrophin receptors, *TrkA* and *TrkB*, were upregulated in the SAMP8 treated group (P = 0.001, 0.0337, respectively; **Figure 4B**). Then, we quantified the levels of well-established synaptic plasticity proteins. In the case of postsynaptic density protein 95 (PSD95), we observed significantly increased levels in the SAMP8 mice treated with a G9ai compared to the control group (P = 0.0407; **Figure 4C** and **D**). In contrast, in the case of PSD93 and synapsin IIa (SYN IIa), a positive tendency was observed after pharmacological treatment (**Figure 4C**, **E**, and **F**). In terms of neurogenesis markers, doublecortin (*Dcx*) gene expression levels were increased in the SAMP8-treated group compared to the control groups (P = 0.0001); however, no differences were observed in SRY-Box transcription factor 2 (*Sox2*) gene expression levels between both experimental groups (**Figure 4G** and **H**). Finally, protein levels of neuronal nuclei (NeuN) were increased in the SAMP8 treated with G9ai *versus* the Control SAMP8 group (P = 0.0165; **Figure 4I** and **J**).

Discussion

In this study, we have identified and explored an unknown molecular pathway based on PPARγ/GADD45α transcriptional repression controlled by G9a which also modulates miRNAs. Several studies suggest that G9a is a contributing factor to neuroinflammation and is upregulated in AD patients (Zheng et al., 2019; Bellver-Sanchis et al., 2023). In addition, a recent study stated that G9a is necessary to produce pro-inflammatory cytokines and reactive oxygen species, which are associated with OS (Mourits et al., 2021). It has been

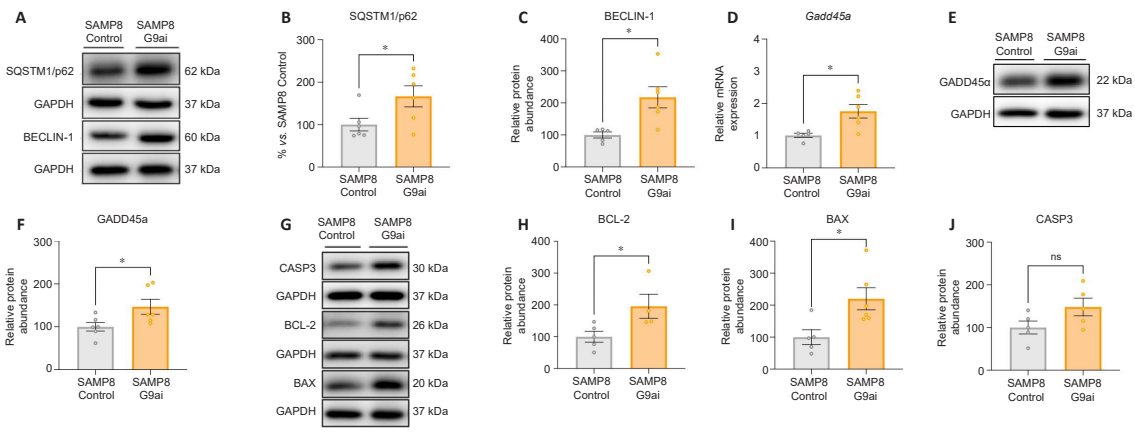

Figure 3 | **Upregulation of peroxisome-proliferator activator receptor γ (PPARγ) by G9ai enhances the expression of genes involved in DNA damage responses, apoptosis, and autophagy.**

Autophagy pathway: (A–C) Representative western blot bands and quantification of sequestosome-1 (SQSTM1/p62) and BECLIN-1. (D) Gene expression levels of growth arrest and DNA damage 45 alpha (*Gadd45a*). (E, F) Representative western blot bands and quantification of GADD45α. Apoptosis pathway: (G–J) Representative western blot bands and quantification of B-cell lymphoma 2 (BCL-2), Bcl-2 Associated X-protein (BAX), and Caspase-3 (CASP3). Values are presented as the mean ± SEM (SAMP8 Control n = 6, and SAMP8 G9ai (UNC0642, 5 mg/kg) n = 6). *P < 0.05 (Student's t-test). ns: Not significant; SAMP8: senescence-accelerated mouse-prone 8.

NEURAL REGENERATION RESEARCH
www.nrronline.org

Research Article

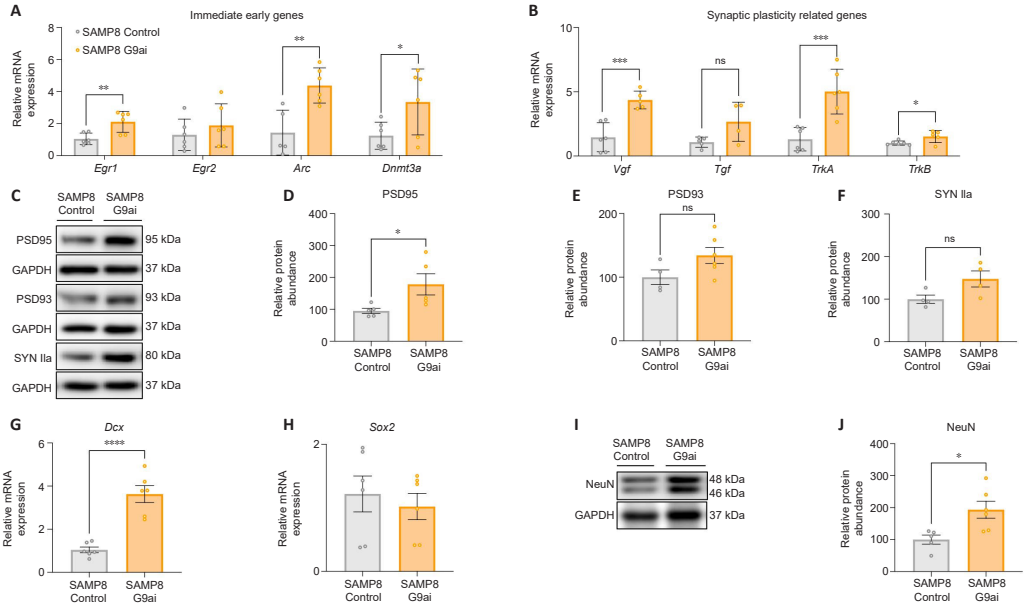

Figure 4 | **PPARγ/GADD45α might contribute to the enhancement of synaptic plasticity and neurogenesis after G9a inhibition.**
(A) Expression of immediate early genes, *Egr1*, *Egr2*, *Arc*, and DNA methyltransferase (*Dnmt3a*) (grey: SAMP8 Control; Orange: SAMP8 G9ai). (B) Expression of synaptic plasticity-related genes, such as *Vgf*, *Tgf*, *TrkA*, and TrkB (grey: SAMP8 control; orange: SAMP8 G9ai). (C–F) Synaptic plasticity pathway: representative western blot bands and quantification of PSD95, PSD93, and SYN IIa protein levels. (G, H) Gene expression of *Dcx* and *Sox2*. (I, J) Representative western blot bands and quantification of NeuN protein levels. Values are presented as the mean ± SEM (SAMP8 control $n = 6$, and SAMP8 G9ai (UNC0642, 5 mg/kg) $n = 6$). $^*P < 0.05$, $^{**}P < 0.01$, $^{***}P < 0.001$ (Student's *t*-test). Arc: Activity regulated cytoskeleton associated protein; Dcx: doublecortin; Dnmt3a: DNA methyltransferase; Egr: early growth response 1; G9ai: G9a inhibitor; GADD45α: growth arrest and DNA damage 45 alpha; NeuN: neuronal nuclei; PPARγ: peroxisome-proliferator activator receptor gamma; SAMP8: senescence-accelerated mouse-prone 8; Tgf: transforming growth factor; Vgf: VGF nerve growth factor inducible; Sox2: SRY-Box transcription factor 2.

suggested that G9a is also necessary for the maintenance of epigenetic marks since it can promote or repress gene expression, and thereby affects the expression of several miRNAs (Shankar et al., 2013). Thus, there is evidence of the crosstalk between G9a, miRNAs, OS, and neuroinflammation and its contribution to the pathogenesis of AD.

Specific miRNAs participate in the initiation and progression of neurodegenerative diseases, including AD (Kumar and Reddy, 2020). Indeed, several miRNAs play a role in the control of key components of neuronal functions such as learning and memory formation (Saab and Mansuy, 2014). Furthermore, as aforementioned, miRNAs regulate gene expression at the post-transcriptional level (Gurtan and Sharp, 2013). At first, by overlaying transcriptomic analyses, we identified several miRNAs (*miR-1298*, *miR-669*, *miR-677*, and *miR-128*) that were modified. The KEGG enrichment analysis revealed the association of G9a with cholinergic synapse, axon guidance, and cAMP signaling pathway, among others. But what is more noteworthy is that KEGG enrichment analysis showed that G9ai treatment modulates the MAPK and FOXO signaling pathways, which is further confirmed throughout the work. An example of one of the modulated miRNAs was *miR-1298*, which is downregulated in different pathological conditions and is associated with hypermethylation of its upstream DNA CpG sites (Hu et al., 2015). Accordingly, our results showed a downregulation of *miR-1298* in SAMP8 mice, which was reverted after G9ai, indicating a reduction in DNA methylation levels, allowing the upregulation of this miRNA and thus, modifying the gene transcription of different important neuroprotective genes. We also found an upregulation in *miR-669* after G9a inhibition with UNC0642 in SAMP8 mice. These results are in agreement with recent work from Kolosowska et al. (2020), which showed that the upregulation of *miR-669c-3p* promotes neuroprotective effects in a mouse model of ischemic stroke through induction of the expression of anti-inflammatory microglial markers and PPARγ. The latter is the one we have focused on in this study. Moreover, we found downregulation in *miR-677* and *miR-128* after G9a inhibition. *miR-677* has a role in protein synthesis directly associated with neurodegenerative disease, including AD, such as protein related to neuroactive ligand-receptor, autophagy, and Wnt signaling pathway as we found in SAMP8 after G9ai. Last but not least, *miR-128* is involved in the development of the nervous system as well as the regulation of neuronal plasticity, neuronal death, and cognitive impairment (Hu et al., 2015; Kolosowska et al., 2020). Importantly, recently published research has shown that *miR-128* is increased in the hippocampus of AD human brains (Siedlecki-Wullich et al., 2021). More importantly, *miR-128* downregulation improved cognitive deficits and reduced A pathology in 3×Tg-AD mice (Liu et al., 2019). Furthermore, this improvement in cognition was associated with increased levels of PPARγ. PPARγ is targeted by *miR-128* (Liu et al., 2019). In our case, we found reduced levels of *miR-128* in SAMP8-treated mice with UNC0642, which were correlated with better cognitive performance, as we demonstrated in our previously published manuscript (Bellver-Sanchis et al., 2023), suggesting the regulation of *miR-128* by G9a.

Downloaded from http://journals.lww.com/nrronline by BhDMf5ePHKav1zEoum1tQfN4a+kJLhEZgbsIHo4XMi0hCywCX1AWnYQp/IlQrHD3i3D0OdRyi7TvSFl4Cf3VC4/OAVpDDa8K2+Ya6H515kE= on 01/16/2024

Downloaded from http://journals.lww.com/nrronline by BhDMf5ePHKav1zEoum1tQfN4a+kJLhEZgbsIHo4XMi0hCywCX1AWnYQp/IlQrHD3i3D0OdRyi7TvSFl4Cf3VC4/OAVpDDa8K2+Ya6H515kE= on 01/16/2024

PPARγ is an essential nuclear receptor involved in energy homeostasis and inflammation, which promotes growth interconnection of various pathways, such as the nuclear factor erythroid 2 related factor 2 (NRF2), Wnt/β-catenin, and FOXO (Polvani et al., 2012). Also, several studies have shown that PPARγ is implicated in the OS response, which involves an imbalance between pro-oxidation and anti-oxidation forces that may lead to cell death (Polvani et al., 2012; Vallée and Lecarpentier, 2018; Beheshti et al., 2022). In this regard, we evaluated gene expression related to this molecular pathway. On one hand, the expression of the antioxidant genes evaluated in this work was increased after treatment with G9ai, both for *in vitro* and *in vivo* studies. In the same way, the expression of the pro-oxidant markers was downregulated in the treated SAMP8 mice. It has been observed that PPARγ agonists protected cells from oxidative stress after ischemia by suppressing COX2 expression in a PPARγ-dependent manner (Zhao et al., 2006). On the other hand, one of the more important upregulated signaling pathways in SAMP8-treated mice was FOXO. In accordance with our results, it has been reported that G9a protein levels were elevated and FOXO1 protein levels were decreased in human colon cancer patients (Chae et al., 2019). Hence, to our knowledge, herein we described for the first time the upregulation of the FOXO signaling pathway in the SAMP8 brain after treatment with UNC0642. Interestingly, in the FOXO1-dependent mechanism, AMPK controls the expression of antioxidant enzymes, and therefore this enzyme may have an important role in the maintenance of redox homeostasis (Yun et al., 2014). Accordingly, the increased expression of some of the OS markers evaluated in this work, such as CAT3 or SOD1 (Ding et al., 2007; Yu et al., 2008), is directly related to all PPAR isoforms (Muzio et al., 2021). For example, increased PPARγ has been shown to correlate with increased levels of glutathione synthetase (Ferguson et al., 2009), and HMOX1 (Krönke et al., 2007; Bilban et al., 2009; Ferguson et al., 2009; Polvani et al., 2012). Altogether, these data suggest the activation of molecular pathways that can revert the neuronal damage presented in AD.

In the same manner, the PPARγ/AMPK axis also regulates autophagy (Wang et al., 2022). It is well-known that G9a represses the expression of genes involved in the autophagic process (Artal-Martinez de Narvajas et al., 2013), and its inhibition promotes the activation of the autophagic pathway (Griñán-Ferré et al., 2019). According to this, here we found an induction of autophagy markers (BECLIN-1, SQSTM1/p62, among others) that are associated with the completion of the beneficial effects of the autophagic process after pharmacological inhibition of G9a in SAMP8-treated animals.

PPARγ is found to be correlated with GADD45α protein (Fujiki et al., 2009). GADD45α protein interacts with PPARγ, recruiting demethylation proteins to CpG island promoters, and consequently upregulating its transcriptional activity (Arab et al., 2019), and consequently upregulating transcriptional activity of PPARγ (Fujiki et al., 2009). Indeed, it has been described that *Gadd45* is widely expressed in the mouse brain, including the cerebral cortex and hippocampus, both fundamental regions for memory formation (Matsunaga et al., 2015; Aparisi Rey et al., 2019). Recently, it was shown that *Gadd45a*-deficient mice displayed alterations in hippocampal memory and long-term potentiation, associated with reduced mRNA levels of genes related to memory (Leach et al., 2012). Thus, we evaluated the gene expression levels of IEGs after the pharmacological treatment of SAMP8 mice and found changes in *Egr1* and *Dnmt3a* gene expression, suggesting the improvement in cognition previously demonstrated (Vasilopoulou et al., 2022). Furthermore, these results were accompanied by increased gene expression of neurotrophin receptors, *TrkA* and *TrkB*. Then, we proceed to evaluate the levels of well-established synaptic plasticity proteins. In the case of the protein levels of PSD95, PSD93, and SYN IIa, as well as neurogenesis markers, *Dcx* gene expression levels as well as protein levels of NeuN were increased in the SAMP8 treated with G9ai versus the Control SAMP8 group. Those results were consistent with previous published results by us and others, that showed that elevated H3K9me2 and G9a levels are present in the hippocampus of several AD mice models, promoting diminished synaptic transmission, and learning and memory deficits (Griñán-Ferré et al., 2019; Zheng et al., 2019). Those processes were ameliorated by G9a inhibition with UNC0642 or BIX01294 treatment, pointing to the participation in synaptic dysfunction and cognitive decline of G9a. However, the exact mechanisms by which G9a inhibition promotes miRNA changes remain unclear and require further studies.

The main limitation of this study could be to describe in depth the direct modulation of *miR-128*/*Pparg* by pharmacological inhibition of G9a. Further studies with gene editing or also using a pharmacological approach would be helpful to confirm this. These experiments could provide more robustness to our results, confirming the direct link between G9a and *miR-128*/*Pparg*. However, it has been noted that all the evidence already cited throughout the manuscript agrees with our findings, as well as we report the changes in the miRNome profile after pharmacological treatment of G9a in a well-established AD mice model, the SAMP8.

In conclusion, this study demonstrates that G9a inhibition with UNC0642 improves the gene expression profile of mRNAs and miRNAs in the SAMP8 mouse model. The differentially expressed miRNAs after UNC0642 treatment promote the activation of the PPARγ/GADD45α axis, leading to changes in crucial molecular pathways associated with age-related cognitive decline. Therefore, these results suggest that G9a and miRNAs are promising diagnostic biomarkers and therapeutic targets for neurodegenerative diseases such as AD.

Author contributions: *CGF conceived the study. ABS, CGF, PAAL, IT, MRV, and DVG performed the experiments. ABS, CGF, AG, PAAL, IT, and CP designed the experiments and analyzed the data. ABS, DB, LL, GC, AG, MP, and CGF wrote the manuscript. All authors read and approved the final manuscript.*
Conflicts of interest: *None of the authors has any disclosures to declare.*
Data availability statement: *No additional data are available.*
Open access statement: *This is an open access journal, and articles are distributed under the terms of the Creative Commons AttributionNonCommercial-ShareAlike 4.0 License, which allows others to remix, tweak, and build upon the work non-commercially, as long as appropriate credit is given and the new creations are licensed under the identical terms.*

NEURAL REGENERATION RESEARCH
www.nrronline.org

Research Article

Additional files:

Additional Table 1: *Reagents and kits used in this study.*
Additional Table 2: *TaqMan probes used in this study.*
Additional Table 3: *SYBR Green primers analyzed in this study.*
Additional Table 4: *Antibodies used in western blot assay in this study.*
Additional Table 5: *Differentially expressed miRNAs.*
Additional Table 6: *miRNAs targets.*

References

Agarwal V, Bell GW, Nam JW, Bartel DP (2015) Predicting effective microRNA target sites in mammalian mRNAs. Elife 4:e05005.

Aparisi Rey A, Karaulanov E, Sharopov S, Arab K, Schäfer A, Gierl M, Guggenhuber S, Brandes C, Pennella L, Gruhn WH, Jelinek R, Maul C, Conrad A, Kilb W, Luhmann HJ, Niehrs C, Lutz B (2019) Gadd45α modulates aversive learning through post-transcriptional regulation of memory-related mRNAs. EMBO Rep 20:e46022.

Arab K, Karaulanov E, Musheev M, Trnka P, Schäfer A, Grummt I, Niehrs C(2019) GADD45A binds R-loops and recruits TET1 to CpG island promoters. Nat Genet 51:217-223.

Artal-Martinez de Narvajas A, Gomez TS, Zhang JS, Mann AO, Taoda Y, Gorman JA, Herreros-Villanueva M, Gress TM, Ellenrieder V, Bujanda L, Kim DH, Kozikowski AP, Koenig A, Billadeau DD (2013) Epigenetic regulation of autophagy by the methyltransferase G9a. Mol Cell Biol 33:3983-3993.

Beheshti F, Gholami M, Ghane Z, Nazari SE, Salari M, Shabab S, Hosseini M (2022) PPARγ activation improved learning and memory and attenuated oxidative stress in the hippocampus and cortex of aged rats. Physiol Rep 10:e15538.

Bellver-Sanchis A, Geng Q, Navarro G, Ávila-López PA, Companys-Alemany J, Marsal-García L, Larramona-Arcas R, Miró L, Perez-Bosque A, Ortuño-Sahagún D, Banerjee DR, Choudhary BS, Soriano FX, Poulard C, Pallàs M, Du HN, Griñán-Ferré C (2023) G9a inhibition promotes neuroprotection through GMFB regulation in Alzheimer's disease. Aging Dis doi: 10.14336/AD.2023.0424-2

Betel D, Wilson M, Gabow A, Marks DS, Sander C (2008) The microRNA.org resource: targets and expression. Nucleic Acids Res 36:D149-153.

Bilban M, Haslinger P, Prast J, Klinglmüller F, Woelfel T, Haider S, Sachs A, Otterbein LE, Desoye G, Hiden U, Wagner O, Knöfler M (2009) Identification of novel trophoblast invasion-related genes: heme oxygenase-1 controls motility via peroxisome proliferator-activated receptor gamma. Endocrinology 150:1000-1013.

Butterfield DA, Poon HF (2005) The senescence-accelerated prone mouse (SAMP8): a model of age-related cognitive decline with relevance to alterations of the gene expression and protein abnormalities in Alzheimer's disease. Exp Gerontol 40:774-783.

Chae YC, Kim JY, Park JW, Kim KB, Oh H, Lee KH, Seo SB (2019) FOXO1 degradation via G9a-mediated methylation promotes cell proliferation in colon cancer. Nucleic Acids Res 47:1692-1705.

Chen EY, Tan CM, Kou Y, Duan Q, Wang Z, Meirelles GV, Clark NR, Ma'ayan A (2013) Enrichr: interactive and collaborative HTML5 gene list enrichment analysis tool. BMC Bioinformatics 14:128.

Cho YW, Hong S, Jin Q, Wang L, Lee JE, Gavrilova O, Ge K (2009) Histone methylation regulator PTIP is required for PPARgamma and C/EBPalpha expression and adipogenesis. Cell Metab 10:27-39.

Cosín-Tomás M, Álvarez-López MJ, Companys-Alemany J, Kaliman P, González-Castillo C, Ortuño-Sahagún D, Pallàs M, Griñán-Ferré C (2018) Temporal integrative analysis of mRNA and microRNAs expression profiles and epigenetic alterations in female SAMP8, a model of age-related cognitive decline. Front Genet 9:596.

Ding G, Fu M, Qin Q, Lewis W, Kim HW, Fukai T, Bacanamwo M, Chen YE, Schneider MD, Mangelsdorf DJ, Evans RM, Yang Q (2007) Cardiac peroxisome proliferator-activated receptor gamma is essential in protecting cardiomyocytes from oxidative damage. Cardiovasc Res 76:269-279.

Duclot F, Kabbaj M (2017) The role of early growth response 1 (EGR1) in brain plasticity and neuropsychiatric disorders. Front Behav Neurosci 11:35.

Eid A, Mhatre I, Richardson JR (2019) Gene-environment interactions in Alzheimer's disease: A potential path to precision medicine. Pharmacol Ther 199:173-187.

Ferguson HE, Thatcher TH, Olsen KC, Garcia-Bates TM, Baglole CJ, Kottmann RM, Strong ER, Phipps RP, Sime PJ (2009) Peroxisome proliferator-activated receptor-gamma ligands induce heme oxygenase-1 in lung fibroblasts by a PPARgamma-independent, glutathione-dependent mechanism. Am J Physiol Lung Cell Mol Physiol 297:L912-919.

Friedman RC, Farh KK, Burge CB, Bartel DP (2009) Most mammalian mRNAs are conserved targets of microRNAs. Genome Res 19:92-105.

Fujiki K, Kano F, Shiota K, Murata M (2009) Expression of the peroxisome proliferator activated receptor gamma gene is repressed by DNA methylation in visceral adipose tissue of mouse models of diabetes. BMC Biol 7:38.

Garcia DM, Baek D, Shin C, Bell GW, Grimson A, Bartel DP (2011) Weak seed-pairing stability and high target-site abundance decrease the proficiency of lsy-6 and other microRNAs. Nat Struct Mol Biol 18:1139-1146.

Ge C, Cawthorn WP, Li Y, Zhao G, Macdougald OA, Franceschi RT (2016) Reciprocal control of osteogenic and adipogenic differentiation by ERK/MAP kinase phosphorylation of Runx2 and PPARγ transcription factors. J Cell Physiol 231:587-596.

Grimson A, Farh KK, Johnston WK, Garrett-Engele P, Lim LP, Bartel DP (2007) MicroRNA targeting specificity in mammals: determinants beyond seed pairing. Mol Cell 27:91-105.

Griñán-Ferré C, Corpas R, Puigoriol-Illamola D, Palomera-Ávalos V, Sanfeliu C, Pallàs M (2018) Understanding epigenetics in the neurodegeneration of Alzheimer's disease: SAMP8 mouse model. J Alzheimers Dis 62:943-963.

Griñán-Ferré C, Marsal-García L, Bellver-Sanchis A, Kondengaden SM, Turga RC, Vázquez S, Pallàs M (2019) Pharmacological inhibition of G9a/GLP restores cognition and reduces oxidative stress, neuroinflammation and β-Amyloid plaques in an early-onset Alzheimer's disease mouse model. Aging (Albany NY) 11:11591-11608.

Gupta-Agarwal S, Franklin AV, Deramus T, Wheelock M, Davis RL, McMahon LL, Lubin FD (2012) G9a/GLP histone lysine dimethyltransferase complex activity in the hippocampus and the entorhinal cortex is required for gene activation and silencing during memory consolidation. J Neurosci 32:5440-5453.

Gurtan AM, Sharp PA (2013) The role of miRNAs in regulating gene expression networks. J Mol Biol 425:3582-3600.

Ha M, Kim VN (2014) Regulation of microRNA biogenesis. Nat Rev Mol Cell Biol 15:509-524.

Harman MF, Martín MG (2020) Epigenetic mechanisms related to cognitive decline during aging. J Neurosci Res 98:234-246.

Hildesheim J, Bulavin DV, Anver MR, Alvord WG, Hollander MC, Vardanian L, Fornace AJ Jr (2002) Gadd45a protects against UV irradiation-induced skin tumors, and promotes apoptosis and stress signaling via MAPK and p53. Cancer Res 62:7305-7315.

Houseknecht KL, Cole BM, Steele PJ (2002) Peroxisome proliferator-activated receptor gamma (PPARgamma) and its ligands: a review. Domest Anim Endocrinol 22:1-23.

Hu W, Wang M, Yin H, Yao C, He Q, Yin L, Zhang C, Li W, Chang G, Wang S (2015) MicroRNA-1298 is regulated by DNA methylation and affects vascular smooth muscle cell function by targeting connexin 43. Cardiovasc Res 107:534-545.

Ionescu-Tucker A, Cotman CW (2021) Emerging roles of oxidative stress in brain aging and Alzheimer's disease. Neurobiol Aging 107:86-95.

Jung D, Kim B, Freishtat RJ, Giri M, Hoffman E, Seo J (2015) miRTarVis: an interactive visual analysis tool for microRNA-mRNA expression profile data. BMC Proc 9:S2

Kapadia R, Yi JH, Vemuganti R (2008) Mechanisms of anti-inflammatory and neuroprotective actions of PPAR-gamma agonists. Front Biosci 13:1813-1826.

Kim S, Kim H, Um JW (2018) Synapse development organized by neuronal activity-regulated immediate-early genes. Exp Mol Med 50:1-7.

Kleinsimon S, Longmuss E, Rolff J, Jäger S, Eggert A, Delebinski C, Seifert G (2018) GADD45A and CDKN1A are involved in apoptosis and cell cycle modulatory effects of viscumTT with further inactivation of the STAT3 pathway. Sci Rep 8:5750.

Kolosowska N, Gotkiewicz M, Dhungana H, Giudice L, Giugno R, Box D, Huuskonen MT, Korhonen P, Scoyni F, Kanninen KM, Ylä-Herttuala S, Turunen TA, Turunen MP, Koistinaho J, Malm T (2020) Intracerebral overexpression of miR-669c is protective in mouse ischemic stroke model by targeting MyD88 and inducing alternative microglial/macrophage activation. J Neuroinflammation 17:194.

Konovalova J, Gerasymchuk D, Parkkinen I, Chmielarz P, Domanskyi A (2019) Interplay between MicroRNAs and Oxidative Stress in Neurodegenerative Diseases. Int J Mol Sci 20:6055.

Krönke G, Kadl A, Ikonomu E, Blüml S, Fürnkranz A, Sarembock IJ, Bochkov VN, Exner M, Binder BR, Leitinger N (2007) Expression of heme oxygenase-1 in human vascular cells is regulated by peroxisome proliferator-activated receptors. Arterioscler Thromb Vasc Biol 27:1276-1282.

Kuleshov MV, Jones MR, Rouillard AD, Fernandez NF, Duan Q, Wang Z, Koplev S, Jenkins SL, Jagodnik KM, Lachmann A, McDermott MG, Monteiro CD, Gundersen GW, Ma'ayan A (2016) Enrichr: a comprehensive gene set enrichment analysis web server 2016 update. Nucleic Acids Re 44:W90- W97.

Downloaded from http://journals.lww.com/nrronline by BhDMf5ePHKav1zEoum1tQfN4a+kJLhEZgbsIHo4XMi0hCywCX1AWnYQp/IlQrHD3i3D0OdRyi7TvSFl4Cf3VC4/OAVpDDa8K2+Ya6H515kE= on 01/16/2024

Downloaded from http://journals.lww.com/nrronline by BhDMf5ePHKav1zEoum1tQfN4a+kJLhEZgbsIHo4XMi0hCywCX1AWnYQp/IlQrHD3i3D0OdRyi7TvSFl4Cf3VC4/OAVpDDa8K2+Ya6H515kE= on 01/16/2024

Kumar S, Reddy PH (2020) The role of synaptic microRNAs in Alzheimer's disease. Biochim Biophys Acta Mol Basis Dis 1866:165937.

Leach PT, Poplawski SG, Kenney JW, Hoffman B, Liebermann DA, Abel T, Gould TJ (2012) Gadd45b knockout mice exhibit selective deficits in hippocampus-dependent long-term memory. Learn Mem 19:319-324.

Lee B, Morano A, Porcellini A, Muller MT (2012) GADD45α inhibition of DNMT1 dependent DNA methylation during homology directed DNA repair. Nucleic Acids Res 40:2481-2493.

Leng F, Edison P (2021) Neuroinflammation and microglial activation in Alzheimer disease: where do we go from here? Nat Rev Neurol 17:157-172.

Lewis BP, Burge CB, Bartel DP (2005) Conserved seed pairing, often flanked by adenosines, indicates that thousands of human genes are microRNA targets. Cell 120:15-20.

Liang Y, Wang L (2021) Inflamma-microRNAs in Alzheimer's disease: from disease pathogenesis to therapeutic potentials. Front Cell Neurosci 15:785433.

Liu B, Liu J, Shi JS (2020) SAMP8 mice as a model of age-related cognition decline with underlying mechanisms in Alzheimer's disease. J Alzheimers Dis 75:385-395.

Liu J, Wang H, Zuo Y, Farmer SR (2006) Functional interaction between peroxisome proliferator-activated receptor gamma and beta-catenin. Mol Cell Biol 26:5827-5837.

Liu Y, Zhang Y, Liu P, Bai H, Li X, Xiao J, Yuan Q, Geng S, Yin H, Zhang H, Wang Z, Li J, Wang S, Wang Y (2019) MicroRNA-128 knockout inhibits the development of Alzheimer's disease by targeting PPARγ in mouse models. Eur J Pharmacol 843:134-144.

Mahringer D, Petersen AV, Fiser A, Okuno H, Bito H, Perrier JF, Keller GB (2019) Expression of c-Fos and Arc in hippocampal region CA1 marks neurons that exhibit learning-related activity changes. BioRxiv doi: https://doi.org/10.1101/644526.

Matsunaga E, Nambu S, Oka M, Iriki A (2015) Comparative analysis of developmentally regulated expressions of Gadd45a, Gadd45b, and Gadd45g in the mouse and marmoset cerebral cortex. Neuroscience 284:566-580.

McGeary SE, Lin KS, Shi CY, Pham TM, Bisaria N, Kelley GM, Bartel DP (2019) The biochemical basis of microRNA targeting efficacy. Science 366:eaav1741.

Meenakshi P, Kumar S, Balaji J (2021) In vivo imaging of immediate early gene expression dynamics segregates neuronal ensemble of memories of dual events. Mol Brain 14:102.

Minatohara K, Akiyoshi M, Okuno H (2016) Role of immediate-early genes in synaptic plasticity and neuronal ensembles underlying the memory trace. Front Mol Neurosci 8:78.

Mourits VP, van Puffelen JH, Novakovic B, Bruno M, Ferreira AV, Arts RJ, Groh L, Crișan TO, Zwaag J, Jentho E, Kox M, Pickkers P, van de Veerdonk FL, Weis S, Oosterwijk E, Vermeulen SH, Netea MG, Joosten LA (2021) Lysine methyltransferase G9a is an important modulator of trained immunity. Clin Transl Immunology 10:e1253.

Muzio G, Barrera G, Pizzimenti S (2021) Peroxisome proliferator-activated receptors (PPARs) and oxidative stress in physiological conditions and in cancer. Antioxidants (Basel) 10:1734.

Nagaraj S, Zoltowska KM, Laskowska-Kaszub K, Wojda U (2019) microRNA diagnostic panel for Alzheimer's disease and epigenetic trade-off between neurodegeneration and cancer. Ageing Res Rev 49:125-143

Park J, Lee K, Kim K, Yi SJ (2022) The role of histone modifications: from neurodevelopment to neurodiseases. Signal Transduct Target Ther 7:217.

Polvani S, Tarocchi M, Galli A (2012) PPARγ and oxidative stress: Con(β) catenating NRF2 and FOXO. PPAR Res 2012:641087.

Rothammer N, Woo MS, Bauer S, Binkle-Ladisch L, Di Liberto G, Egervari K, Wagner I, Haferkamp U, Pless O, Merkler D, Engler JB, Friese MA (2022) G9a dictates neuronal vulnerability to inflammatory stress via transcriptional control of ferroptosis. Sci Adv 8:eabm5500.

Saab BJ, Mansuy IM (2014) Neuroepigenetics of memory formation and impairment: the role of microRNAs. Neuropharmacology 80:61-69.

Salvador JM, Brown-Clay JD, Fornace AJ Jr (2013) Gadd45 in stress signaling, cell cycle control, and apoptosis. Adv Exp Med Biol 793:1-19.

Shankar SR, Bahirvani AG, Rao VK, Bharathy N, Ow JR, Taneja R (2013) G9a, a multipotent regulator of gene expression. Epigenetics 8:16-22.

Shukla S, Tekwani BL (2020) Histone deacetylases inhibitors in neurodegenerative diseases, neuroprotection and neuronal differentiation. Front Pharmacol 11:537.

Siedlecki-Wullich D, Català-Solsona J, Fábregas C, Hernández I, Clarimon J, Lleó A, Boada M, Saura CA, Rodríguez-Álvarez J, Miñano-Molina AJ (2019) Altered microRNAs related to synaptic function as potential plasma biomarkers for Alzheimer's disease. Alzheimers Res Ther 11:46.

Siedlecki-Wullich D, Miñano-Molina AJ, Rodríguez-Álvarez J (2021) microRNAs as early biomarkers of Alzheimer's disease: A synaptic perspective. Cells 10:113.

Smith ML, Ford JM, Hollander MC, Bortnick RA, Amundson SA, Seo YR, Deng CX, Hanawalt PC, Fornace AJ Jr (2000) p53-mediated DNA repair responses to UV radiation: studies of mouse cells lacking p53, p21, and/or gadd45 genes. Mol Cell Biol 20:3705-3714.

Subramanian A, Tamayo P, Mootha VK, Mukherjee S, Ebert BL, Gillette MA, Paulovich A, Pomeroy SL, Golub TR, Lander ES, Mesirov JP (2005) Gene set enrichment analysis: a knowledge-based approach for interpreting genome-wide expression profiles. Proc Natl Acad Sci U S A 102:15545-15550.

Tecalco-Cruz AC, Ramírez-Jarquín JO, Alvarez-Sánchez ME, Zepeda-Cervantes J (2020) Epigenetic basis of Alzheimer disease. World J Biol Chem 11:62-75.

Tront JS, Hoffman B, Liebermann DA (2006) Gadd45a suppresses Ras-driven mammary tumorigenesis by activation of c-Jun NH2-terminal kinase and p38 stress signaling resulting in apoptosis and senescence. Cancer Res 66:8448-8454.

Vairapandi M, Balliet AG, Hoffman B, Liebermann DA (2002) GADD45b and GADD45g are cdc2/cyclinB1 kinase inhibitors with a role in S and G2/M cell cycle checkpoints induced by genotoxic stress. J Cell Physiol 192:327-338.

Vallée A, Lecarpentier Y (2018) Crosstalk between peroxisome proliferator-activated receptor gamma and the canonical WNT/β-catenin pathway in chronic inflammation and oxidative stress during carcinogenesis. Front Immunol 9:745.

Vasilopoulou F, Bellver-Sanchis A, Companys-Alemany J, Jarne-Ferrer J, Irisarri A, Palomera-Ávalos V, Gonzalez-Castillo C, Ortuño-Sahagún D, Sanfeliu C, Pallàs M, Griñán-Ferré C (2022) Cognitive decline and BPSD are concomitant with autophagic and synaptic deficits associated with G9a alterations in aged SAMP8 mice. Cells 11:2603.

Wang L, Jin Q, Lee JE, Su IH, Ge K (2010) Histone H3K27 methyltransferase Ezh2 represses Wnt genes to facilitate adipogenesis. Proc Natl Acad Sci U S A 107:7317-7322.

Wang L, Xu S, Lee JE, Baldridge A, Grullon S, Peng W, Ge K (2013) Histone H3K9 methyltransferase G9a represses PPARγ expression and adipogenesis. EMBO J 32:45-59.

Wang M, Qin L, Tang B (2019) MicroRNAs in Alzheimer's disease. Front Genet 10:153.

Wang S, Li H, Yuan M, Fan H, Cai Z (2022) Role of AMPK in autophagy. Front Physiol 13:1015500.

Wei W, Wang ZY, Ma LN, Zhang TT, Cao Y, Li H (2020) MicroRNAs in Alzheimer's disease: function and potential applications as diagnostic biomarkers. Front Mol Neurosci 13:160.

Xie Z, Bailey A, Kuleshov MV, Clarke DJB, Evangelista JE, Jenkins SL, Lachmann A, Wojciechowicz ML, Kropiwnicki E, Jagodnik KM, Jeon M, Ma'ayan A (2021) Gene set knowledge discovery with Enrichr. Curr Protoc 1:e90.

Yonutas HM, Sullivan PG (2013) Targeting PPAR isoforms following CNS injury. Curr Drug Targets 14:733-742

Yu X, Shao XG, Sun H, Li YN, Yang J, Deng YC, Huang YG (2008) Activation of cerebral peroxisome proliferator-activated receptors gamma exerts neuroprotection by inhibiting oxidative stress following pilocarpine-induced status epilepticus. Brain Res 1200:146-158.

Yun H, Park S, Kim MJ, Yang WK, Im DU, Yang KR, Hong J, Choe W, Kang I, Kim SS, Ha J (2014) AMP-activated protein kinase mediates the antioxidant effects of resveratrol through regulation of the transcription factor FoxO1. FEBS J 281:4421-4438.

Zhao Y, Patzer A, Herdegen T, Gohlke P, Culman J (2006) Activation of cerebral peroxisome proliferator-activated receptors gamma promotes neuroprotection by attenuation of neuronal cyclooxygenase-2 overexpression after focal cerebral ischemia in rats. FASEB J 20:1162-1175.

Zheng Y, Liu A, Wang ZJ, Cao Q, Wang W, Lin L, Ma K, Zhang F, Wei J, Matas E, Cheng J, Chen GJ, Wang X, Yan Z (2019) Inhibition of EHMT1/2 rescues synaptic and cognitive functions for Alzheimer's disease. Brain 142:787-807.

C-Editor: Zhao M; S-Editor: Li CH; L-Editors: Li CH, Song LP; T-Editor: Jia Y

Supplementary Table 1. Reagents and kits used in this work.

Reagent, kits	Source	Catalog number
UNC0642	BLDpharm, Shangai, China	BD630326
2-hydroxypropyl-β-cyclodextrin	Atomole scientific Co. Ltd., Wuhan, Hubei, China	AT-20762
TRItidy G™	PannReac AppliChem, Spain,	A4051, 0,200
High Capacity cDNA Reverse Transcription kit	Applied Biosystems™, Vilnius, Lithuania	4368814
Maxima SYBR Green qPCR Master Mix (2X), ROX solution provided	Thermo Scientific™, Vilnius, Lithuania	K0253
mirVana miRNA Isolation kit with phenol	Invitrogen™, , Foster City, CA, USA	AM1560
TaqMan miRNA Reverse Transcription kit	Thermo Fischer Scientific, Waltham, MA, USA,	4366596
TaqMan™ Universal PCR Master Mix	Applied Biosystems™, Vilnius, Lithuania	4305719
Trypsin-EDTA (0.25%), phenol red	Gibco™, Waltham, MA USA	25200056
DMEM-F12 medium	Gibco™, Waltham, MA USA	12400-024
HyClone Standard Fetal Bovine Serum (FBS)	Cytiva, Marlborough, MA, USA	SH30088.03
Poly-D-lysine	Santa Cruz, Texas, USA	sc-136156
Neurobasal medium	Gibco™, Waltham, MA USA	21103049
B27 supplement	Gibco™, Waltham, MA USA	17504044
GlutaMAX™	Gibco™, Waltham, MA USA	35050061
Penicillin-Streptomycin	Gibco™, Waltham, MA USA	15140-122
LDH assay	Roche, Indianapolis, IN, USA	4744926001
Triton X-100	Sigma-Aldrich, St. Louis, MO, USA	9036-19-5

Supplementary Table 2. TaqMan probes used in this study.

TaqMan probes		
Target	**Product size (bp)**	**Catalog number**
mmu-miR-1298	-	4427975
mmu-miR-677	-	4440886
mmu-miR-669	-	4440886
mmu-miR-128	-	4440886
U6 snRNA	-	4427975

Supplementary Table 3. SYBR Green primers analyzed in this study

SYBR Green Primers		
Target	**Forward primer (5'-3')**	**Forward primer (3'-5')**
Pparg	CATTCTGGCCCACCAACTTTGG	TGGAGATGCAGGCTCCACTTTG
Sod-1	CCACACCTTCACTGGTCCAT	CTAGCGAGTTATGGCGACG
Hmox-1	TGACACCTGAGGTCAAGCAC	GTCTCTGCAGGGGCAGTATC
Gpx	GTCACGGTTTTGGGCTTTCC	CTGGTGACCGAGTGGAACAA
Aox-1	CATAGGCGGCCAGGAACATT	TCCTCGTTCCAGAATGCAGC
Cox-2	TGACCCCCAAGGCTCAAATA	CCCAGGTCCTCGCTTATGATC
Aldh-2	GCAGGCGTACACAGAAGTGA	TGAGCTTCATCCCCTACCCA
Sirt-1	AACACACACACAAAATCCAGCA	TGCAACCTGCTCCAAGGTAT
Gadd45a	CTGCAGAGCAGAAGACCGAA	GGGTCTACGTTGAGCAGCTT
Egr1	CCACCATGGACAACTACCCC	TCATAGGGTTGTTCGCTCGG
Egr2	ACAGGCAGGAGAGAGTCAGT	GAAGATGGTCACCGACGAGG
Arc	GCCCCCAGCAGTGATTCATA	GGAACCCATGTAGGCAGCTT
Dnmt3a	ACGCCAAAGAAGTGTCTGCT	CTTTGCCCTGCTTTATGGAG
Vgf	GTCAGACCCATAGCCTCCC	CTCGGACTGAAATCTCGAAGTTC
Tgf	CAGGGTGAAGGGGAAAACTC	AGTTCGGTCATTCAGTCTCGC
TrkA	CTCCTTCTCGCCAGTGGAC	TGCCCTCAGTAGGGGAAAGA
TrkB	CGTCACTTCGCCAGCAGTAG	CTATACGCCAGGCACCACTC
Dcx	CCAGCAGTCAGCTCTCAACA	GTACAGGTCCTTGTGCCTCC
Sox2	CCCCGGGCTGCAGGAAT	TGTGCATCTTGGGGTTCTCC
ß-actin	CAACGAGCGGTTCCGAT	CAACGAGCGGTTCCGAT

Pparg; Peroxisome Proliferator Activated Receptor Gamma; Sod-1: Superoxide dismutase 1; Hmox-1: Heme Oxygenase 1; Gpx: Glutathione Peroxidase 1; Aox-1: Aldehyde Oxidase 1; Cox-2: Cyclooxygenase 2; Aldh-2: Aldehyde dehydrogenase; Sirt-1: Sirtuin 1; Gadd45a: Growth Arrest And DNA Damage Inducible Alpha; Egr1/2: Early Growth Response 1/2; Arc: Activity Regulated Cytoskeleton Associated Protein; DNMT3a: DNA Methyltransferase 3 Alpha; Vgf; VGF *Nerve Growth Factor Inducible; Tgf: T*ransforming growth factor; TrkA/B: *Receptor tyrosine kinase A/B; Dcx: Doublecortin; Sox2: SRY-Box Transcription Factor 2; ß-actin: Actin beta*

Supplementary Table 4. Antibodies used in western blot assay in this study

Antibody	Host	Source/Catalog/RRID	WB dilution
p-AMPK	Rabbit	Cell Signaling, Danvers, MA, USA/#2532/AB_330331	1:1000
AMPK	Rabbit	Cell Signaling, Danvers, MA, USA /#2537/AB_659805	1:1000
FOXO1a	Rabbit	Cell Signaling, Danvers, MA, USA /#2880/AB_2106495	1:1000
Catalase-3	Rabbit	Cell Signaling, Danvers, MA, USA /#12980/AB_2798079	1:1000
GPX	Rabbit	Novus Biological, CO, USA/NBP1-33620/ AB_10004091	1:1000
SOD-1	Sheep	Millipore, Burlington, MA, USA /574597/AB_2255005	1:1000
GSH	Rabbit	Abcam, Waltham, MA, USA /ab124811/AB_10973222	1:1000
GADD45α	Mouse	Santa Cruz, TX, USA/sc-6850/AB_627653	1:500
BCL-2	Rabbit	Cell Signaling, Danvers, MA, USA /#2870/AB_2290370	1:1000
BAX	Rabbit	Cell signaling/#41162/AB_2924730	1:1000
Caspase-3	Rabbit	BD Transduction Laboratories/C31720/AB_2335903	1:1000
SQSTM1/p62	Mouse	Santa Cruz, TX, USA/sc-28359/AB_628279	1:500
BECLIN-1	Rabbit	Cell Signalling, Danvers, MA, USA /#3738/AB_490837	1:1000
PSD95	Rabbit	Abcam, Waltham, MA, USA /ab18258/AB_444362	1:1000
PSD93	Rabbit	GeneTex, Irvine, CA, USA/GTX133250/AB_2886890	1:1000
SYN IIa	Rabbit	Dako, Santa Clara, CA/CloneSY38	1:1000
NeuN	Mouse	Abcam, Waltham, MA, USA /ab178846/AB_2636859	1:1000
Actin	Mouse	Sigma-Aldrich, St. Louis, MO, USA /A-5441/AB_476744	1:2500
GAPDH	Mouse	Millipore, Burlington, MA, USA/MAB374/AB_2107445	1:5000
Goat-anti-mouse HRP conjugated	Goat	Biorad, Hercules, CA, USA/170-5047/AB_11125753	1:2000
Goat-anti-rabbit HRP conjugated	Goat	Biorad, Hercules, CA, USA /170-6515/AB_11125142	1:2000

(p-)AMPK: (phosphorylated-) Adenosine monophosphate-activated protein kinase; FOXO1a: Forkhead box protein O1; GPX: Glutathione peroxidase; SOD-1: Superoxyde Dismutase 1; GSH: Glutathione; GADD45α: Growth Arrest And DNA Damage Inducible Alpha; BCL-2: B-cell lymphoma 2; BAX: Bcl-2-associated X protein; SQSTM1/p62: Sequestosome 1; PSD95: Postsynaptic density protein 95/93; SYN IIa: Synapsin IIa; NeuN: Neuronal nuclei; GAPDH: GAPDH glyceraldehyde-3-phosphate dehydrogenase

Supplementary Table 5 Differentially expressed miRNAs

miRNA	Log fold change	Log Counts per Million	*p*-value
mmu-let-7j	15.2687362	8.93267811	2.7628E-18
mmu-mir-128-1	7.91104045	3.86978577	2.2849E-09
mmu-miR-677-3p	7.87675113	-1.3732063	0.00057812
mmu-miR-6715-3p	6.53263092	-2.4946678	0.01625387
mmu-miR-6942-3p	6.3646525	-2.6163294	0.02167183
mmu-miR-7646-5p	6.17450633	-2.7482791	0.04072398
mmu-miR-1291	5.07360856	3.62047055	6.6835E-06
mmu-miR-7237-3p	4.51855472	-1.6993221	0.00775791
mmu-miR-802-5p	3.57005461	1.6636214	0.00087489
mmu-miR-690	3.34601258	3.88165459	0.00119641
mmu-mir-128-2	3.10779292	-1.5528322	0.02011138
mmu-miR-1941-3p	2.83854221	0.65391609	0.00769132
mmu-miR-1949	2.74579341	1.68612831	0.00764228
mmu-miR-6929-3p	2.66057011	-1.2558981	0.0359578
mmu-miR-6990-5p	2,55822987	-0,7148019	0.0258626
mmu-miR-6481	2.44209236	5.26687132	0.01343157
mmu-miR-34a-3p	2.22377906	0.60988426	0.03362583
mmu-miR-187-5p	-1.9719857	1.9230752	0.04796803
mmu-miR-877-5p	-2.059489	2.24842384	0.03820115
mmu-miR-7a-2-3p	-2.0595942	4.59869511	0.03478584
mmu-miR-539-5p	-2.1685846	-0.119102	0.04612425
mmu-miR-1298-3p	-2.1973564	4.7557324	0.02516376
mmu-miR-144-3p	-2.3682441	4.77302249	0.01645278
mmu-miR-92b-5p	-2.3773874	2.70168661	0.01740784
mmu-miR-34b-3p	-2.5417088	4.26862977	0.01061103
mmu-miR-1264-5p	-2.5936658	-0.1126349	0.02374869
mmu-miR-34c-3p	-2.6749442	3.25981439	0,00797272
mmu-miR-204-5p	-3.0145851	10.2735647	0.00278358
mmu-miR-1264-3p	-3.0983169	7.65965958	0.0022024
mmu-miR-34c-5p	-3,1327463	6.49555023	0.00202504
mmu-miR-148a-5p	-3.1595987	-1.9930737	0.04615818
mmu-miR-34b-5p	-3.3253556	3.62327107	0.00131442
mmu-miR-204-3p	-3.535278	1.80537606	0.00105262

mmu-miR-1912-5p	-3.9200743	0.56866704	0.00118626
mmu-miR-466d-5p|mmu-miR-466n-5p	-3.9470228	-1.3907703	0.00775791
mmu-miR-448-3p	-4.6805698	6.7736446	1.7266E-05
mmu-miR-7080-5p	-4.8914647	0.24451005	0.00028447
mmu-miR-1912-3p	-6.0065082	4.77360594	3.0439E-07
mmu-miR-452-3p	-6.1996603	-2.4019807	0.02941176
mmu-miR-3572-5p	-6.3235545	-2.312375	0.02167183
mmu-miR-202-5p	-6.4376454	-2.228299	0.01625387
mmu-miR-1298-5p	-6.833234	7.66313366	1.3649E-08
mmu-miR-669l-5p	-6.9798677	-1.8103897	0.00474308
mmu-miR-208b-3p	-8.5571904	-0.4712288	7.244E-05

Supplementary Table 6. miRNAs targets

mmu-miR-34a-3p	***mmu-mir-128-1***	***mmu-mir-128-2***	***mmu-miR-92b-5p***	***mmu-miR-144-3p***	***mmu-miR-34c-5p***	***mmu-miR-204-3p***	***mmu-miR-539-5p***	***mmu-miR-34c-3p***	***mmu-miR-204-5p***	***mmu-miR-208b-3p***	***mmu-miR-148a-5p***	***mmu-miR-34b-5p***	***mmu-miR-448-3p***	***mmu-miR-187-5p***
Mdfic	*Nrp1*	*Nrp1*	*Camk2n1*	*Myo1b*	*Myo1b*	*9430021 M05Rik*	*Hs3st2*	*Myo1b*	*9430021 M05Rik*	*Tes*	*2310014L 17Rik*	*Myo1b*	*Myo1b*	*Lipg*
Il16	*Slc44a5*	*Slc44a5*	*Myo1b*	*Camk4*	*2310014 L17Rik*	*Rcan2*	*Tes*	*2310014 L17Rik*	*Rcan2*	*Gm8179*	*Tes*	*2310014 L17Rik*	*Tes*	*Chrnb3*
A4galt	*Nrp2*	*Nrp2*	*Gm7367*	*Pld5*	*Gadd45a*	*Pla2g4e*	*Camk4*	*Gadd45a*	*Pla2g4e*	*Gch1*	*Pld5*	*Gadd45a*	*Camk4*	*Krt80*
Prlr	*Mdfic*	*Mdfic*	*Egr2*	*Garnl3*	*Xirp2*	*Garnl3*	*Pla2g4e*	*Xirp2*	*Garnl3*	*Col24a1*	*Gadd45a*	*Xirp2*	*Traf5*	*2310014 L17Rik*
Tcfl5	*Car12*	*Car12*	*9430021 M05Rik*	*Snurf*	*N28178*	*Gadd45a*	*Pld5*	*N28178*	*Gadd45a*	*Rorb*	*Cnga4*	*N28178*	*Pld5*	*Mef2c*
Iqch	*Gm119 92*	*Gm119 92*	*Camk4*	*Kcnh5*	*Adamts1 8*	*Xirp2*	*Osbpl3*	*Adamts1 8*	*Xirp2*	*Adcyap1*	*Adcyap1*	*Adamts1 8*	*Kcnh7*	*Gpr88*
Tgtp1	*Pde3a*	*Pde3a*	*Rassf3*	*Gm1329 8*	*Car10*	*Ppp1r1c*	*Garnl3*	*Car10*	*Ppp1r1c*	*Car10*	*Adamts18*	*Car10*	*Cnga4*	*Satb2*
Mfrp	*Htr4*	*Htr4*	*Pld5*	*Pappa2*	*Cd244*	*Ephb6*	*Xirp2*	*Cd244*	*Ephb6*	*Bend7*	*Ephb3*	*Cd244*	*Kcnh5*	*Mkx*
Cdhr1	*Epb4.1l 4a*	*Epb4.1l 4a*	*Hfe2*	*Adamts1 8*	*Tmem13 2d*	*Kcnk3*	*Il12a*	*Tmem13 2d*	*Kcnk3*	*Chrnb3*	*Trib1*	*Gabra3*	*Car10*	*Dusp6*
Htr2c	*Stra6*	*Stra6*	*Lphn2*	*Car10*	*Gabra3*	*Dpp10*	*Gm1329 8*	*Gabra3*	*Dpp10*	*Gpr88*	*Dll4*	*Kcnk3*	*Ppp1r1c*	*Tspan11*
Tmem72	*Lrrc18*	*Lrrc18*	*Adamts1 8*	*Trib1*	*Kcnk3*	*Gpr88*	*Ppp1r1c*	*Kcnk3*	*Gpr88*	*Mafb*	*Mafb*	*Fhod3*	*Serpinb8*	*Arpp19*
St6galna c5	*Dpyd*	*Dpyd*	*Gk2*	*Ppp1r1c*	*Fhod3*	*Mafb*	*Rgs4*	*Fhod3*	*Mafb*	*Pdgfrl*	*Gm15417*	*Arid3b*	*Rgs4*	*Nr4a1*
Shisa2	*Wdr86*	*Wdr86*	*Ppp1r1c*	*Dll4*	*Arid3b*	*Pak7*	*Chrnb3*	*Arid3b*	*Pak7*	*Lgr5*	*Gfra2*	*Krt20*	*Kcnk3*	

Arhgap12	*Gfra1*	*Gfra1*	*Dpp10*	*Chrnb3*	*Krt20*	*Arid3b*	*Gabra3*	*Krt20*	*Arid3b*	*Dtl*	*Wnt10a*	*Grip2*	*Dpp10*
Figf	*Lbp*	*Lbp*	*Mef2c*	*Tnfrsf11b*	*Grip2*	*Tac2*	*Dpp10*	*Grip2*	*Tac2*	*Pcdha12*	*Rgs6*	*Camkk2*	*Usp43*
Col5a2	*A330050F15Rik*	*A330050F15Rik*	*Gpr88*	*Pdgfrl*	*Camkk2*	*Gabrg3*	*Tnfrsf11b*	*Camkk2*	*Gabrg3*		*Ipcef1*	*Tspan11*	*Krt80*
Adamts9	*St6galnac5*	*St6galnac5*	*Pak7*	*Htr2a*	*Tspan11*	*Krt20*	*Dusp1*	*Tspan11*	*Krt20*		*Arpp19*	*Vwa5b2*	*Spata1*
Col9a3	*Cyp7b1*	*Cyp7b1*	*9130024F11Rik*	*Pak7*	*Vwa5b2*	*Camkk2*	*Pdgfrl*	*Vwa5b2*	*Camkk2*		*Slc5a7*	*Mapk12*	*Grip2*
Cachd1	*Slc2a12*	*Slc2a12*	*Gabrg3*	*Pou6f2*	*Mapk12*	*Rasgef1b*	*Cdh22*	*Mapk12*	*Rasgef1b*		*Camk2n1*	*Gpr153*	*Ipcef1*
Ebf3	*Arhgap12*	*Arhgap12*	*Efna5*	*Ipcef1*	*Gpr153*	*C130074G19Rik*	*Pou6f2*	*Gpr153*	*C130074G19Rik*		*Cftr*	*Gm7367*	*Arpp19*
Mettl5	*Figf*	*Figf*	*Foxp2*	*Arpp19*	*Egr1*	*Satb2*	*Gfra2*	*Egr1*	*Satb2*		*Egr2*	*Egr2*	*Pcdha12*
Trpm3	*Col5a2*	*Col5a2*	*Arpp19*	*Pdia5*	*Gm7367*	*Hr*	*9930111J21Rik2*	*Gm7367*	*Hr*		*Gm8179*	*Gm5643*	*Gm7367*
Dcn	*Txnip*	*Txnip*		*Slc5a7*	*Egr2*	*Cux1*	*Ipcef1*	*Egr2*	*Cux1*		*Hgf*	*Satb2*	*Rims3*
Zfp229	*Ndst4*	*Ndst4*		*Camk2n1*	*Gm5643*	*Rorb*	*Arpp19*	*Gm5643*	*Rorb*		*Hkdc1*	*Hr*	*Gm8179*
Dock4	*Gm4951*	*Gm4951*		*Cftr*	*Satb2*	*Pamr1*	*Camk2n1*	*Satb2*	*Pamr1*		*Fos*	*Alpk3*	*Gcnt4*
Tshz2	*Adamts9*	*Adamts9*		*Arl4d*	*Hr*	*Pdzrn3*	*Cftr*	*Hr*	*Pdzrn3*		*Cux1*	*Cux1*	*Hgf*
Marcksl1	*Gpx8*	*Gpx8*		*Gch1*	*Alpk3*	*Xkr7*	*Adra1b*	*Alpk3*	*Xkr7*		*Rorb*	*Rorb*	*Tbr1*
Myh8	*Cachd1*	*Cachd1*		*Gcnt4*	*Cux1*	*Mef2c*	*Scube1*	*Cux1*	*Mef2c*		*Lphn2*	*Pdzrn3*	*Fos*
Acacb	*Trpm3*	*Trpm3*		*Col24a1*	*Pdzrn3*	*BC030499*	*Col24a1*	*Pdzrn3*	*BC030499*		*Pparg*	*BC030499*	*Rorb*
Thsd4	*Dcn*	*Dcn*		*Satb2*	*Arc*	*St6gal2*	*Fos*	*Arc*	*St6gal2*		*Pamr1*	*Cwh43*	*Scn4b*

Fbn2	*Prom2*	*Prom2*	*Ptgfrn*	*BC030499*	*Cobl*	*Lphn2*	*BC030499*	*Cobl*	*Mybl1*	*Klf10*	*Pparg*
					E130012			*E130012*			
Naip6	*F5*	*F5*	*Fos*	*Cwh43*	*A19Rik*	*Rnf152*	*Cwh43*	*A19Rik*	*Mef2c*	*Efna5*	*Mybl1*
Arhgap28	*Wipf3*	*Wipf3*	*Rorb*	*Klf10*	*Rgsl1*	*Pdzrn3*	*Klf10*	*Rgsl1*	*Snap25*	*Dtl*	*Syt6*
Creb3l3	*Gria1*	*Gria1*	*Zfp365*	*Efna5*	*Abi3bp*	*Sema3a*	*Efna5*	*Abi3bp*	*St6gal2*	*Foxp2*	*Sema3a*
	Fam160	*Fam160*									
Pvrl2	*a1*	*a1*	*Pparg*	*Dtl*	*Pik3r6*	*Kcnh1*	*Dtl*	*Pik3r6*	*Cobl*		*Mef2c*
Gpr101	*Epha8*	*Epha8*	*Pamr1*	*Foxp2*	*Efna5*	*Mef2c*	*Foxp2*	*Efna5*	*Wisp1*		*Stard8*
									9130024		
Eomes	*Bhlhe22*	*Bhlhe22*	*Rnf152*		*Dtl*	*Snap25*		*Dtl*	*F11Rik*		*Myl1*
			Gm1374			*BC030499*					
Pcdh8	*Slco1a5*	*Slco1a5*	*9*		*Foxp2*	*9*		*Foxp2*	*Kcnt1*		*Pmaip1*
Slc38a4	*Kit*	*Kit*	*Stard8*			*Klf10*					*Rxfp2*
						9130024					
Zbtb20	*Rxfp3*	*Rxfp3*	*Cobl*			*F11Rik*					*Mkx*
			9130024								
Tcf7l2	*Pkp2*	*Pkp2*	*F11Rik*			*Mkx*					*Dtl*
Drd5	*Dsg2*	*Dsg2*	*Pik3r6*			*Efna5*					*Sytl2*
Col2a1	*Ror1*	*Ror1*	*Dtl*			*Dtl*					
Spint1	*Slc26a4*	*Slc26a4*	*Fnbp1l*			*Foxp2*					
Dgkk	*Thsd4*	*Thsd4*	*Foxp2*			*Chrdl1*					
	Hist1h2	*Hist1h2*									
Col4a3	*ac*	*ac*	*Cyr61*								
Col4a4	*Npr1*	*Npr1*									
Nek10	*Myo5b*	*Myo5b*									

Rreb1	*Lpl*	*Lpl*
Tbx4	*Enpp2*	*Enpp2*
Vwc2l	*Rnf122*	*Rnf122*
Ust	*St18*	*St18*
Fat4	*Egfl6*	*Egfl6*
Ttc16	*Ttr*	*Ttr*
Slc29a4	*Golm1*	*Golm1*
	Pcdh8	*Pcdh8*
	BC030500	*BC030500*
	Steap4	*Steap4*
	Ccdc78	*Ccdc78*
	Ntf3	*Ntf3*
	Ripk4	*Ripk4*
	Slc38a4	*Slc38a4*
	Otx2	*Otx2*
	Zbtb20	*Zbtb20*
	Sh3bgr	*Sh3bgr*
	Zfp618	*Zfp618*
	Tcf7l2	*Tcf7l2*
	Dock10	*Dock10*
	Zic4	*Zic4*
	Rreb1	*Rreb1*

Homer3	*Homer3*
Slc16a1	*Slc16a1*
2	*2*
E03001	*E03001*
3I19Rik	*3I19Rik*
Tbx4	*Tbx4*
Vwc2l	*Vwc2l*
Mpzl3	*Mpzl3*
Igsf1	*Igsf1*
Lrrn4	*Lrrn4*
Ogn	*Ogn*
Mum1l1	*Mum1l1*
Fat4	*Fat4*
Bambi	*Bambi*
Il1r1	*Il1r1*
A2m	*A2m*
Pip5k1b	*Pip5k1b*
Fbn1	*Fbn1*
Zfp608	*Zfp608*

3.4. Publication 4

Structure-Based Virtual Screening and *in vitro* and *in vivo* Analyses Revealed Potent Methyltransferase G9a Inhibitors as Prospective Anti-Alzheimer's Agents.

Aina Bellver-Sanchis[*], Bhanwar Singh Choudhary[*], Júlia Companys-Alemany, Sukanya, Pedro A. Ávila-López,Antón Leandro Martínez Rodríguez, Jose Manuel Brea Floriani, Ruchi Malik, Mercè Pallàs, Belén Pérez, and Christian Griñán-Ferré

ChemMedChem, 2022, 17: e202200002
doi: 10.1002/cmdc.202200002

SUMMARY

Small molecule inhibitors directed against the G9a protein are useful tools for studying its biological functions and further exploring G9a-associated therapeutic hypotheses, especially in the context of neurodegeneration. Several G9ais have been synthesized in the last decade, among which quinazolines and quinolines have been extensively explored. However, existing compounds, including the best-established ones such as BIX01294, UNC0638, and UNC0642, showed limitations in vitro and in vivo studies, including toxicity, poor BBB permeability, and high melting points. Therefore, there is a need to explore new chemical scaffolds to develop G9ais with improved pharmacokinetic properties. Considering our hypothesis that G9a overexpression is associated with the repression of genes involved in learning and memory, this work aims to explore G9ais with new chemical scaffolds that exhibit improved pharmacokinetics, especially focused on AD.

Here, we employed a structure-based virtual screening against G9a to identify potential inhibitors, followed by *in vitro* and *in vivo* screenings. Briefly, our results compile data on IC_{50} against G9a and GLP, in silico ADMET analysis, BBB permeability values, as well as target engagement and efficacy studies in AD transgenic *C. elegans* strain, the CL2006. The results indicated that **E**, **F**, and **H** were the best compounds screened, demonstrating potential CNS pharmacological properties and potent G9a inhibitory activity, also reducing its repressor mark (H3K9me2). Moreover, screening using the CL2006 AD strain demonstrated that the toxicity/function range was safe and resulted in the recovery of age-dependent paralysis. Further characterization involved assessing BBB permeability and examining the impact on Aβ aggregation, revealing encouraging outcomes. Among them, the compound F showed potent G9a inhibitory activity and promising efficacy in reducing Aβ deposition, highlighting its potential as a tool for further *in vivo* AD.

The research findings provide valuable insights into the potential of the identified G9a inhibitors, particularly compound **F**, as prospective anti-AD agents due to their potency, selectivity, and efficacy in *in vitro* and *in vivo* studies. These findings offer promising leads for future research and drug development in the field of AD therapeutics.

Check for updates

ChemMedChem

Research Article
doi.org/10.1002/cmdc.202200002

Chemistry Europe
European Chemical Societies Publishing

www.chemmedchem.org

Structure-Based Virtual Screening and *in vitro* and *in vivo* Analyses Revealed Potent Methyltransferase G9a Inhibitors as Prospective Anti-Alzheimer's Agents

Aina Bellver-Sanchis[+],[a] Bhanwar Singh Choudhary[+],[b, c] Júlia Companys-Alemany,[a] Sukanya,[b] Pedro A. Ávila-López,[d] Antón Leandro Martínez Rodríguez,[e] Jose Manuel Brea Floriani,[e] Ruchi Malik,[b] Mercè Pallàs,[a] Belén Pérez,[f] and Christian Griñán-Ferré*[a]

G9a is a lysine methyltransferase able to di-methylate lysine 9 of histone H3, promoting the repression of genes involved in learning and memory. Novel strategies based on synthesizing epigenetic drugs could regulate gene expression through histone post-translational modifications and effectively treat neurodegenerative diseases, like Alzheimer's disease (AD). Here, potential G9a inhibitors were identified using a structure-based virtual screening against G9a, followed by *in vitro* and *in vivo* screenings. First, screening methods with the AD transgenic *Caenorhabditis elegans* strain CL2006, showed that the toxicity/function range was safe and recovered age-dependent paralysis. Likewise, we demonstrated that the best candidates direct target G9a by reducing H3 K9me2 in the CL2006 strain. Further characterization of these compounds involved the assessment of the blood-brain barrier-permeability and impact on amyloid-β aggregation, showing promising results. Thus, we present a G9a inhibitor candidate, **F**, with a novel and potent structure, providing both leads in G9a inhibitor design and demonstrating their participation in reducing AD pathology.

Introduction

Epigenetic modifications have an important impact on regulating the expression and transcription of genes involved in many human diseases, such as cancer,[1] addiction,[2] psychiatric[3] and neurodegenerative disorders.[4] One of the most relevant epigenetic mechanisms to control gene expression is chromatin remodeling.[5] This is catalyzed by different enzymes and is responsible for the dynamic modification of chromatin structure, enabling or restricting the access of the transcription machinery to condensed genomic DNA. An essential process responsible for the alteration of chromatin architecture is the post-translational modification (PTM) of histones. PTMs are chemical modifications of the amino acid residues of proteins, leading to changes in gene expression. This process is mainly mediated by epigenetic "writer" enzymes, such as histone methyltransferases (HMTs), which are responsible for adding chemical methyl groups in specific residues (lysine (K) or arginine (R)), and as a consequence, leading to active or repressive marks. In general, methylation of H3 K9 and H3 K27 are typical hallmarks of transcription repression, whereas methylation of H3 K4, H3 K36, and H3 K7 are considered active marks. Hence, dysregulation of methylation at specific histone sites has been implicated in many human diseases, highlighting the potential therapeutic value of HMTs as targets.[6]

[a] *A. Bellver-Sanchis,[+] J. Companys-Alemany, Prof. M. Pallàs, Dr. C. Griñán-Ferré*
Pharmacology Section, Department of Pharmacology, Toxicology and Therapeutic Chemistry
Faculty of Pharmacy and Food Sciences
Institute of Neuroscience, Universitat de Barcelona (NeuroUB)
Av. Joan XXIII 27–31, 08028 Barcelona (Spain)
E-mail: christian.grinan@ub.edu
[b] *B. Singh Choudhary,[+] Sukanya, Dr. R. Malik*
Department of Pharmacy
Central University of Rajasthan
Bandarsindari, Ajmer, 305817 (India)
[c] *B. Singh Choudhary[+]*
Department of Pharmaceutical Chemistry and Quality Assurance
Shree S. K. Patel College of Pharmaceutical Education and Research
Ganpat University
Mehsana, Gujarat 384012 (India)
[d] *Dr. P. A. Ávila-López*
Department of Biochemistry and Molecular Genetics
Feinberg School of Medicine
Northwestern University, Chicago, Illinois (USA)
[e] *Dr. A. L. Martínez Rodríguez, Dr. J. M. Brea Floriani*
Centro de Investigación en Medicina Molecular y Enfermedades Crónicas (CIMUS)
Departamento de Farmacología, Farmacia y Tecnología Farmacéutica
Universidad de Santiago de Compostela
15782 Santiago de Compostela (Spain)
[f] *Dr. B. Pérez*
Department of Pharmacology, Therapeutic and Toxicology
Universitat Autònoma de Barcelona, 08193 Barcelona (Spain)
[+] *These authors contributed equally to this work.*

Supporting information for this article is available on the WWW under https://doi.org/10.1002/cmdc.202200002

© 2022 The Authors. ChemMedChem published by Wiley-VCH GmbH. This is an open access article under the terms of the Creative Commons Attribution License, which permits use, distribution and reproduction in any medium, provided the original work is properly cited.

© 2022 The Authors. ChemMedChem published by Wiley-VCH GmbH

ChemMedChem
Research Article
doi.org/10.1002/cmdc.202200002
Chemistry Europe
European Chemical Societies Publishing

18607187, 2022, 13, Downloaded from https://chemistry-europe.onlinelibrary.wiley.com/doi/10.1002/cmdc.202200002 by Readcube (Labtiva Inc.), Wiley Online Library on [18/02/2024]. See the Terms and Conditions (https://onlinelibrary.wiley.com/terms-and-conditions) on Wiley Online Library for rules of use; OA articles are governed by the applicable Creative Commons License

In particular, G9a methyltransferase, also known as euchromatic histone methyltransferase 2 (EHMT2), is an HMT responsible for mono- and di-methylate lysine 9 on histone H3 (H3 K9me1 and H3 K9me2).[7] Consequently, these repressive marks are capable of regulating gene expression.[8] Until now, G9a has been widely explored as an anti-cancer and an anti-malarial target.[9–11] However, interestingly, recent evidence potentially suggests that G9a is a target in neurodegenerative disorders, such as Alzheimer's disease (AD), since its epigenetic marks are related to the repression of transcription in genes involved in learning and memory formation, contributing to cognitive impairment.[12–14]

Small molecule inhibitors of G9a are valuable tools to study this protein's biological functions and further explore the therapeutic hypotheses associated with them, for instance, in the context of neurodegeneration. Several G9a inhibitors have been synthesized and published in the last decade (Figure 1). Among the previously reported G9a inhibitors, quinazolines (1,2,3)[9,10] and quinolines (4)[15,16] are widely explored; others are benzodiazepines (5),[17] amino-indoles (6),[18] 6H-anthra[1,9-cd]isoxazol-6-one (7),[19] pseudodehydrocorydaline (8),[20] 2,4-diamino-6-methylpyrimidines (9),[21] Chaetocin (10)[22–24] and Epidithiodiketopiperazine (11).[25] The first G9a inhibitor identified by high-throughput screening (HTS) was BIX01294 (Figure 1), which resulted in active cell-based assay and reduced H3 K9methylation levels in several G9a target genes. However, this compound had a toxicity/function ratio lower than 6 (determined by dividing the half-maximal effective concentration (EC50) value of observed toxicity by the half-maximal inhibitory concentration (IC_{50}) value of the functional potency), so to overcome its cytotoxicity, more specific and potent molecules need to be discovered.[26,27] Crystallographic studies based on BIX01294 identified other inhibitory compounds to improve the therapeutic range. Further optimization of UNC0638 led to potent and selective G9a inhibitors with a better toxicity/function ratio than BIX01294 (>100). However, these two and the other published compounds were less effective in *in vitro* and *in vivo* studies and had poor blood-brain barrier (BBB) permeability and very high melting points. Thus, there is a need to explore new chemical scaffolds other than quinazolines and quinolines, which exhibit improved pharmacokinetic properties.

In brief, this work is based on the hypothesis that overexpression of G9a and its repressive mark serve as a driver of repression of genes involved in learning and memory. Therefore, we explored an extensive chemical database (Chembridge CNS MPO database) using structure-based virtual screening against G9a, to provide potent inhibitors with novel chemical scaffolds as a research tool to study the function of this protein in biological processes, mainly focused on AD.

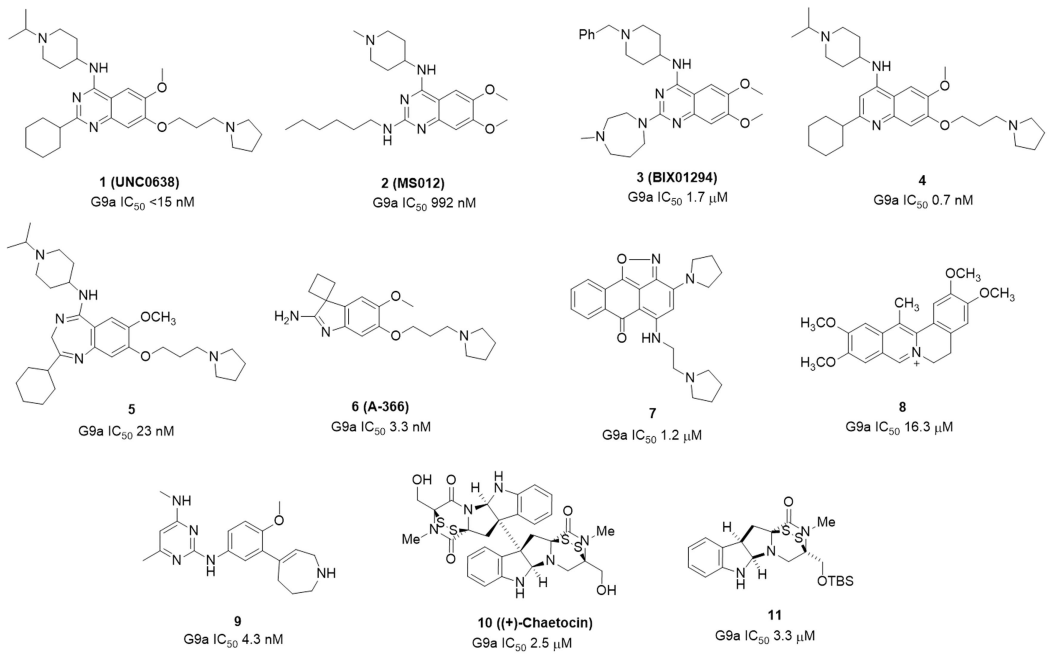

Figure 1. Structures of previously reported G9a inhibitors (IC_{50} values are dependent on the assay conditions used).

© 2022 The Authors. ChemMedChem published by Wiley-VCH GmbH

ChemMedChem
Research Article
doi.org/10.1002/cmdc.202200002
Chemistry Europe
European Chemical Societies Publishing

Results and Discussion

Identification of novel G9a inhibitors through structure-based virtual screening

Protein Data Bank (PDB) id 5TTF is selected for creating a docking model based on its 1.72 Å resolution, the sequence length of 283 amino acids, no Ramachandran outliers, and quinazoline derivative MS012 (Figure 1) as a co-crystallized compound. The crystal structure of G9a bound to MS012 (PDB ID: 5TTF) was retrieved from the RCSB portal and prepared using the protein preparation wizard of Maestro. The enrichment-based validation of the docking protocol was performed, showing the receiver operating characteristic (ROC) graph where docking results were plotted between valid positive rate (sensitivity) and false-positive rate (1-specificity). The ROC graph reflects the probability of a higher ranking of randomly selected active compounds over randomly selected decoy molecules. The results of Glide SP docking showed ROC values of 0.97 for 5TTF (Figure 2). The RMSD of co-crystallized and docked MS012 was found 1.165 Å (Figure S1a).

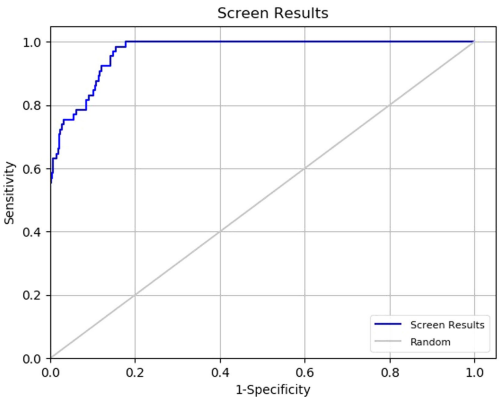

Figure 2. ROC graphs of the docking results for assessing the reliability of the docking protocol.

Table 1. Dock score, MM-GBSA dG score, interacting residues, and G9a IC_{50} (nM) of selected screened molecules.

Compound	Dock Score	MM-GBSA dG	G9a IC_{50} [nM]
UNC0638	−5.049	−70.31	9.4
A	−10.346	−106.68	>100
B	−12.553	−116.98	9.4
C	−10.809	−90.21	1.7
D	−10.552	−101.76	10.5
E	−11.548	−106.01	2.1
F	−10.202	−95.02	1.8
G	−10.487	−93.42	5.8
H	−10.331	−96.43	2.5
I	−11.253	−91.44	3.9

A hierarchical stepwise virtual screening was performed using Glide HTVS, SP, and XP docking for the Chembridge database of 496644 compounds and XP docking of UNC0638 as a reference compound. The top 100 compounds were selected, based on docking scores from the central nervous system multiparameter optimization (CNS MPO) database of Chembridge Corporation, for further analysis. The docking scores of the top 100 compounds ranged from −13.592 kcal/mol to −10.105 kcal/mol. The Molecular Mechanics-Generalized Born Surface Area (MM-GBSA) dG binding affinity of these 100 compounds ranged from −116.98 kcal/mol to −51.09 kcal/mol. 9 molecules were selected based on the Glide XP dock score, MM-GBSA dG binding affinity, hydrogen bond mediated interaction with G9a active residues, i.e. Aspartate (Asp)1074, Asp1083, Leucine (Leu)1086, Asp1088, and hydrophobic interaction with Tyrosine (Tyr)1154, and Phenylalanine (Phe)1158[9,28–30] and scaffold novelty (Figure 3a, 5, S5, Table 1 and Table S1). These selected molecules were further subjected

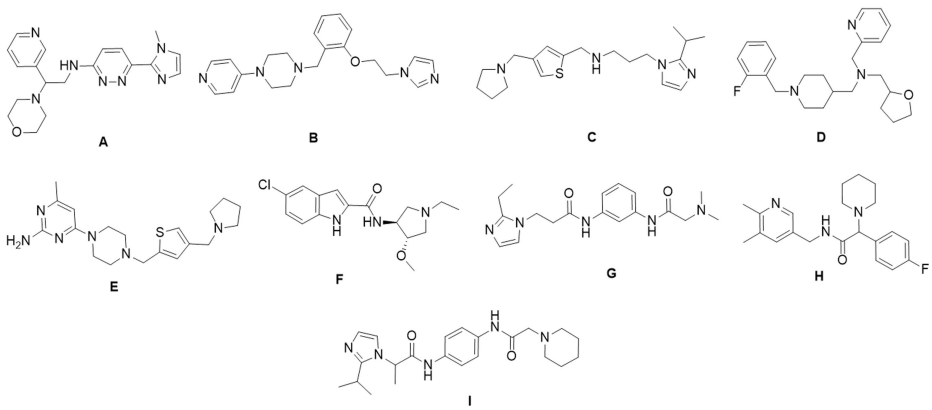

Figure 3. Structure of virtually screened and selected molecules.

© 2022 The Authors. ChemMedChem published by Wiley-VCH GmbH

18607187, 2022, 13, Downloaded from https://chemistry-europe.onlinelibrary.wiley.com/doi/10.1002/cmdc.202200002 by Readcube (Labtiva Inc.), Wiley Online Library on [18/02/2024]. See the Terms and Conditions (https://onlinelibrary.wiley.com/terms-and-conditions) on Wiley Online Library for rules of use; OA articles are governed by the applicable Creative Commons License

ChemMedChem
Research Article
doi.org/10.1002/cmdc.202200002
Chemistry Europe
European Chemical Societies Publishing

18607187, 2022, 13, Downloaded from https://chemistry-europe.onlinelibrary.wiley.com/doi/10.1002/cmdc.202200002 by Readcube (Labtiva Inc.), Wiley Online Library on [18/02/2024]. See the Terms and Conditions (https://onlinelibrary.wiley.com/terms-and-conditions) on Wiley Online Library for rules of use; OA articles are governed by the applicable Creative Commons License

to Pan-assay interference compounds (PAINS) filter and all were found to be non-PAINS.[31]

In vitro G9a inhibition assay

The percentages of G9a activity for the 10 selected molecules were determined at 100 μM S-adenosylmethionine (SAM) and peptide substrate using AlphaLISA® technology. These percentages were used to calculate the IC_{50}. As a control, we used the well-established G9a inhibitor, **UNC0638**. The IC_{50} against G9a of the UNC0638 was 9.4 nM, in accordance with reported studies that have described an $IC_{50} < 15$ nM. No significant inhibition was observed by A, and it was therefore considered as not active ($IC_{50} > 100$ nM). Meanwhile, **D** presented higher IC_{50} in comparison with either **UNC0638** or the other compounds ($IC_{50} = 10.5$ nM), and therefore these compounds were excluded for further studies. Compound **B** reached an IC_{50} equal to that of **UNC0638** ($IC_{50} = 9.4$ nM). The rest of compounds were at least 4-fold more potent as G9a inhibitors than **UNC0638** (IC_{50} **C** = 1.7 nM; IC_{50} **E** = 2.1 nM; IC_{50} **F** = 1.8 nM; IC_{50} **G** = 5.8 nM; IC_{50} **H** = 2.5 nM; IC_{50} **I** = 3.9 nM) (Table 1, Figure S2 and Table S2).

In silico ADMET analysis

Moreover, physicochemical descriptors and pharmaceutically relevant properties of the selected compounds were calculated with Schrödinger QikProp,[32] an ADME program useful for predicting the CNS-relevant drug properties. For instance, CNS activity was predicted using a scale, with the highest activity for those that scored +2, as was the case for **E**, **F**, **G**, and **I**; otherwise, the lowest activity was presented by **B**, **D**, with 0 as their score. Aqueous solubility (logS) could significantly affect the compounds' absorption and distribution. All selected compounds presented a similar value, fitting the recommended range (−6.5–0.5). Other properties calculated were total solvent accessible surface area (SASA), octanol/water partition coefficient (logPo/w), apparent Caco-2 cell permeability (PCaco), brain/blood partition coefficient, apparent MDCK cell permeability (PMDCK), skin permeability (logKp), binding to human serum albumin (logKhsa), Van der Waals surface area of polar atoms (PSA) and the number of Lipinski's rule of five violations. Moreover, human oral absorption (HOA) and the percent of HOA (%HOA) were predicted, resulting high in all of them, although the %HOA of **E** was not strictly superior to 80%. Additionally, hydrogen bond acceptor and donor (HBA, and HBD, respectively). A total of 3 compounds **A** (HBA = 9.2), **G** (HBA = 8.5), and **I** (HBA = 8.5) were not able to pass the qualifying limit for the number of HBA. UNC0638 is can also not pass the qualifying limit for SASA, logKhsa, and Lipinski rule of 5. To balance these properties, 6 compounds that showed CNS drug properties were considered potential hit compounds as drug candidates (Table S3).

In vivo efficacy studies in Caenorhabditis elegans (C. elegans)

Keeping in mind that our main goal in this work is to provide new and potent chemical scaffolds to treat AD pathology, we proposed to use the *C. elegans* model to evaluate their effect on amyloid-β (Aβ)-mediated neurodegeneration. First, food consumption by the *C. elegans* strain N2 (Wild-Type) (N2 (WT)) was assessed by the variation in the optical density (OD_{595}) of bacteria over time as a measure of compounds toxicity, expecting a normal development and well-being of the animals in each dose tested. Although **UNC0638** is a published compound described as a non-toxic compound in *in vivo* studies, we also used it as a control in the assay (Figure S3). The OD_{595} of all compounds at different concentrations was not different from the respective OD_{595} of the negative control in a statistically significant manner (Figure S3). Thus, all of them were classified as safe, as the OD_{595} decrease was parallel to that of the negative control samples, and visual inspection confirmed the average growth of the animals.

Locomotion assay

One of the best-characterized transgenic AD strains in *C. elegans* is the CL2006 strain, which contains the Punc-54::$A\beta_{1-42}$ transgene, showing a progressive adult-onset paralysis. Then, to establish a dose-response profile, the pharmacological impact of G9a inhibition was evaluated in a locomotion assay with this *C. elegans* strain. We performed a motility assay where animals were placed in the center of a seeded plate and allowed to explore the environment freely. After 1 min, the animals that did not cross 1 cm circumference were scored as motor defective. N2 (WT), and CL2006 strain were treated with dimethyl sulfoxide (DMSO) 1%, used as a vehicle, which should not cause a relevant locomotor defective phenotype. As expected, the percentage of locomotion defects in N2 (WT) animals was the lowest (~16%); whereas, as a result of the age-dependent paralysis, CL2006 strain showed a significant percentage of defects in their motility (~60%) (Figure S4a), verifying that locomotor behavior is statistically different between the two strains of *C. elegans* allowing us to study the impact of G9a inhibitors after chronic treatment. The motor index for each condition was calculated using the motor performance of Bristol (N2) (WT, 100%) and the transgenic AD strain (CL2006, 0%) animals as reference. The well-establishing inhibitor, **UNC0638**, was tested and used as a control compared to the other selected compounds (Figure 4).

By correlating *in silico* and *in vitro* G9a activity results, it is proved that interactions mediated by HBD, water bridge (WB), salt bridge (SB), and π-cation (π-cat) with the amino acid residues Asp1074, Asp1083, Asp 1084, Leu1086, Asp1088, and Tyr1154 are essential for the potent activity of G9a inhibitors. The pyrrolidine, morpholine, oxazepane, piperidine, piperazine, imidazole, pyridine, pyrimidine, indole, etc. moieties were present in the screened moiety. Nitrogen atoms present in these moieties interacted with G9a through a hydrogen bond, salt bridge, and π-cation interactions. These moieties interacted

© 2022 The Authors. ChemMedChem published by Wiley-VCH GmbH

ChemMedChem
Research Article
doi.org/10.1002/cmdc.202200002
Chemistry Europe
European Chemical Societies Publishing

18607187, 2022, 13, Downloaded from https://chemistry-europe.onlinelibrary.wiley.com/doi/10.1002/cmdc.202200002 by Readcube (Labtiva Inc.), Wiley Online Library on [18/02/2024]. See the Terms and Conditions (https://onlinelibrary.wiley.com/terms-and-conditions) on Wiley Online Library for rules of use; OA articles are governed by the applicable Creative Commons License

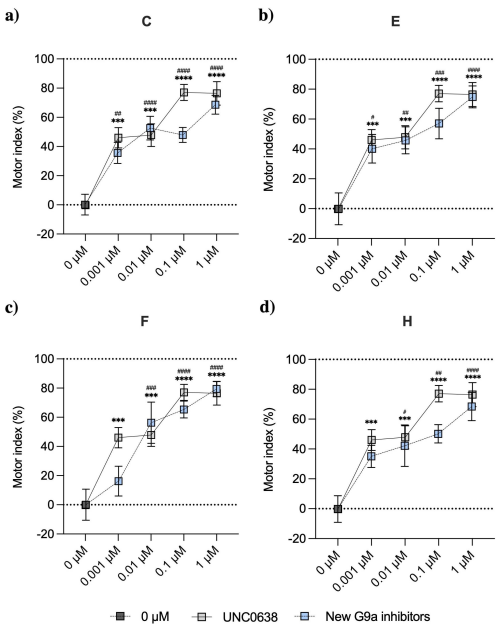

Figure 4. a-d) Treatment with G9a inhibitors ameliorates motor dysfunction of CL2006 worms. For dose-response: Values represented are mean ± Standard error of the mean (SEM); n = 3 with at least 90–100 worms in each group. Statistical analysis: One-Way ANOVA, followed by Dunnett post-hoc analysis. 0 µM Vs. UNC0638 treatment: ***$p < 0.001$; ****$p < 0.0001$. 0 µM Vs. new G9a inhibitor treatment: #$p < 0.05$; ##$p < 0.01$; ###$p < 0.001$; ####$p < 0.0001$.

with Asp1083, Asp1084, Asp1086, and Asp1088 (Figure 5, Figure S5). Although some of these interactions were present in compound **B**, the dose-response profile did not show an improved performance against the motor indexes of the control **UNC0638** (Figure S4b). Moreover, as aforementioned, we described that both IC_{50} were very similar, and it did not present better properties among the selected compounds, such as the CNS activity, justifying its exclusion from the study. NH of amide and 2° amine group in **C**, **F**, **G**, **H**, and **I** are equally important and responsible for interaction with Asp1083, Asp1086, and Asp1088. In parallel fashion, **E** showed SB interaction with the Asp1088, WB interaction with the Asp1083, and HBD interaction with Leu1086 being essential interactions for potent inhibitory activity of G9a. The dose-response profile of **I** showed the lowest motor index in the maximum and minimum dose tested, and in the case of **G** the motor index decreased progressively as the dose decreased (Figure S4c,d). However, due to **G** and **I** not passing the qualifying limit of all of the CNS drug properties described above, these compounds were discarded. **C**, **E**, **F**, and **H** motor index decreased progressively with the doses tested, ameliorating the paralysis presented by CL2006. Moreover, the motor indexes of each dose were not statistically different from the profile of the control UNC0638 (Figure 4a–d). The NH of amide group interacted with water bridge mediated hydrogen bond donor interaction with Asp1083 and Ser1084, NH of indole ring interacted through hydrogen bond donor interaction with Asp1088 of **F**; such interaction is not present in other compounds, and possibly because of this interaction, **F** is the most potent compound with an IC_{50} of 1.8 nM (Figure 5c, Figure S2e). In the same way, the motor index of **F** decreased progressively with the doses tested.

Effects of the best G9a inhibitor candidates on the repressive mark H3 K9me2

Considering the results described heretofore, we selected four compounds to go deeper into their effects on AD pathology. Firstly, to demonstrate that these compounds directly target G9a, we quantified the levels of its repressive mark H3 K9me2 after each drug treatment (Figure 6). First, we compared the ratio H3 K9me2/H3 total levels in the N2 (WT) strain compared to the AD transgenic strain (CL2006). Interestingly, the CL2006 presented higher levels of H3 K9me2, confirming the link between this repressive mark and AD pathology. Regarding each compound, we observed that the ratio H3 K9me2/H3 total levels after each drug intervention were reduced, suggesting that our compounds target G9a directly (Figure 6b).

Inhibition of Aβ aggregation in C. elegans

Furthermore, we evaluated the impact after the pharmacological inhibition of G9a treatment on the deposition of Aβ aggregates, as an important hallmark of AD, using Thioflavin-S (ThS) staining. The transgenic AD strain CL2006 is characterized by the expression of human $A\beta_{1\text{-}42}$ under the control of a muscle-specific promoter, making it suitable to answer this objective in our work. As we mentioned above, **UNC0638** was used as a positive control. Thus, as expected, **UNC0638** reduced the Aβ deposition by approximately 25%. For the four proposed candidates from our tested library, all of them showed the same tendency but in a statistically different way. Similarly, in **UNC0638**, the reduction in the number of deposits by compound **E** was approximately 25%. **F** reduced Aβ aggregation by approximately 40% compared to the vehicle group, being more effective in reducing Aβ aggregation than UNC0638. Unfortunately, treatment with **H** could not alleviate the aggregation of Aβ plaques (3%), although previous *in silico* and *in vitro* results were promising (Figure 7).

In vitro BBB penetration study

Then, we performed the parallel artificial membrane permeation assay (PAMPA) to predict BBB penetration (PAMPA-BBB), obtaining important information for compound selection and synthesis guidance for desirable CNS properties. The selected compounds **E**, **F**, and **H** had *in vitro* permeability (P_e) values of $2.2\times10^{-6}\pm0.1$ cm·s^{-1}, $10.9\times10^{-6}\pm0.4$ cm·s^{-1} and 17.4×10^{-6}

© 2022 The Authors. ChemMedChem published by Wiley-VCH GmbH

ChemMedChem
Research Article
doi.org/10.1002/cmdc.202200002
Chemistry Europe
European Chemical Societies Publishing

18607187, 2022, 13, Downloaded from https://chemistry-europe.onlinelibrary.wiley.com/doi/10.1002/cmdc.202200002 by Readcube (Labtiva Inc.), Wiley Online Library on [18/02/2024]. See the Terms and Conditions (https://onlinelibrary.wiley.com/terms-and-conditions) on Wiley Online Library for rules of use; OA articles are governed by the applicable Creative Commons License

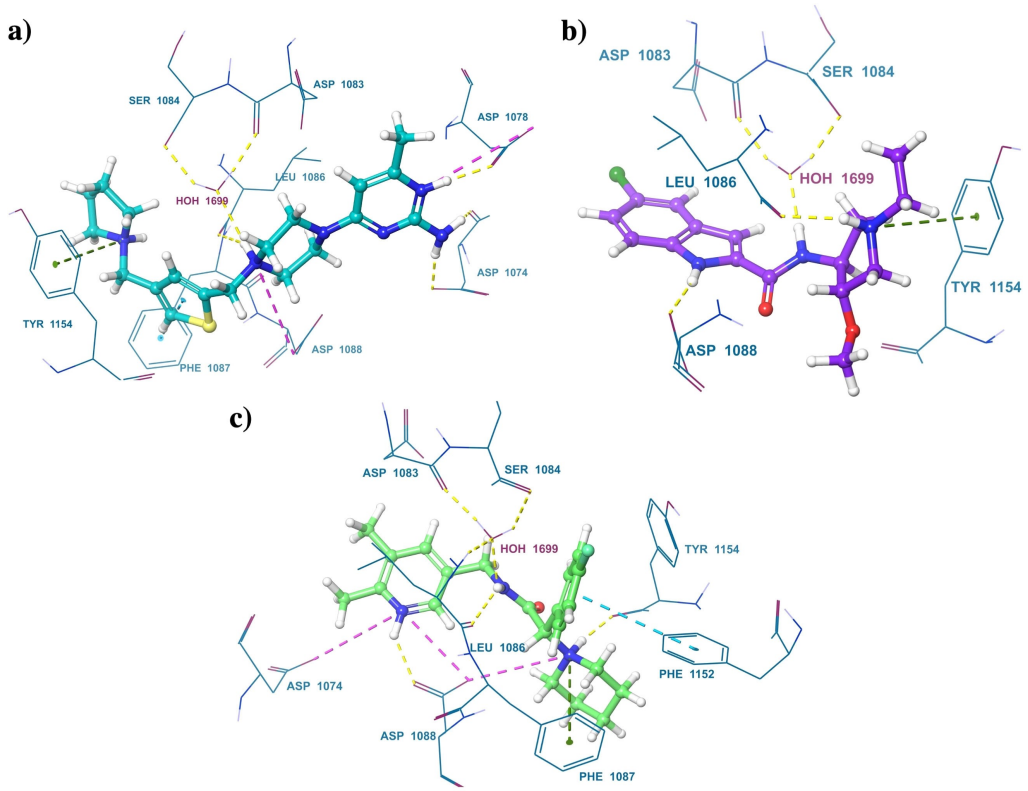

Figure 5. 3D interactions diagram of a) E–G9a, b) F–G9a, and c) H–G9a. Protein-ligand Interactions were denoted by a dotted line. Hydrogen bond: Yellow; Salt bridge: Pink; π-π stacking: blue; π-cation: Green.

± 2.4 cm·s^{-1}, respectively (Table 2). The compound **E** had lower P_e compromising its permeability, being lower than the P_e value of the control **UNC0638** (PAMPA – BBB $P_e = 6.2 \times 10^{-6}$ cm·s^{-1}). Nevertheless, the compounds **F** and **H** presented positive BBB permeation, being able to cross the BBB and reach their biological target in the CNS. Therefore, the compound **F** is a promising tool for *in vivo* AD studies with mammalian models.

Table 2. Permeability (P_e 10^{-6} cm·s^{-1}) in the PAMPA-BBB assay of 14 commercial drugs and tested compounds and predictive penetration in the CNS.

Compound	Bibliography value[33]	Compound	Bibliography value[33]
Verapamil	16.0	25.9 ± 0.8	
Testosterone	17.0	26.6 ± 0.9	
Corticosterone	5.1	6.7 ± 0.1	
Clonidine	5.3	6.5 ± 0.06	
Ofloxacin	0.8	0.1 ± 0.09	
Lomefloxacin	0.0	0.8 ± 0.05	
Progesterone	9.3	14.7 ± 0.3	
Promazine	8.8	13.8 ± 0.4	
Imipramine	13.0	16.8 ± 0.3	
Hydrocortisone	1.9	1.4 ± 0.06	
Piroxicam	2.5	2.0 ± 0.08	
Desipramine	12.0	17.8 ± 0.2	
Cimetidine	0.0	0.7 ± 0.02	
Norfloxacin	0.1	8.8 ± 0.4	
E		2.2 ± 0.1	CNS +/-
F		10.9 ± 0.4	CNS +
H		17.4 ± 2.4	CNS +

Evaluation of EHMT1 (GLP) activity by luminescence assay

Last, but not least, further characterization of the best candidates was performed assessing their selectivity. Thus, we tested them against EHMT1 (G9a-like protein, GLP). Most remarkably, all of the new G9a inhibitors showed very low, almost non-existent, specificity against EHMT1 compared to the well-established **UNC0638** (Table 3). We found that **E** did not inhibit EHMT1 from to 0.01 μM 10 μM. In contrast, compounds **F** and **H** showed slight activity against EHMT1 at low doses.

© 2022 The Authors. ChemMedChem published by Wiley-VCH GmbH

ChemMedChem
Research Article
doi.org/10.1002/cmdc.202200002
Chemistry Europe
European Chemical Societies Publishing

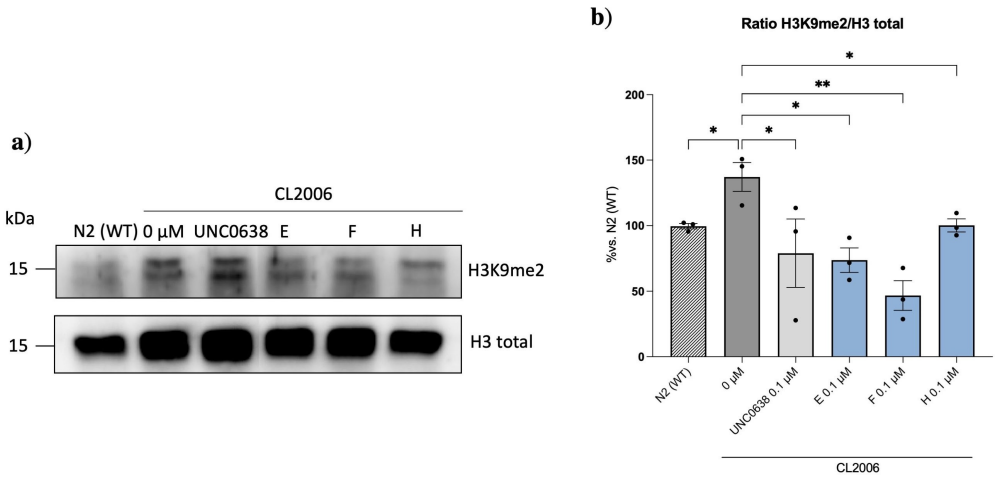

Figure 6. a-b) Representation of western blotting and quantification of the total H3 K9me/H3 ratio after treatments with the best candidates to inhibit G9a. Values represented are mean ± Standard error of the mean (SEM); n = 3 with at least 200 worms in each group. Statistical analysis: One-Way ANOVA, followed by Dunnett post-hoc analysis: 0 µM Vs. UNC0638, E, and F treatment: *p < 0.05;**p < 0.01. Statistical analysis: Unpaired t-test: N2 (WT) Vs. 0 µM: *p < 0.05; 0 µM Vs. H: *p < 0.05.

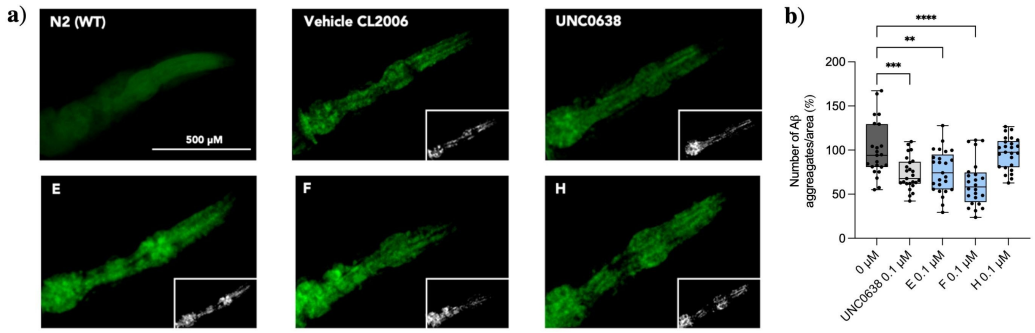

Figure 7. a) Representative images from each group tested. b) Quantification of Thioflavin S-positive particles in the head region of CL2006 strain. Values represented are mean ± Standard error of the mean (SEM); n = 3 with 25 worms in each group. Statistical analysis: One-Way ANOVA, followed by Dunnett post-hoc analysis. Vehicle Vs. new G9a inhibitor treatment: **p < 0.001; ***p < 0.001; ****p < 0.0001.

Table 3. Activity against of EHMT1 (GLP) measured by luminescence assay.

Compound	% Inhibition of EHMT1 0.01 µM	0.1 µM	1 µM	10 µM
UNC0638	2_±1	41_±4	66_±4	84_±1
E	2_±1	4_±2	3_±3	8_±3
F	26_±5	14_±3	4_±2	1_±2
H	14_±1	7_±1	4_±1	2_±1

However, they presented a very low percentage, and furthermore this trend was not observed at high doses.

Conclusion

To sum up, we have identified new G9a inhibitors through *in silico* and *in vitro* screens, with different scaffolds to those previously published inhibitors, and more potent. **E**, **F**, and **H** were further studied in *in vivo* assays. Interestingly, our selected compounds were able to reduce H3 K9me2 levels similar to **UNC0638**, suggesting the G9a is the direct target for them. On the one hand, the effect on the impact of Aβ aggregates reduction was similar for **UNC0638** and **E**. Also, this compound showed promising pharmacokinetics results; however, its predicted BBB-permeability was lower than **UNC0638**, possibly because of decreased lipophilicity due to lower logPo/w, logBB

© 2022 The Authors. ChemMedChem published by Wiley-VCH GmbH

18607187, 2022, 13, Downloaded from https://chemistry-europe.onlinelibrary.wiley.com/doi/10.1002/cmdc.202200002 by Readcube (Labtiva Inc.), Wiley Online Library on [18/02/2024]. See the Terms and Conditions (https://onlinelibrary.wiley.com/terms-and-conditions) on Wiley Online Library for rules of use; OA articles are governed by the applicable Creative Commons License

ChemMedChem
Research Article
doi.org/10.1002/cmdc.202200002
Chemistry Europe
European Chemical Societies Publishing

18607187, 2022, 13, Downloaded from https://chemistry-europe.onlinelibrary.wiley.com/doi/10.1002/cmdc.202200002 by Readcube (Labtiva Inc.), Wiley Online Library on [18/02/2024]. See the Terms and Conditions (https://onlinelibrary.wiley.com/terms-and-conditions) on Wiley Online Library for rules of use; OA articles are governed by the applicable Creative Commons License

value, and higher PSA (Table S3). On the other hand, **H** did not show a positive effect related to Aβ deposition, albeit the *in silico* and *in vitro* results were promising, achieving the best predicted BBB permeability to date published for a G9a inhibitor. Nevertheless, it is noteworthy that compound **F** reduced Aβ deposition by approximately 40%, thereby suggesting a promising role for this compound in AD pathology. Strikingly, **F** has an $IC_{50} = 1.8$ nM (Figure S2e), and none of the previously reported G9a inhibitors have such nanomolar efficacy. Besides, in comparison to the well-established G9a inhibitor (**UNC0638**), **F** exhibited a higher permeability to BBB, as well as a higher selectivity for G9a, as it exhibited low activity against EHMT1. Therefore, these outcomes highlight an important difference and reinforce the potential use in neurodegenerative diseases of these novel G9a inhibitors. Hereinafter, future perspective will be to address the biological activity of our best candidate, **F** (5-chloro-N-((3S,4S)-1-ethyl-4-methoxypyrrolidin-3-yl)-1H-indole-2-carboxamide) and its biological differentiation from other known G9a inhibitors. Then, our study will help future research establish the structure-activity relationship (SAR) of **F** analogs to G9a, improving potency and BBB permeability as well as reducing one of the main AD hallmarks the Aβ plaques.

Experimental Section

Structure-based virtual screening

PDB id of G9a for developing docking model was selected based on resolution, sequence length, PDB validation, and co-crystallized molecule. The crystal structure of G9a bound to MS012 (Figure 1) (PDB ID: 5TTF) was retrieved from the RCSB portal.[34] Refinement of protein was performed using a protein preparation wizard. The active site was defined around the co-crystallized MS012 using the receptor grid generation module of Glide.[35] The protocol resulting from a crystal structure (PDB ID: 5TTF) was validated using receiver operator characteristic (ROC) metrics and docking of co-crystallized MS012 into the G9a (5TTF). The ROC analysis actives dataset was merged with the Schrodinger decoy set containing 1000 drug-like decoy compounds.[36,37] The combined dataset was docked into the protein using the SP docking method in glide. ROC plots were plotted using Enrichment Calculator in Maestro.[38] A Chembridge CNS MPO library of 496.644 compounds was downloaded from the Chembridge portal were prepared with LigPrep using OPLS 2005 forcefield.[35] The prepared Chembridge CNS MPO library was screened using virtual screening workflow docking protocols (HTVS, SP, and XP docking) of the Schrodinger software package on the selected crystal structure (PDB ID- 5TTF) carrying forward 10% each from HTVS to SP and SP to XP and top 100 kept in XP docking. These selected top 100 molecules in XP docking were subjected to the binding affinity (dG) calculation using the Prime-MM-GBSA method. From these top 100 molecules, 9 molecules were selected based on the Glide XP docking score, dG of binding, nature of interaction with G9a active site key residues (Asp1074, Asp1083, and Asp1088),[29,34,39] and scaffold novelty.

In silico analysis of CNS drugability

QikProp module of the Schrodinger software package was used for determining the drug properties. The 9 best scoring hits were taken for study resulting in basic physicochemical properties and *in silico* pharmacokinetic for CNS drugability.[32,40]

Compound preparation

G9a inhibitors were serially diluted between 5 nM and 0.001 nM in 100% DMSO (Sigma, St. Louis, USA). Then, respective concentrations were subsequently diluted in MilliQ purified water to reach a final concentration ranging between 50 and 0.001 μM in 1% DMSO in well.

G9a homogenous assay

G9a activity was measured using the G9a Homogeneous Assay Kit (Catalog #52051, BPS Bioscience, San Diego, CA, USA). The G9a Homogeneous Assay Kit was set up in AlphaLISA® format on an optiplate-384-wells. Briefly, a sample containing the G9a enzyme is incubated with the biotinylated substrate plus inhibitor solution for two hours. Next, acceptor beads and primary antibody is added, followed by donor beads. Finally, the Alpha-counts were read using an AlphaScreen microplate reader. The experiment was run per triplicate.

$$\text{G9a activity } (\%) = (C - Cb)/(Ct - Cb) \times 100$$

Ct = The chemiluminescence reading in the absence of the compound. The data set here is defined as 100% activity in the absence of the compound.

Cb = The chemiluminescence reading in absence of enzyme. The data set here is defined as 0% activity in the absence of the enzyme.

C = The chemiluminescence reading in the presence of the compound.

C. elegans strains, and maintenance

The WT *C. elegans* strain (N2), and the transgenic CL2006 (dvIs2 [pCL12(unc-54/human Aβ peptide 1–42 minigene) + rol-6(su1006)]) provided by the *C. elegans* Genetic Center were used. Standard methods were used for culturing and observing *C. elegans*. N2 were propagated at 20 °C, while CL2006 worms were maintained at 16 °C in a temperature-controlled incubator on solid nematode growth medium (NGM) seeded with Escherichia coli (E. coli) OP50 strain as a food source.

Food clearance assay

N2 (WT) worms were subjected to a drug assay in liquid format. Worms were grown with continuous shaking at 180 rpm at 20 °C for 7 days. Each well contained a final volume of 60 μL, comprising 25–30 animals in the larva 1 (L1) stage diluted in S-medium solution, G9a inhibitor at the appropriate dose, and OP50 inactivated by freeze-thaw cycles suspended in S-medium complete solution to a final OD_{595} of 0.7 measured in the microplate reader. Tested concentrations ranged between 1 μM to 0.001 μM. For control wells were used DMSO 1%(vehicle) and DMSO 5% (toxic condition); and for blank wells were used S-medium and S-medium complete only, without eggs or OP50, respectively. The effect of compounds on *C. elegans* physiology was monitored by the rate at which the OP50 suspension was consumed, as a readout for *C. elegans* growth, survival, or fecundity. The OD_{595} was measured daily. Assays were run in triplicates (n = 3), with a total of at least 150 animals tested per compound concentration.

© 2022 The Authors. ChemMedChem published by Wiley-VCH GmbH

ChemMedChem
Research Article
doi.org/10.1002/cmdc.202200002
Chemistry Europe
European Chemical Societies Publishing

18607187, 2022, 13, Downloaded from https://chemistry-europe.onlinelibrary.wiley.com/doi/10.1002/cmdc.202200002 by Readcube (Labtiva Inc.), Wiley Online Library on [18/02/2024]. See the Terms and Conditions (https://onlinelibrary.wiley.com/terms-and-conditions) on Wiley Online Library for rules of use; OA articles are governed by the applicable Creative Commons License

Locomotion assay

Locomotion assay of G9a inhibitors was assessed to obtain dose-response profile, evaluating the impact of the pharmacology treatment in motor dysfunction presented by the transgenic strains CL2006. Nematodes were synchronized by alkaline hypochlorite treatment, and drug assay was performed as described above, except for the OP50 bacteria OD_{595} adjusted to 0.9, and the duration of the treatment was 5 days. N2 (WT), and the transgenic strain CL2006 were treated in liquid media for 4 days at 20 °C and 180 rpm, starting at the L1 stage. On day 5 of age, worms were transferred from the 96-well plates onto an unseeded NGM plate for 45 minutes before starting the trial, allowing the plates to dry and worms. Locomotion assays were performed in 30 mm NGM plates, in which the whole surface of the plate was covered by OP50. 5 to 10 adult nematodes were placed in the center of a circle (with 1 cm of diameter) in the seeded 30 mm NGM plates. After 1 min, the number of animals remaining inside the circle was scored as a locomotor defect. Motor behavior assays were run in triplicates (n = 3), with a total of at least 100 animals tested per compound concentration. Motor index establishes a score where treated animals showing the same motor defect as CL2006 have an index of 0%. By contrast, when animals improve motor behavior comparable to the WT (N2) they get an index of 100%. All the results shown in the figures are calculated using the following formula:

$$\text{Motor index } (\%) = (\text{LD CL2006}_{\text{vehicle}} - \text{LD CL2006}_{\text{drug}}) \,/\, (\text{LD CL2006}_{\text{vehicle}} - \text{LD WT}_{\text{vehicle}}) \times 100$$

LD = locomotion defective

Thioflavin-S staining Aβ aggregation

After 5 days of treatment, adult CL2006 *C. elegans* were fixed in 4% Paraformaldehyde/Phosphate-buffered saline (PBS) (pH 7.5), for 24 hours at 4 °C. Then, worms were permeabilized in 5% fresh β-mercaptoethanol, 1% Triton X-100, 125 mm Tris (pH 7.5), at 37 °C for another 24 hours. On the last day, nematodes were stained with 0.125% Thioflavin-S (ThS) (Sigma, CAS# 1326–12-1) in 50% ethanol (EtOH) for 2 min, destained in 50% EtOH for 2 min, washed 3 times with PBS. To prepare the glass slide for microscopy, approximately 10 μL volume was transferred on a droplet of Fluoromount G (Electron Microscopy Sciences, CAT#17984-25). Fluorescence images were acquired using a 20 Å~ objective of a fluorescence microscope. Aβ in the head region of worms were quantified by counting the number of Th–S positive spots using ImageJ and were expressed as Aβ deposits/anterior area. Aβ aggregates were scored by an investigator blinded to G9a inhibitors treatments.

Western blotting

To determine the ratio of H3 K9me2/H3 total N2 (WT) and CL2006 animals were incubated in liquid culture with vehicle (DMSO 1%), or 0.1 μM of G9a inhibitor in a 96-well plate format as already mentioned. For chronic treatment, four-day-old animals were collected with M9 buffer. Histone extraction was performed following the manufacturer's instructions (EpiQuik Total Histone Extraction HT Kit, EpiGentek, #OP-0007-192). The samples were resolved in a 14% SDS-gel, as previously described.[12] To capture chemiluminescence signals were used Amersham Imager 680 and Western blot quantifications were performed using ImageLab software (Bio-Rad). Immunoblots were probed with anti-H3 K9me2 (1:1000) (Epigentek, #A-4035), and anti-H3 total (1:1000) (Cell signaling, #9715).

PAMPA-BBB assay

To evaluate the brain penetration of the different compounds, a parallel artificial membrane permeation assay for BBB was used, following the method described by Di et al..[33] The *in vitro* P_e of fourteen commercial drugs through lipid extract of porcine brain membrane together with the test compounds were determined. Commercial drugs and assayed compounds were tested using a mixture of PBS:EtOH (70:30). Assay validation was made by comparing the experimental permeability with the reported values of the commercial drugs by bibliography, and linear correlation between experimental and reported permeability of the fourteen commercial drugs using the parallel artificial membrane permeation assay was evaluated ($y = 1.572x - 1.147$; $R^2 = 0.9452$). From this equation and taking into account the limits established by Di et al.[33] for BBB permeation, we established the ranges of permeability as compounds of high BBB permeation (CNS+): P_e (10^{-6} cm·s^{-1}) > 5.14; compounds of low BBB permeation(CNS-): P_e (10^{-6} cm·s^{-1}) < 1.99 and compounds of uncertain BBB permeation(CNS+/−):5.14 Pe (10^{-6} cm·s^{-1}) > 1.99.

EHMT1 (GLP) chemiluminescence assay kit

The assay was carried out using EHMT1 (GLP) Chemiluminescent Assay kit. Compounds were added on a 96-well plate precoated with histone substrate supplied by kit. 30 μL of master mixture SAM were added and the reaction was initiated adding 20 μL of diluted EHMT1 (GLP) enzyme. The reaction was incubated at room temperature (RT) for 1 hour. The plate was washed three times with 200 μl TBST buffer. 100 μL of Blocking buffer were added to every well and the plate was incubated at RT for 10 minutes with shaking. Supernatant was removed and 100 μl of Primary antibody were added per well. The plate was incubated at RT for 1 hour with slow shaking. The plate was washed three times with 200 μl TBST buffer. 100 μL of Blocking buffer were added to every well and the plate was incubated at RT for 10 minutes with shaking. 100 μl of Secondary HRP-labeled antibody were added per well and the plate was incubated at RT for 30 minutes with slow shaking. The plate was washed three times with 200 μl TBST buffer. Finally, 100 μl of substrate mix were added and the luminescence was measurement with integration time of 1 second in in Perkin Elmer EnSpire Multimode plate reader.

Statistical analysis

Data analysis was conducted using GraphPad Prism ver. 9 statistical software. The statistical outliers were identified with Grubb's test and excluded from the analysis. Group comparisons were carried out with a One-way Analysis of variance (ANOVA), followed by the Dunnett post hoc test. In some cases, comparison between groups was also performed by unpaired t-test or One-way ANOVA, followed by Fisher's LSD post hoc test. For the calculation of IC_{50}, non-linear regressions were performed. Regarding food clearance assay, results were compared non-linear regression model for sigmoidal curves against the negative control. Values are shown as the mean ± Standard error of the mean (SEM) of at least n = 3. Statistical significance was considered when p values were < 0.05.

© 2022 The Authors. ChemMedChem published by Wiley-VCH GmbH

ChemMedChem
Research Article
doi.org/10.1002/cmdc.202200002
Chemistry Europe
European Chemical Societies Publishing

18607187, 2022, 13, Downloaded from https://chemistry-europe.onlinelibrary.wiley.com/doi/10.1002/cmdc.202200002 by Readcube (Labtiva Inc.), Wiley Online Library on [18/02/2024]. See the Terms and Conditions (https://onlinelibrary.wiley.com/terms-and-conditions) on Wiley Online Library for rules of use; OA articles are governed by the applicable Creative Commons License

Acknowledgements

B.S.C. and S. are grateful to Council for Scientific and Industrial Research, India, for Senior Research Fellowship (Grant No. 09/1131(0004)/2016-EMR-I and 09/1131(0026)/2019-EMR-I) and Central University of Rajasthan for providing computational facilities. A.B-S acknowledge the Agència de Gestió d'Ajuts Universitaris i de Recerca (AGAUR) for her FI-SDUR fellowship (2021 FISDU 00182). J.C-A acknowledge the Ministry of Economy and Competitiveness (MINECO) for her FPI fellowship (MDM-2017-0729-19-2). C. elegans *strains were provided by the Caenorhabditis Genetics Center (CGC), which is funded by NIH Office of Research Infrastructure Programs (P40 OD010440). We thank Gemma Triola from the Institute of Advanced Chemistry of Catalonia (IQAC-CSIC) and her lab for offering the possibility of using the AlphaScreen microplate reader.*

Conflict of Interest

The authors declare no conflict of interest.

Data Availability Statement

The data that support the findings of this study are available from the corresponding author upon reasonable request.

Keywords: Alzheimer's disease · epigenetics · G9a methyltransferase · amyloid-β · structure based virtual screening

[1] Z. Zhao, A. Shilatifard, *Genome Biol.* **2019**, *20*, 1–16.
[2] P. J. Hamilton, E. J. Nestler, *Curr. Opin. Neurobiol.* **2019**, *59*, 128–136.
[3] J. Richetto, U. Meyer, *Biol. Psychiatry* **2020**.
[4] A. Berson, R. Nativio, S. L. Berger, N. M. Bonini, *Trends Neurosci.* **2018**, *41*, 587–598.
[5] A. Portela, M. Esteller, *Nat. Biotechnol.* **2010**, *28*, 1057–1068.
[6] K. P. Bhat, H. Ü. Kaniskan, J. Jin, O. Gozani, *Nat. Rev. Drug Discovery* **2021**, *20*, 265–286.
[7] M. Tachibana, J. Ueda, M. Fukuda, N. Takeda, T. Ohta, H. Iwanari, T. Sakihama, T. Kodama, T. Hamakubo, Y. Shinkai, *Genes Dev.* **2005**, *19*, 815–826.
[8] S. R. Shankar, A. G. Bahirvani, V. K. Rao, N. Bharathy, J. R. Ow, R. Taneja, *Epigenetics* **2013**, *8*, 16–22.
[9] M. R. C. Charles, A. Dhayalan, H.-P. Hsieh, M. S. Coumar, *Future Med. Chem.* **2019**, *11*, 993–1014.
[10] H. Cao, L. Li, D. Yang, L. Zeng, X. Yewei, B. Yu, G. Liao, J. Chen, *Eur. J. Med. Chem.* **2019**, *179*, 537–546.
[11] C. Poulard, L. M. Noureddine, L. Pruvost, M. Le Romancer, *Life* **2021**, *11*, 1082.
[12] C. Griñán-Ferré, L. Marsal-García, A. Bellver-Sanchis, S. M. Kondengaden, R. C. Turga, S. Vázquez, M. Pallàs, *Aging (Albany NY)* **2019**, *11*, 11591–11608.
[13] Y. Zheng, A. Liu, Z. J. Wang, Q. Cao, W. Wang, L. Lin, K. Ma, F. Zhang, J. Wei, E. Matas, J. Cheng, G. J. Chen, X. Wang, Z. Yan, *Brain* **2019**, *142*, 787–807.
[14] J. L. T. Han, K. K. L. Pang, S. R. X. Ang, M. Sharma, S. Sajikumar, *Transl. Neurodegener.* **2021**, *10*, 1–3.
[15] O. Rabal, J. A. Sánchez-Arias, E. San Jose-Eneriz, X. Agirre, I. de Miguel, L. Garate, E. Miranda, E. Saez, S. Roa, J. A. Martínez-Climent, *J. Med. Chem.* **2018**, *61*, 6546–6573.
[16] O. Rabal, E. San José-Enériz, X. Agirre, J. A. Sánchez-Arias, I. de Miguel, R. Ordoñez, L. Garate, E. Miranda, E. Sáez, A. Vilas-Zornoza, *J. Med. Chem.* **2021**, *64*, 3392–3426.
[17] C. Milite, A. Feoli, J. R. Horton, D. Rescigno, A. Cipriano, V. Pisapia, M. Viviano, G. Pepe, G. Amendola, E. Novellino, S. Cosconati, X. Cheng, S. Castellano, G. Sbardella, *J. Med. Chem.* **2019**, *62*, 2666–2689.
[18] R. F. Sweis, M. Pliushchev, P. J. Brown, J. Guo, F. Li, D. Maag, A. M. Petros, N. B. Soni, C. Tse, M. Vedadi, *ACS Med. Chem. Lett.* **2014**, *5*, 205–209.
[19] W.-L. Chen, Z.-H. Wang, T.-T. Feng, D.-D. Li, C.-H. Wang, X.-L. Xu, X.-J. Zhang, Q.-D. You, X.-K. Guo, *Bioorg. Med. Chem.* **2016**, *24*, 6102–6108.
[20] J. Chen, X. Lin, K. J. Park, K. R. Lee, H.-J. Park, *J. Comput.-Aided Mol. Des.* **2018**, *32*, 917–928.
[21] K. Katayama, K. Ishii, E. Tsuda, K. Yotsumoto, K. Hiramoto, M. Suzuki, I. Yasumatsu, W. Igarashi, M. Torihata, T. Ishiyama, *Bioorg. Med. Chem. Lett.* **2020**, *30*, 127475.
[22] D. Greiner, T. Bonaldi, R. Eskeland, E. Roemer, A. Imhof, *Nat. Chem. Biol.* **2005**, *1*, 143–145.
[23] E. Iwasa, Y. Hamashima, S. Fujishiro, E. Higuchi, A. Ito, M. Yoshida, M. Sodeoka, *J. Am. Chem. Soc.* **2010**, *132*, 4078–4079.
[24] F. L. Cherblanc, K. L. Chapman, J. Reid, A. J. Borg, S. Sundriyal, L. Alcazar-Fuoli, E. Bignell, M. Demetriades, C. J. Schofield, P. A. DiMaggio Jr, *J. Med. Chem.* **2013**, *56*, 8616–8625.
[25] S. Fujishiro, K. Dodo, E. Iwasa, Y. Teng, Y. Sohtome, Y. Hamashima, A. Ito, M. Yoshida, M. Sodeoka, *Bioorg. Med. Chem. Lett.* **2013**, *23*, 733–736.
[26] F. Liu, X. Chen, A. Allali-Hassani, A. M. Quinn, G. A. Wasney, A. Dong, D. Barsyte, I. Kozieradzki, G. Senisterra, I. Chau, A. Siarheyeva, D. B. Kireev, A. Jadhav, J. M. Herold, S. V. Frye, C. H. Arrowsmith, P. J. Brown, A. Simeonov, M. Vedadi, J. Jin, *J. Med. Chem.* **2009**, *52*, 7950–7953.
[27] Y. Chang, T. Ganesh, J. R. Horton, A. Spannhoff, J. Liu, A. Sun, X. Zhang, M. T. Bedford, Y. Shinkai, J. P. Snyder, X. Cheng, *J. Mol. Biol.* **2010**, *400*, 1–7.
[28] F. Liu, X. Chen, A. Allali-Hassani, A. M. Quinn, G. A. Wasney, A. Dong, D. Barsyte, I. Kozieradzki, G. Senisterra, I. Chau, A. Siarheyeva, D. B. Kireev, A. Jadhav, J. M. Herold, S. V. Frye, C. H. Arrowsmith, P. J. Brown, A. Simeonov, M. Vedadi, J. Jin, *J. Med. Chem.* **2009**, *52*, DOI 10.1021/jm901543 m.
[29] M. Vedadi, D. Barsyte-Lovejoy, F. Liu, S. Rival-Gervier, A. Allali-Hassani, V. Labrie, T. J. Wigle, P. A. DiMaggio, G. A. Wasney, A. Siarheyeva, A. Dong, W. Tempel, S.-C. Wang, X. Chen, I. Chau, T. J. Mangano, X. Huang, C. D. Simpson, S. G. Pattenden, J. L. Norris, D. B. Kireev, A. Tripathy, A. Edwards, B. L. Roth, W. P. Janzen, B. A. Garcia, A. Petronis, J. Ellis, P. J. Brown, S. V. Frye, C. H. Arrowsmith, J. Jin, *Nat. Chem. Biol.* **2011**, *7*, DOI 10.1038/nchembio.599.
[30] M. Ramya Chandar Charles, H.-P. Hsieh, M. Selvaraj Coumar, *J. Biomol. Struct. Dyn.* **2019**, *37*, DOI 10.1080/07391102.2018.1491422.
[31] J. B. Baell, G. A. Holloway, *J. Med. Chem.* **2010**, *53*, 2719–2740.
[32] A. K. Ghose, T. Herbertz, R. L. Hudkins, B. D. Dorsey, J. P. Mallamo, *ACS Chem. Neurosci.* **2012**, *3*, DOI 10.1021/cn200100 h.
[33] L. Di, E. H. Kerns, K. Fan, O. J. McConnell, G. T. Carter, *Eur. J. Med. Chem.* **2003**, *38*, 223–232.
[34] Y. Xiong, F. Li, N. Babault, A. Dong, H. Zeng, H. Wu, X. Chen, C. H. Arrowsmith, P. J. Brown, J. Liu, *J. Med. Chem.* **2017**, *60*, 1876–1891.
[35] G. Madhavi Sastry, M. Adzhigirey, T. Day, R. Annabhimoju, W. Sherman, *J. Comput.-Aided Mol. Des.* **2013**, *27*, DOI 10.1007/s10822-013-9644–8.
[36] R. A. Friesner, J. L. Banks, R. B. Murphy, T. A. Halgren, J. J. Klicic, D. T. Mainz, M. P. Repasky, E. H. Knoll, M. Shelley, J. K. Perry, D. E. Shaw, P. Francis, P. S. Shenkin, *J. Med. Chem.* **2004**, *47*, DOI 10.1021/jm0306430.
[37] T. A. Halgren, R. B. Murphy, R. A. Friesner, H. S. Beard, L. L. Frye, W. T. Pollard, J. L. Banks, *J. Med. Chem.* **2004**, *47*, DOI 10.1021/jm030644 s.
[38] J.-F. Truchon, C. I. Bayly, *J. Chem. Inf. Model.* **2007**, *47*, DOI 10.1021/ci600426e.
[39] F. Liu, X. Chen, A. Allali-Hassani, A. M. Quinn, G. A. Wasney, A. Dong, D. Barsyte, I. Kozieradzki, G. Senisterra, I. Chau, *J. Med. Chem.* **2009**, *52*, 7950–7953.
[40] R. Malik, B. S. Choudhary, S. Srivastava, P. Mehta, M. Sharma, *J. Biomol. Struct. Dyn.* **2017**, *35*, DOI 10.1080/07391102.2016.1253503.

Manuscript received: January 1, 2022
Revised manuscript received: April 11, 2022
Accepted manuscript online: April 12, 2022
Version of record online: May 19, 2022

© 2022 The Authors. ChemMedChem published by Wiley-VCH GmbH

ChemMedChem

Supporting Information

Structure-Based Virtual Screening and *in vitro* and *in vivo* Analyses Revealed Potent Methyltransferase G9a Inhibitors as Prospective Anti-Alzheimer's Agents

Aina Bellver-Sanchis[+], Bhanwar Singh Choudhary[+], Júlia Companys-Alemany, Sukanya, Pedro A. Ávila-López, Antón Leandro Martínez Rodríguez, Jose Manuel Brea Floriani, Ruchi Malik, Mercè Pallàs, Belén Pérez, and Christian Griñán-Ferré*

Table of contents

Page S2 Figure S1: Superimposed co-crystallized and docked MS012.

Page S3 Table S1: 2D interaction diagram of selected screened molecules.

Page S4 Figure S2: IC_{50} curve for each compound tested Vs. well established G9a inhibitor, UNC0638.

Page S5 Table S2: Raw data of the percentage of G9a activity.

Page S6 Table S3: Predicted QikProp properties for CNS drugability.

Page S7 Figure S3: Toxicity of G9a inhibitors through the food clearance assay.

Page S8 Figure S4: Locomotor defect exhibited by N2 strain and the transgenic AD strain, CL2006. Dose-response profile of the excluded G9a inhibitors.

Page S9 Figure S5: 3D interaction diagram of a) A-G9a, b) B-G9a, c) C-G9a. d) D-G9a, e) G-G9a, and f) I-G9a.

Page S10-S18 LC-MS purity data for screened compounds.

Page S19 PAINS analysis results

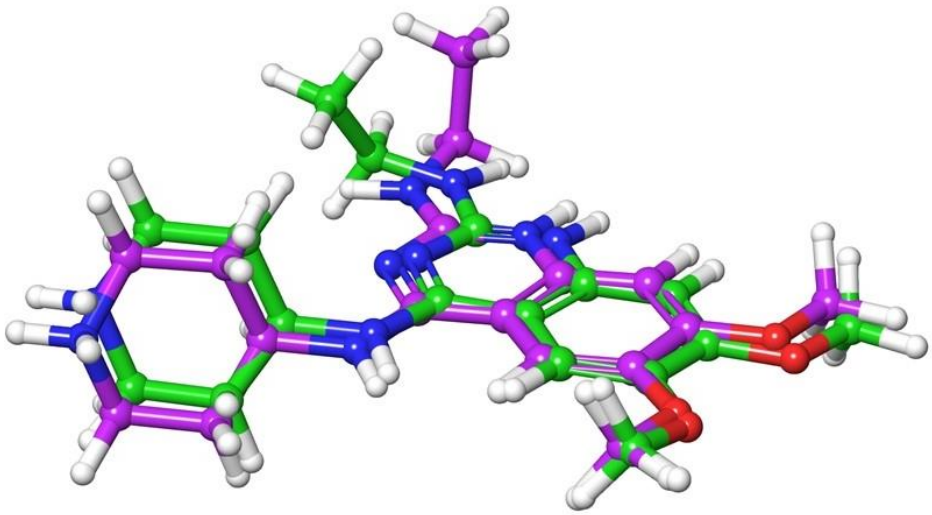

Figure S1. Superimposed co-crystallized (green) and docked (violet) MS012.

Table S1. 2D interaction diagram of selected screened molecules.

S. No.	ID	Code	Interaction type & Interacting residues
1	29352686	A	WB: Asp1083, Ser1084; π-π: Phe1087; π-cat: Tyr1154; SB: Asp1083; HBD: Asp1083, Leu1086
2	55607373	B	SB: Asp1074, Asp1078, Asp1083, Asp1088; π-π: Tyr1067, phe1087, Tyr1154; HBD: Asp1078, Ser1084, Leu1086
3	43631981	C	WB: Asp1083, Ser1084; π-π: Phe1087; SB: Asp1074, Asp1088; π-cat: Tyr1154, Arg1175, HBD: Asp1074, Asp1088, Leu1086
4	15589586	D	SB: Asp1082; HBD: Leu1086, Asp1088
5	55517816	E	SB: Asp1088; π-π: Phe1087; π-cat: Tyr1154; WB: Asp1083, Ser1084; HBD: Asp1074, Asp1078, Leu1086
6	31871543	F	WB: Asp1083, Ser1084; π-cat: Tyr1154; HBD: Leu1086, Asp1088
7	20839262	G	WB: Leu1086; HBD: Asp1078, Asp1088; SB: Asp1083
8	27379251	H	WB: Asp1083, Ser1084, Leu1086; SB: Asp1074, Asp1088; π-cat: Phe1087; π-π-: Phe1152; HBD: Leu1086, Asp1088, Tyr1154
9	12814353	I	WB: Asp1083, Ser1084; π-cat: Tyr1154; SB: Asp1083; HBD: Asp1083, Leu1086; HBA: Arg1157

WB: water bridge; SB: salt bridge; HBD: hydrogen bond donor; HBA: hydrogen bond acceptor; π-cat: π-cation interaction; π-π: π-π interaction; Asp: Aspartate; Leu: Leucine; Tyr: Tyrosine; Phe: Phenylalanine; Arg: Arginine; Ser: Serine.

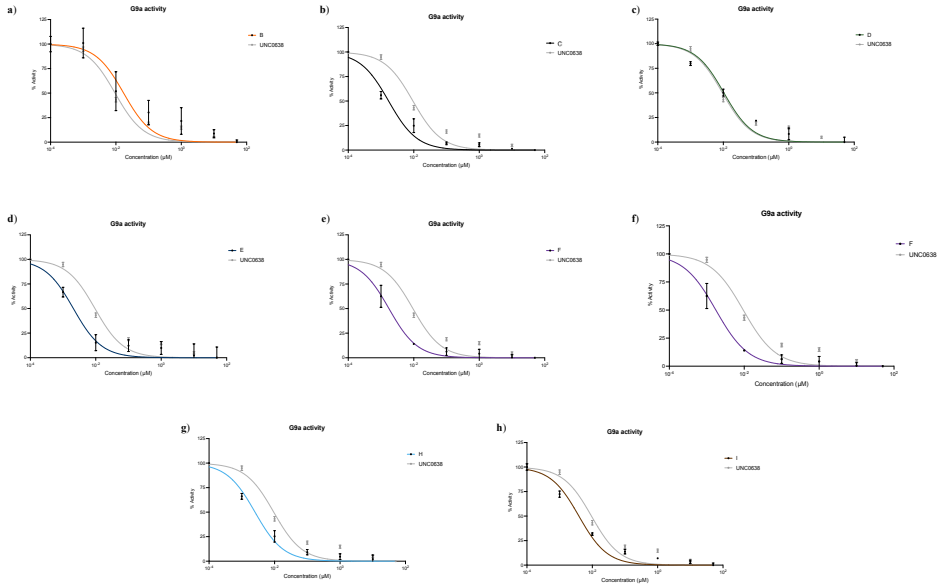

Figure S2. IC_{50} curve for each compound tested Vs. well established G9a inhibitor, UNC0638. (B: orange; C: black; D: green; E: navy blue; F: purple; G: pink; H: light blue; I: brown; UNC0638: grey.)

Table S2. Raw data of the percentage of G9a activity.

	% G9a activity									
µM	A	B	C	D	E	F	G	H	I	UNC0638
50	-0.4	0.2	10.7	9.9	10.3	12.3	7.7	4.2	5.9	0.1
10	10.0	0.9	10.9	8.3	10.6	12.8	8.5	4.9	6.6	1.9
1	14.8	1.2	11.5	11.5	13.7	13.8	8.7	6.1	6.8	5.2
0.1	22.8	2.1	12.0	15.8	14.4	14.0	11.4	7.6	8.2	7.9
0.01	22.9	3.5	15.1	23.0	14.6	14.7	17.6	11.8	13.5	17.0
0.001	27.8	8.7	22.2	29.3	30.3	24.6	26.0	27.8	24.0	34.1
0.0001	31.0	9.3	32.8	33.0	37.1	28.8	29.6	37.9	30.9	36.4

	% G9a activity									
µM	A	B	C	D	E	F	G	H	I	UNC0638
50	0.9	0.6	10.9	12.1	15.5	12.3	9.1	6.9	4.8	0.7
10	11.3	1.6	11.3	10.3	16.3	12.0	9.1	7.6	5.7	2.6
1	15.1	3.8	12.4	14.2	16.9	12.3	10.3	8.0	7.3	5.8
0.1	22.7	5.3	12.6	15.9	17.3	12.7	12.3	9.4	9.3	6.8
0.01	30.7	7.3	19.5	21.5	18.6	14.6	16.1	15.5	12.8	15.3
0.001	30.6	11.6	23.9	28.4	27.9	20.8	28.7	25.9	22.5	35.7
0.0001	32.1	10.8	32.7	33.8	37.3	29.0	33.7	37.5	29.3	37.2

	% G9a activity									
µM	A	B	C	D	E	F	G	H	I	UNC0638
50	0.3	0.4	10.8	11.0	12.9	12.3	8.4	5.6	5.3	0.3
10	10.6	1.2	11.1	9.3	13.5	12.4	8.8	6.2	6.2	1.9
1	15.0	2.5	12.0	12.8	15.3	13.0	9.5	7.0	7.1	6.3
0.1	22.7	3.7	12.3	15.9	15.9	13.4	11.9	8.5	8.7	7.0
0.01	26.8	5.4	17.3	22.2	16.6	14.6	16.8	13.7	13.2	16.1
0.001	29.2	10.1	23.1	28.8	29.1	22.7	27.4	26.8	23.2	34.9
0.0001	31.6	10.0	32.8	33.4	37.2	28.9	31.7	37.7	30.1	36.8

Table S3. Predicted QikProp properties for CNS drugability.

S. No.	Code	CNS	SASA	HBD	HBA	logPo/w	logS	PCaco	logBB	PMDCK	logKp	logKhsa	HOA	%HOA	PSA	Rule of 5
1	UNC0638	2	883.549	1	8	5.311	-5.371	413.395	-0.614	233.048	-4.919	1.165	2	78.956	46.568	2
2	A	1	654.894	1	9.2	2.142	-2.779	497.612	-0.064	257.398	-3.317	-0.222	3	87.754	72.923	0
3	B	1	696.62	0	7.25	3.363	-3.426	586.707	-0.085	307.553	-2.685	0.015	3	96.185	44.722	0
4	**C**	2	716.157	1	5	4.173	-3.768	342.913	0.643	344.802	-4.717	0.655	3	96.754	31.054	0
5	D	2	753.337	0	6.7	4.309	-3.408	476.039	0.844	436.6	-3.951	0.441	3	100	26.969	0
6	**E**	1	719.535	2	7	2.685	-3.675	85.439	0.169	69.055	-6.459	0.408	3	77.241	58.683	0
7	**F**	1	616.786	2	6.2	2.656	-3.717	617.29	0.249	799.747	-3.741	0.078	3	92.442	63.815	0
8	G	0	711.78	2	8.5	2.279	-3.618	233.856	-0.717	113.799	-3.928	-0.092	3	82.691	92.633	0
9	**H**	1	682.052	1	5.5	3.506	-4.117	611.772	0.306	895.879	-3.261	0.29	3	100	45.83	0
10	I	1	773.591	2	8.5	3.356	-4.817	356.15	-0.444	179.307	-3.807	0.359	3	92.265	88.391	0

*Cell denoted with red color fall outside the limits of CNS drugability.

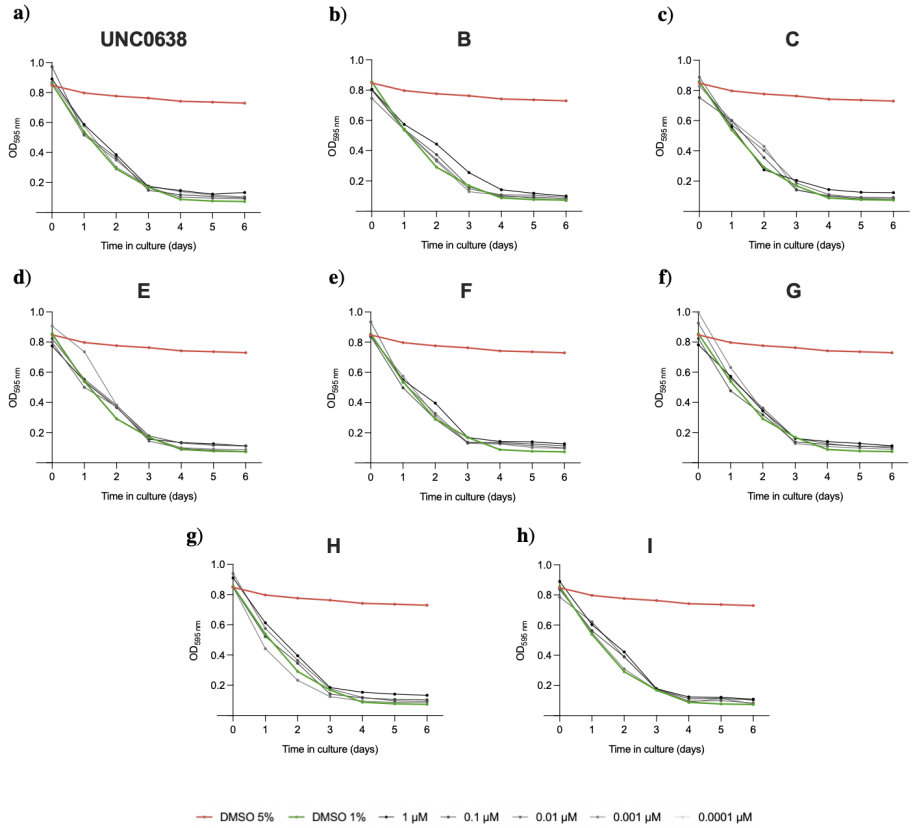

Figure S3. Toxicity of G9a inhibitors was performed through the food clearance assay. The optical density (OD_{595}) of *E. coli* OP50 suspension was measured daily in N2 *C. elegans* treated with the eight compounds in a dose range between 0.001 µM up to 1 µM (greyscale lines), starting at L1 stage. The mean OD_{595} was calculated for each day from six samples and plotted during the 6 days of the experiment. DMSO 5% (red line) was used as a positive control (toxic concentration); DMSO 1% (green line) was used as negative control (non-toxic concentratation), representing the normal development of the animals. Statistical analysis: Application of a non-linear regression model for sigmoidal curves against DMSO 1%.

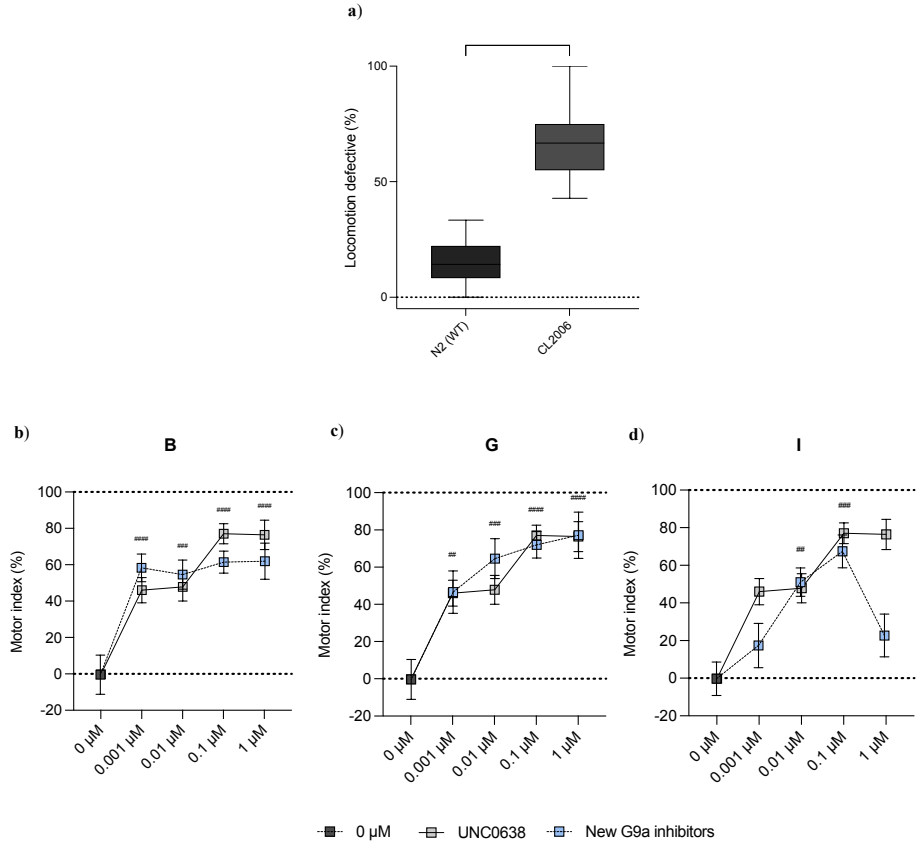

Figure S4. a) Representation for the locomotor defect exhibited by N2 strain and the transgenic AD strain, CL2006. b-d) Dose-response profile of the excluded G9a inhibitors**.** For the percent of locomotion defective: Values represented are mean ± Standard error of the mean (SEM); n = 3 with at least 90-100 worms in each group. Statistical analysis: One-Way ANOVA, followed by Dunnett post-hoc analysis. ****p<0.0001. For dose-response: Values represented are mean ± SEM; n = 3 with at least 90-100 worms in each group. Statistical analysis: One-Way ANOVA, followed by Dunnett post-hoc analysis. 0 µM Vs. UNC0638 treatment:***p<0.001; ****p<0.0001. 0 µM Vs. New G9a inhibitor treatment: $^{\#\#}$p<0.01; $^{\#\#\#}$p<0.001; $^{\#\#\#\#}$p<0.0001.

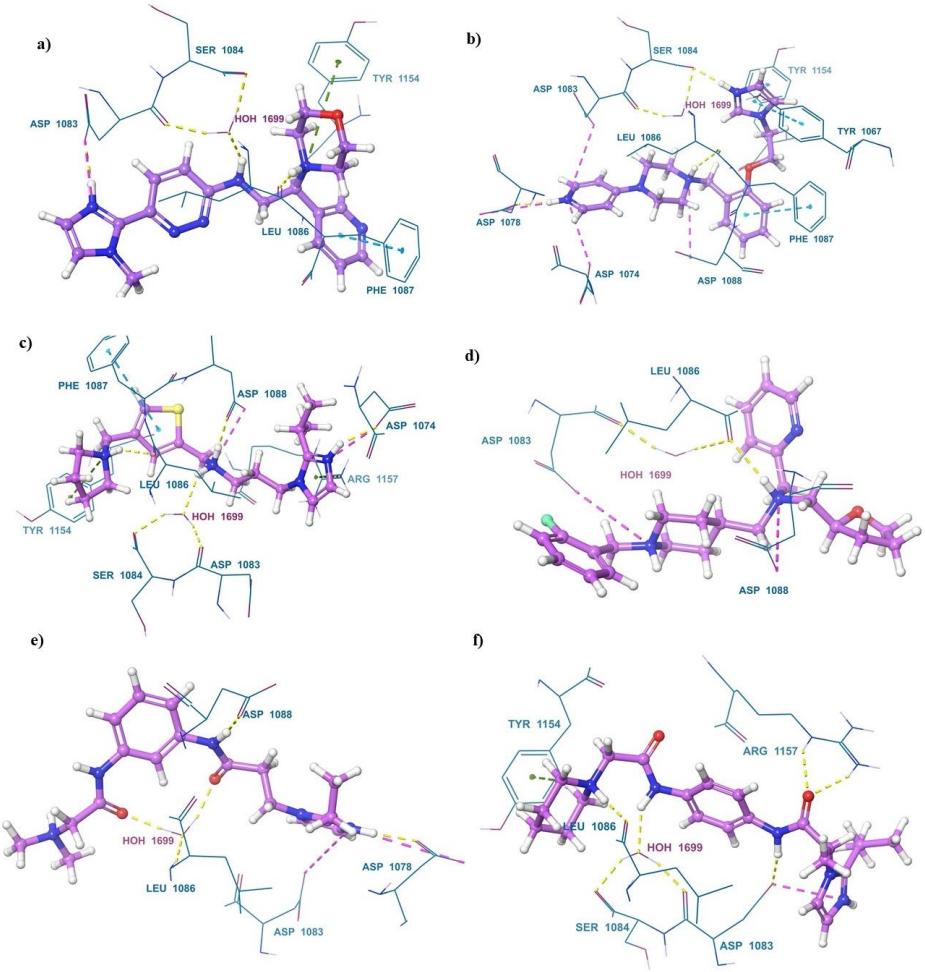

Figure S5. 3D interaction diagram of a) A-G9a, b) B-G9a, c) C-G9a, d) D-G9a, e) G-G9a and f) I-G9a. Protein-ligand Interactions were denoted by a dotted line. Hydrogen bond: Yellow; Salt bridge: Pink; π-π stacking: Blue; π-cation: Green.

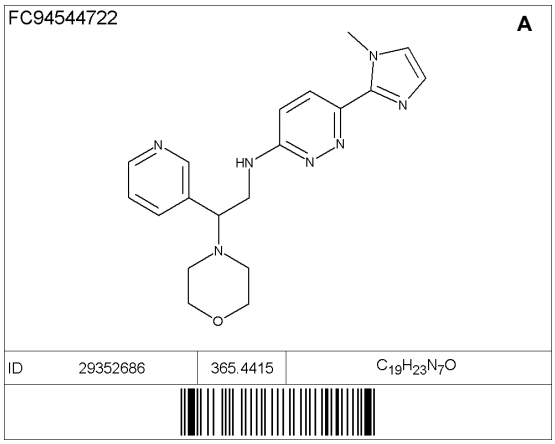

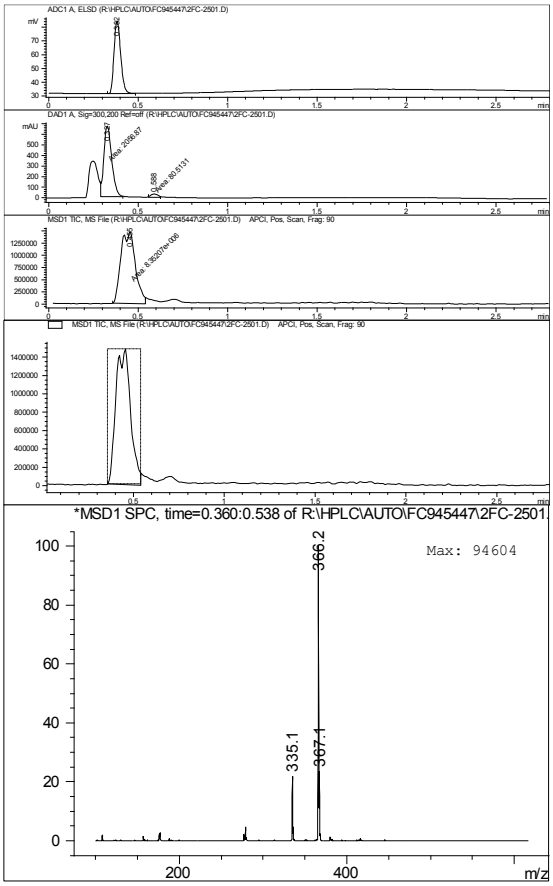


```
Data File R:\HPLC\AUTO\FC945447\2FC-2501.D
Sample Name: FC945447P2-F-03
Instrument 1 26/09/11 11:11:29
PMP1, Solvent A          : 0.1%TFA in Acn/H2O (2.5:97.5)
PMP1, Solvent B          : 0.1% TFA in AcN
PMP1, Solvent C          : 0.1%FA in ACN/H2O (2.5:97.5)
PMP1, Solvent D          : 0.1%FA in ACN
Ionization mode             :    APCI Positive

Signal 1: ADC1 A, ELSD
Peak RetTime Type  Width     Area      Height     Area
  #   [min]        [min]    [mV*s]      [mV]        %
----|-------|----|-------|----------|----------|--------|
   1   0.382 PB    0.0414  137.03101   52.63791 100.0000
Totals :                   137.03101   52.63791


Signal 2: DAD1 A, Sig=300,200 Ref=off
Peak RetTime Type  Width     Area      Height     Area
  #   [min]        [min]   [mAU*s]     [mAU]       %
----|-------|----|-------|----------|----------|--------|
   1   0.327 MM    0.0513 2056.87305  668.02240  96.2331
   2   0.588 MM    0.0455   80.51310   29.52247   3.7669
Totals :                  2137.38615  697.54487


Signal 3: MSD1 TIC, MS File
Peak RetTime Type  Width     Area      Height     Area
  #   [min]        [min]                          %
----|-------|----|-------|----------|----------|--------|
   1   0.455 MM    0.0937 8.35207e6  1.48519e6  100.0000
Totals :                  8.35207e6  1.48519e6
```

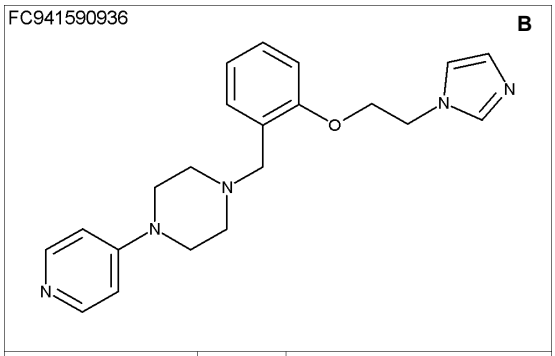

ID	55607373	363.4663	$C_{21}H_{25}N_5O$

```
Data File R:\HPLC\AUTO\1DE-3201.D
Sample Name: FC9415909P1-D-05
Instrument 1 05/08/2014 18:13:30
Column: Onyx C18 50x4.6mm | 3.75ml/min | Columns Reg Valve
Gradient: "A"->@2.2min->"B"(Hold 0.4min)->@0.2min->"A"->PostRun
PMP1, Solvent A          : 0.1%TFA in Acn/H2O (2.5:97.5)
PMP1, Solvent B          : 0.1%TFA in AcN
PMP1, Solvent C          : 0.1%FA in Acn/H2O (2.5:97.5)
PMP1, Solvent D          : 0.1%FA in AcN
Ionization mode             :    APCI Positive

Signal 1: ADC1 B, ELSD
Peak RetTime Type  Width     Area      Height     Area
  #   [min]        [min]   [mAu*s]     [mAu]       %
----|-------|----|-------|----------|----------|-------|
   1   0.754 MM    0.0184    1.80391    1.63314   1.2903
   2   0.809 MF    0.0372  128.73773   57.72703  92.0813
   3   0.879 FM    0.0614    9.26716    2.51536   6.6285
Totals :                   139.80880   61.87553


Signal 2: DAD1 A, Sig=300,200 Ref=off
Peak RetTime Type  Width     Area      Height     Area
  #   [min]        [min]   [mAU*s]     [mAU]       %
----|-------|----|-------|----------|----------|-------|
   1   0.699 MF    0.0394   26.17825   11.06329   1.5820
   2   0.768 MF    0.0448 1550.68164  577.10406  93.7122
   3   0.842 FM    0.0343   51.59457   25.05865   3.1180
   4   1.041 MM    0.0306   26.27340   14.28967   1.5878
Totals :                  1654.72787  627.51569


Signal 3: MSD1 TIC, MS File
Peak RetTime Type  Width     Area      Height     Area
  #   [min]        [min]                          %
----|-------|----|-------|----------|----------|-------|
   1   0.795 MM    0.0494 2.78428e6  9.40117e5  100.0000
Totals :                  2.78428e6  9.40117e5
```

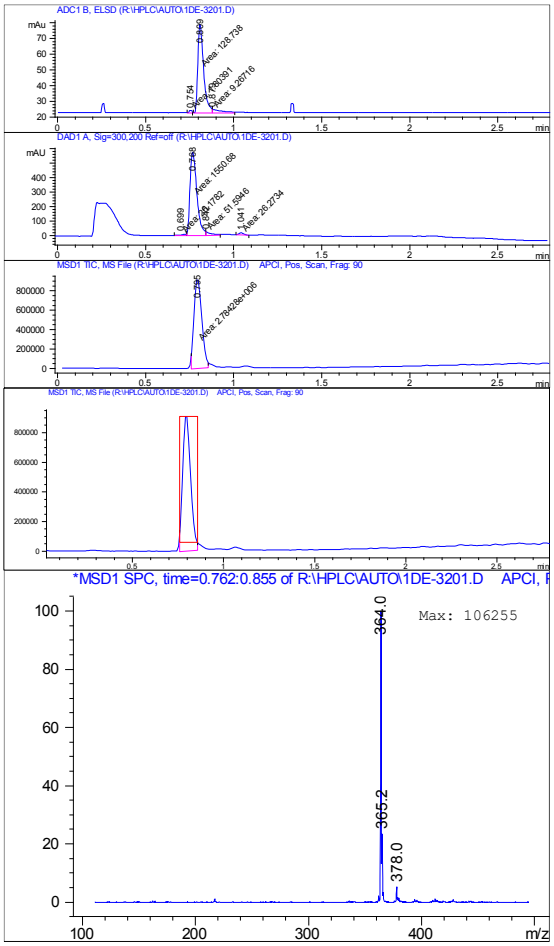

FC942332308 **C**

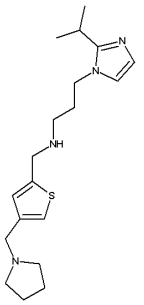

ID	43631981	346.5418	$C_{19}H_{30}N_4S$

```
Data File D:\FC9423~2\1HA-0901.D
Sample Name: FC9423323P1-H-01
Instrument 1 18/09/2017 13:45:19
Column: Onyx C18 50x4.6mm | 3.75ml/min | Columns Reg Valve
Gradient: "A"->@2.0min->"B"(Hold 0.6min)->@0.2min->"A"->PostRun
PMP1, Solvent A          : 0.1%TFA in Acn/H2O (2.5:97.5)
PMP1, Solvent B          : 0.1%TFA in AcN
PMP1, Solvent C          : 0.1%FA in Acn/H2O (2.5:97.5)
PMP1, Solvent D          : 0.1%FA in AcN
Ionization mode             :    APCI Positive

Signal 1: ADC1 B, ELSD
Peak RetTime Type  Width     Area      Height     Area
  #   [min]        [min]    [mAu*s]     [mAu]       %
----|-------|----|-------|----------|----------|-------|
   1   0.520 PB    0.0605  128.23772   30.87906 100.0000
Totals :                   128.23772   30.87906

Signal 2: DAD1 A, Sig=300,200 Ref=off
Peak RetTime Type  Width     Area      Height     Area
  #   [min]        [min]    [mAU*s]     [mAU]       %
----|-------|----|-------|----------|----------|-------|
   1   0.473 PP    0.0650  836.74414  184.24127 100.0000
Totals :                   836.74414  184.24127

Signal 3: MSD1 TIC, MS File
Peak RetTime Type  Width     Area      Height     Area
  #   [min]        [min]                           %
----|-------|----|-------|----------|----------|-------|
   1   0.505 BB    0.0858 3.98199e6  7.01022e5  100.0000
Totals :                  3.98199e6  7.01022e5
```

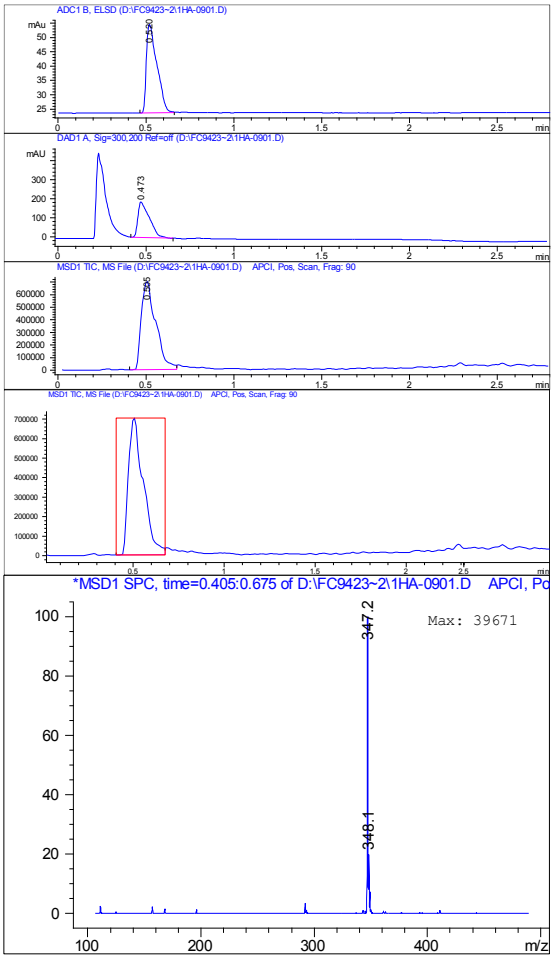

PH10250647 **D**

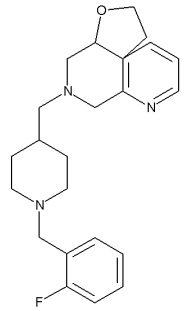

ID	15589586	397.5405	$C_{24}H_{32}FN_3O$

Data File C:\HPCHEM\1\DATA\424\2GF-9301.D
Sample Name: PH102506P2-G-06
Instrument 1 18/06/2006 07:45:38 lcms#6
Column: Hi-Q C18 5um 50x4.6mm | 3.75ml/min
Gradient: "A"->@2.4min->"B"(Hold 0.3min)->@0.1min->"A"->PostRun
PMP1, Solvent A : 0.1% TFA in AcN/Water (5:95)
PMP1, Solvent B : 0.1% TFA in AcN
PMP1, Solvent C : 10mM CH3COONH4 in AcN/Water (2.5:75.5)
PMP1, Solvent D : 10mM CH3COONH4 in AcN/Water (90:10)
Ionization mode : APCI Positive

Signal 1: ADC1 A, ELSD

Peak #	RetTime [min]	Type	Width [min]	Area [mV*s]	Height [mV]	Area %
1	1.092	BP	0.0534	20.30906	5.86045	100.0000
Totals :				20.30906	5.86045	

Signal 2: DAD1 A, Sig=260,2 Ref=off

Peak #	RetTime [min]	Type	Width [min]	Area [mAU*s]	Height [mAU]	Area %
1	0.779	BV	0.0631	214.16794	50.87011	3.3699
2	0.875	VV	0.0558	171.88681	45.80094	2.7046
3	1.053	VV	0.0606	5036.19385	1261.80518	79.2433
4	1.188	VV	0.0529	201.90080	54.88534	3.1769
5	1.288	VV	0.0782	257.65500	46.79729	4.0541
6	1.379	VB	0.1439	473.55078	41.89930	7.4512
Totals :				6355.35518	1502.05817	

Signal 3: MSD1 TIC, MS File

Peak #	RetTime [min]	Type	Width [min]	Area	Height	Area %
1	1.125	PB	0.0963	6.47657e7	1.01304e7	100.0000
Totals :				6.47657e7	1.01304e7	

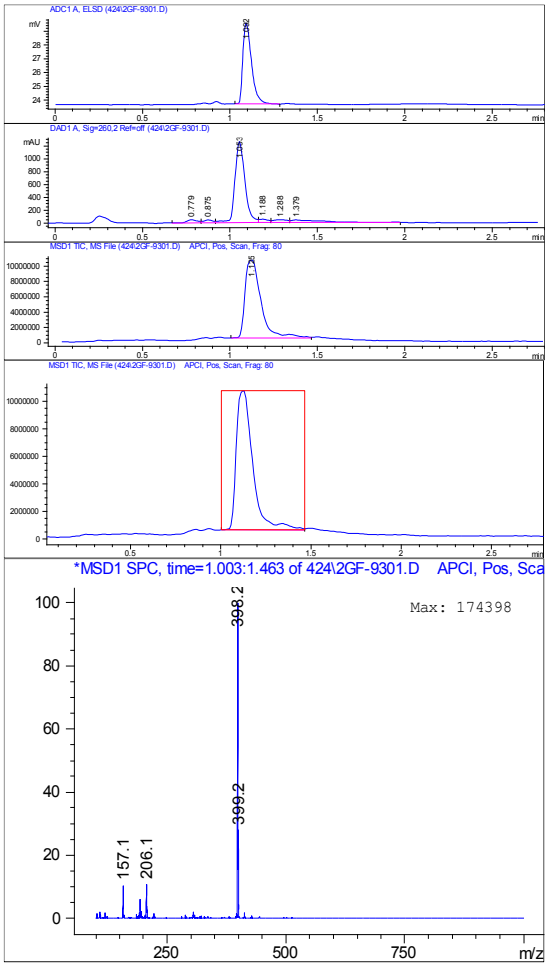

FC942237731 **E**

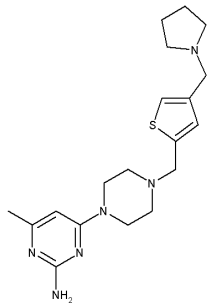

ID	55517816	372.5392	$C_{19}H_{28}N_6S$

```
Data File D:\FC9422~2\2GD-7101.D
Sample Name: FC9422377P2-G-04
Instrument 1 19/05/2017 12:01:10
Column: Onyx C18 50x4.6mm | 3.75ml/min | Columns Reg Valve
Gradient: "A"->@2.2min->"B"(Hold 0.4min)->@0.2min->"A"->PostRun
PMP1, Solvent A          : 0.1%TFA, 2.5%AcN in H2O
PMP1, Solvent B          : 0.1%TFA in AcN
PMP1, Solvent C          : --NOT USED--
PMP1, Solvent D          : --NOT USED--
Ionization mode             :    API-ES Positive
```

Signal 1: ADC1 B, ELSD

Peak #	RetTime [min]	Type	Width [min]	Area [mV*s]	Height [mV]	Area %
1	0.830	BB	0.0338	155.88422	69.21435	100.0000
Totals :				155.88422	69.21435	

Signal 2: DAD1 A, Sig=300,200 Ref=off

Peak #	RetTime [min]	Type	Width [min]	Area [mAU*s]	Height [mAU]	Area %
1	0.728	BB	0.0258	1182.20801	697.45557	100.0000
Totals :				1182.20801	697.45557	

Signal 3: MSD1 TIC, MS File

Peak #	RetTime [min]	Type	Width [min]	Area	Height	Area %
1	0.771	PB	0.0552	1.45094e6	4.20406e5	100.0000
Totals :				1.45094e6	4.20406e5	

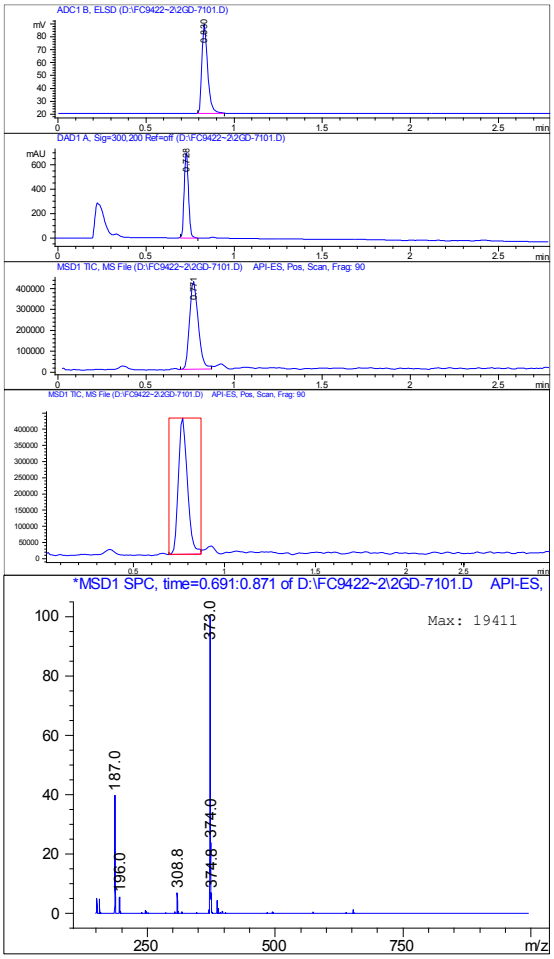

FC941705836 **F**

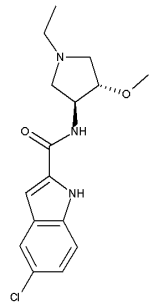

ID	31871543	321.8097	$C_{16}H_{20}ClN_3O_2$

```
Data File D:\FC9417~2\2DE-3601.D
Sample Name: FC9417058P2-D-05
Instrument 1 07/05/2015 10:41:39
Column: Onyx C18 50x4.6mm | 3.75ml/min | Columns Reg Valve
Gradient: "A"->@2.2min->"B"(Hold 0.4min)->@0.2min->"A"->PostRun
PMP1, Solvent A          : 0.1%TFA, 2.5%AcN/W
PMP1, Solvent B          : 0.1%TFA/AcN
PMP1, Solvent C          : --NOT USED--
PMP1, Solvent D          : --NOT USED--
Ionization mode             :    API-ES Positive

Signal 1: ADC1 B, ELSD
Peak RetTime Type  Width     Area      Height     Area
  #   [min]        [min]   [mV*s]      [mV]        %
----|-------|----|-------|----------|----------|--------|
   1   1.235 MM    0.0569 1700.08313  498.27438 100.0000
Totals :                  1700.08313  498.27438

Signal 2: DAD1 A, Sig=300,200 Ref=off
Peak RetTime Type  Width     Area      Height     Area
  #   [min]        [min]   [mAU*s]     [mAU]       %
----|-------|----|-------|----------|----------|--------|
   1   1.172 MM    0.0760 5175.48926 1135.61267  98.6859
   2   1.652 MM    0.0454   68.91638   25.30288   1.3141
Totals :                  5244.40564 1160.91555

Signal 3: MSD1 TIC, MS File
Peak RetTime Type  Width     Area      Height     Area
  #   [min]        [min]                          %
----|-------|----|-------|----------|----------|--------|
   1   1.198 MM    0.0754 8.32205e6  1.84024e6  100.0000
Totals :                  8.32205e6  1.84024e6
```

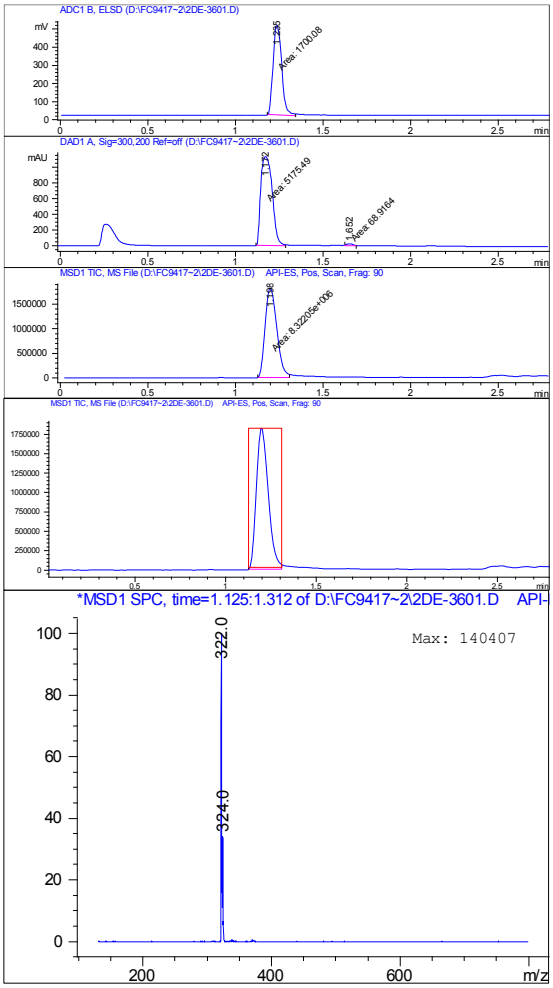

FC942323248 **G**

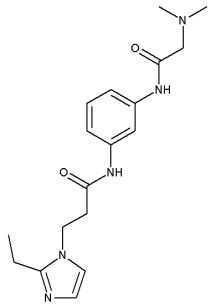

ID	20839262	343.4323	$C_{18}H_{25}N_5O_2$

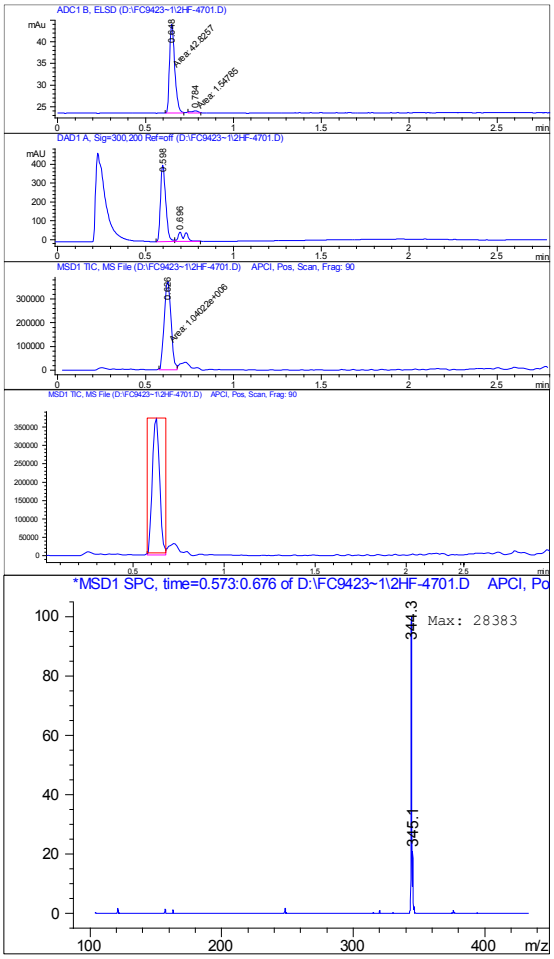


```
Data File D:\FC9423~1\2HF-4701.D
Sample Name: FC9423232P2-H-06
Instrument 1 04/09/2017 13:58:00
Column: Onyx C18 50x4.6mm | 3.75ml/min | Columns Reg Valve
Gradient: "A"->@2.0min->"B"(Hold 0.6min)->@0.2min->"A"->PostRun
PMP1, Solvent A          : 0.1%TFA in Acn/H2O (2.5:97.5)
PMP1, Solvent B          : 0.1%TFA in AcN
PMP1, Solvent C          : 0.1%FA in Acn/H2O (2.5:97.5)
PMP1, Solvent D          : 0.1%FA in AcN
Ionization mode             :    APCI Positive

Signal 1: ADC1 B, ELSD
Peak RetTime Type  Width     Area      Height     Area
  #   [min]        [min]   [mAu*s]     [mAu]       %
----|-------|----|-------|----------|----------|--------|
   1   0.648 MM    0.0345   42.82569   20.67672  96.5118
   2   0.784 MM    0.0473    1.54785 5.45230e-1   3.4882
Totals :                    44.37354   21.22195


Signal 2: DAD1 A, Sig=300,200 Ref=off
Peak RetTime Type  Width     Area      Height     Area
  #   [min]        [min]   [mAU*s]     [mAU]       %
----|-------|----|-------|----------|----------|--------|
   1   0.598 PB    0.0346  840.42780  397.98636  84.6199
   2   0.696 BB    0.0433  152.75237   47.80603  15.3801
Totals :                   993.18016  445.79239


Signal 3: MSD1 TIC, MS File
Peak RetTime Type  Width     Area      Height     Area
  #   [min]        [min]                          %
----|-------|----|-------|----------|----------|--------|
   1   0.626 MM    0.0456 1.04022e6  3.80027e5  100.0000
Totals :                  1.04022e6  3.80027e5
```

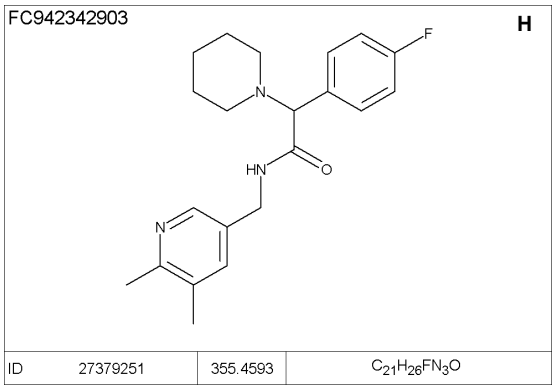

ID	27379251	355.4593	$C_{21}H_{26}FN_3O$

```
Data File R:\HPLC\DENIS\ST\FC9423~2\1CA-0301.D
Sample Name: FC9423429P1-C-01
Instrument 1 29/09/2017 13:25:04
Column: Onyx C18 50x4.6mm | 3.75ml/min | Columns Reg Valve
Gradient: "A"->@2.2min->"B"(Hold 0.4min)->@0.2min->"A"->PostRun
PMP1, Solvent A          : 0.1%TFA, 2.5%AcN in H2O
PMP1, Solvent B          : 0.1%TFA in AcN
PMP1, Solvent C          : --NOT USED--
PMP1, Solvent D          : --NOT USED--
Ionization mode             :    API-ES Positive
```

Signal 1: ADC1 B, ELSD

Peak #	RetTime [min]	Type	Width [min]	Area [mV*s]	Height [mV]	Area %
1	0.970	MF	0.0449	43.00430	15.96386	98.9855
2	1.044	FM	0.0214	4.40752e-1	3.43719e-1	1.0145
Totals :				43.44505	16.30758	

Signal 2: DAD1 A, Sig=300,200 Ref=off

Peak #	RetTime [min]	Type	Width [min]	Area [mAU*s]	Height [mAU]	Area %
1	0.870	MF	0.0342	404.97916	197.24895	97.9496
2	0.934	FM	0.0312	8.47769	4.52932	2.0504
Totals :				413.45684	201.77827	

Signal 3: MSD1 TIC, MS File

Peak #	RetTime [min]	Type	Width [min]	Area	Height	Area %
1	0.896	MM	0.0491	2.53011e6	8.59311e5	100.0000
Totals :				2.53011e6	8.59311e5	

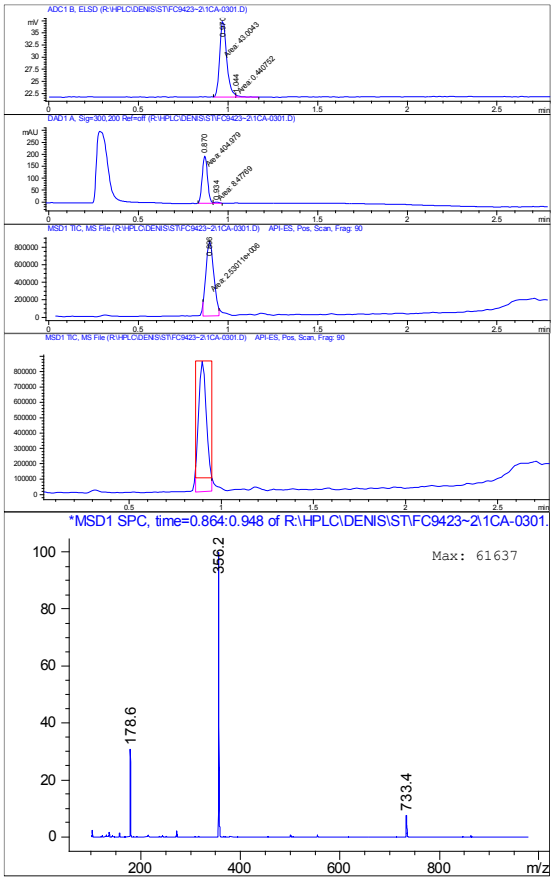

FC942284317 **I**

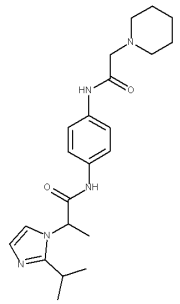

ID	12814353	397.5247	$C_{22}H_{31}N_5O_2$

```
Data File D:\DATA\411\1AC-1901.D
Sample Name: FC9422843P1-A-03
Instrument 1 14/07/2017 15:47:48  N6
Column: Onyx Monolithic C18 50x4.6mm | 3.75ml/min | Columns Reg
Valve
Gradient: "A"->@2.2min->"B"(Hold 0.4min)->@0.2min->"A"->PostRun
PMP1, Solvent A          : 0.1%TFA in Acn/H2O (2.5:97.5)
PMP1, Solvent B          : 0.1%TFA in AcN
PMP1, Solvent C          : 0.1%FA in Acn/H2O (2.5:97.5)
PMP1, Solvent D          : 0.1%FA in AcN
Ionization mode             :    APCI Positive

Signal 1: ADC1 B, ELSD
Peak RetTime Type  Width     Area      Height     Area
  #   [min]        [min]   [mAu*s]     [mAu]       %
----|-------|----|-------|----------|----------|--------|
   1   0.940 BB    0.0277  104.46929   58.95369 100.0000
Totals :                   104.46929   58.95369


Signal 2: DAD1 A, Sig=300,200 Ref=off
Peak RetTime Type  Width     Area      Height     Area
  #   [min]        [min]   [mAU*s]     [mAU]       %
----|-------|----|-------|----------|----------|--------|
   1   0.888 PB    0.0284 1351.10828  772.64844 100.0000
Totals :                  1351.10828  772.64844


Signal 3: MSD1 TIC, MS File
Peak RetTime Type  Width     Area      Height     Area
  #   [min]        [min]                          %
----|-------|----|-------|----------|----------|--------|
   1   0.921 PB    0.0461 2.10541e6  7.03687e5  100.0000
Totals :                  2.10541e6  7.03687e5
```

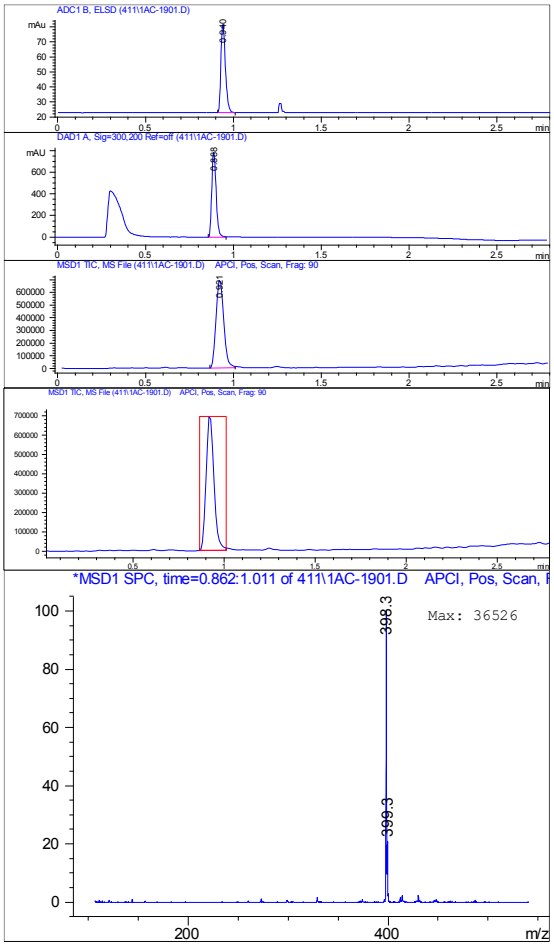

False Positive Remover

Welcome Created 12-2009

Main Page>>Retrieve Structure

Return

Totally 9 Compound(s) passed the filter.Download (Smiles format)
The following are the structure(s) of compound(s) that passed the filter

736748.sdf	736748.sdf 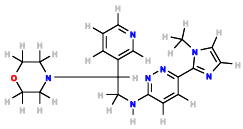	736748.sdf 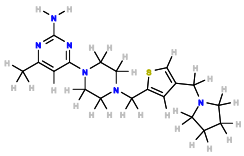	736748.sdf 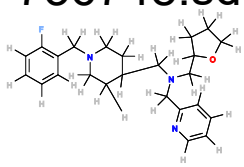
736748.sdf 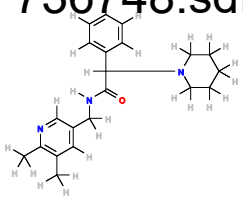	736748.sdf 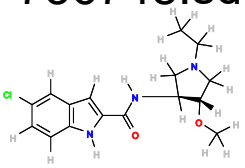	736748.sdf	736748.sdf 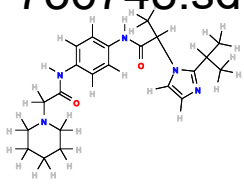
736748.sdf 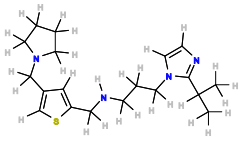			

Return

1

3.5. Publication 5

Repurposing of Raltitrexed as an Effective G9a/EHMT2 Inhibitor and Promising Anti-Alzheimer's Agent.

Abhisek Jana[*], **Aina Bellver-Sanchis**[*], Christian Griñán-Ferré[‡], and Deb Ranjan Banerjee[‡]

ACS Medicinal Chemistry Letter, 2023, 14: 1531−1536

doi: 10.1021/acsmedchemlett.3c00344

SUMMARY

The challenges associated with existing G9ais emphasize the need for effective and safe treatment options. G9a is an excellent epigenetic target with no clinically passed inhibitor due to adverse *in vivo* ADMET toxicities. Interestingly, drug repurposing aims to identify new therapeutic applications for existing drugs, taking advantage of their established safety profiles and known pharmacokinetics to accelerate the drug development process and potentially address unmet medical needs more efficiently. In this line, a systematic 3D QSAR screening was conducted. This screening began with a database containing 400,000 candidates and ultimately identified Raltitrexed as the top virtual lead, suggesting its potential to compete with substrate binding against G9a. Moreover, while Raltitrexed is recognized as an anti-cancer drug, its potential connection to G9a inhibition or AD has not been previously documented. Therefore, our aim was to investigate the potential of repurposing Raltitrexed as a potential AD treatment by G9a inhibition.

Here, we utilized *in silico*, *in vitro,* and *in vivo* analyses to investigate the potential of repurposing the drug **Raltitrexed** as a G9a/EHMT2i. A detailed *in silico* ADMET/TOPKAT analysis of **Raltitrexed** was conducted to validate its toxicity and safety profile. Accordingly, toxicity analyses through food consumption measurements in *C. elegans* demonstrated that **Raltitrexed**'s toxicity/function range was safer than the well-established G9ai, **UNC0642**. Then, we reported the inhibition of G9a by **Raltitrexed** at 120 nM and its reduction of H3K9me2 levels in AD transgenic *C. elegans* strain (CL2006), CL2006. Besides, **Raltitrexed** was found to enhance the locomotive function in a dose-dependent manner and reduced Aβ aggregates in CL2006 up to 47%, suggesting its potential in AD treatment.

Overall, in this work, we identified **Raltitrexed** as a promising G9ai with potential anti-AD effects, providing detailed *in vitro* and *in vivo* evidence supporting its efficacy and safety. Therefore, the findings open new possibilities for repurposing **Raltitrexed** as a therapeutic agent for AD and underline the importance of further investigating and exploring its therapeutic potential not only for cancer but also for neurodegenerative diseases.

ACS Medicinal Chemistry Letters

pubs.acs.org/acsmedchemlett Letter

Repurposing of Raltitrexed as an Effective G9a/EHMT2 Inhibitor and Promising Anti-Alzheimer's Agent

Published as part of ACS Medicinal Chemistry Letters virtual special issue "Many Faces of Medicinal Chemistry".

Abhisek Jana,[‡] Aina Bellver-Sanchis,[‡] Christian Griñán-Ferré,[*] and Deb Ranjan Banerjee[*]

Cite This: *ACS Med. Chem. Lett.* 2023, 14, 1531−1536 Read Online

ACCESS | Metrics & More | Article Recommendations | Supporting Information

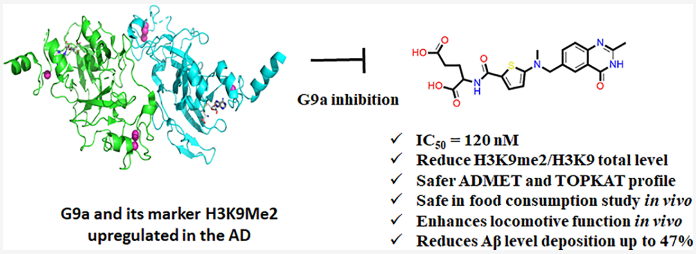

ABSTRACT: Herein, we report for the first time the G9a/EHMT2 inhibition and anti-Alzheimer's activities of the drug raltitrexed. G9a is a lysine methyltransferase that mainly dimethylates the H3K9 of chromatin, which triggers the repression of genes epigenetically, leading to various diseased conditions, including Alzheimer's disease (AD). First, we demonstrate that raltitrexed inhibits G9a at 120 nM. Moreover, raltitrexed lowers the total H3K9me2/H3K9 levels in AD transgenic *C. elegans* CL2006 worms, indicating that raltitrexed targets G9a directly. As toxicity is the bottleneck in G9a drug discovery, we conducted detailed *in silico* toxicity (TOPKAT) analyses of raltitrexed and measured the food consumption by *C. elegans*, demonstrating that raltitrexed's toxicity/function range is safe for the worm's growth. Moreover, we demonstrate that raltitrexed enhances the locomotive function of worms dose-dependently. Finally, we show that raltitrexed reduced the Aβ aggregates in worms up to 47%, highlighting the potential of raltitrexed in AD treatment.

KEYWORDS: *G9a/EHMT2, Methyltransferase, Inhibitor, Epigenetics, Alzheimer's disease, Quinazoline*

Downloaded via UNIV DE BARCELONA on February 18, 2024 at 22:10:20 (UTC).
See https://pubs.acs.org/sharingguidelines for options on how to legitimately share published articles.

Expression and transcription of genes, which are essential for different biochemical activities, are not solely dependent on the transcription factors and DNA sequence but also on epigenetic regulation.[1,2] The state of the chromatin commands epigenetic regulation. Changes in the chromatin state can be achieved in multiple ways, encompassing nucleosome-remodeling of histone variants, DNA methylation, and post-translational modification (PTM) of the side chain of histones.[3,4] The PTM of histones is involved in chromatin compaction, gene expression, transcriptional regulation, cell differentiation, and other important cellular processes.[5−7] Among those enzymes, the most explored PTMs are "writers" that have been identified as potential targets in many human diseases, including various cancers, addiction, and neurodegenerative disorders.[8,9] Histone methyltransferases (HMTs), also known as protein methyltransferases (PMTs), are methyl group writers of the histone code, and they methylate non-histone proteins as well.[10] HMTs relocate the methyl group from the co-factor *S*-5-adenosyl-methionine (SAM) to some specific residues of either lysine (K) or arginine (R). Based on the specific histone residues, HMTs are classified into protein lysine methyltransferases (PKMTs) and protein arginine methyltransferases (PRMTs).[11] The activation or repression of gene expression and transcription depends on the state and location of the histone methylation in a context-specific manner. Methylation at histone H3 lysine 4 (H3K4), histone H3 lysine 36 (H3K36), and histone H3 lysine 79 (H3K79) is connected to transcription activation, and methylation at histone H3 lysine 9 (H3K9) and histone H3 lysine 27 (H3K27) is a typical hallmark of transcriptional repression.[10,12] Overall, PKMTs that modulate protein synthesis and various

Received: August 6, 2023
Accepted: October 9, 2023
Published: October 12, 2023

ACS Publications © 2023 American Chemical Society

https://doi.org/10.1021/acsmedchemlett.3c00344
ACS Med. Chem. Lett. 2023, 14, 1531−1536

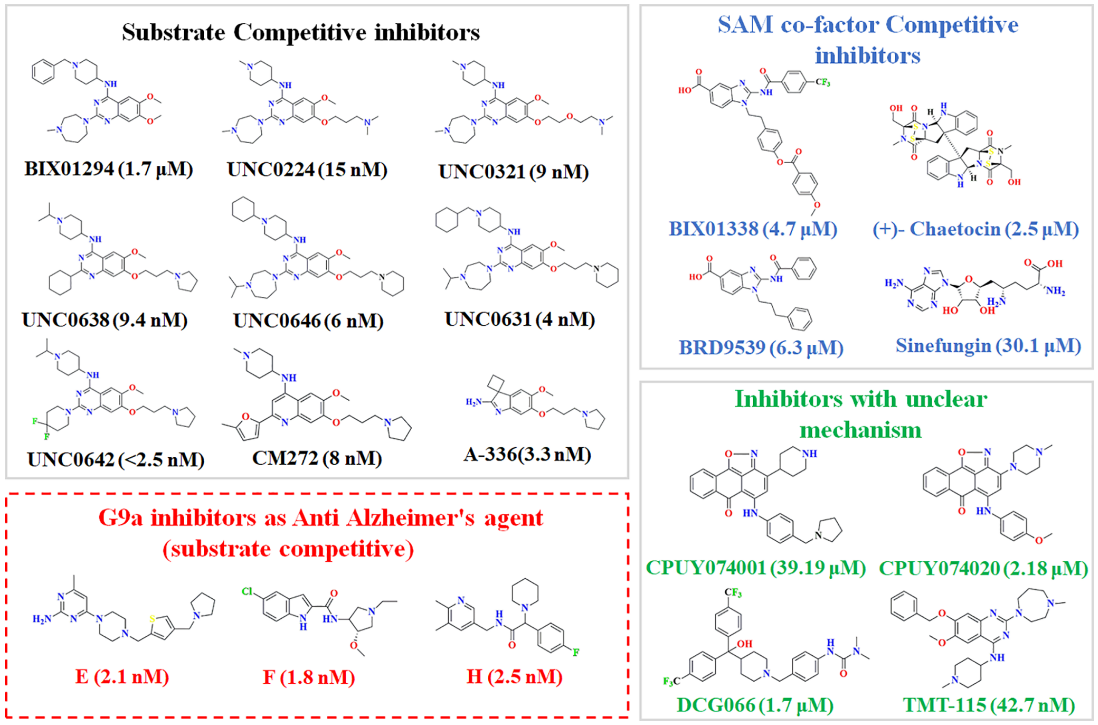

Figure 1. Structures of previously reported G9a inhibitors. Inhibitors are classified into substrate competitive, SAM co-factor competitive, and random inhibitors, as shown in the black, blue, and green boxes. A limited number of G9a inhibitors reported as anti-Alzheimer's agents are shown in the red box. IC_{50} values shown here are dependent on the assay conditions.

crucial biological activities appear to be promising new targets for drug discovery to remedy diverse diseases.[10−13]

G9a (also known as EHMT2 or KMT1C) is an H3K9 methyltransferase which is overexpressed in several human cancers, such as leukemia,[14] lung cancer,[15] prostate cancer,[16] and hepatocellular carcinoma.[17] Recent studies suggest that the processes of synaptic plasticity, learning, and memory are mediated by the "epigenetic code" and that poor regulation of the epigenetic mechanisms accounts for cognitive disorders associated with learning and memory.[18−20] Cross-talk between G9a and other protein complexes modulating the dimethylation of H3K9 is involved in the memory and learning process, suggesting the important role of G9a in Alzheimer's disease (AD).[21,22] Notably, it has been shown that both G9a and H3K9me2 levels are increased in AD patients.[23,24] More interestingly, G9a inhibition rescued memory impairment in different AD models.[25−27] It is also interesting that G9a inhibition induced neuronal plasticity via upregulating the expression of glia maturation factor β (GMFB) in SAMP8 mice.[26] Moreover, the elevation of long-term potentiation (LTP) and its associated mechanisms, like synaptic tagging and capture (STC), is possible by catalytic inhibition of G9a and related complexes.[28−30]

Though a number of G9a inhibitors have been published over the past decade, these reported compounds were less effective in *in vivo* and *in vitro* studies and had toxicities as well as poor blood−brain barrier (BBB) permeability. Moreover, very few G9a inhibitors were tested experimentally to treat AD (Figure 1).[25] Based on these two rationales, a systematic 3D quantitative structure−activity relationship (QSAR)-based screening, starting from a database of 400 000 candidates, was reported by our group, pointing to raltitrexed as a final virtual lead against G9a competing with substrate binding.[31] Though raltitrexed is side-lined as an anti-cancer drug,[32−34] its association with G9a inhibition or AD has never been reported. Continuing the work, herein we report for the first time the G9a inhibition efficacy and anti-Alzheimer's potential of raltitrexed based on detailed *in vitro* and *in vivo* analyses.

Identification of raltitrexed as a virtual lead against G9a was reported earlier by this group elsewhere.[31] Briefly, a 3D QSAR pharmacophore model was developed from 38 structurally diverse G9a inhibitors using the BIOVIA Discovery Studio (DS) Academic Research Suite.[31,35] To probe the properties of the 10 generated pharmacophores, multiple validation procedures were employed, including cost analysis, test set, and Fischer's randomization method, leading to Hypo1 as the best pharmacophore for the screening. Hypo1 contained a total of five features: one hydrogen bond acceptor (HBA), two hydrophobic (HY), one positive ionizable (PI), and one ring aromatic (RA). The features were exactly complementary to those of the G9a active site and targeted specific protein residues, demonstrating that Hypo1 embedded the features of the G9a active site. Next, Hypo1 was used for the screening of a natural products database, COCONUT, containing more than 400 000 candidates. To ensure stringency, additional tiers of criteria such as drug likeness, flexible docking studies, ADMET studies, comparative analysis with reference, and MD simulation were utilized. Raltitrexed was identified as the final

https://doi.org/10.1021/acsmedchemlett.3c00344
ACS Med. Chem. Lett. 2023, 14, 1531−1536

virtual lead against G9a. In the current study, the G9a inhibition efficacy of raltitrexed was measured experimentally using the G9a Chemiluminescent Assay Kit (catalog no. 52001L, BPS Bioscience, San Diego, CA, USA). The well-known G9a inhibitor UNC0642 was used as a reference in this assay. The IC_{50} of UNC0642 was calculated to be 11.97 nM, which is on par with the reported value. Raltitrexed also strongly inhibited G9a with an IC_{50} in the low nanomolar range (120 nM) (Figure 2), proving its G9a inhibition efficacy.

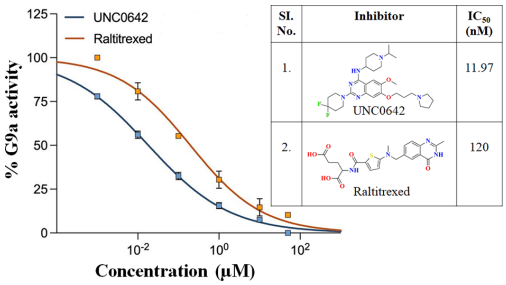

Figure 2. G9a inhibition by raltitrexed (orange line, IC_{50} = 120 nM) vs the well-established G9a inhibitor UNC0642 (black line, IC_{50} = 11.97 nM).

Additionally, we tested the activity of raltitrexed against the G9a-like methyltransferase EHMT1 (GLP) by a chemiluminescence assay. We found that both raltitrexed and our reference UNC0642 inhibited GLP up to 49.98% and 66%, respectively, at 1 μM doses (Table S5).

To demonstrate that raltitrexed directly targets G9a, we quantified the levels of G9a repressive marker H3K9me2 after drug treatment at different doses. The *Caenorhabditis elegans* strain CL2006 was used because it was reported to express higher levels of H3K9me2 compared to the wild-type (WT) *C. elegans* strain N2.[25] Moreover, *C. elegans*, which has been used in AD studies, is an excellent model to evaluate the effect of a new lead on amyloid-β (Aβ)-mediated neurodegeneration. Again, known G9a inhibitor UNC0642 was used as reference, and 1% DMSO was used as vehicle (negative control) in the assay. At a high concentration of inhibitor (50 μM), the levels of H3K9me2 were statistically significantly reduced with both UNC0642 and raltitrexed. It was observed that as the concentration of raltitrexed decreased, the H3K9me2 levels rose, but they were always less elevated than those of the vehicle group (Figure 3 and Figure S1). The observed reduction in total levels of H3K9me2/H3 at different concentrations of raltitrexed demonstrated that raltitrexed targets G9a directly.

Since toxicity is the bottleneck in the existing G9a drug discovery, we carried out detailed *in silico* ADMET/TOPKAT analyses of raltitrexed. The results of *in silico* ADMET/TOPKAT analyses are given in the Supporting Information (Tables S1−S4). In brief, studies of toxicity risks for raltitrexed displayed a good drug score as compared to the reference UNC0642. Encouraged by the TOPKAT toxicity prediction, we measured the food consumption of *C. elegans* worms at increasing concentrations of raltitrexed. Food consumption by the *C. elegans* strain N2 (WT) in the presence of raltitrexed was evaluated by the variation in the optical density (OD_{595}) of bacteria over time as a measure of the compound's toxicity. UNC0642 was used as the reference as it has been reported

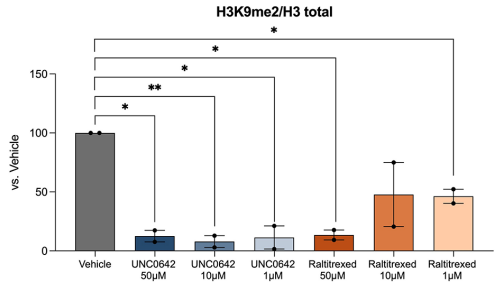

Figure 3. Quantification of the ratio H3K9me2/H3 total. Values are represented as mean ± standard error of the mean (SEM) (n = 2 with at least 250 worms in each biological replicate). One-way ANOVA test followed by Tukey's test and Student's t-test were used when appropriate (*p < 0.05; **p < 0.0).

elsewhere as a non-toxic compound in *in vivo* studies. Additionally, positive control (DMSO 5%) and negative control (DMSO 1%) were employed in the assay. As expected, the statistical difference increased over the days between the positive control and the negative control, demonstrating the toxicity presented by DMSO 5%. In contrast, the OD_{595} values of raltitrexed and UNC0642 at different concentrations (0.01−100 μM) were not significantly different from the OD_{595} of the negative control (Figure 4). Therefore, raltitrexed and

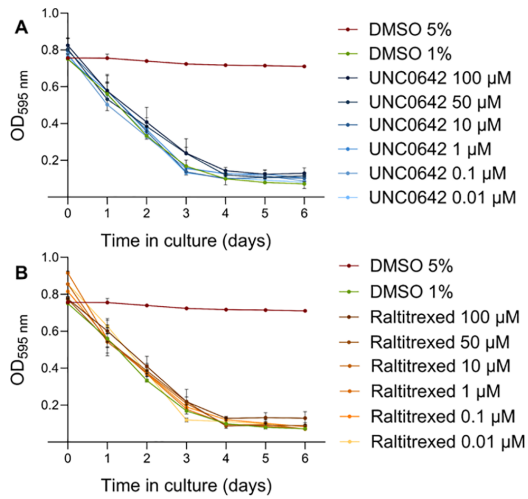

Figure 4. OD_{595} daily measurement during treatments at different doses of (A) UNC0642 and (B) raltitrexed for the food consumption assay. Values are represented as mean ± SEM.

UNC0642 were experimentally verified to be safe for the growth of *C. elegans*, which was also corroborated by visual inspection of the worm's growth. Interestingly, the locomotor behavior of the worm can be quantified using different locomotor parameters, such as worm speed, thrashing frequency, amplitude, and number of bends. A good method for measuring locomotor behavior is the thrashing assay, which can be used to monitor neuronal health when screening anti-Alzheimer's agents in *C. elegans*. Now, *C. elegans* CL2006 is one of the best-characterized transgenic AD strains, containing the

https://doi.org/10.1021/acsmedchemlett.3c00344
ACS Med. Chem. Lett. 2023, 14, 1531−1536

Punc-54::Aβ_{1-42} transgene, which shows progressive adult-onset paralysis. Therefore, to evaluate the pharmacological impact of G9a inhibition by raltitrexed in terms of dose–response, a thrashing assay was conducted. Again, known G9a inhibitor UNC0642 was used as a reference, and 1% DMSO was used as a vehicle (negative control) in the assay. The detailed procedure is given in the Supporting Information; briefly, worms were treated in liquid medium, transferred to a glass slide, and stabilized for 30 s, and their movements were recorded for next 30 s. The total thrashes during 30 s were quantified by counting the total number of proper movements. The *C. elegans* CL2006 specimens displayed significant enhancement in percent of thrashing at different doses (1–50 μM) of UNC0642 and raltitrexed, showing the direct influence of raltitrexed on the locomotor behavior of the worm (Figure 5 and Figure S2).

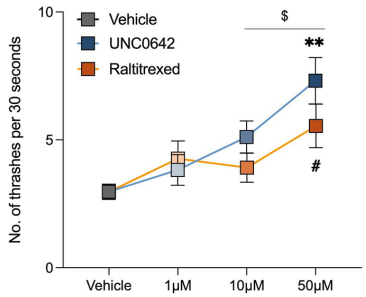

Figure 5. Motility study of *C. elegans* CL2006 as evaluated by the thrashing assay in the presence of reference UNC0642 and raltitrexed. Values are represented as mean ± SEM (n = 27–30 worms/group in each technical replicate). The Kruskal–Wallis test followed by Dunn's test were used when comparing UNC0642 50 μM vs UNC0642 10 μM ($^{\$}p < 0.05$) and when comparing UNC0642 50 μM vs vehicle ($^{**}p < 0.01$), and the Mann–Whitney test was used when comparing raltitrexed 50 μM vs vehicle ($^{\#}p < 0.05$).

Finally, the deposition of Aβ aggregates, an important hallmark in AD, was quantified in *C. elegans* after the pharmacological treatments using thioflavin-S (ThS) staining. As expected, UNC0642 reduced the Aβ deposition by approximately 47%, 35%, and 25% at 50 μM, 10 μM, and 1 μM, respectively. The different doses of raltitrexed reduced the number of Aβ plaques by about 40–47% (Figure 6). Interestingly, a statistically significant reduction in deposition was observed between the 1 μM dose of both treatments, thus highlighting the potency of raltitrexed as a treatment for AD.

In a nutshell, we have reported the G9a/EHMT2 inhibition efficacy and anti-Alzheimer's potential of raltitrexed, a side-lined anti-cancer drug, for the first time. Raltitrexed was previously reported by our group as an *in silico* lead against G9a. Herein, we showed that raltitrexed did inhibit G9a in the low nanomolar range. Moreover, reduction in G9a mediated by dimethylation of its substrate H3K9 at different doses of raltitrexed in *C. elegans* proved that raltitrexed targets G9a directly. As toxicity is the bottleneck in existing G9a drug discovery, we carried out detailed *in silico* ADMET/TOPKAT analyses of raltitrexed and further demonstrated that the toxicity/function range of raltitrexed is safe in the *C elegans* CL2006 strain. To further probe its anti-Alzheimer's potential, we quantified the locomotive function of *C. elegans* CL2006 worms and found that raltitrexed enhanced the locomotive function dose-dependently. Interestingly, we demonstrated *in vivo* that raltitrexed reduced the Aβ aggregates, an important hallmark in AD, in *C. elegans* CL2006 worms up to 47% in a dose-dependent manner, highlighting the potential use of raltitrexed in AD treatment. Owing to the adverse *in vivo* parameters, all known G9a inhibitors, including UNC0642, failed in pre-clinical or clinical testing. Hence, we believe that this is an important work bridging the gap between drug repurposing, G9a inhibition, and anti-Alzheimer's drug discovery. In the future, we are going to quantify and enhance the BBB permeability of raltitrexed with structural derivatives. As raltitrexed is a known thymidylate synthase inhibitor, we may also look into other thymidylate synthase inhibitors,

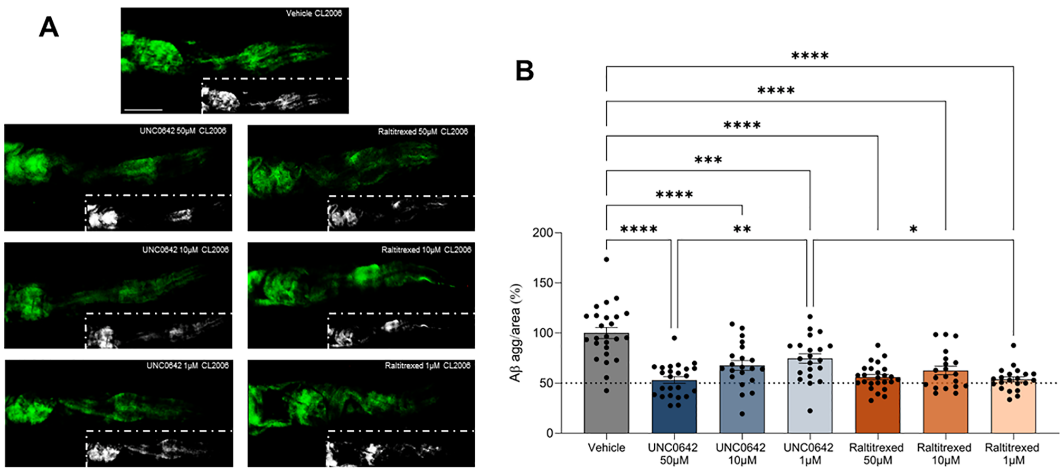

Figure 6. (A) Quantification of ThS-positive aggregates in the head region of the *C. elegans* CL2006 strain. (B) Representative images from each group tested. Values are represented as mean ± SEM (n = 3 with 25 worms in each group; $^{*}p < 0.05$; $^{**}p < 0.01$; $^{***}p < 0.001$; $^{****}p < 0.0001$).

https://doi.org/10.1021/acsmedchemlett.3c00344
ACS Med. Chem. Lett. 2023, 14, 1531–1536

investigating their potential role in G9a-mediated AD epigenetics.

■ ASSOCIATED CONTENT

Supporting Information

The Supporting Information is available free of charge at https://pubs.acs.org/doi/10.1021/acsmedchemlett.3c00344.

Experimental sections (Materials and methods), details of *in silico* ADME/TOPKAT studies, supporting Figures S1 and S2 and Tables S1−S5 (PDF)

■ AUTHOR INFORMATION

Corresponding Authors

Deb Ranjan Banerjee − *Department of Chemistry, National Institute of Technology Durgapur, Durgapur 713209 West Bengal, India;* orcid.org/0000-0002-2058-896X; Email: debranjan.banerjee@ch.nitdgp.ac.in

Christian Griñán-Ferré − *Pharmacology Section, Department of Pharmacology, Toxicology and Therapeutic Chemistry, Faculty of Pharmacy and Food Sciences, Institute of Neuroscience, Universitat de Barcelona (NeuroUB), 08028 Barcelona, Spain; Centro de Investigación en Red, Enfermedades Neurodegenerativas (CIBERNED), Instituto de Salud Carlos III, 28029 Madrid, Spain;* orcid.org/0000-0002-5424-9130; Email: christian.grinan@ub.edu

Authors

Abhisek Jana − *Department of Chemistry, National Institute of Technology Durgapur, Durgapur 713209 West Bengal, India*

Aina Bellver-Sanchis − *Pharmacology Section, Department of Pharmacology, Toxicology and Therapeutic Chemistry, Faculty of Pharmacy and Food Sciences, Institute of Neuroscience, Universitat de Barcelona (NeuroUB), 08028 Barcelona, Spain;* orcid.org/0000-0001-9890-753X

Complete contact information is available at: https://pubs.acs.org/10.1021/acsmedchemlett.3c00344

Author Contributions

‡A.J. and A.B.-S. contributed equally. A.J. initiated the work, carried out the theoretical experiments, and helped write the manuscript. A.B.-S. and C.G.-F. carried out the experimental assays. C.G.-F. contributed with knowledge sharing and language checking. D.R.B. conceived and mentored the research and wrote the manuscript.

Funding

The study was funded by CRG (CRG/2022/002672) and SIRE (SIR/2022/000031) grants from the Science and Engineering Research Board (SERB, DST, India)

Notes

The authors declare no competing financial interest.

■ ACKNOWLEDGMENTS

D.R.B. wants to express his gratitude to the National Institute of Technology Durgapur (NITDGP) for the platform and for the purchase of the BIOVIA Discovery Studio academic research suite. D.R.B. also thanks CRG and SIRE for funding and the DST-FIST program for the purchase of the server node at Chemistry, NIT Durgapur. A.J. thanks the National Institute of Technology Durgapur (NITDGP) for the institute fellowship. A.B-S acknowledges the Agència de Gestió d'Ajuts Universitaris i de Recerca (AGAUR) for her FI-SDUR fellowship (2021 FISDU 00182).

■ ABBREVIATIONS

Aβ, amyloid beta; AD, Alzheimer's disease; DMSO, dimethyl sulfoxide; H3K9, histone H3 lysine 9; IC_{50}, half-maximal inhibitory concentration; PTM, post-translational modification

■ REFERENCES

(1) Jones, P. A.; Baylin, S. B. The Epigenomics of Cancer. *Cell* **2007**, *128* (4), 683−692.

(2) Berger, S. L.; Kouzarides, T.; Shiekhattar, R.; Shilatifard, A. An Operational Definition of Epigenetics. *Genes Dev.* **2009**, *23* (7), 781−783.

(3) Kouzarides, T. Chromatin Modifications and Their Function. *Cell* **2007**, *128* (4), 693−705.

(4) Bernstein, B. E.; Meissner, A.; Lander, E. S. The Mammalian Epigenome. *Cell* **2007**, *128* (4), 669−681.

(5) Bannister, A. J.; Kouzarides, T. Regulation of Chromatin by Histone Modifications. *Cell Res.* **2011**, *21* (3), 381−395.

(6) Miller, J. L.; Grant, P. A. The Role of DNA Methylation and Histone Modifications in Transcriptional Regulation in Humans. *Subcell. Biochem.* **2013**, *61*, 289−317.

(7) Bowman, G. D.; Poirier, M. G. Post-Translational Modifications of Histones That Influence Nucleosome Dynamics. *Chem. Rev.* **2015**, *115* (6), 2274−2295.

(8) Helin, K.; Dhanak, D. Chromatin Proteins and Modifications as Drug Targets. *Nature* **2013**, *502* (7472), 480−488.

(9) Arrowsmith, C. H.; Bountra, C.; Fish, P. V.; Lee, K.; Schapira, M. Epigenetic Protein Families: A New Frontier for Drug Discovery. *Nat. Rev. Drug Discov.* **2012**, *11* (5), 384−400.

(10) Xiong, Y.; Li, F.; Babault, N.; Dong, A.; Zeng, H.; Wu, H.; Chen, X.; Arrowsmith, C. H.; Brown, P. J.; Liu, J.; Vedadi, M.; Jin, J. Discovery of Potent and Selective Inhibitors for G9a-Like Protein (GLP) Lysine Methyltransferase. *J. Med. Chem.* **2017**, *60* (5), 1876−1891.

(11) Kaniskan, H. Ü.; Jin, J. Chemical Probes of Histone Lysine Methyltransferases. *ACS Chem. Biol.* **2015**, *10* (1), 40−50.

(12) Kaniskan, H. Ü.; Martini, M. L.; Jin, J. Inhibitors of Protein Methyltransferases and Demethylases. *Chem. Rev.* **2018**, *118* (3), 989−1068.

(13) Sweis, R. F.; Pliushchev, M.; Brown, P. J.; Guo, J.; Li, F.; Maag, D.; Petros, A. M.; Soni, N. B.; Tse, C.; Vedadi, M.; Michaelides, M. R.; Chiang, G. G.; Pappano, W. N. Discovery and Development of Potent and Selective Inhibitors of Histone Methyltransferase G9a. *ACS Med. Chem. Lett.* **2014**, *5* (2), 205−209.

(14) Montanaro, A.; Kitara, S.; Cerretani, E.; Marchesini, M.; Rompietti, C.; Pagliaro, L.; Gherli, A.; Su, A.; Minchillo, M. L.; Caputi, M.; Fioretzaki, R.; Lorusso, B.; Ross, L.; Alexe, G.; Masselli, E.; Marozzi, M.; Rizzi, F. M. A.; La Starza, R.; Mecucci, C.; Xiong, Y.; Jin, J.; Falco, A.; Knoechel, B.; Aversa, F.; Candini, O.; Quaini, F.; Sportoletti, P.; Stegmaier, K.; Roti, G. Identification of an Epi-Metabolic Dependency on EHMT2/G9a in T-Cell Acute Lymphoblastic Leukemia. *Cell Death Dis.* **2022**, *13* (6), 551.

(15) Pangeni, R. P.; Yang, L.; Zhang, K.; Wang, J.; Li, W.; Guo, C.; Yun, X.; Sun, T.; Wang, J.; Raz, D. J. G9a Regulates Tumorigenicity and Stemness through Genome-Wide DNA Methylation Reprogramming in Non-Small Cell Lung Cancer. *Clin. Epigenetics* **2020**, *12* (1), 88.

(16) Moreira-Silva, F.; Outeiro-Pinho, G.; Lobo, J.; Guimarães, R.; Gaspar, V. M.; Mano, J. F.; Agirre, X.; Pineda-Lucena, A.; Prosper, F.; Paramio, J. M.; Henrique, R.; Correia, M. P.; Jerónimo, C. G9a Inhibition by CM-272: Developing a Novel Anti-Tumoral Strategy for Castration-Resistant Prostate Cancer Using 2D and 3D in Vitro Models. *Biomed. Pharmacother.* **2022**, *150*, 113031.

(17) Yuan, L.-T.; Lee, W.-J.; Yang, Y.-C.; Chen, B.-R.; Yang, C.-Y.; Chen, M.-W.; Chen, J.-Q.; Hsiao, M.; Chien, M.-H.; Hua, K.-T. Histone Methyltransferase G9a-Promoted Progression of Hepatocel-

lular Carcinoma Is Targeted by Liver-Specific Hsa-MiR-122. *Cancers (Basel)* **2021**, *13* (10), 2376.
(18) Bhat, K. P.; Ümit Kaniskan, H.; Jin, J.; Gozani, O. Epigenetics and beyond: Targeting Writers of Protein Lysine Methylation to Treat Disease. *Nat. Rev. Drug Discov.* **2021**, *20* (4), 265−286.
(19) Maze, I.; Covington, H. E.; Dietz, D. M.; LaPlant, Q.; Renthal, W.; Russo, S. J.; Mechanic, M.; Mouzon, E.; Neve, R. L.; Haggarty, S. J.; Ren, Y.; Sampath, S. C.; Hurd, Y. L.; Greengard, P.; Tarakhovsky, A.; Schaefer, A.; Nestler, E. J. Essential Role of the Histone Methyltransferase G9a in Cocaine-Induced Plasticity. *Science* **2010**, *327* (5962), 213−216.
(20) Griñán-Ferré, C.; Corpas, R.; Puigoriol-Illamola, D.; Palomera-Ávalos, V.; Sanfeliu, C.; Pallàs, M. Understanding Epigenetics in the Neurodegeneration of Alzheimer's Disease: SAMP8Mouse Model. *J. Alzheimer's Dis.* **2018**, *62* (3), 943−963.
(21) Han, J. L. T.; Pang, K. K. L.; Ang, S. R. X.; Sharma, M.; Sajikumar, S. Inhibition of Lysine Methyltransferase G9a/GLP Reinstates Long-Term Synaptic Plasticity and Synaptic Tagging/Capture by Facilitating Protein Synthesis in the Hippocampal CA1 Area of APP/PS1Mouse Model of Alzheimer's Disease. *Transl. Neurodegener.* **2021**, *10* (1), 23.
(22) Bellver-Sanchis, A.; Pallàs, M.; Griñán-Ferré, C. The Contribution of Epigenetic Inheritance Processes on Age-Related Cognitive Decline and Alzheimer's Disease. *Epigenomes* **2021**, *5* (2), 15.
(23) Zheng, Y.; Liu, A.; Wang, Z.-J.; Cao, Q.; Wang, W.; Lin, L.; Ma, K.; Zhang, F.; Wei, J.; Matas, E.; Cheng, J.; Chen, G.-J.; Wang, X.; Yan, Z. Inhibition of EHMT1/2 Rescues Synaptic and Cognitive Functions for Alzheimer's Disease. *Brain* **2019**, *142* (3), 787−807.
(24) Griñán-Ferré, C.; Marsal-García, L.; Bellver-Sanchis, A.; Kondengaden, S. M.; Turga, R. C.; Vázquez, S.; Pallàs, M. Pharmacological Inhibition of G9a/GLP Restores Cognition and Reduces Oxidative Stress, Neuroinflammation and β-Amyloid Plaques in an Early-Onset Alzheimer's Disease Mouse Model. *Aging* **2019**, *11* (23), 11591−11608.
(25) Bellver-Sanchis, A.; Singh Choudhary, B.; Companys-Alemany, J.; Sukanya; Ávila-López, P. A.; Martínez Rodríguez, A. L.; Brea Floriani, J. M.; Malik, R.; Pallàs, M.; Pérez, B.; Griñán-Ferré, C. Structure-Based Virtual Screening and in Vitro and in Vivo Analyses Revealed Potent Methyltransferase G9a Inhibitors as Prospective Anti-Alzheimer's Agents. *ChemMedChem* **2022**, *17* (13), No. e202200002.
(26) Bellver-Sanchis, A.; Geng, Q.; Navarro, G.; Ávila-López, P. A.; Companys-Alemany, J.; Marsal-García, L.; Larramona-Arcas, R.; Miró, L.; Perez-Bosque, A.; Ortuño-Sahagún, D.; Banerjee, D. R.; Choudhary, B. S.; Soriano, F. X.; Poulard, C.; Pallàs, M.; Du, H.; Griñán-Ferré, C. G9a Inhibition Promotes Neuroprotection through GMFB Regulation in Alzheimer's Disease. *Aging Dis.* **2023**, DOI: 10.14336/AD.2023.0424-2.
(27) Vasilopoulou, F.; Bellver-Sanchis, A.; Companys-Alemany, J.; Jarne-Ferrer, J.; Irisarri, A.; Palomera-Avalos, V.; Gonzalez-Castillo, C.; Ortuño-Sahagún, D.; Sanfeliu, C.; Pallàs, M.; Griñán-Ferré, C. Cognitive Decline and BPSD Are Concomitant with Autophagic and Synaptic Deficits Associated with G9a Alterations in Aged SAMP8Mice. *Cells* **2022**, *11* (16), 2603.
(28) Sharma, M.; Razali, N. B.; Sajikumar, S. Inhibition of G9a/GLP Complex Promotes Long-Term Potentiation and Synaptic Tagging/Capture in Hippocampal CA1 Pyramidal Neurons. *Cerebral Cortex* **2016**, *27* (6), 3161−3171.
(29) Subbanna, S.; Basavarajappa, B. S. Pre-Administration of G9a/GLP Inhibitor during Synaptogenesis Prevents Postnatal Ethanol-Induced LTP Deficits and Neurobehavioral Abnormalities in Adult Mice. *Exp. Neurol.* **2014**, *261*, 34−43.
(30) Sharma, M.; Dierkes, T.; Sajikumar, S. Epigenetic Regulation by G9a/GLP Complex Ameliorates Amyloid-Beta 1−42 Induced Deficits in Long-Term Plasticity and Synaptic Tagging/Capture in Hippocampal Pyramidal Neurons. *Aging Cell.* **2017**, *16* (5), 1062−1072.
(31) Jana, A.; Naga, R.; Saha, S.; Banerjee, D. R. 3D QSAR Pharmacophore Based Lead Identification of G9a Lysine Methyltransferase towards Epigenetic Therapeutics. *J. Biomol. Struct. Dyn.* **2023**, *41* (18), 8635−8653.
(32) Zhen, H.; Tian, J.; Li, G.; Zhao, P.; Zhang, Y.; Che, J.; Cao, B. Raltitrexed Enhanced Antitumor Effect of Anlotinib in Human Esophageal Squamous Carcinoma Cells on Proliferation, Invasiveness, and Apoptosis. *BMC Cancer* **2023**, *23* (1), 207.
(33) Huang, K.-X.; Pan, Y.-F.; Dai, R.-S.; Xu, L.-S.; Zhu, B.-W.; Zhang, X.-D.; Hu, Y.-W. A Preliminary Study of Immediate Intraperitoneal Chemotherapy for Stage III Colorectal Cancer. *Am. J. Clin. Oncol.* **2023**, *46* (5), 193−198.
(34) Xue, S.; Chen, Y.-X.; Qin, S.-K.; Yang, A.-Z.; Wang, L.; Xu, H.-J.; Geng, H.-Y. Raltitrexed Induces Mitochondrial mediated Apoptosis in SGC7901 Human Gastric Cancer Cells. *Mol. Med. Rep.* **2014**, *10* (4), 1927−1934.
(35) BIOVIA. *BIOVIA Discovery Studio Academic Research Suite*; Dassault Systèmes, San Diego, CA, 2022.

Recommended by ACS

Small-Molecule Heterocyclic Compounds: Gq-Biased Agonists for the 5-HT2A Receptor in Neuropsychiatric Treatment
Robert B. Kargbo.
OCTOBER 19, 2023
ACS MEDICINAL CHEMISTRY LETTERS
READ

Synthesis, Optimization, and Structure–Activity Relationships of Nicotinamide Phosphoribosyltransferase (NAMPT) Positive Allosteric Modulators (N-PAMs)
Zhengnan Shen, Gregory R. J. Thatcher, *et al.*
DECEMBER 14, 2023
JOURNAL OF MEDICINAL CHEMISTRY
READ

Identification of Small Molecule Inhibitors and Ligand Directed Degraders of Calcium/Calmodulin Dependent Protein Kinase Kinase 1 and 2 (CaMKK1/2)
Young Chen, Laura Akullian D'Agostino, *et al.*
NOVEMBER 27, 2023
JOURNAL OF MEDICINAL CHEMISTRY
READ

Identification and Optimization of RNA-Splicing Modulators as Huntingtin Protein-Lowering Agents for the Treatment of Huntington's Disease
Longbin Liu, Celia Dominguez, *et al.*
SEPTEMBER 15, 2023
JOURNAL OF MEDICINAL CHEMISTRY
READ

https://doi.org/10.1021/acsmedchemlett.3c00344
ACS Med. Chem. Lett. 2023, 14, 1531−1536

Supporting Information

Repurposing of Raltitrexed as an effective G9a/EHMT2 inhibitor and promising Anti-Alzheimer's agent

Abhisek Jana[1‡], Aina Bellver-Sanchis[2‡], Christian Griñán-Ferré[2,3*] & Deb Ranjan Banerjee[1*]

[1]Department of Chemistry, National Institute of Technology Durgapur, M G Avenue, Durgapur, West Bengal, India

[2]Pharmacology Section, Department of Pharmacology, Toxicology and Therapeutic Chemistry, Faculty of Pharmacy and Food Sciences, Institute of Neuroscience, Universitat de Barcelona (NeuroUB), Av. Joan XXIII 27–31, 08028 Barcelona (Spain)

[3]Centro de Investigación en Red, Enfermedades Neurodegenerativas (CIBERNED), Instituto de Salud Carlos III, Madrid, Spain

Contents:

- Experimental section: materials and methods (Pages S2 – S6)
- *In silico* ADME and TOPKAT analysis (Page S6)
- Figure S1: Representative Western-Blot for measuring the H3K9me2/H3 total in *C Elegans* CL2006 strain in presence of Raltitrexed and UNC0642. (Page S7)
- Figure S2: Study for motility as estimated by thrashing assay in presence of reference UNC0642 and Raltitrexed. (Page S7)
- Table S1: Predicted ADME properties for CNS drugability. (Page S8)
- Table S2: NTP rodent carcinogenicity prediction of UNC0642 and Raltitrexed (page S8)
- Table S3: FDA rodent carcinogenicity prediction of UNC0642 and Raltitrexed (page S9)
- Table S4: weight of evidence (WOE), Ames mutagenicity, development toxicity potential (DTP), skin irritancy, skin sensitization, ocular irritancy, aerobic biodegradability carcinogenicity prediction of UNC0642 and Raltitrexed. (Page S10)
- Table S5: G9a and GLP inhibition data at 1μM dose of Raltitrexed (Page S11)
- Comparative analysis of ADMET/TOPKAT between UNC0642 and Raltitrexed (S11)
- References (Page S12)

Experimental section: materials and methods

The materials and methods are mentioned pages S1-S6. No unexpected or unusually high safety hazards were encountered during the experiments.

Compounds preparation

The UNC0642 and Raltitrexed were purchased from Sigma-Aldrich (Merck) and the stocks were prepared directly to 10 mM in 100% DMSO (Sigma, St. Louis, USA). Then, stock solutions were diluted in MilliQ purified water to reach a final concentration ranging between 100-0.001 µM in 1% DMSO in final well.

G9a homologous assay

G9a activity was measured using the G9a Chemiluminescent Assay Kit (Catalog # 52001L, BPS Bioscience, San Diego, CA, USA). The kit contained pre-coated wells with histone H3 peptide substrate, the antibody for H3 lysine methylation, the secondary HRP-labeled antibody, the enzyme substrate SAM (S-adenosylmethionine), reaction buffer, and G9a enzyme. For the assay, SAM was incubated with reaction buffer and G9a for 1 hour in presence/absences of inhibitor, followed by incubation of anti-H3K antibody for 1 hour at room temperature. To produce the chemiluminescence output, the secondary HRP-antibody was added and incubated for 30 min, followed by addition of HRP substrate. The chemiluminescence was measured using Varioskan Lux microplate reader (Invitrogen, Thermo Scientific). The experiment was run per duplicate. The percentage of G9a activity was measured using the following equation:

$$\% \text{ G9a activity} = [(C-C_b) / (Ct-C_b)] \text{ X } 100$$

C_t: the chemiluminescence reading in absence of inhibitor.

C_b: the chemiluminescence reading in absence of G9a.

C: the chemiluminescence reading in presence of inhibitor

In Silico ADME and TOPKAT analysis

ADMET descriptors and toxicity prediction (TOPKAT) module of BIOVIA Discovery Studio (DS) Academic Research Suite was utilized to predict the toxicities of the Raltitrexed and UNC0642.[1] The ADME algorithm was used to assess the numerous pharmacokinetic parameters including aqueous solubility, cytochrome CYP2D6 inhibition, blood-brain-barrier penetration (BBB), plasma protein binding (PPB), and human intestinal absorption (HIA). Furthermore, the CNS druggability was checked by calculating the Lipinski's rule parameters.[2] The TOPKAT procedure was used to assess the possible

toxicity and degradation products of the proposed compounds. To predict toxicological end points with relation to probability values, the Quantitative Structure Toxicity Relationship (QSTR) models embedded in TOPCAT program was carefully monitored.

C. elegans strains culture and maintenance

The *C. elegans* Strains used in this work were Bristol strain N2 (WT) and the transgenic strain, CL2006 (dvIs2 [pCL12(unc-54/human Aβ peptide 1-42 minigene) + rol-6(su1006)]). The *C. elegans* Genetic Centre supplied both strains, and they were both used. The *C. elegans* was cultured and observed using conventional techniques. [3] N2 (WT) were propagated at 20ºC, while CL2006 worms were maintained at 16ºC in a temperature-controlled incubator on solid nematode growth medium (NGM) seeded with Escherichia coli (E. coli) OP50 strain as a food source.

Histone extraction and western blotting

The ratio of H3K9me2/H3 total were determined in CL2006 after each treatment in vehicle (DMSO 1%), reference UNC0642 (1, 10, 50 µM), Relitrexed (1, 10, 50 µM), as already mentioned. Four-day-old animals were collected with M9 buffer, and histone extraction was performed following the manufacturer's instructions (EpiQuik Total Histone Extraction HT Kit, EpiGentek, #OP-0007-192). The samples were resolved in a 14 % SDS-gel. Chemiluminescence signals were captured using Amersham Imager 680. To quantify the blots, ImageLab software (Bio-Rad) was used. Immunoblots were probed with anti-H3K9me2 (1: 500) (Epigentek, #A-4035), and anti-H3 total (1: 1000) (Cell signaling, #9715).

Treatment of _C. elegans_

All drug assays were performed in 96-well plate format (liquid culture). [4] Each well contained a final volume of 60 µl, comprising 20–25 animals in egg stage (15 µl), drug at the appropriate concentration (25 µl) , and 20 µl of OP50 inactivated by freeze-thaw cycles and resuspended in S-medium complete solution (30 µL 1 M $MgSO_4$, 30 µL $CaCl_2$, 100 µL 100 x trace metal solution, 100 µL 1 M Potassium citrate (pH = 6.0), 8 µL 5 mg/mL cholesterol, 50 µL Penicillin/Streptomycin, 50 µL Nystatin, and S-basal to 10 ml) to a final OD at 595 nm (OD_{595}) of 0.9 measured in the microplate reader. To obtain the age synchronized population of eggs, 5-day-old adult animals were treated with alkaline hypochlorite solution for 5 min with strong shacking, and centrifuged at 20 ºC and 2000 g, during 1 min. Then, the egg-pellets were washed in M9 buffer 3 times. Egg pellets were resuspended in S-medium (30 µL 1 M $MgSO_4$, 30 µL $CaCl_2$, 100 µL 100 x trace metal solution, 100 µL 1 M Potassium citrate (pH = 6.0), and S-basal to 10 mL), and left with continuous shaking gently for 9 hours at 37 °C until the worms reached the L1 stage. Next day, the L1 animals were transferred to the 96-well plate.

Food clearance assay

The effect of compounds on *C. elegans* physiology was monitored by the rate at which the OP50 suspension was consumed, as a readout for *C. elegans* growth, survival, or fecundity. The OD_{595} was measured daily. N2 (WT) worms were subjected to a toxicity assay in liquid format. Treated worms were grown with continuous shaking at 180 rpm at 20 °C for 6 days, starting at L1 stage as mentioned above in "Treatment *C. elegans*" section. However, in this experiment the final OD_{595} was 0.7. The concentrations of tested compounds were ranged between 100 µM to 0.01 µM. The DMSO was used as control wells in two different concentrations: DMSO 1 % as vehicle, and DMSO 5 % as toxic condition. Additionally, blank control wells were used using S-medium and S-medium complete only, without eggs or OP50, respectively. Assays were run in quartet (n=4), consisting of minimum 150 animals tested per concentration of compound.

Thrashing assay

Thrashing assay was performed to measure the effect of G9a inhibition in locomotive movement of *C. elegans.* Thrashing assays were used to quantify worm motility as a function of neurotransmitter imbalances. To measure this, worms were placed in a liquid medium and counted for lateral swimming (thrashes sec-1). A single thrash involves a complete change in the direction of the mid-body bend. In brief, worms (CL2006 and N2 (WT)) were transferred for 30 minutes to a fresh NGM plate after chronic treatment in liquid culture. First, a small volume of M9 buffer was transferred to the glass slide. Afterward, we selected 25-30 worms, allowed them to stabilize in M9 buffer for 30 seconds, and measured each worm's movement over the following 30 seconds. The number of thrashings was manually counted. This assay was run per duplicate for control and per compound concentration.

Thioflavin-S Staining Aβ Aggregation

We have followed the reported protocol as published elsewhere.[5-7] Briefly, after 4 days of treatments, CL2006 worms were fixed in 4% paraformaldehyde/PBS, pH 7.5, for 24 h at 4 °C, and permeabilized in 5% fresh β-mercaptoethanol, 1% Triton X-100, 125 mm Tris, pH 7.5, at 37 °C for another 24 h. Afterwards, they were stained with 0.125% Thioflavin S (ThS) (CAS# 1326-12-1, Sigma Aldrich, St Louis, MO, USA) in 50% ethanol for 2 min, de-stained with 50% EtOH for 2 min, washed three times with PBS, and transferred to a glass slide with a droplet of Fluoromount G (CAT#17984-25, Electron Microscopy Sciences, Hatfield, PA, USA). Fluorescence images were captured with the 20Å~ objective of a fluorescence microscope. ThS positive particles were quantified using ImageJ. First the image was converted to 8-bit, then the same threshold was set on all images, and finally the option already present in imageJ was selected to quantify the number of particles. With imageJ we also measured

the head area of the worms. The head region in C. elegans is the area delimited by the structure of the pharynx, as you can see in the following figure:

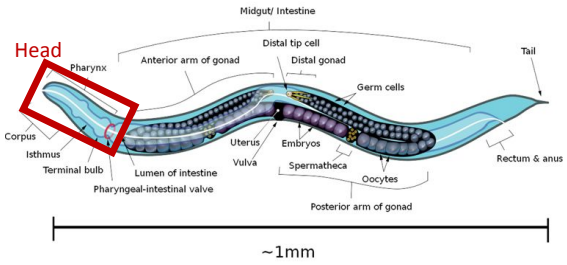

ThS-positive spots on the head regions of the worms were counted using ImageJ and expressed as Aβ deposits/anterior area for G9a inhibitor treated/untreated samples.

Data analysis

The statistical analysis was conducted using GraphPad Prism version 9.2 statistical software. Group size may differ depending on power analysis and expertise of the authors. Shapiro–Wilk test was employed to verify data normality for all groups. Data were expressed as the mean ± Standard Error of the Mean (SEM). For normally distributed data, means were compared in One-Way or Two-Way Analysis of variance (ANOVA), followed by Tukey's post-hoc analysis. Comparison between groups was also performed by a two-tailed Student's t-test for independent samples. In contrast, the Mann-Whitney or Kruskal–Wallis test followed by Dunn's post-hoc analysis was used for non-normally distributed data. Statistical significance was considered when p-values were <0.05. For behavioral tests, a blinded analysis was performed.

EHMT1 (GLP) Chemiluminescent Assay kit

The assay was carried out using EHMT1 (GLP) Chemiluminescent Assay kit as reported previously.[8] Briefly, compounds were added on a 96-well plate precoated with histone substrate supplied by kit. 30 µl of master mixture SAM were added and the reaction was initiated adding 20 µl of diluted EHMT1 (GLP) enzyme. The reaction was incubated at room temperature (RT) for 1 hour. The plate was washed three times with 200µl TBST buffer. 100 µl of Blocking buffer were added to every well and the plate was incubated at RT for 10 minutes with shaking. Supernatant was removed and 100µl of Primary antibody were added per well. The plate was incubated at RT for 1 hour with slow shaking. The plate was washed three times with 200µl TBST buffer. 100 µl of Blocking buffer were added to every well and the plate was incubated at RT for 10 minutes with shaking. 100µl of Secondary HRP-labeled antibody were added per well and the plate was incubated at RT for 30 minutes with slow shaking. The plate was washed three times with 200µl TBST buffer. Finally, 100µl of substrate mix were added

and the luminescence was measurement with integration time of 1 second in in Perkin Elmer EnSpire Multimode plate reader.

***In silico* ADME and TOPKAT analysis**

To further investigate the ADME and toxicology of Raltitrexed, the ADME program embedded in BIOVIA Discovery Suite (DS) Academic Research Suite was utilized for forecasting the CNS-related pharmacological properties, physicochemical descriptors and pharmaceutically relevant properties. The oral bioavailability was determined using Lipinsk's rule of five showing that Raltitrexed as well as reference UNC0642 would have high bioavailability [36]. The **Table S1** depicts the Lipinski's rule along with the molecular weight, number of hydrogen bond donors, number of hydrogen bond acceptors, number of rotatable bonds, and AlogP. The distribution and uptake of the substances may be greatly influenced by their aqueous solubility (logS). Raltitrexed displayed good aqueous solubility in comparison to the reference compound UNC0642. This drug's pharmacokinetics data were encouraging, but its anticipated BBB permeability was lower than UNC0642, presumably due to decreased lipophilicity caused by lower ALogP, logBBB, and higher PSA values (**Table S1**). For medication distribution, the projected PPB value is an essential metric. UNC0642 as well as Raltitrexed were discovered to be strongly attached to plasma protein.

Toxicology prediction by computer assisted technology (TOPKAT), summarized in **Table S2**, **S3**, and **S4** is another technique used to assess the drug's therapeutic compatibility. TOPKAT is a helpful tool for quantitative *in-silico* toxicity prediction and is used in QSTR (quantitative structure-activity relationship) models. Additionally, it calculates probability values and assesses toxicity through them using these QSTR models. The components were checked against the optimal predictive space (OPS) to rule out any false positive. The NTP rodent carcinogenicity models were used to compute the toxicity risk in the UNCO642 and Raltitrexed (**Table S2**). The NTP carcinogenicity profile of Raltitrexed was better compared to the UNC0642, as it was non carcinogenic in all the four NTP predictions (**Table S2**). Another model provided by the USFDA (United States Food and Drug Administration) was used to compute the carcinogenicity. The reference compound UNC0642 was non-carcinogen in all the FDA predictions, on the other hand Raltitrexed was non carcinogenic except for the rat female FDA none *vs* carcinogen prediction (**Table S3**). Additional specific anticipated toxicity parameters such as weight of evidence, development toxicity potential, skin irritancy, skin sensitization, ocular irritancy, and aerobic biodegradability are listed in **Table S4**. The results of toxicity risks for Raltitrexed displayed good drug score as compared to the UNC0642.

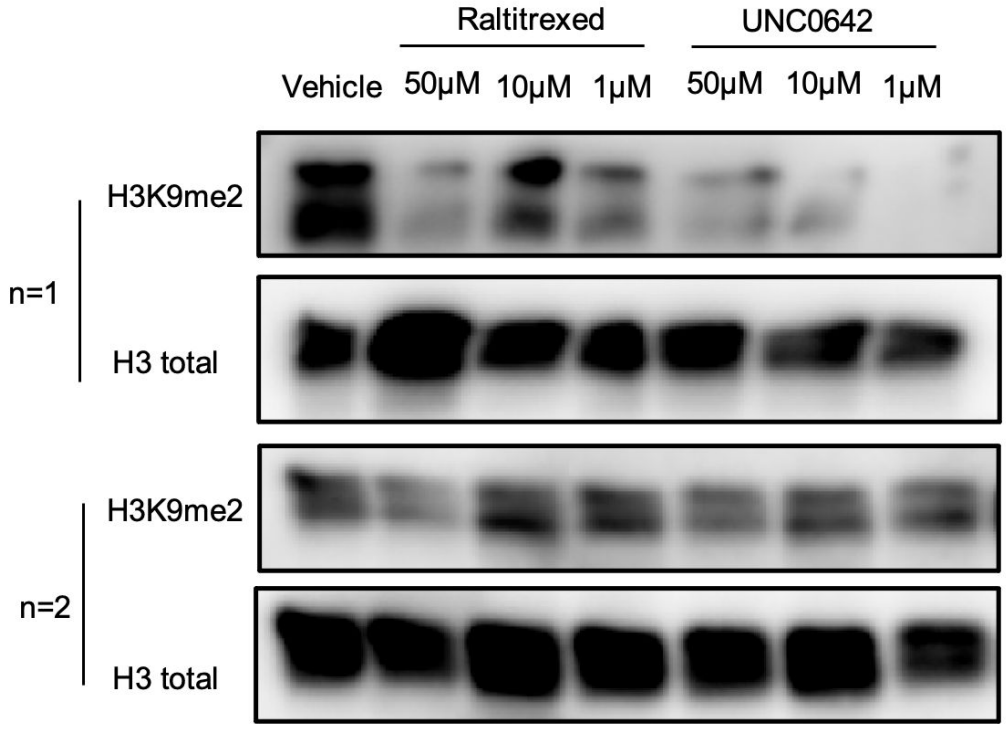

Figure S1: Representative Western-Blot for measuring the H3K9me2/H3 total in *C. elegans* CL2006 strain after treatment with Raltitrexed or UNC0642.

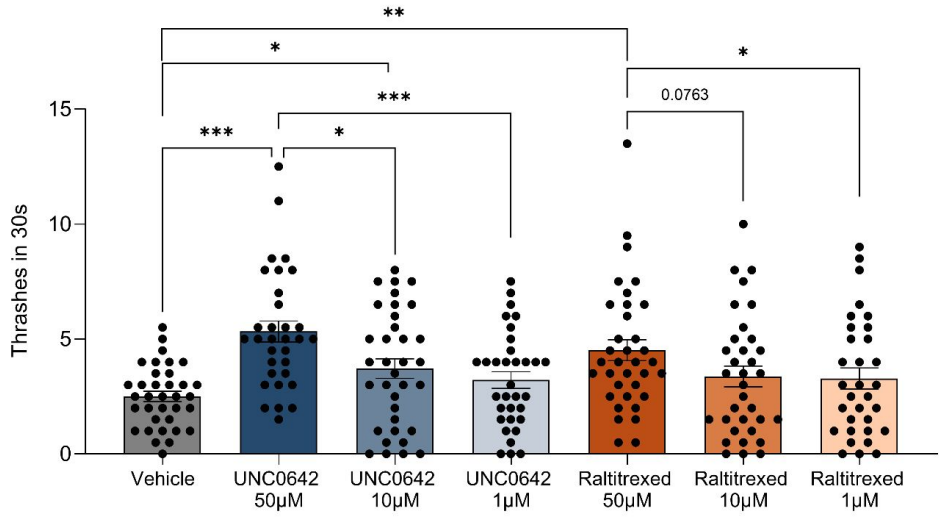

Figure S2: Study for motility as estimated by thrashing assay. Values represented are mean ± standard error of the mean (SEM); (n= 27-30 worms/group in each technical replicate; Kruskal–Wallis test followed by Dunn's, and Student's t-test or Mann-Whitney in when it was appropriate; *p<0.05; **p<0.01; ***p<0.001).

Table S3: FDA rodent carcinogenicity prediction of UNC0642 and Raltitrexed

FDA Prediction	**UNC0642**	**Raltitrexed**
Mouse Female FDA	Non-carcinogen	Non-carcinogen
Mouse male FDA	Non-carcinogen	Non-carcinogen
Rat Female FDA	Non-carcinogen	Non-carcinogen
Rat male FDA	Non-carcinogen	Non-carcinogen
Mouse female FDA none vs carcinogen prediction	Non-carcinogen	Non-carcinogen
Mouse female FDA none vs carcinogen probability	0.22	0.22
Mouse female FDA none vs carcinogen enrichment	0.69	0.69
Mouse female FDA none vs carcinogen enrichment	-12.37	-9.68
Mouse male FDA none vs carcinogen prediction	Non-carcinogen	Non-carcinogen
Mouse male FDA none vs carcinogen probability	0.09	0.22
Mouse male FDA none vs carcinogen enrichment	0.30	0.76
Mouse male FDA none vs carcinogen enrichment	-15.36	-3.59
Rat female FDA none vs carcinogen prediction	Non-carcinogen	carcinogen
Rat female FDA none vs carcinogen probability	0.17	0.33
Rat female FDA none vs carcinogen enrichment	0.54	1.02
Rat female FDA none vs carcinogen enrichment	-11.92	1.33
Rat male FDA none vs carcinogen prediction	Non-carcinogen	Non-carcinogen
Rat male FDA none vs carcinogen probability	0.15	0.29
Rat male FDA none vs carcinogen enrichment	0.45	0.89
Rat male FDA none vs carcinogen enrichment	-11.15	-2.14

Table S4: weight of evidence (WOE), Ames mutagenicity, development toxicity potential (DTP), skin irritancy, skin sensitization, ocular irritancy, aerobic biodegradability carcinogenicity prediction of UNC0642 and Raltitrexed.

TOPKAT predictions	**UNC0642**	**Raltitrexed**
WOE Prediction	Non-carcinogen	Non-carcinogen
WOE probability	0.08	0.43
WOE enrichment	0.16	0.83
WOE score	-19.58	-2.92
Ames prediction	Non-mutagen	Non-mutagen
Ames probability	0.17	0.12
Ames enrichment	0.30	0.21
Ames Score	-14.99	-16.69
DTP prediction	toxic	Non-toxic
DTP probability	0.80	0.49
DTP enrichment	1.53	0.93
DTP score	6.77	-1.65
Skin irritancy	none	None
Skin irritancy none vs irritant prediction	Non-irritant	Non-irritant
Skin irritancy none vs irritant probability	0.89	0.97
Skin irritancy none vs irritant enrichment	0.97	1.05
Skin irritancy none vs irritant score	-2.86	-1.06
Skin sensitization	strong	weak
Skin sensitization none vs sensitizer prediction	irritant	irritant
Skin sensitization none vs sensitizer probability	0.75	0.75
Skin sensitization none vs sensitizer enrichment	1.09	1.09
Skin sensitization none vs sensitizer score	-0.81	0.84
Skin sensitization weak vs strong prediction	strong	weak
Skin sensitization weak vs strong probability	0.87	0.83
Skin sensitization weak vs strong enrichment	1.12	1.07
Skin sensitization weak vs strong score	-0.92	-1.96
Ocular irritancy	severe	moderate
Ocular irritancy none vs irritant prediction	irritant	irritant
Ocular irritancy none vs irritant probability	0.99	0.99
Ocular irritancy none vs irritant enrichment	1.17	1.17
Ocular irritancy none vs irritant score	3.45	1.95
Aerobic biodegradability prediction	Non-degradable	Non-degradable
Aerobic biodegradability probability	0.06	0.22
Aerobic biodegradability enrichment	0.13	0.49
Aerobic biodegradability score	-14.95	-6.64

Table S5: G9a and GLP inhibition data at 1µM dose of Raltitrexed

% G9a inhibition (1µM)		% GLP inhibition (1µM)	
UNC0642	Raltitrexed	UNC0642	Raltitrexed
84.96 ± 0.45	71.49 ± 4.62	66 ± 4	49.98 ± 1.73

Comparative analysis of ADMET/TOPKAT between UNC0642 and Raltitrexed

A computed probability less than 0.3 for a chemical suggests a non-carcinogen, that is, NE (No Evidence) in terms of NTP assignment, while a probability more than 0.7 indicates a carcinogen that is, CE (Clear Evidence) or SE (Some Evidence) in terms of NTP assignment. The "indeterminate" zone (IND) is denoted by a probability range between 0.3 and 0.7. UNC0642 was demonstrated to be a carcinogen in mouse male and rat female model of NTP rodent carcinogenicity module, whereas OPS components of Raltitrexed was within the range for both the predictions and predicted to be non-carcinogen (Table S2). For the weight of evidence (WOE) and Developmental toxicity potential (DTP), same range of probability is applied for the carcinogenicity or toxicity predictions. The DTP probability of UNCO642 is very high as compared to the Raltitrexed, as a result Raltitrexed is non-toxic in DTP prediction. Although WOE probability value UNCO642 is very less compared to the Raltitrexed, both are non-carcinogen in WOE prediction. Computed probability of both UNCO642 and Raltitrexed fall within 0 and 0.3, they are both non-mutagen in nature. The TOPKAT Skin Sensitization Module consists of two modules: one for None vs. Sensitizers and another for Weak vs. Strong Sensitizers. Each module contains two statistically significant and cross-validated quantitative structure-toxicity relationship (QSTR) models applicable to a certain class of chemicals, as well as the data used to generate these models. The discriminant models for the None vs. Sensitizers module compute the chance of a submitted structure being a sensitizer (probability greater than 0.7) or a non-sensitizer (probability less than 0.30). A likelihood of 0.7 or higher implies a strong sensitizer in the Weak vs. Strong Sensitizers module, while a probability of less than 0.30 indicates a weak or moderate sensitizer. Probability values between 0.30 and 0.70 denote an ambiguous range in which decisions should be avoided unless exceptional circumstances exist. Raltitrexed was predicted to be weak skin sensitizer as compared to the UNCO642. In the Draize test, ocular irritancy predicts whether a substance is likely to be an eye irritant and how severe the irritation will be. Raltitrexed and UNCO642 is predicted to be moderate and severe in the ocular irritancy model.

References:

[1] BIOVIA (2022), Dassault Systèmes, BIOVIA Discovery Studio Academic Research Suite, San Diego: Dassault Systems.

[2] Lipinski, C., A.; Lombardo, F.; Dominy, B., W.; Feeney, P., J. Experimental and computational approaches to estimate solubility and permeability in drug discovery and development settings. *Adv Drug Deliv Rev.* **2001***, 46* (1-3), 3–26.

[3] Brenner, S. The genetics of Caenorhabditis elegans. Genetics. **1974**, *77* (1) 71–94.

[4] Voisine, C.; Varma, H.; Walker, N., Bates, E., A.; Stockwell, B., R.; Hart, A., C. Identification of Potential Therapeutic Drugs for Huntington's Disease using Caenorhabditis elegans. *PLoS One.* **2007**, *2* (6), e504.

[5] Yang, Y.; Wang, M.; Yang, P.; Wang, Z.; Huang, L.; Xu, J.; Wang, W.; Yu, M.; Bu, L.; Fei, J.; Huang, F. The Aβ Containing Brain Extracts Having Different Effects in Alzheimer's Disease Transgenic Caenorhabditis elegans and Mice. *Front Aging Neurosci.* **2018**, *10*, 208.

[6] Kang, N.; Luan, Y.; Jiang, Y.; Cheng, W.; Liu, Y.; Su, Z.; Liu, Y.; Tan, P. Neuroprotective Effects of Oligosaccharides in Rehmanniae Radix on Transgenic Caenorhabditis elegans Models for Alzheimer's Disease. *Front Pharmacol*. **2022**, *13*, 878631

[7] Zhang, X.G.; Wang, X.; Zhou, T.T.; Wu, X.F.; Peng, Y.; Zhang, W.Q.; Li, S.; Zhao, J. Scorpion venom heat-resistant peptide protects transgenic Caenorhabditis elegans from β-amyloid toxicity. *Frontiers in pharmacology*. **2016**, *26* (7), 227.

[8] Bellver-Sanchis, A.; Singh Choudhary, B.; Companys-Alemany, J.; Sukanya; Ávila-López, P. A.; Martínez Rodríguez, A. L.; Brea Flori-ani, J. M.; Malik, R.; Pallàs, M.; Pérez, B.; Griñán-Ferré, C. Structure-Based Virtual Screening and in Vitro and in Vivo Analyses Re-vealed Potent Methyltransferase G9a Inhibitors as Prospective Anti-Alzheimer's Agents. *ChemMedChem.* **2022**, *17* (13), e202200002.

4 Discussion

Neurodegenerative diseases, including AD, are a significant cause of disability and mortality worldwide (Deuschl et al., 2020). The research of aging and neurodegeneration focused on mechanisms that govern them are as fascinating as challenging. Advances in sequencing technologies have enabled the mapping of transcriptomic patterns in various neurodegenerative diseases (Nativio et al., 2020). This sheds light on classical neurodegenerative pathways and reveals novel targets, including synaptic degeneration, a common feature of many diseases such as AD (Dharshini et al., 2021; Shademan et al., 2021). Despite thorough genetic evaluations in large patient populations, a significant number of cases of neurodegenerative disease lack a known genetic basis (Blauwendraat et al., 2019). Moreover, several studies on neurodegenerative diseases have shown that adverse environmental factors contribute to neurodegeneration and the subsequent development of pathological and behavioural abnormalities (Hou et al., 2019; Nabi and Tabassum, 2022; Wilson et al., 2023).

The dysregulation of several molecular pathways and intracellular signaling occurs at the sub/cellular level in the brain of individuals with AD. These mechanisms include Aβ and Tau proteostasis, synaptic plasticity, inflammatory-immune responses, and OS (Hampel et al., 2021). Their dysregulation results from a multilayer interaction among genetic, biological, and environmental factors (Castrillo and Oliver, 2016). In this context, epigenetics is crucial in linking the genome to the environment. Epigenetics is a branch of genetics that studies heritable and reversible changes in gene expression without altering the DNA sequence (Cavalli and Heard, 2019). This includes changes such as DNA methylation, histone modifications, and alterations in ncRNA. Of note, epigenetics has been shown to regulate the transcription of genes linked to cell differentiation, learning, and memory (Kosik et al., 2012; Xiao et al., 2020) and is a critical regulator of both development and aging (Brunet and Berger, 2014; Pal and Tyler, 2016), with the latter being the most significant risk factor for AD.

Despite decades of research in the field of AD, most strategies aimed at reversing this pathology are currently limited to treating symptoms and have failed to prevent its progression. For instance, the Aβ hypothesis has been the mainstream concept underlying AD research for over two decades. However, all efforts to develop drugs targeting Aβ have proved

unsuccessful. It has been discovered that healthy patients can exhibit Aβ deposits, while some AD patients may have minimal Aβ deposition (Edison et al., 2007; Li et al., 2008). Additionally, the presence and distribution of Aβ plaques in elderly individuals without dementia can be comparable to those found in dementia patients (Davis et al., 1999; Fagan et al., 2009; Price et al., 2009; Chételat et al., 2013). These findings suggest that Aβ deposition is a natural part of aging and does not necessarily correlate directly with the onset of AD.

In contrast, the progression of AD appears to be strongly correlated with Tau pathology rather than Aβ accumulation. This is because Tau lesions have been reported earlier (Braak and Del Tredici, 2014; Johnson et al., 2015). Recent research has highlighted the importance of plasma p-Tau markers, including p-Thr181, p-Thr217, and p-Thr231, in improving clinical diagnosis and prognosis. These biomarkers show excellent diagnostic utility, especially in the symptomatic stages of AD, with p-Thr217 and p-Thr231 potentially being early indicators of incipient AD, preceding the elevation of p-Thr181 (Ossenkoppele et al., 2022). Reports suggest that suppressing or removing Tau significantly protects against brain damage and neurological impairment (Rapoport et al., 2002; Santacruz et al., 2005; Shipton et al., 2011; Bi et al., 2017). Compounds that prevent Tau's hyperphosphorylation may impact disease progression, but none of the clinical trials have been approved due to their limited benefit.

Thus, the need to identify pathways upstream of Aβ and NFT formation or distinct mechanisms is highlighted (Benayoun et al., 2015). Over the last few decades, several epigenetic mechanisms have been extensively studied and have become important targets for drug development, particularly in the neurosciences. Indeed, aberrant epigenetic marks can silence genes critical for neuronal function while upregulating genes associated with disease progression (Landgrave-Gómez et al., 2015; Bertogliat et al., 2020; Murshid et al., 2022). Thus, epigenetic therapy aims to restore normal gene function by manipulating epigenetic changes, potentially slowing down or halting the progression of neurodegenerative diseases. Several epigenetic targets are currently being studied for treating neurodegenerative diseases (Bustos et al., 2017; Rathore et al., 2021; Kaur et al., 2022).

In brief, this thesis expands our understanding of the HMT G9a and its role in neurodegeneration, particularly in AD. Our research confirms G9a's involvement in the neurodegenerative processes that underlie AD using the SAMP8 mouse model. Further, we demonstrate the therapeutic potential of G9a inhibition in treating AD and identify novel pathways, including GMFB modulation and miRNA regulation, that are affected by G9a inhibition. Aware of the challenges with existing G9ais, we also focused on identifying compounds with improved properties. [redacted] Furthermore, we explored drug repurposing as a cost-effective and less risky strategy and identified **Raltitrexed** as a potential G9ai.

4.1. G9a is a potential target for Alzheimer's disease

G9a is a histone lysine methyltransferase identified as having a critical role in various neurodegenerative diseases, including AD (Park et al., 2022). Therefore, we aimed to validate the hypothesis that overexpression of G9a is present in AD. To address this, we evaluated the expression levels of G9a and its repressive mark, H3K9me2, in the human brains of AD patients and different experimental models such as SAMP8 and *C. elegans*.

As described by Zheng et al. in 2019 (Zheng et al., 2019), our results also confirm the relevance of G9a and its repressor histone mark H3K9me2 in patients with AD. However, it is worth nothing that for the first time, higher levels of H3K9me2 have been correlated with increased levels of the $A\beta_{42}/A\beta_{40}$ ratio, one of the most well-known signs of the disease ((Bellver-Sanchis et al., 2024b) Publication 2), pointing out its role in the neurodegenerative process of AD. Similarly, another study showed elevated levels of H3K9me2 in the occipital cortex of postmortem AD brains compared to the non-demented (ND) group (Lithner et al., 2013).

SAMP8 may be a valuable tool for better understanding the dynamics of the global epigenetic landscape during age-related cognitive decline, as genetic factors cannot fully explain its

phenotype. In previous studies (Cosín-Tomás et al., 2014, 2018; Griñan-Ferré et al., 2016c; Griñán-Ferré et al., 2018), our group identified several epigenetic alterations in SAMP8 compared to SAMR1. These findings reveal the significant interaction between epigenetic mechanisms and gene networks in pathological aging. In addition, it may help to identify markers and therapeutic candidates for AD and other cognitive disorders. In 2019, our group and Zheng et al. conducted PoC studies in 5xFAD mice, focusing on a model of EOAD, and the results showed that G9a is a promising target for AD (Griñán-Ferré et al., 2019; Zheng et al., 2019). However, G9a has yet to be studied in models representing the sporadic form of AD, also known as LOAD. To this end, the SAMP8 mouse model was used in this thesis to characterize the G9a and its repressive mark and evaluate the G9a inhibition as a novel therapeutic approach for AD. Firstly, it was found that SAMP8 mice exhibited specific epigenetic modifications in G9a and H3K9me2, similar to those detected in AD patients. Consistent with data from AD patients, we also identified a correlation between elevated levels of $A\beta_{42}/A\beta_{40}$ and H3K9me2 levels in SAMP8, suggesting a potential involvement of G9a and H3K9me2 in the age-related cognitive decline exhibited by this AD rodent model ((Bellver-Sanchis et al., 2024b) Publication 2). In particular, elevated levels of $A\beta_{40}$ were found in SAMR1 mice compared with SAMP8 mice ((Bellver-Sanchis et al., 2024b) Publication 2). Accordingly, $A\beta_{40}$ is widely recognized to inhibit Aβ deposition *in vivo* (Kim et al., 2007). Therefore, this finding may help how G9a inhibition contributes to the reduction of Aβ aggregation. However, it is essential to note that the exact mechanism has not been extensively explored in this doctoral thesis. Moreover, to better understand the role of G9a in age-related cognitive decline, we assessed its levels in 12-month-old SAMP8 mice. An increase in the overall H3 methylation landscape was associated with higher levels of G9a gene expression in the aged SAMP8 group ((Vasilopoulou et al., 2022) Publication 1).

In addition, to elucidate how G9a contributes to the pathogenesis of AD, we took advantage of the ease of gene manipulation in *C. elegans*. As mentioned earlier, the G9a homolog in worms is known as *set-25* (Towbin et al., 2012; Woodhouse et al., 2018; Woodhouse and Ashe, 2019). Therefore, we used the RNAi approach to generate the *set-25* KD in various AD transgenic strains (CL2006 and CL2355). Within AD *C. elegans* strains, we demonstrated the occurrence of Aβ aggregation and epigenetic changes similar to those identified in AD

patients ((Bellver-Sanchis et al., 2024b) Publication 2). These features were reversed in the *set-25*-KD worms ((Bellver-Sanchis et al., 2024b) Publication 2), confirming our hypothesis about the contribution of G9a to AD-like pathology.

In summary, our analysis of human brain samples, SAMP8 mouse models, and *C. elegans* revealed a correlation between G9a overexpression and AD-related markers, such as the $A\beta_{42}/A\beta_{40}$ ratio. These findings highlight the importance of epigenetic mechanisms in AD and suggest a potential therapeutic avenue through G9a inhibition. However, the mechanism by which G9a promotes neurodegeneration is not well understood. Therefore, the next objective was to elucidate its role at both the behavioural and molecular levels.

4.2. Effects of G9a on cognitive decline and BPSD in SAMP8, a LOAD mouse model

The SAMP8 mouse model is established by phenotypic selection of ARK/J mice and exhibits accelerated senescence, making them suitable to study age-related neurodegenerative diseases such as LOAD (Morley, 2002; Takeda, 2009; E. Morley et al., 2012; Griñán-Ferré et al., 2018; Liu et al., 2020). As our group previously described, SAMP8 presents cognitive symptoms and behavioural alterations similar to those seen in AD, including anxiety and depressive behaviours (Griñan-Ferré, Palomera-Ávalos, et al., 2016; Vasilopoulou et al., 2020). Increasing evidence has linked epigenetic changes with the accelerated aging processes in the SAMP8 brain (Cosín-Tomás et al., 2014, 2018; Griñán-Ferré et al., 2018). Epigenetic mechanisms become dysregulated during pathological aging, contributing to the gradual decline of cognitive and behavioural functions (Harman and Martín, 2020). G9a, a regulator of chromatin structure in the central nervous system, has been associated with brain development, memory consolidation, and cognitive deficits (Gupta-Agarwal et al., 2012; Pang et al., 2019). In addition, Wang et al. (Wang et al., 2018a) demonstrated that chronic treatment with UNC0642 and A-366 reduced anxiety-like behaviours in adult male mice. Therefore, we aimed to assess the potential role of G9a in the cognitive and behavioural changes observed in the SAMP8 model.

As memory loss and cognitive dysfunction are significant symptoms of age-related cognitive decline and AD, various preclinical studies have assessed the cognitive status of SAMP8 mice using cognitive tests such as the Novel Object Recognition Test (NORT, and OLT). Consistent with previous studies by our group and others (Maes et al., 2008), SAMP8 mice exhibited lower discrimination index (DI) in both the 2h short-memory test ((Vasilopoulou et al., 2022) Publication 1; (Bellver-Sanchis et al., 2024b) Publication 2) and the 24h long-memory test ((Bellver-Sanchis et al., 2024b) Publication 2). Additionally, we observed that aged male SAMP8 mice had weaker cognitive performance than age and sex-matched in comparison with old SAMR1 mice ((Vasilopoulou et al., 2022) Publication 1). Regarding the OLT, the DI level in SAMP8 mice was lower compared to SAMR1 mice, indicating impaired spatial memory ((Bellver-Sanchis et al., 2024b) Publication 2). Similarly, studies have shown that inhibitors of KTMs significantly improve cognitive behaviours, including recognition, spatial, and working memory (Artal-Martinez de Narvajas et al., 2013; Cao et al., 2020; Williams et al., 2023). Considering the bibliography and the hypothesis of this doctoral thesis, the effect of pharmacological inhibition of G9a was evaluated in both tests. On the one hand, the results of the NORT revealed that SAMP8 mice treated with G9ai (**UNC0642**, [redacted] exhibited significant improvement in cognitive deficits in both short-term and long-term memory, compared to the SAMP8 Control group of mice ((Bellver-Sanchis et al., 2024b) Publication 2; Annex 1; Annex 2). On the other hand, the outcomes of OLT revealed that SAMP8 mice treated with G9ai (**UNC0642** and [redacted]) displayed an elevated DI compared to the SAMP8 Control group ((Bellver-Sanchis et al., 2024b) Publication 2; Annex 1).

Additionally, the non-cognitive aspects of the disease, such as fear-anxiety and depressive-like behaviour, hold particular significance, as they often contribute to accelerated cognitive decline and eventual social impairments. Managing both memory loss and BPSD is crucial for both patients and caregivers. Nevertheless, there needs to be more research on these distinct specific symptoms in humans (Cerejeira et al., 2012) due to the need for suitable animal models for studying BPSD and age-related emotional changes. Interestingly, Wang's findings in 2018 (Wang et al., 2018a) underscore the significance of G9a in the genesis of anxiety-related behaviours, warranting further investigation in this domain. Therefore, a battery of behavioural tests (OF, EPM, TCT, and RI) were performed on aged SAMP8 mice.

The findings of this doctoral dissertation indicate that aged SAMP8 mice exhibit a thigmotaxis attitude, confirming the elevated anxiety-like behaviour. SAMP8 mice spent more time in the border zone of the OF and slightly less time in the central zone, along with heightened locomotor activity and rearings ((Vasilopoulou et al., 2022) Publication 1). However, the EPM data revealed that SAMP8 mice tended to spend more time in both closed and open arms compared to SAMR1 mice. The contradictory observations regarding SAMP8 could be due to their greater locomotor activity. However, more is needed to fully clarify the interpretation of the EPM data ((Vasilopoulou et al., 2022) Publication 1). In the TCT assessment of social behaviour, 12-month-old male SAMP8 mice exhibited no preference for the chamber and reduced social interaction, indicating deficits in this aspect ((Vasilopoulou et al., 2022) Publication 1). These findings are consistent with previous research describing decreased sociability in SAMP8 mice (Meeker et al., 2013; Companys-Alemany et al., 2020). Alongside social impairments, aggression is a distressing consequence of dementia, mainly due to its direct impact on social functionality (Jackson and Mallory, 2009). We demonstrated that aged SAMP8 males showed increased aggressive behaviour, as evidenced by a shorter latency to attack and a higher total number of attacks. Importantly, this outcome had yet to be previously reported ((Vasilopoulou et al., 2022) Publication 1). Notably, the positive effect of G9ai treatment on social performance has yet to be previously registered. This doctoral dissertation presents the first evidence that G9a inhibition can enhance social behaviour in SAMP8 mice ((Bellver-Sanchis et al., 2024b) Publication 2). The effects of pharmacological inhibition of G9a on the EPM test were not studied in this thesis. However, Anderson and colleagues (Anderson et al., 2018) have described that overexpression of G9a in male rats' nucleus accumbens shell (NAcSh) increases anxiety-like behaviour based on avoidance of open arms. Similarly, another study suggested that G9a knockdown is associated with a reduction in baseline anxiety, although in the context of cocaine self-administration and reinstatement (Anderson et al., 2019).

All this contributes to characterizing BPSD signs in SAMP8 mice, especially at 12 months old. Fear and anxiety-like behaviour have been associated with age-related cognitive deficits in SAMP8 mice (Miyamoto, 2004; Meeker et al., 2013). These results suggest a potential link between anxiety-related parameters and cognitive performance, indicating a plausible

association between emotional disturbances and memory impairment in aged male SAMP8 mice. Furthermore, we identified significant correlations when exploring the relationship between social or aggressive behaviour and cognitive performance. These findings support the consensus that aggression and social impairments in AD and age-related dementias are linked to the degree of cognitive impairment ((Vasilopoulou et al., 2022) Publication 1).

In summary, our study utilizing the SAMP8 mouse model emphasizes the significance of G9a in the cognitive and behavioural manifestations of AD and age-related neurodegenerative processes. Through cognitive tests and behavioural assessments, we demonstrate that pharmacological inhibition of G9a enhances cognitive function and reduces anxiety behaviours in SAMP8 mice. Additionally, the study reveals the complex correlation between cognitive decline and non-cognitive symptoms, including aggression and social disturbances. This suggests a potential association between emotional disturbances and memory impairment in AD. Synaptic function is the primary determinant of cognitive performance, and therefore, synapse loss appears to be the most significant factor contributing to cognitive impairment in AD (Scheff and Price, 2006; Scheff et al., 2007; De Wilde et al., 2016). Thus, we sought to decipher the mechanisms involved in synaptic function modulated by G9a inhibition in SAMP8.

4.3. Molecular insights into the enhancement of synaptic plasticity by inhibition of G9a in SAMP8

As aforementioned, synaptic dysfunction is a significant contributor to AD pathogenesis (Marksteiner et al., 2002; Scheff and Price, 2006; Scheff et al., 2007; Tönnies and Trushina, 2017; Li et al., 2018). Growing evidence suggests that activity-dependent epigenetic modulation is essential for memory and synaptic plasticity (Lattal and Wood, 2013; Zovkic et al., 2013). In particular, the involvement of G9a and its associated repressive mark, H3K9me2, in memory formation and cognition has garnered attention in the last decade. As our group demonstrated in 5xFAD (Griñán-Ferré et al., 2019), the pharmacological G9a

inhibition (**UNC0642**) increased synaptic plasticity in SAMP8 mice, as indicated by increased levels of pre-synaptic (e.g., SYNIIa) and post-synaptic (e.g., PSD95, PSD93) protein levels. Significantly, these changes were associated with the cognitive improvement observed in the mice ((Bellver-Sanchis et al., 2024a) Publication 3).

Neurotrophic factors, such as BDNF and other neurotrophin family members, play a central role in the activity-dependent plasticity affecting neuronal networks' structure and function. NGF and BDNF were first identified for their ability to promote the survival of neurons and neurites (Levi-Montalcini and Cohen, 1956; Barde et al., 1982; Barde, 1989). Other neurotrophins, such as NT-3 and NT-4 (Maisonpierre et al., 1990; Huang and Reichardt, 2001), were then identified through sequence similarity to NGF and BDNF. Additionally, BDNF, NT3, and NGF have been linked to BPSD, including anxiety, depression, and aggressive behaviour (Ernfors et al., 1990; Hohn et al., 1990; Maisonpierre et al., 1990). This doctoral thesis demonstrated decreased *Bdnf*, *NT3,* and *Ngf* gene expression in aged SAMP8 male mice ((Vasilopoulou et al., 2022) Publication 1). Previous research on animal models of AD has consistently shown that reduced levels of BDNF and NGF contribute to neuronal and synaptic dysfunction, ultimately leading to cognitive impairment (Jiao et al., 2016a; Buhusi et al., 2017). It is worth noting that epigenetic mechanisms may influence BDNF transcription. Specifically, inhibiting G9a (**UNC0642**) has been demonstrated to elevate *Bdnf* gene expression in AD mouse models (Peng et al., 2009; Lu et al., 2013; Sharma et al., 2017a). SAMP8 mice treated with a G9ai (**UNC0642**) exhibit up-regulation of the BDNF protein expression levels ((Bellver-Sanchis et al., 2024b) Publication 2), as well as of the *Vgf* and *Transforming growth factor* (*Tgf*) gene expression levels ((Bellver-Sanchis et al., 2024a) Publication 3).

Interestingly, neurotrophins exert their effects by activating two distinct receptor types. Specifically, recent findings indicate that mature neurotrophins primarily engage with Trk receptors, facilitating neuronal survival and enhancing plasticity (Maes et al., 2008; Companys-Alemany et al., 2020). A remarkable downregulation in the gene expression of *TrkA* and *TrkB* was determined in aged SAMP8 mice, corroborating the deficits in the synaptic function of the SAMP8 strain ((Vasilopoulou et al., 2022) Publication 1). In contrast,

SAMP8 showed increased *TrkA* and *TrkB* gene expression levels following G9ai treatment (**UNC0642**) ((Bellver-Sanchis et al., 2024a) Publication 3). Accordingly, phosphorylation of TrkB was observed in SAMP8 treated with G9ai (**UNC0642**) ((Bellver-Sanchis et al., 2024b) Publication 2).

Additionally, G9a has been implicated in both memory consolidation and formation mechanisms (Gupta-Agarwal et al., 2012; Pang et al., 2019), long-lasting forms of synaptic plasticity such as LTP and long-term depression (LTD), both fundamental cellular mechanisms underlying learning and memory (Bliss and Collingridge, 2013). Research has demonstrated that inhibiting G9a can enhance LTP and synaptic associativity deficits in an *in vitro* model of AD. The pharmacological inhibition of the G9a complex (UNC0638 and BIX-01294) improved LTP and enabled it to interact with nearby synaptic populations, resulting in synaptic tagging/capture (STC). BDNF is a critical protein in plasticity that maintains the facilitation of LTP by inhibiting the G9a/GLP complex and the associated STC phenomenon (Sharma et al., 2017b; Han et al., 2021). In addition, research has shown that restoration of Aβ-induced LTP deficits by catalytic inhibition of the G9a/GLP complex depends on protein synthesis and NMDA receptor activity, a physiological correlate of memory (Sharma et al., 2017b, 2017a). The Ca^{2+} influx associated with NMDAR influences the stabilization of LTP by activating intracellular signaling cascades that subsequently promote mRNA and protein synthesis (Kandel et al., 2014), including immediate early genes (IEGs). Among the IEGs, expression of *Early Growth Response-1* (*egr-1*) (also known as *zif268*), *c-fos*, and *Activity regulated cytoskeleton associated protein* (*Arc*) is rapidly and selectively upregulated in subsets of neurons in specific brain regions associated with learning and memory formation (Minatohara et al., 2016). IEG expression has been widely used as a molecular indicator for neuronal populations undergoing plastic changes contributing to long-term memory formation (Minatohara et al., 2016). The gene expression of memory consolidation genes, including *Dnmt3a*, *catechol-O-Methyltransferase* (*Comt*), *egr-1*, and *cFos*, were found to be reduced in the SAMP8 group compared to age-matched SAMR1 mice ((Vasilopoulou et al., 2022) Publication 1). Strikingly, the gene expression levels of *Egr1*, *Arc,* and *Dnmt3a* were increased after the pharmacological inhibition of G9a (**UNC0642**) ((Bellver-Sanchis et al., 2024a) Publication 3).

In the first study ((Vasilopoulou et al., 2022) Publication 1), it was suggested that the downregulation of the expression of neurotrophic factors and IEGs could be associated with the $ERK_{1/2}$ axis, as its activation promotes neuronal plasticity (Ying et al., 2002; Rodrigues et al., 2004). In contrast, downregulation of $ERK_{1/2}$ phosphorylation after G9ai treatment in SAMP8 was observed in the second study ((Bellver-Sanchis et al., 2024b) Publication 2). This downregulation aligned with the neuroinflammatory state observed in SAMP8 after G9ai treatment. Hence, it is challenging to directly attribute a specific role to the MAPK/$ERK_{1/2}$ pathway, as this cascade is part of a more comprehensive network of other complex signaling pathways (Albert-Gascó et al., 2020). For instance, prolonged activation of ERK appears to initiate neurodegeneration (Colucci-D'Amato et al., 2003). Moreover, as discussed above, after pharmacological inhibition of G9a, an increase in the expression of both neurotrophic factors and IEGs was observed in SAMP8 ((Bellver-Sanchis et al., 2024b) Publication 2; (Bellver-Sanchis et al., 2024a) Publication 3). Thus, these findings suggest that G9a plays an upstream regulatory role for genes related to learning and memory formation, leading to their expression. Additionally, these findings indicate an enhancement of the cognitive state in SAMP8, which is consistent with our previous observations in the 5xFAD mouse model (Norrholm and Ouimet, 2001).

Furthermore, synaptic plasticity is essential for maintaining neuronal connections, leading to changes in synaptic structure, dendritic spines, synaptogenesis, and axonal adjustments (Lin and Koleske, 2010; Runge et al., 2020). In the aged brain, there is a loss of synapses (Hof and Morrison, 2004) and a significant reduction in dendritic spine density in AD, which is one of the most prominent features of AD and strongly correlates with cognitive impairment (Masliah et al., 2006; Dorostkar et al., 2015). Altered dendritic spine density has also been reported in models of other neurological conditions, including depression, stress, and aggressive behaviours (Norrholm and Ouimet, 2001; Radley et al., 2008; Medendorp et al., 2018; Patel and Weaver, 2021). As expected, a loss of dendritic spines and reduced length in the cortex of the aged SAMP8 was found compared to the old SAMR1 group ((Vasilopoulou et al., 2022) Publication 1). After the pharmacological treatment of G9ai (**UNC0642**, [redacted] in SAMP8, dendritic spine density and length were significantly increased compared to the SAMP8 Control group ((Bellver-Sanchis et al., 2024b) Publication 2). These

findings are consistent with previous studies where G9a inhibition was observed to enhance the structural plasticity of dendritic spines within neurons of the nucleus accumbens (Zaheer et al., 2001).

Another necessary process that is altered in AD is neurogenesis. Although this doctoral thesis does not cover neurogenesis, only the *Doublecortin* (*Dcx*) gene and Neuronal nurclear antigen (NeuN) protein levels were evaluated in SAMP8. While *Dcx* is a marker for neuro progenitors, indicating maturation of dendritic and neuronal structures, NeuN is a marker for adult neurons (Gusel'Nikova and Korzhevskiy, 2015; Klein et al., 2020). Treatment with G9ai in SAMP8 (**UNC0642**) increased *Dcx* and NeuN levels compared to the Control group. It prevented loss of neurogenesis ((Bellver-Sanchis et al., 2024a) Publication 3), as reported in other *in vitro* studies (**BIX-01294**, **UNC0638**, and **UNC0642**). The relationship between DCX and NGF has been described in line with our findings. Both neurotrophins play specific roles in neuroprotective mechanisms and neuronal repair (Chiaretti et al., 2008; Hou et al., 2021; Rothammer et al., 2022; Zou et al., 2022), thus supporting the beneficial outcomes observed after the pharmacological inhibition of G9a.

Overall, these findings highlight the significant role of G9a in synaptic dysfunction and neurotrophic factor regulation. The study shows that inhibiting G9a pharmacologically improves synaptic plasticity, increases neurotrophic factor and IEG expression, and promotes neuronal branching, dendritic spine density, and neurogenesis in SAMP8 mice. These results underline G9a's potential as a therapeutic target for AD.

4.4. GMFB transduction pathway activation: the key to neuroprotection after G9a inhibition in SAMP8

As the precise mechanisms of G9a activity regulation in cognition are not yet fully understood, this Ph.D. thesis explores the modulation of various molecular pathways that promote neuronal plasticity following G9a inhibition. To enhance our understanding of G9a's role, we employed NGS techniques, including Chip-seq, RNA-seq, and miRNA-seq, after

pharmacological treatment. This allowed us to obtain results on the modulation after G9a inhibition on molecular pathways related to synaptic plasticity and neuroinflammation.

Then, we employed RNA-seq to analyze the transcriptome of SAMP8 mice following pharmacological treatment with G9ai (**UNC0642**). Our differential expression analysis identified 697 genes with altered expression, including 480 genes with increased expression and 217 genes with decreased expression in the G9ai-treated group. The functional analysis revealed the regulation of processes such as neuroactive ligand-receptor interactions, calcium signaling, and G-protein coupled receptor signaling, which are crucial for neural network function and plasticity in the CNS. It is worth noting that genes associated with the sensory perception of the mechanical stimulus were upregulated, which could contribute to the observed behavioural and cognitive improvements. In contrast, genes related to the NF-κB signaling pathway, indicative of neuroinflammation, were downregulated. This suggests that G9a inhibition may be anti-inflammatory ((Bellver-Sanchis et al., 2024b) Publication 2).

Furthermore, enrichment of chromatin methylation processes confirms the impact of G9a inhibition on histone modification. RT-qPCR validation revealed reduced expression of neurodegeneration-associated such as *Synaptosome Associated Protein 25* (*Snap25*), T-Box Brain Transcription Factor 1 (*Tbr1*), and *Camk2g*, along with a significant increase in *Gmfb* expression. It is worth noting that the transcriptional upregulation of GMFB is implicated in neuroplasticity, learning, and memory (Lim and Zaheer, 1996; Zaheer et al., 2001; Goode et al., 2018; Maheshwari et al., 2018). Thus, this finding suggests for the first time that G9a inhibition induces a transcriptional profile that is beneficial for behaviour and cognition by enhancing GMFB expression ((Bellver-Sanchis, Geng et al., 2024) Publication 2).

GMFB is primarily expressed in the CNS and is highly conserved across various animal species, including invertebrates (Zaheer et al., 1993). GMFB regulates neuronal and glial growth and differentiation and is implicated in multiple neurodegenerative diseases. Additionally, it plays diverse roles in inflammatory and immune conditions, with recent research indicating its mono-SUMOylation, which enhances its stability and localization (Sun et al., 2021b). Interestingly, G9a and GMFB are associated with neuroinflammation,

contributing to increased pro-inflammatory cytokines and involvement in neurodegenerative pathways and neuronal plasticity (Zaheer et al., 2011; Kempuraj et al., 2013). However, transcriptional regulation and methylation of GMFB by G9a had yet to be described. This study reveals a novel mechanism in which G9a inhibition increases GMFB levels, influencing its function and mediating neuroprotective effects ((Bellver-Sanchis, Geng et al., 2024) Publication 2).

Moreover, we analyzed public H3K9me2 ChIP-seq data from AML12 cells treated with a G9ai (**UNC0638**) (Yan et al., 2020). Our re-analysis, in collaboration with Dr. Ávila-López, suggests that H3K9me2 plays a role in transcription regulation. Consistent with our RNA-seq data, we observed a reduction of H3K9me2 at TSS and gene body after G9a inhibition. This reduction could decrease H3K9me2 levels in the *Gmfb* gene, potentially promoting an increase in its expression. The observed outcome was remarkable as all the pieces fit together, and thus, we proceeded to see if we could find the mechanism to explain this ambivalent effect ((Bellver-Sanchis et al., 2024b) Publication 2).

Validation of GMFB up-regulation after G9ai treatment (**UNC0642**) in SAMP8 mice was conducted due to its role in inducing the synthesis of essential brain proteins and promoting neurotrophin production, implicated in neuronal growth and regeneration, learning, and memory. GMFB activates p38 MAPK, leading to CREB-mediated up-regulation of BDNF and its receptor, TrkB. It is worth noting that p38 MAPK exhibits significant expression in brain regions that are pivotal for learning and memory (Lim and Zaheer, 1996; Di Giacomo et al., 2009). Furthermore, studies have shown that its activation is essential for facilitating the production of BDNF in the hippocampus of rats (Katoh-Semba et al., 2009). These results suggest that G9a inhibition promotes neuronal plasticity by modulating the GMFB pathway. Additionally, p38 MAPK activation is correlated with dendritic spine morphological changes (Hanley, 2008), as supported by Golgi staining analysis showing increased neuronal complexity ((Bellver-Sanchis et al., 2024b) Publication 2). Altogether, validate the results of previous studies that demonstrated alterations in synaptic plastic genes in the SAMP8 model and were modulated by the inhibition of G9a.

Subsequently, to further confirm GMFB's role in the neuroprotective effects of G9ai, we evaluated cognition, neuronal plasticity, and neuroinflammation status in SAMP8 mice after dual treatment with GMFB and G9a inhibitors. Treatment with a GMFB inhibitor (GMFBi) resulted in decreased social interaction and impaired short- and long-term memory. Besides, SAMP8 mice treated with a GMFBi exhibited a reduced OLT DI. Evaluation of p38 phosphorylation levels revealed reductions in the SAMP8 Control and GMFBi-treated groups. The dendritic spine density and neuron length in mice treated with GMFBi and dual-treated (G9ai + GMFBi) mice were similar to SAMP8 levels, indicating reduced synaptic plasticity ((Bellver-Sanchis et al., 2024b). Publication 2). Furthermore, the creation of *Gmfb* knock-out (KO) mice highlighted their importance in maintaining normal cognitive functions, as their absence promoted the pathological progression of neuroinflammatory disease (Lim et al., 2004). Moreover, an *in vivo* study showed no increase in the expression of neurotrophins, such as BDNF and NGF, in the cerebellum of *Gmfb*-KO mice, which had impaired motor and learning abilities (Zaheer et al., 1999; Lim et al., 2004).

Lastly, we used the RNAi approach to knockdown (KD) *Y50D7A.10*, the *C. elegans* ortholog of human *Gmfb*, in both CL2355 and CL2006 strains. Consistent with previous findings, cognitive deficits persisted in CL2355 (*set-25*; *Y50D7A.10* (RNAi)) and CL2355 (*Y50D7A.10* (RNAi)). Similarly, Aβ aggregation remained unaffected in CL2006 (*Y50D7A.10* (RNAi)) and CL2006 (*set-25*; *Y50D7A.10* (RNAi)). Moreover, these strains exhibited downregulation of *crh-1c/CREB* and upregulation of *I Kappa B homolog* (*ikb-1*), which are target genes of G9a, similar to the Control group ((Bellver-Sanchis et al., 2024b) Publication 2). This suggests an interaction between G9a and GMFB, supporting the idea that inhibiting G9a is crucial for the neuroprotective effects that GMFB mediates.

In brief, through RNA-seq, we identify gene expression alterations related to synaptic plasticity and neuroinflammation. Notably, G9a inhibition leads to the upregulation of GMFB, a protein associated with neuroplasticity and memory function. Functional assays confirm the neuroprotective effects of GMFB, highlighting its importance in modulating cognitive function.

4.4.1. Rebalancing neuroinflammatory pathways via GMFB after the pharmacological treatment of G9a inhibition

A wealth of evidence describes the link between increased levels of inflammatory markers and AD pathogenesis, confirming that neuroinflammation plays a crucial role in neurodegeneration (Kizilarslanoğlu et al., 2015; Ferrucci and Fabbri, 2018; de Oliveira et al., 2021; Thakur et al., 2023). In this line, GMFB expression promotes modulate neuroinflammation through the ERK and NF-κB axis (Zaheer et al., 2007). Hence, the precise mechanism by which GMFB is involved in neurodegeneration or neuroprotection remained unclear. Therefore, assessing pro-inflammatory markers was crucial at this point.

Of note, our RNA-seq data suggests a potential anti-inflammatory effect of the pharmacological G9a inhibition, as genes related to the NF-κB signaling pathway, indicative of neuroinflammation, were down-regulated. Furthermore, Gene Set Enrichment Analysis (GSEA) revealed an increase in the anti-inflammatory cytokine *Il-37* ((Bellver-Sanchis et al., 2024b) Publication 2), suggesting that G9ai may have the potential to alleviate neuroinflammation.

Since NF-κB is a crucial transcription factor in inflammation and pro-inflammatory gene expression (Lawrence and Fong, 2010; Bhatt and Ghosh, 2014), its activation was evaluated after the pharmacological treatment of G9a (**UNC0642**) in SAMP8 to assess its role in AD-related brain inflammation. Strikingly, treatment with a G9ai led to a significant reduction in the $ERK_{1/2}$ phosphorylation, consistent with the NF-κB phosphorylation levels. In addition, the gene expression analysis showed a decrease in pro-inflammatory NF-κB targets (e.g., *Il-6*, *Cxcl10*, *Tnf-a*) in SAMP8 mice treated with a G9ai ((Bellver-Sanchis et al., 2024b) Publication 2).

In parallel, pre-treatment with G9ai (**UNC0642**) significantly reduced cell death caused by Lipopolysaccharide (LPS) and Interferon-gamma (IFN-γ) in primary mixed cultures of neurons and microglia. This indicates that G9ai can alleviate microglial activation induced by these inflammatory agents. On the other hand, pre-treatment with a GMFBi reversed this

effect, highlighting the role of GMFB in modulating neuroinflammation ((Bellver-Sanchis et al., 2024b) Publication 2).

In summary, these results demonstrate that inhibiting G9a can potentially reduce levels of neuroinflammation in SAMP8, as evidenced by the down-regulation of NF-κB signaling and pro-inflammatory gene expression. However, further research was needed to fully understand the mechanisms underlying these effects simultaneously as G9a inhibition upregulated GMFB, the latter of which is associated with neuroinflammation.

4.4.2. G9a methylation of GMFB promotes neurodegeneration

With the above in mind, we aimed to study the methylation dynamics and neuroprotective implications between G9a and GMFB to understand our results. Exogenous G9a constructs were utilized in co-immunoprecipitation assays, revealing an interaction between G9a and GMFB. This interaction was notably absent in Control samples, suggesting a direct link between G9a and GMFB. To explore G9a's potential role in GMFB methylation, we transfected HA-tagged GMFB into HEK 293T cells and observed methylated GMFB forms, indicating G9a-mediated methylation ((Bellver-Sanchis et al., 2024b) Publication 2). We also investigated whether G9a is the methyltransferase responsible for GMFB methylation through two complementary approaches. Firstly, G9a inhibition (**BIX-01294**) significantly reduced the levels of methylated GMFB compared to Control cells. Secondly, G9a-KO also reduced the levels of methylated GMFB, confirming G9a's involvement in GMFB methylation ((Bellver-Sanchis et al., 2024b) Publication 2).

A consensus methylation site encompassing RK/ARK (Poulard et al., 2021), indicative of G9a's preferred targets, was explored. The predictive analysis identified K20 and K25 as potential methylation sites (Chen et al., 2006; Deng et al., 2017). Mutations were introduced at these sites to validate these findings, and their impact on GMFB methylation by G9a was assessed. Mutations at K20R, K25R, or both (2KR) significantly reduced methylation levels. In addition, cell viability assays following LPS exposure revealed that G9a inhibition, mainly targeting K25 of GMFB, greatly enhanced cell survival, consistent with observations in the

double-mutated cells ((Bellver-Sanchis et al., 2024b) Publication 2). This finding highlights the importance of G9a-mediated demethylation at K25 for neuroprotection.

Furthermore, the data suggest that G9a inhibition facilitates GMFB phosphorylation by Protein kinase A (PKA), which is crucial for its activation. When phosphorylated by PKA, GMFB significantly enhances p-38 activity while inhibiting $ERK_{1/2}$ (Lim and Zaheer, 1996; Shi et al., 2006; Fan et al., 2018). It is worth noting the consensus motif found in PKA substrates, which follows the pattern [R/K][R/K/X]X[S/T]. Sequence analysis of GMFB shows that this motif aligns precisely with the LRKFRFRK25ET27 sequence, wherein the PKA phosphorylation site (T27) sits adjacent to the G9a methylation site (K25). Previous research has suggested that PKA phosphorylation of GMFB may be impeded by methylated lysine (Rea et al., 2000).

In short, we demonstrate a direct interaction between G9a and GMFB, with G9a mediating GMFB methylation at specific sites. These findings offer insights into the inhibition of G9a reduced GMFB methylation and enhanced cell survival, highlighting its role in neuroprotection.

4.5. G9a inhibition reveals insights into *miR-128* dysregulation in SAMP8 Mice

As stated in the introduction section, abnormal levels of specific miRNAs have been detected in various regions of the AD brain (Cogswell et al., 2008; Siedlecki-Wullich et al., 2019, 2021). In this doctoral dissertation, an analysis of global miRNA expression was conducted after the pharmacological inhibition of G9a (**UNC0642**) in SAMP8. Our transcriptomic analyses identified several miRNAs, including *miR-1298*, *miR-669*, *miR-677*, and *miR-128*, whose expression was altered by G9a inhibition. In addition, the KEGG enrichment analysis indicated that G9a is involved in pathways related to neurodegenerative processes, such as cholinergic synapse and axon guidance, as well as in MAPK and Forkhead Box O (FOXO=

signaling pathways. It is worth noting that modulation of *miR-1298* and *miR-669* expression was observed after G9a inhibition, with implications for neuroprotection and anti-inflammatory responses (Hu et al., 2015; Kolosowska et al., 2020), consistent with previous research. Besides, the downregulation of *miR-677* and *miR-128* following G9a inhibition suggests potential involvement in protein synthesis, neurodegeneration, and cognitive impairment, with implications for AD pathology (Siedlecki-Wullich et al., 2019; Song et al., 2021; Behera et al., 2022). We focused on *miR-128*, the second most down-regulated miRNA after the G9a inhibition in SAMP8.

Specifically, *miR-128* plays a crucial role in nervous system development and regulates neuronal plasticity, survival, and cognitive function (Liu et al., 2019). Target Scan Human 8.0 analysis revealed a putative 7-nucleotide miR-128 target sequence in the 3'-UTR of PPARG mRNA ((Bellver-Sanchis et al., 2024a) Publication 3). For instance, *miR-128*-KO inhibits the progression of AD pathology in mouse models due to increased PPARγ levels (Liu et al., 2019). The SAMP8 group treated with G9ai (**UNC0642**) consistently showed statistically significantly higher expression levels of the *Pparg* gene. This suggests a regulatory relationship between *miR-128-3p* and PPARG in the context of neuroprotection ((Bellver-Sanchis et al., 2024a) Publication 3). PPARγ is a nuclear hormone receptor superfamily component and functions as a transcription factor activated by ligands. PPARγ regulates essential genes associated with various metabolic processes and cellular fates, maintaining homeostasis and modulating inflammatory reactions (Houseknecht et al., 2002). For example, PPARγ is involved in the inactivation of the NF-κB signaling pathway, reducing levels of proinflammatory markers (Hou et al., 2012). Of note, this finding agrees with ours presented in the second publication ((Bellver-Sanchis et al., 2024b) Publication 2). Moreover, it is also involved in the OS response, and apoptosis following brain injury or neurodegenerative conditions (Kapadia et al., 2008; Yonutas and Sullivan, 2013). Consistent with our findings, one study traced the repression of *Pparg* gene expression through the G9a-dependent addition of H3K9me2 to the entire *Pparg* gene body (Wang et al., 2013).

This study investigates the impact of G9a inhibition on miRNA expression in SAMP8 mice. It highlights *miR-128*, which is involved in neuroprotection and cognitive function through

its regulatory relationship with PPARγ. As PPARγ can modulate several beneficial mechanisms, we decided to investigate them, and the following sections describe our research.

4.5.1. G9a inhibition induces antioxidant response via PPARγ

Our findings reveal an upregulation of antioxidant genes (e.g., *Sod1, Hmox1, Gpx,* and *Aldehyde Oxidase 1* (*Aox1*)) and a downregulation of pro-oxidant markers (e.g., *Cyclooxygenase-2* (*Cox2*) and *Aldehyde dehydrogenase* (*Aldh2*)) in SAMP8 mice following G9a inhibition. These findings are consistent with previous research indicating that PPARγ protects against oxidative stress by regulating various pathways, including NRF2, Wnt/β-catenin, and FOXO (Polvani et al., 2012; Beheshti et al., 2022). After **UNC0642** treatment, we observed an upregulation of the FOXO signaling pathway in SAMP8 brains, which is novel in this context. This finding is consistent with previous observations linking elevated G9a levels and decreased FOXO1 levels in human colon cancer patients (Chae et al., 2019). In addition, we observed an increase in AMPK phosphorylation, a key player in FOXO1-dependent mechanisms, in SAMP8 mice treated with G9ai. This increase correlates with the upregulation of the deacetylase *Sirtuin 1* (*Sirt-1*) gene expression. We also found upregulation of antioxidant enzymes, including CAT3, GPX, and SOD1, in the G9ai-treated SAMP8 group compared to the Control Group ((Bellver-Sanchis et al., 2024a) Publication 3).

To support the antioxidant effects of G9a inhibition, primary neuron cell cultures were exposed to H_2O_2 as an oxidative insult. It was observed that there was a significant increase in cell survival following G9ai treatment compared to the vehicle-only group. Furthermore, the antioxidant enzyme GSH was upregulated after the pharmacological inhibition of G9a ((Bellver-Sanchis et al., 2024a) Publication 3).

To sum up, the downregulation *miR*-128 after the pharmacological inhibition of G9a partially explains oxidative responses in SAMP8.

4.5.2. Upregulation of PPARγ by G9ai could promote the autophagic process

Further investigation into G9a-regulated pathways has revealed its involvement in autophagy repression, a well-described mechanism in neurodegenerative disorders. Previous studies have shown that G9a binds to the promoters of core autophagy-associated genes, inhibiting their activity (Artal-Martinez de Narvajas et al., 2013; Ke et al., 2014; An et al., 2017). In age SAMP8 mice, overexpression of G9a coincided with deficits in the autophagic process. This was characterized by decreased levels of phosphorylated JNK, a key regulator of autophagy, compared to SAMR1 mice. The reduced JNK activity in SAMP8 brains correlated with reductions in crucial autophagic markers levels (e.g., BECLIN-1, SQSTM1/p62, and LC3B-II) ((Vasilopoulou et al., 2022) Publication 1). ChIP experiments have shown that JNK activity is required to prevent G9a-mediated repression of autophagy genes (Artal-Martinez de Narvajas et al., 2013).

Conversely, depleting G9a genetically or inhibiting it pharmacologically may cause it to dissociate from these gene promoters, making it easier to form autophagosome-like structures. The results show an increase in autophagy markers, such as BECLIN-1 and SQSTM1/p62, indicating the activation of the autophagic process after pharmacological G9a inhibition in treated SAMP8 animals ((Bellver-Sanchis et al., 2024a) Publication 3). As previously discussed, G9a inhibition leads to an increase in PPARγ protein expression, which is also involved in the activation of autophagy (Zhou et al., 2009), thus suggesting a possible role of PPARγ in the autophagic process.

In short, these outcomes support the G9a's role in suppressing autophagy, a process linked to neurodegenerative disorders.

4.5.3. GADD45α up-regulation mediated by G9a inhibition ameliorates the DNA damage response and promotes apoptosis

Growth arrest and DNA damage 45 alpha (GADD45α) were modulated miRNA targets observed from our miRNA-seq. GADD45α is crucial in various cellular processes, including DNA repair, apoptosis, cell cycle regulation, angiogenesis, senescence, and DNA demethylation (Smith et al., 2000; Hildesheim et al., 2002; Vairapandi et al., 2002; Tront et al., 2006; Lee et al., 2012). It does this by facilitating the recruitment of demethylation proteins to CpG island promoters (Arab et al., 2019). Moreover, GADD45α interacts with PPARγ, which reduces the recruitment of demethylation proteins to CpG island promoters and subsequently enhances the transcriptional activity of PPARγ (You et al., 2020). Inhibition of G9a in SAMP8 mice increased *Gadd45a* gene expression and protein levels of GADD45α. This up-regulation in GADD45α was accompanied by an increase of apoptotic markers, including BCL-1, BAX, and CASP3, in the treated SAMP8 group compared to the Control group, suggesting a role for GADD45α in apoptosis. It has been described that GADD45 induces activation of JNK and p38, promoting the proapoptotic pathway (Bruemmer et al., 2005), and this was consistent with our results observed in SAMP8.

Furthermore, the absence of *Gadd45a* leads to changes in hippocampal memory and LTP, which are accompanied by a decrease in the levels of memory-related mRNA (Aparisi Rey et al., 2019; Griñán-Ferré et al., 2024). This observation is consistent with the fact that GADD45α is up-regulated after G9a inhibition, indicating that it may also have neuroprotective effects by regulating apoptosis and memory-related processes.

Overall, our study reveals that inhibiting G9a in SAMP8 mice increases the expression of GADD45α, potentially influencing apoptosis, DNA damage response, and memory-related processes.

4.6. Identifying potent G9a inhibitors for Alzheimer's disease

[redacted]

Over the past decade, several small molecule inhibitors of G9a have been synthesized and reported in the literature to investigate the protein's biological functions and explore potential therapeutic applications, as discussed in Section *1.3.5* of the Introduction. Among the previously reported G9ais, quinazolines (Cao et al., 2019; Charles et al., 2019) and quinolines (Rabal et al., 2018, 2021) are widely explored; others are benzodiazepines (Milite et al., 2019), amino-indoles (Sweis et al., 2014), 6H-anthra[1,9-cd]isoxazol-6-one (Chen et al., 2016), pseudodehydrocorydaline (Chen et al., 2018), 2,4- diamino-6-methylpyrimidines (Katayama et al., 2020), Chaetocin (Greiner et al., 2005; Cherblanc et al., 2013) and Epidithiodiketopiperazine (Fujishiro et al., 2013).

Briefly, in the early 2000s, high-throughput screening of a 125,000 compound library against G9a led to the discovery of BIX-01294, the first small molecule G9ai. It inhibits G9a and GLP with an IC_{50} of 1.7 μM and 38 μM, respectively. Although it can reduce H3K9me2 levels, BIX-01294 exhibits cytotoxicity at concentrations exceeding 4.1 μM, which limits its usefulness as a G9a chemical probe (Kubicek et al., 2007). Further investigation of BIX-01294 led to the discovery of UNC0224, which demonstrated a seven-fold increase in G9a inhibitory activity compared to BIX-01294. Structural analysis revealed that UNC0224 had a five-fold binding affinity higher than BIX-01294 (Liu et al., 2009b). Subsequent research developed several G9ais with lysine mimic side chains, including UNC0321, UNC0631, UNC0646 (Liu et al., 2011), UNC0638, UNC0642 (Vedadi et al., 2011), A-366 (Sweis et al., 2014), and CM-272 (José-Enériz et al., 2017), to enhance selectivity and potency.

Among them, UNC0638 was synthesized to improve the toxicity/function ratio of G9ais. Subsequent SAR studies led to UNC0642, a potent G9ai with improved selectivity, reduced cytotoxicity, and better in vivo pharmacokinetics (Vedadi et al., 2011). Specifically, we used Ithese two G9ai compounds to reference our PoCs. Nevertheless, these compounds and others previously published showed limited effectiveness in both *in vitro* and *in vivo* studies. Additionally, they exhibited poor BBB permeability and toxicity problems, among other compromising features.

[redacted]

4.6.1. Compound F: a promising candidate for Alzheimer's disease therapy

In collaboration with Dr. Singh-Choudhary, we performed a structure-based virtual screening to identify potential G9ai from a Chembridge CNS MPO library of 496,644 compounds ((Bellver-Sanchis et al., 2022) Publication 4). First, for further analysis, 100 compounds were selected based on docking scores from the central nervous system multiparameter optimization (CNS MPO) database of Chembridge Corporation. Among them, 9 molecules were chosen from this screening due to their promising *in silico* properties. They were selected based on the Glide XP dock score, Mechanics-Generalized Born Surface Area (MM-GBSA) dG binding affinity, scaffold novelty and hydrogen bond mediated interaction with G9a active resides (e.g. Aspartate (Asp)1074, Asp1083, Asp1088, Leu1086), hydrophobic interaction with Tyr1154, and Phenylalanine (Phe)118 (Liu et al., 2009b; Vedadi et al., 2011; Cao et al., 2019; Ramya Chandar Charles et al., 2019). Moreover, these compounds were not non-Pan assay interreference compounds (PAINS) (Baell and Holloway, 2010). *In vitro* assays were conducted to evaluate the inhibitory activity of these compounds against G9a. Some compounds showed greater potency than **UNC0638**, a well-established G9ai. In

addition, an *in silico* ADMET analysis was conducted to evaluate the pharmacokinetic and pharmacodynamic properties of the selected compounds, providing insights into their drug-like properties, including their potential to penetrate the CNS and other parameters.

In vivo, efficacy studies were performed in *C. elegans*. Interestingly, compounds **E**, **F** and **H** showed promising results in reducing Aβ aggregation and locomotion defects in *C. elegans* (CL2006), supporting the therapeutic potential of the identified compounds in treating AD. In addition, these compounds demonstrated direct targeting of G9a by reducing levels of its repressive mark H3K9me2. In addition, *in vitro* BBB penetration evaluation suggested that compounds **F** and **H** have the potential to cross the BBB, making them suitable candidates for further *in vivo* studies. Finally, the selectivity of the compounds against GLP/EHMT1 was evaluated (GLP) ((Bellver-Sanchis et al., 2022) Publication 4).

In summary, compound **E** showed promising pharmacokinetic properties but lower BBB permeability compared to **UNC0638**, possibly due to reduced lipophilicity. Compound **H** did not positively affect Aβ deposition despite promising *in silico* and *in vitro* results. However, compound **F** showed a remarkable 40% reduction in Aβ deposition and unprecedented nanomolar potency (IC_{50} = 1.8 nM). In addition, it showed higher BBB permeability (2.2 x 10^{-6} ± 0.1 $cm \cdot s^{-1}$) and selectivity for G9a over GLP compared to **UNC0638** (GLP inhibition at 1µM: for compound F: 4±1%; for **UNC0638**: 66±1%) ((Bellver-Sanchis et al., 2022) Publication 4). Thus, these findings underscore the potential therapeutic of compound **F** as a novel G9ai.

4.6.2. [redacted] compound [redacted]

[redacted]

[redacted]

4.6.4. The repurposing approach: The Raltitrexed

As indicated above, the repurposing approach was of interest to us because it offers a strategic and efficient drug discovery and development strategy, potentially getting novel treatments to patients more quickly and cost-effectively than traditional methods (Cha et al., 2018). Thus, in collaboration with Jana and Dr. Rajan Banerjee, a systematic 3D QSAR-based screening was performed (Jana et al., 2023b), identifying Raltitrexed, an anti-cancer agent as a promising inhibitor against G9a ((Jana et al., 2023a) Publication 5).

In vitro assays showed that **Raltitrexed** effectively inhibits G9a activity, with an IC_{50} of 120 nM. Additionally, we evaluated the activity of **Raltitrexed** against GLP and found that it can deter up to 49.98% at a 1µM dose. To confirm the direct targeting of G9a, we quantified levels

of H3K9me2 using the AD transgenic *C. elegans* model (CL2006). Both pharmacological treatments, **UNC0642** and **Raltitrexed**, resulted in a reduction in repressive mark levels. *In silico* analyses (TOPKAT) showed that raltitrexed has a more favorable toxicity profile than the reference inhibitor, **UNC0642**. This was further supported by experiments demonstrating no significant toxicity in *C. elegans*. **Raltitrexed** treatment led to a dose-dependent improvement in locomotor function in CL2006, as observed with **UNC0642** treatment. Furthermore, the quantification of Aβ deposition showed a significant decrease in response to **Raltitrexed** treatment, indicating its potential as a therapeutic agent for AD ((Jana et al., 2023a) Publication 5).

Overall, although **Raltitrexed** showed a similar profile to the reference compound **UNC0642** in many experiments and sometimes even performed worse, it is essential to consider the advantages of the repurposing approach. The approval of **Raltitrexed** by AstraZeneca in Canada and some European countries could accelerate clinical trials to evaluate its efficacy, as it has already been proven safe and tolerable.

4.7. Final considerations

AD is the most prevalent neurodegenerative disease globally and is responsible for an estimated 60-80% of dementia cases (Association, 2019). Despite decades of research, none of the approved AD treatments have been entirely successful. Most of these treatments aim to target Aβ accumulation (Cummings et al., 2023). Therefore, it is essential to identify pathways upstream of both Aβ and NFT formation or distinct mechanisms.

Around 1% of AD cases are caused by several different single-gene mutations characterized by early onset and an autosomal dominant inheritance pattern. However, in most cases, AD has a complex etiology likely to involve multiple susceptibility genes and environmental factors (Eid et al., 2019). Recent investigations into the human epigenome have focused on histone modifications in AD, providing insight into their contribution to disease development and progression. Research has shown that while some histone marks decrease in AD, others

increase, highlighting the complexity of histone modifications in the disease (Marzi et al., 2018; Klein et al., 2019; MacBean et al., 2020; Nativio et al., 2020). G9a is a histone lysine methyltransferase that is a crucial regulator of human disease. Specifically, it is responsible for di-methylating H3K9, a repressive mark for learning and memory formation genes. Postmortem AD brains show an increase in the repressive mark H3K9me2 because of G9a upregulation (Zheng et al., 2019), highlighting its potential as a treatment for AD.

Our findings confirm previous observations of G9a dysregulation in AD, demonstrating its overexpression and association with pathological features such as Aβ aggregation and cognitive impairment. Importantly, our studies in SAMP8 mice and *C. elegans* models provide compelling evidence for the therapeutic potential of G9a inhibition in mitigating AD-related phenotypes.

Moreover, our research extends beyond the direct effects of G9a inhibition on cognitive function to explore its broader implications in modulating neuroinflammation, synaptic plasticity, OS, autophagy, apoptosis, and DNA damage responses. Strikingly, through comprehensive transcriptomic analyses, we have described the new neuroprotective through GMFB regulation after G9a inhibition for the first time. Besides, we have also elucidated the intricate interplay between G9a and microRNAs, such as *miR-128*, which play crucial roles in neuronal plasticity, protein synthesis, and cognitive function. These findings highlight the intricate regulatory role of G9a in orchestrating molecular cascades involved in AD pathogenesis.

In addition, our research endeavors have also explored innovative strategies for developing G9ais with enhanced therapeutic efficacy and safety profiles [redacted] Finally, our exploration of drug repurposing strategies has unveiled **Raltitrexed**'s ability to target G9a, offering a novel approach to AD therapy.

In conclusion, AD remains a significant challenge. G9a inhibition shows promise in mitigating AD-related symptoms and modulating various molecular pathways. Thus, developing G9ais, including novel compounds and repurposed drugs, presents potential therapeutic strategies for AD.

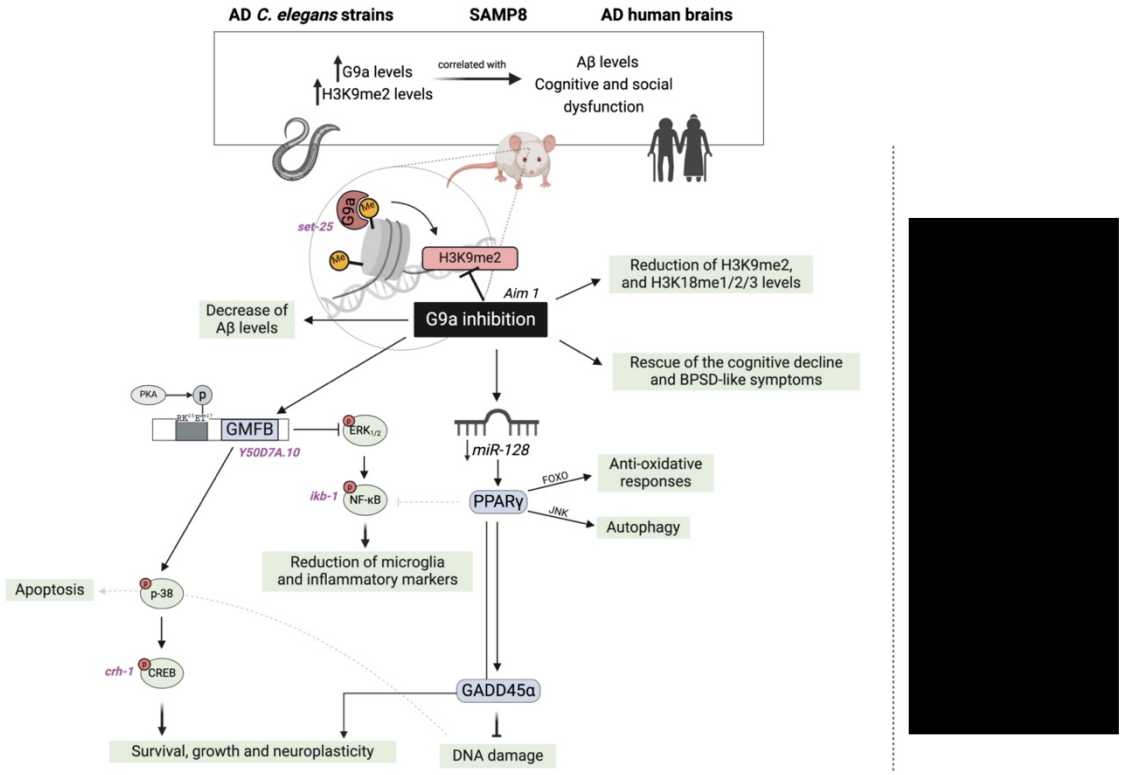

Figure 11. Schematic representations of the beneficial effects of G9a inhibition leading to neuroprotection in the context of Alzheimer's disease. Proposal of different strategies for obtaining G9a inhibitors as candidates for treatment of Alzheimer's disease. Black lines: pathways studied in this doctoral thesis. Grey dashed lines: pathways proposed based on the literature. In purple, the orthologues of the genes in the *C. elegans* model.

5 Conclusions

The present doctoral thesis has made significant contributions to our knowledge of the role of G9a in age-related cognitive decline and AD, highlighting its potential as a therapeutic target. Moreover, our research has developed novel compounds targeting G9a, focusing on enhanced efficacy, selectivity, and safety profiles. By bridging the gap between research on the role of G9a in AD and the development of new pharmacological interventions, this thesis lays the basis for potential future therapies in AD.

The conclusions of the thesis are:

1. Identification of the overexpression of both G9a and its repressive mark (H3K9me2) as a potential target against age-related cognitive decline and AD, as seen in human patient samples and experimental models of AD (*C. elegans* and SAMP8 mouse model).
2. Overexpression G9a might be partially responsible for the deregulation of AD-related pathways, which correlates with impaired cognitive and behavioural state and BPSD-like phenotype in aged SAMP8 mice.
3. Levels of Aβ decrease after the pharmacological inhibition of G9a in both *C. elegans* (**F** and [redacted] and SAMP8 (**UNC0642** and [redacted]). Furthermore, [redacted]
4. Administration of G9ais (**UNC0642** and [redacted]) partially rescues cognitive impairment and socially defective behaviour in the SAMP8 mouse model.
5. The neuroprotective effect of G9ai treatments (**UNC0642**, [redacted]) is further reflected by an increase in synaptic plasticity markers (*Vgf*, Ngf, BDNF, PSD95, PSD93, SYN IIa) and changes in both dendritic spine length and density length in SAMP8 mouse model.
6. Pharmacological inhibition of G9a enhances neuroprotective effects by demethylating the K25R position of GMFB. Accordingly, gene edition using cell cultures and *C. elegans*, as well as pharmacological inhibition of GMFB in the SAMP8 mouse model, confirmed this.

7. G9a inhibition (**UNC0642**) attenuates the neuroinflammatory process in SAMP8 by decreasing the expression of inflammatory cytokines *(Il-6, Cxcl10, Tnf-α)* via the ERK-NF-κB signaling pathway.
8. Administration of a G9ai (**UNC0642**) provides an overall beneficial effect that, according to our miRNome analysis, could be due, at least in part, to miR-128's modulation of PPARγ-dependent pathways.
9. Design of novel, more stable, selective, and less toxic epigenetic drugs targeting G9a is a promising strategy to improve neuronal function and delay AD progression. [redacted]
11. Repurposing of raltitrexed could constitute a new therapeutic strategy due to its ability to inhibit G9a.

6 Bibliography

Agatonovic-Kustrin S, Kettle C, Morton DW. A molecular approach in drug development for Alzheimer's disease. Biomedicine & Pharmacotherapy. 2018;106:553–565.

Akhter R, Shao Y, Shaw M, Formica S, Khrestian M, Leverenz JB, Bekris LM. Regulation of ADAM10 by miR-140-5p and potential relevance for Alzheimer's disease. Neurobiol Aging. 2018;63:110–119.

Akiguchi I, Pallàs M, Budka H, Akiyama H, Ueno M, Han J, Yagi H, Nishikawa T, Chiba Y, Sugiyama H. SAMP8 mice as a neuropathological model of accelerated brain aging and dementia: Toshio Takeda's legacy and future directions. Neuropathology. 2017;37(4):293–305.

Albert-Gascó H, Ros-Bernal F, Castillo-Gómez E, Olucha-Bordonau FE. MAP/ERK signaling in developing cognitive and emotional function and its effect on pathological and neurodegenerative processes. Int J Mol Sci. 2020;21(12):4471.

Allen SJ, Watson JJ, Shoemark DK, Barua NU, Patel NK. GDNF, NGF and BDNF as therapeutic options for neurodegeneration. Pharmacol Ther. 2013;138(2):155–175.

Alvarez-Venegas R, Avramova Z. SET-domain proteins of the Su (var) 3-9, E (z) and trithorax families. Gene. 2002;285(1–2):25–37.

Alzheimer's Association, Association A. 2019 Alzheimer's disease facts and figures. Alzheimer's & dementia. 2019;15(3):321–387.

An PNT, Shimaji K, Tanaka R, Yoshida H, Kimura H, Fukusaki E, Yamaguchi M. Epigenetic regulation of starvation-induced autophagy in Drosophila by histone methyltransferase G9a. Sci Rep. 2017;7(1):1–14.

Anderson EM, Larson EB, Guzman D, Wissman AM, Neve RL, Nestler EJ, Self DW. Overexpression of the histone dimethyltransferase G9a in nucleus accumbens shell increases cocaine self-administration, stress-induced reinstatement, and anxiety. Journal of Neuroscience. 2018;38(4):803–813.

Anderson EM, Sun H, Guzman D, Taniguchi M, Cowan CW, Maze I, Nestler EJ, Self DW. Knockdown of the histone di-methyltransferase G9a in nucleus accumbens shell decreases cocaine self-administration, stress-induced reinstatement, and anxiety. Neuropsychopharmacology. 2019;44(8):1370–1376.

Aparisi Rey A, Karaulanov E, Sharopov S, Arab K, Schäfer A, Gierl M, Guggenhuber S, Brandes C, Pennella L, Gruhn WH. Gadd45α modulates aversive learning through post-transcriptional regulation of memory-related mRNAs. EMBO Rep. 2019;20(6):e46022.

Arab K, Karaulanov E, Musheev M, Trnka P, Schäfer A, Grummt I, Niehrs C. GADD45A binds R-loops and recruits TET1 to CpG island promoters. Nat Genet. 2019;51(2):217–223.

Arciniegas Ruiz SM, Eldar-Finkelman H. Glycogen Synthase Kinase-3 Inhibitors: Preclinical and Clinical Focus on CNS-A Decade Onward. Front Mol Neurosci. 2022;14:349.

Arioka M, Tsukamoto M, Ishiguro K, Kato R, Sato K, Imahori K, Uchida T. τ protein kinase II is involved in the regulation of the normal phosphorylation state of τ protein. J Neurochem. 1993;60(2):461–468.

Arriagada P V, Growdon JH, Hedley-Whyte ET, Hyman BT (1992) Neurofibrillary tangles but not senile plaques parallel duration and severity of Alzheimer's disease. Neurology 42:631.

Artal-Martinez de Narvajas A, Gomez TS, Zhang JS, Mann AO, Taoda Y, Gorman JA, Herreros-Villanueva M, Gress TM, Ellenrieder V, Bujanda L, Kim DH, Kozikowski AP, Koenig A, Billadeau DD. Epigenetic Regulation of Autophagy by the Methyltransferase G9a. Mol Cell Biol. 2013;33(20):3983–3993.

Association A. 2019 Alzheimer's disease facts and figures. Alzheimer's & dementia. 2019;15(3):321–387.

Ayton S, Wang Y, Diouf I, Schneider JA, Brockman J, Morris MC, Bush AI. Brain iron is associated with accelerated cognitive decline in people with Alzheimer pathology. Mol Psychiatry. 2020;25(11):2932–2941.

Babu A, Verma RS. Chromosome structure: euchromatin and heterochromatin. Int Rev Cytol. 1987;108:1–60

Baby N, Alagappan N, Dheen ST, Sajikumar S. MicroRNA-134-5p inhibition rescues long-term plasticity and synaptic tagging/capture in an Aβ (1–42)-induced model of Alzheimer's disease. Aging Cell. 2020;19(1):e13046.

Baell JB, Holloway GA. New substructure filters for removal of pan assay interference compounds (PAINS) from screening libraries and for their exclusion in bioassays. J Med Chem. 2010;53(7):2719–2740.

Bakulski KM, Dolinoy DC, Sartor MA, Paulson HL, Konen JR, Lieberman AP, Albin RL, Hu H, Rozek LS. Genome-wide DNA methylation differences between late-onset Alzheimer's disease and cognitively normal controls in human frontal cortex. Journal of Alzheimer's Disease. 2012;29(3):571–588.

Balusu S, Horré K, Thrupp N, Craessaerts K, Snellinx A, Serneels L, T'Syen D, Chrysidou I, Arranz AM, Sierksma A. MEG3 activates necroptosis in human neuron xenografts modeling Alzheimer's disease. Science. 2023;381(6663):1176–1182.

Bamberger ME, Landreth GE. Inflammation, apoptosis, and Alzheimer's disease. The Neuroscientist. 2002;8(3):276–283.

Banks WA, Farr SA, Morley JE, Wolf KM, Geylis V, Steinitz M. Anti-amyloid beta protein antibody passage across the blood–brain barrier in the SAMP8 mouse model of Alzheimer's disease: an age-related selective uptake with reversal of learning impairment. Exp Neurol. 2007;206(2):248–256.

Bao L, Chen Y, Lai HT, Wu S-Y, Wang JE, Hatanpaa KJ, Raisanen JM, Fontenot M, Lega B, Chiang CM. Methylation of hypoxia-inducible factor (HIF)-1α by G9a/GLP inhibits HIF-1 transcriptional activity and cell migration. Nucleic Acids Res. 2018;46(13):6576–6591.

Barbato C, Giacovazzo G, Albiero F, Scardigli R, Scopa C, Ciotti MT, Strimpakos G, Coccurello R, Ruberti F. Cognitive decline and modulation of alzheimer's disease-related genes after inhibition of MicroRNA-101 in Mouse hippocampal neurons. Mol Neurobiol. 2020;57:3183–3194.

Barde YA, Edgar D, Thoenen H. Purification of a new neurotrophic factor from mammalian brain. EMBO J. 1982;1(5):549–553.

Barde YA. Trophic factors and neuronal survival. Neuron. 1989;2(6):1525–1534.

Barghout SH, Machado RAC, Barsyte-Lovejoy D. Chemical biology and pharmacology of histone lysine methylation inhibitors. Biochimica et Biophysica Acta (BBA)-Gene Regulatory Mechanisms. 2022;1865(6):194840.

Barwari T, Joshi A, Mayr M. MicroRNAs in cardiovascular disease. J Am Coll Cardiol. 2016;68(23):2577–2584.

Batool A, Kamal MA, Rizvi S, Rashid S. Topical discoveries on multi-target approach to manage Alzheimer's disease. Curr Drug Metab. 2018;19(8):704–713.

Baudier J, Cole RD. Interactions between the microtubule-associated tau proteins and S100b regulate tau phosphorylation by the Ca2+/calmodulin-dependent protein kinase II. Journal of Biological Chemistry. 1988;263(12):5876–5883.

Behera JK, Bhattacharya M, Mishra P, Mishra A, Dash AA, Kar NB, Behera B, Patra BC. Regulatory role of miRNAs in Wnt signaling pathway linked with cardiovascular diseases. Current Research in Pharmacology and Drug Discovery. 2022;3:100133.

Beheshti F, Gholami M, Ghane Z, Nazari SE, Salari M, Shabab S, Hosseini M. PPARγ activation improved learning and memory and attenuated oxidative stress in the hippocampus and cortex of aged rats. Physiol Rep. 2022;10(24):e15538.

Bellver-Sanchis A, Ávila-López PA, Tic I, Valle-García D, Ribalta-Vilella M, Labrador L, Banerjee DR, Guerrero A, Casadesus G, Poulard C. Neuroprotective effects of G9a inhibition through modulation of peroxisome-proliferator activator receptor gamma-dependent pathways by miR-128. Neural Regen Res. 2024a;10–4103

Bellver-Sanchis A, Geng Q, Navarro G, Ávila-López PA, Companys-Alemany J, Marsal-García L, Larramona-Arcas R, Miró L, Perez-Bosque A, Ortuño-Sahagún D. G9a inhibition promotes neuroprotection through GMFB regulation in Alzheimer's disease. Aging Dis. 2024b;15(1):311.

Bellver-Sanchis A, Singh Choudhary B, Companys-Alemany J, Ávila-López PA, Martínez Rodríguez AL, Brea Floriani JM, Malik R, Pallàs M, Pérez B, Griñán-Ferré C. Structure-Based Virtual Screening and in vitro and in vivo Analyses Revealed Potent Methyltransferase G9a Inhibitors as Prospective Anti-Alzheimer's Agents. ChemMedChem. 22;17(13):e202200002.

Benayoun BA, Pollina EA, Brunet A. Epigenetic regulation of ageing: linking environmental inputs to genomic stability. Nat Rev Mol Cell Biol. 2015;16(10):593–610.

Berson A, Nativio R, Berger SL, Bonini NM. Epigenetic Regulation in Neurodegenerative Diseases. Trends Neurosci. 2018;41(9):587–598.

Bertogliat MJ, Morris-Blanco KC, Vemuganti R. Epigenetic mechanisms of neurodegenerative diseases and acute brain injury. Neurochem Int. 2020;133:104642.

Bhatt D, Ghosh S. Regulation of the NF-κB-mediated transcription of inflammatory genes. Front Immunol. 2014;5:71.

Bi M, Gladbach A, Van Eersel J, Ittner A, Przybyla M, Van Hummel A, Chua SW, Van Der Hoven J, Lee WS, Müller J. Tau exacerbates excitotoxic brain damage in an animal model of stroke. Nat Commun. 2017;8(1):473

Blauwendraat C, Pletnikova O, Geiger JT, Murphy NA, Abramzon Y, Rudow G, Mamais A, Sabir MS, Crain B, Ahmed S. Genetic analysis of neurodegenerative diseases in a pathology cohort. Neurobiol Aging. 2019;76:214-e1.

Bliss TVP, Collingridge GL. Expression of NMDA receptor-dependent LTP in the hippocampus: bridging the divide. Mol Brain. 2013;6(1):1–14.

Braak H, Del Tredici K. Are cases with tau pathology occurring in the absence of Aβ deposits part of the AD-related pathological process? Acta Neuropathol. 2014;128:767–772.

Brenner S. The genetics of Caenorhabditis elegans. Genetics. 1974;77(1):71–94.

Brown SE, Campbell RD, Sanderson CM. Novel NG36/G9a gene products encoded within the human and mouse MHC class III regions. Mammalian genome. 2001;12(12):916–924.

Bruemmer D, Blaschke F, Law R. New targets for PPARγ in the vessel wall: implications for restenosis. Int J Obes. 2005;Suppl 1:S26-30.

Brunet A, Berger SL. Epigenetics of aging and aging-related disease. Journals of Gerontology - Series A Biological Sciences and Medical Sciences. 2014;69(Suppl 1):17–20.

Buhusi M, Etheredge C, Granholm AC, Buhusi C V. Increased hippocampal ProBDNF contributes to memory impairments in aged mice. Front Aging Neurosci. 2017;9:1–15.

Busche MA, Hyman BT. Synergy between amyloid-β and tau in Alzheimer's disease. Nat Neurosci. 2020;23(10):1183–1193.

Bustos FJ, Ampuero E, Jury N, Aguilar R, Falahi F, Toledo J, Ahumada J, Lata J, Cubillos P, Henríquez B, Guerra MV, Stehberg J, Neve RL, Inestrosa NC, Wyneken U, Fuenzalida M, Härtel S, Sena-Esteves M, Varela-Nallar L, Rots MG, Montecino M, van Zundert B. Epigenetic editing of the Dlg4/PSD95 gene improves cognition in aged and Alzheimer's disease mice. Brain. 2017;140(12):3252–3268.

Butterfield DA, Poon HF. The senescence-accelerated prone mouse (SAMP8): A model of age-related cognitive decline with relevance to alterations of the gene expression and protein abnormalities in Alzheimer's disease. Exp Gerontol. 2005;40(10):774–783.

Byers AL, Covinsky KE, Barnes DE, Yaffe K. Dysthymia and depression increase risk of dementia and mortality among older veterans. The American Journal of Geriatric Psychiatry. 2012;20(8):664–672.

Calissano P, Matrone C, Amadoro G. Apoptosis and in vitro Alzheimer's disease neuronal models. Commun Integr Biol. 2009;2(2):163–169.

Calsolaro V, Edison P. Neuroinflammation in Alzheimer's disease: current evidence and future directions. Alzheimer's & Dementia. 2016;12(6):719–732.

Campagna MP, Xavier A, Lechner-Scott J, Maltby V, Scott RJ, Butzkueven H, Jokubaitis VG, Lea RA. Epigenome-wide association studies: current knowledge, strategies and recommendations. Clin Epigenetics. 2021;13(1):1–24.

Cao H, Li L, Yang D, Zeng L, Yewei X, Yu B, Liao G, Chen J. Recent progress in histone methyltransferase (G9a) inhibitors as anticancer agents. Eur J Med Chem. 2019;179:537–546.

Cao Q, Wang W, Williams JB, Yang F, Wang Z-J, Yan Z. Targeting histone K4 trimethylation for treatment of cognitive and synaptic deficits in mouse models of Alzheimer's disease. 2020;6(50):eabc8096.

Castrillo JI, Oliver SG. Alzheimer's as a systems-level disease involving the interplay of multiple cellular networks. Systems Biology of Alzheimer's Disease. 2016;3–48.

Cavalli G, Heard E. Advances in epigenetics link genetics to the environment and disease. Nature. 2019;571(7766):489–499

Cerejeira J, Lagarto L, Mukaetova-Ladinska EB. Behavioral and psychological symptoms of dementia. Front Neurol. 2012;3:73.

Cha Y, Erez T, Reynolds IJ, Kumar D, Ross J, Koytiger G, Kusko R, Zeskind B, Risso S, Kagan E. Drug repurposing from the perspective of pharmaceutical companies. Br J Pharmacol. 2018;175(2):168–180.

Chae YC, Kim JY, Park JW, Kim KB, Oh H, Lee KH, Seo SB. FOXO1 degradation via G9a-mediated methylation promotes cell proliferation in colon cancer. Nucleic Acids Res. 2019;47(4):1692–1705.

Chang L, Wang Y, Ji H, Dai D, Xu X, Jiang D, Hong Q, Ye H, Zhang X, Zhou X. Elevation of peripheral BDNF promoter methylation links to the risk of Alzheimer's disease. PLoS One. 2014;9(11):e110773.

Chang Y, Ganesh T, Horton JR, Spannhoff A, Liu J, Sun A, Zhang X, Bedford MT, Shinkai Y, Snyder JP, Cheng X. Adding a lysine mimic in the design of potent inhibitors of histone lysine methyltransferases. J Mol Biol. 2010;400(1):1–7

Chang Y, Sun L, Kokura K, Horton JR, Fukuda M, Espejo A, Izumi V, Koomen JM, Bedford MT, Zhang X. MPP8 mediates the interactions between DNA methyltransferase Dnmt3a and H3K9 methyltransferase GLP/G9a. Nat Commun. 2011;2(1):533.

Chang Y, Zhang X, Horton JR, Upadhyay AK, Spannhoff A, Liu J, Snyder JP, Bedford MT, Cheng X. Structural basis for G9a-like protein lysine methyltransferase inhibition by BIX-01294. Nat Struct Mol Biol. 2009;16(3):312–317.

Charles MRC, Dhayalan A, Hsieh HP, Coumar MS. Insights for the design of protein lysine methyltransferase G9a inhibitors. Future Med Chem. 2019;11(09):993–1014.

Charles MRC, Mahesh A, Lin SY, Hsieh HP, Dhayalan A, Coumar MS. Identification of novel quinoline inhibitor for EHMT2/G9a through virtual screening. Biochimie. 2020;168:220–230.

Chen GH, Wang YJ, Wang XM, Zhou JN. Accelerated senescence prone mouse-8 shows early onset of deficits in spatial learning and memory in the radial six-arm water maze. Physiol Behav. 2004;82(5):883–890.

Chen H, Dzitoyeva S, Manev H. Effect of aging on 5-hydroxymethylcytosine in the mouse hippocampus. Restor Neurol Neurosci. 2012;30(3):237–245.

Chen H, Xue Y, Huang N, Yao X, Sun Z. MeMo: a web tool for prediction of protein methylation modifications. Nucleic Acids Res. 2006;34(suppl_2):W249–W253.

Chen J, Lin X, Park KJ, Lee KR, Park HJ. Identification of protoberberine alkaloids as novel histone methyltransferase G9a inhibitors by structure-based virtual screening. J Comput Aided Mol Des. 2018;32(9):917–928.

Chen WL, Wang ZH, Feng TT, Li DD, Wang CH, Xu XL, Zhang XJ, You QD, Guo XK. Discovery, design and synthesis of 6H-anthra [1, 9-cd] isoxazol-6-one scaffold as G9a inhibitor through a combination of shape-based virtual screening and structure-based molecular modification. Bioorg Med Chem. 2016;24(22):6102–6108.

Chen X, Barclay JW, Burgoyne RD, Morgan A. Using C. elegans to discover therapeutic compounds for ageing-associated neurodegenerative diseases. Chem Cent J. 2015;9(1):1–20.

Chen X, Comish PB, Tang D, Kang R. Characteristics and biomarkers of ferroptosis. Front Cell Dev Biol. 2021;9:637162.

Cheng C, Li W, Zhang Z, Yoshimura S, Hao Q, Zhang C, Wang Z. MicroRNA-144 is regulated by activator protein-1 (AP-1) and decreases expression of Alzheimer disease-related a disintegrin and metalloprotease 10 (ADAM10). Journal of Biological Chemistry. 2013;288(19):13748–13761.

Cherblanc FL, Chapman KL, Reid J, Borg AJ, Sundriyal S, Alcazar-Fuoli L, Bignell E, Demetriades M, Schofield CJ, DiMaggio Jr PA. On the histone lysine methyltransferase activity of fungal metabolite chaetocin. J Med Chem. 2013;56(21):8616–8625.

Chételat G, La Joie R, Villain N, Perrotin A, de La Sayette V, Eustache F, Vandenberghe R. Amyloid imaging in cognitively normal individuals, at-risk populations and preclinical Alzheimer's disease. Neuroimage Clin. 2013;2:356–365.

Chiaretti A, Antonelli A, Genovese O, Pezzotti P, Di Rocco C, Viola L, Riccardi R. Nerve growth factor and doublecortin expression correlates with improved outcome in children with severe traumatic brain injury. Journal of Trauma and Acute Care Surgery. 2008;65(1):80–85.

Choi J, Jang H, Kim H, Lee JH, Kim ST, Cho EJ, Youn HD. Modulation of lysine methylation in myocyte enhancer factor 2 during skeletal muscle cell differentiation. Nucleic Acids Res. 2014;42(1):224–234.

Chuang JC, Jones PA. Epigenetics and microRNAs. Pediatr Res. 2007;61(5 Part 2):24R.

Ciccacci C, Di Fusco D, Cacciotti L, Morganti R, D'Amato C, Greco C, Rufini S, Novelli G, Sangiuolo F, Spallone V. MicroRNA genetic variations: association with type 2 diabetes. Acta Diabetol. 2013;50(6):867–872.

Cipriani PG, Piano F. RNAi methods and screening: RNAi based high-throughput genetic interaction screening. In: Methods in cell biology, Elsevier; 2011; pp. 89–111.

Clapier CR, Iwasa J, Cairns BR, Peterson CL. Mechanisms of action and regulation of ATP-dependent chromatin-remodelling complexes. Nat Rev Mol Cell Biol. 2017;18(7):407–422.

Cogswell JP, Ward J, Taylor IA, Waters M, Shi Y, Cannon B, Kelnar K, Kemppainen J, Brown D, Chen C. Identification of miRNA changes in Alzheimer's disease brain and

CSF yields putative biomarkers and insights into disease pathways. Journal of Alzheimer's disease. 2008;14(1):27–41.

Collins RE, Northrop JP, Horton JR, Lee DY, Zhang X, Stallcup MR, Cheng X. The ankyrin repeats of G9a and GLP histone methyltransferases are mono-and dimethyllysine binding modules. Nat Struct Mol Biol. 2008;15(3):245.

Colquitt BM, Allen WE, Barnea G, Lomvardas S. Alteration of genic 5-hydroxymethylcytosine patterning in olfactory neurons correlates with changes in gene expression and cell identity. Proceedings of the National Academy of Sciences. 2013;110(36):14682–14687.

Colucci-D'Amato L, Perrone-Capano C, di Porzio U. Chronic activation of ERK and neurodegenerative diseases. Bioessays. 2003;25(11):1085–1095.

Companys-Alemany J, Turcu AL, Bellver-Sanchis A, Loza MI, Brea JM, Canudas AM, Leiva R, Vázquez S, Pallàs M, Griñán-Ferré C. A novel NMDA receptor antagonist protects against cognitive decline presented by senescent mice. Pharmaceutics 12. 2020;12(3):284.

Consortium TC elegans S. Genome sequence of the nematode C. elegans: a platform for investigating biology. Science. 1998;2012–2018.

Coppieters N, Dieriks B V, Lill C, Faull RLM, Curtis MA, Dragunow M. Global changes in DNA methylation and hydroxymethylation in Alzheimer's disease human brain. Neurobiol Aging. 2014;35(6):1334–1344.

Corsi AK, Wightman B, Chalfie M. A transparent window into biology: a primer on Caenorhabditis elegans. Genetics. 2015;200(2):387–407.

Cosín-Tomás M, Álvarez-López MJ, Companys-Alemany J, Kaliman P, González-Castillo C, Ortuño-Sahagún D, Pallàs M, Griñán-Ferré C. Temporal integrative analysis of mRNA and microRNAs expression profiles and epigenetic alterations in female SAMP8, a model of age-related cognitive decline. Front Genet. 2018;9:596.

Cosín-Tomás M, Alvarez-López MJ, Sanchez-Roige S, Lalanza JF, Bayod S, Sanfeliu C, Pallàs M, Escorihuela RM, Kaliman P. Epigenetic alterations in hippocampus of SAMP8 senescent mice and modulation by voluntary physical exercise. Front Aging Neurosci. 2014;6:1–10;.

Counts SE, Nadeem M, Lad SP, Wuu J, Mufson EJ. Differential expression of synaptic proteins in the frontal and temporal cortex of elderly subjects with mild cognitive impairment. J Neuropathol Exp Neurol. 2006;65(6):592–601.

Courtney C, Farrell D, Gray R, Hills R, Lynch L, Sellwood E, Edwards S, Hardyman W, Raftery J, Crome P, Lendon C, Shaw H, Bentham P; AD2000 Collaborative Group. Long-term donepezil treatment in 565 patients with Alzheimer's disease (AD2000): randomised double-blind trial. The Lancet. 2004;363(9427):2105-15.

Cui D, Xu X. Dna methyltransferases, dna methylation, and age-associated cognitive function. Int J Mol Sci. 2018;19(5):1315.

Cui M, Han M. Roles of chromatin factors in C. elegans development. WormBook: The Online Review of C elegans Biology. 2007;3:1-16.

Cummings JL, Osse AML, Kinney JW. Alzheimer's Disease: Novel Targets and Investigational Drugs for Disease Modification. Drugs. 2023;83(15):1387–1408.

Davis DG, Schmitt FA, Wekstein DR, Markesbery W. Alzheimer neuropathologic alterations in aged cognitively normal subjects. J Neuropathol Exp Neurol. 1999;58(4):376–388.

Dawson MA, Kouzarides T. Cancer epigenetics: from mechanism to therapy. Cell. 2012;150(1):12–27.

de Freitas Silva M, Dias KST, Gontijo VS, Ortiz CJC, Viegas Jr C. Multi-target directed drugs as a modern approach for drug design towards Alzheimer's disease: an update. Curr Med Chem. 2018;25(29):3491–3525.

de Oliveira J, Kucharska E, Garcez ML, Rodrigues MS, Quevedo J, Moreno-Gonzalez I, Budni J. Inflammatory cascade in Alzheimer's disease pathogenesis: A review of experimental findings. Cells. 2021;10(10):2581.

de Vink PJ, Andrei SA, Higuchi Y, Ottmann C, Milroy LG, Brunsveld L. Cooperativity basis for small-molecule stabilization of protein–protein interactions. Chem Sci. 2019;10(10):2869–2874.

De Wilde MC, Overk CR, Sijben JW, Masliah E. Meta-analysis of synaptic pathology in Alzheimer's disease reveals selective molecular vesicular machinery vulnerability. Alzheimer's & dementia. 2016;12(6):633–644.

DeKosky ST, Scheff SW. Synapse loss in frontal cortex biopsies in Alzheimer's disease: correlation with cognitive severity. Annals of Neurology: Official Journal of the

American Neurological Association and the Child Neurology Society. 1990;27(5):457–464.

Del Ser T, Steinwachs KC, Gertz HJ, Andres M V, Gomez-Carrillo B, Medina M, Vericat JA, Redondo P, Fleet D, Leon T. Treatment of Alzheimer's disease with the GSK-3 inhibitor tideglusib: a pilot study. Journal of Alzheimer's Disease. 2013;33(1):205–215.

Deng W, Wang Y, Ma L, Zhang Y, Ullah S, Xue Y. Computational prediction of methylation types of covalently modified lysine and arginine residues in proteins. Brief Bioinform. 2017;18(4):647–658.

DeTure MA, Dickson DW. The neuropathological diagnosis of Alzheimer's disease. Mol Neurodegener. 2019;14(1):1–18.

Deuschl G, Beghi E, Fazekas F, Varga T, Christoforidi KA, Sipido E, Bassetti CL, Vos T, Feigin VL. The burden of neurological diseases in Europe: an analysis for the Global Burden of Disease Study 2017. Lancet Public Health. 2020;5(10):e551–e567

Deverman BE, Patterson PH. Cytokines and CNS development. Neuron. 2009;64(1):61–78.

DeVorkin L, Choutka C, Gorski SM. The Interplay between Autophagy and Apoptosis. Autophagy: Cancer, Other Pathologies, Inflammation, Immunity, Infection, and Aging. 2014;3:369–383.

Dharshini SAP, Jemimah S, Taguchi YH, Gromiha MM. Exploring common therapeutic targets for neurodegenerative disorders using transcriptome study. Front Genet. 2021;12:639160.

Di Giacomo V, Sancilio S, Caravatta L, Rana RA, Di Pietro R, Cataldi A. Regulation of CREB activation by p38 mitogen activated protein kinase during human primary erythroblast differentiation. Int J Immunopathol Pharmacol. 2009;22(3):679–688.

Di Leva G, Garofalo M, Croce CM. MicroRNAs in cancer. Annual Review of Pathology: Mechanisms of Disease. 2014;9:287–314.

Dillon SC, Zhang X, Trievel RC, Cheng X. The SET-domain protein superfamily: protein lysine methyltransferases. Genome Biol. 2005;6:1–10.

DiMasi JA, Feldman L, Seckler A, Wilson A. Trends in risks associated with new drug development: success rates for investigational drugs. Clin Pharmacol Ther. 2010;87(3):272–277.

DiMasi JA, Grabowski HG, Hansen RW. Innovation in the pharmaceutical industry: new estimates of R&D costs. J Health Econ. 2016;47:20–33.

Ding H, Dolan PJ, Johnson GVW. Histone deacetylase 6 interacts with the microtubule-associated protein tau. J Neurochem. 2008a;106(5):2119–2130.

Ding N, Zhou H, Esteve PO, Chin HG, Kim S, Xu X, Joseph SM, Friez MJ, Schwartz CE, Pradhan S. Mediator links epigenetic silencing of neuronal gene expression with x-linked mental retardation. Mol Cell. 2008b;31(3):347–359.

DiSabato DJ, Quan N, Godbout JP. Neuroinflammation: the devil is in the details. J Neurochem . 2016;139:136–153.

Dixon SJ, Lemberg KM, Lamprecht MR, Skouta R, Zaitsev EM, Gleason CE, Patel DN, Bauer AJ, Cantley AM, Yang WS (2012) Ferroptosis: an iron-dependent form of nonapoptotic cell death. Cell. 2012;149(5):1060–1072.

Dixon SJ. Ferroptosis: bug or feature? Immunol Rev. 2017;277(1):150–157.

Dorostkar MM, Zou C, Blazquez-Llorca L, Herms J. Analyzing dendritic spine pathology in Alzheimer's disease: problems and opportunities. Acta Neuropathol. 2015;130(1):1–19.

Drewes G, Ebneth A, Preuss U, Mandelkow E-M, Mandelkow E. MARK, a novel family of protein kinases that phosphorylate microtubule-associated proteins and trigger microtubule disruption. Cell. 1997;89(2):297–308.

Dunham I, Sargent CA, Kendall E, Duncan Campbell R. Characterization of the class III region in different MHC haplotypes by pulsed-field gel electrophoresis. Immunogenetics. 1990;32:175–182.

E. Morley J, A. Farr S, B. Kumar V, J. Armbrecht H, E Morley J, A Farr S, B Kumar V, J Armbrecht H. The SAMP8 mouse: a model to develop therapeutic interventions for Alzheimer's disease. Curr Pharm Des. 2012;18(8):1123–1130.

Edison P, Archer HA, Hinz R, Hammers A, Pavese N, Tai YF, Hotton G, Cutler D, Fox N, Kennedy A. Amyloid, hypometabolism, and cognition in Alzheimer disease: an [11C] PIB and [18F] FDG PET study. Neurology. 2007;68(7):501–508.

Eid A, Mhatre I, Richardson JR. Gene-environment interactions in Alzheimer's disease: A potential path to precision medicine. Pharmacol Ther. 2019;199:173–187.

Ernfors P, Ibanez CF, Ebendal T, Olson L, Persson H. Molecular cloning and neurotrophic activities of a protein with structural similarities to nerve growth factor: developmental

and topographical expression in the brain. Proceedings of the National Academy of Sciences. 1990;87(14):5454–5458.

Estève P-O, Chin HG, Smallwood A, Feehery GR, Gangisetty O, Karpf AR, Carey MF, Pradhan S. Direct interaction between DNMT1 and G9a coordinates DNA and histone methylation during replication. Genes Dev. 2006;20(22):3089–3103.

Fagan AM, Mintun MA, Shah AR, Aldea P, Roe CM, Mach RH, Marcus D, Morris JC, Holtzman DM. Cerebrospinal fluid tau and ptau181 increase with cortical amyloid deposition in cognitively normal individuals: implications for future clinical trials of Alzheimer's disease. EMBO Mol Med. 2009;1(8-9):371–380.

Falnes PØ, Jakobsson ME, Davydova E, Ho A, Małecki J. Protein lysine methylation by seven-β-strand methyltransferases. Biochemical Journal. 2016;473(14):1995–2009.

Fan J, Fong T, Chen X, Chen C, Luo P, Xie H. Glia maturation factor-β: A potential therapeutic target in neurodegeneration and neuroinflammation. Neuropsychiatr Dis Treat. 2018;14:495–504.

Fang S, Miao J, Xiang L, Ponugoti B, Treuter E, Kemper JK. Coordinated recruitment of histone methyltransferase G9a and other chromatin-modifying enzymes in SHP-mediated regulation of hepatic bile acid metabolism. Mol Cell Biol. 2007;27(4):1407–1424.

Fatouros C, Pir GJ, Biernat J, Koushika SP, Mandelkow E, Mandelkow E-M, Schmidt E, Baumeister R. Inhibition of tau aggregation in a novel Caenorhabditis elegans model of tauopathy mitigates proteotoxicity. Hum Mol Genet. 2012;21(16):3587–3603.

Femminella GD, Ferrara N, Rengo G. The emerging role of microRNAs in Alzheimer's disease. Front Physiol. 2015;6:40.

Feng J, Xing W, Xie L. Regulatory roles of microRNAs in diabetes. Int J Mol Sci. 2016;17(10):1729.

Ferrucci L, Fabbri E. Inflammageing: chronic inflammation in ageing, cardiovascular disease, and frailty. Nat Rev Cardiol. 2018;15(9):505–522.

Finkbeiner S, Tavazoie SF, Maloratsky A, Jacobs KM, Harris KM, Greenberg ME. CREB: a major mediator of neuronal neurotrophin responses. Neuron. 1997;19(5):1031–1047.

Fischer ES, Böhm K, Lydeard JR, Yang H, Stadler MB, Cavadini S, Nagel J, Serluca F, Acker V, Lingaraju GM. Structure of the DDB1–CRBN E3 ubiquitin ligase in complex with thalidomide. Nature. 2014;512(7512):49–53.

Francis YI, Fà M, Ashraf H, Zhang H, Staniszewski A, Latchman DS, Arancio O. Dysregulation of histone acetylation in the APP/PS1 mouse model of Alzheimer's disease. Journal of Alzheimer's disease. 2009;18(1):131–139.

Fujishiro S, Dodo K, Iwasa E, Teng Y, Sohtome Y, Hamashima Y, Ito A, Yoshida M, Sodeoka M. Epidithiodiketopiperazine as a pharmacophore for protein lysine methyltransferase G9a inhibitors: reducing cytotoxicity by structural simplification. Bioorg Med Chem Lett. 2013;23(3):733–736.

García JJ, Piñol-Ripoll G, Martínez-Ballarín E, Fuentes-Broto L, Miana-Mena FJ, Venegas C, Caballero B, Escames G, Coto-Montes A, Acuña-Castroviejo D. Melatonin reduces membrane rigidity and oxidative damage in the brain of SAMP8 mice. Neurobiol Aging. 2011;32(11):2045–2054.

García-Domínguez DJ, Hajji N, López-Alemany R, Sánchez-Molina S, Figuerola-Bou E, Morón Civanto FJ, Rello-Varona S, Andrés-León E, Benito A, Keun HC. Selective histone methyltransferase G9a inhibition reduces metastatic development of Ewing sarcoma through the epigenetic regulation of NEU1. Oncogene. 2022;41(18):2638–2650.

Gatz M, Reynolds CA, Fratiglioni L, Johansson B, Mortimer JA, Berg S, Fiske A, Pedersen NL. Role of genes and environments for explaining Alzheimer disease. Arch Gen Psychiatry. 2006;63(2):168–174.

Gaugler J, James B, Johnson T, Reimer J, Solis M, Weuve J, Buckley RF, Hohman TJ. 2022 Alzheimer's disease facts and figures. Alzheimers & Dementia. 2022;18(4):700–789.

Genin E, Hannequin D, Wallon D, Sleegers K, Hiltunen M, Combarros O, Bullido MJ, Engelborghs S, De Deyn P, Berr C. APOE and Alzheimer disease: a major gene with semi-dominant inheritance. Mol Psychiatry. 2011;16(9):903–907.

Gerstein MB, Lu ZJ, Van Nostrand EL, Cheng C, Arshinoff BI, Liu T, Yip KY, Robilotto R, Rechtsteiner A, Ikegami K. Integrative analysis of the Caenorhabditis elegans genome by the modENCODE project. Science. 2010;330(6012):1775–1787.

Goate A, Chartier-Harlin MC, Mullan M, Brown J, Crawford F, Fidani L, Giuffra L, Haynes A, Irving N, James L. Segregation of a missense mutation in the amyloid precursor protein gene with familial Alzheimer's disease. Nature. 1991;349(6311):704–706.

Godin SK, Seo J, Tsai LH. Neurodegenerative Diseases and the Aging Brain. In: The Molecular and Cellular Basis of Neurodegenerative Diseases, Elsevier. 2018; pp. 509–526.

Goedert M, Spillantini MG, Jakes R, Rutherford D, Crowther RA. Multiple isoforms of human microtubule-associated protein tau: sequences and localization in neurofibrillary tangles of Alzheimer's disease. Neuron. 1989;3(4):519–526.

González JF, Alcántara AR, Doadrio AL, Sánchez-Montero JM. Developments with multi-target drugs for Alzheimer's disease: An overview of the current discovery approaches. Expert Opin Drug Discov. 2019;14(9):879–891.

González-Aguilera C, Palladino F, Askjaer P. C. elegans epigenetic regulation in development and aging. Brief Funct Genomics. 2014;13(3):223–234.

Gonzalez-Zuniga M, Contreras PS, Estrada LD, Chamorro D, Villagra A, Zanlungo S, Seto E, Alvarez AR. c-Abl stabilizes HDAC2 levels by tyrosine phosphorylation repressing neuronal gene expression in Alzheimer's disease. Mol Cell. 2014;56(1):163–173.

Goode BL, Sweeney MO, Eskin JA. GMF as an actin network remodeling factor. Trends Cell Biol. 2018;28(9):749–760.

Govindarajan N, Agis-Balboa RC, Walter J, Sananbenesi F, Fischer A. Sodium butyrate improves memory function in an Alzheimer's disease mouse model when administered at an advanced stage of disease progression. Journal of Alzheimer's Disease. 2011;26(1):187–197.

Greer EL, Shi Y. Histone methylation: a dynamic mark in health, disease and inheritance. Nat Rev Genet. 2012;13(5):343–357.

Greiner D, Bonaldi T, Eskeland R, Roemer E, Imhof A. Identification of a specific inhibitor of the histone methyltransferase SU (VAR) 3-9. Nat Chem Biol. 2005;1(3):143–145.

Griñán-Ferré C, Corpas R, Puigoriol-Illamola D, Palomera-Ávalos V, Sanfeliu C, Pallàs M. Understanding Epigenetics in the Neurodegeneration of Alzheimer's Disease: SAMP8 Mouse Model. Journal of Alzheimer's Disease. 2018;62(3):943–963.

Griñán-Ferré C, Jarne-Ferrer J, Bellver-Sanchis A, Ribalta-Vilella M, Barroso E, Salvador JM, Jurado-Aguilar J, Palomer X, Vázquez-Carrera M, Pallàs M. Deletion of Gadd45a Expression in Mice Leads to Cognitive and Synaptic Impairment Associated with Alzheimer's Disease Hallmarks. Int J Mol Sci. 2024;25(5):2595.

Griñán-Ferré C, Marsal-García L, Bellver-Sanchis A, Kondengaden SMSM, Turga RCRC, Vázquez S, Pallàs M. Pharmacological inhibition of G9a/GLP restores cognition and reduces oxidative stress, neuroinflammation and ß-Amyloid plaques in an early-onset Alzheimer's disease mouse model. Aging. 2019;11(23):11591–11608.

Griñan-Ferré C, Palomera-Ávalos V, Puigoriol-Illamola D, Camins A, Porquet D, Plá V, Aguado F, Pallàs M. Behaviour and cognitive changes correlated with hippocampal neuroinflammaging and neuronal markers in female SAMP8, a model of accelerated senescence. Exp Gerontol. 2016a;80(57):69.

Griñan-Ferré C, Pérez-Cáceres D, Gutiérrez-Zetina SM, Camins A, Palomera-Avalos V, Ortuño-Sahagún D, Rodrigo MT, Pallàs M, Griñán-Ferré C, Pérez-Cáceres D, Gutiérrez-Zetina SM, Camins A, Palomera-Avalos V, Ortuño-Sahagún D, Rodrigo MT, Pallàs M. Environmental Enrichment Improves Behavior, Cognition, and Brain Functional Markers in Young Senescence-Accelerated Prone Mice (SAMP8). Mol Neurobiol. 2016b;53(4):2435–2450.

Griñan-Ferré C, Puigoriol-Illamola D, Palomera-Ávalos V, Pérez-Cáceres D, Companys-Alemany J, Camins A, Ortuño-Sahagún D, Rodrigo MT, Pallàs M. Environmental enrichment modified epigenetic mechanisms in SAMP8 mouse hippocampus by reducing oxidative stress and inflammaging and achieving neuroprotection. Front Aging Neurosci. 2016c;8:241.

Griñán-Ferré C, Sarroca S, Ivanova A, Puigoriol-Illamola D, Aguado F, Camins A, Sanfeliu C, Pallàs M. Epigenetic mechanisms underlying cognitive impairment and Alzheimer disease hallmarks in 5XFAD mice. Aging. 2016;8(4):664–684.

Grishok A. RNAi mechanisms in Caenorhabditis elegans. FEBS Lett. 2005;579(26):5932–5939.

Gu M, Toh TB, Hooi L, Lim JJ, Zhang X, Chow EKH. Nanodiamond-mediated delivery of a G9a inhibitor for hepatocellular carcinoma therapy. ACS Appl Mater Interfaces. 2019;11(49):45427–45441.

Guillaumet-Adkins A, Yañez Y, Peris-Diaz MD, Calabria I, Palanca-Ballester C, Sandoval J. Epigenetics and Oxidative Stress in Aging. Oxid Med Cell Longev. 2017;2017:9175806.

Gupta-Agarwal S, Franklin A V, DeRamus T, Wheelock M, Davis RL, McMahon LL, Lubin FD. G9a/GLP histone lysine dimethyltransferase complex activity in the hippocampus and the entorhinal cortex is required for gene activation and silencing during memory consolidation. Journal of Neuroscience. 2012;32(16):5440–5453.

Gusel'Nikova V V, Korzhevskiy D. NeuN as a neuronal nuclear antigen and neuron differentiation marker. Acta Naturae. 2015;7(2 (25)):42–47.

Gyenesei A, Moody J, Semple CAM, Haley CS, Wei WH. High-throughput analysis of epistasis in genome-wide association studies with BiForce. Bioinformatics. 2012;28(15):1957–1964.

Győry I, Wu J, Fejér G, Seto E, Wright KL. PRDI-BF1 recruits the histone H3 methyltransferase G9a in transcriptional silencing. Nat Immunol. 2004;5(3):299–308.

Hadar A, Milanesi E, Walczak M, Puzianowska-Kuźnicka M, Kuźnicki J, Squassina A, Niola P, Chillotti C, Attems J, Gozes I. SIRT1, miR-132 and miR-212 link human longevity to Alzheimer's Disease. Sci Rep. 2018;8(1):8465.

Hambright WS, Fonseca RS, Chen L, Na R, Ran Q. Ablation of ferroptosis regulator glutathione peroxidase 4 in forebrain neurons promotes cognitive impairment and neurodegeneration. Redox Biol. 2017;12:8–17.

Hamilton JP. Epigenetics: principles and practice. Digestive diseases. 2011;29(2):130–135.

Hampel H, Hardy J, Blennow K, Chen C, Perry G, Kim SH, Villemagne VL, Aisen P, Vendruscolo M, Iwatsubo T. The amyloid-β pathway in Alzheimer's disease. Mol Psychiatry. 2021;26(10):5481–5503.

Han JLT, Pang KKL, Ang SRX, Sharma M, Sajikumar S. Inhibition of lysine methyltransferase G9a/GLP reinstates long-term synaptic plasticity and synaptic tagging/capture by facilitating protein synthesis in the hippocampal CA1 area of APP/PS1 mouse model of Alzheimer's disease. Transl Neurodegener. 2021;10(1):1–3.

Hanger DP, Anderton BH, Noble W. Tau phosphorylation: the therapeutic challenge for neurodegenerative disease. Trends Mol Med. 2009;15(3):112–119.

Hanley JG. AMPA receptor trafficking pathways and links to dendritic spine morphogenesis. Cell Adh Migr. 2008;2(4):276–282.

Harman MF, Martín MG. Epigenetic mechanisms related to cognitive decline during aging. J Neurosci Res. 2020;98(2):234-246

He X, Hui Z, Xu L, Bai R, Gao Y, Wang Z, Xie T, Ye XY. Medicinal chemistry updates of novel HDACs inhibitors (2020 to present). Eur J Med Chem. 2022;227:113946.

Hébert SS, Horré K, Nicolaï L, Papadopoulou AS, Mandemakers W, Silahtaroglu AN, Kauppinen S, Delacourte A, De Strooper B. Loss of microRNA cluster miR-29a/b-1 in sporadic Alzheimer's disease correlates with increased BACE1/β-secretase expression. Proc Natl Acad Sci. 2008;105(17):6415–6420.

Heckmann BL, Teubner BJW, Boada-Romero E, Tummers B, Guy C, Fitzgerald P, Mayer U, Carding S, Zakharenko SS, Wileman T. Noncanonical function of an autophagy protein prevents spontaneous Alzheimer's disease. Sci Adv. 2020;6(33):eabb9036.

Heerboth S, Lapinska K, Snyder N, Leary M, Rollinson S, Sarkar S. Use of epigenetic drugs in disease: an overview. Genet Epigenet. 2014;6:GEG-S12270.

Heneka MT, Carson MJ, El Khoury J, Landreth GE, Brosseron F, Feinstein DL, Jacobs AH, Wyss-Coray T, Vitorica J, Ransohoff RM. Neuroinflammation in Alzheimer's disease. Lancet Neurol. 2015;14(4):388–405.

Hernandez-Rapp J, Rainone S, Goupil C, Dorval V, Smith PY, Saint-Pierre M, Vallée M, Planel E, Droit A, Calon F. microRNA-132/212 deficiency enhances Aβ production and senile plaque deposition in Alzheimer's disease triple transgenic mice. Sci Rep. 2016;6(1):30953.

Hildesheim J, Bulavin D V, Anver MR, Alvord WG, Hollander MC, Vardanian L, Fornace Jr AJ. Gadd45a protects against UV irradiation-induced skin tumors, and promotes apoptosis and stress signaling via MAPK and p53. Cancer Res. 2002;62(24):7305–7315.

Hof PR, Morrison JH. The aging brain: morphomolecular senescence of cortical circuits. Trends Neurosci. 2004;27(10):607–613.

Hohn A, Leibrock J, Bailey K, Barde YA. Identification and characterization of a novel member of the nerve growth factor/brain-derived neurotrophic factor family. Nature. 1990;344(6264):339–341.

Hou QQ, Xiao Q, Sun XY, Ju XC, Luo ZG. TBC1D3 promotes neural progenitor proliferation by suppressing the histone methyltransferase G9a. Sci Adv. 2021;7(3):eaba8053.

Hou Y, Dan X, Babbar M, Wei Y, Hasselbalch SG, Croteau DL, Bohr VA. Ageing as a risk factor for neurodegenerative disease. Nat Rev Neurol. 2019;15(10):565–581.

Hou Y, Moreau F, Chadee K. PPARγ is an E3 ligase that induces the degradation of NFκB/p65. Nat Commun. 2012;3:1300.

Houseknecht KL, Cole BM, Steele PJ. Peroxisome proliferator-activated receptor gamma (PPARγ) and its ligands: a review. Domest Anim Endocrinol. 2002;22(1):1–23.

Hu W, Wang M, Yin H, Yao C, He Q, Yin L, Zhang C, Li W, Chang G, Wang S. MicroRNA-1298 is regulated by DNA methylation and affects vascular smooth muscle cell function by targeting connexin 43. Cardiovasc Res. 2015;107(4):534–545.

Huang EJ, Reichardt LF. Neurotrophins: roles in neuronal development and function. Annu Rev Neurosci. 2001;24(1):677–736.

Huang J, Dorsey J, Chuikov S, Zhang X, Jenuwein T, Reinberg D, Berger SL. G9a and Glp methylate lysine 373 in the tumor suppressor p53. Journal of Biological Chemistry. 2010;285(13):9636–9641.

Hui C, Ye T. Synthesis of lysine methyltransferase inhibitors. Front Chem. 2015;3:44.

Ibrahim MM, Gabr MT. Multitarget therapeutic strategies for Alzheimer's disease. Neural Regen Res. 2019;14(3):437.

Iqbal K, Grundke-Iqbal I. Alzheimer's disease, a multifactorial disorder seeking multitherapies. Alzheimer's & Dementia. 2010;6(5):420–424.

Iqbal K, Liu F, Gong CX. Tau and neurodegenerative disease: the story so far. Nat Rev Neurol. 2016;12(1):15–27

Ishiguro K, Kitajima H, Niinuma T, Maruyama R, Nishiyama N, Ohtani H, Sudo G, Toyota M, Sasaki H, Yamamoto E. Dual EZH2 and G9a inhibition suppresses multiple myeloma cell proliferation by regulating the interferon signal and IRF4-MYC axis. Cell Death Discov. 2021;7(1):7.

Ishiguro K, Takamatsu M, Tomizawa K, Omori A, Takahashi M, Arioka M, Uchida T, Imahori K. Tau protein kinase I converts normal tau protein into A68-like component of paired helical filaments. Journal of Biological Chemistry. 1992;267(15):10897–10901.

Iwatsubo T, Odaka A, Suzuki N, Mizusawa H, Nukina N, Ihara Y. Visualization of Aβ42 (43) and Aβ40 in senile plaques with end-specific Aβ monoclonals: evidence that an initially deposited species is Aβ42 (43). Neuron. 1994;13(1):45–53.

Izquierdo V, Palomera-Ávalos V, Pallàs M, Griñán-Ferré C. Resveratrol supplementation attenuates cognitive and molecular alterations under maternal high-fat diet intake: epigenetic inheritance over generations. Int J Mol Sci. 2021;22(3):1453.

J Allen S, J Watson J, Dawbarn D. The neurotrophins and their role in Alzheimer's disease. Curr Neuropharmacol. 2011;9(4):559–573.

Jackson JL, Mallory R. Aggression and violence among elderly patients, a growing health problem. J Gen Intern Med. 2009;24(10):1167–1168.

Jana A, Bellver-Sanchis A, Griñán-Ferré C, Banerjee DR. Repurposing of Raltitrexed as an Effective G9a/EHMT2 Inhibitor and Promising Anti-Alzheimer's Agent. ACS Med Chem Lett. 2023a;14(11)1531–1536.

Jana A, Naga R, Saha S, Banerjee DR. 3D QSAR pharmacophore based lead identification of G9a lysine methyltransferase towards epigenetic therapeutics. J Biomol Struct Dyn. 2023b;41(18):8635–8653

Janczura KJ, Volmar CH, Sartor GC, Rao SJ, Ricciardi NR, Lambert G, Brothers SP, Wahlestedt C. Inhibition of HDAC3 reverses Alzheimer's disease-related pathologies in vitro and in the 3xTg-AD mouse model. Proceedings of the National Academy of Sciences. 2018;115(47):E11148–E11157.

Jenuwein T, Laible G, Dorn R, Reuter G. SET domain proteins modulate chromatin domains in eu-and heterochromatin. Cell Mol Life Sci. 1998;54:80–93.

Jeong H, Mendizabal I, Berto S, Chatterjee P, Layman T, Usui N, Toriumi K, Douglas C, Singh D, Huh I. Evolution of DNA methylation in the human brain. Nat Commun. 2021;12(1):2021.

Jiang D, Li T, Guo C, Tang TS, Liu H. Small molecule modulators of chromatin remodeling: from neurodevelopment to neurodegeneration. Cell Biosci. 2023;13(1):1–32.

Jiao SS, Shen LL, Zhu C, Bu XL, Liu YH, Liu CH, Yao XQ, Zhang LL, Zhou HD, Walker DG, Tan J, Götz J, Zhou XF, Wang YJ. Brain-derived neurotrophic factor protects against tau-related neurodegeneration of Alzheimer's disease. Transl Psychiatry 6. 2016a;6(10):e907.

Jiao Y, Kong L, Yao Y, Li S, Tao Z, Yan Y, Yang J. Osthole decreases beta amyloid levels through up-regulation of miR-107 in Alzheimer's disease. Neuropharmacology. 2016b; 2016b;108:332–344.

Johnson JW, Glasgow NG, Povysheva N V. Recent insights into the mode of action of memantine and ketamine. Curr Opin Pharmacol. 2015;20:54–63.

Jones RS, Gelbart WM. The Drosophila Polycomb-group gene Enhancer of zeste contains a region with sequence similarity to trithorax. Mol Cell Biol. 1993;13(10):6357-66.

José-Enériz ES et al. (2017) Discovery of first-in-class reversible dual small molecule inhibitors against G9a and DNMTs in hematological malignancies. Nat Commun 8.

Kametani F, Hasegawa M. Reconsideration of amyloid hypothesis and tau hypothesis in Alzheimer's disease. Front Neurosci. 2018;12:25.

Kandel ER, Dudai Y, Mayford MR. The molecular and systems biology of memory. Cell. 2014;157(1):163–186.

Kapadia R, Yi J-H, Vemuganti R. Mechanisms of anti-inflammatory and neuroprotective actions of PPAR-gamma agonists. Front Biosci. 2008;13:1813.

Kashyap G, Bapat D, Das D, Gowaikar R, Amritkar RE, Rangarajan G, Ravindranath V, Ambika G. Synapse loss and progress of Alzheimer's disease-A network model. Sci Rep. 2019;9:6555.

Katayama K, Ishii K, Tsuda E, Yotsumoto K, Hiramoto K, Suzuki M, Yasumatsu I, Igarashi W, Torihata M, Ishiyama T. Discovery of novel histone lysine methyltransferase G9a/GLP (EHMT2/1) inhibitors: Design, synthesis, and structure-activity relationships of 2, 4-diamino-6-methylpyrimidines. Bioorg Med Chem Lett. 2020;30(20):127475.

Katoh-Semba R, Kaneko R, Kitajima S, Tsuzuki M, Ichisaka S, Hata Y, Yamada H, Miyazaki N, Takahashi Y, Kato K. Activation of p38 mitogen-activated protein kinase is required for in vivo brain-derived neurotrophic factor production in the rat hippocampus. Neuroscience. 2009;163(1):352–361.

Kaur G, Rathod SSS, Ghoneim MM, Alshehri S, Ahmad J, Mishra A, Alhakamy NA. DNA Methylation: a promising approach in management of Alzheimer's disease and other neurodegenerative disorders. Biology (Basel) 2022:11(1):90.

Ke XX, Zhang D, Zhu S, Xia Q, Xiang Z, Cui H. Inhibition of H3K9 methyltransferase G9A repressed cell proliferation and induced autophagy in neuroblastoma cells. PLoS One. 2014;9(9):e106962

Kempuraj D, Khan MM, Thangavel R, Xiong Z, Yang E, Zaheer A. Glia maturation factor induces interleukin-33 release from astrocytes: implications for neurodegenerative diseases. Journal of Neuroimmune Pharmacology. 2013;8(3):643–650.

Kerchner KM, Mou T-C, Sun Y, Rusnac D-V, Sprang SR, Briknarová K (2021) The structure of the cysteine-rich region from human histone-lysine N-methyltransferase EHMT2 (G9a). J Struct Biol X 5:100050.

Kim J, Onstead L, Randle S, Price R, Smithson L, Zwizinski C, Dickson DW, Golde T, McGowan E. Aβ40 inhibits amyloid deposition in vivo. Journal of Neuroscience. 2007;27(3):627–633.

Kim J, Yoon H, Chung D, Brown JL, Belmonte KC, Kim J. miR-186 is decreased in aged brain and suppresses BACE 1 expression. J Neurochem. 2016;137(3):436–445.

Kim JK, Esteve PO, Jacobsen SE, Pradhan S. UHRF1 binds G9a and participates in p21 transcriptional regulation in mammalian cells. Nucleic Acids Res. 2009;37(2):493–505.

Kitamura Y, Shimohama S, Kamoshima W, Ota T, Matsuoka Y, Nomura Y, Smith MA, Perry G, Whitehouse PJ, Taniguchi T. Alteration of proteins regulating apoptosis, Bcl-2, Bcl-x, Bax, Bak, Bad, ICH-1 and CPP32, in Alzheimer's disease. Brain Res. 1998;780(2):260–269.

Kizilarslanoğlu MC, Kara Ö, Yeşil Y, Kuyumcu ME, Öztürk ZA, Cankurtaran M, Rahatli S, Pakaştiçali N, Çinar E, Halil MG, Sener B, Cankurtaran ES, Arioğul S. Alzheimer disease, inflammation, and novel inflammatory marker: resistin. Turk J Med Sci. 2015;45(5):1040–1046.

Klein B, Mrowetz H, Kreutzer C, Rotheneichner P, Zaunmair P, Lange S, Coras R, Couillard-Despres S, Rivera FJ, Aigner L. DCX+ neuronal progenitors contribute to new oligodendrocytes during remyelination in the hippocampus. Sci Rep. 2020;10(1):20095.

Klein HU, McCabe C, Gjoneska E, Sullivan SE, Kaskow BJ, Tang A, Smith R V, Xu J, Pfenning AR, Bernstein BE. Epigenome-wide study uncovers large-scale changes in histone acetylation driven by tau pathology in aging and Alzheimer's human brains. Nat Neurosci. 2019;22(1):37–46.

Knopman DS, Jones DT, Greicius MD. Failure to demonstrate efficacy of aducanumab: An analysis of the EMERGE and ENGAGE trials as reported by Biogen, December 2019. Alzheimer's & Dementia. 2021;17(4):696–701.

Kolosowska N, Gotkiewicz M, Dhungana H, Giudice L, Giugno R, Box D, Huuskonen MT, Korhonen P, Scoyni F, Kanninen KM. Intracerebral overexpression of miR-669c is protective in mouse ischemic stroke model by targeting MyD88 and inducing alternative microglial/macrophage activation. J Neuroinflammation. 2020;17(1):1–21.

Konze KD, Pattenden SG, Liu F, Barsyte-Lovejoy D, Li F, Simon JM, Davis IJ, Vedadi M, Jin J. A chemical tool for in vitro and in vivo precipitation of lysine methyltransferase G9a. ChemMedChem. 2014;9(3):549–553.

Koper MJ, Van Schoor E, Ospitalieri S, Vandenberghe R, Vandenbulcke M, von Arnim CAF, Tousseyn T, Balusu S, De Strooper B, Thal DR. Necrosome complex detected in granulovacuolar degeneration is associated with neuronal loss in Alzheimer's disease. Acta Neuropathol. 2020;139:463–484.

Krönke J, Fink EC, Hollenbach PW, MacBeth KJ, Hurst SN, Udeshi ND, Chamberlain PP, Mani DR, Man HW, Gandhi AK. Lenalidomide induces ubiquitination and degradation of CK1α in del (5q) MDS. Nature. 2015;523(7559):183–188.

Kubicek S, O'Sullivan RJ, August EM, Hickey ER, Zhang Q, Teodoro MLL, Rea S, Mechtler K, Kowalski JA, Homon CA, Kelly TA, Jenuwein T. Reversal of H3K9me2 by a Small-Molecule Inhibitor for the G9a Histone Methyltransferase. Mol Cell. 2007;25(3):473–481.

Kumar A, Tiwari A, Sharma A. Changing paradigm from one target one ligand towards multi-target directed ligand design for key drug targets of Alzheimer disease: an important role of in silico methods in multi-target directed ligands design. Curr Neuropharmacol. 2018;16(6):726–739.

Lachance V, Wang Q, Sweet E, Choi I, Cai CZ, Zhuang XX, Zhang Y, Jiang JL, Blitzer RD, Bozdagi-Gunal O. Autophagy protein NRBF2 has reduced expression in Alzheimer's brains and modulates memory and amyloid-beta homeostasis in mice. Mol Neurodegener. 2019;14(1):1–13.

Landgrave-Gómez J, Mercado-Gómez O, Guevara-Guzmán R. Epigenetic mechanisms in neurological and neurodegenerative diseases. Front Cell Neurosci. 2015;9:58.

Lang AL, Eulalio T, Fox E, Yakabi K, Bukhari SA, Kawas CH, Corrada MM, Montgomery SB, Heppner FL, Capper D. Methylation differences in Alzheimer's disease neuropathologic change in the aged human brain. Acta Neuropathol Commun. 2022;10(1):1–17.

Lattal KM, Wood MA. Epigenetics and persistent memory: implications for reconsolidation and silent extinction beyond the zero. Nat Neurosci. 2013;16(2):124–129.

Lauretti E, Dincer O, Praticò D. Glycogen synthase kinase-3 signaling in Alzheimer's disease. Biochimica et Biophysica Acta (BBA)-Molecular Cell Research. 2020;1867(5):118664.

Lawrence T, Fong C. The resolution of inflammation: anti-inflammatory roles for NF-κB. Int J Biochem Cell Biol. 2010;42(4):519–523.

Ledesma MD, Correas I, Avila J, Diaz-Nido J. Implication of brain cdc2 and MAP2 kinases in the phosphorylation of tau protein in Alzheimer's disease. FEBS Lett. 1992;308(2):218–224.

Lee B, Morano A, Porcellini A, Muller MT. GADD45α inhibition of DNMT1 dependent DNA methylation during homology directed DNA repair. Nucleic Acids Res. 2012;40(6):2481–2493.

Lee DY, Northrop JP, Kuo M-H, Stallcup MR. Histone H3 lysine 9 methyltransferase G9a is a transcriptional coactivator for nuclear receptors. Journal of Biological Chemistry. 2006;281(13):8476–8485.

Lee JS, Kim Y, Bhin J, Shin H-JR, Nam HJ, Lee SH, Yoon J-B, Binda O, Gozani O, Hwang D. Hypoxia-induced methylation of a pontin chromatin remodeling factor. Proceedings of the National Academy of Sciences. 2011;108(33):13510–13515.

Lee JS, Kim Y, Kim IS, Kim B, Choi HJ, Lee JM, Shin HJR, Kim JH, Kim JY, Seo S-B. Negative regulation of hypoxic responses via induced Reptin methylation. Mol Cell. 2010;39(1):71–85.

Lei X, Lei L, Zhang Z, Zhang Z, Cheng Y. Downregulated miR-29c correlates with increased BACE1 expression in sporadic Alzheimer's disease. Int J Clin Exp Pathol. 2015;8(2):1565.

Leroy K, Boutajangout A, Authelet M, Woodgett JR, Anderton BH, Brion JP. The active form of glycogen synthase kinase-3β is associated with granulovacuolar degeneration in neurons in Alzheimer's disease. Acta Neuropathol. 2002;103:91–99.

Leroy K, Yilmaz Z, Brion J (2007) Increased level of active GSK-3β in Alzheimer's disease and accumulation in argyrophilic grains and in neurones at different stages of neurofibrillary degeneration. Neuropathol Appl Neurobiol. 2007;33(1):43–55.

Levi-Montalcini R, Cohen S. In vitro and in vivo effects of a nerve growth-stimulating agent isolated from snake venom. Proceedings of the National Academy of Sciences. 1956;42(9):695–699.

Levinsky AJ, McEdwards G, Sethna N, Currie MA. Targets of histone H3 lysine 9 methyltransferases. Front Cell Dev Biol. 2022;10:1026406.

Li D, Guo B, Wu H, Tan L, Lu Q. TET Family of Dioxygenases: Crucial Roles and Underlying Mechanisms. Cytogenet Genome Res. 2015;146(3):171–180.

Li JG, Barrero C, Merali S, Praticò D. Five lipoxygenase hypomethylation mediates the homocysteine effect on Alzheimer's phenotype. Sci Rep. 2017;7(1):46002.

Li K, Li J, Zheng J, Qin S. Reactive astrocytes in neurodegenerative diseases. Aging Dis. 2019a;10(3):664.

Li K, Wei Q, Liu FF, Hu F, Xie A ji, Zhu LQ, Liu D. Synaptic Dysfunction in Alzheimer's Disease: Aβ, Tau, and Epigenetic Alterations. Mol Neurobiol. 2018;55(4):3021–3032.

Li L, Qiu Y, Miao M, Liu Z, Li W, Zhu Y, Wang Q. Reduction of Tet2 exacerbates early stage Alzheimer's pathology and cognitive impairments in 2× Tg-AD mice. Hum Mol Genet. 2020;29(11):1833–1852.

Li P, Marshall L, Oh G, Jakubowski JL, Groot D, He Y, Wang T, Petronis A, Labrie V. Epigenetic dysregulation of enhancers in neurons is associated with Alzheimer's disease pathology and cognitive symptoms. Nat Commun. 2019b;10(1):2246.

Li W, Li X, Xin X, Kan PC, Yan Y. MicroRNA-613 regulates the expression of brain-derived neurotrophic factor in Alzheimer's disease. Biosci Trends. 2016;10(5):372–377.

Li Y, Rinne JO, Mosconi L, Pirraglia E, Rusinek H, DeSanti S, Kemppainen N, Någren K, Kim BC, Tsui W. Regional analysis of FDG and PIB-PET images in normal aging, mild cognitive impairment, and Alzheimer's disease. Eur J Nucl Med Mol Imaging. 2008;35:2169–2181.

Li Z, Jiao X, Di Sante G, Ertel A, Casimiro MC, Wang M, Katiyar S, Ju X, Klopfenstein D V, Tozeren A. Cyclin D1 integrates G9a-mediated histone methylation. Oncogene. 2019c;38(22):4232–4249.

Lim R, Zaheer A, Khosravi H, Freeman Jr JH, Halverson HE, Wemmie JA, Yang B. Impaired motor performance and learning in glia maturation factor-knockout mice. Brain Res. 2004;1024(1–2):225–232.

Lim R, Zaheer A. In vitro enhancement of p38 mitogen-activated protein kinase activity by phosphorylated glia maturation factor. Journal of Biological Chemistry. 1996;271(38):22953–22956

Lin L, Liu A, Li H, Feng J, Yan Z. Inhibition of histone methyltransferases EHMT1/2 reverses amyloid-β-induced loss of AMPAR currents in human stem cell-derived cortical neurons. Journal of Alzheimer's Disease. 2019;70(4):1175–1185.

Lin YC, Koleske AJ. Mechanisms of synapse and dendrite maintenance and their disruption in psychiatric and neurodegenerative disorders. Annu Rev Neurosci. 2010;33:349–378.

Ling BMT, Bharathy N, Chung TK, Kok WK, Li S, Tan YH, Rao VK, Gopinadhan S, Sartorelli V, Walsh MJ. Lysine methyltransferase G9a methylates the transcription factor MyoD and regulates skeletal muscle differentiation. Proceedings of the National Academy of Sciences. 2012;109(3):841–846.

Link CD. Expression of human beta-amyloid peptide in transgenic Caenorhabditis elegans. Proceedings of the National Academy of Sciences. 1995;92(20):9368–9372.

Link CD. Invertebrate models of Alzheimer's disease. Genes Brain Behav. 2005;4(3):147–156.

Lithner CU, Lacor PN, Zhao WQ, Mustafiz T, Klein WL, Sweatt JD, Hernandez CM. Disruption of neocortical histone H3 homeostasis by soluble Aβ: Implications for Alzheimer's disease. Neurobiol Aging. 2013;34(9):2081–2090.

Liu B, Liu J, Shi JS. SAMP8 mice as a model of age-related cognition decline with underlying mechanisms in Alzheimer's disease. Journal of Alzheimer's Disease. 2020;75(2):385–395.

Liu CG, Wang JL, Li LEI, Wang PC. MicroRNA-384 regulates both amyloid precursor protein and β-secretase expression and is a potential biomarker for Alzheimer's disease. Int J Mol Med. 2014;34(1):160–166.

Liu F, Barsyte-Lovejoy D, Allali-Hassani A, He Y, Herold JM, Chen X, Yates CM, Frye S V., Brown PJ, Huang J, Vedadi M, Arrowsmith CH, Jin J. Optimization of cellular

activity of G9a inhibitors 7-aminoalkoxy- quinazolines. J Med Chem. 2011;54(17):6139–6150.

Liu F, Barsyte-Lovejoy D, Li F, Xiong Y, Korboukh V, Huang XP, Allali-Hassani A, Janzen WP, Roth BL, Frye S V., Arrowsmith CH, Brown PJ, Vedadi M, Jin J. Discovery of an in vivo chemical probe of the lysine methyltransferases G9a and GLP. J Med Chem. 2013;56(21):8931–8942.

Liu F, Chen X, Allali-Hassani A, Quinn AM, Wasney GA, Dong A, Barsyte D, Kozieradzki I, Senisterra G, Chau I, Siarheyeva A, Kireev DB, Jadhav A, Herold JM, Frye SV, Arrowsmith CH, Brown PJ, Simeonov A, Vedadi M, Jin J. Discovery of a 2,4-diamino-7-aminoalkoxyquinazoline as a potent and selective inhibitor of histone lysine methyltransferase G9a. J Med Chem. 2009a;52(24):7950–7953.

Liu F, Chen X, Allali-Hassani A, Quinn AM, Wasney GA, Dong A, Barsyte D, Kozieradzki I, Senisterra G, Chau I, Siarheyeva A, Kireev DB, Jadhav A, Herold JM, Frye SV, Arrowsmith CH, Brown PJ, Simeonov A, Vedadi M, Jin J. Discovery of a 2,4-diamino-7-aminoalkoxyquinazoline as a potent and selective inhibitor of histone lysine methyltransferase G9a. J Med Chem. 2009b;52(24):7950–7953.

Liu F, Chen X, Allali-Hassani A, Quinn AM, Wigle TJ, Wasney GA, Dong A, Senisterra G, Chau I, Siarheyeva A, Norris JL, Kireev DB, Jadhav A, Herold JM, Janzen WP, Arrowsmith CH, Frye SV, Brown PJ, Simeonov A, Vedadi M, Jin J. Protein lysine methyltransferase g9a inhibitors: Design, synthesis, and structure activity relationships of 2,4-diamino-7-aminoalkoxy-quinazolines. J Med Chem 2010;53(15):5844–5857.

Liu F, Liang Z, Wegiel J, Hwang Y-W, Iqbal K, Grundke-Iqbal I, Ramakrishna N, Gong C-X. Overexpression of Dyrk1A contributes to neurofibrillary degeneration in Down syndrome. The FASEB Journal. 2008;22(9):3224.

Liu R, Wu J, Guo H, Yao W, Li S, Lu Y, Jia Y, Liang X, Tang J, Zhang H. Post-translational modifications of histones: Mechanisms, biological functions, and therapeutic targets. MedComm. 2023;4(3):e292.

Liu W, Liu C, Zhu J, Shu P, Yin B, Gong Y, Qiang B, Yuan J, Peng X. MicroRNA-16 targets amyloid precursor protein to potentially modulate Alzheimer's-associated pathogenesis in SAMP8 mice. Neurobiol Aging. 2012;33(3):522–534.

Liu Y, Zhang Y, Liu P, Bai H, Li X, Xiao J, Yuan Q, Geng S, Yin H, Zhang H. MicroRNA-128 knockout inhibits the development of Alzheimer's disease by targeting PPARγ in mouse models. Eur J Pharmacol. 2019;843:134–144.

Llorens-Marítin M, Jurado J, Hernández F, Ávila J. GSK-3β, a pivotal kinase in Alzheimer disease. Front Mol Neurosci 2014;7:46.

Long JM, Holtzman DM. Alzheimer disease: an update on pathobiology and treatment strategies. Cell. 2019;179(2):312–339.

Long JM, Lahiri DK. MicroRNA-101 downregulates Alzheimer's amyloid-β precursor protein levels in human cell cultures and is differentially expressed. Biochem Biophys Res Commun. 2011;404(4):889–895.

Long JM, Maloney B, Rogers JT, Lahiri DK. Novel upregulation of amyloid-β precursor protein (APP) by microRNA-346 via targeting of APP mRNA 5′-untranslated region: Implications in Alzheimer's disease. Mol Psychiatry. 2019;24(3):345–363.

Long JM, Ray B, Lahiri DK. MicroRNA-339-5p down-regulates protein expression of β-site amyloid precursor protein-cleaving enzyme 1 (BACE1) in human primary brain cultures and is reduced in brain tissue specimens of Alzheimer disease subjects. Journal of Biological Chemistry. 2014;289(8):5184–5198.

López-Otín C, Blasco MA, Partridge L, Serrano M, Kroemer G, López-Otín C, Blasco MA, Kroemer G, Partridge L, Serrano M, Kroemer G. The hallmarks of aging. Cell. 2013;153(6):1194.

López-Otín C, Blasco MA, Partridge L, Serrano M, Kroemer G. Hallmarks of aging: An expanding universe. Cell. 2023;186(2):243–278.

Lovestone S, Boada M, Dubois B, Hüll M, Rinne JO, Huppertz HJ, Calero M, Andrés M V, Gómez-Carrillo B, León T. A phase II trial of tideglusib in Alzheimer's disease. Journal of Alzheimer's Disease. 2015;45(1):75–88.

Lovestone S, Reynolds CH, Latimer D, Davis DR, Anderton BH, Gallo JM, Hanger D, Mulot S, Marquardt B, Stabel S. Alzheimer's disease-like phosphorylation of the microtubule-associated protein tau by glycogen synthase kinase-3 in transfected mammalian cells. Current Biology. 1994;4(12):1077–1086.

Lu B, Nagappan G, Guan X, Nathan PJ, Wren P. BDNF-based synaptic repair as a disease-modifying strategy for neurodegenerative diseases. Nat Rev Neurosci. 2013;14(6):401–416

Lu DC, Soriano S, Bredesen DE, Koo EH. Caspase cleavage of the amyloid precursor protein modulates amyloid β-protein toxicity. J Neurochem. 2003;87(3):733–741.

Lu Y, Christian K, Lu B. BDNF: a key regulator for protein synthesis-dependent LTP and long-term memory? Neurobiol Learn Mem. 2008;89(3):312–323.

Lucin KM, O'Brien CE, Bieri G, Czirr E, Mosher KI, Abbey RJ, Mastroeni DF, Rogers J, Spencer B, Masliah E. Microglial beclin 1 regulates retromer trafficking and phagocytosis and is impaired in Alzheimer's disease. Neuron. 2013;79(5):873–886.

Lucin KM, Wyss-Coray T. Targeting autophagy for disease therapy. Nat Biotechnol. 2013;31(4):322–323

Ma A, Yu W, Li F, Bleich RM, Herold JM, Butler K V., Norris JL, Korboukh V, Tripathy A, Janzen WP, Arrowsmith CH, Frye S V., Vedadi M, Brown PJ, Jin J. Discovery of a selective, substrate-competitive inhibitor of the lysine methyltransferase SETD8. J Med Chem. 2014;57(15):6822–6833.

MacBean LF, Smith AR, Lunnon K. Exploring beyond the DNA sequence: a review of epigenomic studies of DNA and histone modifications in dementia. Curr Genet Med Rep. 2020;8:79–92.

Maes OC, An J, Sarojini H, Wang E. Murine microRNAs implicated in liver functions and aging process. Mech Ageing Dev. 2008;129(9):534–541.

Maheshwari D, Shukla VK, Jain A, Tripathi S, Kumar D, Arora A. Solution structure and dynamics of glia maturation factor from Caenorhabditis elegans. Biochimica et Biophysica Acta (BBA)-Proteins and Proteomics. 2018;1866(10):1008–1020.

Maisonpierre PC, Belluscio L, Squinto S, Ip NY, Furth ME, Lindsay RM, Yancopoulos GD. Neurotrophin-3: a neurotrophic factor related to NGF and BDNF. Science. 1990;247(4949):1446–1451.

Marksteiner J, Kaufmann WA, Gurka P, Humpel C. Synaptic proteins in Alzheimer's disease. Journal of Molecular Neuroscience. 2002;18:53–63.

Marzi SJ, Leung SK, Ribarska T, Hannon E, Smith AR, Pishva E, Poschmann J, Moore K, Troakes C, Al-Sarraj S. A histone acetylome-wide association study of Alzheimer's

disease identifies disease-associated H3K27ac differences in the entorhinal cortex. Nat Neurosci. 2018;21(11):1618–1627.

Masliah E, Crews L, Hansen L. Synaptic remodeling during aging and in Alzheimer's disease. Journal of Alzheimer's disease. 2006;9(s3):91–99.

Massone S, Vassallo I, Fiorino G, Castelnuovo M, Barbieri F, Borghi R, Tabaton M, Robello M, Gatta E, Russo C. 17A, a novel non-coding RNA, regulates GABA B alternative splicing and signaling in response to inflammatory stimuli and in Alzheimer disease. Neurobiol Dis. 2011;41(2):308–317.

Mauger O, Klinck R, Chabot B, Muchardt C, Allemand E, Batsché E. Alternative splicing regulates the expression of G9A and SUV39H2 methyltransferases, and dramatically changes SUV39H2 functions. Nucleic Acids Res. 2015;43(3):1869–1882.

Maze I, Covington III HE, Dietz DM, Laplant Q, Renthal W, Russo SJ, Mechanic M, Mouzon E, Neve RL, Stephen J, Ren Y, Sampath SC, Hurd YL, Greengard P, Tarakhovsky A, Schaefer A, Nestler EJ. Essential Role of the Histone Methyltransferase G9a in Cocaine-induced Plasticity. Science. 2010;327(5962):213–217.

McQuown SC, Barrett RM, Matheos DP, Post RJ, Rogge GA, Alenghat T, Mullican SE, Jones S, Rusche JR, Lazar MA. HDAC3 is a critical negative regulator of long-term memory formation. Journal of Neuroscience. 2011;31(2):764–774.

Medendorp WE, Petersen ED, Pal A, Wagner L-M, Myers AR, Hochgeschwender U, Jenrow KA. Altered behavior in mice socially isolated during adolescence corresponds with immature dendritic spine morphology and impaired plasticity in the prefrontal cortex. Front Behav Neurosci. 2018;12:87.

Medina M, Avila J. New insights into the role of glycogen synthase kinase-3 in Alzheimer's disease. Expert Opin Ther Targets. 2014;18(1):69–77.

Meeker HC, Chadman KK, Heaney AT, Carp RI. Assessment of social interaction and anxiety-like behavior in senescence-accelerated-prone and-resistant mice. Physiol Behav. 2013;118:97–102.

Mellén M, Ayata P, Dewell S, Kriaucionis S, Heintz N. MeCP2 binds to 5hmC enriched within active genes and accessible chromatin in the nervous system. Cell. 2012;151(7):1417–1430.

Micheau O, Tschopp J. Induction of TNF receptor I-mediated apoptosis via two sequential signaling complexes. Cell. 003;114(2):181–190.

Migliore L, Coppedè F. Gene–environment interactions in Alzheimer disease: the emerging role of epigenetics. Nat Rev Neurol. 2022;18(11):643–660.

Milà-Alomà M, Ashton NJ, Shekari M, Salvadó G, Ortiz-Romero P, Montoliu-Gaya L, Benedet AL, Karikari TK, Lantero-Rodriguez J, Vanmechelen E, Day TA, González-Escalante A, Sánchez-Benavides G, Minguillon C, Fauria K, Molinuevo JL, Dage JL, Zetterberg H, Gispert JD, Suárez-Calvet M, Blennow K. Plasma p-tau231 and p-tau217 as state markers of amyloid-β pathology in preclinical Alzheimer's disease. Nat Med. 2022;28(9):1797–1801

Milite C, Feoli A, Horton JR, Rescigno D, Cipriano A, Pisapia V, Viviano M, Pepe G, Amendola G, Novellino E, Cosconati S, Cheng X, Castellano S, Sbardella G. Discovery of a Novel Chemotype of Histone Lysine Methyltransferase EHMT1/2 (GLP/G9a) Inhibitors: Rational Design, Synthesis, Biological Evaluation, and Co-crystal Structure. J Med Chem. 2019;62(5):2666–2689.

Millán-Zambrano G, Burton A, Bannister AJ, Schneider R (2022) Histone post-translational modifications—cause and consequence of genome function. Nat Rev Genet. 2022;23(9):563–580.

Millar AH, Heazlewood JL, Giglione C, Holdsworth MJ, Bachmair A, Schulze WX. The scope, functions, and dynamics of posttranslational protein modifications. Annu Rev Plant Biol. 2019;70:119–151.

Milner CM, Campbell RD. The G9a gene in the human major histocompatibility complex encodes a novel protein containing ankyrin-like repeats. Biochemical Journal. 1993;290(3):811–818.

Minatohara K, Akiyoshi M, Okuno H. Role of immediate-early genes in synaptic plasticity and neuronal ensembles underlying the memory trace. Front Mol Neurosci. 2016;8:78.

Mishra A, Kim HJ, Shin AH, Thayer SA. Synapse loss induced by interleukin-1β requires pre-and post-synaptic mechanisms. Journal of neuroimmune pharmacology. 2012;7:571–578.

Miyamoto M. Emotional disorders and memory deficits in senescence-accelerated mice, SAMP8 and SAMP10. In: International Congress Series, Elsevier; 2004; pp. 99–106.

Modarresi F, Faghihi MA, Patel NS, Sahagan BG, Wahlestedt C, Lopez-Toledano MA. Knockdown of BACE1-AS nonprotein-coding transcript modulates beta-amyloid-related hippocampal neurogenesis. Int J Alzheimers Dis. 2011;2011:929042.

Mohs RC, Greig NH. Drug discovery and development: Role of basic biological research. Alzheimer's & Dementia: Translational Research & Clinical Interventions. 2017;3(4):651–657.

Monti N, Cavallaro RA, Stoccoro A, Nicolia V, Scarpa S, Kovacs GG, Fiorenza MT, Lucarelli M, Aronica E, Ferrer I. CpG and non-CpG Presenilin1 methylation pattern in course of neurodevelopment and neurodegeneration is associated with gene expression in human and murine brain. Epigenetics. 2020;15(8):781–799.

Moore LL, Morrison M, Roth MB. HCP-1, a protein involved in chromosome segregation, is localized to the centromere of mitotic chromosomes in Caenorhabditis elegans. J Cell Biol. 1999;147(3):471–480.

Morley JE. The SAMP8 mouse: a model of Alzheimer disease? Biogerontology. 2002;3:57–60.

Moujalled D, Strasser A, Liddell JR. Molecular mechanisms of cell death in neurological diseases. Cell Death Differ. 2021;28(7):2029–2044.

Mozzetta C, Pontis J, Fritsch L, Robin P, Portoso M, Proux C, Margueron R, Ait-Si-Ali S. The histone H3 lysine 9 methyltransferases G9a and GLP regulate polycomb repressive complex 2-mediated gene silencing. Mol Cell. 2014;53(2):277–289.

Mulligan P, Westbrook TF, Ottinger M, Pavlova N, Chang B, Macia E, Shi Y-J, Barretina J, Liu J, Howley PM (2008) CDYL bridges REST and histone methyltransferases for gene repression and suppression of cellular transformation. Mol Cell 32:718–726.

Murshid NM, Lubis FA, Makpol S. Epigenetic Changes and Its Intervention in Age-Related Neurodegenerative Diseases. Cell Mol Neurobiol. 2022;42(3):577-595.

Mus E, Hof PR, Tiedge H. Dendritic BC200 RNA in aging and in Alzheimer's disease. Proceedings of the National Academy of Sciences. 2007;104(25):10679–10684.

Myung NH, Zhu X, Kruman II, Castellani RJ, Petersen RB, Siedlak SL, Perry G, Smith MA, Lee H. Evidence of DNA damage in Alzheimer disease: phosphorylation of histone H2AX in astrocytes. Age (Omaha). 2008;30:209–215.

Nabi M, Tabassum N. Role of environmental toxicants on neurodegenerative disorders. Frontiers in toxicology. 2022;4:837579.

Nagano T, Mitchell JA, Sanz LA, Pauler FM, Ferguson-Smith AC, Feil R, Fraser P. The Air noncoding RNA epigenetically silences transcription by targeting G9a to chromatin. Science. 2008;322(5908):1717–1720.

Nagata T, Kobayashi N, Ishii J, Shinagawa S, Nakayama R, Shibata N, Kuerban B, Ohnuma T, Kondo K, Arai H. Association between DNA methylation of the BDNF promoter region and clinical presentation in Alzheimer's disease. Dement Geriatr Cogn Dis Extra. 2015;5(1):64–73.

Naik RS, Hartmann J, Kiewert C, Duysen EG, Lockridge O, Klein J. Effects of rivastigmine and donepezil on brain acetylcholine levels in acetylcholinesterase-deficient mice. Journal of Pharmacy & Pharmaceutical Sciences. 2009;12(1):79-85.

Namzaric (memantine hydrochloride extended-release/donepezil hydrochloride) capsules. US Food and Drug Administration. 2014 [cited 2024 Jan 7]. Available from: https://www.accessdata.fda.gov/drugsatfda_docs/nda/2014/206439Orig1s000TOC.cfm

Narlikar GJ, Sundaramoorthy R, Owen-Hughes T. Mechanisms and functions of ATP-dependent chromatin-remodeling enzymes. Cell. 2013;154(3):490–503.

Nativio R, Lan Y, Donahue G, Sidoli S, Berson A, Srinivasan AR, Shcherbakova O, Amlie-Wolf A, Nie J, Cui X. An integrated multi-omics approach identifies epigenetic alterations associated with Alzheimer's disease. Nat Genet. 2020;52(10):1024–1035.

Nelson TJ, Xu Y. Sting and p53 DNA repair pathways are compromised in Alzheimer's disease. Sci Rep. 2023;13(1):8304.

Nishida M, Kato M, Kato Y, Sasai N, Ueda J, Tachibana M, Shinkai Y, Yamaguchi M. Identification of ZNF200 as a novel binding partner of histone H3 methyltransferase G9a. Genes to Cells. 2007;12(7):877–888.

Nishigaya Y, Takase S, Sumiya T, Kikuzato K, Sato T, Niwa H, Sato S, Nakata A, Sonoda T, Hashimoto N, Namie R, Honma T, Umehara T, Shirouzu M, Koyama H, Yoshida M, Ito A, Shirai F. Discovery of Novel Substrate-Competitive Lysine Methyltransferase G9a Inhibitors as Anticancer Agents. J Med Chem. 2023;66(6):4059-4085.

Nishio H, Walsh MJ. CCAAT displacement protein/cut homolog recruits G9a histone lysine methyltransferase to repress transcription. Proceedings of the National Academy of Sciences. 2004;101(31):11257–11262.

Nixon RA. The role of autophagy in neurodegenerative disease. Nat Med. 2013;19(8):983–997.

Norrholm SD, Ouimet CC. Altered dendritic spine density in animal models of depression and in response to antidepressant treatment. Synapse. 2001;42(3):151–163.

O'Brien RJ, Wong PC. Amyloid precursor protein processing and Alzheimer's disease. Annu Rev Neurosci. 2011;34:185–204.

Obulesu M, Lakshmi MJ. Apoptosis in Alzheimer's disease: an understanding of the physiology, pathology and therapeutic avenues. Neurochem Res. 2014;39:2301–2312.

Oh ST, Kim K-B, Chae YC, Kang JY, Hahn Y, Seo SB. H3K9 histone methyltransferase G9a-mediated transcriptional activation of p21. FEBS Lett. 2014;588(5):685–691.

Olsen A, Vantipalli MC, Lithgow GJ. Using Caenorhabditis elegans as a model for aging and age-related diseases. Ann N Y Acad Sci. 2006;1067(1):120–128.

Ossenkoppele R, van der Kant R, Hansson O. Tau biomarkers in Alzheimer's disease: towards implementation in clinical practice and trials. Lancet Neurol. 2022;21(8):726–734.

Overk CR, Masliah E. Pathogenesis of synaptic degeneration in Alzheimer's disease and Lewy body disease. Biochem Pharmacol. 2014;88(4):508–516.

Ownby RL, Crocco E, Acevedo A, John V, Loewenstein D. Depression and risk for Alzheimer disease: systematic review, meta-analysis, and metaregression analysis. Arch Gen Psychiatry. 2006;63(5):530–538.

Ozaki Y, Yoshino Y, Yamazaki K, Sao T, Mori Y, Ochi S, Yoshida T, Mori T, Iga J, Ueno S. DNA methylation changes at TREM2 intron 1 and TREM2 mRNA expression in patients with Alzheimer's disease. J Psychiatr Res. 2017;92:74–80..

Pačesová A, Holubová M, Hrubá L, Strnadová V, Neprašová B, Pelantová H, Kuzma M, Železná B, Kuneš J, Maletínská L. Age-related metabolic and neurodegenerative changes in SAMP8 mice. Aging (Albany NY). 2022;14(18):7300.

Padeken J, Methot SP, Gasser SM. Establishment of H3K9-methylated heterochromatin and its functions in tissue differentiation and maintenance. Nat Rev Mol Cell Biol. 2022;23(9):623–640.

Padilla PA, Garcia AM, Ladage ML, Toni LS. Caenorhabditis elegans: an old genetic model can learn new epigenetic tricks. Integr Comp Biol. 2014;54(1):52–60.

Pal S, Tyler JK. Epigenetics and aging. Sci Adv. 2016;2(7):e1600584.

Pallas M, Camins A, Smith MA, Perry G, Lee H, Casadesus G. From aging to Alzheimer's disease: unveiling "the switch" with the senescence-accelerated mouse model (SAMP8). Journal of Alzheimer's Disease. 2008;15(4):615–624.

Pallàs M. Senescence-Accelerated Mice P8: A Tool to Study Brain Aging and Alzheimer's Disease in a Mouse Model. ISRN Cell Biol. 2012;2012:917167.

Pan MRR, Hsu MCC, Chen LTT, Hung WCC. Orchestration of H3K27 methylation: mechanisms and therapeutic implication. Cellular and molecular life sciences. 2018;75(2):209–223.

Pang KKL, Sharma M, Sajikumar S. Epigenetics and memory: Emerging role of histone lysine methyltransferase G9a/GLP complex as bidirectional regulator of synaptic plasticity. Neurobiol Learn Mem. 2019;159:1–5.

Pao PC, Patnaik D, Watson LA, Gao F, Pan L, Wang J, Adaikkan C, Penney J, Cam HP, Huang WC. HDAC1 modulates OGG1-initiated oxidative DNA damage repair in the aging brain and Alzheimer's disease. Nat Commun. 2020;11(1):2484.

Park G, Nhan HS, Tyan SH, Kawakatsu Y, Zhang C, Navarro M, Koo EH. Caspase activation and caspase-mediated cleavage of APP is associated with amyloid β-protein-induced synapse loss in Alzheimer's disease. Cell Rep. 2020;31(13).

Park J, Lee K, Kim K, Yi SJ. The role of histone modifications: From neurodevelopment to neurodiseases. Signal Transduct Target Ther. 2022;7(1):217.

Park SE, Yi HJ, Suh N, Park Y-Y, Koh JY, Jeong SY, Cho DH, Kim CS, Hwang JJ. Inhibition of EHMT2/G9a epigenetically increases the transcription of Beclin-1 via an increase in ROS and activation of NF-κB. Oncotarget. 2016;7(26):39796.

Patel MR, Weaver AM. Astrocyte-derived small extracellular vesicles promote synapse formation via fibulin-2-mediated TGF-β signaling. Cell Rep. 2021;34(10):108829.

Paweletz N. Walther Flemming: pioneer of mitosis research. Nat Rev Mol Cell Biol. 2001;2(1):72–75.

Pei JJ, Braak E, Braak H, Grundke-Iqbal I, Iqbal K, Winblad B, Cowburn RF. Distribution of active glycogen synthase kinase 3β (GSK-3β) in brains staged for Alzheimer disease neurofibrillary changes. J Neuropathol Exp Neurol. 1999;58(9):1010–1019.

Pei JJ, Braak E, Braak H, Grundke-Iqbal I, Iqbal K, Winblad B, Cowburn RF. Localization of active forms of C-jun kinase (JNK) and p38 kinase in Alzheimer's disease brains at different stages of neurofibrillary degeneration. Journal of Alzheimer's Disease. 2001;3(1):41–48.

Peng S, Garzon DJ, Marchese M, Klein W, Ginsberg SD, Francis BM, Mount HTJ, Mufson EJ, Salehi A, Fahnestock M. Decreased brain-derived neurotrophic factor depends on amyloid aggregation state in transgenic mouse models of Alzheimer's disease. Journal of Neuroscience. 2009;29(29):9321–9329.

Peng Y, Croce CM. The role of microRNAs in human cancer. Signal Transduct Target Ther 1. 2016;1:1500.

Pickford F, Masliah E, Britschgi M, Lucin K, Narasimhan R, Jaeger PA, Small S, Spencer B, Rockenstein E, Levine B. The autophagy-related protein beclin 1 shows reduced expression in early Alzheimer disease and regulates amyloid β accumulation in mice. J Clin Invest. 2008;118(6):2190–2199.

Pless O, Kowenz-Leutz E, Knoblich M, Lausen J, Beyermann M, Walsh MJ, Leutz A. G9a-mediated lysine methylation alters the function of CCAAT/enhancer-binding protein-β. Journal of Biological Chemistry. 2008;283(39):26357–26363.

Poewe W, Seppi K, Tanner CM, Halliday GM, Brundin P, Volkmann J, Schrag AE, Lang AE Parkinson disease Nat Rev Dis Primers. 2017;3:17013.

Polvani S, Tarocchi M, Galli A. PPARγ and oxidative stress: Con (β) catenating NRF2 and FOXO. PPAR Res. 2012;2012:641087.

Poulard C, Bittencourt D, Wu D, Hu Y, Gerke DS, Stallcup MR. A post-translational modification switch controls coactivator function of histone methyltransferases G9a and GLP. EMBO Rep. 2017;18(8):1442–1459.

Poulard C, Kim HN, Fang M, Kruth K, Gagnieux C, Gerke DS, Bhojwani D, Kim Y-M, Kampmann M, Stallcup MR. Relapse-associated AURKB blunts the glucocorticoid sensitivity of B cell acute lymphoblastic leukemia. Proceedings of the National Academy of Sciences. 2019;116(8):3052–3061.

Poulard C, Noureddine LM, Pruvost L, Le Romancer M. Structure, Activity, and Function of the Protein Lysine Methyltransferase G9a. Life. 2021;11(10):1082.

Price JL, McKeel Jr DW, Buckles VD, Roe CM, Xiong C, Grundman M, Hansen LA, Petersen RC, Parisi JE, Dickson DW. Neuropathology of nondemented aging: presumptive evidence for preclinical Alzheimer disease. Neurobiol Aging. 2009;30(7):1026–1036.

Purcell DJ, Jeong KW, Bittencourt D, Gerke DS, Stallcup MR. A distinct mechanism for coactivator versus corepressor function by histone methyltransferase G9a in transcriptional regulation. Journal of Biological Chemistry. 2011;286(49):41963–41971.

Purcell DJ, Khalid O, Ou C, Little GH, Frenkel B, Baniwal SK, Stallcup MR. Recruitment of coregulator G9a by Runx2 for selective enhancement or suppression of transcription. J Cell Biochem. 2012;113(7):2406–2414.

Pushpakom S, Iorio F, Eyers PA, Escott KJ, Hopper S, Wells A, Doig A, Guilliams T, Latimer J, McNamee C. Drug repurposing: progress, challenges and recommendations. Nat Rev Drug Discov. 2019;18(1):41–58.

Qazi TJ, Quan Z, Mir A, Qing H. Epigenetics in Alzheimer's disease: perspective of DNA methylation. Mol Neurobiol. 2018;55:1026–1044.

Qian C, Zhou MM. SET domain protein lysine methyltransferases: Structure, specificity and catalysis. Cell Mol Life Sci. 2006;63:2755–2763.

Rabal O, San José-Enériz E, Agirre X, Sánchez-Arias JA, De Miguel I, Ordoñez R, Garate L, Miranda E, Saéz E, Vilas-Zornoza A, Pineda-Lucena A, Estella A, Zhang F, Wu W, Xu M, Prosper F, Oyarzabal J. Design and Synthesis of Novel Epigenetic Inhibitors Targeting Histone Deacetylases, DNA Methyltransferase 1, and Lysine Methyltransferase G9a with in Vivo Efficacy in Multiple Myeloma. J Med Chem. 2021;64(6):3392–3426.

Rabal O, Sánchez-Arias JA, José-Enériz ES, Agirre X, De Miguel I, Garate L, Miranda E, Sáez E, Roa S, Martínez-Climent JA, Liu Y, Wu W, Xu M, Prosper F, Oyarzabal J. Detailed Exploration around 4-Aminoquinolines Chemical Space to Navigate the Lysine Methyltransferase G9a and DNA Methyltransferase Biological Spaces. J Med Chem. 2018;61(15):6546–6573.

Radi E, Formichi P, Battisti C, Federico A. Apoptosis and oxidative stress in neurodegenerative diseases. Journal of Alzheimer's disease. 2014;42(s3):S125–S152

Radley JJ, Rocher AB, Rodriguez A, Ehlenberger DB, Dammann M, McEwen BS, Morrison JH, Wearne SL, Hof PR. Repeated stress alters dendritic spine morphology in the rat medial prefrontal cortex. Journal of Comparative Neurology. 2008;507(1):1141–1150.

Rahman Z, Bazaz MR, Devabattula G, Khan MA, Godugu C. Targeting H3K9 methyltransferase G9a and its related molecule GLP as a potential therapeutic strategy for cancer. J Biochem Mol Toxicol. 2021;35(3):e22674.

Ramazi S, Allahverdi A, Zahiri J. Evaluation of post-translational modifications in histone proteins: A review on histone modification defects in developmental and neurological disorders. J Biosci. 2020;45:1–29.

Ramya Chandar Charles M, Hsieh HP, Selvaraj Coumar M. Delineating the active site architecture of G9a lysine methyltransferase through substrate and inhibitor binding mode analysis: a molecular dynamics study. J Biomol Struct Dyn. 2019;37(10):2581-2592

Ranganathan K, Sivasankar V. MicroRNAs-Biology and clinical applications. J Oral Maxillofac Pathol. 2014;18(2):229.

Rao JS, Keleshian VL, Klein S, Rapoport SI. Epigenetic modifications in frontal cortex from Alzheimer's disease and bipolar disorder patients. Transl Psychiatry. 2012;2(7):e132.

Rapoport M, Dawson HN, Binder LI, Vitek MP, Ferreira A. Tau is essential to β-amyloid-induced neurotoxicity. Proceedings of the National Academy of Sciences. 2002;99(9):6364–6369.

Rathore AS, Birla H, Singh S Sen, Zahra W, Dilnashin H, Singh R, Keshri PK, Singh SP. Epigenetic modulation in Parkinson's disease and potential treatment therapies. Neurochem Res. 2021;46(7):1618–1626.

Ravanelli F, Musazzi L, Barbieri SS, Rovati G, Popoli M, Barbon A, Ieraci A. Differential Epigenetic Changes in the Dorsal Hippocampus of Male and Female SAMP8 Mice: A Preliminary Study. Int J Mol Sci. 2023;24(17):13084.

Rea S, Eisenhaber F, O'Carroll D, Strahl BD, Sun ZW, Schmid M, Opravil S, Mechtier K, Ponting CP, Allis CD, Jenuwein T. Regulation of chromatin structure by site-specific histone H3 methyltransferases. Nature. 2000;406(6796):593–599.

Reisberg B, Doody R, Stöffler A, Schmitt F, Ferris S, Möbius HJ. Memantine in moderate-to-severe Alzheimer's disease. New England Journal of Medicine. 2003;348(14):1333–1341.

Reitz C, Rogaeva E, Beecham GW. Late-onset vs nonmendelian early-onset Alzheimer disease: A distinction without a difference? Neurol Genet. 2020;6(5):e512.

Reynolds CH, Betts JC, Blackstock WP, Nebreda AR, Anderton BH. Phosphorylation sites on tau identified by nanoelectrospray mass spectrometry: differences in vitro between the mitogen-activated protein kinases ERK2, c-Jun N-terminal kinase and P38, and glycogen synthase kinase-3β. J Neurochem. 2000;74(4):1587-95.

Ricobaraza A, Cuadrado-Tejedor M, Pérez-Mediavilla A, Frechilla D, Del Río J, García-Osta A. Phenylbutyrate ameliorates cognitive deficit and reduces tau pathology in an Alzheimer's disease mouse model. Neuropsychopharmacology. 2009;34(7):1721–1732.

Rodrigues SM, Schafe GE, LeDoux JE. Molecular mechanisms underlying emotional learning and memory in the lateral amygdala. Neuron. 2004;44(1):75–91.

Rogaev E. Familial Alzheimer's disease in kindreds with missense mutation in a gene on chromosome 1 related to the Alzheimer's disease type 3 gene. Nature. 1995;376:600–602.

Roopra A, Qazi R, Schoenike B, Daley TJ, Morrison JF. Localized domains of G9a-mediated histone methylation are required for silencing of neuronal genes. Mol Cell. 2004;14(6):727–738.

Roos WP, Kaina B. DNA damage-induced cell death by apoptosis. Trends Mol Med. 2006;12(9):440–450.

Rose MR. Adaptation, aging, and genomic information. Aging (Albany NY). 2009;1(5):444.

Rossi D, Volterra A. Astrocytic dysfunction: insights on the role in neurodegeneration. Brain Res Bull. 2009;80(4–5):224–232.

Rothammer N, Woo MS, Bauer S, Binkle-Ladisch L, Di Liberto G, Egervari K, Wagner I, Haferkamp U, Pless O, Merkler D. G9a dictates neuronal vulnerability to inflammatory stress via transcriptional control of ferroptosis. Sci Adv. 2022;8(31):eabm5500.

Roy J, Sarkar A, Parida S, Ghosh Z, Mallick B. Small RNA sequencing revealed dysregulated piRNAs in Alzheimer's disease and their probable role in pathogenesis. Mol Biosyst. 2017;13(3):565–576.

Runge K, Cardoso C, De Chevigny A. Dendritic spine plasticity: function and mechanisms. Front Synaptic Neurosci. 2020;12:36.

Salminen A, Kaarniranta K, Haapasalo A, Hiltunen M, Soininen H, Alafuzoff I. Emerging role of p62/sequestosome-1 in the pathogenesis of Alzheimer's disease. Prog Neurobiol. 2012;96(1):87–95.

Sanchez-Mut J V, Gräff J. Epigenetic Alterations in Alzheimer's Disease. Front Behav Neurosci. 2015;9:347.

Santa-Maria I, Alaniz ME, Renwick N, Cela C, Fulga TA, Van Vactor D, Tuschl T, Clark LN, Shelanski ML, McCabe BD. Dysregulation of microRNA-219 promotes neurodegeneration through post-transcriptional regulation of tau. J Clin Invest. 2015;125(2):681–686.

Santacruz K, Lewis J, Spires T, Paulson J, Kotilinek L, Ingelsson M, Guimaraes A, DeTure M, Ramsden M, McGowan E. Tau suppression in a neurodegenerative mouse model improves memory function. Science. 2005;309(5733):476–481

Santana DA, Smith M de AC, Chen ES. Histone modifications in alzheimer's disease. Genes (Basel). 2023;14(2):347.

Santos M, Coelho PA, Maciel P. Chromatin remodeling and neuronal function: exciting links. Genes Brain Behav. 2006;5:80–91.

Santosh B, Varshney A, Yadava PK. Non-coding RNAs: biological functions and applications. Cell Biochem Funct. 2015;33(1):14–22.

Schapira M. Suppl 1: Structural Chemistry of Human SET Domain Protein Methyltransferases. Curr Chem Genomics. 2011;5:85.

Scheff SW, Neltner JH, Nelson PT. Is synaptic loss a unique hallmark of Alzheimer's disease? Biochem Pharmacol. 2014;88(4):517–528.

Scheff SW, Price DA, Schmitt FA, DeKosky ST, Mufson EJ. Synaptic alterations in CA1 in mild Alzheimer disease and mild cognitive impairment. Neurology. 2007;68(18):1501–1508.

Scheff SW, Price DA, Schmitt FA, Mufson EJ. Hippocampal synaptic loss in early Alzheimer's disease and mild cognitive impairment. Neurobiol Aging. 2006;27(10):1372–1384.

Scheff SW, Price DA, Schmitt FA, Scheff MA, Mufson EJ. Synaptic loss in the inferior temporal gyrus in mild cognitive impairment and Alzheimer's disease. Journal of Alzheimer's Disease. 2011;24(3):547–557.

Scheff SW, Price DA. Alzheimer's disease-related alterations in synaptic density: neocortex and hippocampus. Journal of Alzheimer's Disease. 2006;9(s3):101–115.

Schneider LS, Mangialasche F, Andreasen N, Feldman H, Giacobini E, Jones R, Mantua V, Mecocci P, Pani L, Winblad B. Clinical trials and late-stage drug development for A lzheimer's disease: an appraisal from 1984 to 2014. J Intern Med. 2014;275(3):251–283.

Scholes NS, Mayor-Ruiz C, Winter GE. Identification and selectivity profiling of small-molecule degraders via multi-omics approaches. Cell Chem Biol. 2021;28(7):1048–1060.

Schultz C, Del Tredici K, Braak H. Neuropathology of Alzheimer's disease. In: Alzheimer's disease: A physician's guide to practical management, Springer; 2004; pp. 21–31.

Sen P, Shah PP, Nativio R, Berger SL. Epigenetic Mechanisms of Longevity and Aging. Cell. 2016;166(4):822–839

Serenó L, Coma M, Rodriguez M, Sánchez-Ferrer P, Sánchez MB, Gich I, Agulló JM, Pérez M, Avila J, Guardia-Laguarta C. A novel GSK-3β inhibitor reduces Alzheimer's pathology and rescues neuronal loss in vivo. Neurobiol Dis. 2009;35(3):359–367.

Serrano-Pozo A, Frosch MP, Masliah E, Hyman BT. Neuropathological alterations in Alzheimer disease. Cold Spring Harb Perspect Med 1. 2011;1(1):a006189.

Sevigny J, Chiao P, Bussière T, Weinreb PH, Williams L, Maier M, Dunstan R, Salloway S, Chen T, Ling Y. The antibody aducanumab reduces Aβ plaques in Alzheimer's disease. Nature. 2016;537(7618):50–56.

Shademan B, Biray Avci C, Nikanfar M, Nourazarian A. Application of next-generation sequencing in neurodegenerative diseases: opportunities and challenges. Neuromolecular Med. 2021;23:225–235.

Shadfar S, Parakh S, Jamali MS, Atkin JD. Redox dysregulation as a driver for DNA damage and its relationship to neurodegenerative diseases. Transl Neurodegener. 2023;12(1):18.

Shankar SR, Bahirvani AG, Rao VK, Bharathy N, Ow JR, Taneja R. G9a, a multipotent regulator of gene expression. Epigenetics. 2013;8(1):16–22.

Sharma M, Dierkes T, Sajikumar S. Epigenetic regulation by G9a/GLP complex ameliorates amyloid-beta 1-42 induced deficits in long-term plasticity and synaptic tagging/capture in hippocampal pyramidal neurons. Aging Cel. 2017a;16(5):1062–1072.

Sharma M, Razali NB, Sajikumar S. Inhibition of G9a/GLP Complex Promotes Long-Term Potentiation and Synaptic Tagging/Capture in Hippocampal CA1 Pyramidal Neurons. Cerebral Cortex. 2017b;27(6):3161–3171.

Sharma VK, Singh TG, Singh S, Garg N, Dhiman S. Apoptotic pathways and Alzheimer's disease: probing therapeutic potential. Neurochem Res. 2021;46:3103–3122.

Shaye DD, Greenwald I. OrthoList: a compendium of C. elegans genes with human orthologs. PLoS. 2011;6(5):e20085.

Sherrington R, Rogaev EI, Liang Y al, Rogaeva EA, Levesque G, Ikeda M, Chi H, Lin C, Li G, Holman K. Cloning of a gene bearing missense mutations in early-onset familial Alzheimer's disease. Nature. 1995;375(6534):754–760.

Shi Y, Chen L, Liotta LA, Wan H-H, Rodgers GP. Glia maturation factor gamma (GMFG): a cytokine-responsive protein during hematopoietic lineage development and its functional genomics analysis. Genomics Proteomics Bioinformatics. 2006;4(3):145–155.

Shinosaki K, Nishikawa T, Takeda M. Neurobiological basis of behavioral and psychological symptoms in dementia of the Alzheimer type. Psychiatry Clin Neurosci. 2000;54(6):611–620.

Shipton OA, Leitz JR, Dworzak J, Acton CEJ, Tunbridge EM, Denk F, Dawson HN, Vitek MP, Wade-Martins R, Paulsen O. Tau protein is required for amyloid β-induced impairment of hippocampal long-term potentiation. Journal of Neuroscience. 2011;31(5):1688–1692.

Shu F, Xiao H, Li QN, Ren X-S, Liu ZG, Hu BW, Wang HS, Wang H, Jiang GM. Epigenetic and post-translational modifications in autophagy: Biological functions and therapeutic targets. Signal Transduct Target Ther. 2023;8(1):32.

Siedlecki-Wullich D, Català-Solsona J, Fábregas C, Hernández I, Clarimon J, Lleó A, Boada M, Saura CA, Rodríguez-Álvarez J, Miñano-Molina AJ. Altered microRNAs related to synaptic function as potential plasma biomarkers for Alzheimer's disease. Alzheimers Res Ther. 2019;11(1):46.

Siedlecki-Wullich D, Miñano-Molina AJ, Rodríguez-Álvarez J. microRNAs as early biomarkers of Alzheimer's disease: A synaptic perspective. Cells. 2021;10(1):113.

Siegmund KD, Connor CM, Campan M, Long TI, Weisenberger DJ, Biniszkiewicz D, Jaenisch R, Laird PW, Akbarian S. DNA methylation in the human cerebral cortex is dynamically regulated throughout the life span and involves differentiated neurons. PLoS One. 2007;2(9):e895.

Sievers QL, Petzold G, Bunker RD, Renneville A, Słabicki M, Liddicoat BJ, Abdulrahman W, Mikkelsen T, Ebert BL, Thomä NH. Defining the human C2H2 zinc finger degrome targeted by thalidomide analogs through CRBN. Science. 2018;362(6414):eaat0572.

Sims R, Hill M, Williams J. The multiplex model of the genetics of Alzheimer's disease. Nat Neurosci. 2020;23(3):311–322.

Singh J, Sah B, Shen Y, Liu L. Histone methyltransferase inhibitor UNC0642 promotes breast cancer cell death by upregulating TXNIP-dependent oxidative stress. Chem Biol Interact. 2023;385:110720.

Singh TJ, Grundke-Iqbal I, Iqbal K. Differential phosphorylation of human tau isoforms containing three repeats by several protein kinases. Arch Biochem Biophys. 1996a;328(1):43–50.

Singh TJ, Zaidi T, Grundke-Iqbal I, Iqbal K. Non-proline-dependent protein kinases phosphorylate several sites found in tau from Alzheimer disease brain. Mol Cell Biochem. 1996b;154:143–151.

Sironi JJ, Yen S-H, Gondal JA, Wu Q, Grundke-Iqbal I, Iqbal K. Ser-262 in human recombinant tau protein is a markedly more favorable site for phosphorylation by CaMKII than PKA or PhK. FEBS Lett. 1998;436(3):471–475.

Smallwood A, Estève P-O, Pradhan S, Carey M. Functional cooperation between HP1 and DNMT1 mediates gene silencing. Genes Dev. 2007;21(10):1169–1178.

Smith ML, Ford JM, Hollander MC, Bortnick RA, Amundson SA, Seo YR, Deng C-X, Hanawalt PC, Fornace Jr AJ (2000) p53-mediated DNA repair responses to UV

radiation: studies of mouse cells lacking p53, p21, and/or gadd45 genes. Mol Cell Biol. 2000;20(10):3705–3714.

Song H, Shen R, Liu X, Yang X, Xie K, Guo Z, Wang D. Histone post-translational modification and the DNA damage response. Genes Dis. 2022;10(4):1429-1444.

Song Z, Qu Y, Xu Y, Zhang L, Zhou L, Han Y, Zhao W, Yu P, Zhang Y, Li X. Microarray microRNA profiling of urinary exosomes in a 5XFAD mouse model of Alzheimer's disease. Animal Model Exp Med. 2021;4(3):233–242.

Spiliopoulou P, Spear S, Mirza H, Garner I, McGarry L, Grundland-Freile F, Cheng Z, Ennis DP, Iyer N, McNamara S. Dual G9A/EZH2 inhibition stimulates antitumor immune response in ovarian high-grade serous carcinoma. Mol Cancer Ther. 2022;21(4):522–534.

Spires TL, Meyer-Luehmann M, Stern EA, McLean PJ, Skoch J, Nguyen PT, Bacskai BJ, Hyman BT. Dendritic spine abnormalities in amyloid precursor protein transgenic mice demonstrated by gene transfer and intravital multiphoton microscopy. Journal of Neuroscience. 2005;25(31):7278–7287.

Spires-Jones TL, Hyman BT. The intersection of amyloid beta and tau at synapses in Alzheimer's disease. Neuron. 2014;82(4):756–771.

Srimongkolpithak N, Sundriyal S, Li F, Vedadi M, Fuchter MJ. Identification of 2,4-diamino-6,7-dimethoxyquinoline derivatives as G9a inhibitors. Medchemcomm. 2014;5(12):1821–1828.

Strahl BD, Allis CD. The language of covalent histone modifications. Nature. 2000;403(6765):41.

Sugeno N, Jäckel S, Voigt A, Wassouf Z, Schulze-Hentrich J, Kahle PJ. α-Synuclein enhances histone H3 lysine-9 dimethylation and H3K9me2-dependent transcriptional responses. Sci Rep. 2016;6(1):1–11.

Sun L, Cho HJ, Sen S, Arango AS, Huynh TT, Huang Y, Bandara N, Rogers BE, Tajkhorshid E, Mirica LM. Amphiphilic distyrylbenzene derivatives as potential therapeutic and imaging agents for soluble and insoluble amyloid β aggregates in Alzheimer's disease. J Am Chem Soc. 2021a;143(27):10462–10476.

Sun W, Wang J, Zhang J, Gao F, Ou Q, Tian H, Jin C, Xu J, Zhang J, Xu GT. SUMOylation of GMFB regulates the stability and function of GMFB in RPE cells under oxidative stress and inflammation. bioRxiv. 2021-03.

Sweis RF, Pliushchev M, Brown PJ, Guo J, Li F, Maag D, Petros AM, Soni NB, Tse C, Vedadi M, Michaelides MR, Chiang GG, Pappano WN. Discovery and development of potent and selective inhibitors of histone methyltransferase G9a. ACS Med Chem Lett . 2014;5(2):205–209.

Tachibana M, Matsumura Y, Fukuda M, Kimura H, Shinkai Y. G9a/GLP complexes independently mediate H3K9 and DNA methylation to silence transcription. EMBO J. 2008;27(20):2681–2690.

Tachibana M, Sugimoto K, Fukushima T, Shinkai Y. Set domain-containing protein, G9a, is a novel lysine-preferring mammalian histone methyltransferase with hyperactivity and specific selectivity to lysines 9 and 27 of histone H3. Journal of Biological Chemistry. 2001;276(27):25309–25317.

Tachibana M, Sugimoto K, Nozaki M, Ueda J, Ohta T, Ohki M, Fukuda M, Takeda N, Niida H, Kato H. G9a histone methyltransferase plays a dominant role in euchromatic histone H3 lysine 9 methylation and is essential for early embryogenesis. Genes Dev. 2002;16(14):1779–1791.

Tachibana M, Ueda J, Fukuda M, Takeda N, Ohta T, Iwanari H, Sakihama T, Kodama T, Hamakubo T, Shinkai Y. Histone methyltransferases G9a and GLP form heteromeric complexes and are both crucial for methylation of euchromatin at H3-K9. Genes Dev. 2005;19(7):815–826.

Tahiliani M, Mei P, Fang R, Leonor T, Rutenberg M, Shimizu F, Li J, Rao A, Shi Y. The histone H3K4 demethylase SMCX links REST target genes to X-linked mental retardation. Nature. 2007;447(7144):601–605.

Tajes M, Gutierrez-Cuesta J, Folch J, Ferrer I, Caballero B, Smith MA, Casadesus G, Camins A, Pallás M. Lithium treatment decreases activities of tau kinases in a murine model of senescence. J Neuropathol Exp Neurol. 2008;67(6):612–623.

Tajes M, Gutierrez-Cuesta J, Folch J, Ortuño-Sahagun D, Verdaguer E, Jiménez A, Junyent F, Lau A, Camins A, Pallàs M. Neuroprotective role of intermittent fasting in senescence-accelerated mice P8 (SAMP8). Exp Gerontol. 2010;45(9):702–710.

Takeda T. Senescence-accelerated mouse (SAM) with special references to neurodegeneration models, SAMP8 and SAMP10 mice. Neurochem Res. 2009;34(4):639–659.

Takeda T. Senescence-accelerated mouse (SAM): a biogerontological resource in aging research. Neurobiol Aging. 1999;20(2):105–110.

Tan L, Yu JT, Tan L. Causes and consequences of microRNA dysregulation in neurodegenerative diseases. Mol Neurobiol. 2015;51(3):1249–1262.

Tang Y, Bao JS, Su JH, Huang W. MicroRNA-139 modulates Alzheimer's-associated pathogenesis in SAMP8 mice by targeting cannabinoid receptor type 2. Genet Mol Res. 2017;16(19166):10–4238.

Tang YP, Gershon ES. Genetic studies in Alzheimer's disease. Dialogues Clin Neurosci. 2003;5(1):17–26.

Taylor WR, Xiao B, Gamblin SJ, Lin K. A knot or not a knot? SETting the record 'straight'on proteins. Comput Biol Chem. 2003;27(1):11–15.

Terry RD, Masliah E, Salmon DP, Butters N, DeTeresa R, Hill R, Hansen LA, Katzman R. Physical basis of cognitive alterations in Alzheimer's disease: synapse loss is the major correlate of cognitive impairment. Annals of Neurology: Official Journal of the American Neurological Association and the Child Neurology Society. 1991;30(4):572–580.

Thakur S, Dhapola R, Sarma P, Medhi B, Reddy DH. Neuroinflammation in Alzheimer's disease: current progress in molecular signaling and therapeutics. Inflammation. 2023;46(1):1–17.

Tian N, Cao Z, Zhang Y. MiR-206 decreases brain-derived neurotrophic factor levels in a transgenic mouse model of Alzheimer's disease. Neurosci Bull. 2014;30:191–197.

Tönnies E, Trushina E. Oxidative Stress, Synaptic Dysfunction, and Alzheimer's Disease. J Alzheimers Dis. 2017;57(4):1105–1121.

Towbin BD, González-Aguilera C, Sack R, Gaidatzis D, Kalck V, Meister P, Askjaer P, Gasser SM. Step-wise methylation of histone H3K9 positions heterochromatin at the nuclear periphery. Cell. 2012;150(5):934–947.

Trievel RC, Beach BM, Dirk LMA, Houtz RL, Hurley JH. Structure and catalytic mechanism of a SET domain protein methyltransferase. Cell. 2002;111(1):91–103.

Trojer P, Zhang J, Yonezawa M, Schmidt A, Zheng H, Jenuwein T, Reinberg D. Dynamic histone H1 isotype 4 methylation and demethylation by histone lysine methyltransferase G9a/KMT1C and the Jumonji domain-containing JMJD2/KDM4 proteins. Journal of Biological Chemistry. 2009;284(13):8395–8405.

Tront JS, Hoffman B, Liebermann DA. Gadd45a suppresses Ras-driven mammary tumorigenesis by activation of c-Jun NH2-terminal kinase and p38 stress signaling resulting in apoptosis and senescence. Cancer Res. 2006;66(17):8448–8454.

Ukaegbu UE, Zhang X, Heinberg AR, Wele M, Chen Q, Deitsch KW. A unique virulence gene occupies a principal position in immune evasion by the malaria parasite Plasmodium falciparum. PLoS Genet. 2015;11(5):e1005234.

Vairapandi M, Balliet AG, Hoffman B, Liebermann DA. GADD45b and GADD45g are cdc2/cyclinB1 kinase inhibitors with a role in S and G2/M cell cycle checkpoints induced by genotoxic stress. J Cell Physiol. 2002;192(3):327–338.

van den Hove DLA, Riemens RJM, Koulousakis P, Pishva E. Epigenome-wide association studies in Alzheimer's disease; achievements and challenges. Brain Pathology. 2020;30(5):978-983.

van Dyck CH, Swanson CJ, Aisen P, Bateman RJ, Chen C, Gee M, Kanekiyo M, Li D, Reyderman L, Cohen S, Froelich L, Katayama S, Sabbagh M, Vellas B, Watson D, Dhadda S, Irizarry M, Kramer LD, Iwatsubo T. Lecanemab in early Alzheimer's disease. New England Journal of Medicine. 2023;388(1):9-21.

Vanheer LN, Kafsack BFC. Activity comparison of epigenetic modulators against the hemoprotozoan parasites babesia divergens and plasmodium falciparum. ACS Infect Dis. 2021;7(8):2277–2284.

Vanheer LN, Zhang H, Lin G, Kafsack BFC. Activity of epigenetic inhibitors against Plasmodium falciparum asexual and sexual blood stages. Antimicrob Agents Chemother. 2020;64(7):10–1128.

Vasilopoulou F, Bellver-Sanchis A, Companys-Alemany J, Jarne-Ferrer J, Irisarri A, Palomera-Ávalos V, Gonzalez-Castillo C, Ortuño-Sahagún D, Sanfeliu C, Pallàs M. Cognitive decline and BPSD are concomitant with autophagic and synaptic deficits associated with G9a alterations in aged SAMP8 mice. Cells. 2022;11(16):2603.

Vedadi M, Barsyte-Lovejoy D, Liu F, Rival-Gervier S, Allali-Hassani A, Labrie V, Wigle TJ, Dimaggio PA, Wasney GA, Siarheyeva A, Dong A, Tempel W, Wang SC, Chen X, Chau I, Mangano TJ, Huang XP, Simpson CD, Pattenden SG, Norris JL, Kireev DB, Tripathy A, Edwards A, Roth BL, Janzen WP, Garcia BA, Petronis A, Ellis J, Brown PJ, Frye SV, Arrowsmith CH, Jin J. A chemical probe selectively inhibits G9a and GLP methyltransferase activity in cells. Nat Chem Biol. 2011;7(8):566–574.

Verma J, Khedkar VM, Coutinho EC. 3D-QSAR in drug design-a review. Curr Top Med Chem. 2010;10(1):95–115.

Vinson DA, Stephens KE, O'Meally RN, Bhat S, Dancy BCR, Cole RN, Yegnasubramanian S, Taverna SD. De novo methylation of histone H3K23 by the methyltransferases EHMT1/GLP and EHMT2/G9a. Epigenetics Chromatin. 2022;15(1):1–13.

Vossel K, Ranasinghe KG, Beagle AJ, La A, Pook KA, Castro M, Mizuiri D, Honma SM, Venkateswaran N, Koestler M. Effect of levetiracetam on cognition in patients with Alzheimer disease with and without epileptiform activity: a randomized clinical trial. JAMA Neurol. 2021;78(11):1345–1354.

Walker MP, Laferla FM, Oddo SS, Brewer GJ. Reversible epigenetic histone modifications and Bdnf expression in neurons with aging and from a mouse model of Alzheimer's disease. Age (Omaha). 2013;35(3):519–531.

Wang DY, Kosowan J, Samsom J, Leung L, Zhang KL, Li YX, Xiong Y, Jin J, Petronis A, Oh G, Wong AHC. Inhibition of the G9a/GLP histone methyltransferase complex modulates anxiety-related behavior in mice. Acta Pharmacol Sin. 2018a;39(5):866–874.

Wang J, Grundke-Iqbal I, Iqbal K. Kinases and phosphatases and tau sites involved in Alzheimer neurofibrillary degeneration. European Journal of Neuroscience. 2007;25(1):59–68.

Wang L, Xu S, Lee J, Baldridge A, Grullon S, Peng W, Ge K. Histone H3K9 methyltransferase G9a represses PPARγ expression and adipogenesis. EMBO J. 2013;32(1):45–59.

Wang X, Zhang M, Liu H. LncRNA17A regulates autophagy and apoptosis of SH-SY5Y cell line as an in vitro model for Alzheimer's disease. Biosci Biotechnol Biochem. 2019;83(4):609–621.

Wang Y, Branicky R, Noë A, Hekimi S. Superoxide dismutases: Dual roles in controlling ROS damage and regulating ROS signaling. Journal of Cell Biology. 2018b;39(5):866–874.

Wang Y, Zhang J, Su Y, Shen Y, Jiang D, Hou Y, Geng M, Ding J, Chen Y. G9a regulates breast cancer growth by modulating iron homeostasis through the repression of ferroxidase hephaestin. Nat Commun. 2017;8(1):274.

Wang Z, Yang D, Zhang X, Li T, Li J, Tang Y, Le W. Hypoxia-induced down-regulation of neprilysin by histone modification in mouse primary cortical and hippocampal neurons. PLoS One. 2011;6(4):e19229.

Weiland A, Wang Y, Wu W, Lan X, Han X, Li Q, Wang J. Ferroptosis and its role in diverse brain diseases. Mol Neurobiol. 2019;56:4880–4893.

Weiss T, Hergeth S, Zeissler U, Izzo A, Tropberger P, Zee BM, Dundr M, Garcia BA, Daujat S, Schneider R. Histone H1 variant-specific lysine methylation by G9a/KMT1C and Glp1/KMT1D. Epigenetics Chromatin. 2010;3:1–13.

Wenzel D, Palladino F, Jedrusik-Bode M. Epigenetics in C. elegans: facts and challenges. Genesis. 2011;49(8):647–661.

Wilcock GK, Lilienfeld S, Gaens E. Efficacy and safety of galantamine in patients with mild to moderate Alzheimer's disease: multicentre randomised controlled trial. Galantamine International-1 Study Group. BMJ. 2000;321(7274):1445-9.

Williams JB, Cao Q, Wang W, Lee YH, Qin L, Zhong P, Ren Y, Ma K, Yan Z. Inhibition of histone methyltransferase Smyd3 rescues NMDAR and cognitive deficits in a tauopathy mouse model. Nat Commun. 2023;14(1):91.

Wilson DM, Cookson MR, Van Den Bosch L, Zetterberg H, Holtzman DM, Dewachter I. Hallmarks of neurodegenerative diseases. Cell. 2023;186(4):693–714.

Woodhouse RM, Ashe A. Transgenerational Epigenetic Inheritance Is Revealed as a Multi-step Process by Studies of the SET-Domain Proteins SET-25 and SET-32. Epigenet Insights. 2019;12:1–4.

Woodhouse RM, Buchmann G, Hoe M, Harney DJ, Low JKK, Larance M, Boag PR, Ashe A. Chromatin Modifiers SET-25 and SET-32 Are Required for Establishment but Not Long-Term Maintenance of Transgenerational Epigenetic Inheritance. Cell Rep. 2018;25(8):2259-2272.e5.

Woods YL, Cohen P, Becker W, Jakes R, Goedert M, Wang X, Proud CG. The kinase DYRK phosphorylates protein-synthesis initiation factor eIF2Bε at Ser539 and the microtubule-associated protein tau at Thr212: potential role for DYRK as a glycogen synthase kinase 3-priming kinase. Biochemical Journal. 2001;355(3):609–615.

Wu H, Chen X, Xiong J, Li Y, Li H, Ding X, Liu S, Chen S, Gao S, Zhu B. Histone methyltransferase G9a contributes to H3K27 methylation in vivo. Cell Res. 2011;21(2):365–367.

Xie L, Sheehy RN, Xiong Y, Muneer A, Wrobel JA, Park K-S, Velez J, Liu J, Luo Y-J, Li Y-D. Novel brain-penetrant inhibitor of G9a methylase blocks Alzheimer disease proteopathology for precision medication. medRxiv 2023;2010–2023.

Xiong Y, Li F, Babault N, Dong A, Zeng H, Wu H, Chen X, Arrowsmith CH, Brown PJ, Liu J. Discovery of potent and selective inhibitors for G9a-like protein (GLP) lysine methyltransferase. J Med Chem. 2017;60(5):1876–1891.

Yamaguchi H, Ishiguro K, Uchida T, Takashima A, Lemere CA, Imahori K. Preferential labeling of Alzheimer neurofibrillary tangles with antisera for tau protein kinase (TPK) I/glycogen synthase kinase-3β and cyclin-dependent kinase 5, a component of TPK II. Acta Neuropathol. 1996;92:232–241.

Yan Z, Ji L, Huo X, Wang Q, Zhang Y, Wen B. G9a/GLP-Sensitivity of H3K9me2 Demarcates Two Types of Genomic Compartments. Genomics Proteomics Bioinformatics. 2020;18(4):359-370.

Yang S, Zhang R, Wang G, Zhang Y. The development prospection of HDAC inhibitors as a potential therapeutic direction in Alzheimer's disease. Transl Neurodegener. 2017;6(1):1–6.

Yang TT, Liu CG, Gao SC, Zhang Y, Wang PC. The serum exosome derived MicroRNA− 135a,− 193b, and− 384 were potential Alzheimer's disease biomarkers. Biomedical and Environmental Sciences. 2018;31(2):87–96.

Yao Q, Chen Y, Zhou X. The roles of microRNAs in epigenetic regulation. Curr Opin Chem Biol. 2019;51:11–17.

Ying S-W, Futter M, Rosenblum K, Webber MJ, Hunt SP, Bliss TVP, Bramham CR. Brain-derived neurotrophic factor induces long-term potentiation in intact adult hippocampus:

requirement for ERK activation coupled to CREB and upregulation of Arc synthesis. Journal of Neuroscience. 2002;22(5):1532–1540.

Yonutas HM, Sullivan PG. Targeting PPAR isoforms following CNS injury. Curr Drug Targets. 2013;14(7):733–742.

Yoon SS, Jo SA. Mechanisms of amyloid-β peptide clearance: potential therapeutic targets for Alzheimer's disease. Biomol Ther. 2012;20(3):245.

You W, Xu Z, Sun Y, Valencak TG, Wang Y, Shan T. GADD45α drives brown adipose tissue formation through upregulating PPARγ in mice. Cell Death Dis. 2020;11(7):585.

Yu N, Liu J, Yi G, Ye F, Xiao J, Guo F. DNA methylation is necessary for erythropoietin to improve spatial learning and memory in SAMP8 mice. Exp Gerontol. 2015;69:111–115.

Yuan Y, Wang Q, Paulk J, Kubicek S, Kemp MM, Adams DJ, Shamji AF, Wagner BK, Schreiber SL. A small-molecule probe of the histone methyltransferase G9a induces cellular senescence in pancreatic adenocarcinoma. ACS Chem Biol. 2012;7(7):1152–1157.

Zaheer A, Fink BD, Lim R. Expression of glia maturation factor β mRNA and protein in rat organs and cells. J Neurochem. 1993;60(3):914–920.

Zaheer A, Weiss JL, Goyal P, Lim R. Enhanced expression of neurotrophic factors by C6 rat glioma cells after transfection with glia maturation factor. Neurosci Lett. 1999;265(3):203–206.

Zaheer A, Yorek MA, Lim R. Effects of glia maturation factor on signal transduction, transcription factors and neurotrophin secretion. Neurochem Res. 2001;26(12):1293-9.

Zaheer A, Zaheer S, Sahu SK, Knight S, Khosravi H, Mathur SN, Lim R. A novel role of glia maturation factor: induction of granulocyte-macrophage colony-stimulating factor and pro-inflammatory cytokines. J Neurochem. 2007;101(2):364–376.

Zaheer S, Thangavel R, Sahu SK, Zaheer A. Augmented expression of glia maturation factor in Alzheimer's disease. Neuroscience. 2011;194:227–233.

Zang L, Kondengaden SM, Zhang Q, Li X, Sigalapalli DK, Kondengadan SM, Huang K, Li KK, Li S, Xiao Z, Wen L, Zhu H, Babu BN, Wang L, Che F, Wang PG. Structure based design, synthesis and activity studies of small hybrid molecules as HDAC and G9a dual inhibitors. Oncotarget. 2017;8(38):63187–63207.

Zhang C, Rodriguez C, Spaulding J, Aw TY, Feng J. Age-dependent and tissue-related glutathione redox status in a mouse model of Alzheimer's disease. Journal of Alzheimer's Disease. 2012;28(3):655–666.

Zhang D, Wang W, Sun X, Xu D, Wang C, Zhang Q, Wang H, Luo W, Chen Y, Chen H. AMPK regulates autophagy by phosphorylating BECN1 at threonine 388. Autophagy. 2016a;12(9):1447–1459

Zhang J, Hu M, Teng Z, Tang Y-P, Chen C. Synaptic and cognitive improvements by inhibition of 2-AG metabolism are through upregulation of microRNA-188-3p in a mouse model of Alzheimer's disease. Journal of Neuroscience. 2014;34(45):14919–14933.

Zhang W, Zhao H, Wu Q, Xu W, Xia M. Knockdown of BACE1-AS by siRNA improves memory and learning behaviors in Alzheimer's disease animal model. Exp Ther Med. 2018;16(3):2080–2086.

Zhang X, Tamaru H, Khan SI, Horton JR, Keefe LJ, Selker EU, Cheng X. Structure of the Neurospora SET domain protein DIM-5, a histone H3 lysine methyltransferase. Cell. 2002a;111(1):117–127.

Zhang XG, Wang X, Zhou TT, Wu XF, Peng Y, Zhang WQ, Li S, Zhao J. Scorpion venom heat-resistant peptide protects transgenic Caenorhabditis elegans from β-amyloid toxicity. Front Pharmacol. 2016b;7:1–9.

Zhang Y, Li Q, Liu C, Gao S, Ping H, Wang J, Wang P. MiR-214-3p attenuates cognition defects via the inhibition of autophagy in SAMP8 mouse model of sporadic Alzheimer's disease. Neurotoxicology. 2016c;56:139–149.

Zhang Y, McLaughlin R, Goodyer C, LeBlanc A. Selective cytotoxicity of intracellular amyloid β peptide1–42 through p53 and Bax in cultured primary human neurons. J Cell Biol. 2002b;156(3):519–529.

Zhao J, Huai J (2023) Role of primary aging hallmarks in Alzheimer´s disease. Theranostics. 2023;13:197–230.

Zhao M, Zhu Z, Li H, Wang W, Cheng S, Qin X, Wu H, Liu D, Pan F. Effects of traumatic stress in adolescence on PTSD-like behaviors, dendrite development, and H3K9me2/BDNF expression in the amygdala of male rats. J Affect Disord. 2022;296:388–399.

Zhao W, Soejima H, Higashimoto K, Nakagawachi T, Urano T, Kudo S, Matsukura S, Matsuo S, Joh K, Mukai T. The essential role of histone H3 Lys9 di-methylation and MeCP2 binding in MGMT silencing with poor DNA methylation of the promoter CpG island. J Biochem. 2005;137(3):431–440.

Zhao Y, Zhao B. Oxidative stress and the pathogenesis of Alzheimer's disease. Oxid Med Cell Longev. 2013;2013:316523.

Zheng H, Dai Q, Yuan Z, Fan T, Zhang C, Liu Z, Chu B, Sun Q, Chen Y, Jiang Y. Quinazoline-based hydroxamic acid derivatives as dual histone methylation and deacetylation inhibitors for potential anticancer agents. Bioorg Med Chem. 2022;53:116524.

Zheng Y, Liu A, Wang ZJ, Cao Q, Wang W, Lin L, Ma K, Zhang F, Wei J, Matas E, Cheng J, Chen GJ, Wang X, Yan Z. Inhibition of EHMT1/2 rescues synaptic and cognitive functions for Alzheimer's disease. Brain. 2019;142(3):787–807.

Zhong Z, Yuan K, Tong X, Hu J, Song Z, Zhang G, Fang X, Zhang W. MiR-16 attenuates β-amyloid-induced neurotoxicity through targeting β-site amyloid precursor protein-cleaving enzyme 1 in an Alzheimer's disease cell model. Neuroreport. 2018;29(16):1365–1372.

Zhou J, Zhang W, Liang B, Casimiro MC, Whitaker-Menezes D, Wang M, Lisanti MP, Lanza-Jacoby S, Pestell RG, Wang C. PPARγ activation induces autophagy in breast cancer cells. Int J Biochem Cell Biol. 2009;41(11):2334–2342.

Zhou L, McInnes J, Wierda K, Holt M, Herrmann AG, Jackson RJ, Wang Y-C, Swerts J, Beyens J, Miskiewicz K. Tau association with synaptic vesicles causes presynaptic dysfunction. Nat Commun. 2017;8(1):15295.

Zhou SS, Jin JP, Wang JQ, Zhang ZG, Freedman JH, Zheng Y, Cai L. MiRNAS in cardiovascular diseases: Potential biomarkers, therapeutic targets and challenges review-article. Acta Pharmacol Sin. 2018;39(7):1073–1084.

Zhu HC, Wang LM, Wang M, Song B, Tan S, Teng JF, Duan DX. MicroRNA-195 downregulates Alzheimer's disease amyloid-β production by targeting BACE1. Brain Res Bull. 2012;88(6):596–601.

Zou J, Walter TJ, Barnett A, Rohlman A, Crews FT, Coleman Jr LG. Ethanol induces secretion of proinflammatory extracellular vesicles that inhibit adult hippocampal neurogenesis through G9a/GLP-epigenetic signaling. Front Immunol. 2022;13:866073.

Zovkic IB, Guzman-Karlsson MC, Sweatt JD. Epigenetic regulation of memory formation and maintenance. Learning & memory. 2013;20(2):61–74.

A. Annex

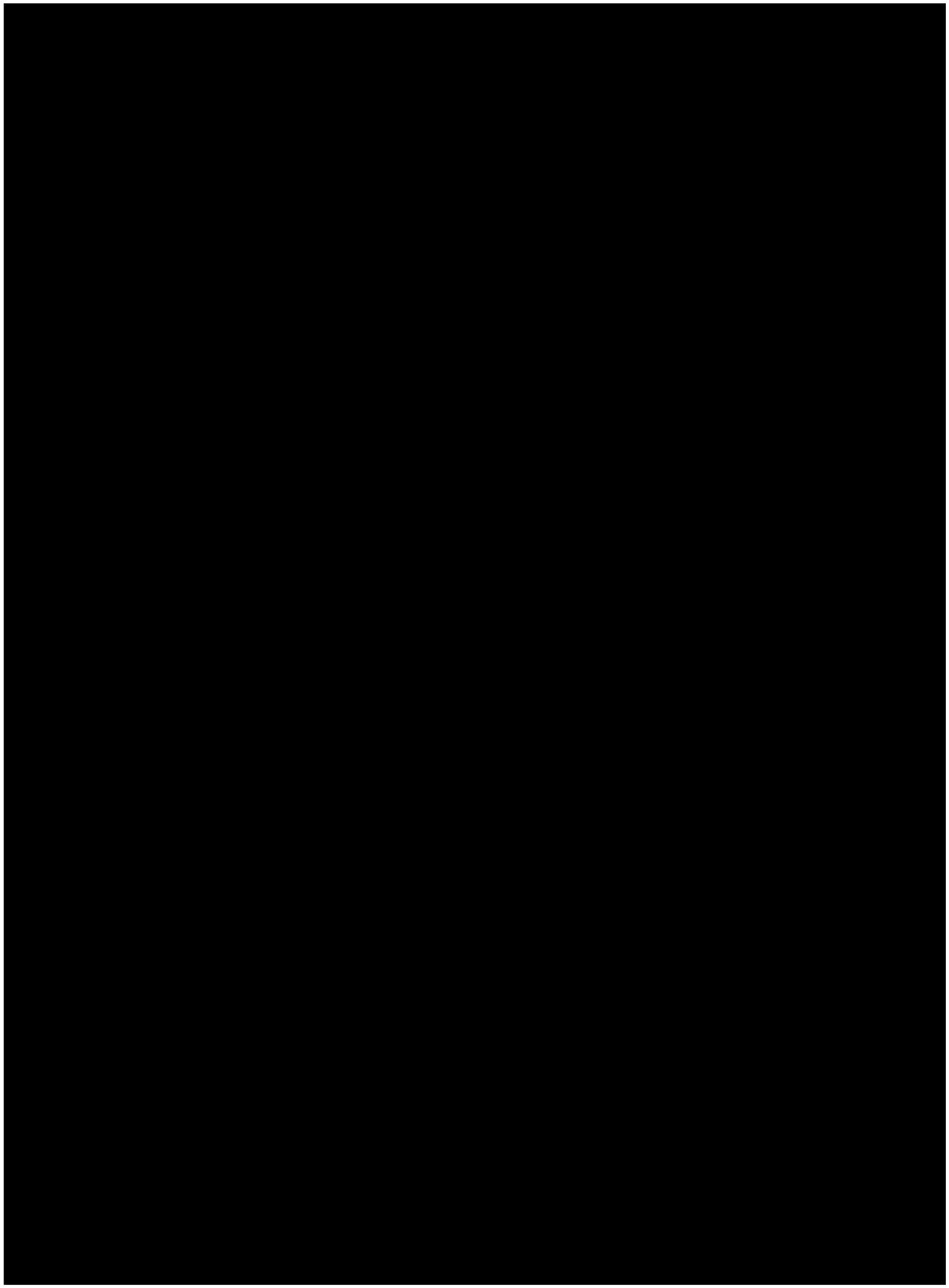

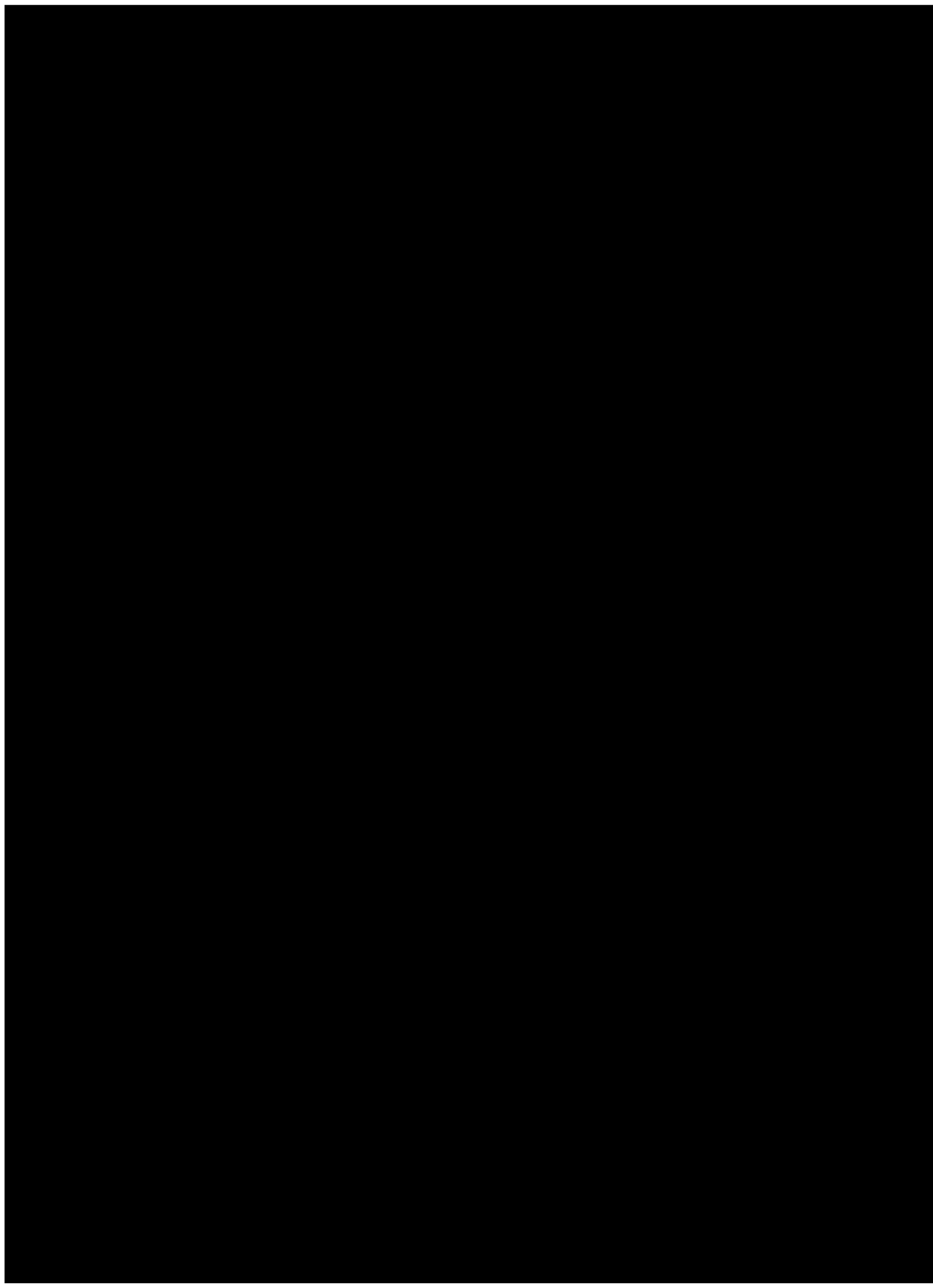

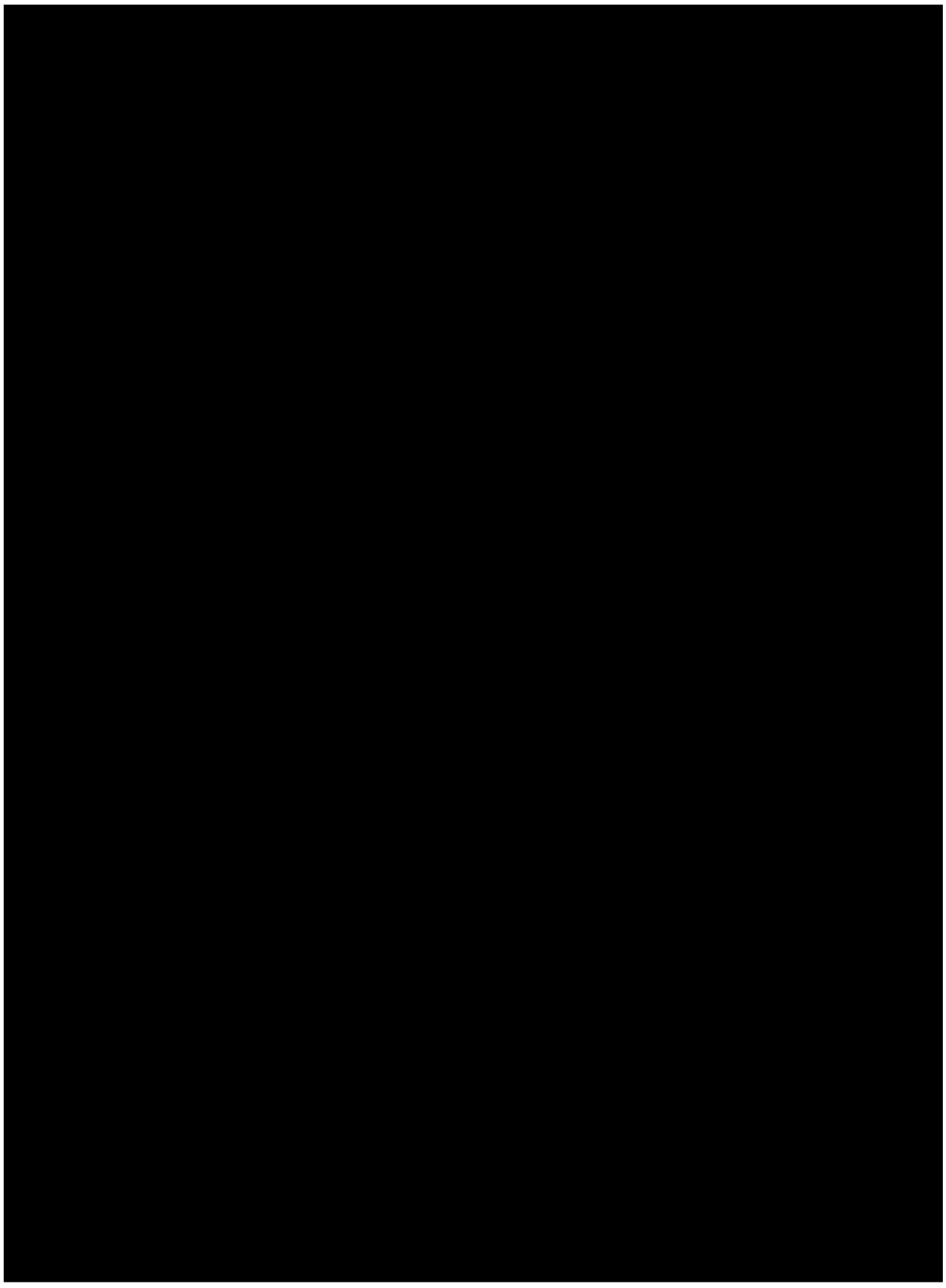

[redacted]

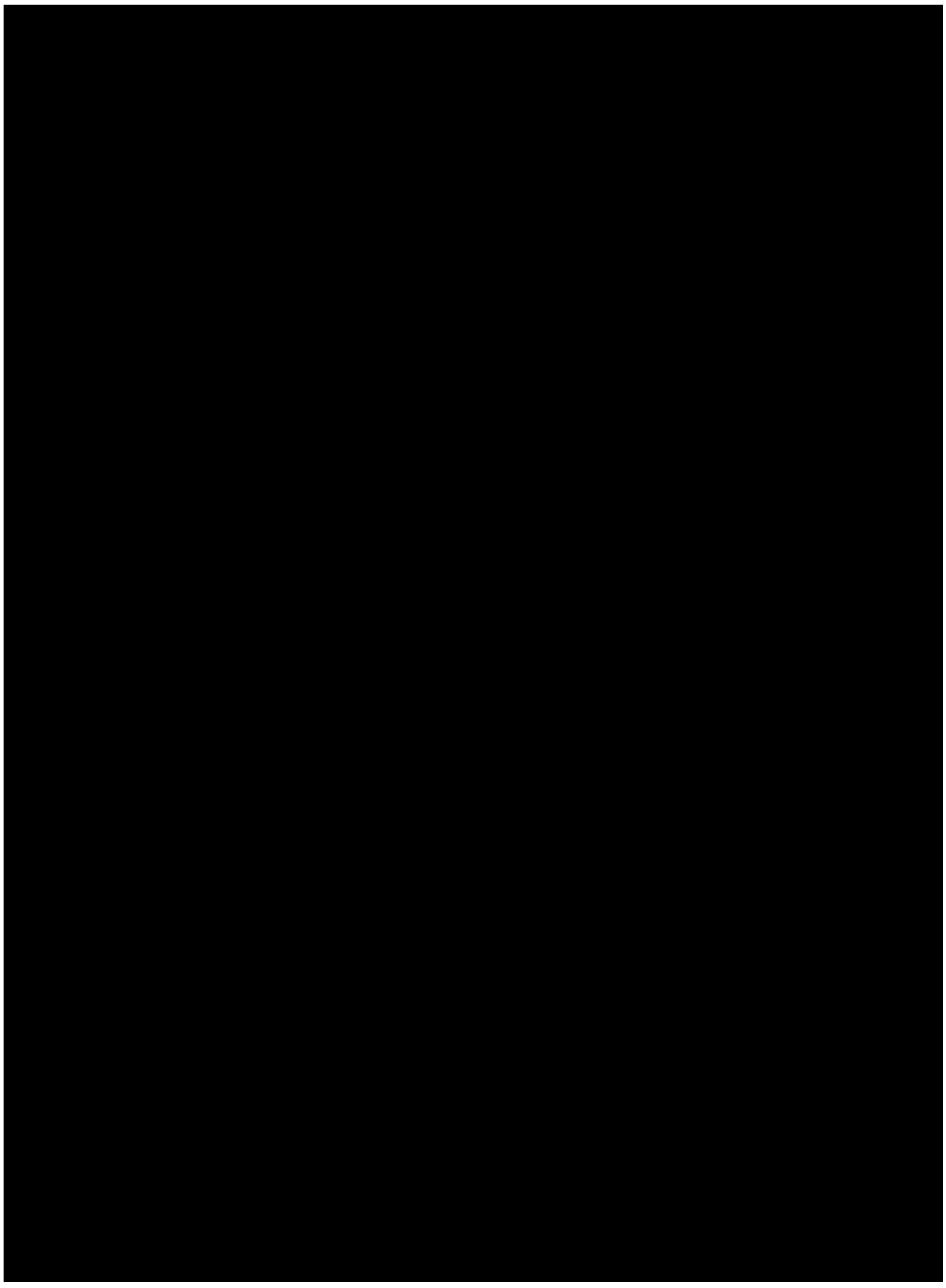

[redacted]

[redacted]

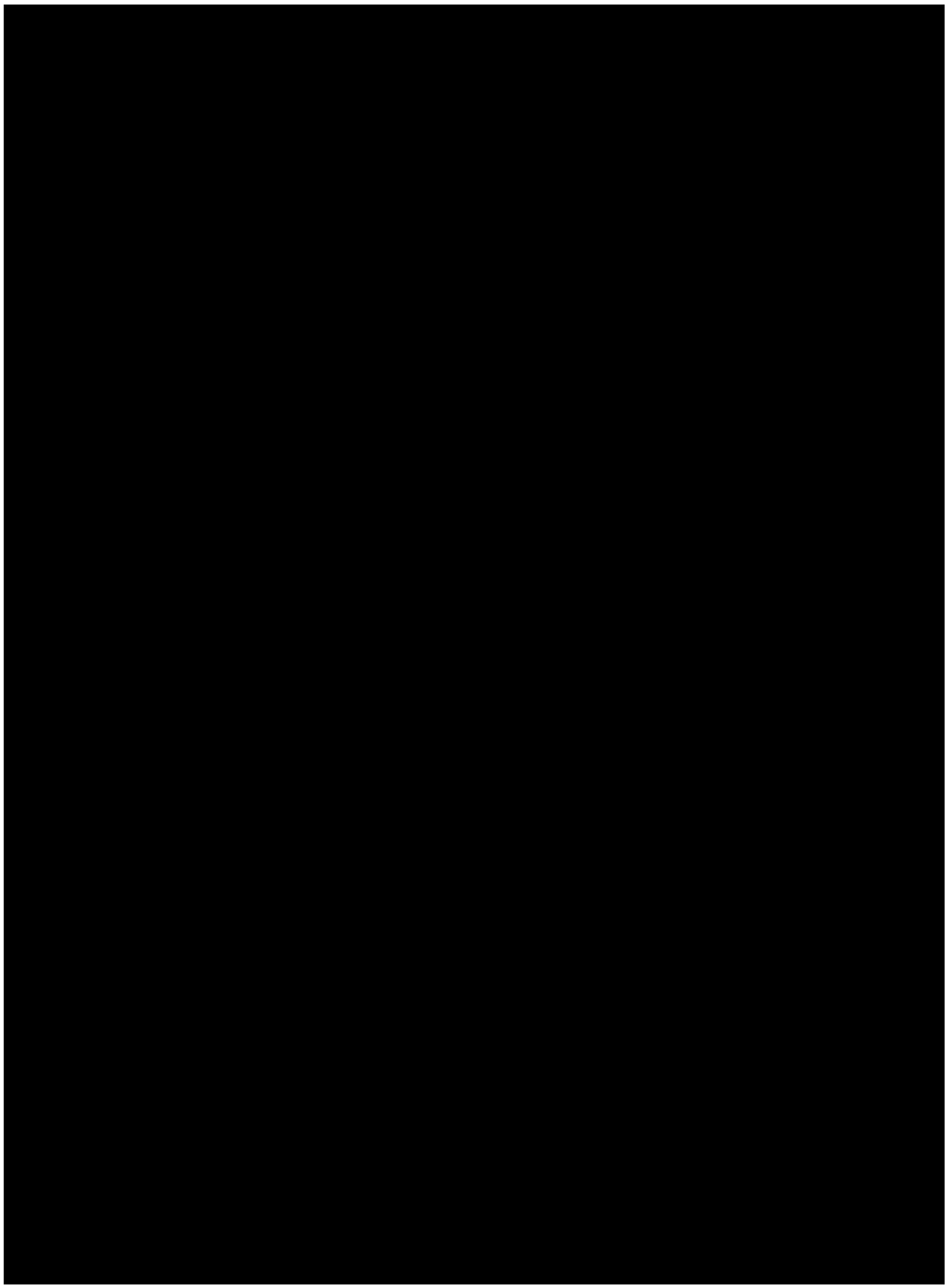

[redacted]

[redacted]

[redacted]

[redacted]

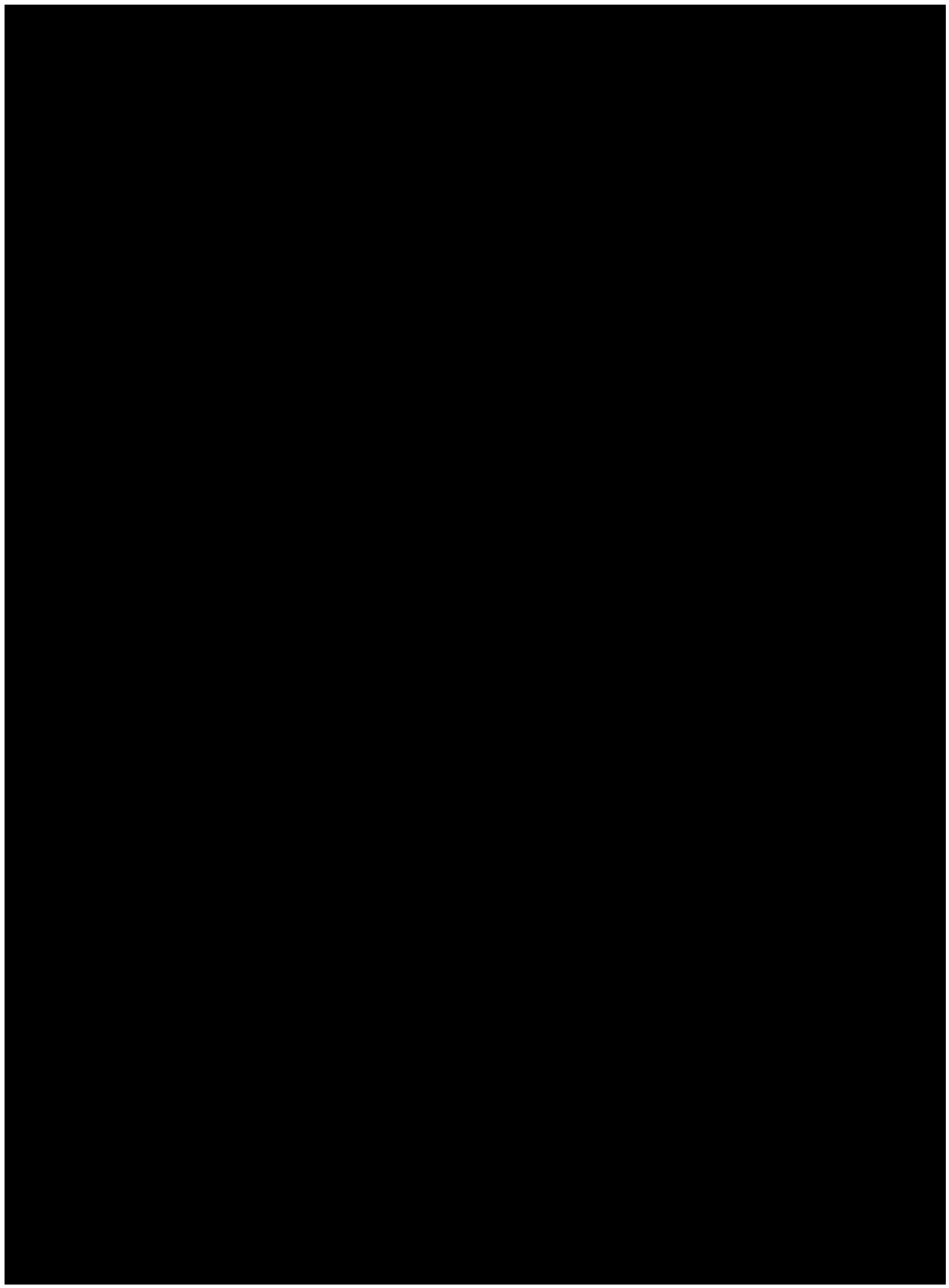

[redacted]

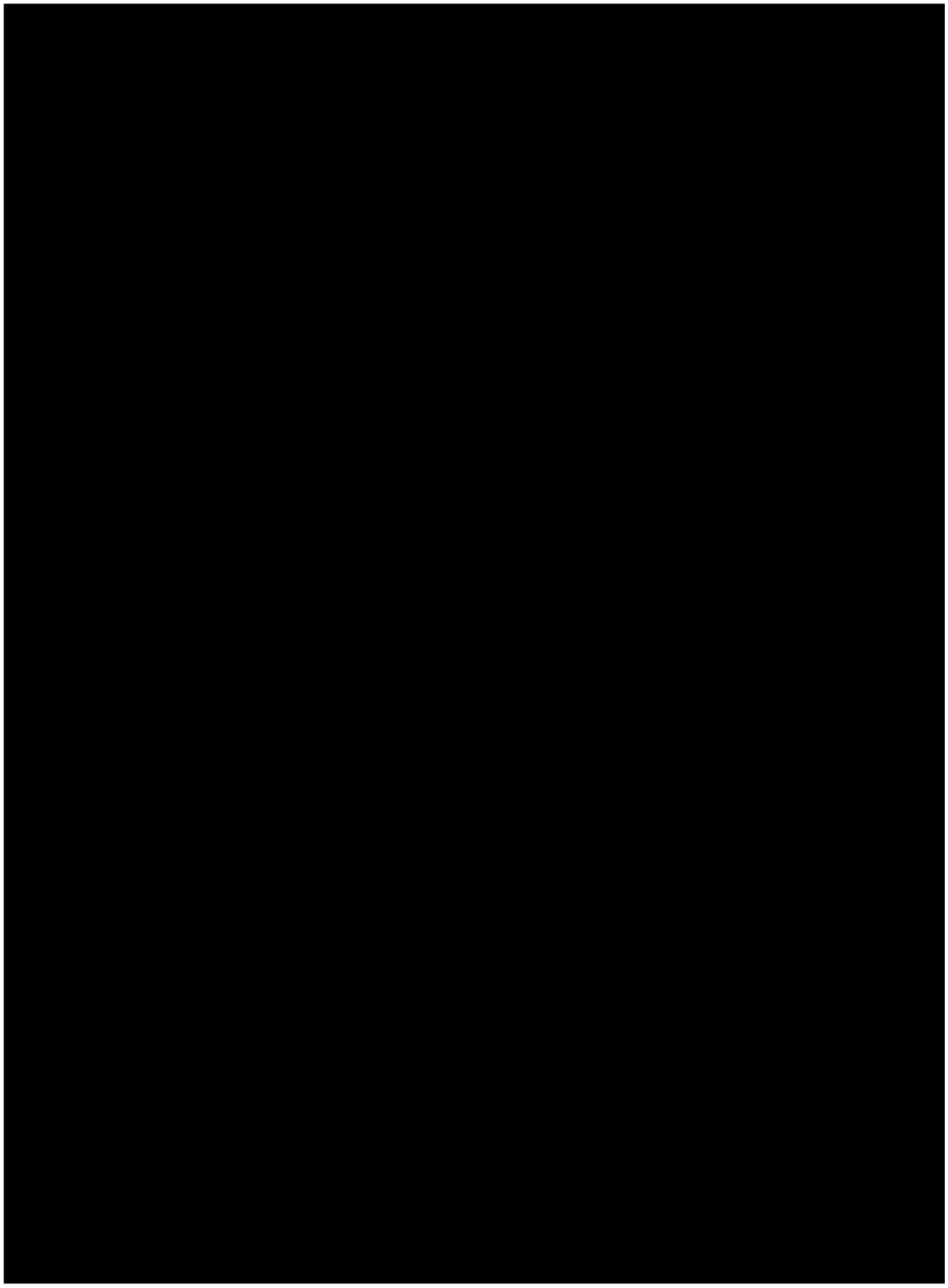

[redacted]

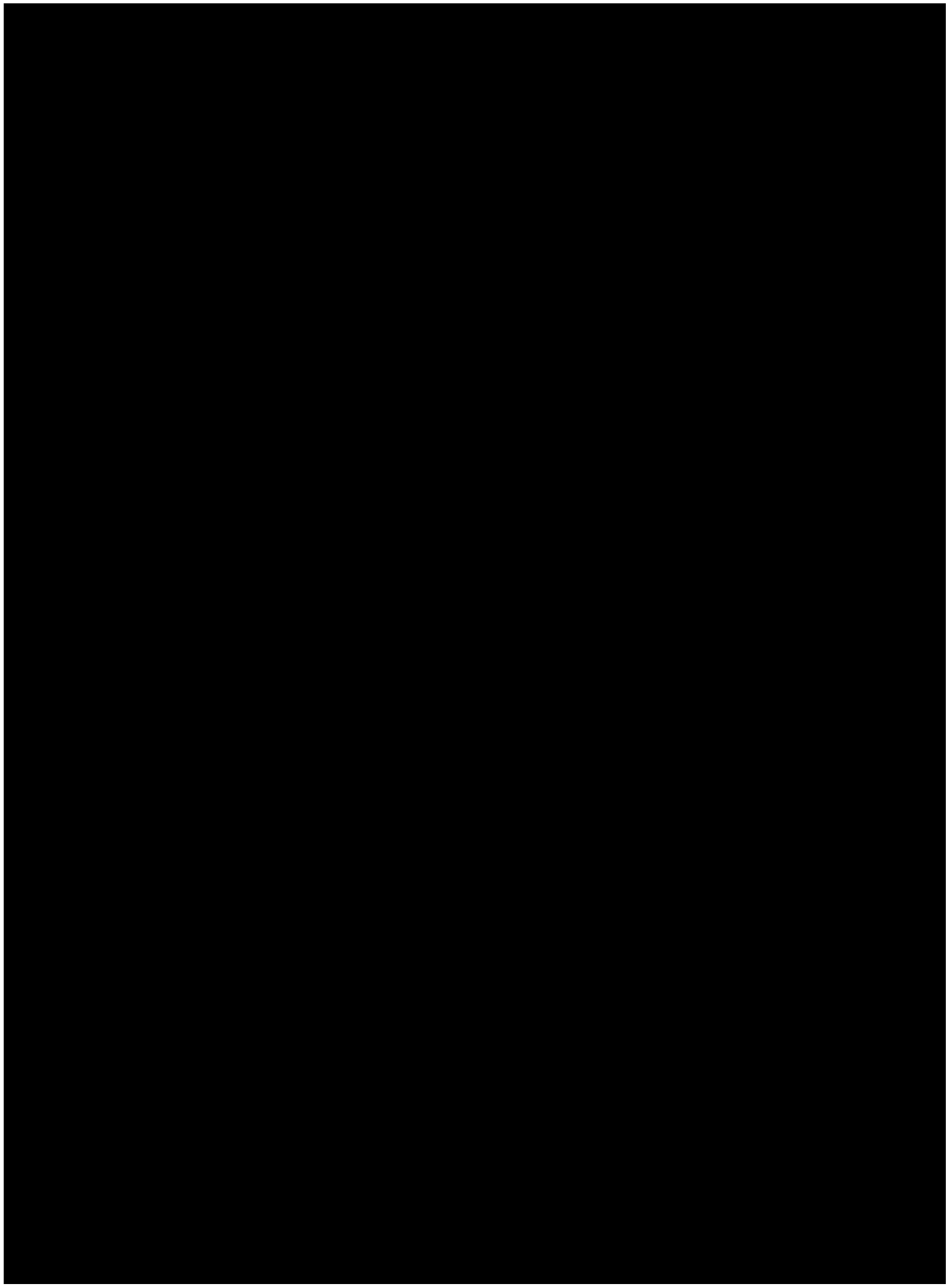

[redacted]

[redacted]

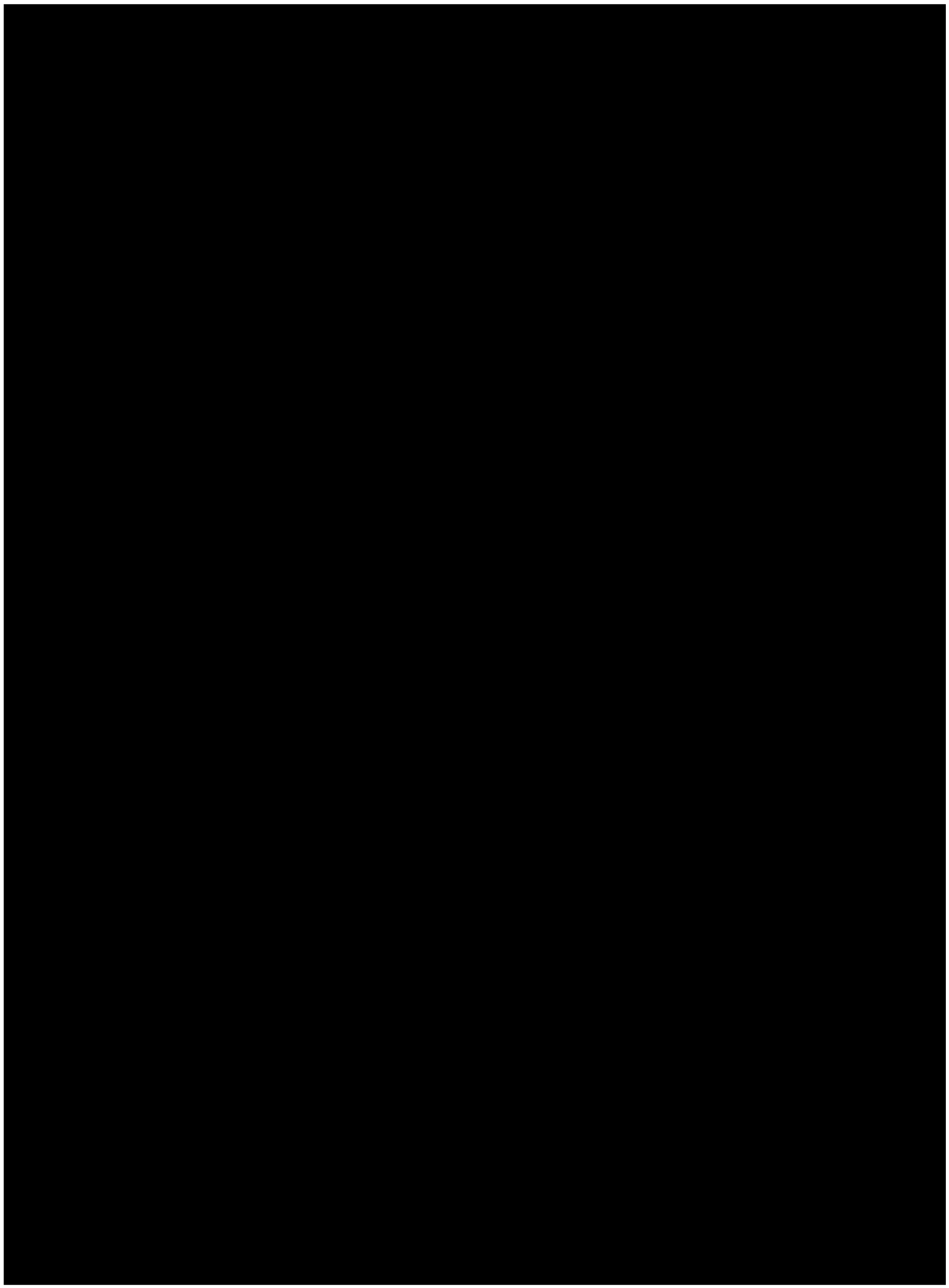

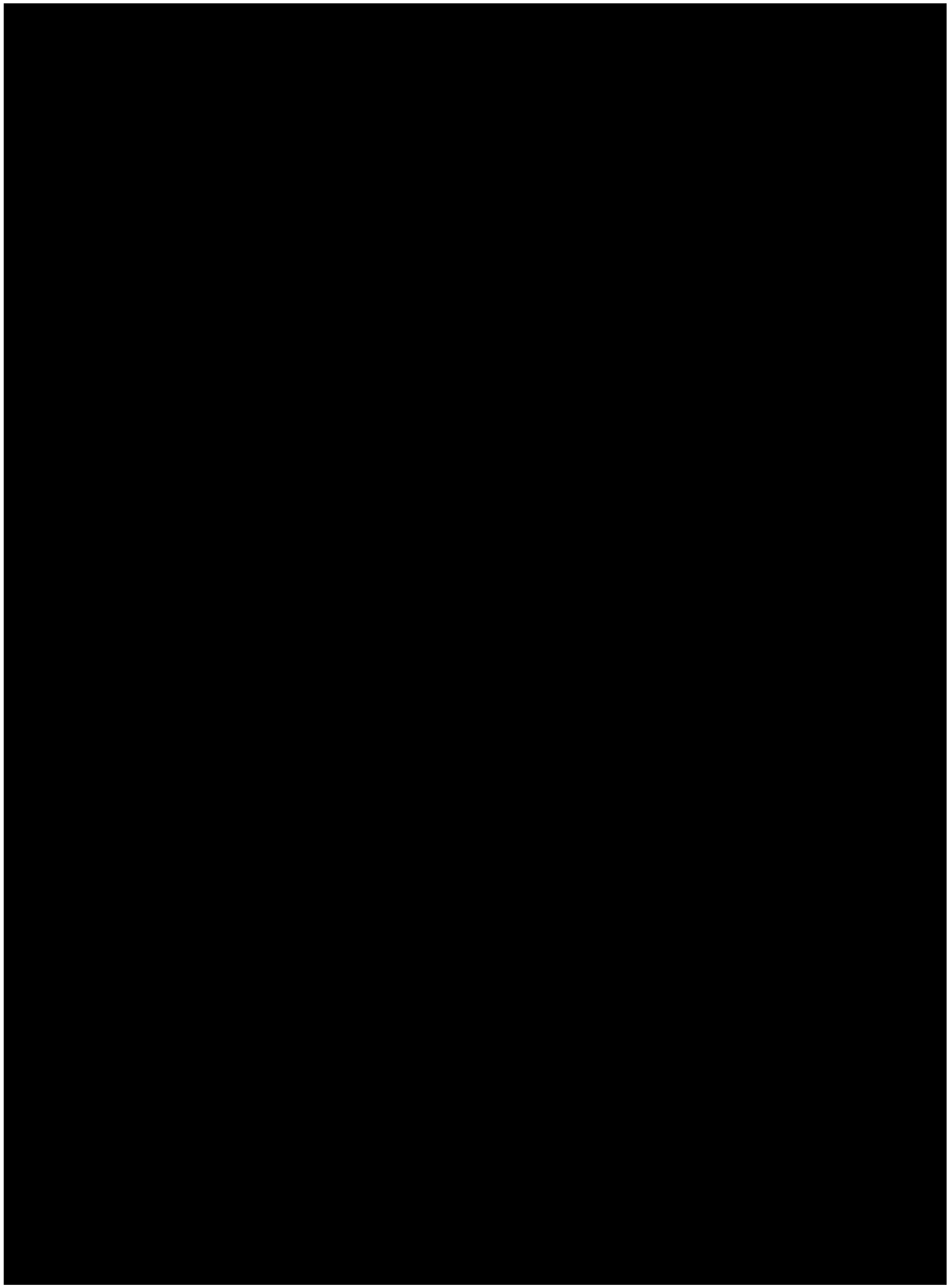

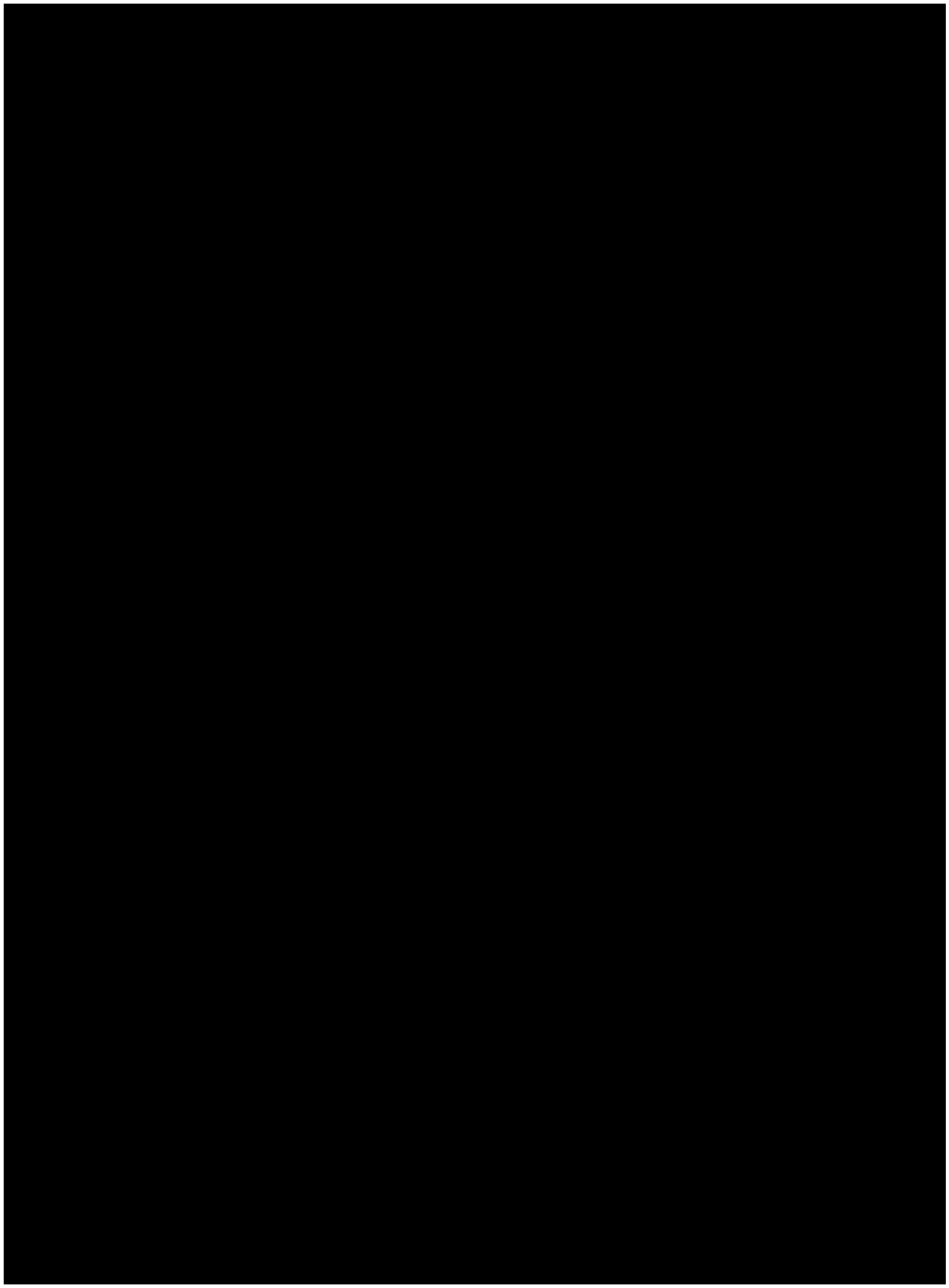

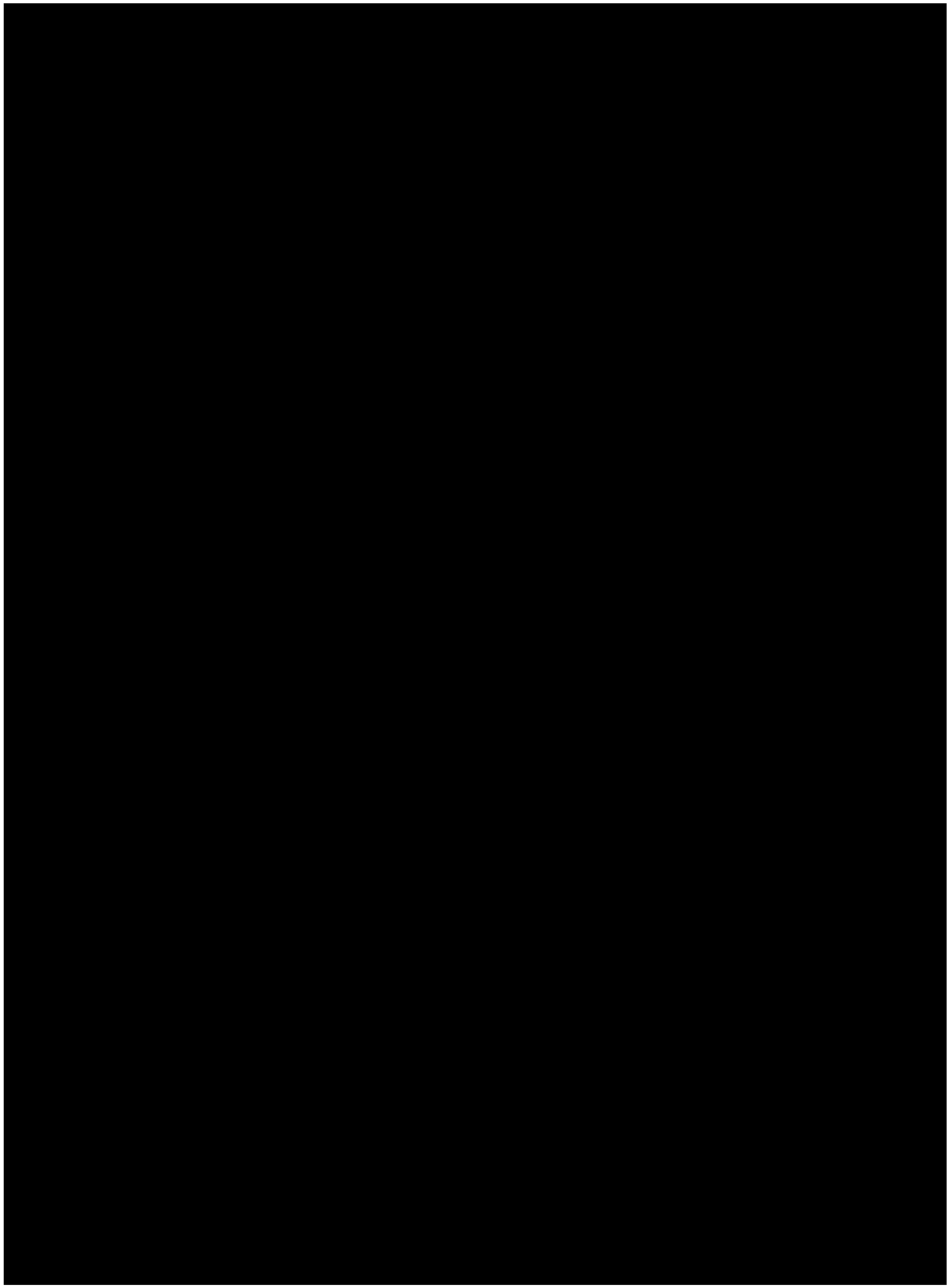

[redacted]

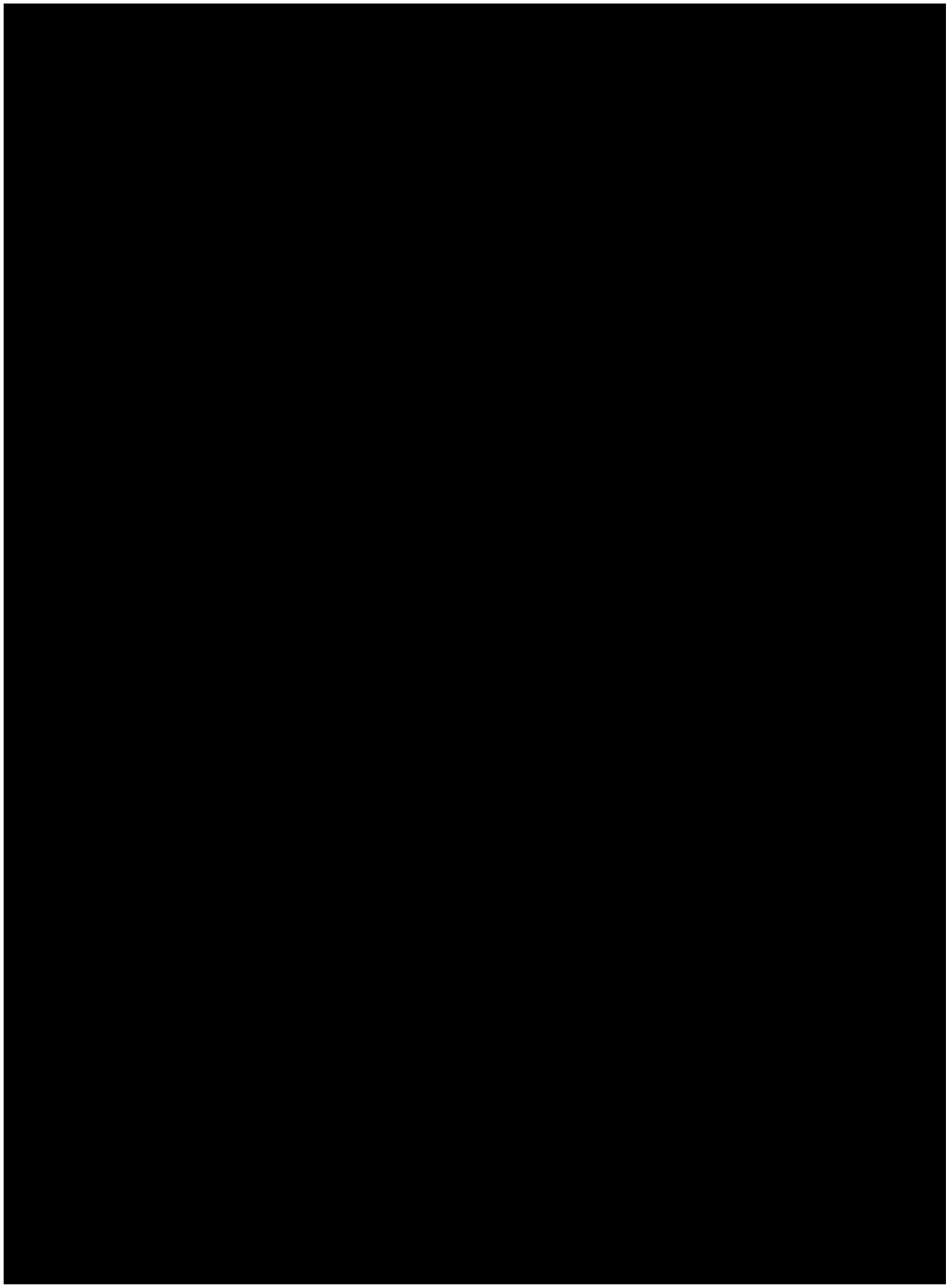

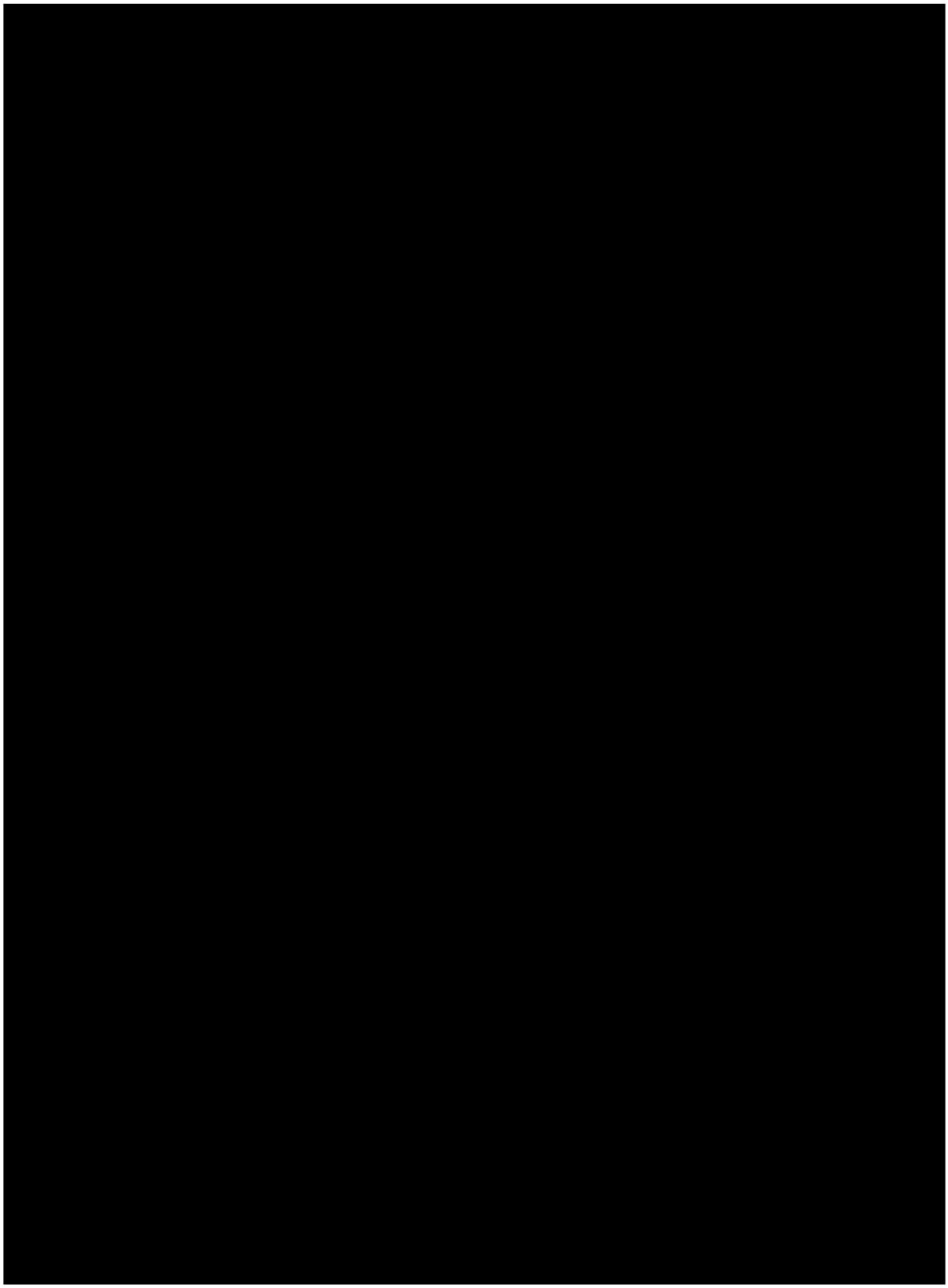

[redacted]

diseases: GSK-3 and CSK-3β as therapeutic targets

[redacted]

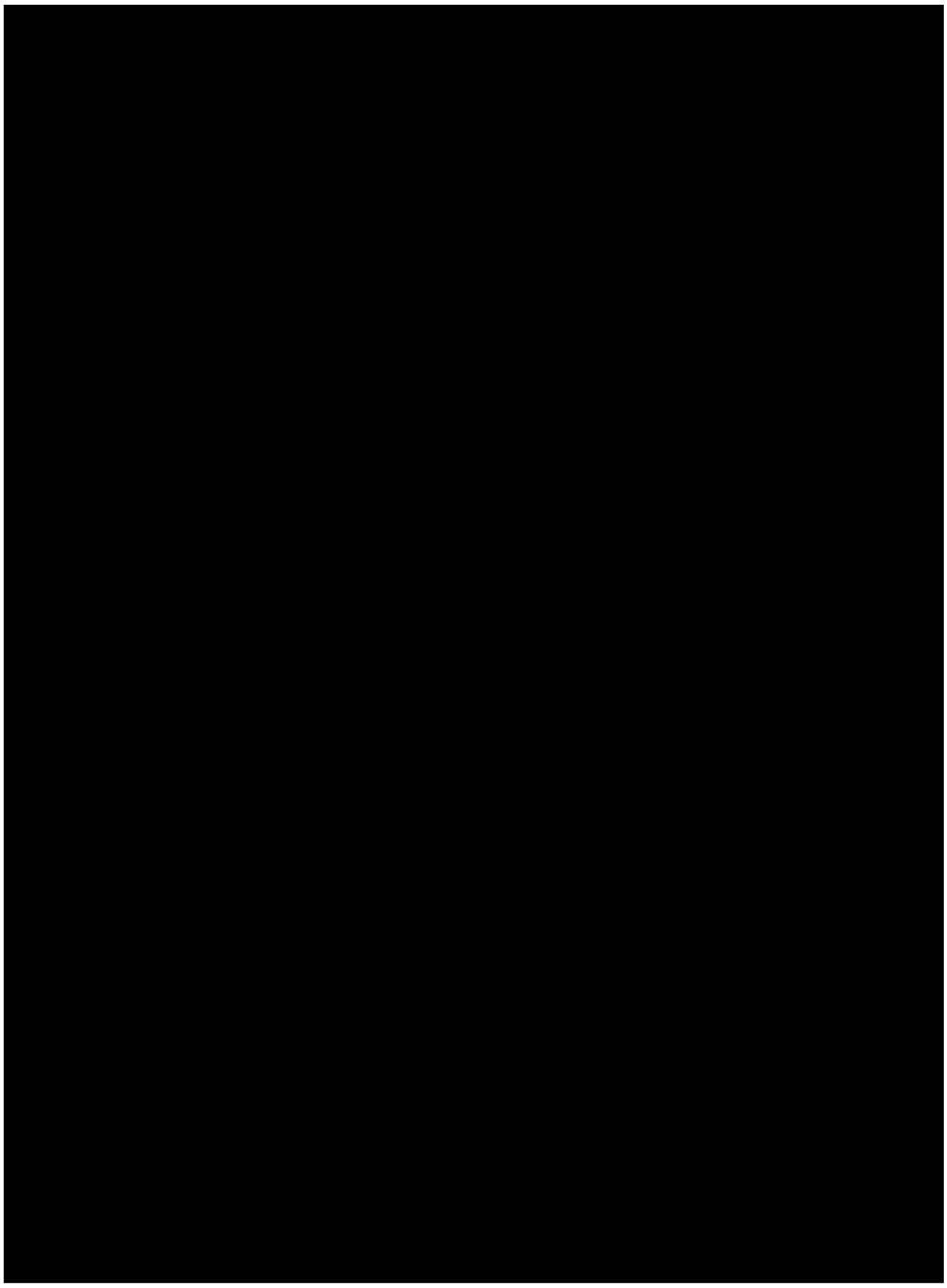

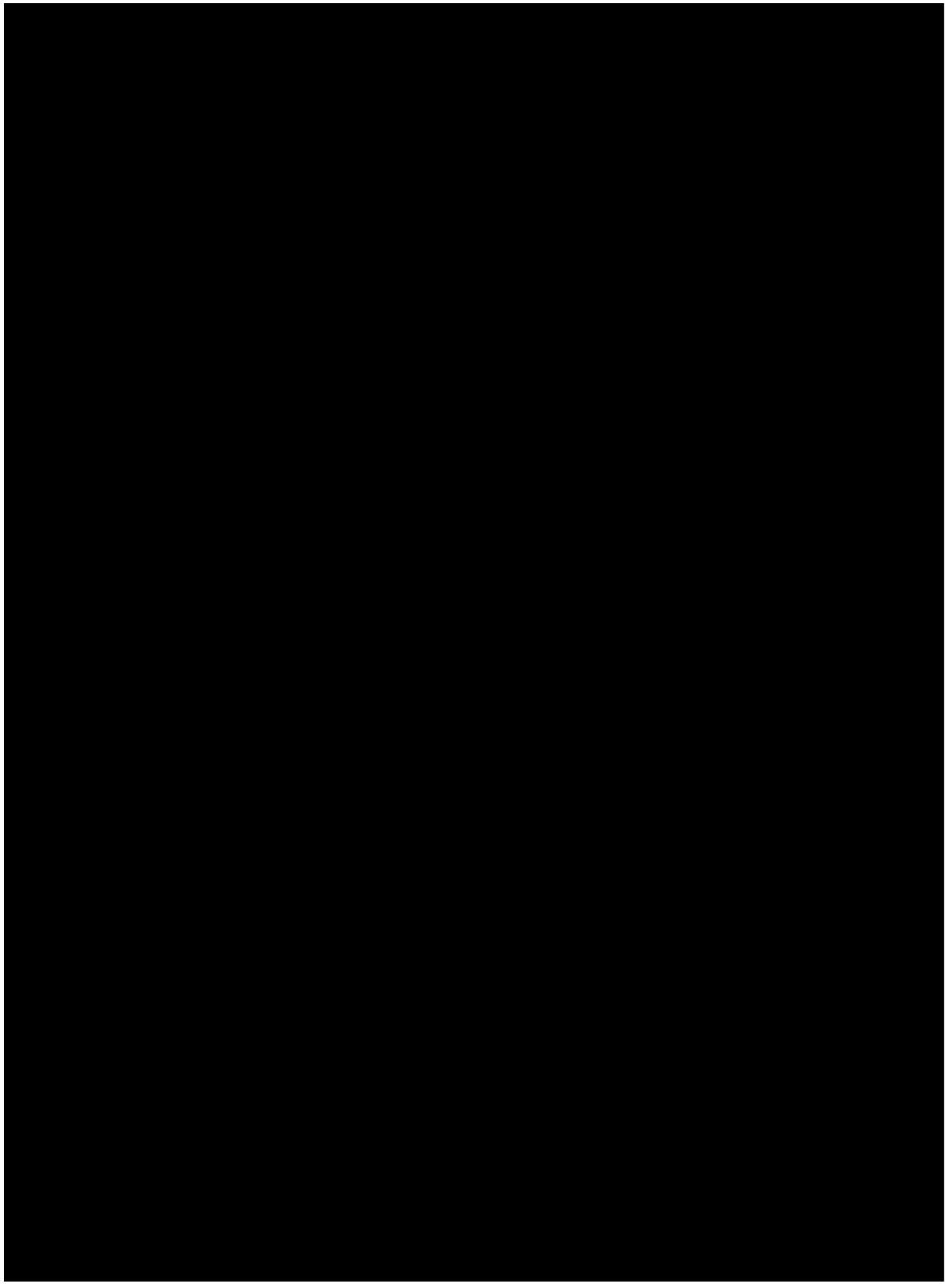

[redacted]

[redacted]

[redacted]

[redacted]

[redacted]

[redacted]

[redacted]

[redacted]

[redacted]

[redacted]

[redacted]

[redacted]

[redacted]

[redacted]

[redacted]

[redacted]

[redacted]

[redacted]

[redacted]

[redacted]

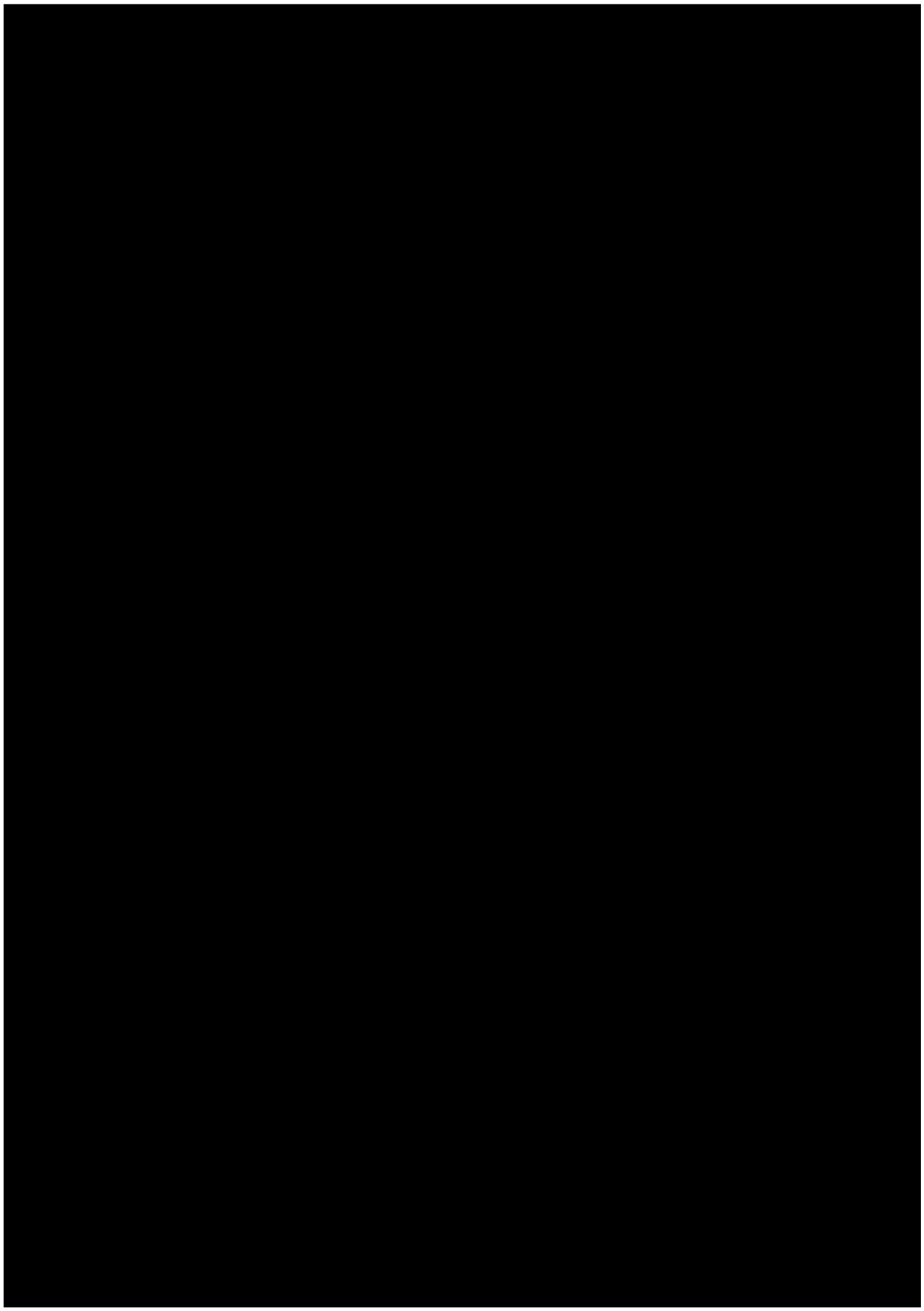

[redacted]

ANNEX 3

Supplementary information – Chapter 1. Introduction

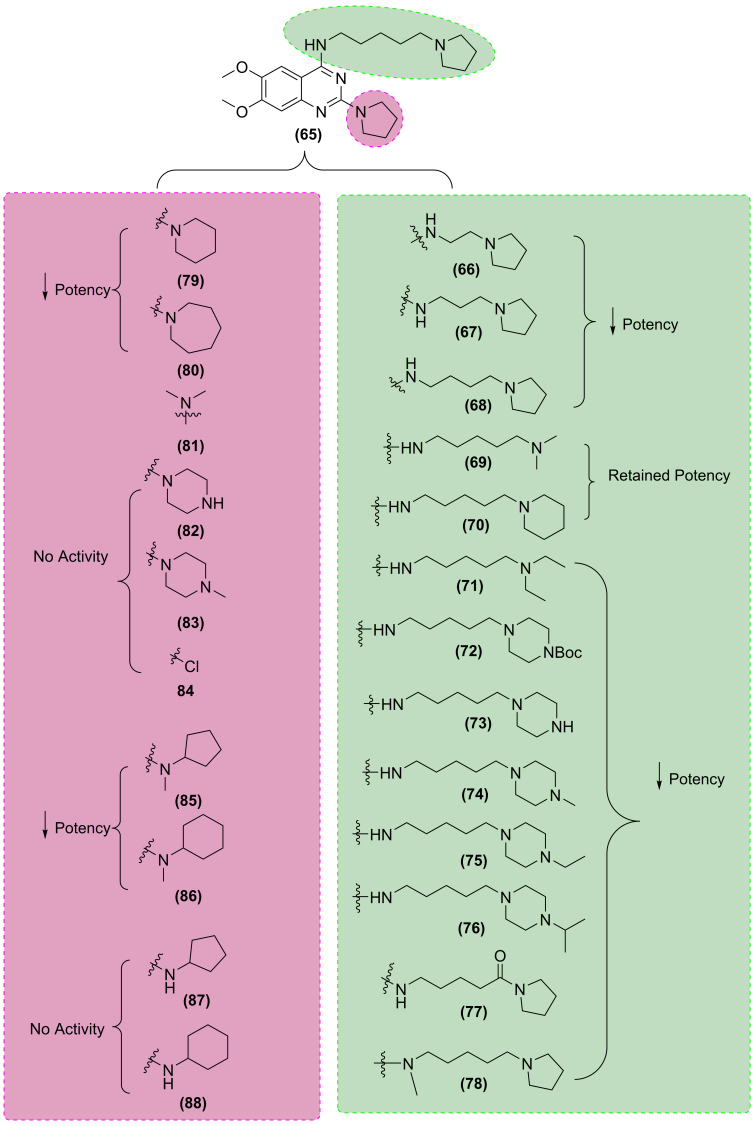

Supplementary Figure 1. Part IV: Rationing, design, and synthesis of G9a inhibitors.

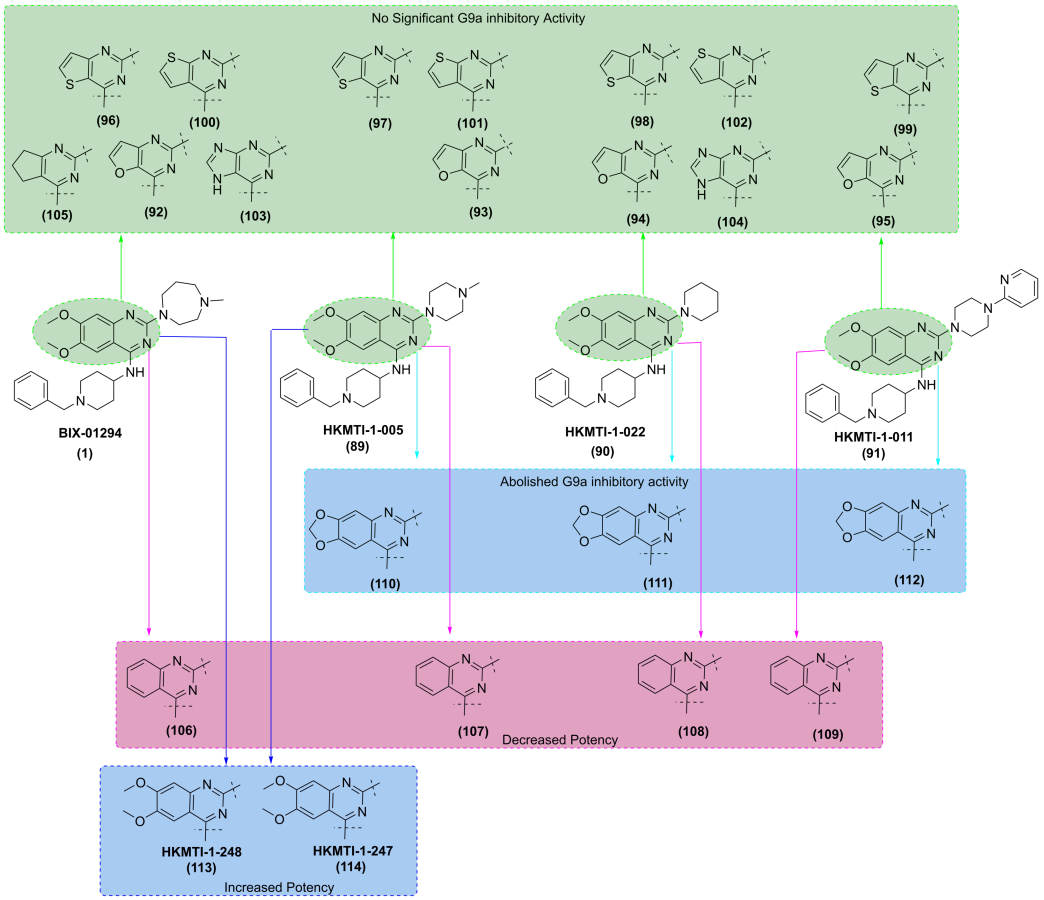

Supplementary Figure 2. Part V: Rationing, design, and synthesis of G9a inhibitors.

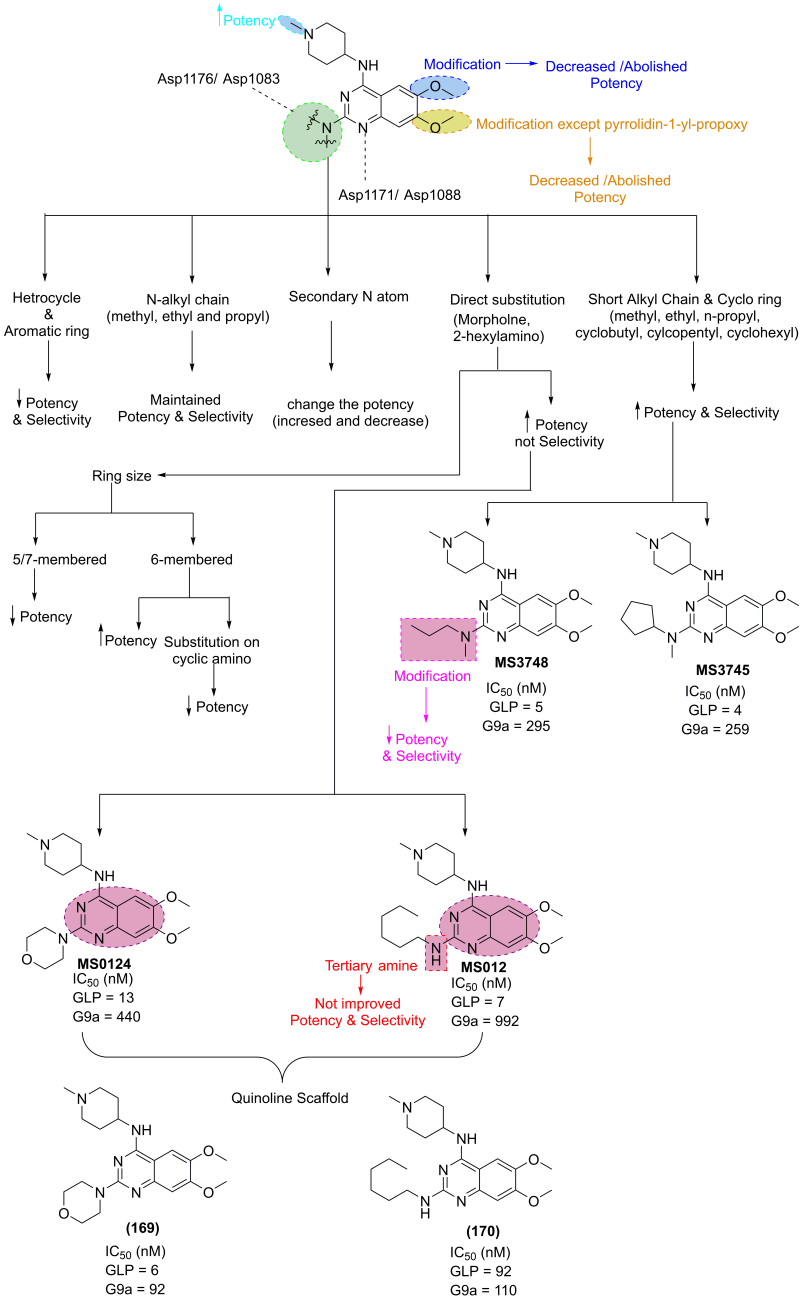

Supplementary Figure 3. Part VI: Rationing, design, and synthesis of G9a inhibitors.

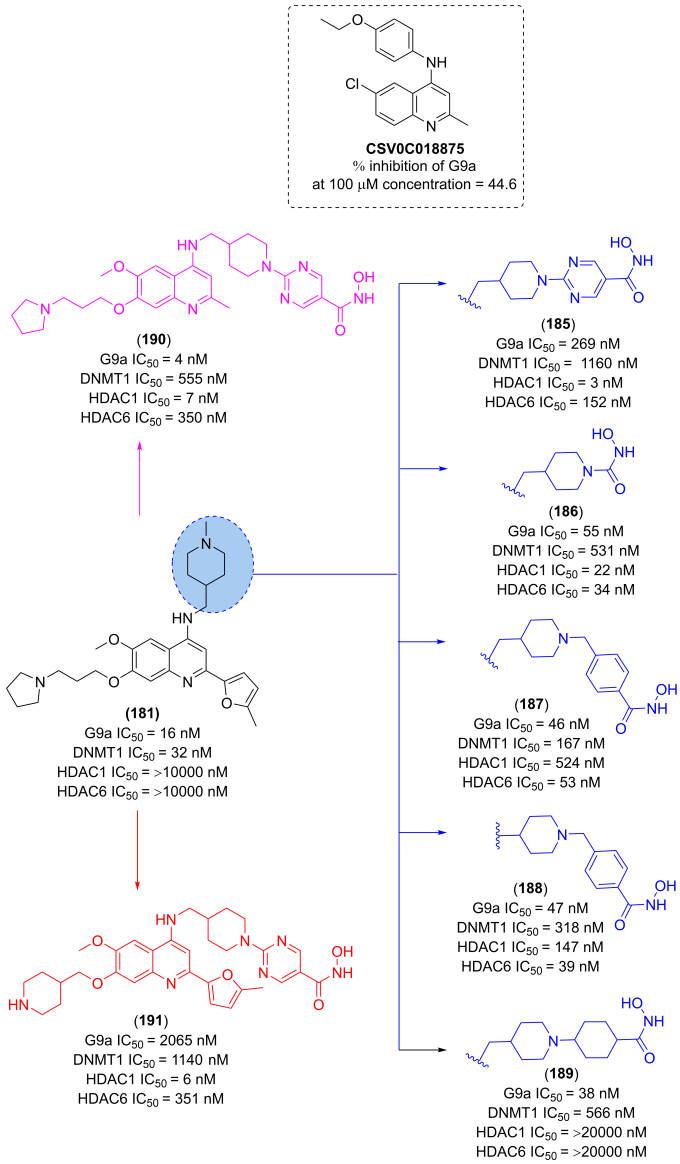

Supplementary Figure 4. Part VII: Rationing, design, and synthesis of G9a inhibitors.

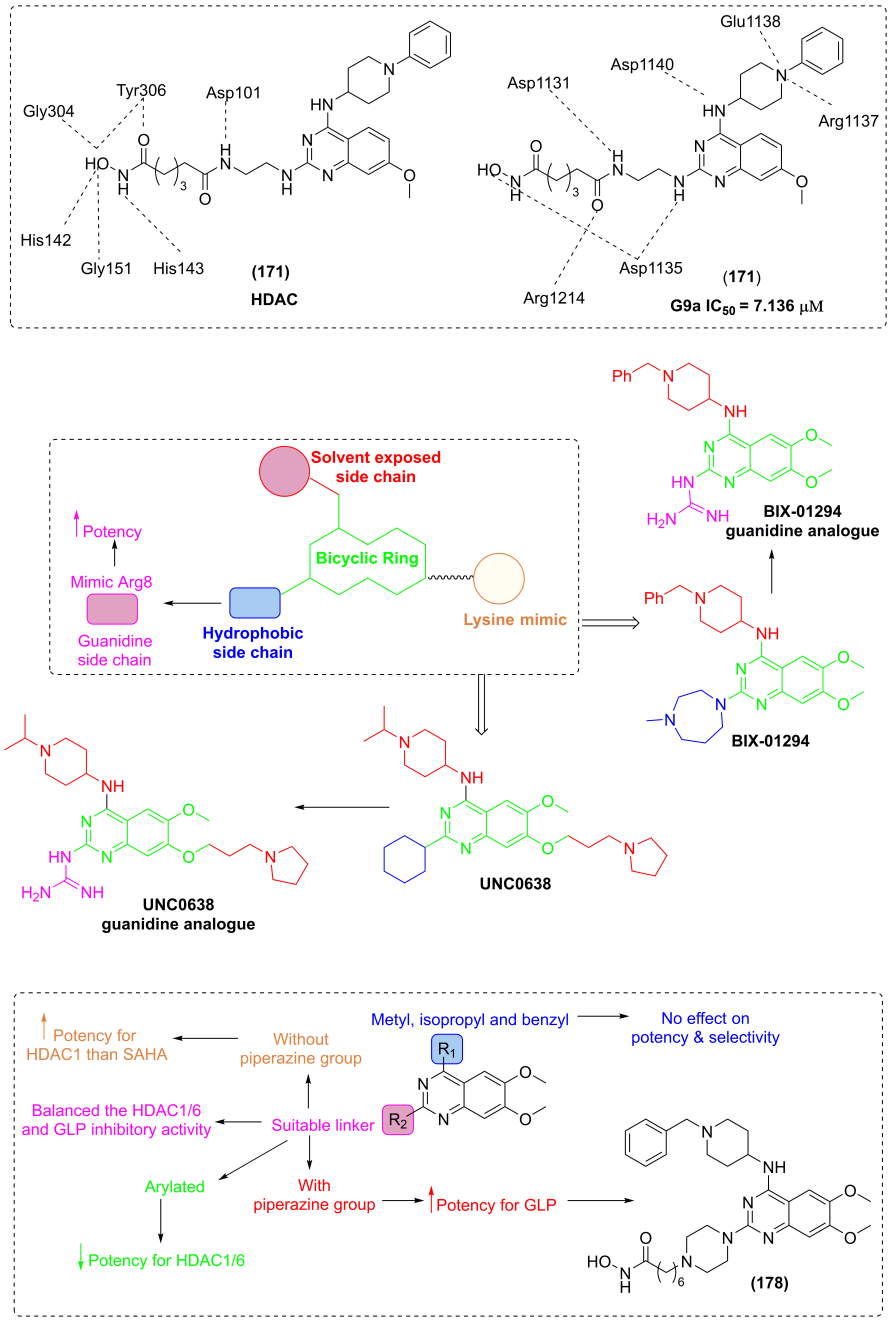

Supplementary Figure 5. Part VIII: Rationing, design, and synthesis of G9a inhibitors.

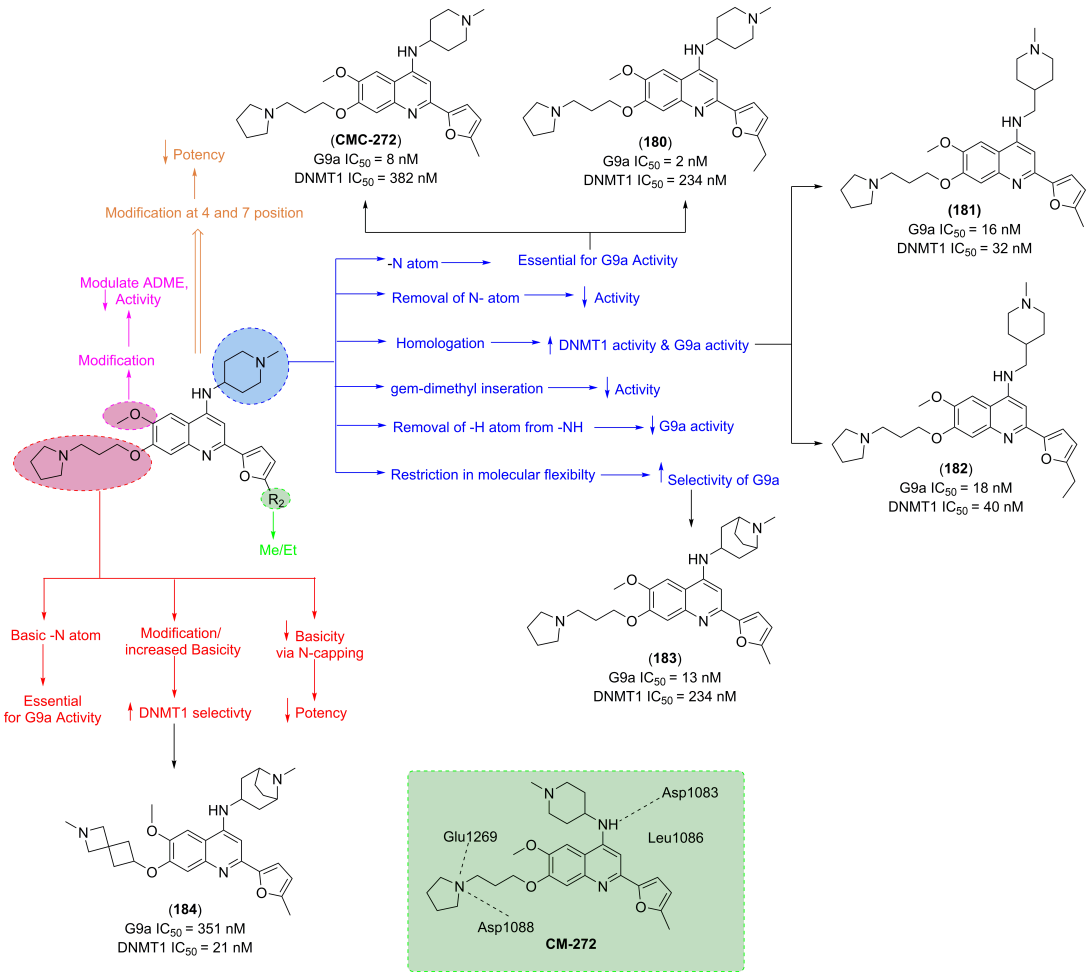

Supplementary Figure 6. Part IX: Rationing, design, and synthesis of G9a inhibitors.